kOMUNIKÁCIE
COMMUNICATIONS

A - OPERATION AND ECONOMICS

B - MECHANICAL ENGINEERING

C - ELECTRICAL ENGINEERING

D - CIVIL ENGINEERING IN TRANSPORT

E - MANAGEMENT SCIENCE AND INFORMATICS

F - SAFETY AND SECURITY ENGINEERING

ASSESSING THE ENERGY EFFICIENCY OF AN ELECTRIC CAR

František Synák[1,*], Matej Kučera[2], Tomáš Skrúcaný[1]

[1]Department of Road and Urban Transport, Faculty of Operation and Economics of Transport and Communications, University of Zilina, Zilina, Slovakia
[2]Department of Measurement and Applied Electrical Engineering, Faculty of Electrical Engineering and Information Technology, University of Zilina, Zilina, Slovakia

*E-mail of corresponding author: frantisek.synak@fpedas.uniza.sk

Resume
Electric car does not supply all the electric energy, obtained from the electric network, to the wheels in the form of mechanical energy. During such a transformation, a part of this energy is lost. The article endeavours to determine the energy efficiency of selected electric car. The electric car used for measurements is not from the batch production since that is a vehicle designed at University of Zilina. The efficiency has been observed while driving under the conditions of amended methodology of New European Driving Cycle (NEDC). The measured value of electric car's efficiency is being analyzed from the energy consumption, as well as emission production, points of view.

Article info
Received 31 March 2020
Accepted 16 May 2020
Online 22 October 2020

Keywords:
electric car,
energy efficiency,
emissions,
road traffic

Available online: https://doi.org/10.26552/com.C.2021.1.A1-A13

ISSN 1335-4205 (print version)
ISSN 2585-7878 (online version)

1 Introduction

Energy input to an electric car in the form of electric energy obtained from the electric network is regulated before being supplied to the wheels in the form mechanical energy; there is a change in the value of electric current and voltage and it is further stored in the accumulator and transformed into mechanical energy in the electric motor. These processes are connected to energy losses [1]. Scientific publications, in many cases, pay attention only to particular components of electric cars, mostly to energy efficiency of electric car‘s batteries [2-4], or to efficiency of hybrid vehicles [5-7].

The article aims to determine the energy efficiency of an electric car. Through the measurements, the amount of energy obtained from the electric network and the amount of energy supplied to the dynamometer's cylinders, by means of which the measurements were performed, have been compared. The value of energy efficiency of electric car affects several aspects. One of those aspects is the amount of energy consumed that is needed for overcoming a certain distance. For instance, when increasing the overall energy efficiency of electric car from 60% to 80%, the energy consumption needed for 100 km to be driven would decrease by 20%. In the case of average value of energy consumption of 20 kWh . 100 km^{-1}, the 20%-increase in efficiency would lead to decrease in energy consumption to 16 kWh . 100 km^{-1}. What is more, every single kWh of electric energy consumed is connected with a certain amount of emissions produced, certain amount of non-renewable energy resources consumed as well as certain amount of money spent on electric energy purchase [8-9].

The value of energy efficiency of electric car also affects the value of its coasting, or the needed capacity of electric car's batteries. Such a capacity closely relates to mass of the batteries. Increasing of battery capacity by 10 kWh means increase in mass of electric car by about 15 kg depending on the battery type. Such an increase can cause a difference in energy consumption, according to driving cycle parameters [10], up to 1 kWh . 100 km^{-1}. When increasing the battery capacity, as well as the unladed mass of electric car, it leads to decrease in vehicle load capacity [11].

There is also a relation between the amount of emissions produced and the energy efficiency and consumption of an electric car [12]. A theoretical amount of selected emissions produced in connection with production of electric energy used for the electric car to be driven has been calculated, as well. Such a theoretical production of emissions of carbon dioxide, carbon monoxide, nitrogen oxides and particulate matters has been calculated per unit of energy consumed. The reason of the comparison of emissions produced by electric cars and combustion engine vehicles lies in the fact that the road transport is a major producer of the above-mentioned gaseous emissions [13].

Carbon dioxide CO_2 is considered as a gas causing the greenhouse effect with approximately 55% share on it. In the EU, the transport is the only sector in which there

Figure 1 *Vehicle used for measuring*

Table 1 *Technical parameters of vehicle used for measuring [16]*

parameter	value
electric motor	AC, AKOE 15/30 kW, 80 V
controller	Curtis 1238
batteries	Thunder Sky LiFeYPO4, 300 Ah
gross vehicle weight	1300 kg
maximal speed	80 $km.h^{-1}$
frame	steel tube space frame
body	steel/plastic
length	3100 mm
wheelbase	2130 mm
width	1550 mm

was no reduction, but an increase in the greenhouse gases production when comparing to 1990 [13].

Carbon monoxide CO is a colourless and odourless gas, which is highly toxic for humans. It can bind with haemoglobin up to 300 times more efficiently than oxygen resulting in a limited transportation of oxygen from lungs into the tissues and thus the tissues and cells are being damaged. The longer exposure of humans, together with its higher concentration in blood, causes coma or death [14].

Specific chemical compounds, known as nitrogen oxides $NO_{x,}$ affect the greenhouse effect, acid rains and health of population negatively.

Particulate matters PM have a negative impact on population's health. They also cause faster ice melting due to their higher absorption of light resulting from black colour [15].

Concerning the electric car operation, the amounts of emissions produced have been compared to values calculated for combustion engine vehicles.

Devices through which is the energy for the wheels to be driven coming can be divided into those that operate only with electric energy and those that operate only with mechanical energy. There is an exception seen in the electric motor's shaft in which the transformation of electric energy to mechanical energy during the wheel driving mode and the transformation of mechanical energy to electric energy during the recuperation mode, are being under way.

The electric car used for measurements has all of its devices, from the electric socket up to electric motor's shaft, operating only with electric energy and from the electric motor's shaft up to wheels, operating only with mechanical energy. Not taking into consideration mechanical losses, conducting the vehicle coasting test on the dynamometer has enabled to determine the efficiency of particular parts of vehicle that operate with electric or mechanical energy. The mechanical losses in electric motor are caused only by two rolling bearings and thus, it can be assumed that they are not of significant value and their share on the result accuracy can be neglected.

The article contributes an insight into the efficiency of energy transmission by electric cars from several points of view.

2 Measurement methodology

In the form of mechanical energy, there has been the transmission energy efficiency, taken from electric energy to dynamometer's cylinders, determined.

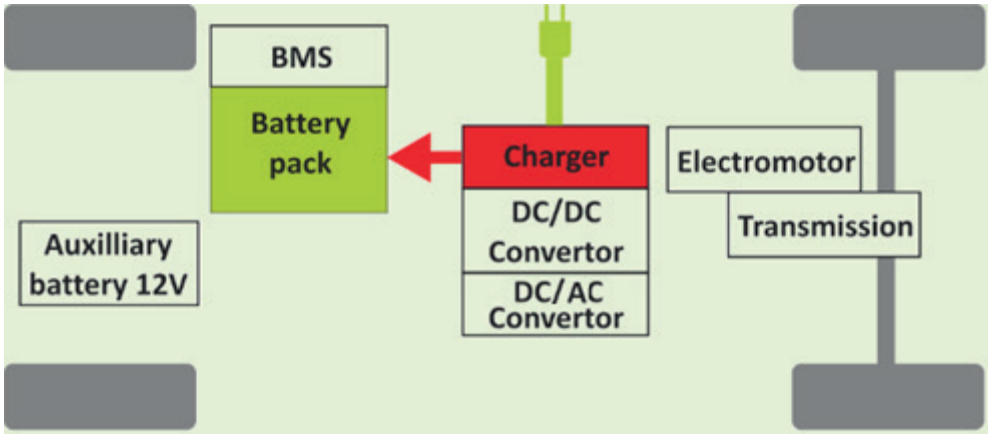

Figure 2 *Mode of battery charging [16]*

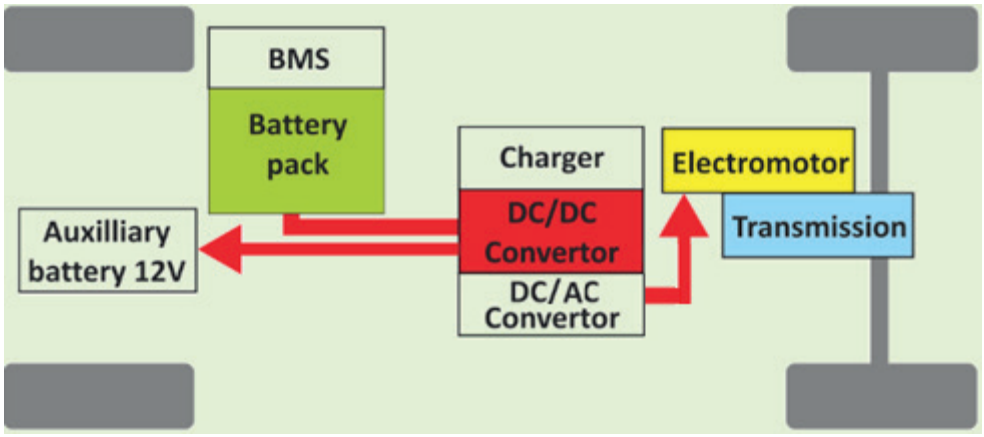

Figure 3 *Mode of wheel driving [16]*

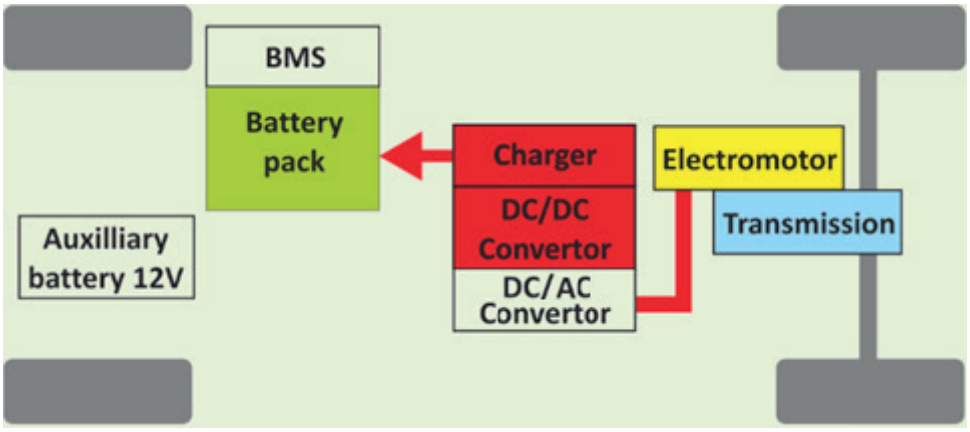

Figure 4 *Recuperation mode [16]*

2.1 Vehicle used for measuring

Figure 1 shows the vehicle used for measuring. It is called Edison II and its production was at University of Zilina.

The technical parameters are given in Table 1.

The basic vehicle modes comprise charging, wheel driving and recuperation. Particular modes are controlled via battery management system. The energy flow during the charging mode is displayed in Figure 2.

As seen from Figure 2, while charging, the energy is transmitted from the socket to the battery pack via charger together with convertor.

Figure 3 displays the flow of energy while wheel driving.

During the mode of wheel driving, the electric energy from batteries is being transmitted through the DC/DC convector into the electric motor in which it is converted into mechanical energy. This energy is further transmitted through the planetary gear to the wheels. Electric energy in

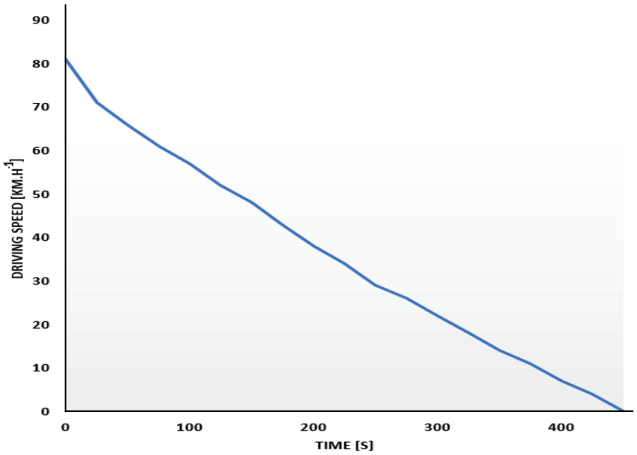

Figure 5 *Vehicle deceleration during coasting deceleration measurement*

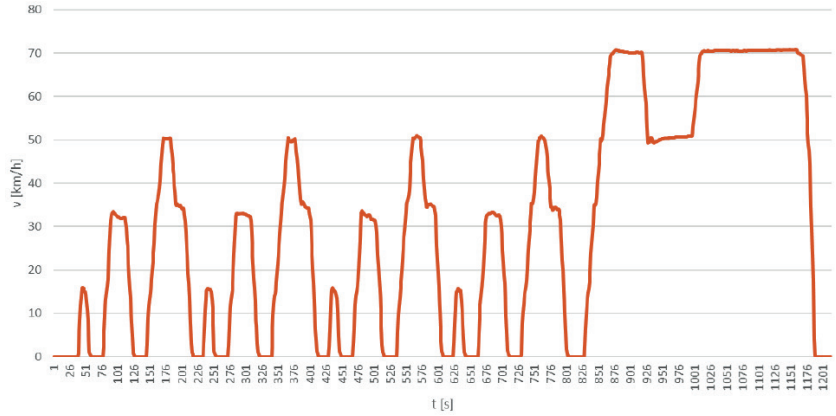

Figure 6 *Real driving speed according to amended methodology of the NEDC*

the vehicle is also necessary for on-board computer, vehicle headlights, windscreens and other devices to be connected. It is, therefore, also transmitted from the DC/DC convector to 12 V auxiliary battery intended for the above-mentioned devices to be plugged-in.

While vehicle is running, there is no need to bring the driving force on the wheels. It can be seen while engine braking for example when driving downhill [17]. The energy flow during the recuperation is shown in Figure 4.

During the mode of energy recuperation, mechanical energy from the wheels is being transmitted through the transmission to electric motor. The electric motor converts the mechanical energy into electric energy, which is further transmitted through the controller and DC/DC convertor to the charger and subsequently to the batteries.

2.2 Device used for measuring

The device used for measuring was a dynamometer MAHA MSR 1050. The measurement deviation of this device is +/-2% from the measured value according to the manufacturer. The dynamometer enables a simulation of a vehicle driving by simulating the real driving resistances via braking or cylinder driving. At the same time, it provides the better accuracy in comparison to measurements while road driving and it also enables to record a value of mechanical energy delivered from the wheels on its cylinders [18]. In order to have the cylinder values at the level of situation in which a vehicle is road driving, it is necessary to introduce these values into the cylinder test station's control computer. The values are achieved by the coasting deceleration measurement of vehicle resistance under the conditions of Standard EN 30 0556 [19]. Such measurement relies on a vehicle with prescribed laden mass, which is accelerated up to the speed about of 80 km.h^{-1}; disconnection between the engine and wheels, and on the recording of vehicle coasting [20]. Figure 5 depicts the vehicle deceleration during measurement.

The recorded vehicle speed that depends on the time of disconnection between the engine and wheels is further introduced into the cylinder test station's computer. Based on these values and measurement results, the computer sets values of deceleration or acceleration directly at the cylinders during the particular driving modes. At the same time, based on the coasting test, the computer is calculating the difference in values of the rolling resistance between the road and cylinder driving since the rolling resistance has an increasing character on the cylinders compared to road surface. Thus, the cylinder test station can fully provide a road driving simulation [21].

2.3 Measurement process

Measurement of the transmission energy efficiency has been performed while the vehicle driving according to amended new European driving cycle, known as NEDC [22]. Such amendment of NEDC cycle comprises a change in the maximum driving speed from 121 km.h^{-1} to 70 km.h^{-1}. The instantaneous speed deviation, opposite to the prescribed one, has been of ± 2 km.h^{-1}. The real course of driving, according to amended methodology of the NEDC, is shown in Figure 6.

While vehicle driving under the NEDC conditions, various driving modes are changing such as vehicle acceleration, driving at the stabilised speed, or vehicle deceleration as seen in Figure 5. Thus, while driving, there are both driving modes active, wheel driving and recuperation modes.

According to conditions of the NEDC, the transmission energy efficiency has been determined while vehicle driving under the comparison of the amount of energy supplied to vehicle from the electrical socket and energy delivered from the vehicle into dynamometer's cylinders.

An electricity meter has been used for measuring the energy delivered from the socket since it is a designated measuring device, which is tested according to [23]. The electricity meter displays the amount of energy consumed in kilowatt-hours. A kilowatt-hour is not a part of the International System of Units (SI), although it is derived from the watt unit. According to SI, the unit that corresponds to the energy is a joule. One joule is one watt-second. In order to calculate the amount of energy delivered in the joules, the relation below has been used:

$$EE_s = EE_{sk} \cdot 36 \cdot 10^5 , \tag{1}$$

where:
EEs - electric energy delivered in [J],
EE_{sk} - electric energy delivered in [kWh].

Value of electric energy delivered has been determined by subtraction of the value seen in the electricity meter at the end of charging from the value seen at the beginning. While charging the electric car from the socket, to which the electricity meter was connected, there was no electric energy taken by any other device.

The dynamometer has recorded the power supplied to the cylinders by the wheels 10 times per second. In order to compare the energy supplied to the dynamometer's cylinders with the energy delivered from the socket, it was necessary to calculate the energy supplied to the cylinders firstly according to relation:

$$EM_{sc} = \frac{P_c}{T_m} , \tag{2}$$

where:
EM_{sr} - mechanical energy supplied to the cylinders [kWh],
P_c - average value of power supplied to the dynamometer's cylinders [kW],
T_m - time of measuring [hours].

Subsequently, the energy supplied to the cylinders and calculated in kWh was recalculated into joules according to relation (1).

By the theoretical calculations, it was also possible to determine an approximate energy loss between the electric socket and electric motor's shaft as well as between the electric motor's shaft and cylinders of dynamometer. This calculation has been made based on the measurement between the power of electric motor's shaft and power transmitted on the dynamometer's cylinders.

2.4 Calculation of average energy consumption

Average energy consumption, given per 100 km of the distance driven, has been determined, as well. Based on the average energy consumption per one amended NEDC cycle and its average length, the energy consumption has been calculated. On the grounds of transmission energy efficiency, the energy consumption has been calculated as an energy consumption taken from the socket, energy consumption in the electric motor's shaft and energy consumption on the dynamometer's cylinders.

The energy consumption on the cylinders of dynamometer has been calculated according to relation:

$$EC_c = \frac{E_{dc}}{D} \tag{3}$$

where:
EC_c - energy consumption on dynamometer's cylinders [kJ.100km^{-1}],
E_{dc} - energy delivered to dynamometer's cylinders [kJ],
D - trajectory driven while measuring [m] [24].

Similarly, the energy consumption in connection with energy taken from the electric socket has been calculated, however, there is a difference. Instead of energy delivered to the dynamometer's cylinders, the energy taken from the socket has been taken into consideration within the formula of calculation.

In order to calculate the energy consumption in connection with electric motor shaft, the same relation has been used, though there has been also the transmission energy efficiency from the electric motor's shaft on the dynamometer's cylinders borne in mind.

3 Results

Figure 7 displays the curves showing the courses of power measured by Edison II vehicle on the cylinder test station MAHA MSR 1050. The abscissa displays the driving speed, the left ordinate axis displays the power and the right ordinate axis shows the torque.

Data from Figure 7 can also be obtained from the control computer of MAHA MSR 1050 numerically. By averaging the data values of power on the dynamometer's cylinders and torque, it is possible to find out that the transmission power efficiency from the electric motor's

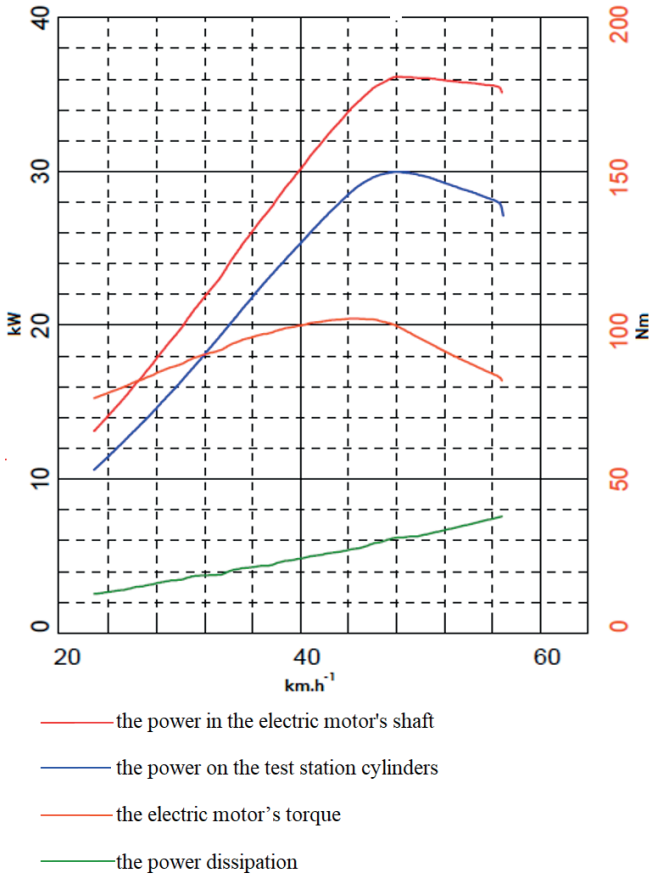

Figure 7 *The course of power and torque in Edison vehicle*

Table 2 *The values of selected parameters during measurement*

number of measuring	time of measuring (s)	average driving speed ($km.h^{-1}$)	distance driven (m)	average cylinders power (kW)
1.	1324	28.14	10349	2.643
2.	1345	27.97	10449	2.607
3.	1321	27.82	10208	2.640
4.	1336	28.02	10398	2.617
5.	5394	27.03	40499	2.563

shaft on dynamometer's cylinders is 82%. Thus, there is an energy loss of 18% between the electric motor's shaft and cylinders. When assessing results of calculations, it is necessary to take into consideration that besides losses in the vehicle there are also losses caused by the wheels' rolling resistance along the dynamometer's cylinders. Therefore, the calculation cannot be regarded as accurate but approximate [25]. The values measured during one amended NEDC cycle correspond to measurements from the number 1 up to 4 and the results measured during four successive amended NEDC cycles and subsequent charging correspond to measurement number 5.

The parameters of particular measurements according to amended NEDC cycle are shown in Table 2.

Results of the transmission energy efficiency are given in Table 3.

The transmission energy efficiency from the electric socket on the dynamometer's cylinders has been 45% that is quite a low value [26]. However, it is necessary to bear in mind that there is a rolling resistance added into the efficiency [27]. On the other hand, the rolling resistance, as well as the other driving resistances, is always seen when vehicle driving.

Table 4 shows the value of energy according to the place of its dissipation, that means its conversion into other energy than mechanical, supplied to the dynamometer's cylinders.

As seen from Table 4, there are large energy losses between the socket and electric motor's shaft.

Based on the data from Tables 2 and 3, it is possible to calculate an average energy consumption of Edison II per 100 km while driving according to amended NEDC cycle.

Table 3 *Transmission energy efficiency from the electric socket on dynamometer's cylinders*

number of measuring	energy delivered (kJ)	energy on cylinders (kJ)	efficiency (%)
1.	7711	3499	45
2.	7715	3506	45
3.	7672	3488	45
4.	7711	3496	45
5.	30924	13824	45

Table 4 *Reduction of electric car efficiency*

number of measuring	overall energy lost (kJ)	energy lost in front of the electric motor's shaft (kJ)	energy lost in front of the electric motor's shaft (%)	energy lost behind the electric motor's shaft (kJ)	energy lost behind the electric motor's shaft (%)
1.	4212	3454	82	758	18
2.	4209	3451	82	758	18
3.	4184	3431	82	753	18
4.	4215	3456	82	759	18
5.	17100	14022	82	3078	18

Table 5 *Average energy consumption*

place of energy consumption calculation	dynamometer's cylinders ($kJ.100km^{-1}$)	electric motor's shaft ($kJ.100km^{-1}$)	electric socket ($kJ.100km^{-1}$)
energy consumption	33958	40071	75373

Table 6 *Emission production depending on how a vehicle is driven*

vehicle	emission ($g.kwh^{-1}$)			
	CO	CO_2	NO_x	PM
heavy goods vehicles	1.5	-	0.4	0.01
SI engines for M1 vehicles	0.989	253	0.06	0.06
electric energy from power plants in EU	0.186	459.2	0.348	0.019

The average energy consumption pursuant to the above-mentioned conditions is given in Table 5.

As seen from Table 5, the wheels' energy consumption has been 45% of the energy consumption taken from the electric socket. The energy consumption of electric motor's shaft represented 53% of the energy consumption of electric socket. That means there was 47% energy from the electric socket lost between the electric socket and electric motor's shaft.

Publication [28] shows the theoretical calculation of the amount of selected emissions produced per energy unit. There is emission production compared between the combustion engine vehicles and vehicles with electric motors. Concerning the vehicles with electric motor, the data are calculated for electric energy made in European Union. Since the Standard [29] sets the emissions in kilowatt-hour, the data are also set so. Values have been calculated based on data from the Euro 6 standard and according to values given by the power plants in the case of electric cars. The data are calculated for the motor's shaft energy output and can be seen in Table 6.

Concerning the heavy goods vehicles and SI engines for M1 vehicles, it is considered that only a certain part of the chemical energy from the fuel is converted into mechanical energy on the motor's shaft energy output, depending on the energy efficiency of combustion engine. On the other hand, in the case of electric cars, it is considered that all of the energy delivered from the electric socket is being converted into mechanical energy on the output of the motor's shaft. However, that is not a true fact as proved in the previous part of the article. Based on the measurement results, it is possible to add a value of theoretical production of selected emissions to Table 6 by taking into consideration the energy efficiency of energy transmission measured from the electric socket up to electric motor's shaft that is seen in Table 7.

Table 7 *Emission production depending on efficiency of electric car's transmission energy and how a vehicle is driven_*

vehicle	emission (g.kwh^{-1})			
	CO	CO_2	NO_x	PM
heavy goods vehicles	1.5	-	0.4	0.01
SI engines for M1 vehicles	0.989	253	0.06	0.06
electric energy from power plants in EU, 100% efficiency	0.186	459.2	0.348	0.019
electric energy from power plants in EU, real efficiency	0.273	675	0.512	0.028

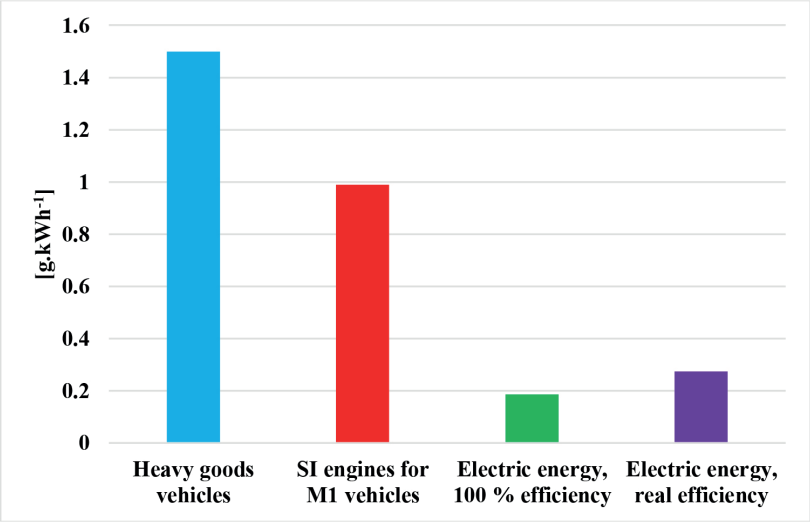

Figure 8 *Comparison of theoretical CO production*

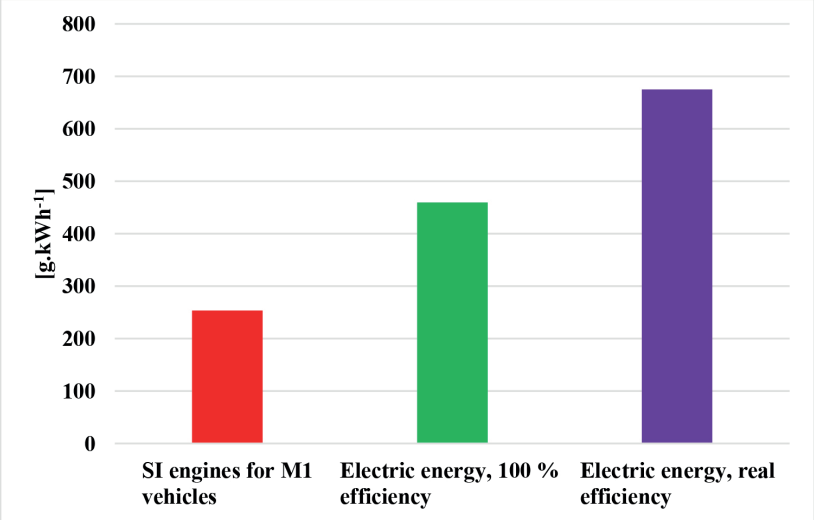

Figure 9 *Comparison of theoretical CO_2 production*

For better transparency, the results are also given in graphs in Figures 8-11.

As seen from Figure 8, the electric cars should not produce more CO than the combustion engine vehicles. CO is a gas, which affects the health of population negatively, and thus, it is important that electric cars do not produce CO directly while running.

Figure 9 shows the comparison of CO_2 production. Since the CO_2 production is not being assessed within the heavy goods vehicles, it is not given in Figure 9 either.

The theoretical production of the greenhouse gas CO_2, relating to the operation of electric cars is significantly higher as for the SI engine vehicles. When taking into consideration the real efficiency of energy transmission from the electric socket on the electric motor's shaft, the theoretical production of CO_2 within the electric cars has increased from the value of 459 g.kWh^{-1} to 675 g.kWh^{-1}. Considering the combustion engines, CO_2 production is being proportional to the fuel consumption [24]. Assuming the higher engine energy efficiency of heavy goods vehicles,

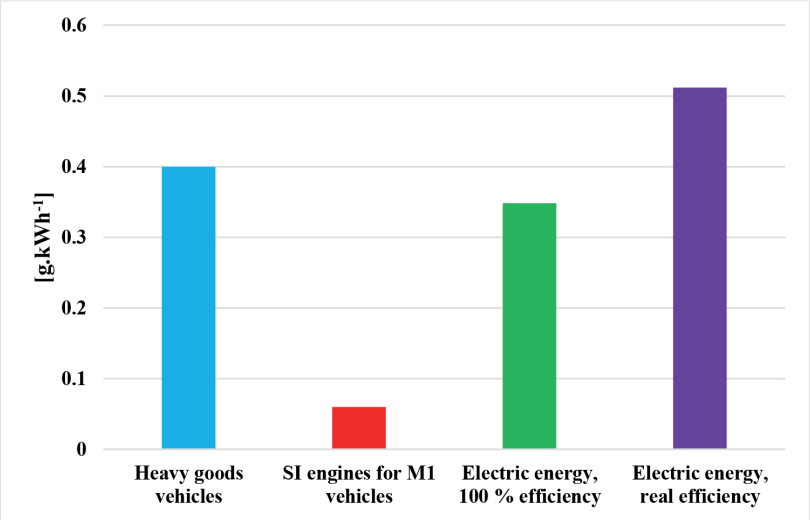

Figure 10 *Comparison of theoretical NO_x production*

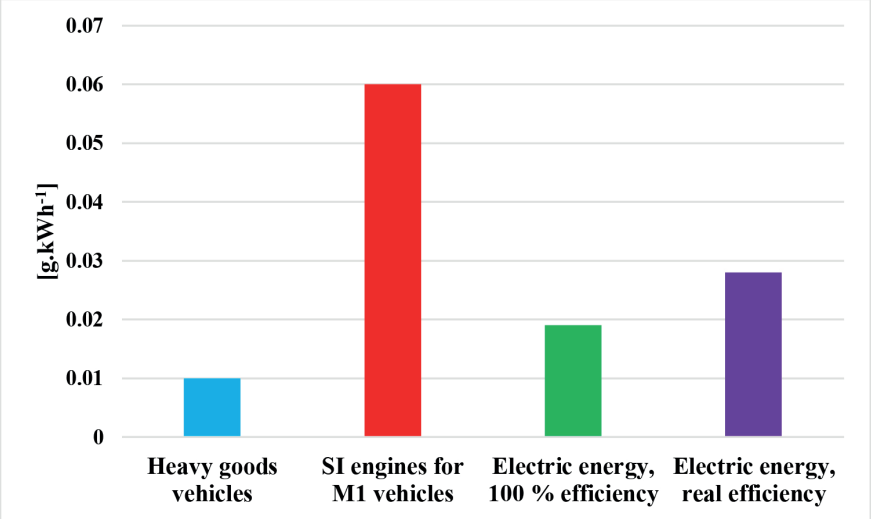

Figure 11 *Comparison of theoretical PM production*

it is possible to expect lower production of CO_2 grams per one kWh within the framework of these vehicles.

After taking into consideration the real efficiency, the greatest producers of NO_x, albeit indirectly, are the electric vehicles.

The theoretical production of PM within the electric cars is higher than within the heavy goods vehicles, however, concerning the SI engines for M1 vehicles, it is lower.

4 Discussion

Concerning the electric cars, the comparison of values of the energy input and output has shown their energy efficiency issues.

The power measured on the Edison II has been higher (Figure 7) than the power given in its documentation (Table 1). The power in the documentation is the assumed one and, in the case of electric cars, there is a common phenomenon that the power measured is the higher than power given by the manufacturer [30].

The losses measured between the electric motor's shaft and dynamometer have reached 18% of energy transmitted. These losses are predominantly of mechanical character [31]. In comparison to combustion engine vehicles, such loss has shown as lower. Concerning the combustion engine vehicles, the losses reach up to 25% and more, mainly due to their construction design, primarily and foremost due to simplification of the transmission system [32]. The vehicle Edison II has a planetary transmission with three gears of speed. Thus, the transmission mechanism of a vehicle used has substantially fewer parts in which it could lead to mechanical losses [33].

Concerning particular measurements, the data from Table 1 slightly vary. While driving according to amended NEDC cycle, some deviations were noticed in time of measuring, average speed, distance driven and in an average value of power supplied to dynamometer's cylinders, as well. The reason of these deviations lies in a fact that drivers were not always driving precisely according to conditions of amended NEDC cycle. This requires a long time practice by the driver. However, the deviations between particular

measurements do not have a negative impact on needs for the article's research.

The transmission energy efficiency from the electric socket on the dynamometer's cylinders was 45% under the conditions set in this article. It is quite a low value and it is necessary to take into consideration that the value was not measured on the wheels directly, but on the cylinders of dynamometer [34-35]. It means that the efficiency was decreased by the rolling resistance of tires along the cylinders. If the efficiency is increased by the rolling resistance, the transmission energy efficiency will be still low, up to 55% and less. The reason lies in various factors. The first one represents the charging during which it must lead to the voltage transformation and its rectification [36]. The second one is the storage of electric energy in accumulators and its further transmission through the DC/DC convertor into electric motor, as seen in Figure 3 [37-38]. There are also some energy losses depending on design of accumulator. The Li-ion accumulators have the efficiency of 80-90%, the PB accumulators have 50 up to 92%, and the NiMH accumulators have the efficiency of about 66% [39-41]. Thus, the storage and further deliver of electric energy from the accumulators are accompanied with energy losses. Those losses can be also seen between the engine and wheels due to mechanical resistances of the transmission system. The last place in which the losses can be seen is tire. However, there is a part of energy used for the on-board computer and other appliances to be plugged-in.

The measurements have been done at the surrounding temperature of about 22 °C. In the case of lower temperatures, the efficiency would have lower values [42]. While driving according to amended NEDC cycle, there is also vehicle deceleration. Here, it can be assumed that the driving mode of recuperation, i.e. vehicle accumulator charging, is applied.

From Table 4 can be seen an obvious difference in average energy consumption if assessing it on the dynamometer's cylinders and as taken from the electric socket. The cylinders of dynamometer have the average energy consumption calculated as 33958 [kJ.100km^{-1}], resp. 9.43 kWh . 100 km^{-1}, the electric socket has had 75373 [kJ.100km^{-1}], resp. 20.93 kWh . 100 km^{-1}.

5 Conclusion

Measurements have shown a great difference between the amount of energy taken from the electric socket and amount of energy delivered to the dynamometer's cylinders.

Efficiency of the transmission energy from the electric socket on the dynamometer's cylinders has been 45% within the electric car used for the measurement. Thus, 55% of the energy taken from the electric socket has not been used for the wheels to be driven. In other words, under these conditions, only 5 kWh from every 10 kWh of energy taken from the electric socket is being delivered to wheels in the form of electric energy. This value of efficiency is relatively low. Such a value has been probably affected by using the vehicle of serial production. However, whether using serial or individual vehicles, the efficiency of energy transmission has a significant impact on energy efficiency of electric cars.

As also stated in the article's introduction, the devices through which the energy in electric car, used for the measurement, is coming can be divided into electric and mechanical ones. The electric devices especially include charger, convertors, battery pack, electric conductors and part of the electric motor's shaft (Figures 2 - 4). Mechanical parts consist predominantly of transmissions gear, shafts and wheel bearings. All of the vehicle's electrical parts, used in the measurement, are placed between the electric socket and electric motor's shaft and the mechanical parts are placed between the electric motor's shaft and wheels. Through the vehicle coasting driving test on the dynamometer it was possible to determine losses of mechanical energy between the electric motor's shaft and cylinders of dynamometer. The energy taken from the socket has been delivered to electric motor's shaft in the amount of 53%. The losses have had up to 82% in electric devices and 18% in mechanical devices from the overall amount of energy lost. Thus, the electric part of a vehicle has had substantially higher share on the overall energy losses than its mechanical part. It is necessary to take into consideration that losses also have included a part of electric energy delivered from the electric socket that has been used for an on-board indicator to be plugged in. Lights, ventilators and other electronic devices have been switched off during the measurement.

The value of the electric car energy efficiency has a large impact on the harmful emission production, as well, as seen in Table 7 and in Figures 8-11. Knowing the value of efficiency of energy transmission from the electric socket onto the electric motor's shaft has enabled a comparison of theoretical production of selected emission production within the combustion engines as there has been a theoretical production of emission calculated for them having considered the engine's energy efficiency.

Concerning the theoretical production of CO, a considerably lower CO production within the electric cars was found out, even having made calculations with the real efficiency of energy transmission onto the electric motor's shaft. It is important to know that the electric cars do not produce CO directly during the driving, but indirectly, during the electric energy production. Thus, to introduce the electric car driving in the cities is positive.

Concerning the CO_2 production, the highest theoretical value of production of gas causing the greenhouse effect has been calculated within the production of electric energy in relation to operation of electric vehicles. Therefore, it can be said that from the local point of view the electric vehicles can contribute to reduction of CO concentration in densely populated areas. However, from the global point of view, using the electric vehicles does not weigh in on slowing down global warming.

Taking into consideration the efficiency of energy transmission from the electric socket onto the electric

motor's shaft, the theoretical production of nitrogen oxides has increased from the value of 0.348 g.kWh^{-1} up to 0.512 g.kWh^{-1} (Figure 10). Thus, when considering such energy efficiency, the indirect production of nitrogen oxides by electric cars is higher than in the case of heavy goods vehicles.

Due to considering the real efficiency of energy transmission from the electric socket onto the electric motor's shaft, the theoretical production of PM within electric cars has increased from the value of 0.019 g.kWh^{-1} up to 0.028 g.kWh^{-1} (Figure 11).

Results of this article point out that it is important to take the energy efficiency into consideration when thinking about electric cars.

Acknowledgement

This contribution/publication is the result of the project implementation:

VEGA no. 1/0436/18 - Externalities in road transport, an origin, causes and economic impacts of transport measures.

References

[1] WU, Z., LING, R., TANG, R. Dynamic battery equalization with energy and time efficiency for electric vehicles. *Energy Procedia* [online]. 2017, **141**, p. 937-948. ISSN 1876-6102. Available from: https://doi.org/10.1016/j.energy.2017.09.129

[2] HAMSAVARTHINI, Y., KANTHALAKSHMI, S. Technologies in battery management system - a review. *International Journal of Scientific and Technology Research*. 2020, **9**(2), p. 1324-1330. ISSN 2277-8616.

[3] AJANOVIC, A., HAAS, R. Economic and environmental prospects for battery electric- and fuel cell vehicles: a review. *Fuel cells* [online]. 2019, **19**(5), p. 515-529. eISSN 1615-6854. Available from: https://doi.org/10.1002/fuce.201800171

[4] HUANG, Y. Q., MEI, P., LU, Y. J., HUANG, R., YU, X., CHEN, Z., ROSKILLY, A. P. A novel approach for Lithium-ion battery thermal management with streamline shape mini channel cooling plates. *Applied Thermal Engineering* [online]. 2019, **157**, 113623. ISSN 1359-4311. Available from: https://doi.org/10.1016/j.applthermaleng.2019.04.033

[5] WANG, S., LI, J., SHI, D., Sun, X., Yao, Y. Energy management strategy of dual planetary hybrid electric vehicle based on optimal transmission efficiency. *Journal of Theoretical and Applied Mechanics* [online]. 2019, **57**(2), p. 383-396. ISSN 1429-2955, eISSN 2543-6309. Available from: https://doi.org/10.15632/jtam-pl/104591

[6] CHEN, B., EVANGELOU, SA., LOT, R. Hybrid electric vehicle two-step fuel efficiency optimization with decoupled energy management and speed control. *IEEE Transactions on Vehicular Technology* [online]. 2019, **68**(12), p. 11492-11504. ISSN 0018-9545. Available from: https://doi.org/10.1109/TVT.2019.2948192

[7] WANG, F., ZHANG, J., XU, X., CAI, Y., ZHOU, Z., SUN, X. A comprehensive dynamic efficiency-enhanced energy management strategy for plug-in hybrid electric vehicles. *Applied Energy* [online]. 2019, **247**, p. 657-669. ISSN 0306-2619. Available from: https://doi.org/10.1016/j.apenergy.2019.04.016

[8] HUBKA, L. Electric cars in the Czech Republic - the analysis of CO_2 emissions reduction. In: 2019 20th International Carpathian Control Conference: proceedings [online]. ICCC, 2019. Available from: https://doi.org/10.1109/CarpathianCC.2019.8765971

[9] CANALS, C., MARTINEZ-LASERNA, E., AMANTE-GARCIA, B., NIETO, N. Sustainability analysis of the electric vehicle use in Europe for CO2 emissions reduction. *Journal of Cleaner Production* [online]. 2016, **127**, p. 425-437. ISSN 0959-6526. Available from: https://doi.org/10.1016/j.jclepro.2016.03.120

[10] WEISS, M., CLOOS, KC., HELMERS, E. Energy efficiency trade-offs in small to large electric vehicles. *Enviromental Science Europe* [online]. 2020, **32**(1), 46. eISSN 2190-4715. Available from: https://doi.org/10.1186/s12302-020-00307-8

[11] JAGELCAK, J., KIKTOVA, M., STOPKOVA, M. The application of the verified gross mass of intermodal loading units in the conditions of the Slovak Republic. *Nase More* [online]. 2018, **65**(4), p. 218-223. Available from: https://doi.org/10.17818/NM/2018/4SI.10

[12] MASSIANI, J., WEINMANN, J., Estimating electric car's emissions in Germany: an analysis through a pivotal marginal method and comparison with other methods. *Economics and Policy of Energy and the Environment*. 2012, **2**. ISSN 2280-7659.

[13] Transport emissions - Eurostat [online]. 2018. Available from: https://ec.europa.eu/clima/policies/transport_en

[14] KONECNY, V., PETRO, F. Calculation of selected emissions from transport services in road public transport. In: 18th International Scientific Conference Logi: proceedings [online]. 2017. Available from: https://doi.org/10.1051/matecconf/201713400026

[15] OSIPOWOCZ, T., ABRAMEK, K. F., MATUSZAK, Z., JASKIEWICZ, M., LUDWINEK, K., POLIAK, M. The analysis of technical condition common rail fuel system components. In: 11th International Science and Technical Conference Automotive Safety Automotive Safety: proceedings [online]. 2018. Available from: https://doi.org/10.1109/AUTOSAFE.2018.8373304

[16] Project of electric vehicle - Edison [online] [accessed 2019-12-21]. Available from: http://www.edison.uniza.sk/en/electric_vehicle

[17] QIN, Z., ZHANG, D., HAN, Y., LUO, Y. Dynamic coordinated control of a downhill safety assistance system for hybrid electric buses. *Proceedings of the Institution of Mechanical Engineers, Part D: Journal of Automobile Engineering* [online]. 2017, **231**(8), p. 1034-1045. ISSN 0954-4070, eISSN 2041-2991. Available from: https://doi.org/10.1177/0954407016670295

[18] MAHA MSR 1050. User manual.

[19] EN 30 0556. Road vehicles. Speed characteristics. Test methods.

[20] SARKAN, B., STOPKA, O. Quantification of road vehicle perormance parameters under laboratory conditions. *Advances in Science and Technology - Research Journal* [online]. 2018, **12**(3), p. 16-23. ISSN 2299-8624. Available from: https://doi.org/10.12913/22998624/92107

[21] SARKAN, B., STOPKA, O., CHOVANCOVA, M., KURANC, A. Simulating real driving conditions on the single roller dynamometer: a case study in terms of the fuel consumption measurement. In: 11th International Scientific and Technical Conference on Automotive Safety: proceedings. 2018.

[22] Commission Regulation (EU) No 1014/2010 of 10 November 2010 on monitoring and reporting of data on the registration of new passenger cars pursuant to Regulation (EC) No 443/2009 of the European Parliament.

[23] EN 50470-1/A1. Electricity metering equipment (a.c.). Part 1: General requirements, tests and test conditions. Metering equipment (class indexes A, B and C).

[24] MILOJEVIC, S. Sustainable application of natural gas as engine fuel in city buses-benefit and restrictions. *Journal of Applied Engineering Science* [online]. 2017, **15**(1), p. 81-88. ISSN 2247-3769. Available from: https://doi.org/10.5937/jaes15-12268

[25] JILEK, P., SEFCIK, I., VERNER, J., BERG, J. System allowing adhesion force change of road vehicle. In: 18th International Scientific Conference on Engineering for Rural Development ERD 2019: proceedings. 2019. p. 1876-1882. Available from: https://doi.org/10.22616/ERDev2019.18.N051

[26] SHEN, Y., VIEHMANN, A., RINDERKNECHT, S. Investigation of the power losses of the hybrid transmission DE-REX based on modeling and measurement. *Proceedings of the Institution of Mechanical Engineers Part D - Journal of Automobile Engineering* [online]. 2019, **233**(14), p. 3646-3657. ISSN 0954-4070, eISSN 2041-2991. Available from: https://doi.org/10.1177/0954407019829655

[27] VRABEL, J., STOPKA, O., RIEVAJ, V., SARKAN, B., PRUSKOVA, K., MICHALK, P. Measuring the resistance of tires for passenger vehicle against the rolling and sliding on loading area of the flatbed truck when providing the transport services. *Communications - Scientific Letters of the University of Zilina* [online]. 2016, **18**(2), p. 124-128. ISSN 1335-4205. Available from: http://komunikacie.uniza.sk/index.php/communications/article/view/343

[28] RIEVAJ, V., GANA, J., SYNAK, F. Comparison of emissions depending on the type of vehicle engine. *Logistics and Sustainable Transport* [online]. 2019, **10**(1), p. 45-54. eISSN 2232-4968. Available from: https://doi.org/10.2478/jlst-2019-0004

[29] Corrigendum to Commission Regulation (EU) 2017/1154.

[30] CHEN, Z., LIU, Y., FU, Y., XU, X. Motor-torque-limited power-on upshift control in electric vehicles with automatic transmissions. *Proceedings of the Institution of Mechanical Engineers Part D: Journal of Automobile Engineering* [online]. 2016, **230**(1), p. 18-36. ISSN 0954-4070, eISSN 2041-2991. Available from: https://doi.org/10.1177/0954407015577309

[31] HUI, C., WANG, Y. Effects analysis and modeling of different transmission running conditions for transmission efficiency. In: SAE 2016 World Congress and Exhibition: proceedings [online]. 2016. ISSN 0148-7191, eISSN 2688-3627. Available from: https://doi.org/10.4271/2016-01-1096

[32] PHILIPS, P. J., ORPE, M., VASQUEZ, G. Decoupling vehicle work from powertrain properties in vehicle fuel consumption. *SAE Intarnational Journal of Fuels and Lubricants*. 2018, **11**(4), p. 533-543. ISSN 1946-3952, eISSN 1946-3960. Available from: https://doi.org/10.4271/2018-01-0322

[33] JABLONICKY, J., HUJO, L., TKAC, Z., KOSIBA, J., ZIKLA, A. Comparison of two designs of differential planetary gear with differential in output. *Materials, Technologies and Quality Assurance* [online]. 2013, **801**, p. 13-18. ISSN 1662-8985. Available from: https://doi.org/10.4028/www.scientific.net/AMR.801.13

[34] TAVARESS, A. A., FORNASA, I., CALIPA-LUGUE, J. C. Power losses analysis and efficiency evaluation of an electric vehicle conversion. In: IEEE International Conference on Electrical Systems for Aircraft, Railway, Ship Propulsion and Road Vehicles and International Transportation Electrification Conference ESARS-ITEC: proceedings [online]. 2018. Available from: https://doi.org/10.1109/ESARS-ITEC.2018.8607322

[35] ZHU, C., CHEN, Q., ZHUANG, Y., GAO, B., TIAN, M. Research on tire stiffness and rolling resistance matching of in-wheel-motor direct drive electric vehicle. *Jixie Gongcheng Xuebao / Journal of Mechanical Engineering* [online]. 2019, **55**(22), p. 41-51. ISSN 0577-6686. Available from: https://doi.org/10.3901/JME.2019.22.041

[36] KHALIGH, A., D'ANTONIO, M. Global trends in high-power on board chargers for electric vehicles. *IEEE Transactions on Vehicular Technology* [online]. 2019, **68**(4), p. 3306-3324. ISSN 0018-9545. Available from: https://doi.org/10.1109/TVT.2019.2897050

[37] DING, Z. Electric vehicle controller driving efficiency and power batteries pack capacity detecting test-bed design. *IPPTA: Quarterly Journal of Indian Pulp and Paper Technical Association*. 2018, **30**(5). ISSN 0379-5462.

[38] RAJABZADEH, M., BATHAEE, S. M. T., GOLKAR, M. A. Advanced DC-link voltage regulation of fuel-cell electric vehicle. *COMPEL - The International Journal for Computation and Mathematics in Electrical and Electronic Engineering* [online]. 2016, **35**(3), p. 943-958. ISSN 0332-1649. Available from: https://doi.org/10.1108/COMPEL-04-2015-0166

[39] SHAROVA, V., MORETTI, A., DIEMANT, T., VARZI, A., BEHM, R. J., PASSERINI, S. Comparative study of imide-based Li salts as electrolyte additives for Li-ion batteries. *Journal of Power Source* [online]. 2018, **375**, p. 43-52. ISSN 0378-7753. Available from: https://doi.org/10.1016/j.jpowsour.2017.11.045

[40] SANTOS, A. G., VIEIRA, M. R. S., URTIGA, S. L., SILVA, F. J., Influence of Sn addition on the corrosion resistance and recharge capacity of Pb-1, 5 wt% Sn alloy for positive grids of lead acid batteries. *Materia* [online]. 2019, **24**(1). ISSN 1517-7076. Available from: https://doi.org/10.1590/S1517-707620190001.0640

[41] ZHUFRI, A., ZHANG, J. An electrical model for energy efficiency evaluation of NiMh batteries. In: 30th Annual IEEE Canadian Conference on Electrical and Computer Engineering IEEE CCECE 2017: proceedings. 2017. ISBN: 978-1-5090-5538-8.

[42] LEBKOWSKI, A. Studies of energy consumption by a city bus powered by a hybrid energy storage system in variable road conditions. *Energies* [online]. 2019, **12**(5), 951. ISSN eISSN 1996-1073. Available from: https://doi.org/10.3390/en12050951

INFLUENCE OF SELECTED FACTORS ON IMPLEMENTATION OF THE PPP PROJECTS IN TRANSPORT

Beata Zagożdżon*, Andrzej Rogowski

Faculty of Transport, Electrical Engineering and Computer Science, Kazimierz Pulaski University of Technology and Humanities in Radom, Radom, Poland

*E-mail of corresponding author: b.zagozdzon@uthrad.pl

Resume

Countries seek to use the knowledge and capital of the private sector to minimise the gap between the transport infrastructure needs and the capacity of their budgets. A form of private investor involvement is usually a public-private partnership PPP. However, success in implementing the PPP projects requires appropriate economic, legal and institutional conditions.

The article presents results of research aimed at identifying the PPP success factors in Poland and assessing the strength of impact of individual factors on the implementation of projects. An analysis of the subject literature was carried out, based on which the success factors were determined. Next, econometric modelling methods were applied (correlation and regression), which were used to measure the degree of correlation between the variables and showed the relationships of variables to each other.

Article info

Received 30 March 2020
Accepted 15 May 2020
Online 23 October 2020

Keywords:

critical success factors for PPP,
transport,
PPP in Poland

Available online: https://doi.org/10.26552/com.C.2021.1.A14-A20

ISSN 1335-4205 (print version)
ISSN 2585-7878 (online version)

1 Introduction

Public-private partnership (PPP) as a form of cooperation between the public and private partners, who act together while realizing a project, keeping their own goals and interests, has been an area of scientific research since the 1980s. Initially, directions of this research included such issues as: risk management, managing relations between project partners, project financing system or public procurement procedures. However, the global financial crisis in 2007-2008 intensified the research of scientists on the PPP issues. Governments around the world are trying to use the knowledge and capital of the private sector to minimize the gap between the needs for infrastructure, especially transport and possibilities of their budgets. The subject of particular interest of governments is the transport infrastructure, which determines economic and social development, and in the current state of quantity and quality requires large investment outlays. These include European rail, road and air transport systems, as well as urban transport systems, which are suffering from effects of congestion and citizens expect a rapid improvement of current transport systems. At the same time, the previous practice of the PPP implementation and the conducted research have shown that the success of a partnership requires appropriate economic, legal, institutional and social conditions. Therefore, at present, the main area of research on the PPP is to identify success factors and determine influence of particular factors, their strength of influence on the process of successful project implementation [1]. Result of this research is to determine the best ways of planning and realizing the PPP investment projects.

The aim of the undertaken research was to identify the success factors of the PPP in Poland and to assess the strength of influence of particular factors on implementation of projects. The notion of success is understood very synthetically (because it is not the main subject of research) and means of a PPP project that was performed in accordance with the budget, schedule and service quality standard. The adopted aim of the research implied in the first stage - a review of the subject literature and then - developing statistical data and applying econometric modelling methods. A qualitative research approach was used, based on conceptual and comparative analysis of the secondary data, scientific literature and reports of international institutions. Then, in the next stage of research, correlation and regression analysis were applied. The former was used to measure the degree of correlation between the variables and the latter showed the quantitative dependence of one variable on another.

2 Background of the PPPs

As a result of the financial crisis in the 1980s, governments have focused their attention on the private sector as a source of financing for investments of general interest. One of the first scientists who dealt with this

issue was a professor at Columbia University - E. S. Savas [2-3]. Research concerning not only the financing, but the operation and management of public infrastructure by the private sector as well, was conducted in the 1990s by D. Osborne and T. Gaebler [4]. Among European countries, the United Kingdom implemented various forms of cooperation between the public and private sector at the earliest and the largest scale. On the initiative of the government agency - The Private Finance Initiative, a lot of theoretical and research work on the role of the private sector in the sphere of public infrastructure and services was created [5-7]. Initially, the research directions covered such issues as: risk management, management of relations between the project partners, project financing system or public procurement procedures. However, in the last twenty years the main area of research are the success factors of the PPP, described in the literature as critical success factors (CSF). Their detailed review was presented by the author in an earlier publication [8], therefore only the most important of them will be discussed here.

Based on the literature research, it can be assumed that classification of determinants of the PPP success includes four groups of factors: economic and financial, political and legal, technical and social. Moreover, they can be divided according to the level of analysis. Determinants that are shaped by the government and its institutions can be defined as factors at the macro level. On the other hand, those that affect practical implementation at the stage of project preparation and feasibility assessment concern the micro-level.

The research undertaken has focused on the macro-level factors as they provide a fundamental framework for functioning of the partnership. Without them the PPP formula will not exist at all, let alone successful implementation. Thus, the research conducted by Chou et al. [9] shows that at the macro level the following factors have the strongest impact: stable macroeconomic conditions, economic and political support of the government, legal system, availability of financing, competent advisory public agencies, social support, transparent procurement process, competition in the procurement process. Osei-Kyei and Chan [1] also point out in their research the importance of stable macroeconomic conditions, a favourable legal framework, political and social support and a clear procurement system. In general, the conducted research shows that the PPPs are more common in countries where there are strong and effective legal institutions and in countries where legal regulations well protect investors' rights [10]. All this creates a good atmosphere for investors and has a positive impact on trust between the government and the private consortium. Mutual trust is important for success of the PPPs [11].

Moreover, the already mentioned studies by Osei-Kyei and Chan [1], underline the importance of factors such as the appropriate allocation and sharing of risks and presence of the strong private consortia on the economic market. According to studies, undertaken by Esmaeili, Pellicer and Molenaar [12], the following factors proved to be the most important: a strong private consortium, appropriate risk allocation and available financial market.

Out of these factors, the most important for the transport infrastructure projects, as highlighted by Hammami et al. [10] and Chou et al. [9], is the country's stable macro-economic condition and, in particular, such indicators as: the GDP level and growth, market size, customer purchasing power. Good macroeconomic conditions, according to Mansoor and Klein [13], are able to attract investors and increase the level of financial resources. In contrast, the size of the market affects the volume of demand and the purchasing power of customers at the level of future fees, which, in turn, determines the revenues and liquidity of the private consortium. Efficient financial intermediation, free access to capital and financial services are also important factors. Involvement of multilateral lenders and credit agencies in the transport project strengthens the positive outcome of this investment [14]. The factor related to the government's economic policy and legal system is the transparent (transparent) public procurement process and the level of competitiveness of the procurement market. Intensity of competition means a large number of complex bids, which gives the possibility to choose a better supplier and carry out an ex-ante evaluation.

The conceptual and comparative analysis of the scientific literature has allowed identification of the critical success factors for the PPP projects that will be further investigated. These included: macroeconomic conditions, the legal framework (including the level of democracy and corruption) and availability of funding and competitiveness of the public procurement system.

3 Methodology and research results

The tests carried out consisted of two main stages:

- in the first stage, the critical success factors for the PPPs were assigned macroeconomic quantities and the quantitative indicators that are appropriate for them, characterize them, constitute an aggregated set of information; these quantities were established based on the statistical data and reports of international institutions and covered the period 2009-2018,
- in the second stage, the correlation and regression analyses were used and the constructed models made it possible to measure the degree of correlation between the variables and interdependencies occurring between them.

Thus, in order to characterise the macro-economic conditions, the basic macro-economic quantities, expressed in monetary terms, were selected: gross domestic product - GDP, exports, deficit, public debt. The international investment position of a country, which indicates whether a given country is a creditor or a net debtor to the foreign country, was also taken into account [15]. Positive values show that the country is a creditor and negative values - a debtor. This indicator is presented both in monetary units, as well as in relation to GDP, because the preliminary

Table 1 *Indicators (explanatory variables) included in the surveys*

a group of success factors	indicators
macroeconomic conditions	gross domestic product GDP, exports, deficit, public debt, international investment position (EUR billion), international investment position (% of GDP)
availability of financing	bank assets (EUR billion), bank assets (% of GDP), private sector debt, private sector credit
legal framework, level of democracy	rule of law index, democracy index, corruption index
competitiveness of the public procurement process	competitiveness indicator

studies have shown its great influence on success of the PPP projects.

The rule of law indicator was used to assess the legal regulations and the general level of standards of operation of the state and its institutions (scale from 0 to 1; where 1 means the strongest compliance with the rule of law) [16], democracy (scale from 0 to 10; where 10 means a fully democratic state) [17] and a corruption indicator [18]. The latter shows how national entrepreneurs assess the level of corruption in the public sector. The indicator value of 0 means the highest level of corruption and 100 means the lowest level of corruption.

Another group of indicators allows assessing availability of financing. The following indicators were taken into account: bank assets, debt and private sector credit. The first one, due to its importance for the successful implementation of the PPP projects, is presented in EUR billion and in % of the GDP. The other two, however, are presented only in % of the GDP [15]. Debt of the private sector is the state of liabilities of enterprises, households and non-commercial institutions acting for the benefit of households, calculated cumulatively in subsequent years. Private sector credit is the net amount of liabilities of private entities, incurred in a given year.

The competitiveness of the public procurement process was assessed by means of an indicator that reflects several aspects of public procurement, including competition and red tape. The indicator measures the percentage of contracts awarded for which there was only one bidder [19]. A larger number of bidders is more advantageous because it means that public purchasers have more options and can obtain the better value for the money.

Table 1 summarises indicators that have been assigned to each PPP success factor.

In the second stage of research, the correlation and regression analyses was used. The first is used to measure the degree of correlation between the variables. The regression analysis is an extension of the analysis, which allows for a quantitative description of a relationship between one variable and another. The subject of the research was the degree of connection between the value and number of the PPP agreements concluded in a given year and indicators assigned to particular groups of the PPP success factors (Table 1). The two econometric (regression) models are given, expressing the value of agreements (Wu) and number of the PPP agreements (Lu) concluded in a given year. Calculations were made in an Excel spreadsheet. Selected regression models are presented in Table 2 and in Figures 1 and 2. Next, the linear correlation coefficients, Spearman's RHO (RHO Spearman) and linear regression functions were determined (Table 3).

It is worth noting that in the case of number of models estimating the number of the PPP agreements, the adjustment measured by the coefficient of determination R2 is much better than in the case of agreement values. Both models Wu1 and Wu2 are models of generalised log-hyperbolic regression; Lu1 is a model of exponential regression and Lu2 of hyperbolic regression. It is important to note that the best suited contract count models are those with six and five explanatory variables (indicators), contract count models use seven indicators. The average annual value of the PPP contracts in Poland in the years 2009-2018 amounted to 0.1405 billion Euro (standard deviation 0.1384 billion Euro) and the average number of contracts 13.1 (standard deviation = 5.7). Thus, the average error in estimating the value of contracts, according to the given models, represents for Wu1 20.7% and Wu2 21.4% of the average value of contracts and for Lu1 4.0% and Lu2 4.5% of the average number of contracts.

There is a significant positive correlation between the GDP, value of exports, level of public debt and a negative correlation between the international investment position and the deficit and number of contracts concluded. In the case of the value of contracts, the correlation with these macroeconomic indicators is much weaker. Level of the GDP value indicates the size, potential of the internal market that generates demand. This is an important factor for possible charges for use of the transport infrastructure. Correlation coefficients also show that growth of the GDP and value of export, i.e. generally the economic development of the country, causes an increase in number of the PPP agreements. On the other hand, a deterioration of the international position, i.e. an increase in the country's debt to foreign countries, results in an increase in both the number and value of concluded agreements. In addition, an increase in the public debt level positively influences an increase in the number of agreements. Based on that, one can formulate an assumption that an increase in the level of debt, i.e. generally the government's willingness to take on obligations and then an increase in money supply in the economy, contributes to development of the PPP, both in terms of the number of concluded agreements and their value. However, it is a conclusion that requires even further, in-depth research and analysis. Undoubtedly, however,

Table 2 *Selected econometric models (regression) of the PPP agreements concluded in a given year in years 2009-2018 in Poland: Wu value of agreements [billion EUR], Lu number of agreements*

W	equation	R^2	$\bar{x}_d$ (bln EUR)	s_d (bln EUR)	$\frac{s_d}{\bar{x}}$ (%)
Wu1	$\hat{y} = \exp\left(\frac{38111.33}{x_9} - \frac{5158.27}{x_9} - \frac{3608.38}{x_6} + \frac{16549.21}{x_5} + \frac{481.79}{x_4} - \frac{1199.27}{x_2} - 27.8616\right)$	0.8908	0.02904	0.03724	128.2
Wu2	$\hat{y} = \exp\left(\frac{36115.2}{x_9} - \frac{5128.85}{x_9} - \frac{3539.19}{x_6} + \frac{16185.69}{x_5} + \frac{636.52}{x_2} - 24.3909\right)$	0.8822	0.03000	0.03879	129.3
Lu1	$\hat{y} = \exp(0.18542x_{13} - 0.08103x_9 + 0.26490x_8 - 1.37281x_6 - 0.37548x_5 + 0.00565x_4 - 0.08754x_2 + 6.36924)$	0.9874	0.52	0.40	77.7
Lu2	$\hat{y} = \frac{0.09056}{x_{13}} - \frac{0.22300}{x_9} - \frac{0.83611}{x_8} + \frac{3.18745}{x_6} - \frac{0.91355}{x_5} + \frac{0.04327}{x_4} - \frac{0.18879}{x_2} + 6.50$	0.9847	0.59	0.42	71.4

W - specification

$\bar{x}_d = \frac{1}{n}\sum_{i=1}^{n}|y_i - \hat{y}_i|$ - mean absolute deviation of model values from actual values, where y_i actual value, $\hat{y}_i$ model value (regression function),

s_d - standard deviation of the absolute deviation of model values from actual values,

R^2 - determination factor,

x_i - explanatory variables, according to the Table 3.

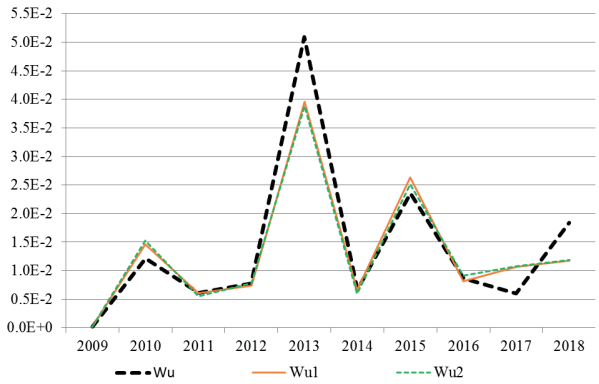

Figure 1 *Value of the PPP agreements in Poland in 2009-2018 and their estimation with regression models Wu1 and Wu2 from Table 2*

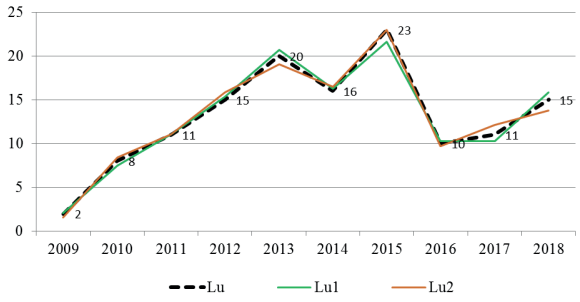

Figure 2 *Number of the PPP agreements in Poland in 2009-2018 and their estimation with regression models Lu1 and Lu2 from Table 2*

the increase in the budget deficit in a given year limits the number of concluded agreements. In the case of other indicators, the correlation is at most very weak.

There is a strong correlation between the rule of law and number of the PPP agreements concluded. Stable, clear regulations and compliance with the law are the factors that have the greatest impact on development of the PPP projects. In the case of the influence of this factor on the value of concluded agreements, one can only speak of a weak linear correlation. The value of the correlation coefficient for the number of contracts, which is 0.78, indicates a very strong correlation, which in practice means a large increase in number of contracts with a low level of corruption. Impact of this factor on value of contracts can be described as relatively weak, although significantly stronger than the rule of law. Nevertheless, the low level of corruption contributes to the value of contracts. The level of democracy, on the other hand, can be considered a very insignificant factor for the PPP projects.

There is a significant correlation between the level of financial assets of banks and the number of concluded PPP agreements - an increase in assets also in relation to the GDP, causes an increase in number of agreements. However, the level of private sector debt has the greatest impact, among the financial instruments taken into account. A progressive increase in the private sector debt implies an increase in the number of concluded agreements. On the other hand, credit flows of the private sector in a given year clearly influence, primarily the value of concluded agreements and, to a lesser extent, their number. It is a negative correlation - an increase in the level of private sector credit liabilities in a given year limits the value of concluded PPP agreements to a greater extent than the number of projects.

Table 3 *Linear correlation coefficient, Spearman's rank correlation coefficient, directional coefficient and linear regression (y = ax +b)*

	specification	linear correlation factor		spearman's rank correlation factor		linear regression directional factor *a* ($y = ax + b$)	
		value of contracts concluded in a given year (Wu)	number of contracts concluded in a given year (Lu)	value of contracts concluded in a given year (Wu)	number of contracts concluded in a given year (Lu)	value of contracts concluded in a given year (Wu)	number of contracts concluded in a given year (Lu)
1	GDP	0.1789	0.4980	0.3333	0.5061	0.00051	0.05860
2	exports	0.1816	0.4913	0.2970	0.4207	0.00069	0.07751
3	deficit	-0.1110	-0.4302	-0.1758	-0.3598	-0.00222	-0.35650
4	public debt	0.3571	0.5341	0.3697	0.3476	0.00218	0.13500
5	international investment position (EUR billion)	-0.2475	-0.5066	-0.2606	-0.4268	-0.00154	-0.13031
6	international investment position (%GDP)	-0.3860	-0.4501	-0.3455	-0.4573	-0.02919	-1.41120
7	private sector credit	-0.4493	-0.3244	-0.3222	-0.2844	-0.05884	-1.76102
8	private sector debt	0.2115	0.5989	0.3212	0.5061	0.00614	0.72089
9	bank assets (EUR billion)	0.1609	0.5016	0.2970	0.4207	0.00039	0.04970
10	bank assets (%GDP)	0.1447	0.5272	0.2606	0.3354	0.00437	0.66030
11	democracy	-0.0594	0.0047	-0.2646	0.1238	-0.03378	0.11148
12	rule of law	0.2849	0.6670	0.3084	0.7187	1.64243	159.375
13	corruption	0.3874	0.7848	0.4602	0.6543	0.01342	1.12657
14	competitiveness of the public procurement	-0.0285	0.1175	-0.1184	0.1442	-0.17826	30.4704

The last of the examined factors - competitiveness of the public procurement market in practice has no impact on number of concluded contracts and value of those contracts.

The Spearman's rank correlation coefficient shows that a positive moderate correlation appears between the size of the GDP, level of exports, private sector debt and assets of banks. A moderate negative correlation occurs in the case of international investment position and number of contracts. On the other hand, when analysing the strength of the correlation between the value of contracts and individual characteristics, one should pay attention to the significant correlation with corruption. The strength of the correlation between the other features is low.

Analysis of the directional coefficient and linear regression allows formulating a conclusion that appropriate legal regulations and observance of the rule of law can have a very significant influence on increase in number of the PPP agreements. An analogous situation, however, the expected changes will not be so decisive, occurs in the case of increasing competitiveness of the public procurement market. Important factors are also private sector credit commitments in a given year and the international investment position of the country. An increase in credit debt may cause a decrease in number of agreements concluded in a given year. The opposite situation occurs when the investment position deteriorates, since an increase in foreign debt generates an increase in number of contracts. However, with respect to the value of contracts concluded in a given year, none of the factors, apart from a minor impact of the rule of law, have a practical significance.

The conducted research and analysis of its results allowed identifying the following critical success factors of CSF for the PPP projects in Poland:

macroeconomic situation: GDP volume, public debt level, international investment position;

legal regulations: rule of law, corruption;

availability of financing: the level of private sector debt, bank assets and private sector credit debt in a given year.

Legal regulations and compliance with the rule of law, as well as the low level of corruption, have the greatest influence on success of the PPP. Among economic factors, the international investment position of the country, the level of banks' assets and private sector debt (calculated cumulatively) and its credit debt in a given year, are important.

4 Conclusions

When considering factors that determine the success of implementation of the PPP concept in the area of

infrastructure, especially transport infrastructure, the main factors include: the macroeconomic situation, the wider rule of law and the availability of financing.

The most critical factors with the greatest impact on functioning and development of the PPP market in Poland are the legal framework, compliance with the rule of law and low levels of corruption. Results of research by Chou et al. [9] and Osei-Kyei and Chan [1] also show that these factors are fundamental for the PPP. Hammami et al. [10] emphasized that PPP is more common in countries where there are strong legal institutions and in countries where legal regulations well protect investors' rights. However, in the economic and financial aspect of the Polish economy, the size, internal market potential, as well as the international investment position of the country or the level of banks' assets, are very important. These factors were pointed out by Mansoor and Klein [13] and the team: Esmaeili, Pellicer and Molenaar [12]. Good macroeconomic conditions are able to attract investors and increase the possibility of obtaining funds. Therefore, the conducted research generally confirms the conclusions formulated earlier by other scientists. However, in Poland, deterioration of the international investment position, increase in the level of public and private sector debt contributes both to the increase in number of agreements concluded in a given year and their value. Based on that, it can be assumed that the PPP projects in Poland are based, above all, on the long-term external (foreign) financing, both on the side of the public and private partner. However, as it has already been mentioned before, this hypothesis requires further, in-depth research.

The results presented are of practical and academic importance. In economic practice, the knowledge of the critical success factors of the PPP gives experts and institutions the opportunity to shape an effective, efficient policy for the implementation of the PPP enterprises. The results can also be incorporated into government guidelines to inform local practitioners about the best ways to manage projects. Assessment of the success factors at the initial stage is essential for both large transport infrastructure projects and provision of the transport services, for example by private operators in public transport.

From an academic point of view, it is worthwhile to expand the research to include further critical success factors, to conduct an in-depth analysis, using statistical methods and econometric models. The research could include such factors as: activity of advisory public agencies or, in relation to the private partner, activity of strong consortia. Another direction of research, even at the current stage of the CSF identification, using the adopted methodology, could be to increase its scale, e.g. by Central European countries (Slovakia, Czech Republic, Hungary) and to conduct comparative analysis.

References

[1] OSEI-KYEI, R., CHAN, A. Review of studies on the critical success factors for public-private partnership (PPP) projects from 1990 to 2013. *International Journal of Project Management* [online]. 2015, **33**(6), p. 1335-1346. ISSN 0263-7863. Available from: https://doi.org/10.1016/j.ijproman.2015.02.008

[2] SAVAS, E. S. *Privatizing the public sector: how to shrink government*. New York: Chatham House, 1982. ISBN 978-0934540155.

[3] SAVAS, E. S. *Privatization and public-private partnerships.* New York: Chatham House, 2000. ISBN 978-1566430739.

[4] OSBORNE, D., GAEBLER, T. *Reinventing government - how the entrepreneurial spirit is transforming the public sector.* New York: Plume, 1993. ISBN 978-0452269422.

[5] GAYLE, D. J., GOODRICH, J. N. *Privatisation and deregulation in global perspective.* New York: Quorum Books, 1990. ISBN 0861871200.

[6] JACKSON, P., PRICE, C. *Privatization and Regulation.* A Review of the Issues. Longman Group Ltd., Essex, 1994.

[7] WALKER, C., SMITH, A. J. *Privatized Infrastructure: The Build Operate Transfer Approach.* Thomas Telford, London, 1995.

[8] ZAGOZDZON, B. Conditions for the development of public-private partnership PPP - analysis based on an example of transport infrastructure in Poland. *Communications - Scientific Letters of the University of Zilina* [online]. 2020, **22**(1), p. 35-41. ISSN 1335-4205, eISSN 2585-7878. Available from: https://doi.org/10.26552/com.C.2020.1.35-41

[9] CHOU, J.-S., TSERNG, H. P., LIN, CH., YEH, CH.-P. Critical factors and risk allocation for PPP policy: Comparison between HSR and general infrastructure projects. *Transport Policy* [online]. 2012, **22**, p. 36-48. ISSN 0967-070X. Available from: https://doi.org/10.1016/j.tranpol.2012.05.009

[10] HAMMAMI, M., RUHASHYANKIKO, J. F., YEHOUE, E. *Determinants of public-private partnerships in infrastructure.* IMF, Working Paper WP/06/99. IMF Institute, 2006.

[11] PARKER, D., HARTLEY, K. Transaction costs, relational contracting and public private partnerships: a case study of UK defence. *Journal of Purchasing and Supply Management* [online]. 2003, **3**(9), p. 97-108. ISSN 1478-4092. Available from: https://doi.org/10.1016/S0969-7012(02)00035-7

[12] ESMAEILI, B., PELLICER, E., MOLENAAR, K. R. Critical success factors for construction projects. In: *Project Management and Engineering Research, 2014* [online]. MUNOZ, J. L. A., BLANCO, J. L. Y., CAPUZ-RIZO, S. F. (eds.). Cham: Springer, 2016. ISBN 978-3-319-26457-8, eISBN 978-3-319-26459-2. Available from: https://doi.org/10.1007/978-3-319-26459-2

[13] MANSOOR, D., KLEIN, M. *Government support to private infrastructure projects in emerging markets*. Policy Research Working Paper, 1688. Washington: World Bank, 2007.

[14] BUTKIEWICZ, J., YANIKKAYA, H. The effects of IMF and World Bank lending on long-run economic growth: an empirical analysis. *World Development* [online]. 2005, **33**(3), p. 371-391. ISSN 0305-750X. Available from: https://doi.org/10.1016/j.worlddev.2004.09.006

[15] Eurostat. European Commission [online]. Available from: https://ec.europa.eu/eurostat

[16] *The WJP rule of law index 2009-2018* - World Justice Project, Washington, U.S.A., 2010-2019 [online]. Available from: https://worldjusticeproject.org

[17] Democracy index 2009-2018. A report by The Economist Intelligence Unit [online]. Available from: https://www.eiu.com/topic/democracy-index

[18] Corruption Perceptions Index 209-2018 - Transparency International [online]. Available from: https://www.transparency.org

[19] Single market scoreboard. Public procurement 2009-2018 - European Commission [online]. Available from: https://ec.europa.eu/internal_market/scoreboard

THE TRANSPORT SERVICE OF SMALL TOWNS

Jozef Gnap[1,*], Jana Kupčuljaková[1], Ľubomír Černický[1], Grzegorz Dydkowski[2]

[1]Department of Road and Urban Transport, Faculty of Operation and Economics of Transport and Communications, University of Zilina, Zilina, Slovakia
[2]Department of Transport, University of Economics in Katowice, Katowice, Poland

*E-mail of corresponding author: jozef.gnap@fpedas.uniza.sk

Resume
The paper is focused on assessment of the transport services in small towns. Current legislation in the Slovak Republic, however, does not clearly determine which cities must provide the urban public transport (UPT). Analysis of the current state of the UPT evaluated 71 district towns of the SR and it was found out that 21 towns did not provide operation of the UPT. Another criterion for evaluation was the number of inhabitants of the city over 10,000 in Slovakia and selected regions of the Czech Republic and Poland. The paper presents results of a research conducted in the area of a transport operation, along with a proposal for the content of the methodology, based on a multi-criterial analysis to assess the need to introduce the UPT. The EU research results, regarding dependency of a GDP size and transport performances in UPT in selected EU states, Switzerland and Norway, are presented, as well.

Article info
Received 3 April 2020
Accepted 18 June 2020
Online 23 October 2020

Keywords:
urban public transport,
transport operation plan,
UPT accessibility,
multi-criterial analysis

Available online: https://doi.org/10.26552/com.C.2021.1.A21-A31

ISSN 1335-4205 (print version)
ISSN 2585-7878 (online version)

1 Introduction

In the Slovak Republic (SR), the transport operation plans are required to be prepared by the Act on road transport and the Act on transport on the railways in towns, which nowadays act as an order party of the urban public transport. The transport operation plan is a source for granting the transport licences to the UPT lines, for making contracts on transport services in public interest and for drawing up schedules. However, the applicable law in the EU does not specify which towns must have and order UPT. The EU has committed to reduce the air pollution from transport in towns; however, it has not set even minimum requirements for obligation to establish the UPT in towns, e.g. depending on the number of their residents. The EU supports the UPT infrastructure through structural funds, but it does not interfere in the legislation of states in that sense which towns shall provide UPT and to what extent. In the SR, there exists a whole series of district towns (or other towns) with a significant railway station or stop, which is also part of an integrated transport system without any UPT in the town. Thus, in majority of cases the area or time accessibility is not provided. The issue of accessibility, mainly in suburban areas, is for example dealt with in [1].

This paper presents results from research projects for towns and the main goal of the paper was to assess the UPT accessibility in all the district towns of the SR and in some regions of Poland and the Czech Republic, neighbouring with the SR. In addition, the objective was to propose a methodology to determine the need for the UPT based on a multi-criterial analysis.

Within the SR, there is a lag behind in building the integrated transport systems, one reason for which is the non-existence of a law on public passenger transport and a disunity of ordering the urban public transport [2-4].

2 Analysis of the current state in the Slovak Republic and abroad

Analysis of the current state of the UPT was evaluated in 71 district towns of the SR and it was found that 21 towns (29 %) did not provide operation of the UPT (Figure 1, left). Out of 50 towns with the UPT, only 12 operators are members of the Association of operators of the public transport for people in conurbations of the Slovak Republic (Figure 1, right).

A duty to operate UPT is neither defined by the law, nor specified exactly. The literature states that in the case of an average transport distance of 2 km it is possible to use calculations to find out that public transport is desirable when the number of residents of an urban settlement exceeds 15,000 people [5-6]. Considering this fact, it was found that in two district towns (Pezinok and Senec) the number of residents significantly exceeds the required limit. In one town (Detva), the number of residents approaches that limit (Figure 2).

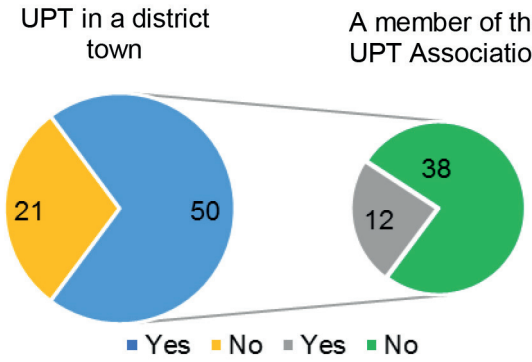

Figure 1 *The UPT in district towns (left); members of the Association of operators of the public transport for people in conurbations of the Slovak Republic (right)*

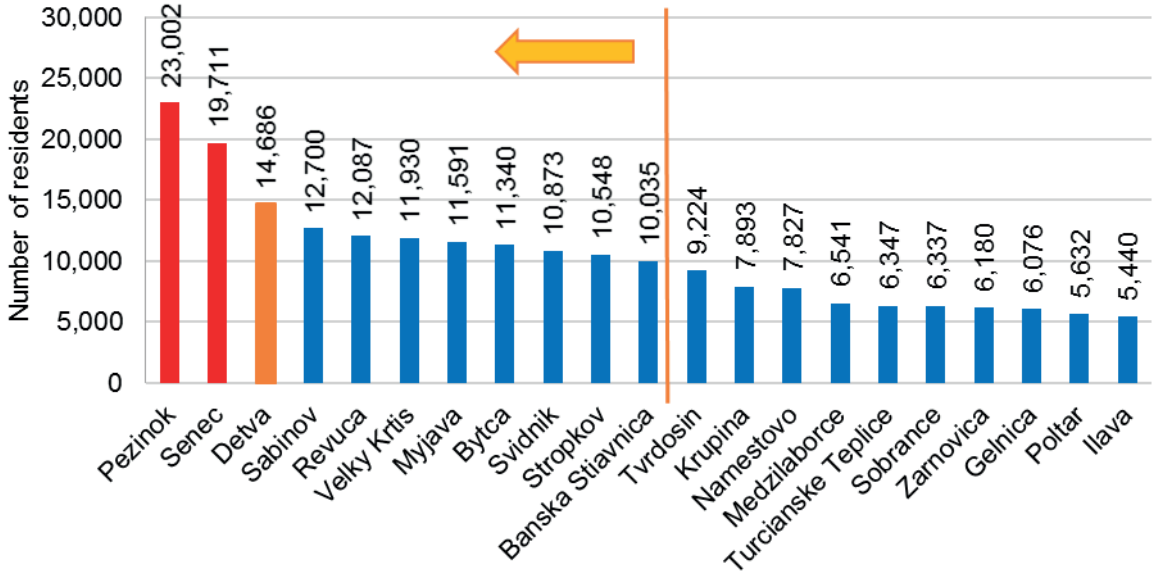

Figure 2 *The number of residents of towns without the UPT operation, based on [7]*

Table 1 *Evaluation of facilities in towns without the UPT, [9-10]*

	bus station	railway station	hospital	secondary school	university
yes	13	17	12	20	1
no	8	4	9	1	20

However, it is necessary to note that building the UPT system is not affected only by the number of residents, but by many other factors, as well. Some additional factors are the town area or town residential area (built-up area), the fact if there is a bus or railway station in the town, if the town is a catchment area from the point of view of health services (a hospital in the territory of the town), as well as education (secondary schools and universities). Thus, one may assume some higher requirements to provide transport operation not only for town residents, but also for commuters. The need for the UPT in smaller towns and development of the integrated transport systems are dealt with by Nigro et al. [8]. Due to this reason, the need to build the UPT is justified even in towns with a smaller number of residents. Table 1 lists the results found for the investigated towns.

Analysis revealed that there is a railway station in Revuca and Velky Krtis, however, passenger transport is currently disrupted on the line. The highest number of secondary schools is in Svidnik (8), Banska Stiavnica (6), Pezinok, Revuca, Stropkov and Namestovo (4) and only in Ilava there is no secondary school. The university is situated only in Banska Stiavnica.

In the case of a foreign country, analysis was performed for Poland and part of the Czech Republic - for Moravia-Silesia region. Analysis of Poland implies that urban public transport is not operated in 77 towns (46 %), out of total 167 towns investigated. The number of residents in these towns is represented in Figure 3; in 13 towns the number of residents exceeds 15,000. In the case of Zawiercie, this value is exceeded several times. Regarding the town facilities, a railway station is

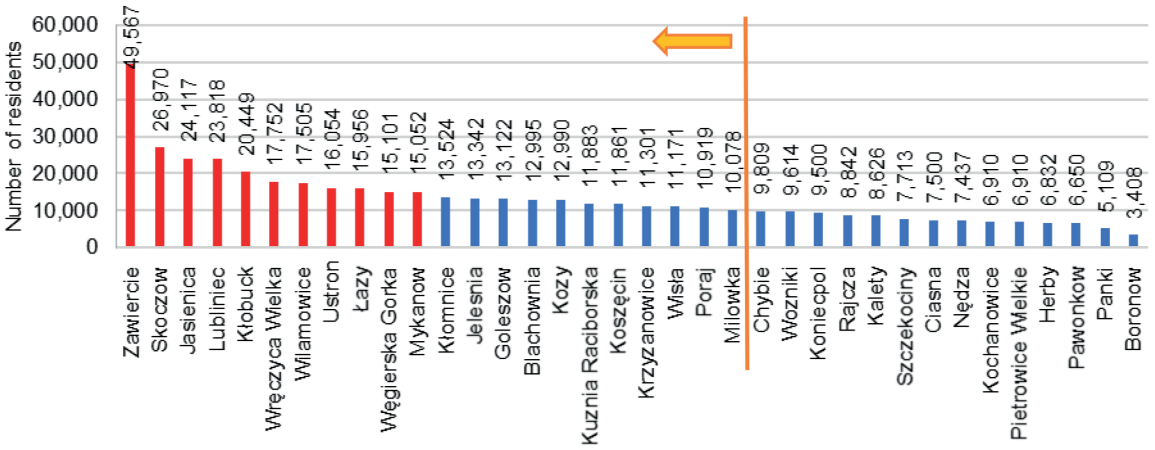

Figure 3 *Number of residents of towns without the UPT operation in Poland, based on [11]*

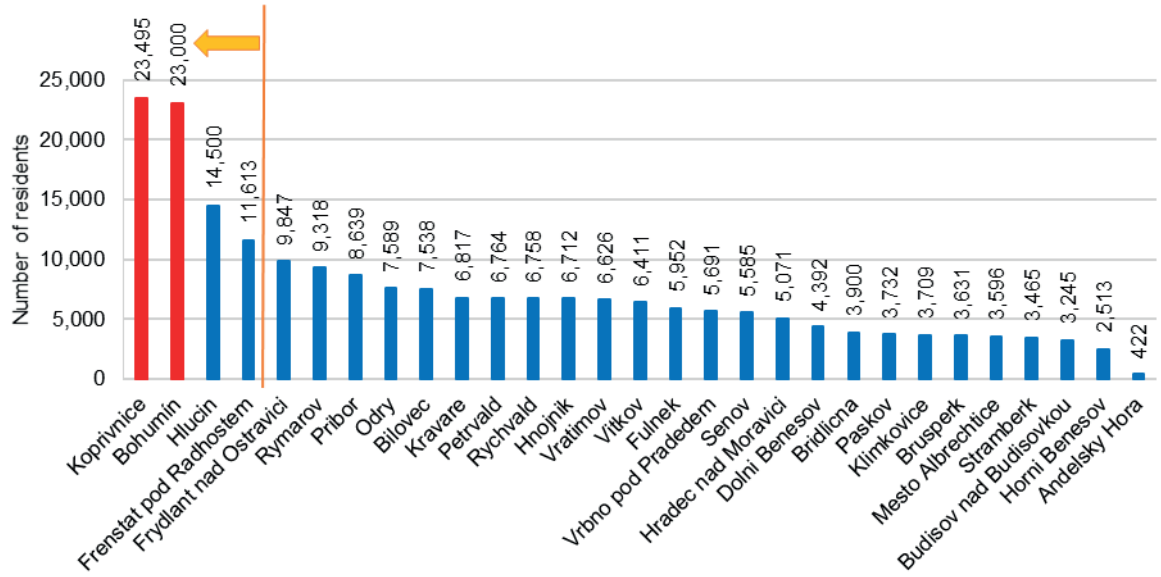

Figure 4 *Number of residents in towns without the UPT operation in Moravia-Silesia region in the Czech Republic, based on [12]*

situated in 29 towns, a hospital is situated only in 6 towns, secondary schools are in 31 towns and universities are not established in any of the evaluated towns without the UPT operation. The bus station facilities were not investigated in these towns.

In the case of analysis of the Moravia-Silesia region, it was found that the urban public transport is not operated in 29 towns, which represents 70%, out of total 41 towns investigated. However, this is partially affected by the fact that the transport operation of multiple towns is performed by the suburban lines (a partial replacement of urban public transport), which are part of the integrated transport system ODIS (Integrated Transport System of Moravia-Silesia region). An overview of the number of residents of towns, where the UPT is not operated, is represented in Figure 4, which makes it clear that in 2 towns the number of residents exceeds the value of 20,000.

Regarding the town facilities, a railway station is situated in 23 towns, hospital is situated in 4 towns, a secondary school exists in 13 towns and there is no university in any of the towns (with no UPT). The bus station facilities were not investigated in these towns.

3 Methods of solution

3.1 The study of relation between the transport performances within the UPT and the gross domestic product in selected states of the EU

The decision to study the relation between the transport performances of the UPT and the gross domestic product (GDP) was made by authors, because in the SR the UPT is operated in most of the towns where the UPT was funded through the national budget before 2003. In that year, the UPT was funded this way in 49 district towns; out of those towns, the UPT is currently not operated only in towns of Sabinov and Svidnik. To the contrary, in Piestany, Brezno and Skalica the UPT is operated even though it was not funded through the national budget in 2003.

Table 2 *Results of correlation between the transport performances in the UPT (passenger kilometres) and the GDP in selected EU states, Switzerland and Norway*

	country	correlation coefficient	determination coefficient	coefficient *a*	coefficient *b*	P-value *a*	P-value *X*	significance *F*
strong direct dependency	Switzerland	0.9709	0.9989	0	0.0128	x	0.000	0.000
	Romania	0.9421	0.9954	0	0.1015	x	0.000	0.000
	Macedonia	0.9205	0.9426	0	0.2079	x	0.000	0.000
	Austria	0.8702	0.9968	0	0.0333	x	0.000	0.000
moderate direct dependency	France	0.7606	0.9847	0	0.0258	x	0.000	0.000
	Denmark	0.5682	0.9598	0	0.0427	x	0.000	0.000
	Spain	0.4091	0.9886	0	0.0500	x	0.000	0.000
weak direct dependency	Croatia	0.2469	0.9868	0	0.0825	x	0.000	0.000
	Poland	0.2161	0.9415	0	0.1047	x	0.000	0.000
	Latvia	0.1517	0.9552	0	0.1514	x	0.000	0.000
	Estonia	0.0532	0.9387	0	0.1509	x	0.000	0.000
	Lithuania	0.0289	0.9442	0	0.1053	x	0.000	0.000
	Finland	0.0257	0.9916	0	0.0424	x	0.000	0.000
weak indirect dependency	Bulgaria	-0.0949	0.9469	0	0.2853	x	0.000	0.000
moderate indirect dependency	Czech Republic	-0.3062	0.9699	0	0.1042	x	0.000	0.000
	Hungary	-0.4599	0.9777	0	0.1764	x	0.000	0.000
	Portugal	-0.5000	0.8921	0	0.0440	x	0.000	0.000
	Norway	-0.5344	0.9821	0	0.0133	x	0.000	0.000
	Great Britain	-0.7674	0.9680	0	0.0235	x	0.000	0.000
strong indirect dependency	Slovenia	-0.8110	0.9622	0	0.0953	x	0.000	0.000
	Netherlands	-0.9345	0.9445	0	0.0097	x	0.000	0.000
	Slovakia	-0.9384	0.7055	0	0.1120	x	0.000	0.000
	Sweden	-0.9795	0.9627	0	0.0239	x	0.000	0.000

Towns of Bratislava, Banska Bystrica, Kosice, Presov and Zilina received subsidies for the urban public transport, which included regular, as well as capital expenditures. Other towns with the urban public transport received the so-called current transfers for the self-governing regions in order to provide regular public bus transport for the year 2003. Those transfers were intended to cover a decrease in incomes arising from the provision of discount travels and to provide the operation of the territory. At that time, the state also dictated the amounts of discounts for selected groups of passengers.

Since 2004, the direct subsidies from the national budget have been granted to urban public transport in Bratislava, Banska Bystrica, Kosice, Presov and Zilina, but there have been no subsidies for other urban public transports. The national budget, however, has found a subsidy for the self-governing regions to compensate for a loss, completely or partially, or to provide another compensation for carriers, while providing performances in public interest in regular public bus transport and to provide the operation of the territory. Since 2005, on the territory of the SR (and based on a change of responsibilities), funding of the UPT, determination of prices, as well as selection of a carrier, have lien within the full authority of towns. Towns or self-governing regions have been funding the UPT from current transfers from the national budget or their own incomes [13].

Hypothesis 01: If the gross domestic product increases, then the state tax revenues, as well as share of taxes for towns, increase, which should be manifested in support for the UPT and thus in an increase of the transport performances.

This hypothesis was verified on a sample of data on EUROSTAT from selected states of the European Union (EU), Switzerland and Norway, presented in Table 2, covering the years 1998-2017. The results of correlation between the transport performances in the UPT and the GDP, in selected EU states, are presented in Table 2.

In order to determine the intensity of correlation, the following criteria were established:

- weak dependency, if $0 < |r| < 0.3$,
- moderate strong dependency, if $0.3 \leq |r| < 0.8$,

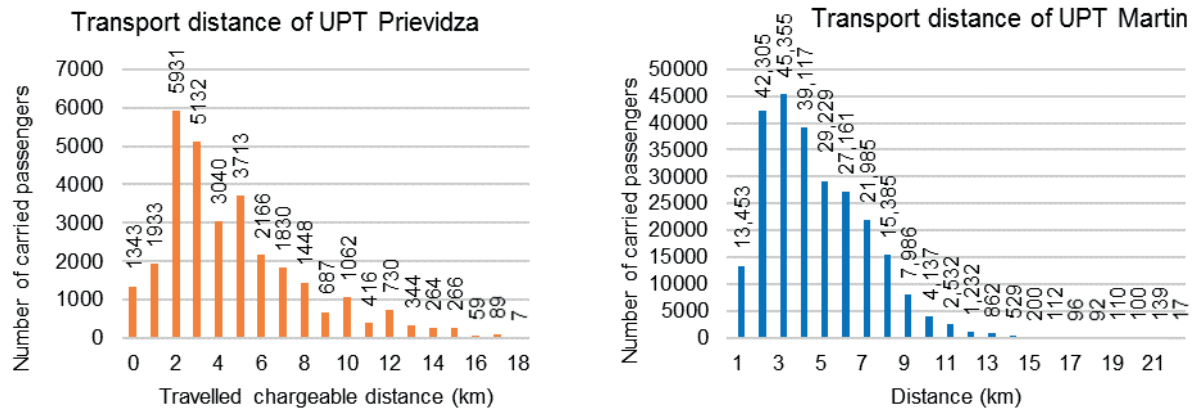

Figure 5 *Distribution of the transport distance in the UPT Prievidza (left) and in the UPT Martin (right) in km, based on [14-15]*

- strong dependency, if $0.8 \leq |r| < 1$.

The studied dependency was modelled using a linear function in the form):

$$y = a + bx. \quad (1)$$

The significance level was selected at the level $\alpha = 0.01$.

Initially, the linear regression model was created for each country. Based on the comparison of the significance level $\alpha = 0.01$ to the P-value, it was determined that the localising constant a was not significant in at least 75 % of cases. Due to that, it was decided to create the linear regression models without a constant. Then, the form of a regression relation is as follows:

$$y = bx. \quad (2)$$

In analyses' results (Table 2), the individual states are sorted according to the correlation coefficients, starting from the strongest direct dependency to the strongest indirect dependency. Results imply that the GDP change impact on demand for the passenger transport by the UPT differs in the studied European countries.

The **strong direct dependency** is observed in Switzerland, Romania, Macedonia and Austria. France, Denmark and Spain fall into the category with the **moderate strong direct dependency**. The **weak direct dependency** can be seen in Croatia, Poland, Latvia, Estonia, Lithuania and Finland.

In the case of Bulgaria, the weak indirect dependency was discovered. The moderate indirect dependency is observed in the Czech Republic, Hungary, Portugal, Norway and Great Britain. Slovenia, Netherlands, Slovakia and Sweden feature the strong indirect dependency.

In the case of all the models, the significance level is less than 0.01, which means that all the models are significant. The results mentioned above indicate a different impact of the GDP on transport performances in the UPT. With respect to differences in the UPT funding, which is in majority of countries fully dependent on towns and their authorities, the transport performances in the UPT are also affected by regulation of individual automobile transport, employment rate, pricing policy, etc. Thus, the hypothesis 01 has not been confirmed.

3.2 Selected experience from creating transport operation plans in UPT

As a part of the towns' transport operation plans creation, one may state that not all the towns in the SR, which feature the UPT or urban bus transport, have worked out the transport operation plans. Effective as of April 2019, the Ministry of Transport and Construction of the SR imposed a fine from 500 Euro to 10,000 Euro upon a municipality (town) for failing to perform the obligation under the Article 20 Paragraph 4, Act No. 56/2012 Coll. on the road transport (preparation of the transport operation plan). If even after three months from the date of entry into force of the relevant decision on imposing the previous fine, the obligation were not performed, the fine would be imposed repeatedly until the obligation is performed. The transport operation plans are to be worked only for towns that already had the UPT. There are 21 district towns in the SR without the UPT. Do the residents of these towns not need UPT? Can they manage their mobility by foot, by bike or car? Do they have no problems with parking their cars in the town centres?

Even within district towns, the UPT is utilised for relatively long distances. For example, in the UPT Prievidza – Bojnice it was found that the majority of passengers travel for the distance of 2 km, then the distances of 3.5 and 4 km follow (Figure 5). An average transport distance in Prievidza was discovered even at the level of 4.7 km.

In the case of Martin, it was found that the highest number of passengers is transported for the distance of 3 km; then follow the distances of 2, 4 and 5 km. The average transport distance was discovered at the level of 4.2 km.

Another criterion is the spatial accessibility of the public passenger transport. As part of working the transport operation plans out, one always assesses distribution of the UPT stops, as well as stops of the suburban bus transport

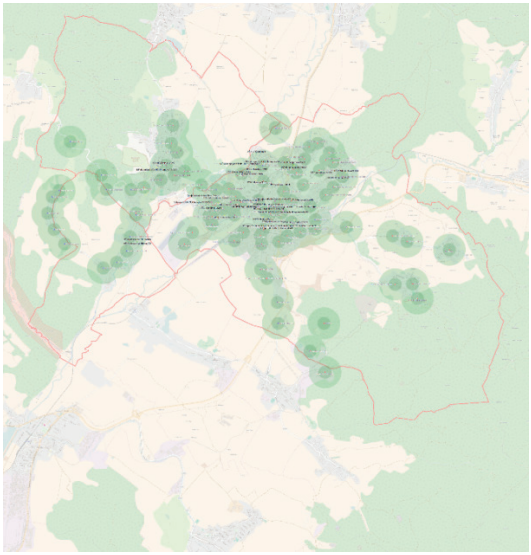

Figure 6 *Representation of isochrones of the stops accessibility in the UPT Prievidza - Bojnice and village Opatovce nad Nitrou and accessibility of schools, based on [14]*
Legend: Dark green circle of UPT The stop accessibility less than 2 min. by foot
Light green circle of UPT The stop accessibility less than 5 min. by foot

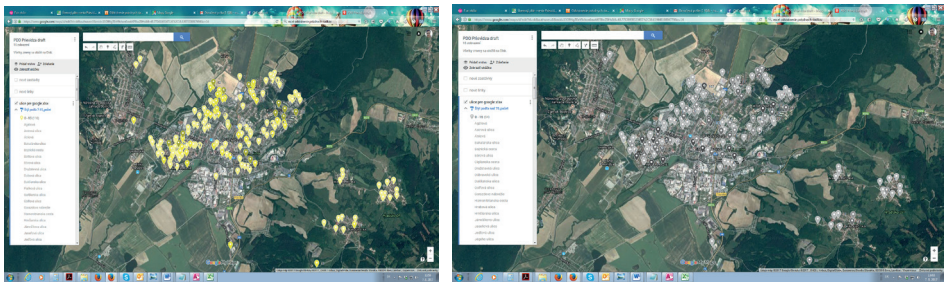

Figure 7 *The graphical representation of streets with an above-average number of residents at the age of 7-15 years (left) and at the age above 70 years (right) in towns of Prievidza and Bojnice; a darker colour means a higher number, based on [14]*

and railway transport on the territory of the given town and their accessibility from the built-up area [14-15]. The spatial accessibility of the UPT is evaluated through depicting the isochrones of the time accessibility for individual stops, which, at the same time, will evaluate the area operation of the town. Places without the UPT operation are defined, as well (Figure 6). It is not possible to expect that the suburban bus transport lines, with very small area coverage of stops, would suffice for commuting to schools (children), or to health care institutions, or that citizens would commute to and from the stops for the distance of 1.5-2 km.

The passengers require an attendance distance to the UPT stop (the so-called spatial accessibility of the UPT), which is derived from conducted questionnaire surveys within the management of transport operation plans; in the town of Prievidza it was discovered at the level of 300 m (71.6 % of responses) [14].

Since not all the residents of the town or commuters (especially schoolchildren and pensioners above 70) are given the option to get to their destination in the town using other transport means than the UPT, the transport operation plans also include a study of the town residents' distribution from the point of view of the age structure by individual streets (Figure 7). The routing of lines and the time position of individual connections can then reflect requirements of the residents with a higher share in the given urban part.

A detailed study of the access by foot, including the quality of pavement surface, to the UPT stops was conducted in Ljubljana, Slovenia [16]. Modelling of the UPT stops accessibility in smaller towns is in the centre of interest of Lamotte, O. et al. [17]. They state that in Europe and France it is basically anticipated that residents are close to a UPT stop if its distance is not more than 400 m [17]. This statement was also confirmed by results of research realised in the Slovak Republic. In addition, thanks to studying different towns, especially in South Korea, a multi-criterial analysis was worked out, which also considers deploying the advanced public transport modes (APTM) with respect to building the new types of towns, [7].

Figure 8 implies that the pedestrian traffic is only counted with for the distance of up to 1 km; in the case of the bike transport, it is something more than 2 km. Still, the utilisation of the bus transport with a combination of accelerated lines is counted with. One can see that foreign

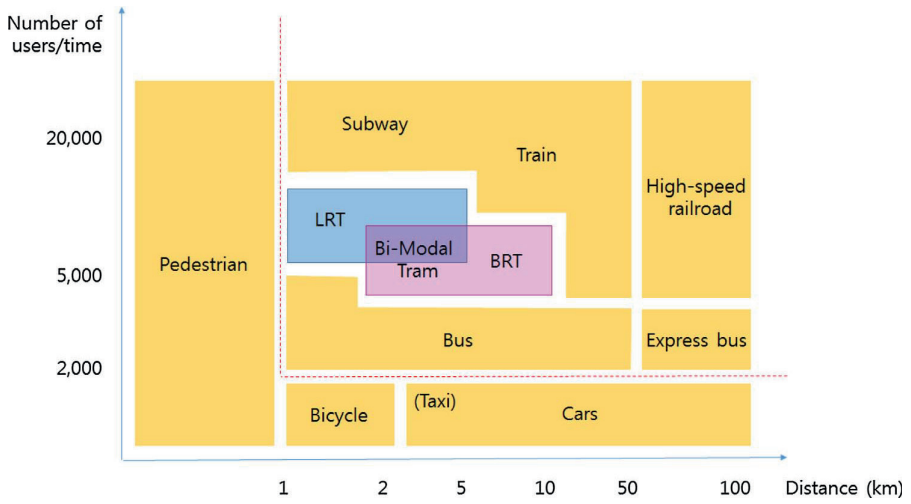

Figure 8 *Characteristics of the advanced public transport modes (APTM) and existing options for the transport modes, [7]*

countries deal in detail with the question what kinds of public passenger transport should be applied in towns. In the SR, part of residents from bigger towns, with respect to the growing prices of flats and a lack of building lands, moves to the countryside where the satellite built-up areas of family houses and flat complexes arise without sufficient facilities of schools and health care institutions, etc. and often even without a link to the public passenger transport [18].

4 Application of the multi-criterial analysis and discussion

As a part of the decisions making about the need to provide the UPT, it is necessary to take into account many more factors than the number of the town residents only. The authors studied a whole series of other factors besides those already mentioned. In fact, it is a problem of a multi-criterial decision making which is also applied to logistics [19].

In case of a multi-criterial decision-making, the decisive subject evaluates individual variants through the multiple criteria when the objectification of the decision process depends on a number of evaluative aspects. If the number of evaluative criteria and variants is small, the decisive subject can make the decision based on their intuition. However, if the number of criteria is higher and the decision situation is more complex, it is necessary to apply formalised procedures. An appropriate formalised procedure is determination of the evaluative criteria weights and aggregation of the partial evaluations into a complex evaluation [20]. Fiala, Jablonsky and Manas [21] introduce that in case of the multi-criterial evaluation of variants the task is specified explicitly with a set of alternatives A = {a1, a2..., etc.}. In here presented case, it is created with options to choose a transport means and maybe specific carriers and with a set of evaluative criteria F = {f1, f2..., fk}, which is created with selected bank products and with evaluation of selected variants via individual criteria in the form of the so-called criteria matrix:

$$\begin{array}{c} \\ a_1 \\ a_2 \\ . \\ . \\ a_p \end{array} \begin{array}{c} \begin{array}{cccccc} f_1 & f_2 & . & . & f_k \end{array} \\ \begin{bmatrix} y_{11} & y_{12} & . & . & y_{1k} \\ y_{21} & y_{22} & . & . & y_{2k} \\ . & . & . & . & . \\ . & . & . & . & . \\ y_{p1} & y_{p2} & . & . & y_{pk} \end{bmatrix} \end{array} \tag{3}$$

Elements of the criteria matrix, y_{ij}, i = 1, 2..., p, j = 1, 2..., k, express information on evaluation of alternatives by individual criteria. The information may take the following form:

- cardinal information - it represents the actual value achieved with individual variants during the evaluation by the given criteria,
- ordinal information - it expresses the order of a certain variant by individual criteria, i.e. sorting the criteria by their importance,
- relative information - it compares pair variants between each other by individual criteria [21].

The next criterion of the decision-making about the UPT provision is reduction of the attendance distance by foot or by the bike transport to the railway or bus station and thus reduction of individual automobile transport effects on environment in the town, reduction of congestions, enhancement of road transport safety, etc. [22]. Moreover, it is very important to study how the behaviour of residents in smaller towns is affected by quality of the UPT. A factor analysis can be applied here [23].

Furthermore, a very important issue is the setting of the UPT offering via lines, connections and operation time [24]. They are bound to provide accessibility of the UPT to health care institutions, schools, offices and last, but not the least, regular commuting to work. Provision of transport to work is a separate specific area of studying the mobility of the population.

Based on the assessments conducted by the authors, eight criteria to be taken into account when deciding on the necessity of establishing the UPT were defined. Standardized scales of importance and reference values were defined for individual criteria (Table 3). The ranking method was used to determine the scales of importance,

Table 3 *Defined criteria with assigned scales of importance and reference values*

criteria	scales of importance	reference values
number of inhabitants	0.22	50,000
number of pupils and students of all the schools	0.19	2,000
number of employers with 100 or more employees	0.17	10
number of medical facilities (ambulances / wards in the hospital)	0.14	100
number of public authorities (district office, building office, labour office, etc.)	0.11	50
railway station equipment (number of passenger rail connections)	0.08	100
bus station equipment (number of bus connections)	0.06	500
preference for ecological modes of transport	0.03	1/0

*In the case of medical facilities of superregional importance, value of the scales of importance needs to be adjusted

Table 4 *Application of the methodical procedure*

	information's of the city under assessment	fulfilment of the criterion [%]	achieved evaluation
30,000	inhabitants	60	13.2
1,500	pupils and students	75	14.25
3	employers with 100 or more employees	30	5.1
30	ambulances / wards in the hospital	30	4.2
10	public authorities	20	2.2
21	passenger rail connections	21	1.68
130	bus connections	26	1.56
1	the city wants to prefer an ecological mode of transport	100	3
total			45.19
minimum value for ordering the UPT			60
necessary UPT			no

where the order of the criteria was ranked by the authors based on their experience with the creation of transport operation plans. Defined reference values for each criterion take into account the fact that the methodology is proposed for small towns, where values were determined by expert authors estimate. Determination of the precise reference values will be the subject of further more detailed research.

The methodological procedure is based on the percentage assessment of fulfilment of the defined criteria reference values. The achieved evaluation of the criteria corresponds to the value of the performance multiplied by the scales of importance for the given criterion. The sum of the subtotal is determined final value, whereby it is possible to decide on the need for setting up the UPT. The authors set the minimum value of the final evaluation at the level of 60 points, which corresponds to fulfilment of the reference values at the level of 60%. An example of application of the methodological procedure is given in Table 4.

The decision-making also includes the criterion weight of impacts of a specific transport mode, or a combination of transport means on the environment. Except for the costs, the so-called carbon footprint on specific transport means used may be calculated [25]. Alternatively, in the case of railway passenger transport, which uses the electricity as its source of energy, calculation of the so-called indirect emissions, which arise during its production, will be taken into account [26-27].

As a part of the further research, the authors would like to focus on completing the methodology for application of the multi-criterial analysis to the decision process on providing the UPT in smaller towns with less than 50,000 or 30,000 residents. The objective is its application in the SR and Poland, the Czech Republic and some other EU states, using experts on the UPT.

In this case, the Delphi method was used to verify the correctness of the established criteria and defined the scales of importance and it is assumed to verify the accuracy of the defined methodology, as well.

5 Conclusion

In the case of important strategic decisions on provision of the UPT and its scope, the following strategic documents should definitely be helpful in the SR: a transport operation plan of a town, or a transport operation plan of a self-governing region; here the methods of a multi-criterial decision making are required to be applied. It is recommended that the decisive subject - a town or a self-governing region - evaluates individual variants using the multiple criteria, when the objectification of the decision process depends on a number of evaluative aspects and on the accuracy of inputs, e.g. from transport operation plans, which, unfortunately, are still worked out in a varied quality.

For the decision process on provision of the UPT and choice of the transport means, one may also utilise the latest decision techniques and potential engineer applications, which can evaluate a whole series of data obtained online within a transport chain; e.g. Collaborative Filtering Bandits method can be applied here [28-29]. In the case of the multi-criterial analysis application, it is possible to complete the partial evaluation by using other additional and new methods [30].

Of course, it is inevitable to deal with requirements of the town residents, visitors, students, etc. imposed on the urban public transport in view of building a sustainable transport system in the town [31-32].

In the Slovak Republic, the general legislation was amended with a regulation of the Ministry of Transport and Construction of the SR No. 5/2020 Coll., laying down certain provisions related to ordering of the public passenger transport. In addition, it includes standards of transport operation. Under this regulation, special standards for urban transport in municipalities, with the number of residents less than 50,000, are represented by creation of connections, leading mainly to the centres with the occurrence of jobs, schools, health care institutions and public authorities. That includes guaranteed changes, bound to the suburban or long-distance transport to facilities mentioned before, if such centres are at a distances of more than 1,500 m or more than 20 min walk from a stop of the long-distance or suburban transport. Part of the transport operation of a village or a town may also be alternative transport in the form of a hybrid operation of suburban lines with the character of an intra-municipal operation in the territory of a village or town.

Unfortunately, with respect to saving money, such standards set for towns with less than 50,000 residents may lead to the point when, in certain district towns of the SR, the offering of the UPT connections, as well as the spatial accessibility of stops may decrease, especially if the suburban lines are funded by the self-governing region, not the town itself.

As a part of the UPT funding, it is necessary to highlight that the issue does not lie only in the mobility of town residents, but in the financing of an environmentally more friendly form of mobility than a car is, as well. In other words, the subject under consideration is financing a healthier way of life of town residents.

Potential considerations regarding the possibility to replace the UPT by a car sharing in smaller towns, where also the offering of taxi service is not sufficient, are published in [33].

Acknowledgement

The paper was created within the project of an institutional research of the Faculty of Operation and Economics of Transport and Communications No. 7/PEDAS/2019 Plans and Standards of Transport Operation of Towns and Regions as Part of Transport Operation Plans.

References

[1] STANKOVIC, M., GLADOVIC, P., POPOVIC, V., LUKOVAC. V. Selection criteria and assessment of the impact of traffic accessibility on the development of suburbs. *Sustainability*. [online]. 2018, **10**(6), 1997 [accessed 2019-6-10]. ISSN 2071-1050. Available from: https://doi.org/10.3390/su10061977

[2] DYDKOWSKI, G. *Urban transport integration* (in Polish). Katowice: Wydawnictwo Uniwersytetu Ekonomicznego w Katowicach, 2009. ISBN 978-83-7246-452-1.

[3] POLIAK, M., MRNIKOVA, M., JASKIEWICZ, M., JURECKI, R., KACIAKOVA, B. Public transport integration. *Communications - Scientific Letters of the University of Zilina*. [online]. 2017, **19**(2), p. 127-132 [accessed 2019-6-10]. ISSN 1335-4205, eISSN 2585-7878. Available from: http://komunikacie.uniza.sk/index.php/communications/article/view/196

[4] TOMANEK, R. Effectiveness of free of charge public transport in cities (in Polish). *Public Transport* [online]. 2017, **69**(4), p. 18-25 [accessed 2019-6-10]. ISSN 1429-5788, eISSN 2543-6570. Available from: http://komunikacja.kzkgop.com.pl/public_media/fb/files/czasopisma/komunikacja/2017/kp_04_2017_ENG.PDF

[5] SUROVEC, P. *Design of the urban public transport system*. 1. ed. Zilina: EDIS - Publishing house of University of Zilina, 1999. ISBN 80-7100-586-X.

[6] CIBULKA, J.: The increase in transport relations satisfied by traffic that are carried out to work only inside the city territory as a result of increasing distance between home and work. Development of transport with respect to the environment. Usti nad Labem. 1979.

[7] LEE, D. J. A multi criteria approach for prioritizing advanced public transport modes (APTM) considering urban types in Korea. *Transport Research* [online]. 2018, **A111**, p. 148-161 [accessed 2019-6-10]. ISSN 0965-8564. Available from: https://doi.org/10.1016/j.tra.2018.02.005

[8] NIGRO, A., BERTOLINI, L., MOCCIA, F. D. Land use and public transport integration in small cities and towns: assessment methodology and application. *Journal of Transport Geography* [online]. 2019. **74**, p. 110-124 [accessed 2019-6-10]. ISSN 0966-6923. Available from: https://doi.org/10.1016/j.jtrangeo.2018.11.004

[9] Statistical Office of the Slovak Republic [online] [accessed 2019-06-10]. Available from: www.datacube.statistics.sk

[10] The network of school and school facilities in the Slovak Republic - The Ministry of Education, Science, Research and Sport of the Slovak Republic [online] [accessed 2019-06-10]. Available from: www.minedu.sk
[11] Local Data Bank [online] [accessed 2019-05-25]. Available from: https://bdl.stat.gov.pl/BDL
[12] The Czech Statistical Office [online] [accessed 2020-01-15]. Available from: https://www.czso.cz/csu/czso/databaze-demografickych-udaju-za-obce-cr
[13] KONECNY, V., GNAP, J., SIMKOVA, I. Impact of fiscal decentralization on motor vehicle taxation in the Slovak republic. *Transport and Telecommunication Journal* [online]. 2016, **17**(1), p. 28-39 [accessed 2019-6-10]. ISSN 1407-6179. Available from: https://doi.org/10.1515/ttj-2016-0004
[14] GNAP, J., GOGOLA, M., POLIAK, M., KONECNY, V., MAJER, T., CERNICKY, L., KUPCULJAKOVA, J., PALO, J., VARJAN, P., BEREZNY, R. *Transport operation plan of the city of Prievidza - optimal variant* [online]. University of Zilina, 2017 [accessed 2019-05-25] Available from: http://www.prievidza.sk/upload/wsw/files/file/SAMOSPRAVA/MsZ/PDO%20Prievidza%20FIN.pdf
[15] GNAP, J., GOGOLA, M., POLIAK, M., KONECNY, V., MAJER, T., CERNICKY, L., KUPCULJAKOVA, J., PALO, J., SLAVIK, R., SETTEY, T. *Transport operation plan of the city of Martin*. University of Zilina, 2019.
[16] TIRAN, J., LAKNER, M., DROBNE, S. Modelling walking accessibility: a case study of Ljubljana, Slovenia. *Moravian Geographical Reports* [online]. 2019, **27**(4), p. 194-206 [accessed 2019-6-10]. ISSN 2199-6202. Available from: https://doi.org/10.2478/mgr-2019-0015
[17] LAMOTTE, O., GAUD, N., GALLAND, S. Towards the dynamic evaluation of a public bus network for small size urban environments. *Procedia Computer Science* [online]. 2015, **56**, p. 168-176 [accessed 2019-6-10]. ISSN 1877-0509. Available from: https://doi.org/10.1016/j.procs.2015.07.191
[18] GOGOLA, M., HOCOVA, M. Deurbanisation and mobility. *Transportation Research Procedia* [online]. 2016, **14**, p. 1193-1200 [accessed 2019-6-10]. ISSN 2352-1465. Available from: https://doi.org/10.1016/j.trpro.2016.05.190
[19] LEBEAU, O., MACHARIS, C., VAN MIERLO, J., JANJEVIC, M. Improving policy support in city logistics: the contributions of a multi-actor multi-criteria analysis. *Case Studies of Transport Policy* [online]. 2018, **6**(4), p. 554-563 [accessed 2019-6-10]. ISSN 2213-624X. Available from: http://dx.doi.org/10.1016/j.cstp.2018.07.003
[20] REPISKY, J. *Decision theory*. 2. ed. Nitra: Slovak University of Agriculture in Nitra, 2005. ISBN 80-8069-475-3.
[21] FIALA, P., JABLONSKY, J., MANAS, M. *Multi-criterial decision making*. 1. ed. Prague: University of Economics, 1994. ISBN 80- 7079-748-7.
[22] KALASOVA, A., KUBIKOVA, S, MIKULSKI, J. The impact of intelligent transport systems on an accident rate of the chosen part of road communication network in the Slovak republic. *Communications in Computer and Information Science* [online]. 2016, **640**, p. 47-58 [accessed 2019-6-10]. ISSN 1865-0929. Available from: https://doi.org/10.1007/978-3-319-49646-7_5
[23] CHEBA, K., SANIUK, S. Urban mobility - identification, measurement and evaluation. *Transport Research Procedia* [online]. 2016, **14**, p. 1230-1239 [accessed 2019-6-10]. ISSN 2352-1456. Available from: https://doi.org/10.1016/j.trpro.2016.05.194
[24] GNAP, J., KONECNY, V., POLIAK, M. Demand elasticity of public. *Journal of Economics* [online]. 2006, **54**(7), p. 668-684 [accessed 2019-6-10]. ISSN 0013-3035. Available from: https://www.researchgate.net/publication/292548426_Demand_elasticity_of_public_transport
[25] PETRO, F., KONECNY, V. Calculation of emissions from transport services and their use for the internalisation of external costs in road. *Procedia Engineering* [online]. 2017, **192**, p. 677-682 [accessed 2019-6-10]. ISSN 1877-7058. Available from: https://doi.org/10.1016/j.proeng.2017.06.117
[26] SKRUCANY, T., KENDRA, M., SARKAN, B., GNAP, J. Software simulation of an energy consumption and GHG production in transport. Tools of transport telematics. *Communications in Computer and Information Science* [online]. 2015, **531**, p. 151-160 [accessed 2019-6-10]. ISSN 1865-0929. Available from: https://doi.org/10.1007/978-3-319-24577-5_15
[27] SKRUCANY, T., GNAP, J. Energy intensity and greenhouse gases production of the road and rail cargo transport using a software to simulate the energy consumption of a train. In: 14th Transport Systems Telematics Conference TST 2014: proceedings. Vol. 471. Berlin: Springer-Verlag, 2014. ISSN 1865-0929, p 263-272.
[28] LI, S., KARATZOGLOU, A., GENTILE, C. Collaborative filtering bandits. In: 39th ACM SIGIR Conference of Research and Development in Information Retrieval: proceedings. New York: NY, United States: Association for Computing Machinery, 2016. ISBN 978-1-4503-4069-4, p. 539-548.
[29] BOUNEFFOUF, D. Contextual bandit algorithm for risk-aware recommender systems. In: IEEE Congress on Evolutionary Computation CEC held as part of IEEE World Congress on Computational Intelligence IEEE WCCI: proceedings. 2016. p. 4667-4674.
[30] HAO, F., LI; S., MIN, G., KIM, H.-CH., YAU, S. S., YANG, L. T. An efficient approach to generating location-sensitive recommendations in ad-hoc social network environments. *IEEE Transactions on Services Computing* [online]. 2015, **8**(3), p. 520-533 [accessed 2019-06-10]. Available from: https://doi.org/10.1109/TSC.2014.2401833

[31] MASOUMI, H. A discrete choice analysis of transport mode choice causality and perceived barriers of sustainable mobility in the MENA region. *Transport Policy* [online]. 2019, **79**, p. 37-53 [accessed 2019-8-1]. ISSN 0967-070X. Available from: https://doi.org/10.1016/j.tranpol.2019.04.005

[32] GNAP, J., KONECNY, V. Transport policy related to road transport and sustainable development. *Communications - Scientific Letters of the University of Zilina* [online]. 2003, **5**(1), p. 52-61 [accessed 2019-6-10]. ISSN 1335-4205, eISSN 2585-7878. Available from: http://www3.uniza.sk/komunikacie/archiv/2003/1/1_2003en.pdf

[33] ROTARIS, L., DANIELIS, R. The role for car sharing in medium to small-sized towns and in less densely populated rural areas. *Transport Research* [online]. 2018, **A115**, p. 148-161 [accessed 2019-6-10]. ISSN 0965-8564. Available from: https://doi.org/10.1016/j.tra.2017.07.006

ANALYSIS OF TRANSPORTATION COMPANIES IN THE CZECH REPUBLIC BY THE KOHONEN NETWORKS - IDENTIFICATION OF INDUSTRY LEADERS

Jakub Horák*, Petr Šuleř, Jaromír Vrbka

School of Expertness and Valuation, Institute of Technology and Business in Ceske Budejovice, Ceske Budejovice, Czech Republic

*E-mail of corresponding author: horak@mail.vstecb.cz

Resume

Computational models of artificial neural networks are currently used in different areas. Accuracy of results exceeds the performance of traditional statistical techniques. Artificial neural networks as the Kohonen map may be used e.g. to identify industry leaders, thus replacing the traditional cluster analysis and other methods. The aim of this contribution is to analyse the transportation industry in the Czech Republic by the Kohonen networks and identify industry leaders. The data file contains results - division of companies into a total of 100 clusters. Each cluster is subjected to analysis of absolute indicators and several parameters, average, as well as absolute, are examined. In total, 88 firms may be considered as industry leaders. Consequently, a fairly small group of companies has a strong influence on development of the whole transportation industry in the Czech Republic.

Article info

Received 3 March 2020
Accepted 3 June 2020
Online 26 October 2020

Keywords:

Kohonen networks,
artificial intelligence,
industry leaders,
transportation,
cluster analysis

Available online: https://doi.org/10.26552/com.C.2021.1.A32-A43

ISSN 1335-4205 (print version)
ISSN 2585-7878 (online version)

1 Introduction

Artificial neural networks (ANN) have become a frequently addressed topic over the last decade and currently they are inevitable in all the sectors, including transport. With their help, it is possible not only to analyse the large data files, but also to predict future development or to apply them in decision-making processes. Their application in the transport sector offers many advantages, which might become not only competitive. The need to use the ANN is constantly growing, and becoming an advantage that can both save time and improve results of analyses, as well as help where traditional methods are no longer sufficient. A significant deficiency in traditional methods is their inability to work with nonlinear data, or their problem with processing of large data files, and the perfect solution is to use the artificial neural networks. Demand for use of the neural networks in business processes has been constantly growing and range of their application is so wide that they will prove useful to a large number of users. However, using the ANN is not only a useful option, but for some companies it is a question of necessity, because, as already mentioned, there are issues where traditional methods of data processing can no longer be applied. Advantage in neural networks over the traditional methods is also seen by Horak and Krulicky [1], who say that the method of artificial neural networks has many advantages over the conventional methods. In the transport sector, one can find abundant use of the ANN, such as for processing data on consumer behaviour, prediction of train delays based on historical time data, or generally, in comprehensive evaluation of companies which is dealt with, for example, by Vochozka [2]. Neural networks can be also widely used in analysis of companies, as they were used e.g. by Machova and Vochozka [3], who analysed business companies in the Czech Republic using the artificial neural networks and subsequently estimated development of this sector of the national economy. Transport companies abound in a large amount of (not only) company data, which - thanks to their fast and efficient processing - can be transformed into useful outputs that provide companies with many benefits and predictions of the future development. Transport companies form an important component of the national economy in the Czech Republic, whether it is the transport of people, information, or freight. According to Svobodova, Veznik and Hofmann [4], the unprecedented importance of transport in the Czech Republic arises from its position at the crossroads of trans-European routes. Undoubtedly, the interior transport is also of a great importance in the Czech Republic, above all for the import and export of raw materials and products and especially for satisfying the need for interior and international passenger transport.

Artificial neural networks are in fact computational models that are inspired by biological neural networks, namely neuronal behaviour [5]. Use of these networks is,

however, applicable in many different areas. According to Pao [6], neural networks are currently widely used to address potential future problems, in particular for value prediction. Horak, Vochozka and Machova [7] state that results of the neural networks are very promising, and their performance and accuracy when calculating a company's key performance indicators are significantly higher than those of the traditional statistical techniques. Sayadi et al. [8] argue that the main advantages of artificial neural networks are the ability to generalize, the ability to learn, etc. One of disadvantages of networks is that they require high data quality and possibility of illogical behaviour of the artificial neural network [9]. According to Grigoryev et al. [10], this illogical behaviour can be explained by the fact that a trained ANN classifies the observations according to its own criteria, which differ from the usual criteria used by humans. Therefore, using these unusual criteria, ANN can make fundamental errors in the non-standard irregular situations. Thus, some specific additional techniques are needed to detect such illogical behaviour. One of the major disadvantages is also the inability to estimate an error of the result, which is obtained by a neural network.

According to Vochozka and Machova [11], the artificial neural network is one of the most popular methods that is used as a prognostic method that requires a more complex model, uses more variables and tends to be nonlinear. Therefore, this method is suitable for auxiliary adjustments of the financial sector, especially in the stock market. The authors' study proves that the neural network, as a predictive model, could significantly outperform the minimum return.

Vochozka and Sheng [12] used the artificial neural networks to predict potential financial problems in transport companies in the Czech Republic. The result is a neural network, which, with accuracy exceeding 90%, determines if a company is able to overcome potential financial problems, in how many years a company could go bankrupt or whether a company could fail within one calendar year. The model can be used in practice by leading transport companies, investors looking for a suitable company for capital investment, competitors, etc. [13], based on the presented data, demonstrated the classification capability of the Kohonen network model, one of the models of artificial neural networks. Using this approach to analysing a company can help to decide, quickly and easily, whether the company is healthy or in recession with respect to historical data. This is often a crucial requirement for the successful business activity in the area. According to Han and Wang [14], business analysis can be measured in different ways, but Kohonen networks are considered as a very attractive model. These networks can be used to group into different groups. Many experimental results show that Kohonen's networks are very effective for business valuation. Krulicky [15] noted that Kohonen's network is self-organized and is composed of an input layer that is interlinked to the output layer. Since it is an alternative network, it has a wide range of application that can be used for most neural network calculations.

According to Severin [16], separate Kohonen networks can be used to improve the time stability of the financial failure model. This model is successfully used for data mapping and its trajectory allows clustering and visualization of bankruptcy tendencies, offering new insights into models of business expansion in competition [17]. On the other hand, it serves as a tool for predicting the future bankruptcy and much relevant literature suggests such models [18].

Cluster analysis has many uses, not only in the transport sector. For example, Hitka et al. [19] applied the cluster analysis to define three motivationally oriented groups in the category of managers and three similar motivationally oriented groups in the category of employees, using the cluster analysis as a strategic advantage of human resource management in small and medium-sized enterprises in the woodworking industry. Furthermore, e.g. Vrbka and Rowland [20] used the neural networks to forecast stock price developments.

This article explores the Kohonen networks to analyse transport companies and therefore there is a need to briefly describe the specificities of transport companies and introduce some research on a similar topic. Transport companies provide public services and usually operate under the conditions of a natural monopoly [21]. Most authors categorize transport businesses by road, water, air, sea and rail and as public and non-public. As is well known, the process of globalization is a link between existing economies, with transport companies trying to meet the highest leading business standards [22]. This change in the transport market and acceleration of the cycle of external and internal changes in the transport companies brings extraordinary demands on top management in the area of management processes [23]. According to Ou et al. [24], a significant difference between the transport and other businesses is the focus on ecology. Traffic and transport companies have a far greater negative impact on the environment and, therefore, ecological issues of course concern them far more than the most of other companies. The transport sector has been one of the major factors contributing to environmental pollution in recent years. At present, many studies are working on the fuel consumption analysis in transport. Fuel types, including alternative fuel systems, have been compared, leading to a greater fuel technology development and, therefore, environmental protection.

Vochozka, Rowland and Vrbka [25], briefly presented the financial analysis, typical of transport and logistics companies and defined the financial characteristics of the average transport and logistics company in the Czech Republic. Based on the findings, they carried out a financial analysis of the average company, thus revealing the future potential of the transport and logistics sector in the Czech Republic. It can be said that the transport and logistics sector is financially sound and promising in the Czech Republic. Seroka-Stolka, Tomski and Pabian [26] analysed and evaluated the current situation of environmental management

in the Austrian transport sector. The authors sought to identify the specific characteristics of the transport sector with regard to environmental protection. They stated that there are effective ways to increase the overall sustainable performance of transport companies, especially through planned route optimization, pooling or investing in efficient warehouses.

2 Data and methods

In terms of methodology, the text is related to [15]. For the purposes of the contribution, the same set of data is used. A data file was analysed, containing data on 3,989 companies operating in the transport sector in the Czech Republic in 2016. The data file comes from Bisnode's Albertina database. All the enterprises are included in the database in the given year according to the CZ NACE classification of economic activities; in the specified sector H. Those are the complete financial statements of the companies. For the analysis itself, only certain items, expressing the main activity of the company, were used. Those items are not directly value generators, but they can have an impact, albeit indirect, on the company's performance. Those are the total assets (information on the size of the company), fixed assets (the level of technology used and the expected volume of performance - transport machines, i.e. cars, planes, etc.), current assets (the volume of funds, cash equivalents, account receivables and stock inventory), own resources (the degree of business risk), external resources (the external view of potential risks), performance (the production), added value (the value added by the company to the basic input - material), operating profit (how successful the company is in its activities), return on equity (the appreciation of equity) and profit before tax (a success or a failure of the company in its entire activity). The superstructure is to identify the transportation industry leaders in the Czech Republic. The contribution provides a deeper analysis of the previously obtained results.

The data file was subjected to cluster analysis using one type of artificial neural networks without a teacher, namely Kohonen networks. Dell's Statistica software version 12 was used. The data for the analysis was determined - in all the cases there were the continuous predictors. The data file was divided into three parts, of which the first - the training data set - contained 70% of the companies in the file. Based on this data set, a Kohonen network was created. The second part was a test data set, which contained 15% of the data and was used to verify parameters of the created network. The third part was a validation set, which also contained 15% of the data and was used to verify the created network and whether or not it was applicable.

The topology was based on the idea that it should be factually graspable, the length and width should not be too wide or too small (so that the level of detail is ideal). Prior to this research, a topology from 5 x 5 to 20 x 20 was tested and the most suitable one was determined to be 10 x 10. The topology is set in advance; it is a grid in the space of sample neurons. If only a single one was omitted, the grid would be irregular. It was also impossible to omit clusters that were not filled with real data, because in reality there may be a company that belongs to such a cluster. It is also impossible to find fewer clusters than the topology contains - it follows from the structure itself. The topological length and width of the Kohonen map was therefore set to 10. The view was orthogonal, however the distance measured was Euclidean. A sample neuron was created; after that, the distance was measured according to the distance of a real neuron. The neuron was represented by a number. The specification and methodology of creating Kohonen networks in the given software were used. That created a total of 100 clusters, 100 neurons. The number of repetitions of the calculation (iteration) was determined to be 10,000. However, the error level should be crucial - if the parameters did not improve with each subsequent iteration, the training would be terminated earlier. If, on the other hand, the network parameters improved, even during the final iteration, the whole process would be repeated and a higher iteration value would be set.

The results, namely the division of companies into 100 clusters, were imported to an Excel spreadsheet file. Consequently, each cluster was subjected to the analysis of absolute indicators. At this moment, the question should be answered, how an industry leader is understood. Numerous parameters can be selected, including, but not limited to:

- Volume of assets,
- Volume of fixed assets,
- Operating profit,
- Earnings before taxes (EBT).

The analysis has examined both average and absolute parameters of each cluster in order to establish:

- Most successful company clusters in the transportation industry.
- Most successful companies in the transportation industry.

The evaluation of return on assets and return on equity was also included in the analysis of absolute indicators. Return on assets (ROA) has shown the appreciation of capital invested in companies, or company clusters. Return on equity should, among others, document the attractiveness of each cluster for potential investors.

3 Results

Clusters were created using the applied methodology. The breakdown by representation of companies in each cluster of the Kohonen map is shown in Figure 1.

Figure 1 offers three-dimensional display of a Kohonen map and number of companies represented in each cluster. It is obvious from the graph that Cluster (4, 10) has the highest representation of companies. It is followed by Cluster (4, 9) and Cluster (5, 9) comes as the third. A hundred or more companies are also concentrated in Clusters (6, 10), (5, 10), (2, 6), (3, 8) and (1, 6). The

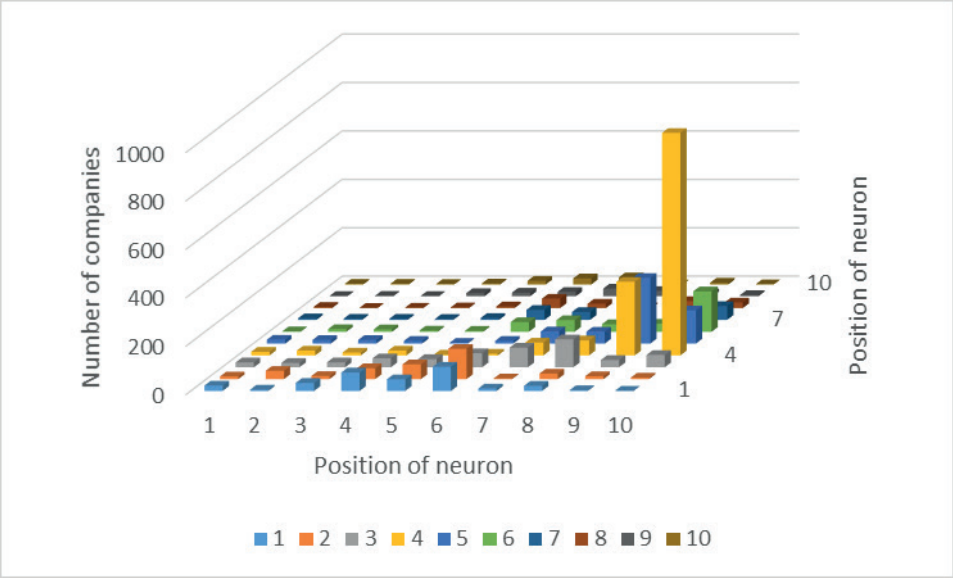

Figure 1 *Breakdown by representation of companies in each cluster of the Kohonen map*

Table 1 *Representation of companies in Kohonen map clusters*

cluster position	1	2	3	4	5	6	7	8	9	10
1	22	5	33	76	48	100*	10	21	3	1
2	11	34	13	45	61	125*	3	23	12	6
3	20	18	20	37	34	58	81	115*	30	51
4	15	20	12	20	3	7	53	62	304*	919*
5	16	15	15	11	3	11	50	49	271*	137*
6	2	11	10	5	4	40	48	31	33	167*
7	7	5	5	4	8	41	33	8	21	57
8	5	1	2	3	7	39	18	3	29	23
9	1	2	1	13	15	18	32	22	12	5
10	3	3	2	4	15	25	29	0	7	1

remaining clusters show a considerably lower number of companies. By the same token, note that only one cluster of the Kohonen map remains unoccupied, namely Cluster (10, 8). Several clusters are formed by a single company: (1, 10), (8, 2), (9, 1), (9, 3) a (10, 10).

Figure 1 is supported by specific values listed in Table 1 to provide a detailed overview of companies in each cluster.

Table 1 shows that apart from the clusters above (marked "*" in the table) no other clusters include more than a hundred of companies.

Further, the transportation companies, or the transportation industry, were analyzed from two points of view:

- The prism of average values of companies represented in each cluster: to determine how companies are characterised in each cluster and to which extent their company activity is successful on average;
- The view of absolute values per cluster: to get information how each cluster affects the future development and success of the transportation industry in the Czech Republic.

3.1 Analysis of average values

The first parameter used is the average value of corporate assets per cluster (Figure 2).

In practice, there is a marginal rate of capital-labour substitution, i.e. the fixed assets for employees. It can be concluded that companies, which own a high volume of fixed assets implement a high number of contracts with a lower number of employees. However, there is a very specific marginal rate of substitution in transportation. It rather varies between modes of transport, e.g. rail transport is a lot more challenging than the road transport. Nevertheless, the volume of the fixed assets may predetermine the volume of incomes realized from a company activity. However, it was expected for that to be the assets necessary for operation (i.e. assets needed by the company to realize income). In the case of transportation companies, a cluster with high average values of assets was identified. It is Cluster (10, 1). It is followed by several clusters with highly above-average average values of the fixed assets. In particular, note Cluster (10, 2) and Cluster (9, 2). Clusters (8, 1), (9, 3), (8, 2) (9, 1) and (8, 3) are also considered as very significant.

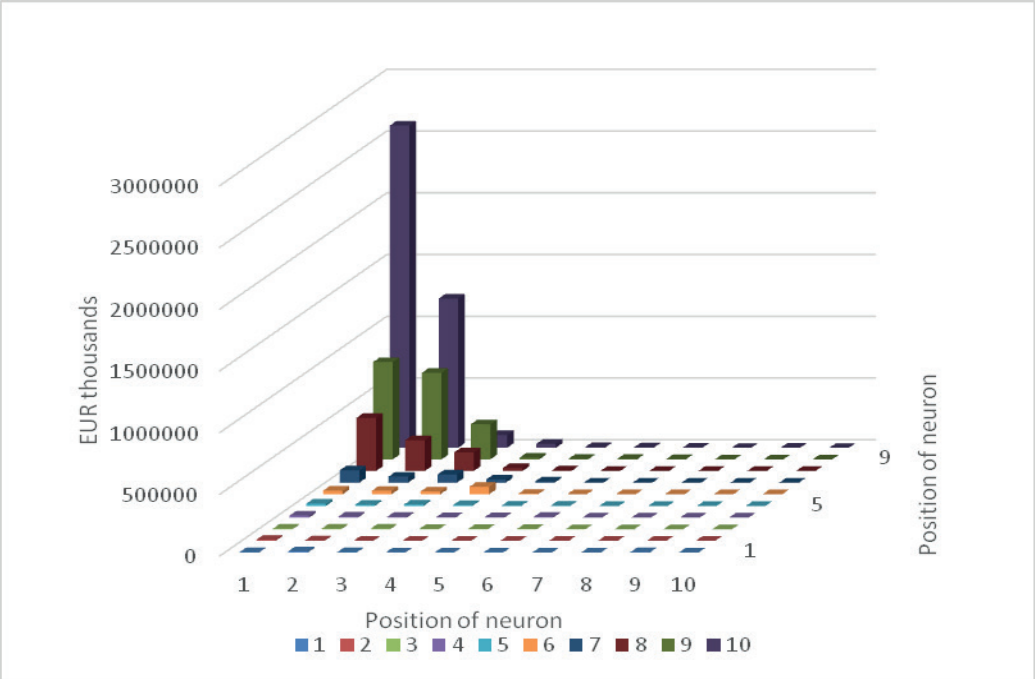

Figure 2 *Average value of corporate fixed assets per cluster*

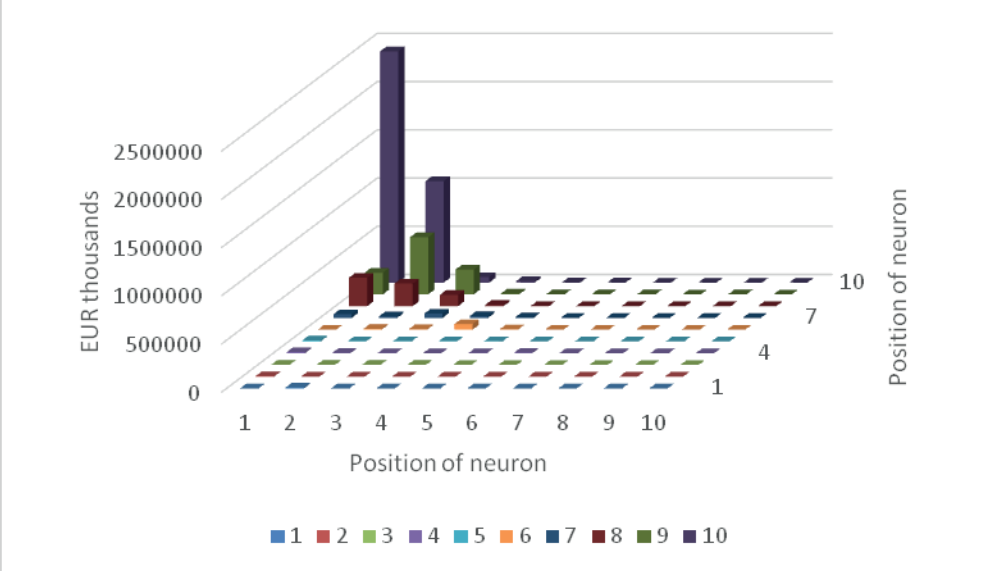

Figure 3 *Average value of total corporate assets per cluster*

In addition to fixed assets, an interesting indicator is total assets of an average company per cluster (Figure 3).

The total volume of assets predetermines the ability of the company to generate production. In particular, they include two out of three production factors [27] - i.e. fixed assets and material. The third production factor, human labour, is impossible to keep on store, thus it cannot be measured before the moment of consumption. The figure shows a very high value of average assets in Cluster (10, 1).

Clusters (10, 2), (9, 2), (8, 1), (9, 3), (8, 2) (9, 1) and (8, 3) show much lower values of the average total assets, however, still higher above the average.

There is another average value, which is very strong, namely operating profit.

The average operating profit (Figure 4) allows comparing the success of companies in different clusters.

Different sizes of companies are compared (although average parameters). Companies in Cluster (10, 2) appear to be the most successful. They are immediately followed by Clusters (10, 1), (9, 2), (6, 1) and (9, 1). In addition, note Clusters (8, 2), (8, 1), (5, 2) and (9, 3). The results of Clusters (6, 1) and (6, 2) are definitely very interesting. In terms of results, both clusters, in particular Cluster (6, 1), may easily compete with companies from clusters, which dispose of much more capital and fixed assets. It means that their management and administration are very effective, or they offer services with high value added. Or additionally, we can assume that sales are partly realized outside the transportation sector and their secondary activity is very

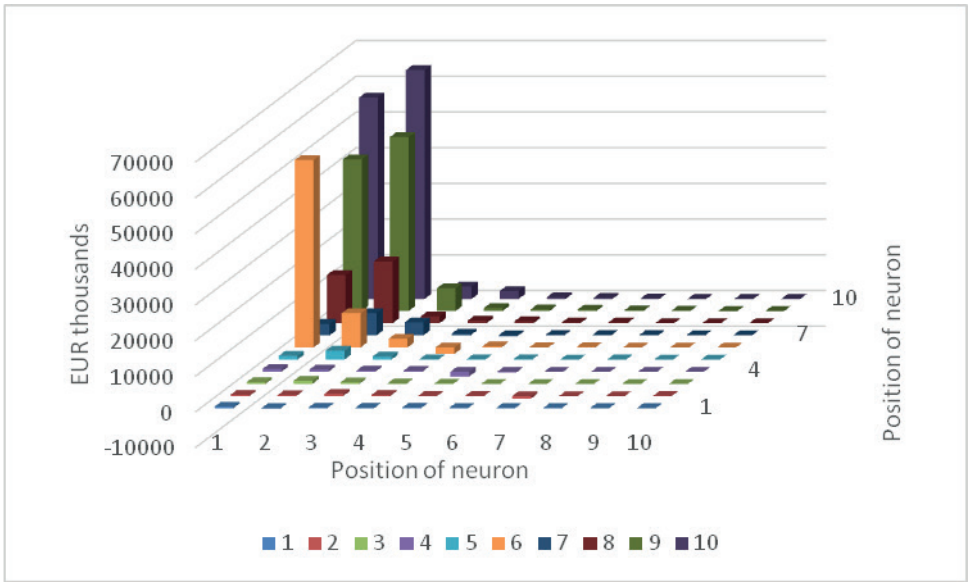

Figure 4 *Average operating profit per cluster*

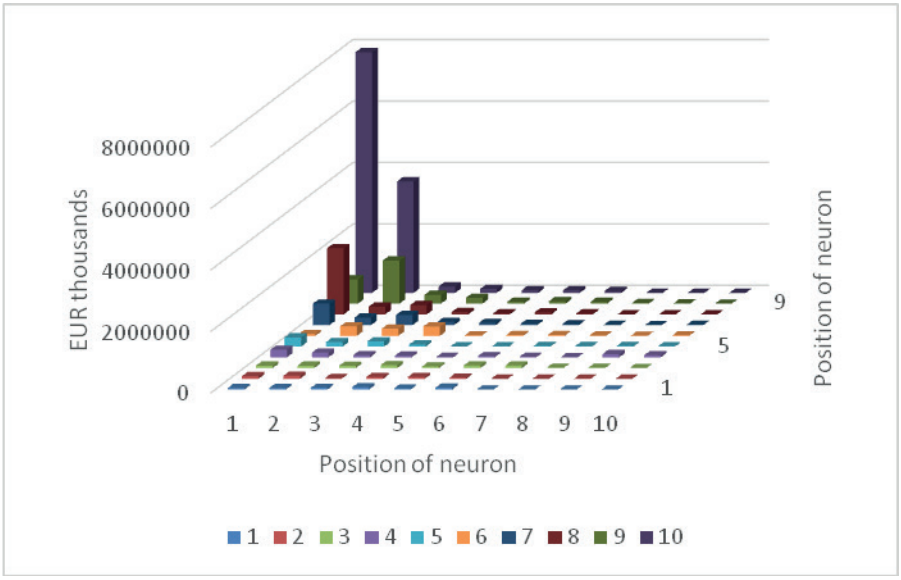

Figure 5 *Assets owned by companies per cluster*

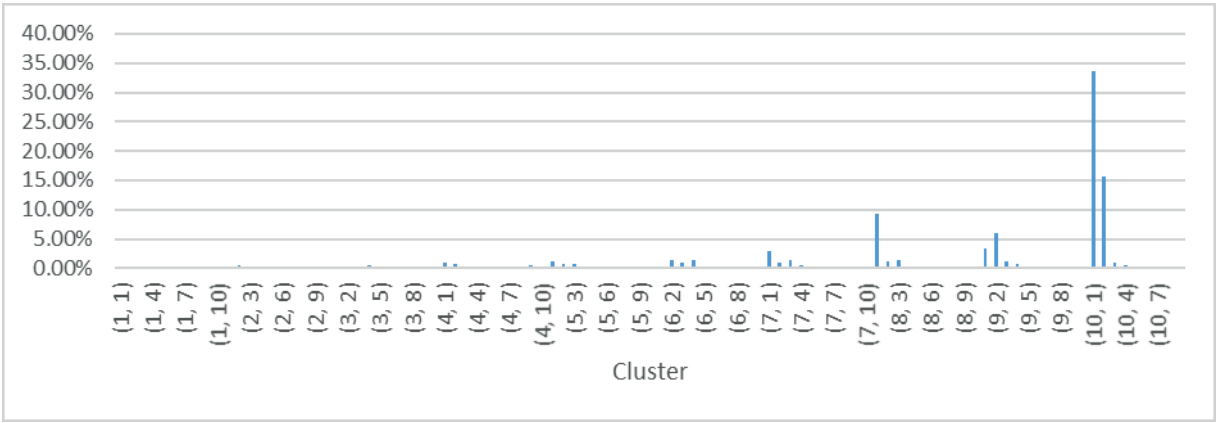

Figure 6 *Cluster shares of assets in the transportation industry*

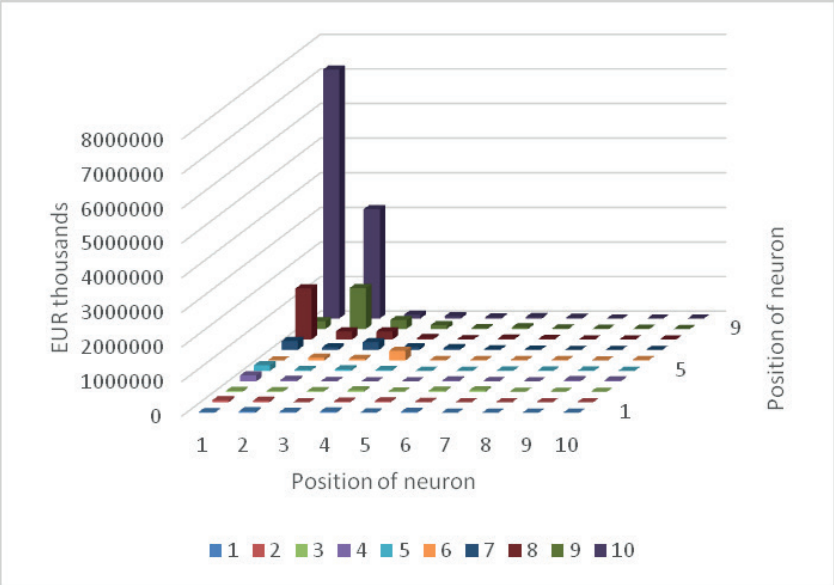

Figure 7 *Fixed assets owned by companies per cluster*

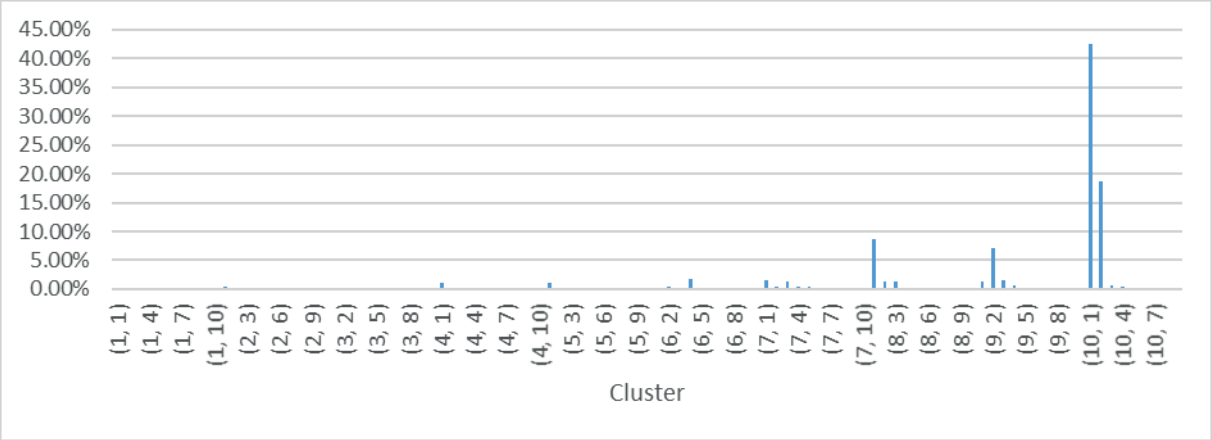

Figure 8 *Cluster shares of fixed assets in the transportation industry*

effective. In terms of efficiency (measured by the total and fixed assets to operating profit ratio), Cluster (6, 1) is considered as the most successful. On the other hand, the least successful companies are included in Cluster (6, 4) with realized operating loss exceeding on average EUR 1.8 million. This loss is in big contrast to their total assets and fixed assets. It can be deduced that the fixed assets are not used efficiently by those companies, or that just a small part of their fixed assets can be referred to as necessary for operation.

3.2 Analysis of absolute indicators

As previously mentioned, the analysis of absolute indicators should reveal how much each company cluster is important for the entire transportation industry in the Czech Republic. The same parameters, as in the case of average values analysis, were analyzed.

Figure 5 shows the absolute amount of fixed assets owned by companies pertaining to the same cluster.

The graph shows that the most of assets are owned by companies in Cluster (10, 1). The companies in this cluster dispose of the total assets amounting to nearly EUR 7,851 billion. The companies in Cluster (10, 2) own total assets exceeding EUR 3.61 billion. The companies allocated to Clusters (8, 1), (9, 2), (9, 1) and (7, 1) also dispose of total assets exceeding EUR 393 million. This interesting information is completed by cluster shares of the owned capital (Figure 6).

The graph shows that companies in Cluster (10, 1) own nearly 35% of all the assets in the transportation sector of the Czech Republic. The companies in Cluster (10, 2) own more than 15% assets of the transportation industry. Eventually, the companies in Cluster (8, 1) own 9.26% of all assets in the transportation sector of the Czech Republic. It has been expected that clusters large in numbers also appear in absolute parameters. However, that was not the case. Cluster (4, 10) representing 919 companies, i.e. more than 23% of the studied companies, represents only 0.28% of the total assets.

The fixed assets was another parameter examined (Figure 7).

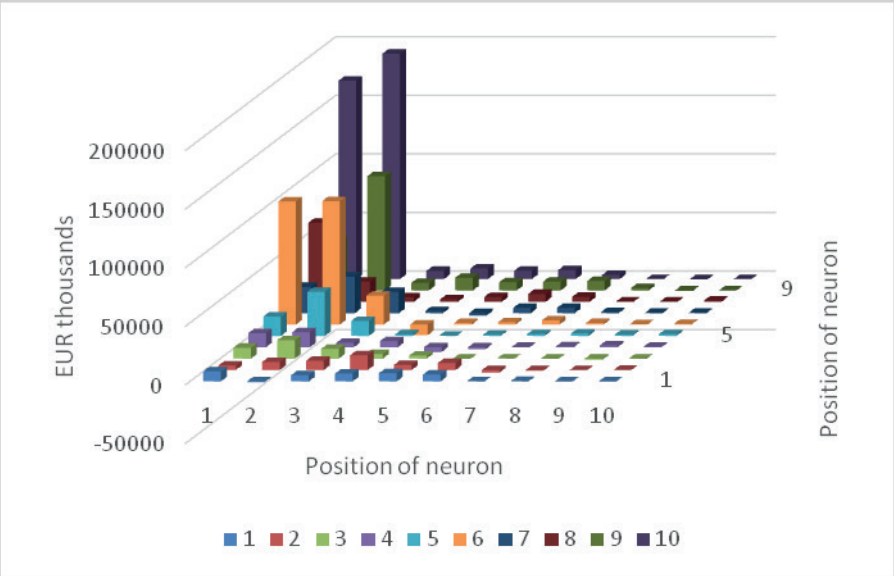

Figure 9 *Realized operating profit of companies per cluster*

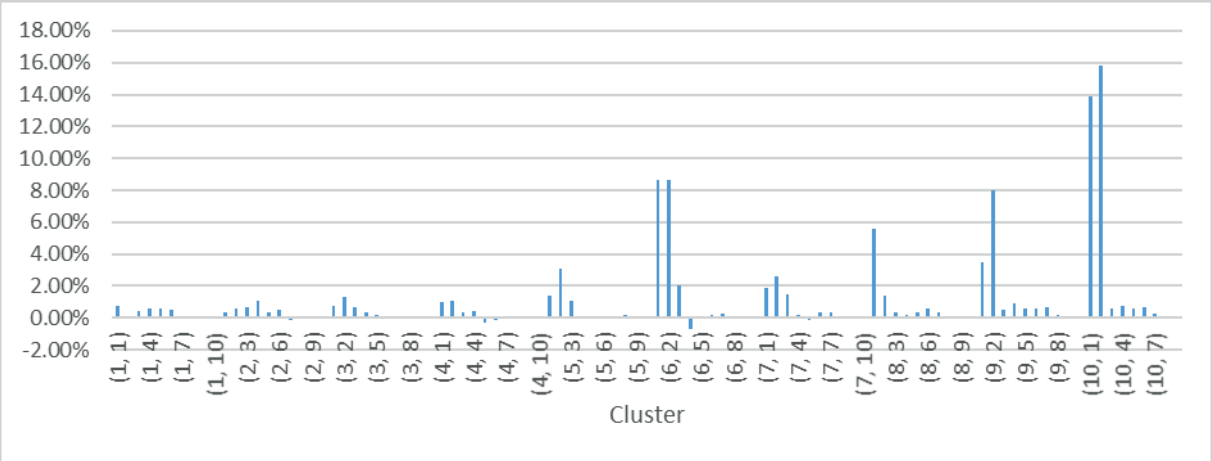

Figure 10 *Cluster shares of the operating profit realized in the transportation industry*

The graph shows again that the most of fixed assets are owned by companies in Cluster (10, 1). They register the aggregate value of fixed assets over EUR 7.18 billion. Clusters (10, 2), (8, 1) and (9, 2) also dispose of considerable fixed assets. All the identified clusters each dispose of fixed assets of billions of EUR. The situation was clarified based on a relative comparison of companies - namely the share of total owned fixed assets in the transportation sector (Figure 8).

The graph in Figure 9 indicates that companies in Cluster (10, 1) own more than 42% of the fixed assets employed in the transportation industry. Then 18.64% belongs to companies in Cluster (10, 2); 8.7% is owned by Cluster (8, 1) and less than 7% by Cluster (9, 2). The percentage of the fixed assets, employed in the transportation industry, owned by companies in Cluster (4, 10) is only 0.19%.

Figure 9 provides a comparison of absolute operating profits.

From the graph results that Cluster (10, 2) is definitely the most successful cluster in terms of operating profit. It generates a total income of less than EUR 192.4 million. It is followed by Cluster (10, 1) with operating profit exceeding EUR 164.9 million. Those two are followed by Clusters (6, 2), (6, 1) (9, 2), (8, 1) and (5, 2). See Figure 10 for illustration.

Figure 10 shows the predominance of Cluster (10, 2). In 2016 it generated nearly 15.8% of operating profit of the entire transportation industry. Cluster (10, 1) realized nearly 15% of operating profit across the Czech transportation industry in the reference period. Clusters (6, 2), (6, 1) and (8, 1) are also ranged above 8% of the total profit from operations in the transportation industry. The largest Cluster (4, 10) shares are - 0.00083% in the profits from operations of the Czech transportation industry.

It was also interesting to compare the return of equity (ROE) of different clusters (see Figure 11 for more details).

The graph does not show ROE values for clusters where companies achieved values outside the interval -500% to + 500%. Those were senseless values of clusters where only one company was represented at each time. The values outside the interval would cause a high distortion of outputs from the graph in Figure 11. Whether the interval was not too large is still a question. The ROE (return

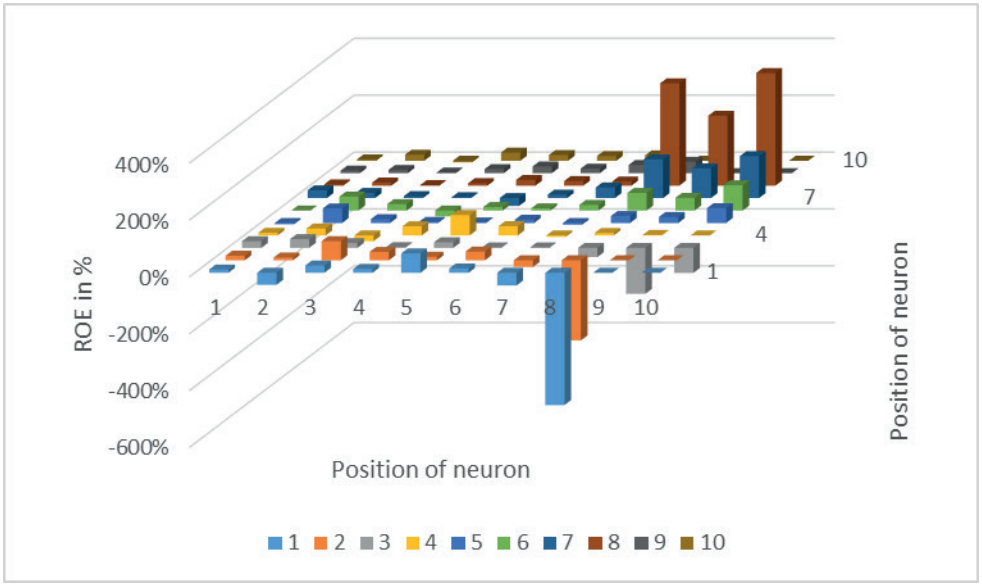

Figure 11 *ROE comparison of clusters in the transportation industry*

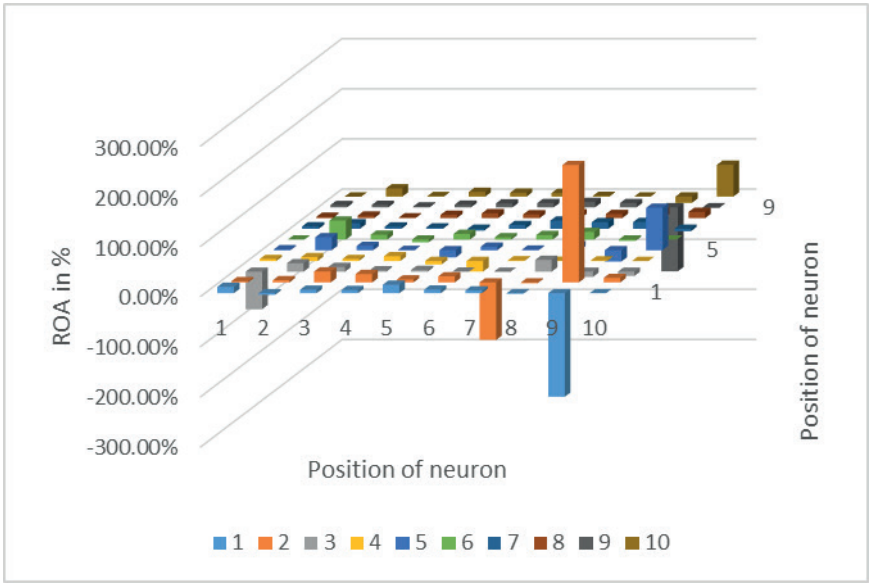

Figure 12 *ROA comparison of company clusters in the transportation industry*

Table 2 *Leaders in the transportation industry 2016*

row description	number of companies in a cluster	fixed assets (in EUR)	total assets (in EUR)	operating profit (in EUR)
(10, 2)	3	3,158,116,467	3,626,118,037	192,304,809
(10, 1)	3	7,193,464,181	7,830,443,415	169,191,482
(6, 2)	11	82,295,388	310,578,842	105,335,191
(6, 1)	2	123,062	58,153,759	103,901,418
(9, 2)	2	1,185,279,686	1,403,650,638	97,468,106
(8, 1)	5	1,473,422,493	2,152,522,473	67,550,854
(9, 1)	1	224,062,807	788,537,782	42,512,267
(5, 2)	61	30,765,810	145,671,717	37,633,091
total	88	13,347,529,890	16,315,676,660	816,998,430
percentage of the total	2.21%	78.77%	70.17%	67.10%

on equity) provides information on the appreciation for deposits of the owners. The best would be only to consider taxed equity for calculation. In this case, however, all the equity was used. The indicator is considered as one of the key indicators of the company's success. The value is typically compared to profitability of other investment opportunities on the market. Weakness of the ROE comes from the fact that it does not take into account the risk of investment opportunities. Several values are visible in the figure. The best results are reported by clusters in another part of the Kohonen map. Specifically, Clusters (8, 10), (8, 8) and (8, 9) followed by Clusters (7, 10), (7, 8) and (7, 9). Conversely, the worst results are presented by Clusters (1, 8) and (2, 8). The most profitable Cluster (10, 2) achieved an ROE of 21.35%. Cluster (10, 1), the largest cluster in terms of the total assets, had an ROE about 4.65%. In terms of operating profit, the successful Cluster (6, 1) achieved an ROE outside of the present range, Cluster (6, 2) then had an ROE of 49%. The largest Cluster (4, 10) achieved an average ROE of -0.19%.

Return on assets (ROA) was analysed as the second ratio indicator (Figure 12).

The ROA as the indicator evaluates the ability of assets to make profit. The value of this indicator is based on the ratio of the two underlying parameters - namely assets and profit. Thus, the relatively small companies may achieve attractive results similar to large companies. The ROA indicator is fairly high for a number of clusters. Cluster (2, 9) is the most successful cluster. The value is about 234.1%. Conversely, the worst result was achieved by Cluster (2, 9). In this case, the cluster value is highly negative, specifically -206.5%.

4 Discussion of results

The aforementioned analyses clearly demonstrate that Clusters (10, 2), (10, 1), (6, 2), (6, 1), (9, 2), (8, 1), (9, 1) and (5, 2) are the most important for the transportation industry in terms of the total assets, fixed assets and profit-making. Clusters (10, 2) and (10, 1) are each formed only by three companies. Still, they dispose of the largest amount of assets and fixed assets as well as they achieve the highest profit from operations in the industry.

Note that the total of 3,989 companies were active in the Czech transportation industry in 2016. Considering all the analyses, one can conclude that industry leaders are the representatives of Clusters (10, 2), (10, 1), (6, 2), (6, 1), (9, 2), (8, 1), (9, 1) and (5, 2). Table 2 summarizes the most successful clusters.

The identified group of leaders in the transportation industry consists of 88 companies, out of which 61 are allocated to Cluster (5, 2), of the total of 3,989. Thus, it makes 2.21% of all the companies that were active in the industry during the reference period. Those 88 companies own 78.77% of all fixed assets allocated to transportation in the Czech Republic. At the same time, they own 70.17% of all the assets concentrated in the industry. A total of 67.10% of the profit from operations in the entire industry is generated by 88 companies.

5 Conclusions

The aim of this paper was to analyse transportation in the Czech Republic with Kohonen networks. The analysis was supposed to identify industry leaders.

The Kohonen networks were used for cluster analysis. There were 3,989 companies active in the transportation industry in 2016 and they were classified into 100 clusters (the Kohonen map was predefined using the mesh topology 10 x 10). All the clusters were analysed. Cluster (4, 10) was the largest one. Still, this cluster is not crucial for development of the transportation industry in the Czech Republic. On the contrary, the transportation industry is strongly influenced by companies of Clusters (10, 1) and (10, 2). Those clusters include only 6 companies. Nevertheless, their average values are highly above those of all the other companies active in the industry. In addition, their absolute indicators surmount all the other clusters. Still, there are other clusters, which have no small influence on development of the transportation industry in the Czech Republic, namely clusters (6, 2), (6, 1), (9, 2), (8, 1), (9, 1) and (5, 2). On overall, 88 companies can be referred to as leaders in the transportation industry although the importance of companies in Cluster (5, 2), which includes 61 companies can be looked at. The conclusion is that a relatively small group of companies have a major influence on development of transportation in the Czech Republic. If one should speculate, it can be said that this group has a great influence on development on the entire national economy. The reason lies in the nature of the transportation industry. The result implies that the future development of the entire transportation industry can be predicted based on results of 88 companies. The other companies, with a view to their number and partial low influence on development of the industry, provide a certain hotbed, which is not going to change a lot in the aggregated form. As a prediction tool, the analysis of 88 companies seems very positive. However, the negative fact is that fluctuations in production (no matter what is the cause) can result in fluctuations in the entire industry if not the entire national economy.

Further research should then focus on:

- Identifying whether the representation of companies in different clusters changes over time, in particular for clusters where leaders in the transportation industry come from (both the number and the form of specific companies - especially for Clusters (10, 1) and (10, 2).
- Verifying the ability to predict development of the transportation industry based on analysis of industry leaders.
- Identifying how potential fluctuations in economic results of the leaders have affected development of the transportation industry, in particular with accent on Clusters (10, 1) and (10, 2).

References

[1] HORAK, J., KRULICKY, T. Comparison of exponential time series alignment and time series alignment using artificial neural networks by example of prediction of future development of stock prices of a specific company. In: SHS Web of Conferences: Innovative Economic Symposium 2018 - Milestones and Trends of World Economy IES2018: proceedings [online]. Vol. 61. SHS Web of Conferences, 2019. eISSN 2261-2424. Available from: https://doi.org/10.1051/shsconf/20196101006

[2] VOCHOZKA, M. Formation of complex company evaluation method through neural networks based on the example of construction companies collection. *Ad Alta: Journal of Interdisciplinary Research*. 2018, **7**(2), p. 232-239. ISSN 2464-6733.

[3] MACHOVA, V., VOCHOZKA, M. Analysis of business companies based on artificial neural networks. In: SHS Web of Conferences: Innovative Economic Symposium 2018 - Milestones and Trends of World Economy IES2018: proceedings [online]. Vol. 61. SHS Web of Conferences, 2019. eISSN 2261-2424. Available from: https://doi.org/10.1051/shsconf/20196101013

[4] SVOBODOVA, H., VEZNIK, A., HOFMANN, E. *Vybrane kapitoly ze socioekonomicke geografie Ceske republiky / Selected chapters from socioeconomic geography of the Czech Republic* (in Czech). 1. ed. Brno: Masaryk University, 2013. ISBN 978-80-210-6229-0.

[5] KLIESTIK, T. Models of autoregression conditional heteroskedasticity GARCH and ARCH as a tool for modeling the volatility of financial time series. *Ekonomicko-manazerske spektrum*. 2013, **7**(1), p. 2-10. ISSN 1337-0839.

[6] PAO, H. A comparison of neural network and multiple regression analysis in modeling capital structure. *Expert Systems with Applications* [online]. 2008, **35**(3), p. 720-727. ISSN 0957-4174. Available from: https://doi.org/10.1016/j.eswa.2007.07.018

[7] HORAK, J., VOCHOZKA, M., MACHOVA, V. Evaluation of transport and forwarding companies by means neural networks. In: Proceedings of the Interdisciplinary Scientific International Conference for PhD Students and Assistants QUAERE 2018: proceedings. 2018. p. 377-385.

[8] SAYADI, A. R., TAVASSOLI, S. M. M., MONJEZI, M., REZAEI, M. Application of neural networks to predict net present value in mining projects. *Arabian Journal of Geosciences* [online]. 2012, **7**(3), p. 1067-1072. ISSN 1866-7511, eISSN 1866-7538. Available from: https://doi.org/10.1007/s12517-012-0750-z

[9] MACHOVA, V., ROWLAND, Z. Value generators of enterprises in the processing industry. In: Proceedings of the 6th International Conference Innovation Management, Entrepreneurship and Sustainability IMES2018: proceedings. 2018. ISBN 978-80-245-2274-6, p. 624-634.

[10] GRIGORYEVA, N. Y., ZHANGIROV, T. R., PERKOV, A. S., IVANOVA, S. A., LISS, A. A. Classifying neural networks and methods of their illogical behaviour revealing. *Journal of Physics: Conference Series* [online]. 2019, **1352**, 012024. ISSN 1742-6588. Available from: https://doi.org/10.1088/1742-6596/1352/1/012024

[11] VOCHOZKA, M., MACHOVA, V. Determination of value drivers for transport companies in the Czech Republic. *Nase More* [online]. 2018, **65**(4), p. 197-201. ISSN 1848-6320. Available from: https://doi.org/10.17818/NM/2018/4SI.6

[12] VOCHOZKA, M., SHENG, P. The application of artificial neural networks on the prediction of the future financial development of transport companies. *Communications - Scientific Letters of the University of Zilina* [online]. 2016, **18**(2), p. 62-67. ISSN 1335-4205, eISSN 2585-7878. Available from: http://komunikacie.uniza.sk/index.php/communications/article/view/331

[13] KONECNY, V., TRENZ, O., SVOBODOVA, E. Classification of companies with the assistance of self-learning neural networks. *Agricultural Economics - Zemedelska Ekonomika* [online]. 2010, **56**(2), p. 51-58. ISSN 0139-570X. Available from: https://doi.org/10.17221/60/2009-AGRICECON

[14] HAN, X., WANG, L. Stock company comprehensive assessment model based on Kohonen network. In: 2008 Second International Conference on Genetic and Evolutionary Computing: proceedings [online]. 2008. ISBN 978-0-7695-3334-6, p. 185-188. Available from: https://doi.org/10.1109/WGEC.2008.97

[15] KRULICKY, T. Using Kohonen networks in the analysis of transport companies in the Czech Republic. In: SHS Web of Conferences: Innovative Economic Symposium 2018 - Milestones and Trends of World Economy: proceedings [online]. 2019. ISBN 978-2-7598-9063-7. Available from: https://doi.org/10.1051/shsconf/20196101010

[16] SEVERIN, E. Self organizing maps in corporate finance: quantitative and qualitative analysis of debt and leasing. *Neurocomputing* [online]. 2010, **73**(10-12), p. 2061-2067. ISSN 0925-2312. Available from: https://doi.org/10.1016/j.neucom.2009.12.024

[17] CHEN, N., RIBEIRO, B., VIEIRA, A., CHEN, A. Clustering and visualization of bankruptcy trajectory using self-organizing map. *Expert Systems with Applications* [online]. 2013, **40**(1), p. 385-393. ISSN 0957-4174. Available from: https://doi.org/10.1016/j.eswa.2012.07.047

[18] LIN, W. Y., HU, Y. H., TSAI, C. F. Machine learning in financial crisis prediction: a survey. *IEEE Transactions on Systems, Man, and Cybernetics, Part C - Applications and Reviews* [online]. 2012, **42**(4), p. 421-436. ISSN 1094-6977. Available from: https://doi.org/10.1109/TSMCC.2011.2170420

[19] HITKA, M., LORINCOVA, S., LIZBETINOVA, L., PAJTINKOVA BARTAKOVA, G., MERKOVA, M. Cluster analysis used as the strategic advantage of human resource management in small and medium-sized enterprises in the wood-processing industry. *BioResources* [online]. 2017, **12**(4), p. 7884-7897. Available from: https://doi.org/10.15376/biores.12.4.7884-7897

[20] VRBKA, J., ROWLAND, Z. Stock price development forecasting using neural networks. In: SHS Web of Conferences: Innovative Economic Symposium 2017 - Strategic Partnerships in International Trade: proceedings [online]. Vol. 39. 2017. Available from: https://doi.org/10.1051/shsconf/20173901032

[21] LEHUTOVA, K., KRIZANOVA, A., KLIESTIK, T. Quantification of equity and debt capital costs in the specific conditions of transport enterprises. In: 17th International Conference on Transport Means: proceedings. 2013. ISSN 1822-296X, p. 258-261.

[22] KAMPF, R., LORINCOVA, S., HITKA, M., STOPKA, O. Generational differences in the perception of corporate culture in European transport enterprises. *Sustainability* [online]. 2017, **9**(9), p. 1-14. ISSN 2071-1050. Available from: https://www.mdpi.com/2071-1050/9/9/1561

[23] HRASKOVA, D., BARTOSOVA, V. Emergent approach to management of the transport company. In: 2nd International Conference on Social Sciences Research: proceedings. 2014. ISBN 978-967-11768-7-0, p. 92-96.

[24] OU, X., YAN, X., ZHANG, X., LIU, Z. Life-cycle analysis on energy consumption and GHG emission intensities of alternative vehicle fuels in China. *Applied Energy* [online]. 2012, **90**(1), p. 218-224. ISSN 0306-2619. Available from: https://doi.org/10.1016/j.apenergy.2011.03.032

[25] VOCHOZKA, M., ROWLAND, Z., VRBKA, J. Financial analysis of an average transport company in the Czech Republic. *Nase More* [online]. 2016, **63**(3), p. 227-236. ISSN 0469-6255. Available from: https://doi.org/10.17818/NM/2016/SI28

[26] SEROKA-STOLKA, O., TOMSKI, P., PABIAN, A. Environmental strategies in the management of transport. In: 4th International Conference on Advanced Logistics and Transport ICALT 2015: proceedings. 2015. ISBN 978-1-4799-8400-8, p. 122-127.

[27] WOHE, G., KISLINGEROVA, E. *Uvod do podnikoveho hospodarstvi / Introduction to business economy* (in Czech). 2. ed. Prague: C. H. Beck, 2007. ISBN 978-80-7179-897-2.

MODELLING OF THE TRAFFIC FLOW BASIC CHARACTERISTICS AT THE ROAD NETWORK SELECTED SECTION

Alica Kalašová*, Simona Skřivánek Kubíková, Veronika Harantová

Department of Road and Urban Transport, Faculty of Operation and Economics of Transport and Communications, University of Zilina, Zilina, Slovakia

*E-mail of corresponding author: alica.kalasova@fpedas.uniza.sk

Resume

Elimination of connection between an increase in transport and economic growth has been the main aim of the transport policy of the EU for a few years and it has not been accomplished yet. Transportation causes considerable external costs that have concrete originators but are not paid by them. The biggest external costs are connected with emissions, noise, accidents and congestions. In this contribution, the problem of congestions, which currently bother drivers in EU was analysed, together with possibilities for their solving, since the congestions' reduction is one of the priorities of the EU's transport policy. The task was to observe a relation between the basic traffic flow characteristics on the specific section of the road no. I/65 and to identify effects on traffic in general, as well as to specify reasons and conditions within the traffic congestions that occurred. These results are a basis for the theoretical proposal of possible solutions of the issue.

Article info

Received 9 April 2020
Accepted 19 June 2020
Online 3 November 2020

Keywords:

road safety,
external costs,
congestions,
traffic flow

Available online: https://doi.org/10.26552/com.C.2021.1.A44-A53

ISSN 1335-4205 (print version)
ISSN 2585-7878 (online version)

1 Introduction

Reduction of external costs is one of the most significant factors affecting increase in the road transport safety. External costs are described as follows. When consumers decide to purchase an item or take a trip, they examine the price of a given option and compare it to the gain or satisfaction they expect. For example, a person who wants to get from place A to place B will consider the price (of using public transport or his/her private car) and quality of the service provided before choosing the suitable transport mode. Users are willing to accommodate a whole array of parameters (speed, frequent/regular service, quality, flexibility, etc.) in the price of transportation that users pay. Consumers of goods or services do not generally foot the full bill for the costs that their decision imposes on society and the environment. These costs are defined as external because they are not reflected in the price paid by users. The main sources of external costs in the transport sector are accidents, congestions, air pollution, noise and climate changes [1-2]. This paper is focused on the congestions that are probably the most negative phenomenon that drivers perceive while driving. The main aim was to try to specify the connections between traffic flow characteristics and why congestions occur. It was decided to observe the traffic characteristics' relationships at the selected section of the road no. I/65. The first part of the paper includes some theoretical knowledge about the traffic flow theory. The next part includes a description of the selected road section, methodology and results of transport survey using the Sierzega microwave radar. Based on those findings, the last part consists of discussion and formulated conclusions.

2 Literature preview

Since the 1960s of 20th century, the generalized relationships between speed, density and the flow rate are defined with the following parameters [3]:

Flow Rate (intensity) - number of vehicles per hour, which pass over a given point or section of a lane or roadway during a given time interval of less than one hour.

Speed - defined as a rate of motion expressed as a distance per unit of time, generally as kilometre per hour (km/h). In characterizing the speed of a traffic flow, a representative value must be used, because a broad distribution of individual speeds is observable in the traffic flow.

Density - the number of vehicles occupying a given length of a lane or roadway at a particular instant. Density is usually expressed as vehicles per kilometre (veh/km).

While diagrams in Figure 1 show continuous curves, in reality there are likely discontinuities, with part of these curves not present. The curves illustrate the following significant points:

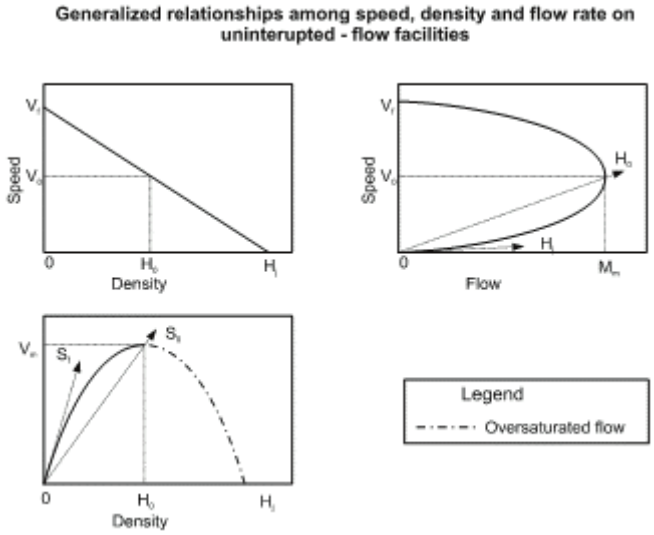

Figure 1 *Basic relationships between the traffic flow characteristics [3]*

A zero flow rate occurs under two different conditions. One is when there are no vehicles on the facility - density is zero and a flow rate is zero. The second is when density becomes so high that all the vehicles must stop - the speed is zero and the flow rate is zero, because there is no movement and vehicles cannot pass a point on the roadway.

Between these two extreme points, dynamics of the traffic flow produces a maximizing effect. As flow increases from zero, density also increases, since more vehicles are on the roadway. When this happens, speed declines because of the interaction of vehicles. This decline is negligible at low and medium densities and flow rates. As the density increases, these generalized curves suggest that speed decreases significantly just before a capacity of the road is reached. The capacity is defined as the product of density and speed resulting in the maximum flow rate. This conditions are shown as optimum speed V_o (often called critical speed), optimum density M_o (sometimes referred to as critical density) and maximum flow V_m.

In accordance with NI [4], the traffic demand is not constant. It can vary significantly depending on the season of the year, the day of the week and even the time of the day. In addition, the capacity is not constant - it can change (sometimes rapidly) because of weather, work zones, traffic incidents, or other events. It is not necessarily simple, either. The physical fact of finiteness and the principle of conservation underlie the traffic stream behaviour. However, the actual performance of a particular section of a freeway, at a particular point in time, is more ambiguous, resulting from variations in individual human behaviour and the mix of vehicle types using the facility. According to KESSELS [5], it may be possible to predict the average behaviour and average capacity and the variances about these averages for a traffic flow, but never the precise behaviour.

The principles of macroscopic models are relations between the essential characteristics of a traffic flow - intensity, density (quantitative characteristics) and speed (a qualitative characteristics). For a complete description, only two of these characteristics are sufficient, the third one can be calculated according to an equation of continuity [6-7]:

$$M = H.V \text{ [veh/h]}, \quad (1)$$

where:
M - intensity [veh/h],
V - speed [km/h],
H - density [veh/km].

The theory of traffic flow recognizes two types of movements:

- movements of one vehicle,
- movements of a group of vehicles in the same driving lane.

A movement of vehicles within a different driving lanes layout

Vehicles change their position during the driving in a certain direction, depending on width conditions, density, speed etc. Different modes of vehicles' behaviour in the traffic flow can be derived from these conditions:

- stream driving in a single lane in a row (overtaking is not possible),
- driving where overtaking is possible (without any issues on the unidirectional two - lane belt, sufficient space in opposite direction on the two - lane belt),
- changing driving lanes on multiple-lanes belt (it is possible in several driving lanes, overtaking in the right lane is dangerous),
- vehicles movements on the two or four lane bi-directional belt (it gives an option of various movement conjunctions; traffic flow imbalance could create danger) [4-5, 8].

Driving of vehicles in a stream

While driving, the situation of vehicles' movements changes (a number of vehicles, speed, structure of traffic flow, weather, etc.). A stream of vehicles is made up of two or more vehicles driving behind each other in the same

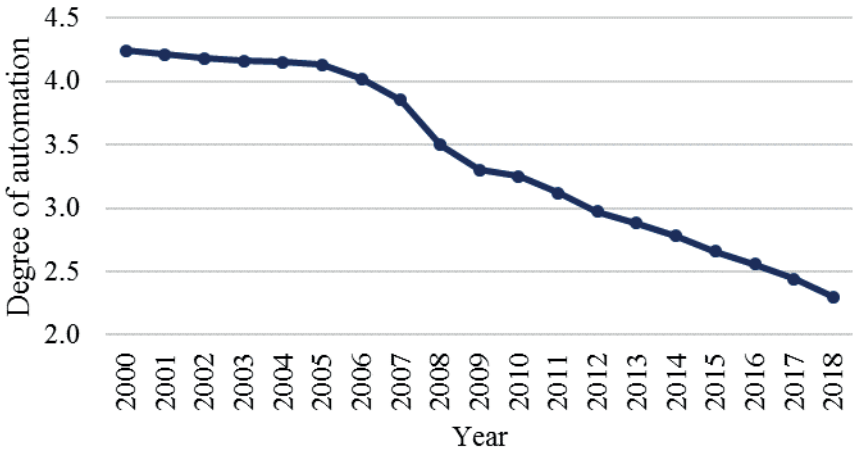

Figure 2 Development of the degree of automation in Slovakia (based on data from the Statistical Office of the SR) [16]

driving lane. Driving is disturbed and has its own specifics, it is different in non - urban areas and in urban areas. It is possible to determine:

- a number of vehicles in a stream - speed of the stream, defined as an average travel speed determined from speed of each vehicle in a stream,
- time consuming of a stream, defined as a difference in passage time of the first and the last vehicle of a stream in the chosen road profile,
- a physical length of a stream, defined as a distance among the first and the last vehicle at the same moment,
- a stream dispersion expressed as a relative change in time and length dimensions of a stream, which is related to a particular profile of a road communication or time point [3, 9-10].

3 Methods and materials

Currently, the road network of 38 985 km of length is used in the Slovak Republic [11]. Regarding increasing intensities mainly on highways and I class roads, the character of traffic departs from the free traffic flow and the proportion of traffic increases with the degree of load, which is approaching value of 1. In this case, individual vehicles affect each other in the traffic flow. In the Slovak republic, in 2018 the number of registered vehicles increased by 4.16% compare to 2017 and reached the value of more than 3.2 million. The increase of individual automobiles (IA) was 4.24% and exceeded 2.3 million [12-13], which represents a degree of automation of 2.34, see Figure 2.

Time losses resulting from congestions are a significant negative effect of overloaded roads, which affect the economic activity of inhabitants indirectly. While in 2000, there was one individual car per 4 inhabitants, in 2018 it was already one IA (individual automobile) per 2.3 inhabitants. One of the significant parameters, which have an impact on individual automobile transportation increase, is rising of the living standard of population and increasing demands on the expected quality of transport [14-15].

The situation in freight transport does not contribute to improving the overall situation either. While the importance of transport modes, suitable for transport of large volumes of goods, without undue burden on infrastructure and the environment, is decreasing or is totally negligible in the total transport volume, transport performances of the road freight transport are rising steeply. Figure 3 presents development of the modal split of the freight transport in Slovakia [14, 17].

Taking into account all of these mentioned issues, it is very important to know and understand theory of the traffic flow and be able to predict under what conditions do congestions occur.

3.1 Methods of traffic flow monitoring using Sierzega microwave radars

The microwave radar Sierzega was used since the idea was to measure the basic traffic flow characteristics.

Radars have recorded vehicles' passage in real time, speed, length and direction of vehicles (this value is recorded only when bidirectional measurement is turned on but it is very inaccurate at higher intensities). The most accurate results are obtained for a single lane road communications. For the multiple lane communications, accuracy declines as traffic flow increases because of the vehicles overlapping. The main reason of this accuracy decline is an implementation of the radar low above the road (see Figure 4), as well as the measurement is running under the angle of 30° and any deviation reduces accuracy, e.g. determination of a vehicle length. Measurement accuracy deviations are according to the manufacturer: speed ± 3%, length of vehicle ± 20%, space between vehicles ± 0.2 s. Another disadvantage is the range of a measurement. A manufacturer declares the range of measurement from 8 to 254 km/h. However, at lower speeds there is a large measurement deviation in the number of recorded vehicles.

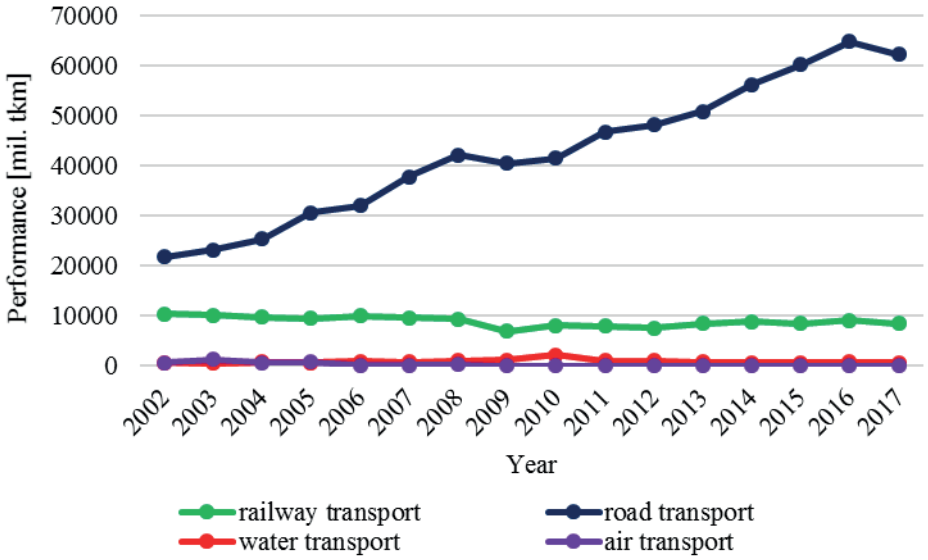

Figure 3 Modal split of freight transport in Slovakia (based on data from the Statistical Office of the SR), [16]

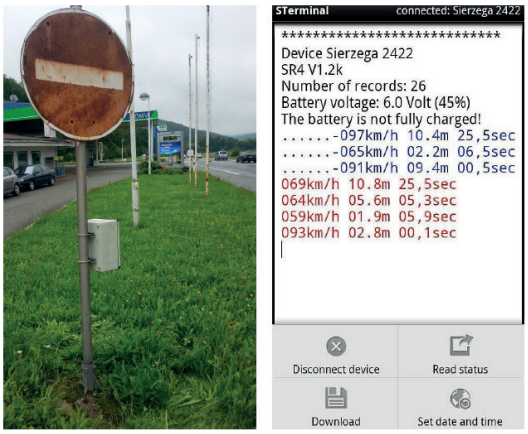

Figure 4 *Radar Sierzega, on the left - hand: implementation of the radar on the traffic sign; on the right - hand: the example of reached data from radar [18]*

An advantage of this device is its mobility, due to small dimensions 400/400/200 mm and a big range of operating temperatures from -20 °C to 60 °C [18-19].

3.2 An analysis of the selected section of road communication

The basis of a research are the transport surveys and their detail analysis, where the data obtained from the radar Sierzega were used, specifically vehicles intensity and travel speed. The vehicles density was calculated using the equation of continuity (1). The main objective of this research was to better understand the behaviour of a traffic flow as well as the relations between vehicles [19-20].

The measurement was carried out on Tuesday, 17th of September 2019 in cadastral city of Martin on the I class road I/65, see Figure 5. The transport survey took 12 hours, from 6 a.m. to 6 p.m. The maximum permitted speed on the chosen section is 50 km/h.

During the measurement, the intensity reached 13 505 vehicles per 12 hours, in both directions. The highest value of the intensity 326 vehicles per 15 minutes, was recorded from 6:30 a.m. to 6:45 a.m. and the peak hour of 1248 vehicles per hour was recorded from 6:30 a.m. to 7:30 a.m. The structure of the traffic flow, according to obtained data, is as follows:

76.3% IA (individual automobile), 10.5% T (Truck), 12.5% HT (Heavy Truck), 0.37% M (Motorcycle), 0.25% Bus and 0.07% B (bicycle).

This is the case of the inhomogeneous traffic flow, because it is predicted that for the homogenous traffic flow a minimum of 80% of vehicles, which have similar properties, is needed (e.g. individual automobiles). The data were divided in accordance with the driving lanes and then speeds and intensities of all the modes of transport were generated. Subsequently, the vehicle densities were determined. Based on that, the following diagrams were created, see Figure 6. [22]

Figure 5 *The chosen section of road I/65 (based on use of the Openstreet maps) [21]*

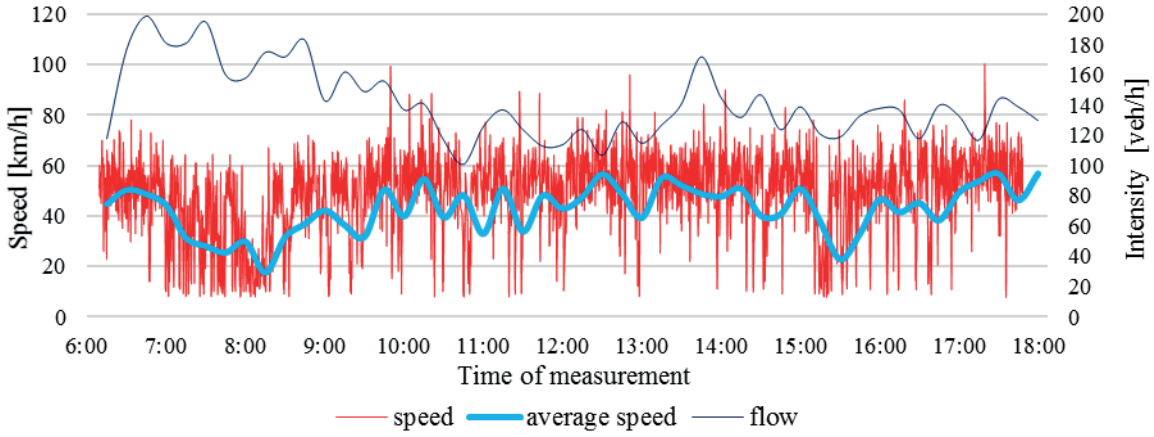

Figure 6 *Running of real vehicles speed and an average vehicles speed during the 15 minutes intervals in the traffic flow - measurement on the lane A*

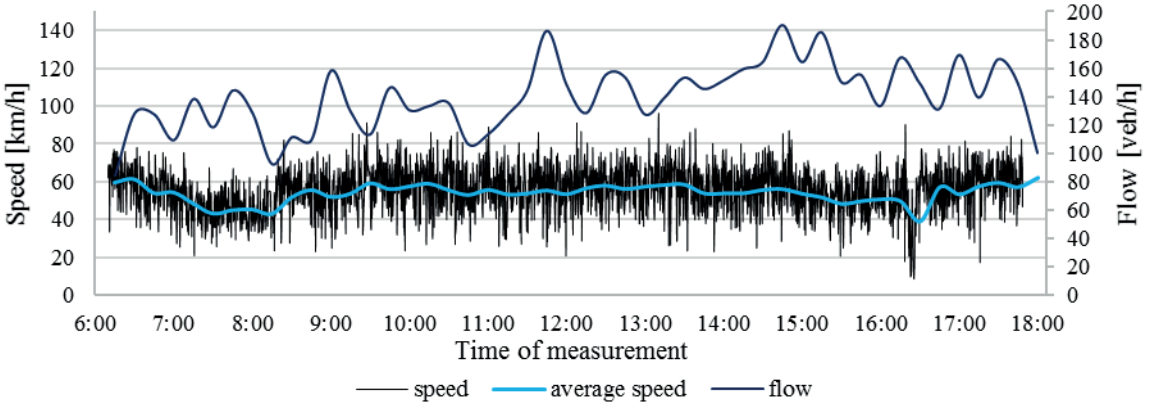

Figure 7 *Running of real vehicles speed and an averaged vehicle speed during the 15 minutes intervals in the traffic flow - measurement on the lane B*

Figure 6 shows that the decrease of vehicles speed was recorded on driving lane A twice approximately at 8 a.m. and in the afternoon at 3 p.m. The highest intensity was recorded at 6:45 a.m. and it gradually declined and then slightly increased again at 1:45 p.m. An average vehicle speed reached value of 54 km/h during the measurement.

The velocity curve on the second lane in the opposite direction, Figure 7, has the lower velocity dispersion than in the first case. However, it can be seen that most vehicles exceeded the speed limit. In this case, the intensity sharply varies. The lowest value was recorded at 8:15 a.m. and, on the other side, the highest value intensity was recorded at 2:45 p.m. An average speed of vehicles reached 42 km/h.

Figure 8 shows the intensity, speed and average speed for both driving lanes. The intensity for both directions first raised sharply and then oscillated around 300 vehicles per hour. The decline occurred at 10:45 a.m., but then the intensity value began to increase and exceeded again

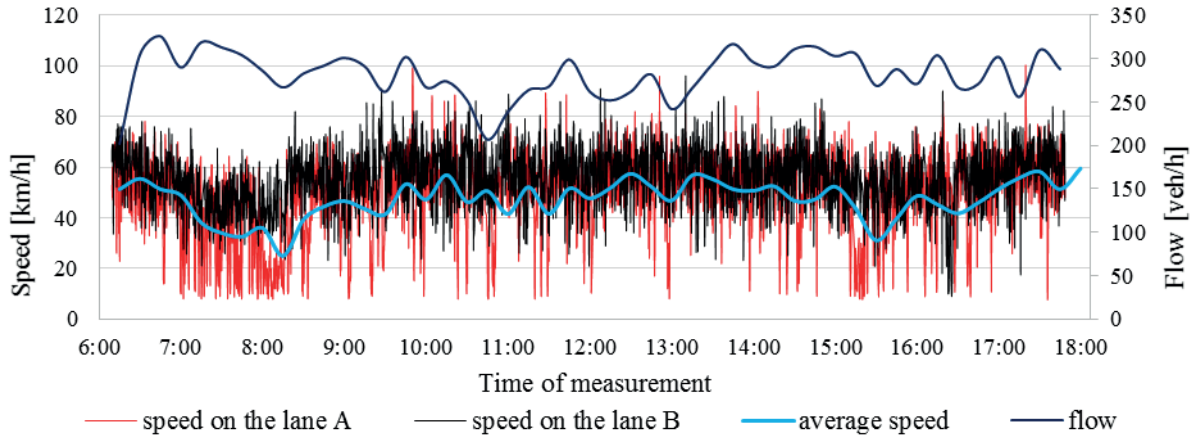

Figure 8 *Running of real vehicles speed and an average vehicle speed during the 15 minutes intervals in the traffic flow - measurement on both lanes*

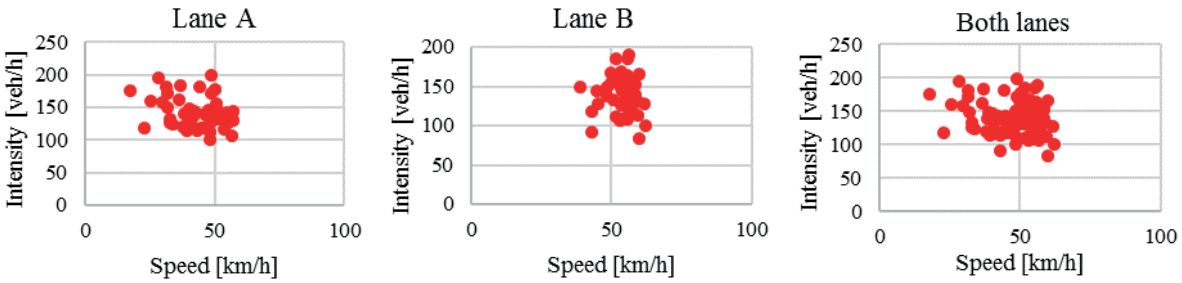

Figure 9 *Graphical dependence between the traffic flow intensity and speed*

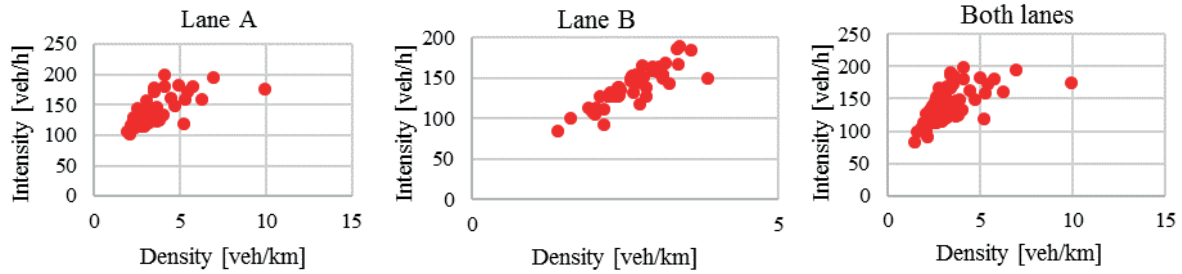

Figure 10 *Graphical dependence between the traffic flow intensity and density*

value of 300 vehicles per hour. The average speed on the monitored section during the measurement reached 45 km/h.

The dependence should create a parabola according to basic relation (Figure 1). However, with increasing speed the intensity should also increase, which represents a linear course. From several points of view, it is obvious that each intersection or communication has maximum capacity. If this capacity were exceeded, intensity should still rise and a speed is decreasing, see Figure 9. The maximum capacity was reached at the optimum speed and due to declining speed intensity it starts to decrease and leads to reducing the gaps between vehicles and increasing density.

Therefore, the relation between intensity and speed is expressed as a parabola. The same rule applies also for intensity - density relation (Figure10).

Correlation coefficient between parameters, shown in Figure 10, also refuted the linear dependence. The value of this coefficient was in range of - 0.299 to - 0.037, which corresponds to very weak linear dependence. However, an interesting thing is that dependence between the intensity and density (Figure 10) became a linear dependence with a high correlation coefficient of 0.653 and 0.859, which is the middle and strong correlation.

The dependence between speed and density has, on the other hand, an exponential running with a confidential level of almost 80% (Figure 11). In principle, if vehicles speed would decrease, the density at the chosen monitored road section would rise and vice versa.

Figure 12 presents dependence of the basic characteristics during each hour of measurement. Between the speed and density, a linear course is very noticeable; if one quantity decreases the other increases and vice versa. The intensity also corresponds to this fact. When the speed decreases, the intensity of vehicles is also decreasing and vice versa.

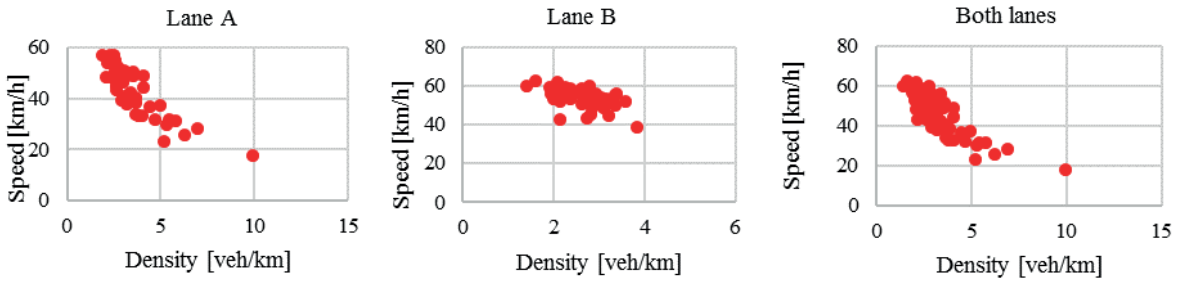

Figure 11 *Graphical dependence between the speed and the traffic flow density*

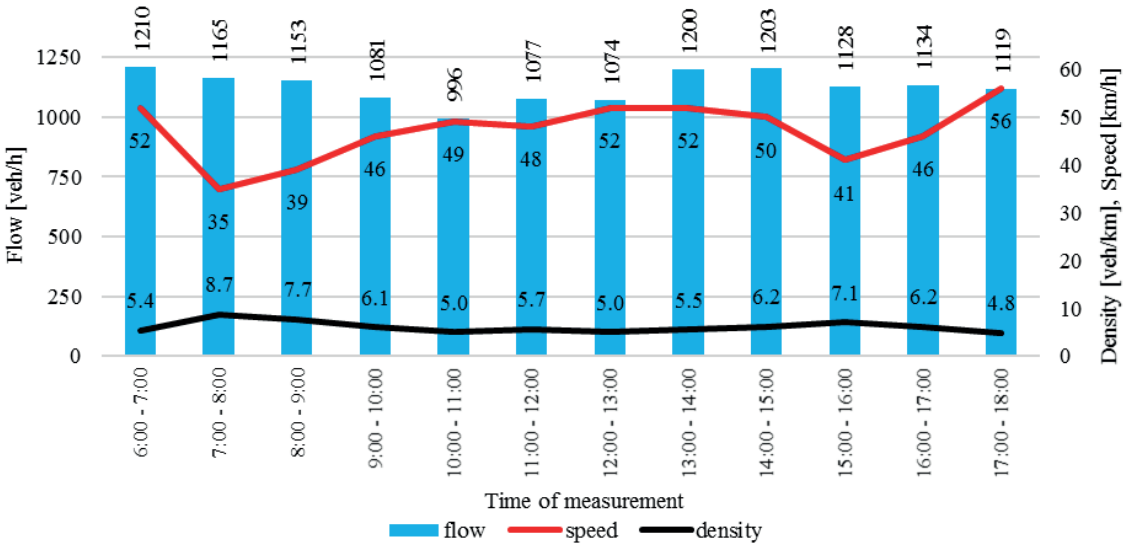

Figure 12 *Running of the basic traffic flow characteristics related to one-hour gap intervals*

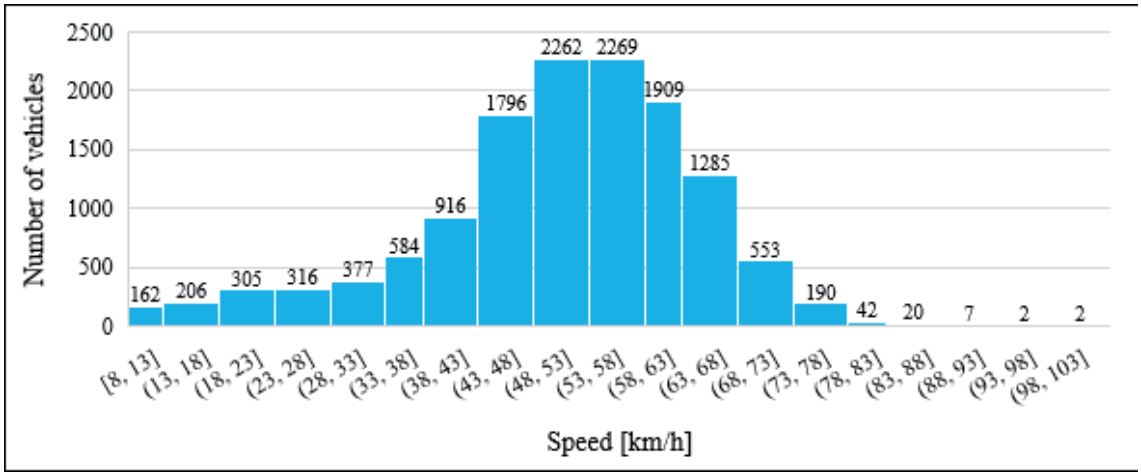

Figure 13 *Division of vehicles' speeds according to their frequency*

The correlation coefficient was calculated also for the speed/ density relation. In this case, the correlation coefficient of dependence between the two parameters is -0.963, which represents a very strong negative correlation.

3.3 Histograms of observing variables

Histogram is a graphical representation of data distribution using the column graph, with columns of the same width, which represents the width of intervals, while the height of column shows a frequency of a monitored variable in the given interval. It is important to choose the suitable width for an interval, because the incorrect width can decrease information value of a histogram.

The range of one class is 5 km/h and there are 20 different classes. Figure 13 shows that the lowest recorded speed of vehicles was 8 km/h and the highest one was 103 km/h. The range of recorded speeds is 95 km/h. These data on speed are generated by the radar, which was used for

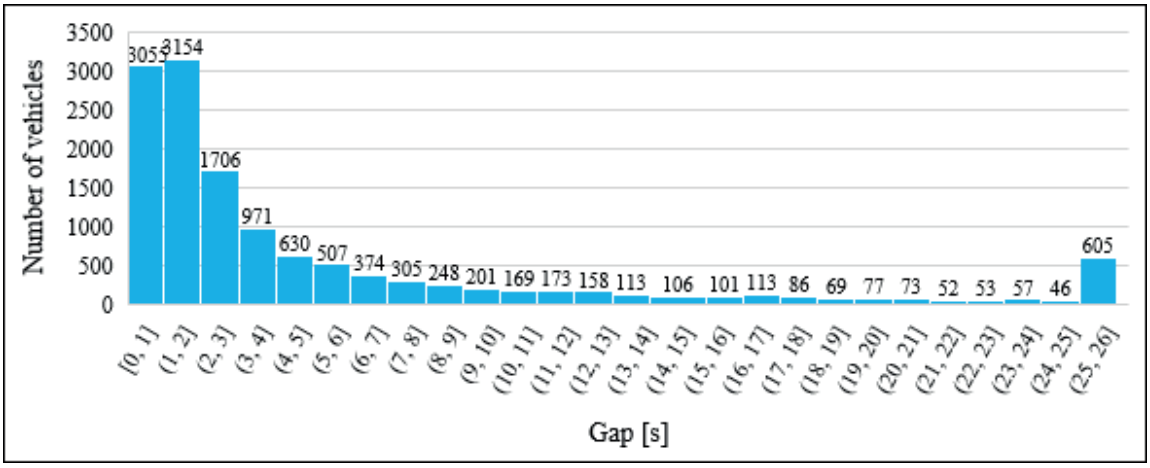

Figure 14 *Division of time gaps to 26 classes with range of one class of 1 sec]*

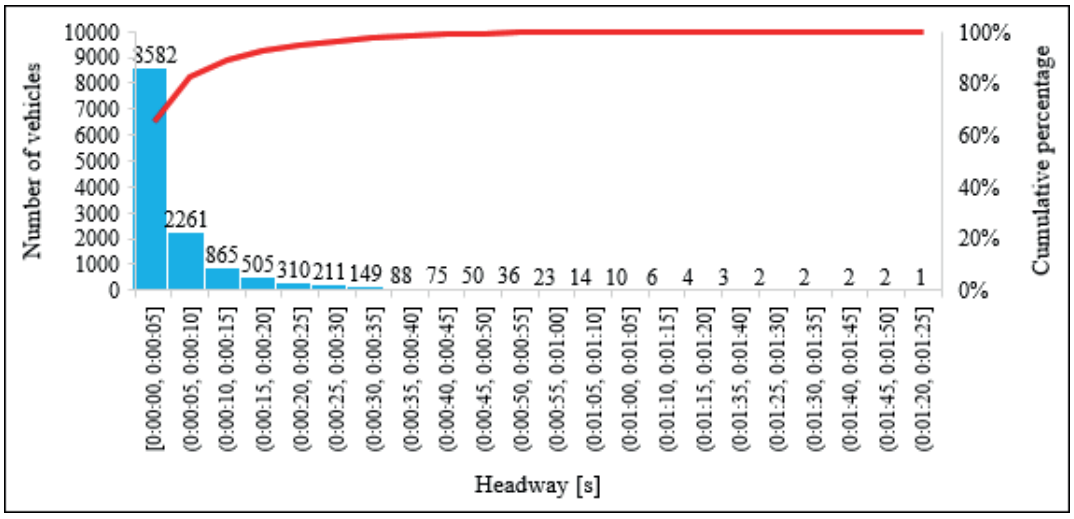

Figure 15 *Division of headways into 5 sec intervals*

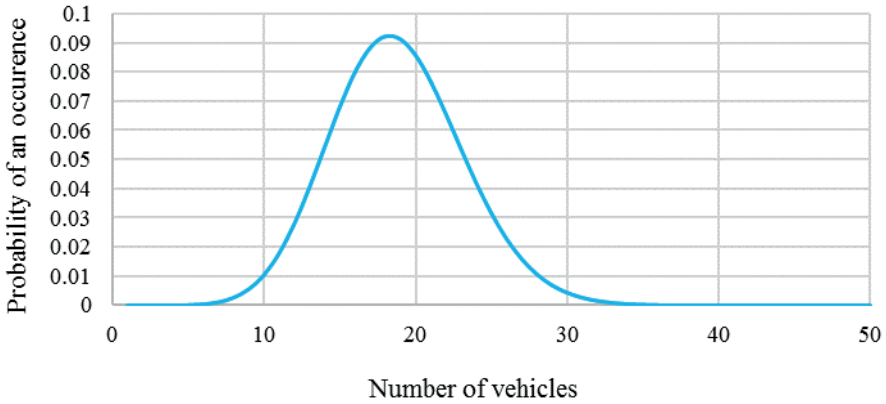

Figure 16 *Probability of vehicles' occurrence during one minute of measurement*

this measurement. In the speed class of 53-58 km/h, was obtained the highest number of vehicles. Considering that the maximum speed at this section of road is 50 km/h, more than 58% of vehicles exceeded the permitted speed. The speed median of 53 km/h reached value, which was for 8 km/h higher than the average one. The most often recorded value of speed was 55 km/h, also called as modus. This probability distribution of speed is called the normal or Gaussian distribution and it is one of the most important probability distributions of continuous stochastic variables [10, 23-25].

Time gaps between vehicles were divided into 26 classes with range of one class of 1s. The most often, gaps between vehicles were 1 and 2 seconds, subsequently

their value decreased (Figure 14). The probability of unpredictable events occurrence, which affect time gaps between vehicles, has an exponential distribution. The next histogram of time lapses between vehicles (Figure 15) has the similar running, i.e. an exponential distribution.

Time lapses were divided to classes from 0 s to 85 s, with class range of 5 s and the number of classes of 22. The graphical representation in Figure 15 is called the Pareto diagram, which is a combination of histogram and line diagram. The line represents a cumulative multiplicity and gradually increases to 100%. The most frequent time lapse was 5 s, which was reached by 8582 vehicles. Approximately 50 vehicles had time lapse of more than a minute. The reason for this could be that vehicles have come in groups.

Figure 16 shows the graphical representation of the number of vehicles per minute, based on the Poisson distribution. According to statistics, that is a discrete probability distribution of occurrence of rare events in a series of a large number of independent experiments.

Based on the survey, there were recorded 18.8 vehicles per minute in average. Thus, the highest probability is that 18.8 vehicles per minute would pass the monitored road section in both directions (λ) and, as the number of vehicles would increase or decrease, this probability decreases.

4 Discussion

As the number of automobile transport increases, density increases and speed of the traffic flow decreases. This fact has the effect on increase of the delay time, travel time and stop time. Mentioned characteristics of the traffic flow vary considerably, depending on time and volume of traffic, often reaching the maximum values. Intersections are the important points of the road network permeability.

Evaluation of transport survey revealed that the highest number of vehicles was recorded from 6:30 to 6:45 a.m., at intensity of 326 vehicles. The average intensity, according to survey results is 1200 vehicles per hour and according to simulation it is 1035 vehicles. The strongest correlation was observed in relationship of density and speed of value of - 0.95, which represents a strong linear dependence. Results of relations between the basic characteristics showed that the traffic flow variables do not always behave according predefined relations. The basic theory behind the interaction is that congestion leads to higher vehicle densities (i.e., more closely spaced vehicles on a roadway), which provides more opportunities for a conflict. Congestion also reduces vehicle speeds. When vehicles are engaged in a crash, the collision forces are lower because of the lower speed and the negative consequences of an accident could be reduced for a driver, as well as for passengers. Another aspect of the model is the concept of "secondary" accidents - accidents that occur due to conditions produced by an existing crash. Some of those conditions - which would not exist without occurrence of the primary accident - include the rapid backward queue formation (as vehicles suddenly stop to avoid the primary accident), rubbernecking by drivers and manoeuvres of emergency vehicles. The details of the relationship between congestion and safety are not well understood.

5 Conclusion

- Based on the limited work that has been performed, a few tentative conclusions may be drawn:
- An accident occurrence probably increases as congestion increases.
- There is a lower proportion of single vehicle crashes (e.g., run-off-road, rollover, collision with fixed object) during the congestions, on the other side, there is a higher proportion of multiple vehicle accidents.
- Accident severities (extent and nature of personal injuries) are lower during the congestion, due to the lower vehicle speeds at the moment of crash impact.

In general, it can be assumed that any operational improvement that reduces congestion would lead to fewer accidents but the consequences of accidents could be harder related to the greater proportion of single vehicle crashes. Knowing these facts can target mitigation strategies to single vehicle crashes and higher severities - such as wider roadside recovery zones, protection on highways and coordination with emergency medical services. Moreover, an operations philosophy must take a systems-oriented view, where the consequences of a specific action must consider the related impacts, such as safety.

Acknowledgment

This contribution is made within project VEGA 1/0436/18 Externalities in road transport, an origin, causes and economic impacts of transport measures.

This contribution is the result of the project implementation: Centre of excellence for systems and services of intelligent transport II, ITMS 26220120050 supported by the Research & Development Operational Programme funded by the ERDF.

References

[1] SCHREYER, CH., SCHNEIDER, CH., MAIBACH, M., ROTHENGATTER, W., DOOL, C., SCHMEDDING, D. *External costs of transport*. Update study, Paris: International Railway Union, 2004. ISBN 2-7461-0891-7.

[2] SYNAK, F., CULIK, K., RIEVAJ, V., GANA, J. Liquefied petroleum gas as an alternative fuel. *Transportation Research Procedia* [online]. 2019, **40**, p. 527-534. ISSN 2352-1465. Available from: https://doi.org/10.1016/j.trpro.2019.07.076

[3] KUHNE, R. Foundations of traffic flow theory I: Greenshields' Legacy - highway traffic. In: Symposium on the Fundamental Diagram: 75 Years - Greenshields 75 Symposium: invited presentations. Massachusetts, United States: Committee on Traffic Flow Theory and Characteristics, 2008.

[4] NI, D. *Traffic flow theory: characteristics, experimental methods and numerical techniques*. 1. ed. Elsevier, 2015. ISBN 978-0128041345, eISBN 9780128041475.

[5] KESSELS, F. *Traffic flow modelling: introduction to traffic flow theory through a genealogy of models* [online]. Berlin Heidelberg: Springer-Verlag, 2019. ISBN 978-3-319-78694-0, eISBN 978-3-319-78695-7. Available from: https://doi.org/10.1007/978-3-319-78695-7

[6] KALASOVA, A., STACHO, M. Decrease in congestions is one of the most important factors for increase in safety in road transport. In: Modern Safety Technologies in Transportation: proceedings. 2005. ISBN 80-969106-1-2.

[7] KALASOVA, A., FAITH, P., PALO. J. *Transportation Engineering I / Dopravne inzinierstvo I* (in Slovak). Zilina: University of Zilina, 2006. ISBN 80-8070-634-4.

[8] LEUTZBACH, W. *Introduction to the theory of traffic flow* [online]. Berlin Heidelberg: Springer-Verlag, 1988. ISBN 978-3-642-64805-2, eISBN 978-3-642-61353-1. Available from: https://doi.org/10.1007/978-3-642-61353-1

[9] TREIBER, M., KESTING, A. *Traffic flow dynamics* [online]. Berlin Heidelberg: Springer-Verlag, 2013. ISBN 978-3-642-32459-8, eISBN 978-3-642-32460-4. Available from: https://doi.org/10.1007/978-3-642-32460-4

[10] Relations between the basic characteristics of the traffic flow / Vztahy zakladnich charakteristik dopravniho proudu (in Czech) [online] [accessed 2020-02-02]. Available from: http://kds.vsb.cz/krivda/www-di(vb3-dos)/02-dopr-proud.pdf

[11] List of countries by road network size - Wikipedia [online] [accessed 2020-02-23]. Available from: https://en.wikipedia.org/wiki/List_of_countries_by_road_network_size

[12] CULIK, K., KALASOVA, A., KUBIKOVA, S. Simulation as an instrument for research of driver-vehicle interaction. *MATEC Web of Conferences* [online]. 2017, **134**, 00008 [accessed 2020-02-03]. eISSN 2261-236X. Available from: https://doi.org/10.1051/matecconf/201713400008

[13] ITE (Institute of Transportation Engineers), WOLSHON, B., PANDE, A. *Traffic engineering handbook*. 7. ed. Wiley Network, 2016. ISBN 978-1-118-76230-1.

[14] Transport Yearbook 2018 / Rocenka dopravy 2018 (in Czech) [online] [accessed 2020-02-03]. Available from: https://www.sydos.cz/cs/rocenka-2018/rocenka/htm_cz/cz18_321000.html

[15] Strategic plan for transport development in the Slovak republic until 2030 / Strategicky plan rozvoja dopravy SR do roku 2030 - Ministry of Transport and Construction of the Slovak Republic (in Slovak) [online] [accessed 2020-01-13]. Available from: https://www.mindop.sk/ministerstvo-1/doprava-3/strategia/strategicky-plan-rozvoja-dopravy-sr-do-roku-2030

[16] Statistical Office of the Slovak Republic [online] [accessed 2020-02-08]. Available from: https://slovak.statistics.sk/

[17] POLIAK, M. The relationship with reasonable profit and risk in public passenger transport in the Slovakia. *Ekonomicky Casopis*. 2016, **61**(2), p. 206-220. ISSN 0013-3035.

[18] Sierzega radar [online] [accessed 2020-02-12]. Available from: https://www.sierzega.com/en-us/home

[19] BARCELO, J., CODINA, E., CASAS, J., FERRER, J. L., GARCIA, D. Microscopic traffic simulation: a tool for the design, analysis and evaluation of intelligent transport systems. *Journal of Intelligent and Robotic Systems* [online]. 2005, **41**(2), p. 173-203. ISSN 0921-0296. Available from: https://doi.org/10.1007/s10846-005-3808-2

[20] KRBALEK, M. Equilibrium distributions in a thermodynamical traffic gas. *Journal of Physics A: Mathematical and Theoretical* [online]. 2007, **40**, p. 5813-5821. ISSN 1751-8113, eISSN 1751-8121. Available from: https://doi.org/10.1088/1751-8113/40/22/004

[21] Open Street Maps [online] [accessed 2020-02-01]. Available from: https://www.openstreetmap.org/#map=15/49.0588/18.9322

[22] TSS - Transport Simulation Systems. Microsimulator and Mesosimulator Aimsun 8.1 User's manual.

[23] Total number of registered cars - Car sales statistics [online] [accessed 2020-02-05]. Available from: https://www.best-selling-cars.com/germany/2018-germany-total-number-registered-cars

[24] ONDRUS, J., KOLLA, E. The impact of ABS system on the braking characteristics of the specified motorcycle on the dry road surface. *IOP Conference Series: Materials Science and Engineering* [online]. 2018, **421**(2), p. 1-11 [accessed 2020-01-19]. ISSN 1757-8981, eISSN 1757-899X. Available from: https://doi.org/10.1088/1757-899X/421/2/022024

[25] ONDRUS, J., CERNICKY, L. Usage of Polcam device for parameter monitoring and traffic flow modelling. *Communications: Scientific Letters of the University of Zilina* [online]. 2016, **18**(2), p. 118-123. ISSN 1335-4205, eISSN 2585-7878. Available from: http://komunikacie.uniza.sk/index.php/communications/article/view/342

CONSOLIDATION OF CARGOS IN THE ROAD TRANSPORT AS A KEY METHOD TO SUCCESS

Zbigniew Łukasik[1], Aldona Kuśmińska-Fijałkowska[1,*], Jacek Kozyra[1], Sylwia Olszańska[2]

[1]Faculty of Transport, Electrical Engineering and Computer Science, Kazimierz Pulaski University of Technology and Humanities in Radom, Radom, Poland
[2]Chair of Logistics and Process Engineering, University of Information Technology and Management in Rzeszow, Rzeszow, Poland

*E-mail of corresponding author: a.kusminska@uthrad.pl

Resume
The problem of consolidation of goods for the provider of logistic services, which is a third part that delivers goods from many suppliers to one business client in time horizon was analysed in this article. Every parcel has a fixed date of reception in the source and delivery schedule in a destination. In the age of highly developed economy, time pressure and costs, outsourcing is a condition necessary to improve the functioning of enterprises. New logistic chains, networks of terminals and intermodal connections are built every year to reduce the transport costs and improve the whole process. In this article, the authors presented the benefits resulting from consolidation of cargos in the road transport. Special emphasis was put on determination of the role of the transport costs reduction using the cargo consolidation services.

Article info
Received 30 March 2020
Accepted 2 June 2020
Online 6 November 2020

Keywords:
cargo transportation,
costs of transport,
efficient transportation,
system transport planning,
consolidation

Available online: https://doi.org/10.26552/com.C.2021.1.A54-A61

ISSN 1335-4205 (print version)
ISSN 2585-7878 (online version)

1 Introduction

Large carriers have more potential to survive any crisis. Therefore, the Polish transport industry, analogically to companies in Western Europe, will have to consolidate. Consolidation allows to transport smaller goods (e.g. put on a few pallets) from distant areas for a reasonable price [1-2] Nowadays, time and price are the most important factors; therefore, consolidation of cargos is a good solution [3]. It is also particular facilitation for smaller exporters. Dense network allows combining parcels, both within national and international connections [4]. Moreover, it is a safe form of transport of goods [5]. The consolidation of parcel to one transport means, above all, one shipping order, one parcel number, one customs clearance and one company that deals with transport service [6-8].

The digitization of transport processes can be achieved thanks to the systems of management of transports and invoices or applications monitoring the position of the transport means [9-11]. Programs of the cost optimization are ideal for enterprises having the networks of terminals, which are the most important on the market due to pressure put on the cost reduction [12]. In the last few years, transport business has drastically changed. Due to globalization of economy, range and frequency of transports have considerably increased. New logistic chains, networks of terminals and intermodal connections are built every year [13-15] to reduce the transport costs and improve the whole process. The movement of goods guarantees the functioning of cities and regions, however, motor trucks, due to their size, pace of moving and frequency of stops cause huge difficulties in the road traffic. In addition, they contribute to formation of hold-ups, increased noise and environmental pollution. These difficulties still have a growing trend; therefore, consolidation of cargos in road transport is the future of knowledge-based. Consolidation of cargos is a combination of a few various shipments into one cargo (Figure 1). Such a solution mainly allows optimizing costs. In the event of smaller shipments from a few suppliers (Client A, Client B, Client C), it would be unprofitable to load a few separate pallets. It is also more comfortable for the clients from logistics point of view. All the cargos are delivered within one delivery, which makes end client more satisfied.

A comprehensive analysis of the transport processes efficiency requires a broad view, taking into account both the organizational and financial aspects. The effectiveness analysis is mainly based on use of a set of indicators assessing the transport process [16], bearing in mind the specificity of transport processes in financial and organizational aspects (Tables 1 and 2). In Tables 1 and 2, examples of the rates of assessment of the transport processes effectiveness, from financial (Table 1) and organizational (Table 2) points of view, were presented. Effectiveness of the transport process

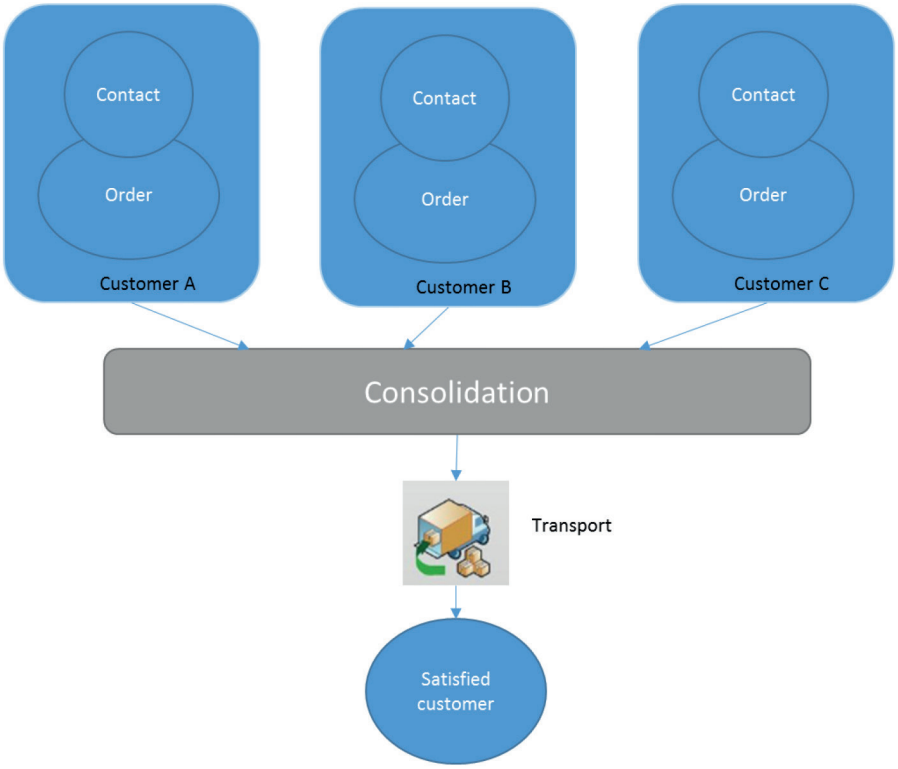

Figure 1 *Cargo consolidation*

Table 1 *Selected indicators for assessing the efficiency of transport processes in organizational terms [16]*

indicator	formula	characteristics	units of measure
load fleet load indicator	$\frac{a}{b}$	a - number of kilometers driven, b - number of means of transport	kg/car
rate of use of the transport means		a- weight of transported load b- number of means of transport	kg/car
transport intensity index		a- transport time, b- total number of deliveries	h/ delivery
timeliness of transport indicator	$\frac{a}{b} \times 100$	a - number of timely journeys b - total number of journeys	%
load damage indicator during the transport		a - load transported (mass or volume) b - load capacity or capacity of the transport fleet	%
cargo planning		a - value of incomplete deliveries b - value of all deliveries	%

is the most visible in a list of meters in the organizational aspect. It is not surprising, because the processes occurring at the operational level have the greatest contribution to the assessment of effectiveness of the transport process.

2 The consolidation of two means of transport illustrated through an example of client B

The fundamental research goal of the authors of this article was determination of the role of reduction of the transport costs using the consolidation services, illustrated through an example of client B. To achieve the goal, the research and analyses presented were conducted. The client is located in Prague. It now uses two systems of transportation (3.5 t and 6 t) that are sent to specific regions of Germany (Table 3 and Table 4).

In the event if the first means of transport, transit is two days, for the second one, one and a half day (Figure 2 and Figure 3).

Average speed accepted for the analysis of transit is 65 km/h. LDM a loading meter is the standard unit of measurement for transport by truck. One meter of cargo space, calculated as the product of the total width of the trailer and one meter of length. Most often, the width of the trailer is 2.4 meters, so 1 LDM - 2.4 m2. LDM calculations can be made using the goodloading.com application. Transport costs based on average rates on the current transport market

Table 2 *Selected indicators for assessing the efficiency of transport processes in financial terms [16]*

indicator	formula	characteristics	units of measure
shipping costs per shipment	$\frac{a}{b}$	a - transport cost b - number of shipments	€
costs of the transport fleet i		a - cost of kilometers travelled b - number of means of transport	€/car
costs of the transport fleet ii		a - value / cost of transported load b - number of means of transport	€/car
transport costs per tkm		a - transport cost b - number of tkm	€/tkm
complaints and returns	$\frac{a}{b} \times 100$	a - value / cost of returns complaints b - value / cost of all supplies of materials and raw materials	%
valuable incompleteness of supply		a - value of incomplete deliveries b - value of all deliveries	%

Table 3 *Transport schedule of client B - means of transport no. 1 - 3.5-ton*

code	city	date	time	distance	working time	driving time	comment
33098	Paderborn	2.07	08:00-09:00	0	1	0	loading
37001	Gottingen	2.07	11:00-12:00	135	3	2	
38440	Wolfsburg	2.07	14:00-15:00	135	5	4	45 min pause on the way to Potsdam
14467	Potsdam	2.07	19:00-20:00	205	10	9	pause 11 hours
8001	Zwickau	3.07	11:30-12:30	278	4.5	4.5	start 7:00
1099	Dresden	3.07	15:00-16:00	116	8	6.5	
10000	Prague	3.07	18:30	149	10.5	9	unloading
				1018			

Table 4 *Transport schedule of client B - means of transport no. 2 - 6-ton*

code	city	date	time	distance	working time	driving time	comment
36001	Fulda	2.07	08:00-09:00	0	0	1	loading
68159	Mannheim	2.07	12:00-13:00	187	4	3	
76131	Karlsruhe	2.07	14:00-15:00	68	5	4	pause 45 min on the way to Augsburg
86150	Augsburg	3.07	19:30-20:30	228	10.5	9	pause 11 hours
93047	Ratisbon	3.07	10:00-11:00	146	2	2	start 8:00
10000	Prague	3.07	16:00	268	8	6	pause 45 minutes unloading on the way
				897			

and consolidation tariff of the company (Table 5). The cost of every additional place of the so-called stop is 25 €.

The first means of transport must cover 1018 km (0.65 €/km), stopping in five places (125 €), generating the costs of 786.7 €. The second means of transport will cover 897 km (0.8 €/km) and will stop in four additional loading places (100 €). In this case, freight rate is 817.6 €.

The utilization of both means of transport stays within the range of 86% (Tables 5-7).

Transport enterprise offers delivery of every cargo within 2 working days. In this case, the cargo loaded on 02/07 shall be available for reception in the warehouse only on 04/07 (Tables 8 and 9).

The cargo will be ready on 4th of July at 9 pm (Table 10). The means of transport that will take goods must be 24-ton and will have to cover 300 km. According to a price list, the rate for such distance is 1.3 €/km (Table 5). Therefore, the cost of this transport will be 390 €.

Transit will last two and a half days, that is, one day longer than now (Figure 4).

Using defined weight tariff that verifies the costs of transport of cargos to the warehouse in Nuremberg in

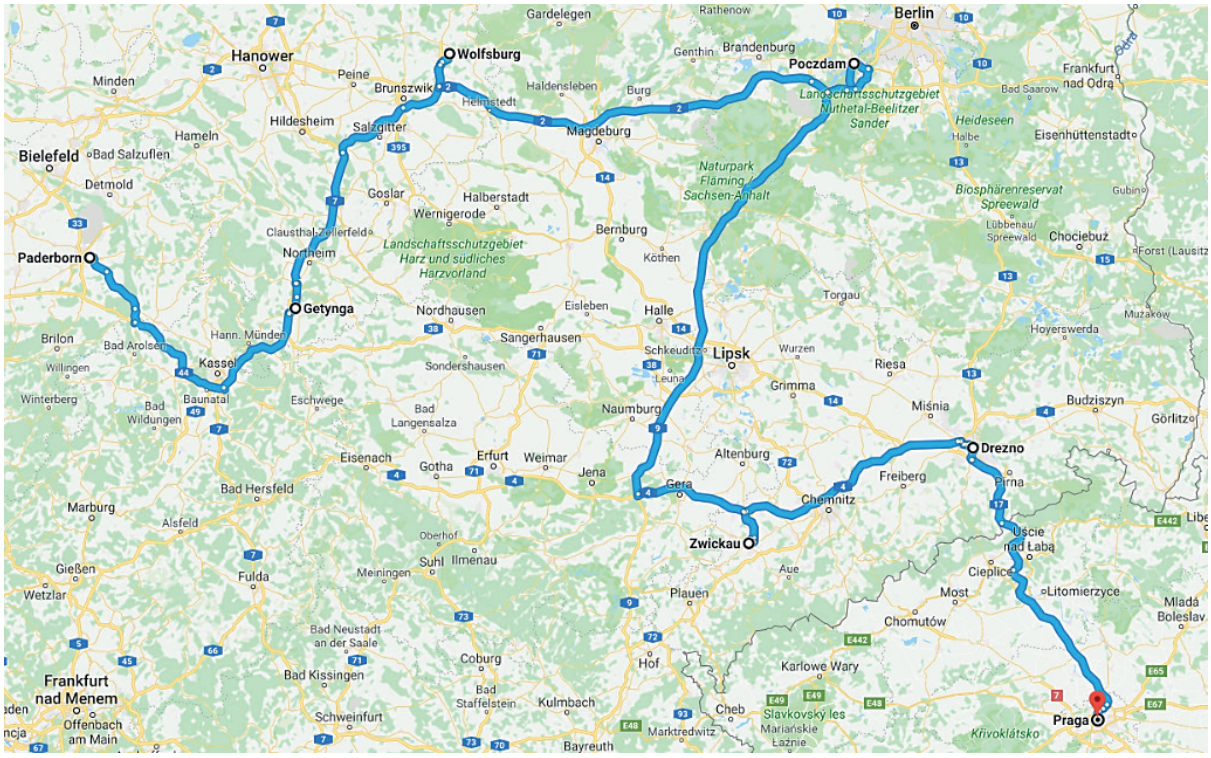

Figure 2 *Current organization of transport of a client B - means of transport no. 1 (based on Google Maps pl)*

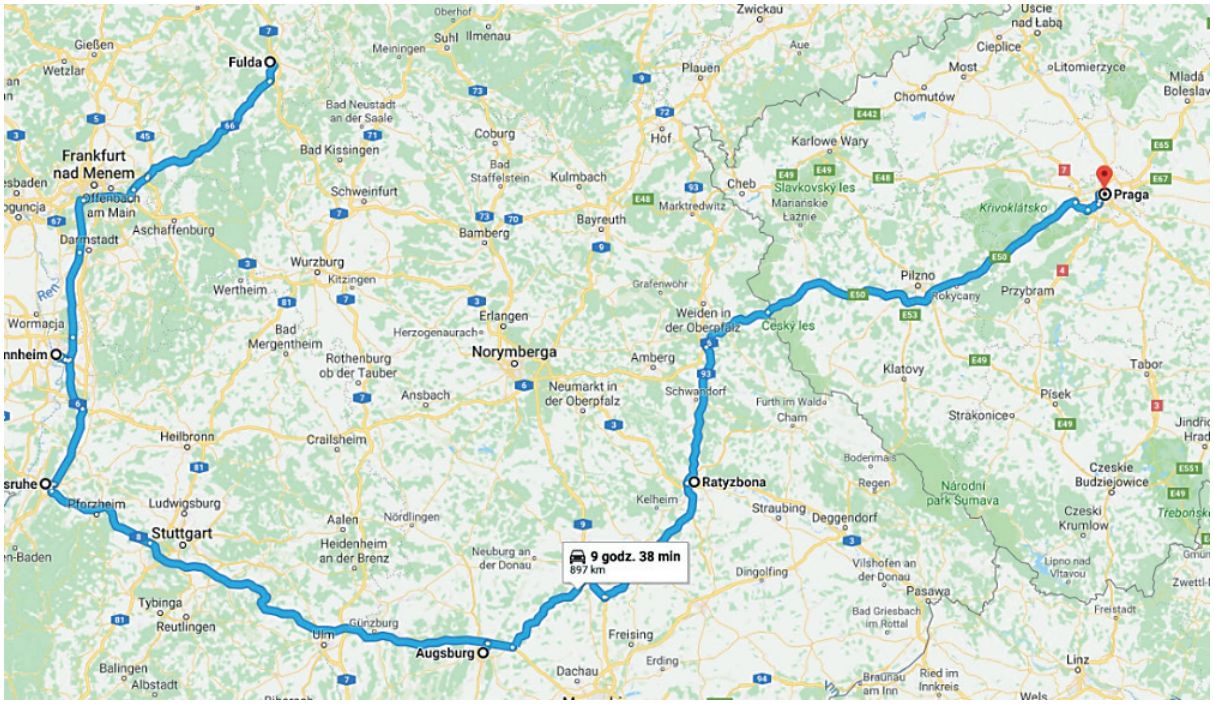

Figure 3 *Current organization of transport of a client B - means of transport no. 2 (based on Google Maps pl)*

Table 5 *The average rates for a kilometre for specific cars (the author's own work)*

car type (t)	dimensions (length / width / height) (m)	0-300 km (€/km)	300-800 km (€/km)	>800 km (€/km)
3.5	6.0/2.4/2.7	0.8	0.75	0.65
6	7.2/2.4/2.7	0.9	0.85	0.8
24	13.6/2.5/3	1.3	1.25	1.2

Table 6 *The cost of consolidation service for client B - means of transport no. 1, LDM -length of a load box*

code	city	number of pallets	LDM (m)	mass (kg)	handling(€)	transport (€)
33098	Paderborn	4	1.6	400	8	62.20
37001	Gottingen	1	0.4	300	2	45.71
38440	Wolfsburg	2	0.8	300	4	49.21
14467	Potsdam	3	1.2	500	6	71.08
8001	Zwickau	2	0.8	800	4	73.27
1099	Dresden	1	0.4	50	2	15.90
	total	13	5.2	2350	26	317.36
		utilization of means of transport	86.67%	78.33%		343.36 €

Table 7 *The cost of consolidation service for client B - means of transport no. 2 LDM - length of a load box)*

code	city	number of pallets	LDM (m)	mass (kg)	handling (€)	transport (€)
36001	Fulda	2	0.4	200	4	26.14
68159	Mannheim	3	0.6	500	6	55.97
76131	Karlsruhe	2	0.8	300	4	41.55
86150	Augsburg	5	2	1000	10	86.80
93047	Ratisbon	6	2.4	1000	12	82.44
	total	18	6.2	3000	36	292.94
		utilization of means of transport	86.11%	78.33%		328.94 €

Table 8 *Delivery time of cargos to Nuremberg (Client B) - means of transport no. 1*

code	city	date	time	code	city	date	time
33098	Paderborn	2.07	08:00	90402	Nuernberg	4.07	08:00
37001	Gottingen	2.07	11:00	90402	Nuernberg	4.07	08:00
38440	Wolfsburg	2.07	14:00	90402	Nuernberg	4.07	08:00
14467	Potsdam	2.07	09:30	90402	Nuernberg	4.07	08:00
8001	Zwickau	2.07	11:30	90402	Nuernberg	4.07	08:00
1099	Dresden	2.07	15:00	90402	Nuernberg	4.07	08:00

Table 9 *Delivery time of cargos to Nuremberg (Client B) - means of transport no. 2*

code	city	date	time	code	city	date	time
36001	Fulda	2.07	08:00	90402	Nuernberg	4.07	08:00
68159	Mannheim	2.07	12:00	90402	Nuernberg	4.07	08:00
76131	Karlsruhe	2.07	14:00	90402	Nuernberg	4.07	08:00
86150	Augsburg	2.07	19:30	90402	Nuernberg	4.07	08:00
93047	Ratisbon	2.07	10:00	90402	Nuernberg	4.07	08:00

Table 10 *Transport of consolidated cargo to Prague*

code	city	date	time	code	city	date	time
90407	Nuernberg	4.07	09:00	10000	Praga	4.07	13:30

terms of postal code of a supplier, the rate of reception of all suppliers and for handling operations is 343.36 € Client B - means of transport no. 1, and for Client B means of transport no. 2 is 328.95 €. Total cost of movements for client B is 1604.3 € per week (Table 11).

There is one issue to be determined yet, the impact of extended transit on the costs frozen in material. The value of cargo and number of production days of the plant are needed. The value of goods is forty-five thousand euro, in six-day production line; it is seven and a half thousand euros a day. Increasing the transit by one day will give negative impact for value of one day, that is, seven and a half thousand euro. Comparing the losses in material and savings in transport, one gets a positive result in

Figure 4 *Nuremberg - Prague (based on use of the Optimizing XYZ)*

Table 11 *The savings of a client B, proposed offer of a transport enterprise*

route	type of a car (t)	distance	feet	costs (€)
suppliers -> client B Prague 1	3.5	1018	5	786.70
suppliers -> client B Prague 2	6	897	4	817.60
actual total cost				1604.30
suppliers -> Nuremberg 1	consolidation			343.4
suppliers -> Nuremberg 2	consolidation			328.9
Nuremberg -> client B Prague	24	300	0	390
proposed total cost				1062.31
weekly saving				-541.99
annual saving				-26015.75

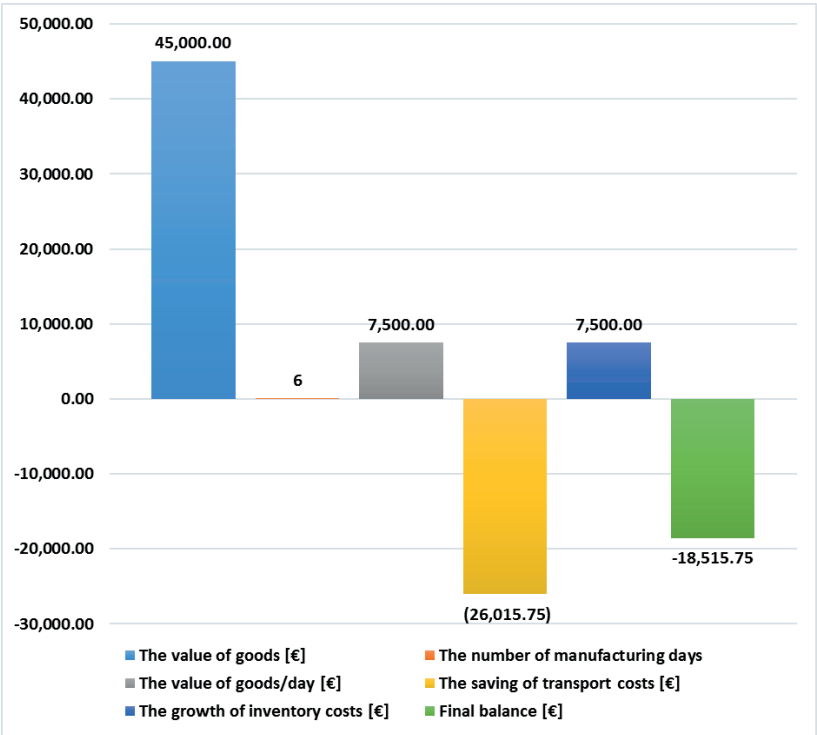

Figure 5 *Comparison of transport savings and inventory losses of a client B*

the form of thirty thousand euros of saving for client B (Figure 5).

3 Conclusions

The fundamental goal of the authors of this article was to determine the role of reduction of transport costs with the use of consolidation service. To achieve the goal, execution of the following plans was used:

- An analysis of current transport organization of a client,
- An assignment of particular suppliers to warehouses towards terminal network of a transport enterprise providing consolidation services,
- Calculation of costs of consolidation service, taking transport and handling costs into account,
- Determination of the impact of transport organization on inventory costs,
- Comparison of current costs with proposed solution,

Conducted analysis allowed to prove that consolidation services reduce the costs of transport of small cargos. In the event of direct transports, the cars must cover many kilometres, only to take one small parcel or pallet. Medium and large cargos are not cost-effective for such organizations, however, direct and consolidation method can be combined to get the optimal results. Impact on inventory costs was also taken into consideration in the analysis. Extended time of transit, caused by use of a consolidation service, should be in majority of cases covered by the transport savings.

References

[1] HANBAZAZAH, A. S., ABRIL, L., ERKOC, M., SHAIKH, N. Freight consolidation with divisible shipments, delivery time windows, and piecewise transportation costs. *European Journal of Operational Research* [online]. 2019, **276**(1), p. 187-201. ISSN 0377-2217. Available from: https://doi.org/10.1016/j.ejor.2018.12.043

[2] BOOKBINDER, J. H., ELHEDHLI, S., LI, Z. The air-cargo consolidation problem with pivot weight: models and solution methods. *Computers and Operations Research* [online]. 2015, **59**(C), p. 22-32. ISSN 0305-0548. Available from: https://doi.org/10.1016/j.cor.2014.11.015

[3] CROXTON, K. L., GENDRON, B., MAGNANTI, T. L. Models and methods for merge-in-transit operations. *Transportation Science* [online]. 2003, **37**(1), p. 1-22. ISSN 0041-1655, eISSN 1526-5447. Available from: https://doi.org/10.1287/trsc.37.1.1.12822

[4] KOLINSKI, A., STAJNIAK, M. *Effectiveness of transport processes: modern problems and development trends / Efektywnosc procesow transportowych: wspolczesne problemy i trendy rozwoju* (in Polish). Radom: Instytut Naukowo-Wydawniczy, 2016. ISBN 978-83-62805-18-1.

[5] NOWACKI, G., KRYSIUK, C., NIEDZICKA, A. Selected transport problems of dangerous goods in the European Union and Poland. In: *Safety of Marine Transport*. 2015. ISBN 978-1-138-02859-3, eISBN 978-1-315-67261-8, p. 297-303.

[6] QIN, H., ZHANG, Z., QI, Z., LIM, A. The freight consolidation and containerization problem. *European Journal of Operational Research* [online]. 2014, **234**(1), p. 37-48. ISSN 0377-2217. Available from: https://doi.org/10.1016/j.ejor.2013.09.015

[7] FAN, Y., BEHDANI, B., BLOEMHOF- RUWAARD, J., ZUIDWIJK, R. Flow consolidation in hinterland container transport: an analysis for perishable and dry cargo. *Transportation Research Part E: Logistics and Transportation Review* [online]. 2019, **130**, p. 128-160. ISSN 1366-5545. Available from: https://doi.org/10.1016/j.tre.2019.08.011

[8] LV, B., YANG, B., ZHU, X., LI, J. Operational optimization of transit consolidation in multimodal transport. *Computers and Industrial Engineering* [online]. 2019, 129, p. 454-464. ISSN 0360-8352. Available from: https://doi.org/10.1016/j.cie.2019.02.001

[9] OLSSON, J., WOXENIUS, J. Localisation of freight consolidation centres serving small road haulers in a wider urban area: barriers for more efficient freight deliveries in Gothenburg. *Journal of Transport Geography* [online]. 2014, **34**, p. 25-33. ISSN 0966-6923. Available from: https://doi.org/10.1016/j.jtrangeo.2013.10.016

[10] NEUMANN, T. Fuzzy routing algorithm in telematics transportation systems. In: *Smart solutions in today's transport* [online]. MIKULSKI, J. (ed.). TST 2017. Communications in computer and information science. Vol. 715. Cham: Springer International Publishing, 2017. ISBN 978-3-319-66250-3, eISBN 978-3-319-66251-0, p. 494-505. Available from: https://doi.org/10.1007/978-3-319-66251-0_40

[11] NEUMANN, T. Automotive and telematics transportation systems. In: International Siberian Conference on Control and Communications SIBCON 2017: proceedings. IEEE, 2017. ISBN 978-1-5090-1081-3, p. 1-4.

[12] KLINCEWICZ, JOHN, G. Solving a freight transport problem using facility location techniques. *Operations Research* [online]. 1990, **38**(1), p. 99-109. ISSN 0030-364X, eISSN 1526-5463. Available from: https://doi.org/10.1287/opre.38.1.99

[13] KUSMINSKA-FIJALKOWSKA, A, KOZYRA, J, OLSZANSKA, S. Analysis of movements of TEU intermodal transshipment terminal in the area of polish. In: International Conference Transport Means: proceedings. 2018. ISSN 1822-296 X, eISSN 2351-7034, p. 849-854.

[14] MOCCIA, L., CORDEAU, J.-F., LAPORTE, G., ROPKE, S., VALENTINI, M. P. Modeling and solving a multimodal transportation problem with flexible-time and scheduled services. *Networks* [online]. 2011, **57**(1), p. 53-68. eISSN 1097-0037. Available from: https://doi.org/10.1002/net.20383

[15] KUSMINSKA-FIJALKOWSKA, A. *Aspect of time in automated processes of TEU flow in a handling terminal / Aspekt czasu w zautomatyzowanych procesach przeplywu TEU w terminalu przeladunkowym* (in Polish). Radom: Wydawnictwo UTH, 2018. ISBN 9788373518490.

[16] HAJDUL, M., STAJNIAK, M., FOLTYNSKI, M. KOLIKOWSKI, A., ANDRZEJCZYK P. *Organization and monitoring of transport processes / Organizacja i monitorowanie procesow transportowych* (in Polish). Poznan: Instytut Logistyki i Magazynowania, 2015.

OPTIMISATION OF DISTRIBUTION ROUTES: A CASE STUDY

Rudolf Kampf, Martina Hlatká, Patrik Gross*

Department of Transport and Logistics, Faculty of Technology, Institute of Technology and Business in Ceske Budejovice, Ceske Budejovice, Czech Republic

*E-mail of corresponding author: gross@mail.vstecb.cz

Resume

This article focuses on optimisation of the distribution routes for a company that produces carpets, floor coverings and tapestries. The optimisation process is based on operational research methods including, without limitations, Mayer's method and the single linkage method. The obtained results are subsequently compared to the current situation and evaluated in terms of time and costs. The conclusion provides the optimised economic solution.

Article info

Received 13 July 2020
Accepted 21 July 2020
Online 12 November 2020

Keywords:

logistics,
transport,
transportation problem,
operational research,
Mayer´s method,
single linkage method

Available online: https://doi.org/10.26552/com.C.2021.1.A62-A73

ISSN 1335-4205 (print version)
ISSN 2585-7878 (online version)

1 Introduction

The modern age is characterised by the rapid technological progress, as facilitated by its creators, and the growing demands being placed on employees. On occasion, this combination of factors may lead to job losses within a company. However, if the adopted technologies fail to meet their potentials, there is a risk that the quality of products and services will fall, resulting in a significant loss of customers. In addition, the current supply of products and services hugely exceeds demand, which calls for greater appreciation of new and current buyers. Customer satisfaction and aftercare should, therefore, be the main objective of all the companies.

The company at the centre of this case study sells carpets, tapestries, floor coverings (PVC, vinyl, wood, laminate, linoleum, cork), mats, associated materials (underlay, glues, skirting boards, sanitizers and detergents), as well as offers related services, such as floor assembly, carpet laying and floor cleaning. The company´s large number of customers means that the company must plan its distribution routes in detail. Long-standing customers (57 companies in South Bohemia) are extended free or reduced shipping costs. The company retains the option to compensate for these costs in the form of goods or services. Offering goods is considered risky due to the fierce competition on the market, so offering services is considered adequate compensation. Since retaining customer loyalty is not very easy nowadays, extra bonuses such as "free shipping" are a great enticement.

2 Methodology

The operational research focused on examining individual operations in terms of a set of scientific fields dealing with decision problems. In his book, Jablonsky refers to operational research as a scientific field - a set of relatively independent disciplines aimed at analysing different types of decision problems [1]. He further points out the impossibility of formulating an exact definition of operational research. However, he offers a rough outlining of what operational research covers by referring to the term as the research of operations. Within this context, other authors applied operational research to all the spheres dealing with analysis and coordination of performed operations (irrespective of their definition) within a system. For example, as a scientific tool for developing and supporting the solution of decision-making problems and the reduction of emergency situations in continuous transport with respect to the environment [1-3].

Operational analysis tries to achieve the highest possible quality of operations, or their mutual relationship, with a view to ensuring the smoothest possible functioning of a system. Setting specific criteria is vital for assessing the proper or unsuitable functioning of a system by means of mathematical modelling, which is an indispensable operational research tool. If one examines a transportation system based on the operational research, it is specifically this analysis that uses a model for that system [4-6].

Table 1 *Design of an economic model for the transportation problem [1]*

sources	sinks	source capacity			
	O_1	O_2	…	O_n	
D_1	c_{11}	c_{12}		c_{1n}	
	x_{11}	x_{12}	…	x_{1n}	a_1
D_2	c_{21}	c_{22}		c_{2n}	
	x_{21}	x_{22}	…	x_{2n}	a_2
.	.	.	.	.	.
.	.	.	.	.	.
.	.	.	.	.	.
D_m	c_{m1}	c_{m2}		c_{mn}	
	x_{m1}	xm_2	…	x_{mn}	a_m
sinks' requirements					$\sum_i a_i$
	b_1	b_2	…	b_n	$\sum_j b_j$

3 The transportation problem

Transportation problems generally are concerned with the scheduling distribution of specific goods or materials from supplier points (sources) to customers (sinks), with the intent to minimise the overall distribution costs [7].

Holoubek argues that transport tasks focus on delivering goods from supplier warehouses to customer storages by maximising the economics of the shipping process [8]. As one can see in Table 1, he points out that for each of m supplier warehouses D_1, D_2…, D_M the maximum amount of a_1, a_2…, a_m to be delivered is defined. For each of n customer storage facilities O_1, O_2…, O_n the maximum amount of b_1, b_2…, b_n to be stored is defined. Capacity and requirements are measured in identical and standard units of measure, i.e. tonne, pieces, etc. The last measured quantity is the transport intensity specifically referred to as shipping (transport) costs between the supplier warehouse i and the customer storage facility j designated as c_{ij}, where $i=1, 2, \ldots, m$ and $j=1, 2, \ldots n$ [8-10].

Resolving the transportation problem also includes case specific consideration for relationships between the total capacity of sources $\sum i\ a_i$ (total of all the partial capacities) and all the requirements of the sinks $\sum j\ bj$ (total of all the requirements), whereby the formula is as follows:

$$\sum i\ a_i = \sum j\ b_j . \tag{1}$$

For purposes of this problem, it will be referred to as the balanced transportation problem, i.e. one that satisfies all the requirements and fills all the capacities.

This transportation problem is calculated as follows:

$$\sum i\ a_i \neq \sum j\ b_j . \tag{2}$$

For purposes of this problem will be referred to as the unbalanced transportation problem, i.e. one caused by the excess supply or demand, resulting in a waste of capacity (over capacity or shortage of).

4 The travelling salesman problem

Pelikan states that the travelling salesman assignments consist of looking for the optimal route for vehicles shipping goods using the travelling salesman technique, whereby distribution network nodes are served (supplied) once or more times, with the start and end of the route usually being the starting point. The key objective is to minimise the overall length of the route, while meeting customers' requirements and adhering to the technological restrictions imposed on the means of transport [11-12].

Other authors analysed the travelling salesman problem, thereby mostly focusing on the most economical way of delivering goods to customers. However, this is not concerned with the typical issue within the concept of the travelling salesman problem where customers are supplied from several points. In this case, goods delivery takes place along one route, starting and ending at the same point. Experts often call it a travelling salesman assignment. This task consists of getting from the starting point (point A1) and delivering goods to places A2, A3 … A(n) at one time (in random order) and then returning to the starting point (A1). The route should be as short as possible with a view to finding the quickest route starting and ending at point A1 [13-15].

5 Single and multiple travelling salesman problems

Subrt defines a simpler single travelling salesman problem, which delivers goods along one route [16].

The mathematical model for the single travelling salesman problem is as follows:

$$\min f = \sum_{i=1}^{m} \sum_{j=1}^{n} c_{ij}\ x_{ij}, \tag{3}$$

for which the following conditions apply:

$\sum_{i=1}^{n} x_{ij} = 1$ for i = 1, 2, …, n,

$\sum_{i=1}^{n} x_{ij} = 1$ for i = 1, 2, …, m,

$u_i - u_j + nx_{ij} \leq n - 1$ for i = 1, 2, …, m and j = 1, 2, …, n,

$x_{ij} \in \{0,1\}$ for i = 1, 2, …, m and j, = 1, 2, …, n.

The first two conditions allow each node to be visited exactly once. The third condition ensures the indivisibility of the resulting Hamiltonian cycle, i.e. the graph cycle visits individual nodes only once, with the exception of the start node, which is also the end node [16-17].

6 Mayer's method

Ziskal and Havlicek argue that Mayer's method also focuses on scheduling routes by selecting minimal elements [18]. They further point to use of the multi-lane assignments with a complete route network and limited capacity. To solve the task based on the Mayer's method, it is necessary to use a symmetric matrix of distances. Inside the model, separate points form a sequence of distance points, whereby the central point is the last (e.g. a warehouse followed by other locations according to their distance). The matrix therefore indicates the farthest point and subsequently those points closer to the final destination - the central warehouse. According to the authors, Mayer's method consists of two steps [18].

The first step involves selection of points for individual routes, so that the first route includes the place farthest from the central position. Unless the vehicle exceeds its capacity, it goes on to the next point closest (shortest distance) to the previous location, followed by a check of the vehicle´s capacity. Unless filled, the lorry, once again, goes to the next point closest (shortest distance) to the previous one, followed by a check of its capacity. The whole cycle repeats itself until the vehicle is packed to capacity. For scheduling of additional routes, the same method is applied.

The second step involves putting points on separate routes into order based on the intuitive decision-making and previous knowledge.

7 Single linkage method

In his publication, Subrt explains that this technique was developed from the distance matrix. The main principle is to determine the starting point and to subsequently find the most convenient connection (the shortest distance) to the next place. This point then serves for finding the closest nexus to a different point [15].

The calculation originated from the rate matrix (distances), with the starting point column, which is the last point, first being ruled out. The starting location line takes on a minimum-rate (distance) cell, which is integrated into the route and removes the designated column, followed by indication of the highest-rate cell in the column that corresponds to the specific location, complementing the route. The whole cycle repeats itself until all the points have been incorporated, whereby the route from the last points leads to the starting point (the central warehouse).

Paper explains that, one by one, all the points become starting points, each of them having an allocated route. In the event of an asymmetric rate matrix, the route must be traced in reverse. Such a situation will result in either the crossing out of lines and the detection of minimum rates in columns or in the whole procedure being conducted on a transposed matrix that results in an option for the most convenient route [19-20].

In her work, Frieblova states that the method in question involves considering each point as a starting point, i.e. picking the closest place from the starting location and subsequently the next closest point (unless already incorporated in the solution, which would mean selecting the second closest point) [21]. The cycle continues until the circuit closes, with the process repeated for all starting points. The so-called quasi-starting points, i.e. those places not identified as starting points, must be allocated with an accordingly adjusted route [21-22].

8 Intuition method

The intuition method always tackles simple and visible problems in the same way. This technique is highly economical.

Intuitively resolving problems embraces use of analogies, experience garnered from previous decisions and/or decisions taken on the basis of first impressions. These resolutions are often subliminal and are made to settle the petty problems [23].

9 Analysis of current situation in the company

The company at the centre of this case study sells carpets, tapestries, floor coverings (PVC, vinyl, wood, laminate, linoleum, cork), mats, associated materials (underlay, glues, skirting boards, sanitizers and detergents), as well as offers related services, such as floor assembly, carpet laying and floor cleaning.

Internal corporate data - customer address, order of unloading, time windows used for planning and meeting deadlines - provided the information necessary for the calculations. The goods register also contributed to scheduling of the distribution routes, which in turn provided information on kilometrage. All the obstacles on roads, for example bridges and other traffic safety restraints, were taken into consideration when working out the current shipping routes.

The company grants free shipping to long-term customers (57 companies in South Bohemia). The large number of customers means supply routes must be planned in detail. This article focuses particularly on the three delivery routes that are followed every week, namely:

- Monday- Jindrichuv Hradec, Pelhrimov, Tabor.
- Tuesday- Strakonice, Pisek, Klatov, Susice.

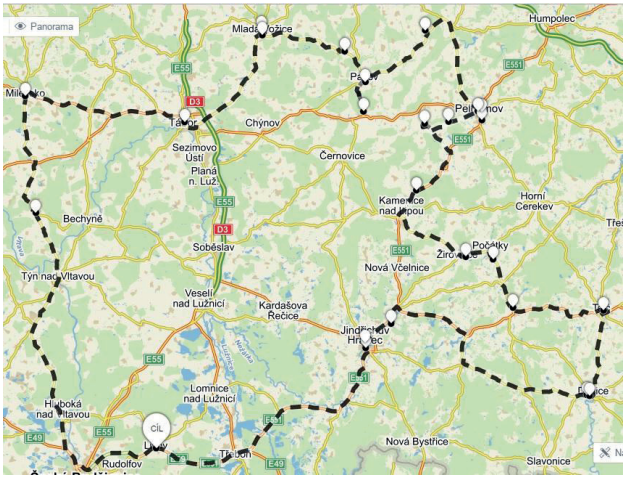

Figure 1 *Route I [24]*

- Wednesday - Kaplice, Cesky Krumlov, Prachatice, Vimperk, Ceske Budejovice.

If a public holiday falls on one of these days a different weekday is fixed.

An employee receives orders from individual customers and compiles a goods register (list and description of products). This is sent to the warehouse by fax. The warehouse workers gather the ordered goods, ordering and labelling pallets and/or boxes accordingly and in such way that the lorry can unload the goods as quickly as possible.

The following day, the driver unloads the ordered goods, making sure to unload the correct goods (incl. amount and quality) in the right place. To optimise the process, the following data were required:

- Vehicle loading capacity in kilograms
- Delivery addresses of customers
- Quantities (in kilograms) being unloaded for individual customers
- Time windows for unloading
- 3 routes run every week (the optimisation of which requires consideration being given to all the restrictions the driver must respect)

10 Analysis of the company's organisational rules

The company's organisational rules are as follows:

- Transport is provided using the company's lorry (capacity: 3.5 tonnes).
- Three different routes, with scheduled delivery to long-term customers each week (shipping goods regularly on Monday, Tuesday and Wednesday to 57 companies in South Bohemia).
- All the routes always begin and end in the town of Lisov.
- Only one driver at a time delivers goods.
- The driver is always accompanied by an assistant - a company employee who helps to unload the freight.
- The driver can choose from two alternatives with regards to work times:
- 6 a.m. start in Lisov and finishing no later than 5.30 p.m. in Lisov;
- flexible starting and finishing times according to customer requirements and the opening hours of unloading places.
- Time windows (e.g. 6.00 a.m. - 4.00 p.m.) shall be respected and goods delivered accordingly.
- The time required to complete the shipping route must not exceed the driver's maximum daily working hours.
- Drivers' breaks, as regulated by law, must be respected.
- Maximum weight limits (in relation to a specific distribution route and/or traffic restrictions) must be respected.
- Height, width and time restrictions imposed on lorries must be respected.
- Force majeure (congestions, drivers' incapacity, lorries' susceptibility to failure).

Microsoft Excel was used to carefully work out the three distribution routes with a view to effectively and efficiently process the collated data.

11 Current distribution routes

In this section, the routes are presented in terms of the exact number and sequence of unloading points on a particular day, kilometrage, average vehicle speed and the time spent on the route.

11.1 Route I

This route is followed on Mondays, involves 19 unloading points, with the town of Lisov being the loading point. The customer locations are as follows: Jindrichuv Hradec I - Jindrichuv Hradec II - Rodvinov - Dacice I - Dacice II - Telc - Studena - Pocatky - Pelhrimov I - Pelhrimov II - Pelhrimov III - Pelhrimov IV - Arnestovice - Pacov I - Pacov II - Mlada Vozice I - Mlada Vozice II - Tabor - Milevsko - Lisov. On Route I, which is 354 km long, it takes 175 minutes (i.e. 2:55 hrs) to unload freight weighing 3 295 kg. The net driving time is 6:65 hrs, excluding a 45-minute mandatory break. The total number of working hours

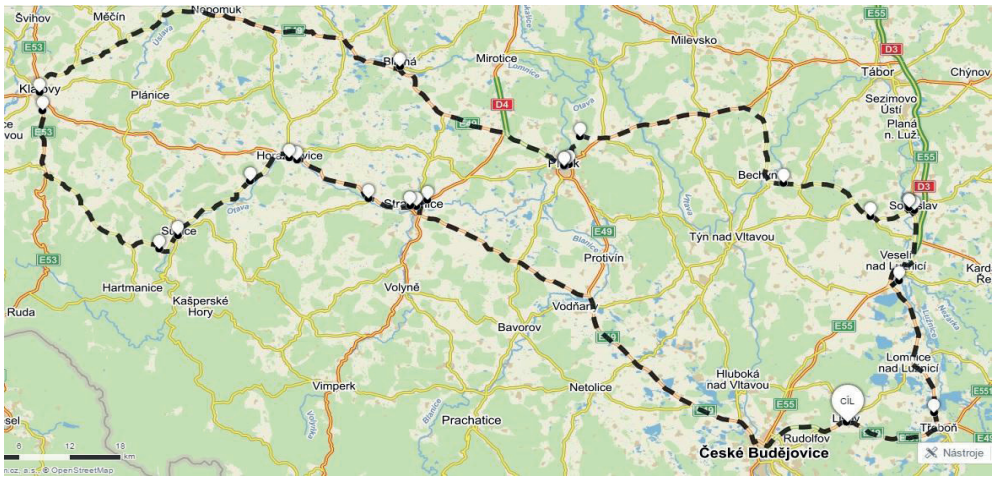

Figure 2 *Route II [24]*

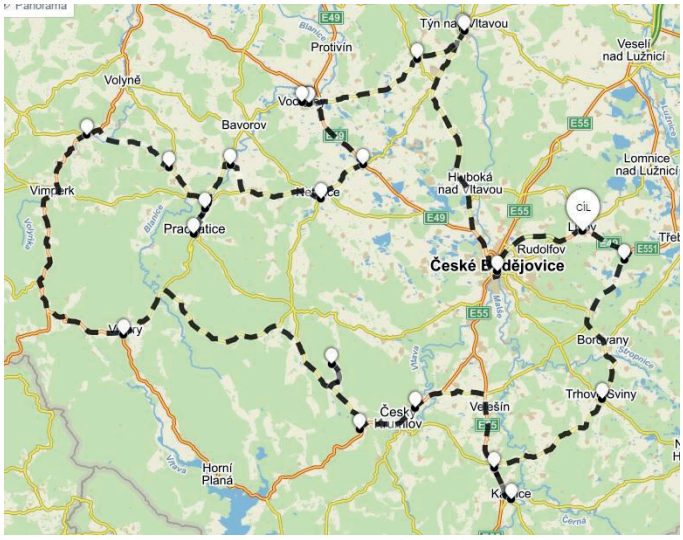

Figure 3 *Route III [24]*

Table 2 *Overview of km/day in relation to driver's working hours*

shipping day	km/day	driver's working hours min/day	driver's working hours hrs/day
Monday	354	636	10:36
Tuesday	331	573	9:33
Wednesday	304	591	9:51
total	989 km/3 days	1 800 min/3 days	30 hrs/3 days

required to complete Monday's route is 10:36 hrs (636 minutes). Figure 1 illustrates the planned route that avoids all road restrictions.

11.2 Route II

This route is followed on Tuesdays, involves 20 unloading points, with the warehouse in the town of Lisov being the loading point. The customer locations are as follows: Veseli nad Luznici - Sobeslav I - Sobeslav II - Sobeslav III - Vrcovice - Pisek I - Pisek II- Pisek III - Blatna - Klatovy I - Klatovy II - Susice - Susice Volsovy - Bojanovice - Horazdovice I - Horazdovice II - Katovice - Strakonice I - Strakonice II - Strakonice III - Lisov. Total kilometrage is 331 km (average speed 55 km/h), total unloading time 165 min, total cargo weight 3 270 kg, and net driving time 6:03 hrs, excluding a 45-minute mandatory break. The total number of working hours required to complete Tuesday's route is 9:33 hrs (573 minutes). Figure 2 shows Route II.

11.3 Route No. III

This route is followed on Wednesdays, involves 18 unloading points, with the warehouse in the town of Lisov being the loading point. The customer locations are as follows: Ceske Budejovice - Tyn nad Vltavou I - Tyn nad Vltavou II - Temelin - Vodnany I - Vodnany II - Vodnany III - Netolice - Strunkovice nad Blanici - Prachatice - Vlachovo

Table 3 *Distance matrix*

	Lisov	J. Hradec I.	J. Hradec II.	Rodvinov	Dacice I.	Dacice II.	Telc	Studena	Pocatky	…
Lisov	0	40.7	41.2	48.1	95.6	94.9	82.6	69.1	62.4	…
J. Hradec I.	40.7	0	1.5	7.2	34.2	34.1	41.8	28.3	21.5	…
J. Hradec II.	41.2	1.5	0	5.6	36	35.8	40.2	26.7	19.9	…
Rodvinov	48.1	7.2	5.6	0	38.2	38.1	36.6	23.1	16.4	…
Dacice I.	95.6	34.2	36	38.2	0	0.55	15.3	20.1	38.3	…
Dacice II.	94.9	34.1	35.8	38.1	0.55	0	15.1	19.9	38.6	…
Telc	82.6	41.8	40.2	36.6	15.3	15.1	0	14.8	25.5	…
Studena	69.1	28.3	26.7	23.1	20.1	19.9	14.8	0	11.1	…
Pocatky	62.4	21.5	19.9	16.4	38.8	38.6	25.5	11.1	0	…
										0

Brezi - Ckyne - Volary - Borova - Kajov - Prisecna - Kaplice - Trhove Sviny - Lisov. Total kilometrage is 304 km (average vehicle speed 51 km/h), total unloading time 185 minutes, total cargo weight 3 460 kg, and net driving time 6:01 hrs, excluding a 45-minute mandatory break. The total number of working hours required to complete Wednesday´s route is 9:51 hrs (591 minutes). Figure 3 shows Route III.

12 Calculation of overall transport costs

The overall transport costs provide an essential indicator of the impact thereof on the company's profits. The lorry's average fuel consumption is 18 l/100 km. Although diesel prices fluctuate, a price of 1.30 EUR/l is used for the price calculation per km, which is as follows:

Calculation of costs of diesel/km: 0.18*1.3 = 0.234 EUR

Driver costs are 0.56 EUR/km with daily remuneration of 36 EUR per day. The difference between the price of diesel per kilometre and the price charged by the shipper per kilometre is 0.33 EUR (0.56 EUR – 0.22 EUR = 0.33 EUR), with the calculated amount being used for vehicle amortization, regular maintenance, road tax, extraordinary events and the driver's remuneration [25].

Table 2 presents the overall transport costs of the company in terms of the total kilometrage per week and total working hours for each day. The costs for Monday, Tuesday and Wednesday are 198.24 EUR, 185.36 EUR, and 170.24 EUR, respectively. This brings total weekly costs to 553.84 EUR + 108 EUR (total remuneration for driver for 3 days) = 661.84 EUR. On a monthly basis, this is equivalent to 2647.36 EUR, and on an annual basis 31768.32 EUR.

13 Optimisation of distribution routes

To optimise the distribution routes of the company, it is necessary to draw up a distance matrix of the individual customer points. The distance matrix must be symmetric, containing 57 lines (customers) and the loading place (warehouse in Lisov), i.e. 58 x 58. Because of its massive size, Table 3 represents only a part of the designed matrix.

The matrix explores the kilometrage within each combination of analysed customer points, which is of critical importance for making final decisions. The model is symmetric, i.e. the kilometrage from point A to point B and vice versa is the same. MSExcel was used to draw up the list of customer points, and googlemaps.com and mapy.cz for compiling the whole pattern.

14 Application of the Mayer's method

The Mayer's method is an important tool with which to determine routes to the closest destinations and for their subsequent integration into a single route. The Mayer's method involves searching for and including individual customer points into the specific circuits. The basis for the application of the method was 58 locations (including the distribution warehouse in Lisov) divided over the three distribution routes and hired drivers for three days a week, with a focus on bringing down the driver costs to 0.56 EUR/km. The task is to optimise these three routes, thereby reducing the total kilometrage, whilst meeting the following requirements:

- Cargo weight must not exceed 3.5 tonnes;
- Time windows for deliveries must be adhered to;
- Driver's daily working hours must not exceed the prescribed limit; if the driving time exceeds 4.5 hrs, the driver is entitled to a 45-minute break, which is to be included in the total working hours.

14.1 Route I

The first step is, with help of the distance matrix, to determine the farthest place from the distribution warehouse in Lisov, which is the customer point identified as Klatovy I. At a distance of 116 km from the distribution warehouse, Klatovy I is therefore the first point on the

Table 4 *Application of the Mayer's method to Route I*

customer place	unloading time (min)	goods weight (kg)	time windows
Klatovy I.	5	60	6 a.m.-6 p.m.
Klatovy II.	10	100	8 a.m.-5 p.m.
Susice	10	120	8 a.m.-5 p.m.
Susice-Volsovy	10	100	8 a.m.-5 p.m.
Horazdovice II.	5	80	8 a.m.-5 p.m.
Bojanovice	10	90	6 a.m.-5 p.m.
Horazdovice I.	5	90	8 a.m.-5 p.m.
Katovice	20	900	6 a.m.-5 p.m.
Strakonice III.	10	140	7 a.m.-5 p.m.
Strakonice II.	5	50	6 a.m.-6 p.m.
Blatna	5	50	6 a.m.-6 p.m.
Strakonice I.	10	130	6 a.m.-6 p.m.
Pisek III.	5	70	8 a.m.-5 p.m.
Pisek II.	20	650	8 a.m.-5 p.m.
Pisek I.	5	90	6 a.m.-6 p.m.
Vodnany III.	10	120	8 a.m.-5 p.m.
Vrcovice	5	80	6 a.m.-6 p.m.
Vodnany I.	5	100	8 a.m.-5 p.m.
Vodnany II.	10	80	8 a.m.-5 p.m.
Milevsko	10	100	6 a.m.-6 p.m.
Temelin	10	110	6 a.m.-6 p.m.
Tyn nad Vlt. I.	10	120	6 a.m.-6 p.m.
Tyn nad Vlt. II.	5	50	6 a.m.-6 p.m.
total	200 Min	3.480 Kg	

designated route. From Klatovy I, the distance model identifies the closest customer point from this town, which is Klatovy II 2.3 km away. The choice of customer point must take into consideration the capacity of the lorry. The total weight of the cargo is 160 kg (Klatovy I 60 kg; Klatovy II 100 kg), therefore within capacity. It is now necessary to cross out the already visited places in the distance matrix so as to prevent repeat visits to these points. After crossing out the lines and columns for Klatovy I and II, the next stop is Susice (total weight of goods 120 kg). This cycle repeats itself until the capacity of the lorry has been filled and/or the 23 customer points have been visited. Table 4 shows the suggested shipping route.

14.2 Route No. II

The second farthest place (not included in Route I) is Arnestovice some 98 km from the distribution warehouse in Lisov. It is now necessary to identify other customer points closest to Arnestovice, but which have not yet been crossed out in the distance matrix and whilst making sure that each customer point is visited only once. The procedure for this is the same as described for Route I. The total weight of the cargo on Route II is 3 465 kg with an unloading time of 190 minutes.

14.3 Route III

The farthest customer point is Volary, 70.8 km from the distribution warehouse in Lisov. Route III only includes 12 customer points: Volary, Prachatice, Vlachovo Brezi, Strunkovice, Ckyne, Netolice, Ceske Budejovice, Prisecna, Trhove Sviny, Kajov, Borova and Kaplice. The total weight of the cargo is 3 070 kg with an unloading time of 140 minutes.

15 Single linkage method

After dividing the customer points over the three routes, through application of the Mayer's method, it is necessary to arrange the customer points by distance in the shortest possible order. The single linkage method involves considering each customer point as a starting point, with the next closest point being identified as the follow-up

Table 5 *Single linkage method - Route I*

route I	distance
Lisov - Strakonice I - Strakonice II - Strakonice III - Katovice - Horazdovice II - Horazdovice I - Bojanovice - Susice - Susice Volsovy - Klatovy II - Klatovy I - Blatna - Pisek III - Pisek II - Pisek I - Vrcovice - Milevsko - Tyn nad Vltavou I - Tyn nad Vltavou II - Temelin - Vodnany I - Vodnany II - Vodnany III - Lisov	346.8 km

Table 6 *Single linkage method - Route II*

route II	distance
Lisov - Veseli nad Luznici - Sobeslav I - Sobeslav II - Sobeslav III - Tabor - Mlada Vozice II - Mlada Vozice I - Pacov I - Pacov II - Arnestovice - Pelhrimov III - Pelhrimov II - Pelhrimov IV - Pelhrimov I - Pocatky - Studena - Telc - Dacice II - Dacice I - Jindrichuv Hradec I - Jindrichuv Hradec II - Rodvinov - Lisov	330.15 km

Table 7 *Single linkage method - Route III*

route III	distance
Lisov - Ceske Budejovice - Trhove Sviny - Kaplice - Prisecna - Kajov - Borova - Netolice - Strunkovice - Vlachovo Brezi - Prachatice - Volary - Ckyne - Lisov	279.9 km

destination (if it is already included in the solution, the second closest customer point is found). This cycle repeats itself until the circuit is closed. The same procedure applies to all the starting points, with exception of the quasi-starting points, which requires suitable modification of the route [26-27].

15.1 Order of customer points on Route I

The order of customer points on Route I, according to the single linkage method, starts in Lisov, goes to Strakonice I and ends in Lisov. The total distance is 346.8 km. Table 5 shows the shortest route.

Based on that, the total time required to cover the route is calculated and compared to the driver's working hours. The overall unloading time is 200 minutes, net driving time 6:31 hrs, average speed 53 km/h, whilst making sure not to exceed the prescribed 9 hours (after 4.5 hrs the driver is obliged to take a 45-minute break) or 10 hours (if the route takes longer than 9 hours, the driver is entitled to a second break of 45 minutes). The total working time amounts to 636 minutes (10:36 hrs) including the mandatory break of 45 minutes. If the driver starts at 5.55 a.m., he should be back in Lisov no later than 4.45 p.m.

15.2 Order of customer points on Route II

The order of customer points on Route II, according to the single linkage method, starts in Lisov, goes to Veseli nad Luznici and ends in Lisov. The total distance is 330.15 km. Table 6 below shows the shortest route.

As before, the total time required to cover the route is calculated and compared to the driver's working hours. The overall unloading time is 190 minutes, net driving time 6:37 hrs, average speed 52 km/h. The total route time amounts to 587 min + 45 min (mandatory driver's pause). The total working time, including the obligatory break, is 632 minutes. If the driver starts at 5.25 a.m., he should therefore be back in Lisov by 3.57 p.m.

15.3 Order of customer points on Route III

The order of customer points on Route III, according to the single linkage method, starts in Lisov, with the first customer point being in Ceske Budejovice. The total distance is 279.9 km. Table 7 shows the shortest route.

If the driver drives at an average speed of 54 km/h, the net driving time is 5:23 hrs, which, with an unloading time of 140 minutes, plus a 45-minute mandatory break, comes to a total of 508 minutes (8:28 hrs). If the driver starts work at 6.40 a.m., this would mean that he would return to Lisov 3.08 p.m.

16 Application of the intuition method

Experimental findings suggest this method produces the best results (lowest kilometrage). The internet application mapy.cz processed the factual data on addresses of the customers, which were placed in the most convenient order.

16.1 Order of customer points on Route I

The distance of Route I could be cut to 330.2 km. The total time this would take is 6:15 hrs (at an average speed of 53 km/h). The driver's number of working hours = 6:15 hrs + 45 minutes (compulsory break) + 200 minutes (unloading time) = 620 min (10:20 hrs).

16.2 Order of customer points on Route II

Applying the intuition method to Route II produces the three significant changes (for Jindrichuv Hradec I, Jindrichuv Hradec II and Rodvinov), with the rest of the

Table 8 *Comparison of methods - Route I*

method	route I	distance
single linkage method	Lisov - Strakonice I - Strakonice II - Strakonice III - Katovice - Horazdovice II - Horazdovice I - Bojanovice - Susice - Susice Volsovy - Klatovy II - Klatovy I - Blatna - Pisek III - Pisek II - Pisek I - Vrcovice - Milevsko - Tyn nad Vltavou I - Tyn nad Vltavou II - Temelin - Vodnany I - Vodnany II - Vodnany III - Lisov	346.8 km
intuition method	Lisov - Temelin - Tyn nad Vltavou I - Tyn nad Vltavou II - Milevsko - Vrcovice - Pisek III - Pisek II - Pisek I - Blatna - Klatovy I - Klatovy II - Susice Volsovy - Susice - Bojanovice - Horazdovice II - Horazdovice I - Katovice - Strakonice III - Strakonice II - Strakonice I - Vodnany III - Vodnany II - Vodnany I - Lisov	330.2 km

Table 9 *Comparison of methods - Route II*

method	route II	distance
single linkage method	Lisov - Veseli - Sobeslav I - Sobeslav II - Sobeslav III - Tabor - Mlada Vozice II - Mlada Vozice I - Pacov I - Pacov II - Pelhrimov I - Pelhrimov IV - Pelhrimov II - Pelhrimov III - Arnestovice - Pocatky - Studena - Telc - Dacice II - Dacice I - Jindrichuv Hradec I - Jindrichuv Hradec II - Rodvinov - Lisov	330.15km
intuition method	Lisov - Veseli - Sobeslav I - Sobeslav II - Sobeslav III - Tabor - Mlada Vozice II - Mlada Vozice I - Pacov I - Pacov II - Pelhrimov I - Pelhrimov IV - Pelhrimov II - Pelhrimov III - Arnestovice - Pocatky - Studena - Telc - Dacice II - Dacice I - Rodvinov - Jindrichuv Hradec I - Jindrichuv Hradec II - Lisov	326.75 km

Table 10 *Comparison of methods - Route III*

method	route III	distance
single linkage method	Lisov - Ceske Budejovice - Trhove Sviny - Kaplice - Prisecna - Kajov - Borova - Netolice - Strunkovice - Vlachovo Brezi - Prachatice - Volary - Ckyne - Lisov	279.9 km
intuition method	Lisov - Trhove Sviny - Kaplice - Prisecna - Kajov - Borova - Volary - Ckyne - Vlachovo Brezi - Prachatice - Strunkovice nad Blanici - Netolice - Ceske Budejovice - Lisov.	268.4 km

route being identical to that of the best solution of the single linkage method. The distance is 326.75 km, and the net driving time 6:18 hrs at an average speed of 52 km/h. In this case, the driver's number of working hours = 6:18 hrs + 45 minutes (compulsory break) + 190 minutes (unloading time) = 613 minutes (10:13 hrs).

16.3 Order of customer points on Route III

Under the intuition method, the distance of Route III dropped to 268.4 km. The net driving time is 5:05 hrs at an average speed of 53 km/h. In this case, the driver's number of working hours = 5:05 hrs + 45 minutes (compulsory break) + 140 minutes (unloading time) = 490 minutes (8:10 hrs).

17 Evaluation of the optimised routes - Comparison of the single linkage method and intuition method

17.1 Route I - Monday

The shortest route identified by the single linkage method produced worse results than that devised by the intuition method. The reason for this is that the single linkage method line does not reflect the closest and most suitable place. This omission may result in a customer point being ruled out because it is situated in an unfavourable location on the route. Table 8 shows results of application of both methods.

17.2 Route II - Tuesday

In this case, the shortest route identified by the single linkage method also produces the worse result than that devised by the intuition method, but only by a margin of 3.4 km. The difference lies in the single linkage method´s approach to the closest possible place, which excludes the most convenient way. For example, the journey from Dacice I to Jindrichuv Hradec I is the shortest, yet not the handiest route. A more suitable route would be for the driver to first go to Rodvinov and then to Jindrichuv Hradec, saving 3.4 km. Table 9 shows results of application of both methods.

17.3 Route III - Wednesday

Table 10 shows results of application of both methods to Route III. Once again, the intuition method produces the best results. On this route, the driver would therefore unload in Trhove Sviny first.

Table 11 *Comparison of driver's working hours*

routes	current situation (hours)	single linkage method (hours)	intuition method (hours)
route I - Monday	10:36	10:36	10:20
route II - Tuesday	9:33	10:32	10:13
route III - Wednesday	9:51	8:28	8:10
total working hours	30	29:36	28:43

18 Calculation of annual costs

The company currently pays annual transport costs of 31768.32 EUR. Under the single linkage approach, this would be 30904.32 EUR, leading to annual savings of 864 EUR. However, under the intuition method, this would fall even further still to 30057.60 EUR, thereby generating annual savings of 1710.72 EUR.

Current situation: 2647.36 *12 = 31768.32 EUR
Single linkage method: 2575.36 *12 = 30904.32 EUR
Intuition method: 2504.80 *12 = 30057.60 EUR

In percentage terms, the annual savings under the single linkage method would be 2.72%, whilst under the intuition method 5.39%.

19 Calculation of time savings

Evaluating the time savings is another variable that requires consideration. Table 11 compares the driver´s current number of working hours for each route (in total 30 hrs over 3days) to that under the single linkage method (29:36 hours over 3 days) and the intuition method (28:43 hours over 3 days).

20 Conclusion

Firstly, the specific terms used in the article, were defined like the operational research, transportation problem, travelling salesman problem and multiple travelling salesman problems.

An analysis of the company's current situation pointed us towards resolving the multiple travelling salesman problem using the Mayer's method. The very first step was to design a symmetric distance matrix (58 x 58 towns/customer points). The second step consisted of dividing the customer points over three routes with symmetric matrices (24 x 24; 23 x 23; and 13 x 13). The applied methodology connected individual customer points, without thinking about appropriateness of the order in which they were visited. The third stage saw towns and cities (customer points) arranged within the travelling salesman problem through application of the two methods, namely the single linkage method and the intuition method.

The single linkage method helped to put the specific customer points in a particular order, thereby producing the lowest kilometrage. The total distance under this method came to 956.85 km. However, the intuition method produced the lower result, namely a distance of 925.35 km. Both methods provided the shortest routes for the relevant shipping days, whilst maintaining the driver's schedule according to the given time windows.

Overall, the intuition method produced the better results. The main reason for this is that in practice, full integration of the shortest distance does not always produce the most suitable route.

The final part of the work focused on a detailed comparison of the original overall annual transport costs (31768.32 EUR) with those under the single linkage method (30904.32 EUR; savings of 2.72%) and the intuition method (30057.60 EUR; savings of 5.34%). Evaluation of these approaches also enabled a comparison to be made of the driver´s working hours on each route and in total according to the two methods applied. Under the current situation this is 30 hrs over 3 days, under the single linkage method 29:36 hrs over 3 days and under the intuition method 28:43 hrs over 3 days.

In conclusion, the optimisation process under the intuition method was found to generate savings of 1710.72 EUR, which is a valuable contribution to the company´s economic results.

References

[1] JABLONSKY, J. *Operational research* (in Czech). 2. ed. Prague: Vysoka skola ekonomicka, 1999. ISBN 80-7079-597-2.

[2] JOVCIC, S., PRUSA, P., DOBRODOLAC, M., SVADLENKA, L. A Proposal for a decision-making tool in third-party logistics (3PL) provider selection based on multi-criteria analysis and the fuzzy approach. *Sustainability* [online]. 2019, **11**(15), 4236. eISSN 2071-1050. Available from: https://doi.org/10.3390/su11154236

[3] STROHMANDL, J., CEMPIREK, M. Experimental measurements used to reduce emergency situations of environmental continuous transport. In: 20th International Scientific Conference Transport Means 2016: proceedings. Kaunas University of Technology, 2016. p. 835-839. FABIANOVA, J., KACMARY, P., JANEKOVA, J. Operative production planning utilising quantitative forecasting and Monte Carlo simulations. *Open Engineering* [online]. 2019, **9**(1), p. 613-622. eISSN 2391-5439. Available from: https://doi.org/10.1515/eng-2019-0071

[4] STOPKA, O., JERABEK, K., STOPKOVA, M. Using the operations research methods to address distribution tasks at a city logistics scale. *Transportation Research Procedia* [online]. 2020, **44**, 348-355. ISSN 2352-1465. Available from: https://doi.org/10.1016/j.trpro.2020.02.032

[5] VIEIRA, C. L. S., LUNA, M. M. M. Models and methods for logistics hub location: a review towards transportation networks design. *Pesquisa Operacional* [online]. 2016, **36**(2), p. 375-397. ISSN 0101-7438, eISSN 1678-5142. Available from: https://doi.org/10.1590/0101-7438.2016.036.02.0375

[6] FEDORKO, G, MOLNAR, V., HONUS, S., NERADILOVA, H., KAMPF, R. The application of simulation model of a milk run to identify the occurrence of failures. *International Journal of Simulation Modelling* [online]. 2018, **17**(3), p. 444-457. ISSN 1726-4529. Available from: https://doi.org/10.2507/Ijsimm17(3)440

[7] MAIOROV, N., FETISOV, V., KRILE, S., MISKOVIC, D. Simulation of the route network and ferry traffic intensity based on the process of discretization and circos plot intensity diagram. *Transport Problems*. 2019, **14**(4), p. 23-30. ISSN 1896-0596, eISSN 2300-861X. Available from: https://doi.org/10.20858/tp.2019.14.4.2

[8] HOLOUBEK, J. *Economic and mathematical methods* (in Czech). 2. ed. Brno: Mendel University in Brno, 2010. ISBN 978-80-7375-411-2.

[9] CEJKA, J., BARTUSKA, L., TURINSKA, L. Possibilities of using transport terminals in South Bohemian region. *Open Engineering* [online]. 2017, **7**(1), p. 55-59. eISSN 2391-5439. Available from: https://doi.org/10.1515/eng-2017-0010

[10] KUBASAKOVA, I., KUBANOVA, J. The usage of simulation road transport for company operating on the market. In: International Conference Transport Means 2019: proceedings. 2019.

[11] PELIKAN, J. *Practicum in operational research* (in Czech). Prague: University of Economics, 1993. ISBN 80-7079-135-7.

[12] GEORGIJEVIC, M., BOJIC, S., BRCANOV, D. The location of public logistic centers: an expanded capacity-limited fixed cost location-allocation modeling approach. *Transportation Planning and Technology* [online]. 2013, **36**(2), p. 218-229. ISSN 0308-1060, eISSN 1029-0354. Available from: https://doi.org/10.1080/03081060.2013.770945

[13] MATTEO, U. D., PEZZIMENTI, P. M., ASTIASO GARCIA, D. Methodological proposal for optimal location of emergency operation centers through multi-criteria approach. *Sustainability*. 2016, **8**(1), 50. eISSN 2071-1050. Available from: https://doi.org/10.3390/su8010050

[14] TOMKOVA, E., MIKUSOVA, N. Application of the competitiveness model in city Poprad. In: Economic and Management Forum PEMF 2019: proceedings. Ruzomberok: Verbum - Catholic University in Ruzomberok Press, 2019. ISBN 978-80-561-0671-6, p. 332-342.

[15] FEDORKO, G., HEINZ, D., MOLNAR, V., BRENNER, T. Use of mathematical models and computer software for analysis of traffic noise. *Open Engineering* [online]. 2020, **10**(1), p. 129-139. eISSN 2391-5439. Available from: https://doi.org/10.1515/eng-2020-0021

[16] SUBRT, T. *Economic and mathematical methods* (in Czech). Plzen: Vydavatelstvi a nakladatelstvi Ales Cenek, 2011. ISBN 978-80-7380-345-2.

[17] SIPUS, D., ABRAMOVIC, B. The possibility of using public transport in rural area. *Procedia Engineering* [online]. 2017, **192**, p. 788-793. ISSN 1877-7058. Available from: https://doi.org/10.1016/j.proeng.2017.06.136

[18] ZISKAL, J., HAVLICEK, J. *Economic mathematical methods: study texts for distance learning* (in Czech). Prague: Credit, 1999. ISBN 80-213-0510-x.

[19] STOPKA, O., BARTUSKA, L., KUBASAKOVA, I. Selecting the most suitable region in the selected country for the placement of the bi-modal freight village using the WSA method. In: 9th International Conference Intelligent Technologies in Logistics and Mechatronics Systems ITELMS 2014: proceedings. 2014. p. 238-243.

[20] MIRCETIC, D., NIKOLICIC, S., MASLARIC, M., RALEVIC, N., DEBELIC, B. Development of S-ARIMA model for forecasting demand in a beverage supply chain. *Open Engineering* [online]. 2016, **1**, p. 407-411. eISSN 2391-5439. Available from: https://doi.org/10.1515/eng-2016-0056

[21] FRIEBELOVA, J. *Operational analysis* (in Czech). Ceske Budejovice: Faculty of Economics of the University of South Bohemia, 2009. ISBN 978-80-7394-193-2.

[22] ZITRICKY, V., GASPARIK, J., PECENY, L. The methodology of rating quality standards in the regional passenger transport. *Transport Problems* [online]. 2015, **10**, p. 59-72. ISSN 1896-0596, eISSN 2300-861X. Available from: https://doi.org/10.21307/tp-2015-062

[23] Methods of systematic and creative problem solving - European Social Fund Prague & EU (in Czech) [online] [accessed 2017-02-02] Prague, 2011. Available at: http://kem.vscht.cz/files/uzel/0012237/7.%20Metody%20systematick%C3%A9ho%20%C5%99e%C5%A1en%C3%AD.pdf?redirected

[24] Mapy.cz (in Czech) [online] [accessed 2017-02-02]. 2017. Available at: https://mapy.cz/zakladni?x=14.0970000&y=49.9847980&z=11

[25] Current price of petrol, price of diesel - Kurzy.cz (in Czech) [online] [accessed 2017-01-02]. 2017. Available at: http://www.kurzy.cz/komodity/benzin-nafta-cena/

[26] GHADI, M., TOROK, A. A comparative analysis of black spot identification methods and road accident segmentation methods. *Accident Analysis and Prevention* [online]. 2019, **128**, p. 1-7. ISSN 0001-4575. Available from: https://doi.org/10.1016/j.aap.2019.03.002

[27] CHEN, K.-H., LIAO, C.-N., WU, L.-C. A selection model to logistic centers based on TOPSIS and MCGP methods: the case of airline industry. *Journal of Applied Mathematics* [online]. 2014, 470128, p. 1-10. ISSN 1110-757X, eISSN 1687-0042. Available from: https://doi.org/10.1155/2014/470128

University of Žilina

In its over 65 years of successful existence, the University of Žilina (UNIZA) has become one of the top universities in Slovakia.

The mission of UNIZA is to develop education on the basis of science, research and art activities within national and democratic traditions, to develop harmonic personality, knowledge, the good and creativity of a man and to contribute to the advancement of education, science, and culture for the welfare of the whole society.

Professional profile of UNIZA is unique and includes transport (road, railway, water, air), transport and postal services, communications, civil engineering construction, electrical engineering, telecommunications, informatics, information and communication technologies, management and marketing, mechanical engineering, materials and technologies, robotics, machinery design, energies, civil engineering, crisis and security management, civil security, fire protection, forensic engineering, applied mathematics, teacher training, library and information sciences, social pedagogy and high mountain biology. Results of science and research activities of the University have an important influence not only on the educational activities but also on the development of international cooperation or interconnection with practice.

UNIVERSITY PARTS
7 faculties
11 research and educational institutes and centres
3 specialized professional and training workplaces
1 economic and administrative department
4 dedicated facilities

SCIENCE AND RESEARCH
688 creative workers
875 000 hours, annual research capacity
200 domestic scientific projects
39 foreign projects
29 scientific and technical journals
60 scientific and professional events per year

EDUCATION
7 faculties
8 000 students
84 000 graduates
180 study programmes

INTERNATIONAL COOPERATION
50 valid university bilateral agreements
255 collaborating universities
29 foreign non-research projects
377 ERASMUS+ agreements

UNIVERSITY OF ŽILINA
Science & Research Department
Univerzitná 8215/1, 010 26 Žilina, Slovakia
Ing. Janka Macurová
tel.: +421 41 513 5143
e-mail: janka.macurova@uniza.sk

INFLUENCE OF THE LOAD DISTRIBUTION AND SIZES ON THE WHEEL GEOMETRY IN PASSENGER CARS

Jarosław Gonera*, Jerzy Napiórkowski, Kamil Ciborowski

Department of Vehicle and Machine Construction and Operation, University of Warmia and Mazury in Olsztyn, Olsztyn, Poland

*E-mail of corresponding author: jaroslaw.gonera@uwm.edu.pl

Resume

This paper discusses impact of changes in the load size and distribution in passenger cars on geometry of the suspension and steering systems. It was found to have a major impact on the road safety. The research was carried out with the four most popular suspension system designs used in modern passenger cars, i.e. multi-link suspension on both front and rear axles, only on the front axle, only on the rear axle and a simple suspension design for both front and rear axles. Eight load variants were used for the tests. Changes in the following wheel geometry parameters were identified: toe-in and camber angles of all the wheels and castors for the front wheels. The numerical relationships were determined between the load distribution and sizes and changes in suspension and steering systems in passenger cars. It was found that cars with multi-link suspension in both front and rear axles adapt best to changes in weight and load distribution.

Article info

Received 23 January 2020
Accepted 11 June 2020
Online 21 October 2020

Keywords:

wheel geometry,
suspension,
simulated weight and load distributions,
cars

Available online: https://doi.org/10.26552/com.C.2021.1.B1-B12

ISSN 1335-4205 (print version)
ISSN 2585-7878 (online version)

1 Introduction

In modern vehicles, manufacturers have introduced numerous changes in design, which contributed to an increase in safety during their operation [1-3]. For modern cars intended to provide good performance to drivers, it is necessary to introduce more safety systems and more advanced structures of suspension and steering systems, which improve driving quality and greatly reduce the risk of accidents [4-6]. It is a common belief that the active safety is related to design of the suspension and steering systems, which provide the possibility of a quick and precise response to prevent occurrence of an accident or a road collision [7-11]. It should be stressed that quite often such factors are listed as having an impact on the active safety of a vehicle along with the technical conditions of the suspension and steering systems and, above all, their correct mounting and alignment, appropriate traction properties and optimal load distribution between the axles, [12-13]. Changes in geometry of the suspension and steering systems reduce a vehicle's stability and may cause problems with controlling the vehicle and maintaining the driving track assumed by the driver under the influence of varied disturbances affecting the vehicle [13-15].

During the vehicle operation, various forces and moments, resulting from traffic conditions, are transferred to vehicle suspension and steering systems, as well as to its body. Those are related to interaction of forces and moments resulting from unavoidable environmental conditions, such as the condition of the road surface, kerbs, etc. [16]. A car is a complex system, which is subjected to influence of varied dynamic forces and environmental conditions with a wide frequency range [17]. The literature distinguishes two main types of loads acting on a vehicle: static and dynamic [18-19]. In the first case, they are related to loading of the car body with a torsional moment, resulting from application of forces from the suspension system, from the surface and the bending moment, resulting from the weight of the vehicles, driver, passengers and transported load. In the latter case, however, they are result of conditions related to the speed and acceleration of the car, as well as the conditions acting on a vehicle when taking a turn, driving on bumps, braking and accelerating [18-20].

The structural changes in contemporary suspension systems are mainly aimed at improving the comfort of the driver and passengers and at improving the precision of driving [21-23]. The suspension system of a modern vehicle largely reduces the forces, reaction forces and vibrations transmitted to the car body from the road [24-25]. The issue of changes in the wheel geometry, depending on the load, was discussed in [26-27]. It was found that in the suspension systems with a simpler and less complex design (e.g. McPherson's column, torsion-beam axle), parameters affecting stiffness and responsible for control of a vehicle (e.g. toe-in, castor) are subject to significant changes depending on the changing load conditions. This limits precise vehicle control and stability during driving. The resulting changes in the wheel geometry may also

Table 1 *Characteristics of the research object*

model	front axle suspension type	rear-axle suspension type
A1	independent - McPherson	independent - multi-link
A2	independent - McPherson	independent - multi-link
B3	independent - McPherson	semi-dependent - with torsional beam
B4	independent - McPherson	semi-dependent - with torsional beam
C5	independent - multi-link	semi-dependent - with torsional beam
C6	independent - multi-link	semi-dependent - with torsional beam
D7	independent - multi-link	independent - multi-link
D8	independent - multi-link	independent - multi-link

a) *b)*

Figure 1 *Autoboss A860: a. control unit with heads; b. measuring head mounted on a wheel*

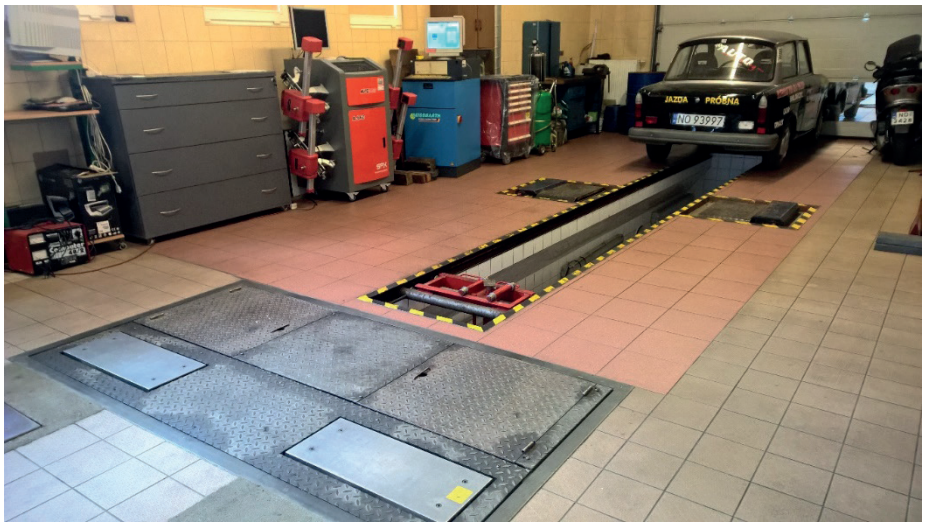

Figure 2 *Beissbarth STL7000 diagnostic line*

contribute to higher tyre wear [28]. Unfortunately, there are still no construction solutions to guarantee driving steering with changes in the load sizes and distribution [21, 23-24, 27].

This study analysed impact of changes in size and distribution of the load in a passenger car on parameters of the wheel geometry in vehicles with different suspension system designs.

2 The test procedure

The study was carried out on passenger cars characterized by varied structure of the front and the suspension system of a rear axle. All of the vehicles were equipped with a rack and pinion steering gear with power steering. This solution is present in most modern passenger cars. The tested vehicles had similar weight and external

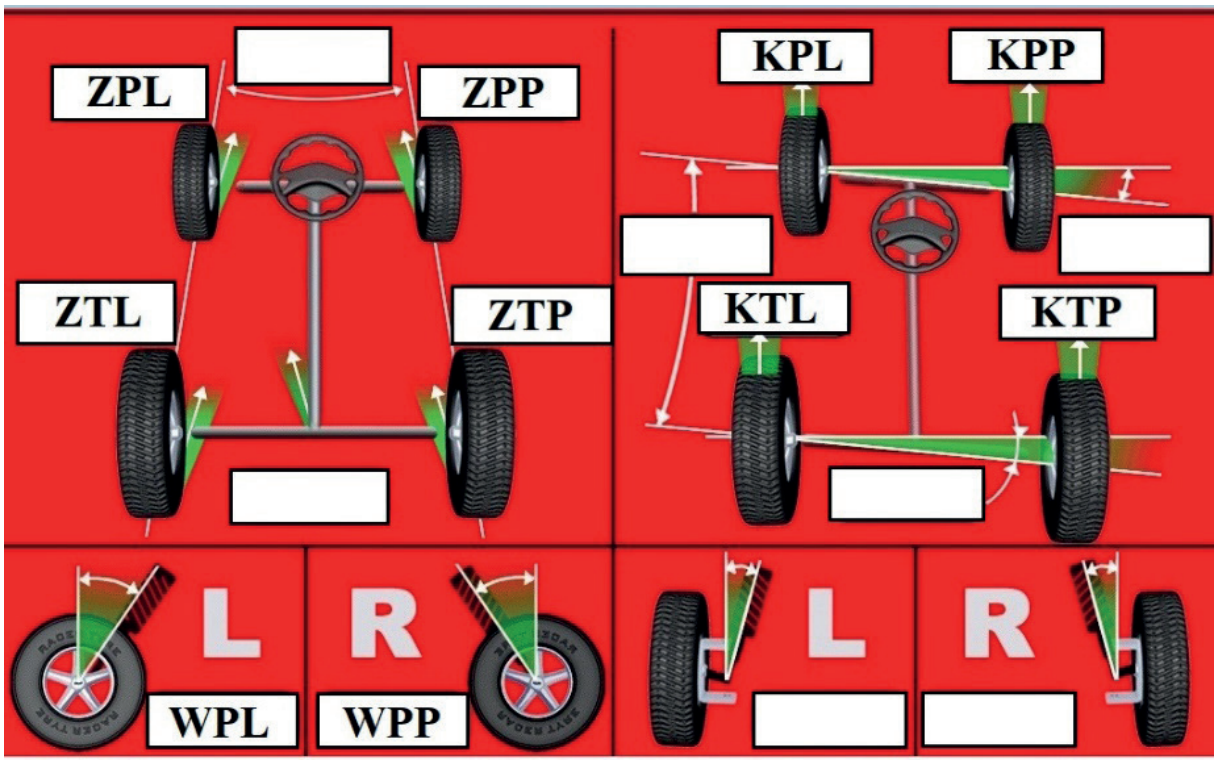

Figure 3 *Parameters related to wheel geometry: ZPL- toe-in for the left front axle wheel; ZPP - toe-in for the right front axle wheel; KPL - camber for the left front axle wheel; KPP - camber for the right front axle wheel; WPL - castor for the left front axle wheel; WPP - castor for the right front axle wheel; ZTL - toe-in for the left back axle wheel; ZTP - toe-in for the right back axle wheel; KTL - camber for the left back axle wheel; KTP - camber for the right back axle wheel*

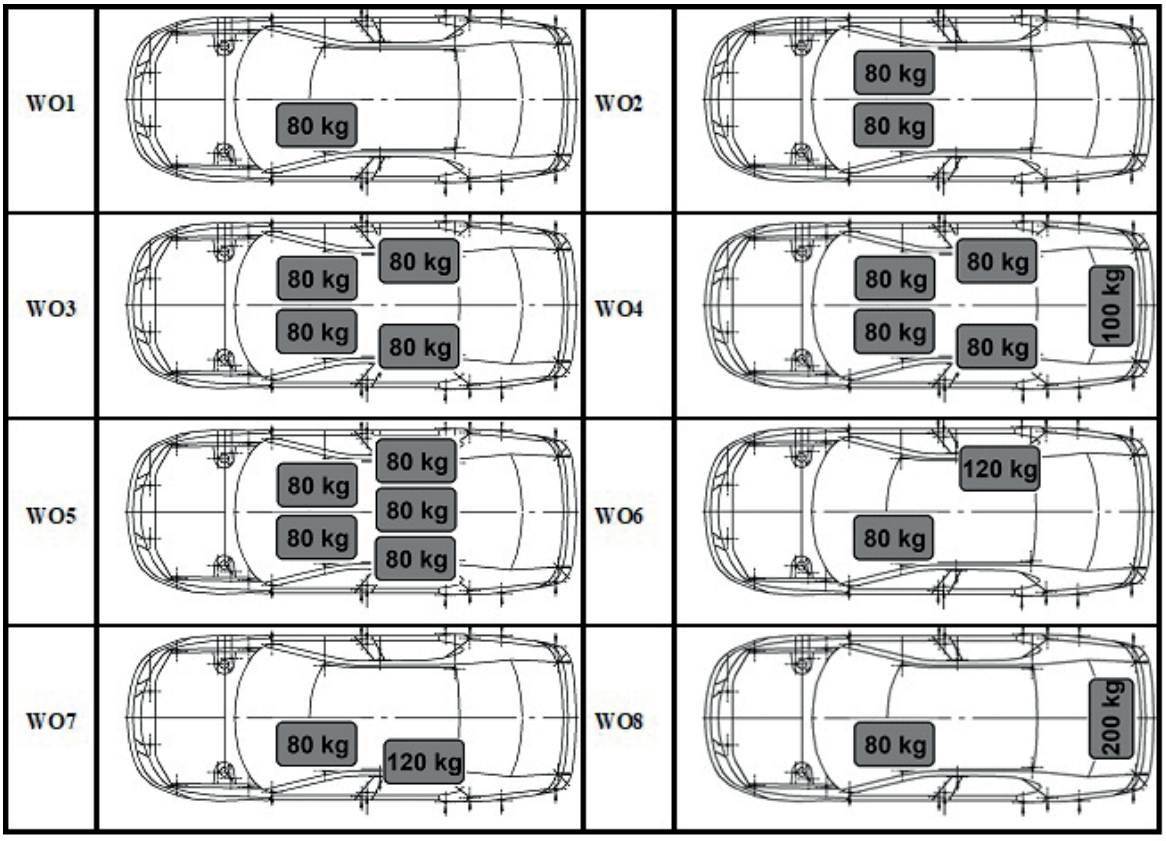

Figure 4 *Simulated weight and load distributions*

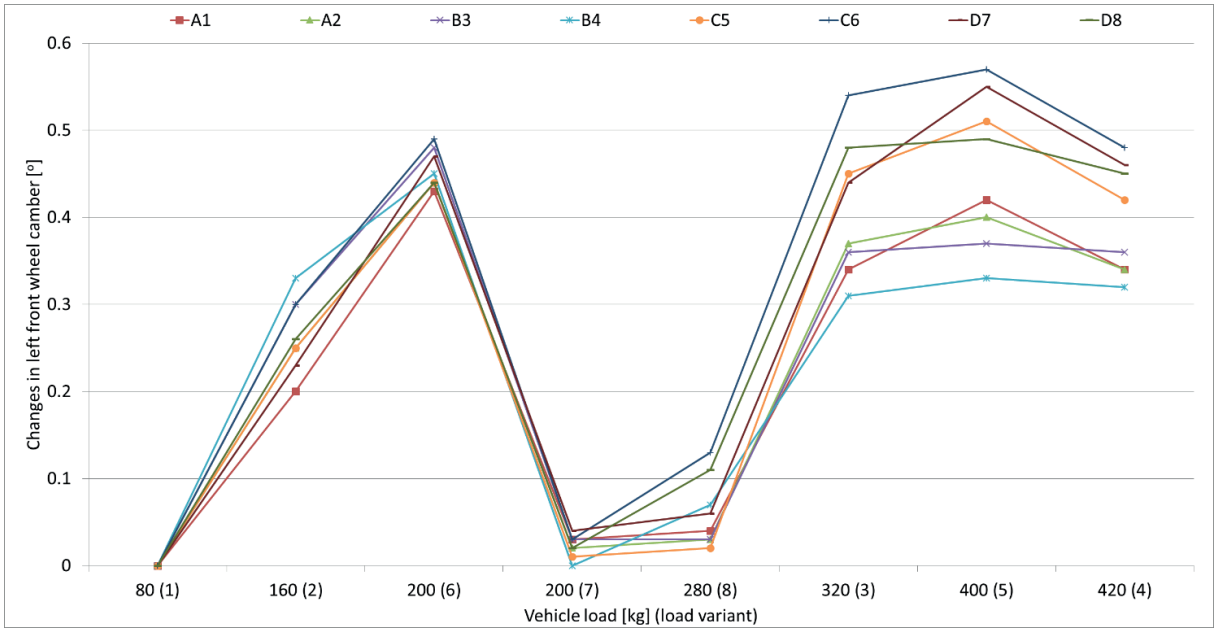

Figure 5 *Dependency of changes in the left front wheel camber on the weight distribution*

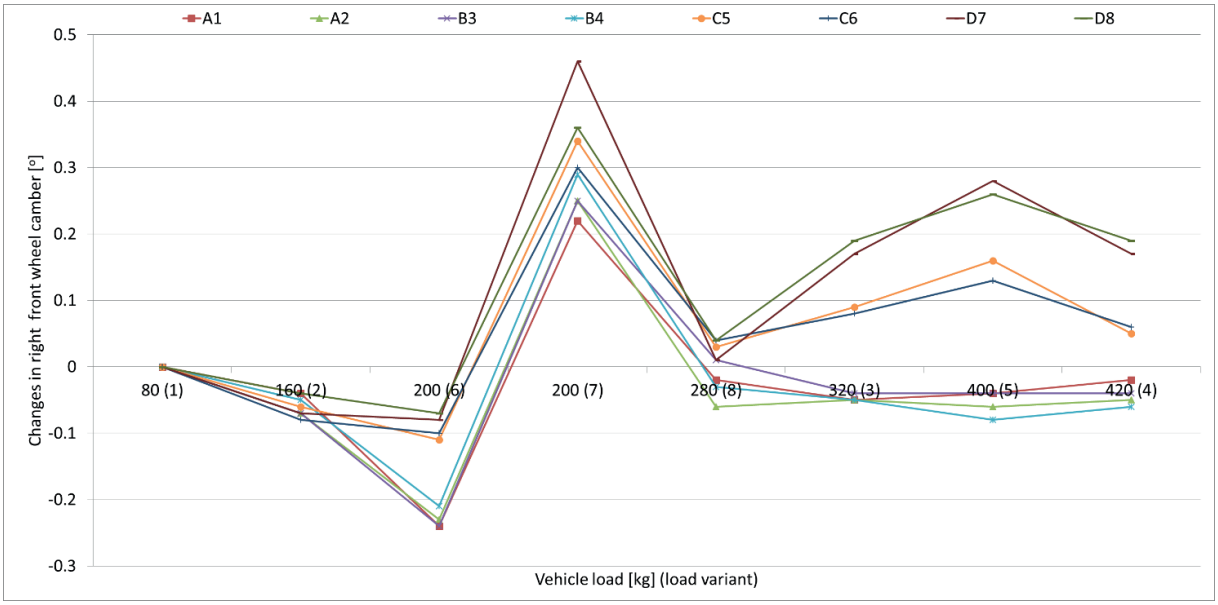

Figure 6 *Dependency of changes in the right front wheel camber on the weight distribution*

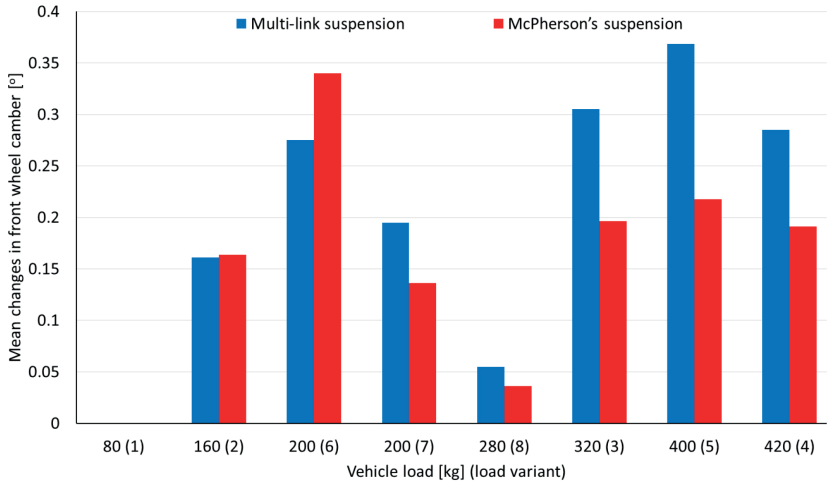

Figure 7 *Breakdown in camber changes for the front wheel depending on the suspension type*

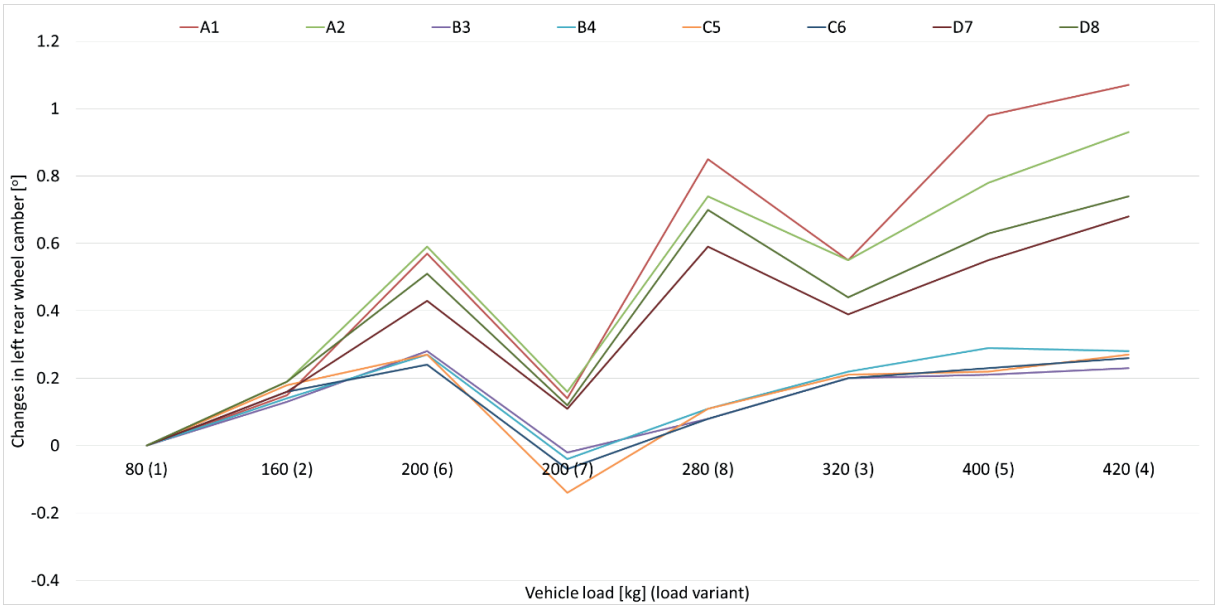

Figure 8 *Dependency of changes in the left rear wheel camber on the weight distribution*

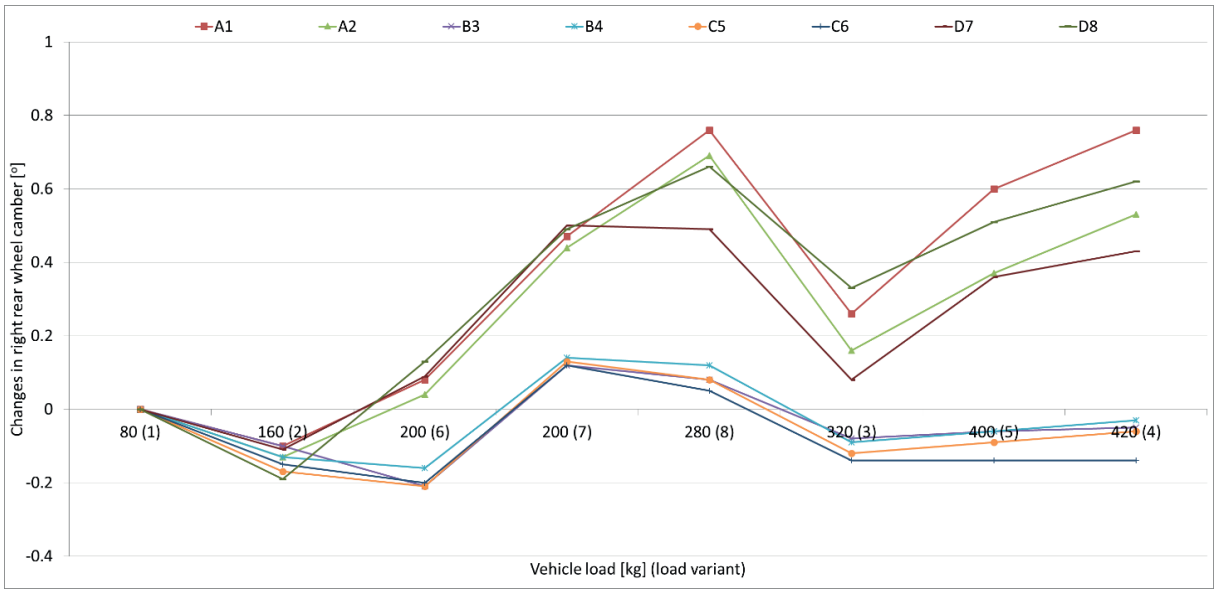

Figure 9 *Dependency of changes in the right rear wheel camber on the weight distribution*

dimensions. Table 1 presents detailed characteristics of vehicles.

Measurements of geometry of the suspension and steering systems were carried out with the Autoboss A860 computer-laser device (Figure 1a) with an accuracy of 1'. It consisted of a Pc-based control unit with a dedicated piece of software installed and four heads (Figure 1b). They were assembled on individual wheels of the vehicle. During the measurements, the heads communicated wirelessly and transmitted information to the control unit. The Beissbarth STL7000 diagnostic line, equipped with the Micro-Swing 6200 module, was used to measure the load and weight distribution on vehicle axles (Figure 2).

During the preliminary tests, it was verified whether the vehicles had correct geometry of the suspension and steering systems. It was found that none of the tested wheel geometry parameters exceeded the permissible values.

During the basic tests, the wheel geometry parameters were measured, as shown in Figure 3.

During the basic tests, each vehicle was loaded with the same weight placed in the same place. Eight load variants were analysed, as graphically shown in Figure 4. The vehicles were loaded with specially prepared lead bars, which were placed on the front seats, back seat and in the boot.

3 Analysis of the test results

The camber of the left front wheel (Figure 5) and the right front wheel (Figure 6) changed significantly with

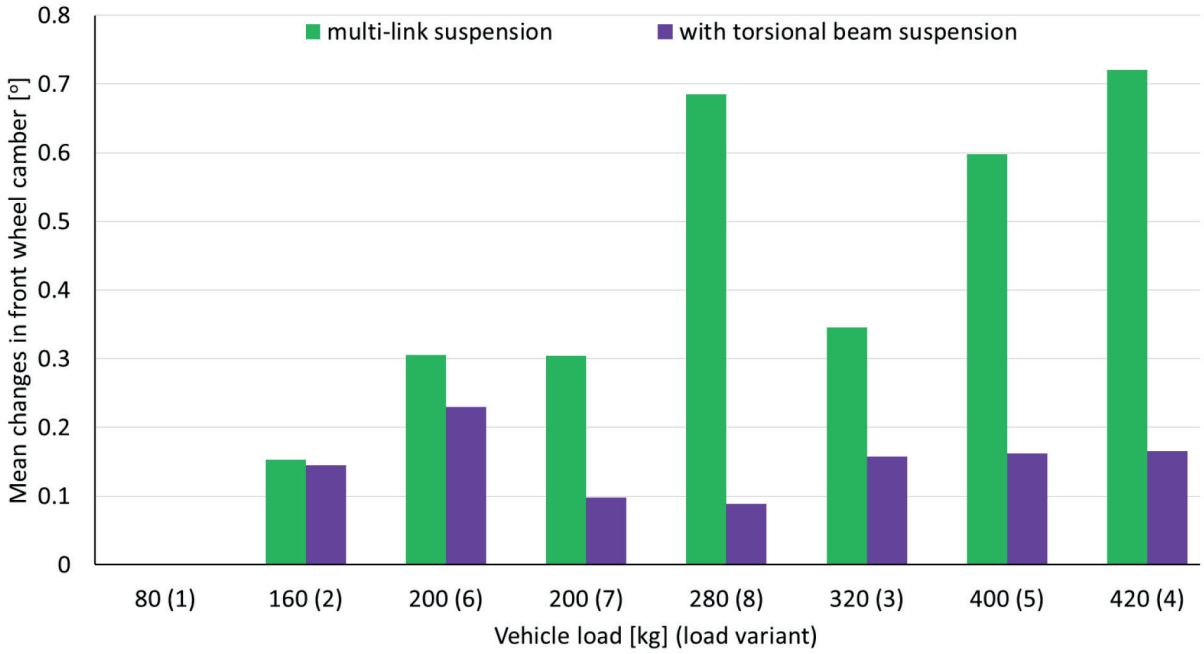

Figure 10 *Breakdown in camber changes for rear wheel depending on the suspension type*

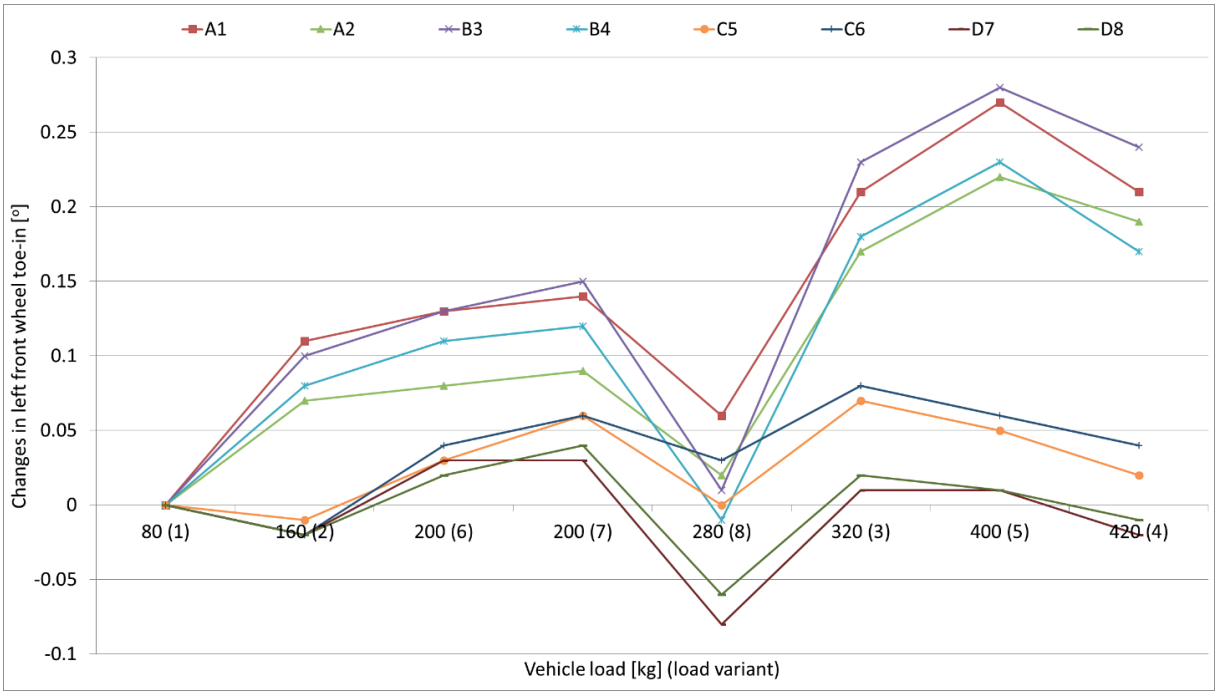

Figure 11 *Dependency of changes in the left front wheel toe-in on the weight distribution*

changes in the load sizes and load distribution. On the left-hand side, this parameter reached top values in most vehicles for variants with heavy load (320, 400 and 420 kg) and symmetrical weight distribution, as well as with asymmetrical weight distribution under relatively low load (200 kg). It was found that in the case of vehicles with multi-link suspension, greater changes for this angle were recorded than in vehicles with McPherson columns. They reached, respectively, +0.58° and +0.4° with the vehicle loaded with a weight of 400 kg, placed in the passenger cabin. In the case of the front right wheel, the top values were already reached for much lower loads with the whole load being on the left-hand side of a vehicle. Change in the right front wheel camber during the simulation of some load variants recorded large positive and negative values for some of the load variants. For example, when the vehicle was loaded with 200 kg, the large positive values of the front right wheel camber were found, reaching up to +0.48°. That was also the case when the weight was placed on the driver's seat and on the back seat on the

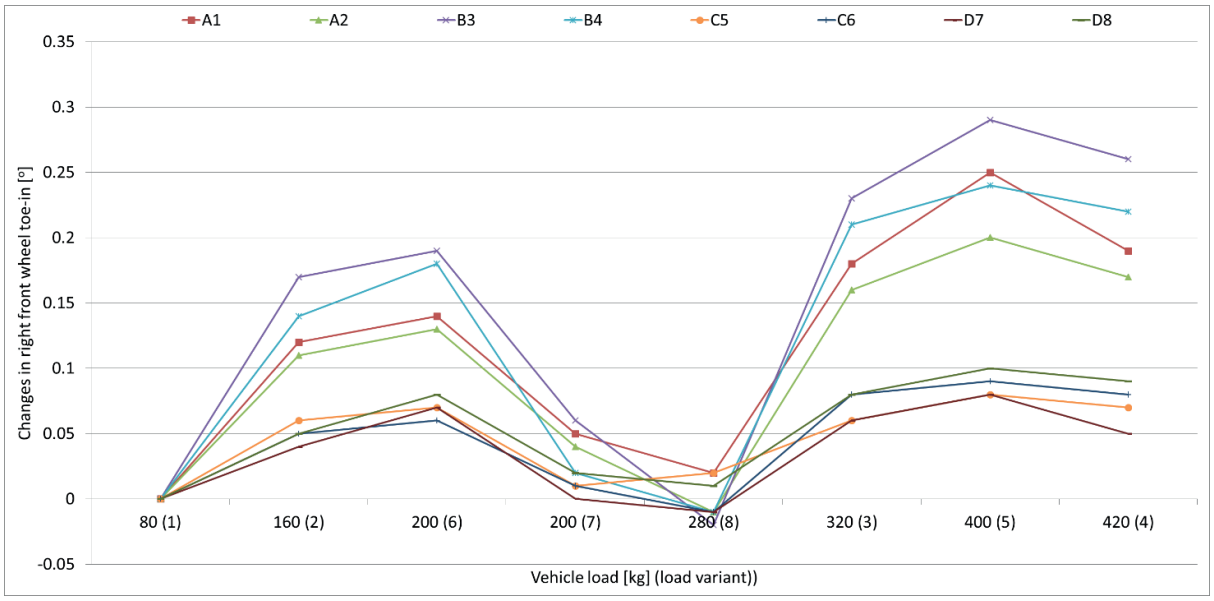

Figure 12 *Dependency of changes in the right front wheel toe-in on the weight distribution*

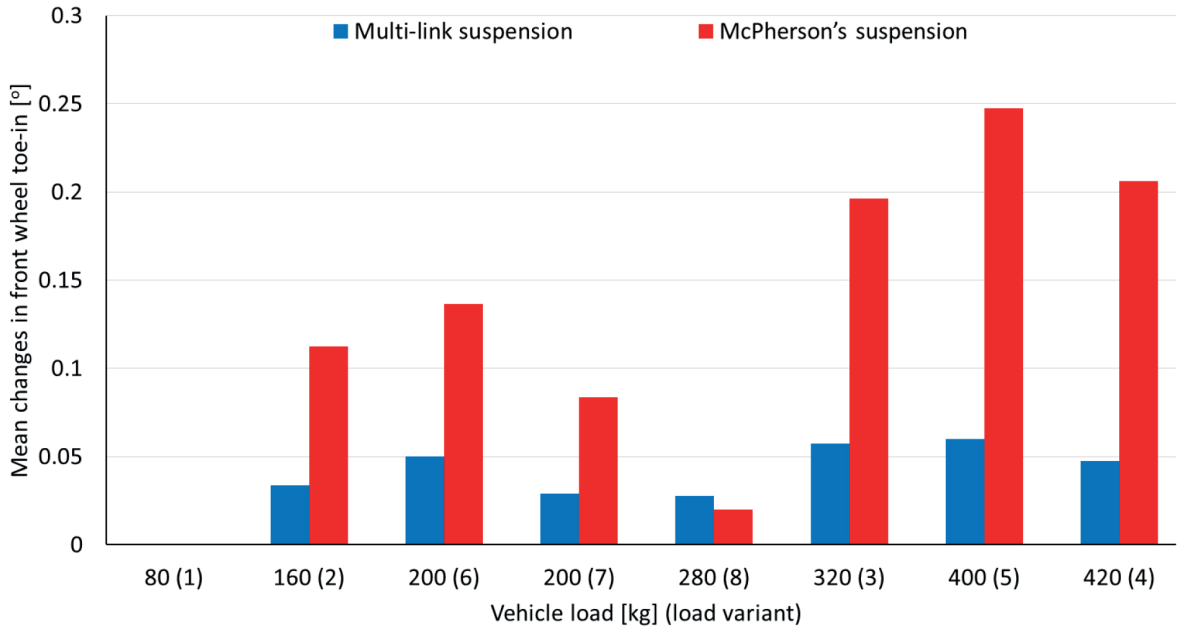

Figure 13 *Breakdown in the toe-in changes for the front wheel depending on the suspension type*

left-hand side of a vehicle. However, the negative values, reaching -0.23°, were observed in cars under the same load but applied to the driver's seat and to the back seat on the right-hand side of a vehicle.

In the case of a camber of both front wheels, larger changes depending on the load were observed in cars with multi-link front axle suspension than in cars with the McPherson column (Figure 7). This is fairly beneficial as it improves grip when taking turns. A car with a multi-link suspension better adapts to changing load conditions and varying weight distribution. Better tyre adhesion to the road surface is also observed when driving straight ahead and braking.

In cars with the multi-link rear axle suspension, changes in load entailed significant changes in the left (Figure 8) and right (Figure 9) rear wheel cambers. In vehicles with the relatively simple rear suspension system, consisting of a torsion beam, those changes were much smaller and amounted to a maximum of +0.28°. For vehicles with multi-link suspension, these changes were several times greater and reached up to +1.07°. In cars with the multi-link rear axle suspension, changes in camber for both rear wheels assumed positive values after loading. On the other hand, in cars with a torsional beam, in most cases, positive values for the left wheel, but negative values for the right wheel were observed. This was related to distribution of weight on specific wheels when loading the vehicle.

In cars with a relatively simple rear axle suspension based on a torsion beam with higher load sizes and symmetrical weight distribution, a change in castor for

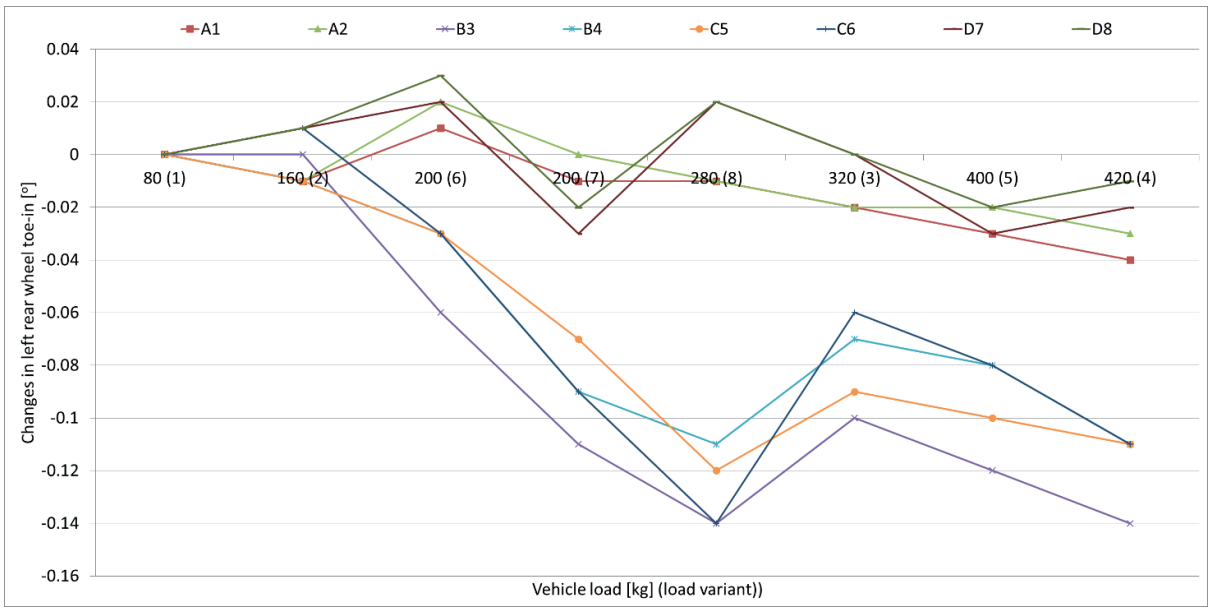

Figure 14 *Dependency of changes in the left rear wheel toe-in on the weight distribution*

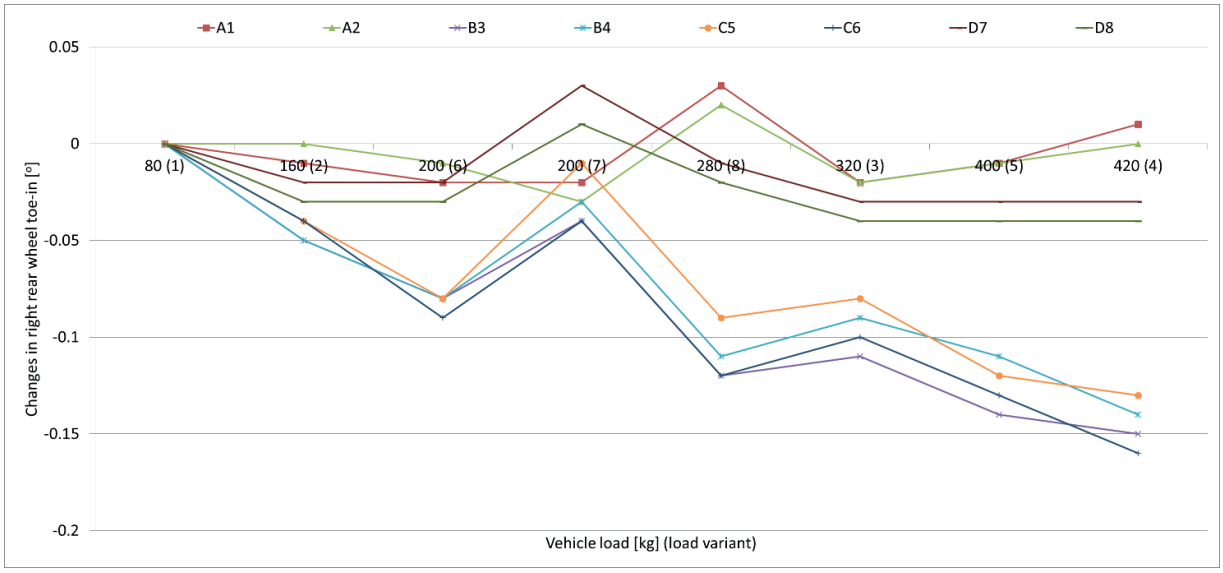

Figure 15 *Dependency of changes in the right rear wheel toe-in on the weight distribution*

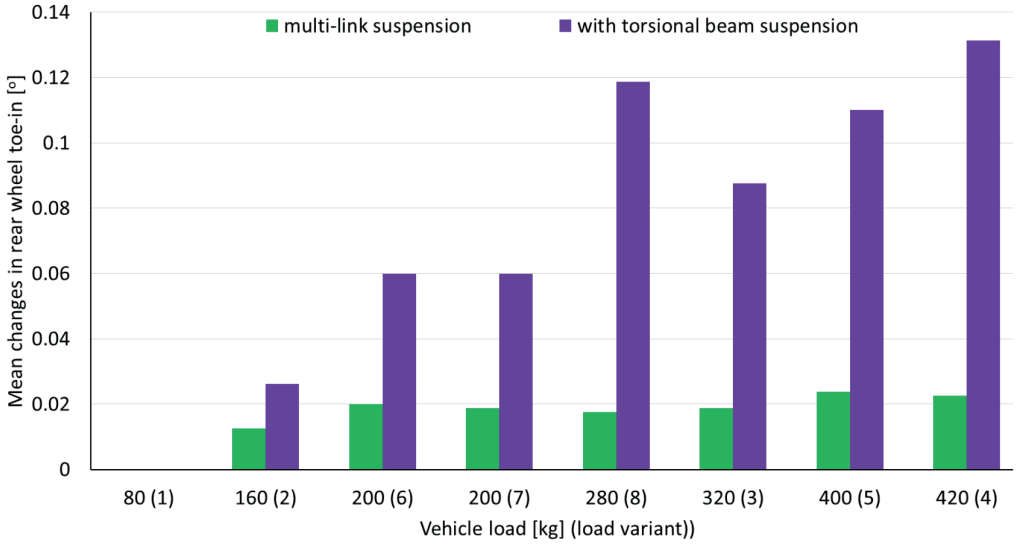

Figure 16 *Breakdown in the toe-in changes for the front wheel depending on the suspension type*

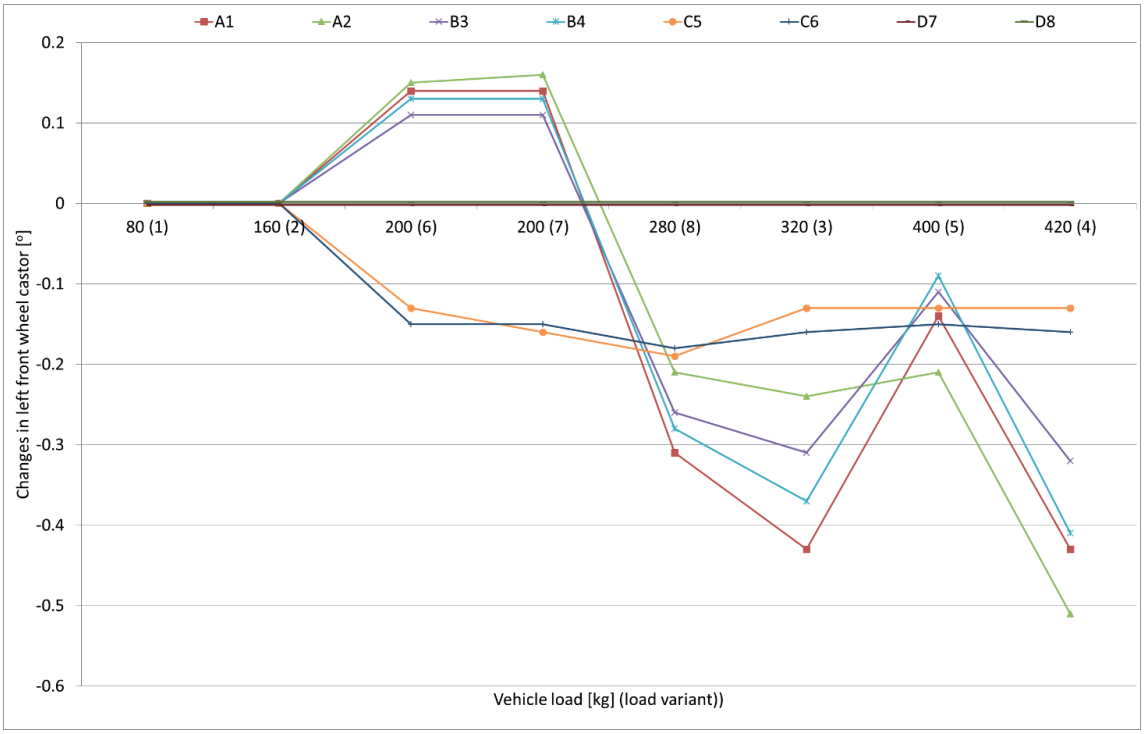

Figure 17 *Dependency of changes in the left front wheel castor on the weight distribution*

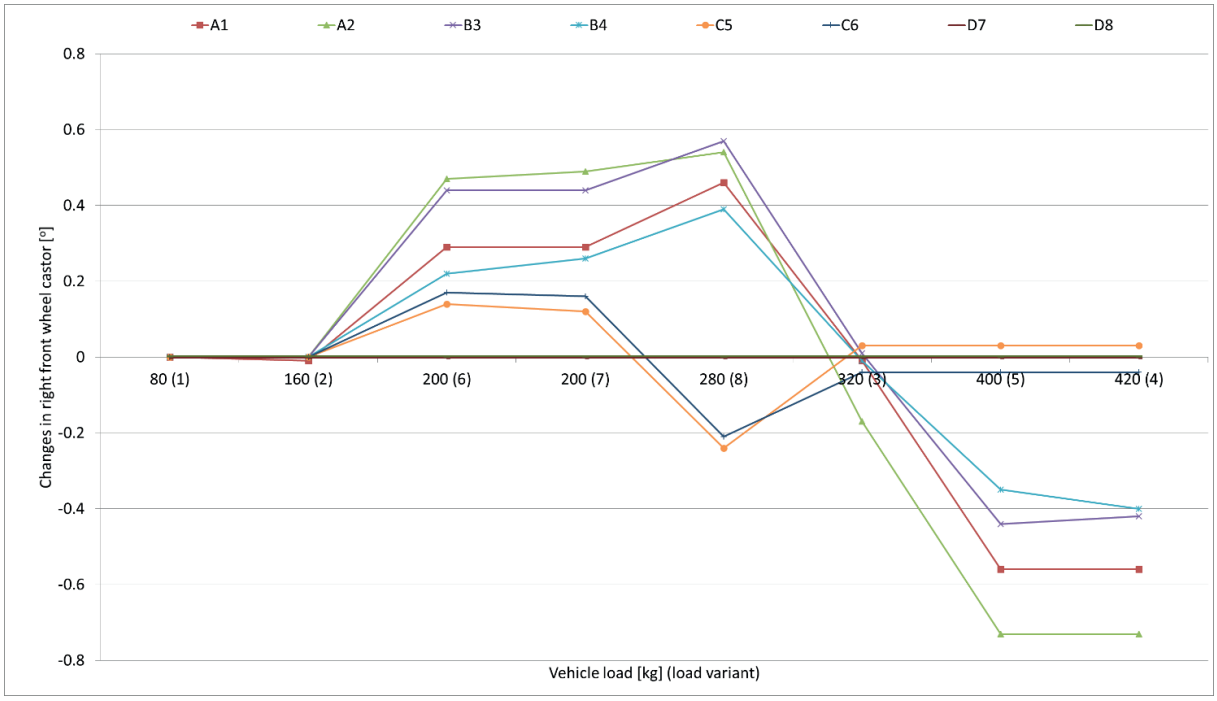

Figure 18 *Dependency of changes in the right front wheel castor on the weight distribution*

both rear wheels (Figure 10) was only observed to a limited extent, despite significant load (320, 400 and 420 kg). Unfortunately, this is an unfavourable feature since, for this reason, the vehicle may drive much worse when loaded. It may lead to wheels not having adequate grip, especially when driving on a curvilinear track.

In each of the tested cars, toe-in for both front wheels changed together with changes in load size and distribution. Much smaller changes occurred in cars with the multi-link front axle suspension. For example, changes of the toe-in of the left front wheel (Figure 11) did not exceed +0.08°. On the other hand, in cars with the McPherson-type

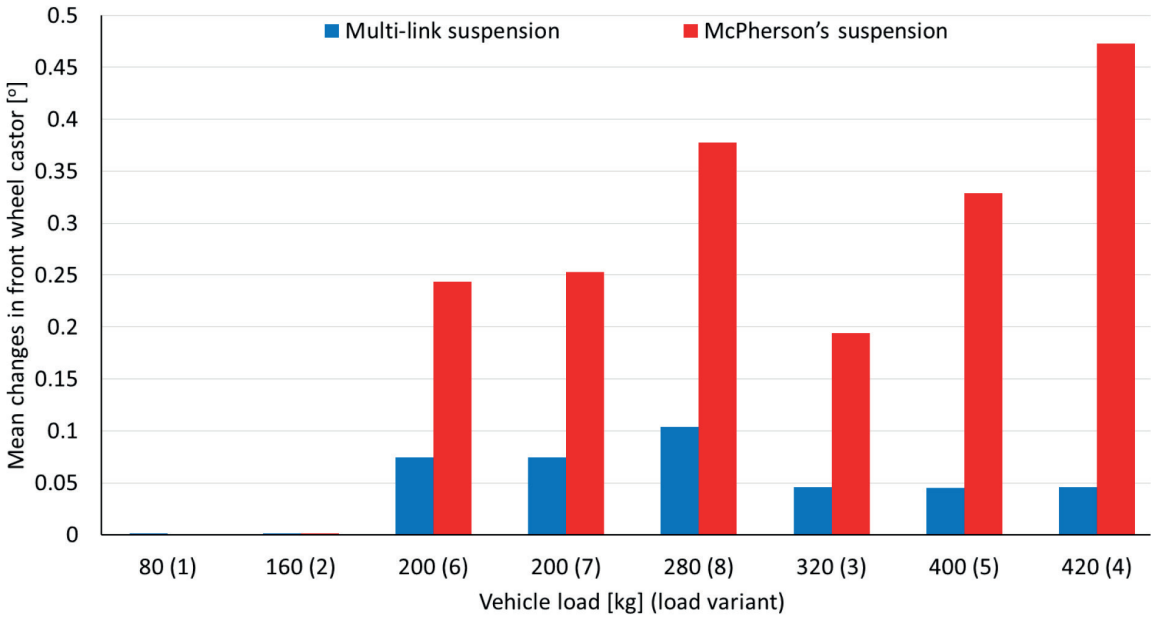

Figure 19 *Breakdown in castor changes for the front wheel depending on the suspension type*

suspension, greater changes were observed, reaching even +0.28° when loaded with 400 kg placed in the passenger space. In cars with the multi-link suspension, changes in the toe-in took both positive and negative values depending on the load, which is due to the specific design of this type of suspension and better adaptation to changes in load, which positively affects driving. Similar values of changes were obtained for the front right wheel toe-in (Figure 12). Values of this parameter increased with practically every simulated load variant in the all cars. In addition, in the case of this parameter, smaller changes in the toe-in after loading occurred in cars with the multi-link suspension, with a maximum of +0.1°. In turn, in cars with the McPherson-type suspension, these changes were almost three times greater (+0.29°).

The toe-in determines stability of a vehicle when driving on a straight track, precision of the response when driving on a curvilinear track and e degree of the tyre wear and fuel consumption. Changes in this parameter are strictly dependent on the vehicle load. In cars with the multi-link suspension, changes in the toe-in of the front axle wheels (Figure 13) were less dependent on the size and distribution of the load during the driving.

For the rear axle toe-in, it is also advantageous that changes in this parameter were as small as possible (depending on the load). For the left rear wheel (Figure 14), relatively small variations in the toe-in were observed depending on the load size and distribution in cars with the multi-link rear axle suspension. These changes did not exceed -0.04°. Much larger changes occurred in vehicles with the torsion beam suspension in the rear axle. In this case, changes were several times greater and reached -0.14°. Particularly large changes occurred after loading the rear part of a vehicle. This was the load variant no 4, where a weight of 320 kg was distributed symmetrically in the passenger cabin and a weight of 100 kg was additionally placed in the boot and variant no 8 in which, in addition to the driver's own weight, the car was also loaded with a 200 kg load placed in the boot. In the simulated load variants, changes in the rear right wheel toe-in (Figure 15) were also much smaller in cars with the multi-link suspension. They did not exceed -0.04°. In cars with the rear axle suspension, based on a torsion beam, particularly large changes in the toe-in were found after loading the vehicle (400 and 420 kg). In this case, the toe-in changes of the rear right wheel were up to four times greater and reached -0.16°.

Similarly, as with the toe-in for the front axle, the rear axle toe-in directly relates to stability of a vehicle when driving on a straight track, as well as to the reaction precision when driving on a curved track. Changes in this parameter are strictly dependent on the vehicle load. In cars with the multi-link suspension, changes in the toe-in of the rear axle wheels after load change (Figure 16) were much smaller, which translates into a smaller impact of the load size and distribution on the vehicle control with this suspension system design.

Analysis of changes in the front left wheel castor (Figure 17) and front right wheel castor (Figure 18) shows that this parameter did not change at all, or changed in a relatively small range (up to -0.22°), in cars with the multi-link front axle suspension. On the other hand, in cars with the McPherson-type suspension, the changes depending on the load were much greater and reached even -0.74°. In some cases, change in castor was positive for both wheels, while in other cases it was negative.

A lack of changes (or minor changes) in castor for both wheels of the front axle (Figure 19), in cars with the multiple-link suspension, together with change in the load distribution and size, are both of a great importance for the vehicle safety. Value of this angle influences the stability of the steering system and contributes to the automatic wheel positioning when driving on a straight track. For the large

changes in castor with varied load variants, changes in the vehicle stability may affect maintaining the correct driving direction.

4 Summary

The suspension systems of many modern passenger cars differ significantly in the type of suspension used for the front and rear axles. Many vehicles still have a relatively simple suspension system of the front axle, based on the McPherson's column and a simple suspension system of the rear axle, based on a torsion beam. When driving cars with such structural solutions, the conditions change depending on the transported load. Type of the suspension system has a significant impact on changes in the wheel geometry parameters.

This study has shown that in all the tested passenger cars, the change in the value and location of the load was accompanied by a change in the wheel geometry parameters. These included toe-in and camber for all the wheels and castor for the front axle wheels. For operation of ae vehicle, it is advantageous when a change in the load size and distribution is accompanied by a greater change in camber. Changes in angle and adjustments to the load are very beneficial as they improve the road adhesion when taking turns. Among the vehicles tested, much larger changes in both the front and rear axle camber were observed in cars with the multi-link suspension systems. Thanks to this, vehicles with multi-link suspension drive can be better controlled and can adapt to changing load conditions and different weight distribution. The better tyre adhesion to the road surface was also observed in curvilinear and straight-line motion, as well as during the braking.

The large changes in the toe-in that were found in cars with relatively simple front axle (McPherson's column) and the rear axle (torsion beam) suspension are unfavourable. This parameter is directly related to stability of a vehicle when driving on a straight track and reaction precision when driving on a curvilinear track. In cars with the multi-link suspension, those changes were much smaller, i.e. the vehicle can be driven in a relatively comparable way with varied load sizes and distribution. For the front axle wheels, castor was also analysed. The smaller changes were observed in cars with the multi-link suspension than in cars with the McPherson's suspension. In the former, castor changed relatively little or not at all, so changes in size and distribution do not significantly affect stability of a vehicle or maintain its driving direction.

It was found that cars with the multi-link suspension in both the front and rear axle adapt best to changes in weight and load distribution, thus drive the best under the variable load conditions.

References

[1] CALVO, J. A., ALVAREZ-CALDAS, C., SAN ROMAN, J. L., COBO, P. Influence of vehicle driving parameters on the noise caused by passenger cars in urban traffic. *Transportation Research Part D: Transport and Environment* [online]. 2012, **17**(7), p. 509-513. ISSN 1361-9209. Available from: https://doi.org/10.1016/j.cub.2016.05.047

[2] CHEN, H., GONG, X., HU, Y. F., LIU, Q. F., GAO, B. Z., GUO, H. Y. Automotive control: the state of the art and perspective. *Acta Automatica Sinica* [online]. 2013, **39**(4), p. 322-346. ISSN 1874-1029. Available from: https://doi.org/10.1016/S1874-1029(13)60033-6

[3] DIONNE, G., MICHAUD, P. C., PINQUET, J. A review of recent theoretical and empirical analyses of asymmetric information in road safety and automobile insurance. *Research in Transportation Economics* [online]. 2013, **43**(1), p. 85-97. ISSN 0739-8859. Available from: https://doi.org/10.1016/j.retrec.2012.12.006

[4] BROUGHTON, J. Car driver casualty rates in Great Britain by type of car. *Accident Analysis and Prevention* [online]. 2008, **40**(4), p. 1543-1552. ISSN 0001-4575. Available from: https://doi.org/10.1016/j.aap.2008.04.002

[5] HELAI, H., HOONG CHOR, C., HAQUE, M. Severity of driver injury and vehicle damage in traffic crashes at intersections: A Bayesian hierarchical analysis. *Accident Analysis and Prevention* [online]. 2008, **40**(1), p. 45-54. ISSN 0001-4575. Available from: https://doi.org/10.1016/j.aap.2007.04.002

[6] KIM, J., RASOULI, S., TIMMERMANS, H. Satisfaction and uncertainty in car-sharing decisions: an integration of hybrid choice and random regret-based models. *Transportation Research Part A: Policy and Practice* [online]. 2016, **95**, p. 13-33. ISSN 1879-2375. Available from: https://doi.org/10.1016/j.tra.2016.11.005

[7] AUST, M. L. Generalization of case studies in road traffic when defining pre-crash scenarios for active safety function evaluation. *Accident Analysis and Prevention* [online]. 2010, **42**(4), p. 1172-1183. ISSN 0001-4575. Available from: https://doi.org/10.1016/j.aap.2010.01.006

[8] BERA, T. K., BHATTACHARYA, K., SAMANTARAY, A. K. Evaluation of antilock braking system with an integrated model of full vehicle system dynamics. *Simulation Modelling Practice and Theory* [online]. 2011, **19**(10), p. 2131-2150. ISSN 1569-190X. Available from: https://doi.org/10.1016/j.simpat.2011.07.002

[9] BOAUAZARA, M., RICHARD, M. J., RAKHEJA, S. Safety and comfort analysis of a 3-D vehicle model with optimal non-linear active seat suspension. *Journal of Terramechanics* [online]. 2006, **43**(2), p. 97-118. ISSN 0022-4898. Available from: https://doi.org/10.1016/j.jterra.2004.10.003

[10] MILANES, V., GONZALEZ, C., NARANJO, J. E., ONIEVA, E., PEDRO, T. D. Electro-hydraulic braking system for autonomous vehicles. *International Journal of Automotive Technology* [online]. 2010, **11**(1), p. 89-95. ISSN 1229-9138. Available from: https://doi.org/10.1007/s12239-010-0012-6

[11] SEPULCRE, M., GOZALVEZ, J., HERNANDEZ, J. Cooperative vehicle-to-vehicle active safety testing under challenging conditions. *Transportation Research Part C: Emerging Technologies* [online]. 2013, **26**, p. 233-255. ISSN 0968-090X. Available from: https://doi.org/10.1016/j.trc.2012.10.003

[12] BERLEMANN, M., MATTHES, A. Positive externalities from active car safety systems. A new justification for car safety regulations. *Journal of Policy Modeling* [online]. 2014, **36**(2), p. 313-329. ISSN 0161-8938. Available from: https://doi.org/10.1016/j.jpolmod.2014.01.004

[13] GONERA, J., NAPIORKOWSKI, J. An analysis of the active safety of a passenger car body during car use. In: 17th International Conference Diagnostics of Machines and Vehicles: proceedings [online]. MATEC Web of Conferences. Vol. 182. 2018. ISSN 2261-236X. Available from: https://doi.org/10.1051/matecconf/201818201022

[14] CIROVIC, V., ALEKSENDRIC, D., SMILJANIC, D. Longitudinal wheel slip control using dynamic neural networks. *Mechatronics* [online]. 2013, **23(**1), p. 135-146. ISSN 0957-4158. Available from: https://doi.org/10.1016/j.mechatronics.2012.11.007

[15] HABIBOVIC, A., DAVIDSSON, J. Causation mechanisms in car-to-vulnerable road user crashes: Implications for active safety systems. *Accident Analysis and Prevention* [online]. 2012, **49**, p. 493-500. ISSN 1879-2057. Available from: https://doi.org/10.1016/j.aap.2012.03.022

[16] AGUILAR, J. J., SANZ, M., GUILLOMIA, D., LOPE, M., BUENO, I. Analysis, characterization and accuracy improvement of optical coordinate measurement systems for car body assembly quality control. *International Journal Advanced Manufacturing Technology* [online]. 2006, **30**(11), p. 1174-1190. ISSN 0268-3768. Available from: https://doi.org/10.1007/s00170-005-0143-5

[17] KONIECZNY, L. *Application of vibratory methods for assessment of technical condition of mechanical and hydropneumatic automotive suspension systems / Wykorzystanie metod drganiowych w ocenie stanu technicznego mechanicznych i hydropneumatycznych zawieszen pojazdow samochodowych* (in Polish). Gliwice: Wydawnictwo Politechniki Slaskiej, 2015. ISBN 9788378803256.

[18] GONERA, J., NAPIORKOWSKI, J. Model for forecasting the geometry of the floor panel of a passenger car during its operation. *Eksploatacja i Niezawodnosc - Maintenance and Reliability* [online]. 2018, **20**(4), p. 689-695. ISSN 1507-2711. Available from: http://dx.doi.org/10.17531/ein.2018.4.20

[19] GONERA, J., NAPIORKOWSKI, J. Effect of the mileage of a passenger car on changes in its body geometry. In: The 18th International Conference on Positron Annihilation AIP 2018: proceedings [online]. AIP Conference Proceedings. Vol. 1946. Iss. 1. ISSN 1551-7616, 020011. Available from: https://doi.org/10.1063/1.5030315

[20] WALLENTOWITZ, H. *Virtual vehicle development - networks as prerequisites for problem solving. success in networks / Virtuelle Fahrzeugentwicklung - Netzwerkeals Voraussetzungenzur Problemlosung. Erfolg in Netzwerken* (in German). Berlin: Springer - Verlag, 2002. ISBN 9783642628535.

[21] BAE, S., LEE, J. M., CHOI, W. J., YUN, J. R., TAK, T. O. Axiomatic approach to the kinematic design of an automotive suspension system with the McPherson strut type. *International Journal of Vehicle Design* [online]. 2003, **31**(1). ISSN 1741-5314. Available from: https://doi.org/10.1504/IJVD.2003.002047

[22] SHAO, X., NAGHDY, F., DU, H., QIN, Y. Coupling effect between road excitation and an in-wheel switched reluctance motor on vehicle ride comfort and active suspension control. *Journal of Sound and Vibration* [online]. 2018, **443**, p. 683-702. ISSN 0022-460X. Available from: https://doi.org/10.1016/j.jsv.2018.12.012

[23] VIDYA, V., DHARMANA, M. M. Model reference based intelligent control of an active suspension system for vehicles. In: International Conference on Circuit, Power and Computing Technologies ICCPCT 2017: proceedings [online]. IEEE. 2017. ISBN 978-1-5090-4967-7. Available from: https://doi.org/10.1109/ICCPCT.2017.8074362

[24] DURMAZ, B. E., KACMAZ, B., MUTLU, I.; SOYLEMEZ, M. T. Implementation and comparison of LQR-MPC on active suspension system. In: 10th International Conference on Electrical and Electronics Engineering ELECO 2017: proceedings. 2017. ISBN 978-605-01-1134-7.

[25] HYNIOVA, K. One-quarter-car active suspension model verification. In: The 2016 International Conference Applied Mathematics, Computational Science and Systems: proceedings [online]. ITM Web of Conferences. Vol. 9. 2017. ISSN 2271-2097. Available from: https://doi.org/10.1051/itmconf/20170903003

[26] SHI, Q., PENG, C., CHEN, Y., HE, J. Robust kinematics design of MacPherson suspension based on a double-loop multi-objective particle swarm optimization algorithm. *Proceedings of the Institution of Mechanical Engineers Part D: Journal of Automobile Engineering* [online]. 2019. ISSN 0954-4070. Available from: https://doi.org/10.1177/0954407018821556

[27] SHIM, T., VELUSAMY, P. C. Suspension design and dynamic analysis of a lightweight vehicle. *International Journal of Vehicle Design* [online]. 2007, **43**(1-4). ISSN 0143-3369. Available from: https://doi.org/10.1504/IJVD.2007.012307

[28] CHEN B., LIU Y., SHI W. Suspension optimization design and virtual prototype simulation analysis of FSAE racing car. *Journal of Physics Conference Series*. 2019, **1176**(5), 052084. ISSN 1742-6588.

ANALYSIS OF TRAFFIC NOISE IN TWO CROSS-SECTIONS AT THE ROAD CROSSING THE CITY

Andrzej Bąkowski*, Leszek Radziszewski

Faculty of Mechatronics and Mechanical Engineering, Kielce University of Technology, Kielce, Poland

*E-mail of corresponding author: abakowski@tu.kielce.pl

Resume

The paper presents an analysis of the noise recorded by the two road traffic noise-monitoring stations. The stations were located in Kielce, Poland, at the road No. 74: on the outskirts of the city and near the center. Based on the experimentally recorded data, an equivalent sound level and acoustic pressure were determined for three sub-intervals of the day: nights, days and evenings. The conducted analyses showed that the average annual values (depending only on the time sub-intervals) of the median do not differ significantly between stations. A similar conclusion can be drawn based on simulations of the median and the C90 percentile of the sound pressure . However, the maximum relative differences in the C99 percentile of the acoustic pressure between stations are around 13%. The maximum relative differences in median pressure between stations are around 15% (for the time sub-interval nights).

Article info

Received 28 April 2020
Accepted 10 June 2020
Online 29 October 2020

Keywords:

urban traffic noise,
monitoring station,
variation of acoustic pressure

Available online: https://doi.org/10.26552/com.C.2021.1.B13-B21

ISSN 1335-4205 (print version)
ISSN 2585-7878 (online version)

1 Introduction

Short- or long-term noise indicators are used to assess the traffic noise, which significantly contributes to environmental pollution and greatly affects the comfort of life [1-2]. In order to monitor the noise and traffic volume of road vehicles, systems of stationary measuring stations operating throughout the year are being built in some cities [3-5]. Results of the noise monitoring are related to changes in the structure and volume of traffic in the city [6-7]. They also indicate the danger associated with the harmful effects of noise on the humans residing in specific areas of the city [8-9]. Kielce has more than ten such stations, installed both in the center and on the outskirts of the city. In this work, an analysis of the measurements results of the equivalent sound level, recorded by the two such stations, located at the large communication artery passing close to the city center, was carried out [10]. Kielce was chosen as an example of a medium-sized city (about 200,000 inhabitants), located in the southern part of central Poland. The temperature throughout the year varies from around -5°C in January to around + 17°C in July. Average monthly precipitation is from 34 mm in October to 96 mm in July. The wind, predominantly from the south and west, reaches an average speed of about 3 m/s over a year. Kielce gets on average 70 days of snow on the ground a year. Tests in Kielce on road No 74 showed that the permissible noise levels were exceeded, during the day - by 6dB(A), evenings - by 5dB(A), nights - by 11dB(A) [10]. Exceedances of applicable normative values are greatest at night. For that reason, the authors decided to conduct a detailed analysis of the road noise generated during this period.

2 Noise monitoring stations

The subject of research, presented in this work, are results of the equivalent sound level measurements recorded by stationary, automatic stations for monitoring noise and vehicle traffic located at Lodzka Rd. (marked as S1 station) and Jesionowa Rd. (marked as S2 station) in Kielce. The location of these stations in the urban layout of Kielce is shown in Figure 1. The distance between these stations is about 2 km.

Streets Lodzka and Jesionowa form one communication route constituting a section of national road No. 74 from the western to eastern borders of the city. Lodzka Street consists of four lanes separated by a 3 m wide green belt. It is the main part of the exit route from the center of Kielce towards Lodz, Warsaw and Krakow. This road is mainly used for transit and suburban traffic. Jesionowa Street consists of five lanes separated by a 5 m wide green belt. It connects Lodzka street with the express road S74. It is intended for the urban and suburban traffic, as well as for transit traffic. These streets are at flat ground level and the technical condition of the bituminous surface is good. There are two large intersections with city roads between the measuring stations. The average daily traffic for S1 station is 20200 vehicles, including 2050 heavy and for S2 station 29500 vehicles, including 1900 heavy. During the night,

Figure 1 *Location of the noise monitoring stations in Lodzka Rd (50.894369 and 20.611445) - station S1 and Jesionowa Rd (50.885759 and 20.636054) - station S2 in the urban layout of Kielce [after Google Maps]*

the number of heavy vehicles registered by each station is similar and amounts to about 450 vehicles. For that time sub-interval, the ratio of light to heavy vehicle traffic is similar for both stations and is about 2:1 [11]. There is also a high railway embankment between the stations located transversely to the analyzed road section. Databases of the sound level measurement results were created in the form of calculated values of the equivalent sound level expressed in decibels. They cover the year 2013 with three time sub-intervals of a 24-hour interval: days, evenings and nights. Due to various technical problems, the databases are not complete. Analysis of data showed that in the period from 02-07-2013 to 28-08-2013 in the case of S1 station and from 02-05-2013 to 13-06-2013 in the case of the S2 station, the stations did not record an equivalent sound level. This increases the uncertainty of the measurement results. Monitoring stations in Kielce are installed on the roadside lighting poles, at a distance of about 20 m from intersections with city roads. The S2 station is located at the intersection with traffic lights. The acoustic measurements were carried out with the SVAN 958A, a four-channel digital vibration analyser and a class 1 sound level meter. A Microtech Gefell MK250 free-field, prepolarised 1/2" condenser microphone with a sensitivity of 50 mV/Pa, and a SV 12L preamplifier with the frequency range from 3.5 Hz to 20 kHz was used during the tests. The dynamic range is from 15dB to 146dB. The device can operate in the temperature range from -50°C to 100°C and it has a membrane made of nickel. The microphone for measuring sound pressure is located 4 m from the road edge at a height of 4 m. The measurements were carried out 24 hours a day. The RMS values of the A sound level were registered in the buffer every 1 s and the results were recorded every 60 seconds. The data collected were the basis for equivalent sound level calculation for three time intervals, i.e., from 6:00 to 18:00, from 18:00 to 22:00 and from 22:00 to 6:00.

3 Results analysis methods

The most commonly used measure for noise assessment is the equivalent sound level ($L_{Aeq,T}$) expressed in dB(A), defined as follows:

$$L_{Aeq,T} = 10 \cdot \log\left[\frac{1}{T}\int_0^T \left(\frac{p_A(t)}{p_0}\right)^2 dt\right] = \\ = 10 \cdot \log\left[\left(\frac{p_{ARMS}}{p_0}\right)^2\right], \quad (1)$$

where:
T - measurement time, s,
$p_A(t)$ - sound pressure corrected by frequency characteristics A, Pa,
p_0 - the standardized reference acoustic pressure of $20 \cdot 10^{-6}$ Pa.

Expanded uncertainty of measurements is determined from [12]:

$$u(t_{\alpha;N-1}) = u = \pm\sqrt{\frac{\sigma^2}{N} + \frac{0.026\sigma^4}{N-1}}\, t_{\alpha;N-1}, \quad (2)$$

where $t_{\alpha;N-1}$ is the quantile of the t - distribution at the confidence level α, standardized at 0.05. Equation (2) can be applied, assuming that the null hypothesis about normal unimodal distributions (H_0) of the measured sound level, independent variables, adequately large quantity of data and low standard deviations, can be accepted. In the case of the traffic noise, those conditions are not always met.

The logarithm function used to represent $L_{Aeq,T}$, determined according to Equation (1), may impede comparative analysis and affect results of the statistical tests. For that reason, the authors decided to additionally determine the RMS value of sound pressure (denoted p_{ARMS}), from Equation (3), in the analyzed time interval T and use this parameter expressed in mPa for further analysis.

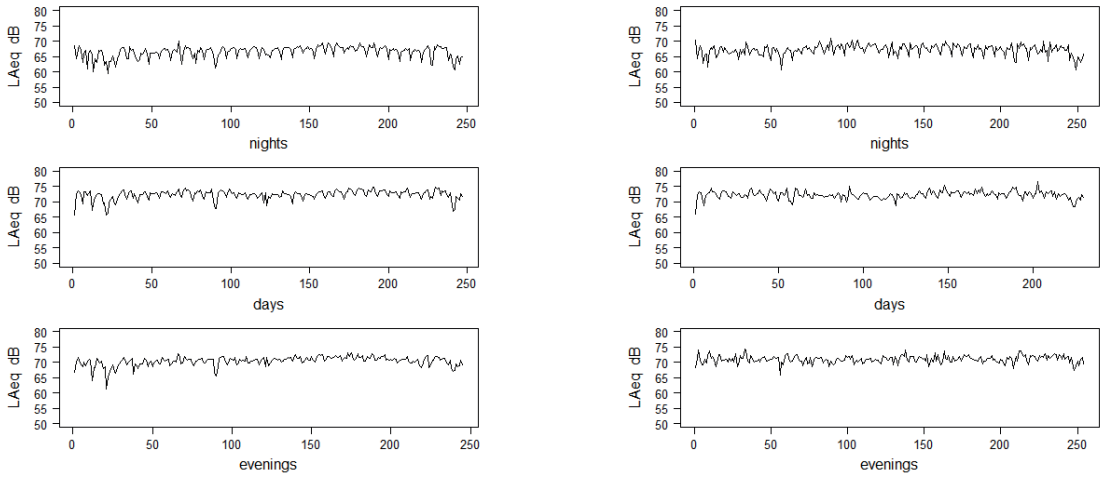

Figure 2 *Equivalent sound levels $L_{Aeq,T}$ for all the measurement days in 2013 split into time sub-intervals; a) station S1, b) station S2 [10]*

$$p_{A_{RMS}} = p_A = \sqrt{10^{(0.1*L_{Aeq,T})} \cdot p_0^2}\,. \tag{3}$$

The analysis carried out in these units allows easier comparison of the constant (expected value, median, percentiles e.g. C_{90} and C_{99}) and variable (e.g. standard deviation, coefficient of variation of the standard deviation) components of the analyzed sound pressure signal. The study of the variable components contained in the analyzed signals was based on analysis of the classical and positional coefficients: standard deviation $(\sigma_{pA_{RMS}})$, coefficient of variation of the standard deviation (denoted COV), positional coefficient of variation (V_{Q31}). In order to make it easier for the reader to evaluate the presented results, below are definitions of all the coefficients analyzed in this paper.

A frequently used measure for analyzing the variable component of sound pressure is the standard deviation, which can be referred to the expected value of the analyzed signal by obtaining the COV coefficient. The COV coefficient can be used to compare directly the variable components of the analyzed parameters. For the sound pressure, it can be expressed as:

$$COV_{pA_{RMS}} = COV = \frac{\sqrt{\frac{1}{n-1}\sum_{i=1}^{i=n}(p_{A_{RMSi}} - \overline{p_{A_{RMS}}})^2}}{\overline{p_{A_{RMS}}}} \cdot 100\%. \tag{4}$$

Values of the classical coefficients of variation are strongly influenced by atypical data that was included in the analyzes. The impact of such data is smaller when using positional variability measures. The measure of dispersion of the analyzed variable is the average quartile deviation. Quartile deviation is an absolute measure that defines the average variance of half of the measurement data around the median after rejecting 25% data with the lowest values $Q_1(p_{A_{RMS}})$ and 25% data of the highest values $Q_3(p_{A_{RMS}})$ of the sound pressure. By relating it to the median, the positional coefficient of variation can be calculated as:

$$V_{Q31} = \frac{0.5 \cdot [Q_3(p_{A_{RMS}}) - Q_1(p_{A_{RMS}})]}{Med} \cdot 100\%. \tag{5}$$

Data that can be considered atypical have less impact on values of this coefficient. The relative differences between the positional statistical parameters, such as the C_X and C_Y percentiles, can be calculated according to the following relationship:

$$\varepsilon_{X-Y} = \frac{C_X - C_Y}{C_Y} \cdot 100\%,, \tag{6}$$

where:

ε_{X-Y} - coefficient of relative difference between percentiles of order X and Y, X > Y,

C_X, C_Y - percentiles of order X and Y, respectively.

This indicator can be used to analyze values of the noise parameters recorded by one measuring station. When analyzing data recorded by several measuring stations, the ratio of relative difference between the X-percentiles can be calculated as follows:

$$\varepsilon_X = \frac{C(S2)_X - C(S1)_X}{C(S1)_X} \cdot 100\%,, \tag{7}$$

where:

$C(S2)_X, C(S1)_X$ - percentiles of order X of the tested parameter determined for the stations S1 and S2, respectively.

4 Measurements results

Examples of diagrams showing recorded $L_{Aeq,T}$ for all the measurement days in 2013, split into 24-hour period sub-intervals, are shown in Figure 2a for station S1 and in Figure 2b for station S2.

Table 1 shows basic average annual statistics of the parameter $L_{Aeq,T}$ for the 24 h periods and three time sub-intervals determined from station S1 measurement data, expressed in dB(A). The Lilliefors and Shapiro-

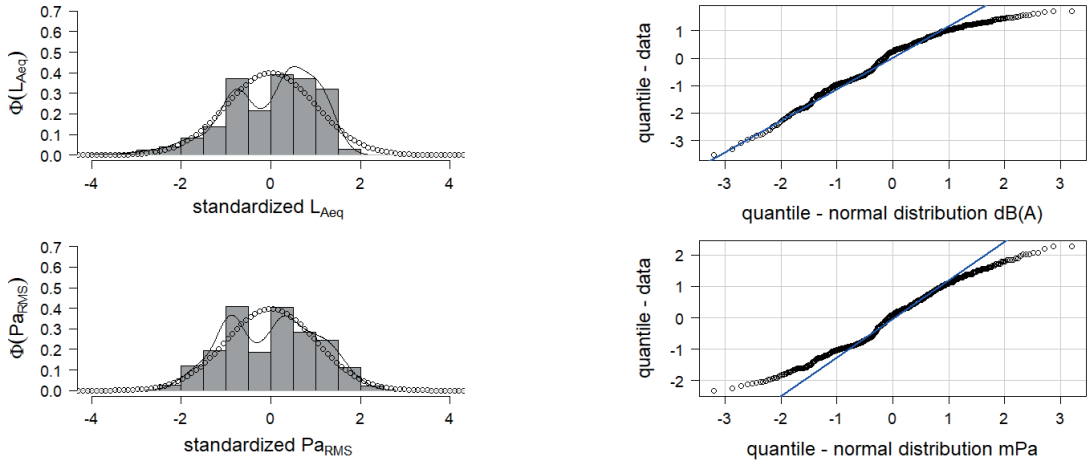

a) *b)*

Figure 3 *Graphs prepared for standardized analyzed values of measurement data recorded by station S1, expressed in dB(A) or mPa a) histograms with the probability density function, b) Q-Q quantile charts*

Table 1 *Average annual values of basic statistical noise measures determined by the station S1 and S2, for all the measurement days in 2013*

period of the day	median $L_{Aeq,T}$ dB(A)	u dB(A)	median p_{ARMS} mPa	u_A mPa	$\overline{p_{ARMS}}$ mPa	σ_{pARMS} mPa	COV %	V_{Q31} %	C_{90} mPa	C_{99} mPa
station S1										
24 h	70.50	0.24	66.99	0.73	64.68	19.93	30.82	24.72	91.42	104.50
night	67.10	0.25	45.29	0.53	43.03	8.35	19.41	10.78	52.00	59.02
day	72.70	0.20	86.30	0.84	83.77	13.18	15.73	9.53	98.41	107.51
evening	70.70	0.20	68.55	0.66	67.24	10.30	15.32	9.02	79.26	88.89
station S2										
24 h	70.68	0.20	68.40	0.67	66.48	18.28	27.50	21.28	88.11	105.31
night	67.43	0.22	47.05	0.54	46.34	8.56	18.47	12.17	56.43	64.89
day	72.29	0.17	82.32	0.77	82.74	11.67	14.10	7.86	96.39	112.50
evening	71.03	0.16	71.21	0.63	71.90	10.02	13.94	8.83	84.06	100.78

Wilk statistical tests rejected hypothesis H_0 because the calculated significance levels were lower than the required level of 0.05. In the cases where the normal distribution of given data was doubtful, the Jarque-Bera test was additionally used. Results of those tests are not included in Table 1, but one can conclude that in the case of data expressed in dB(A) for the S1 and S2 station, in each of the four considered periods of the day, there are grounds to reject the H_0 hypothesis. Figure 3 shows (for comparison) examples of histograms with the probability density function plotted and Q-Q quantile charts for standardized values of analyzed measurement data, expressed in dB(A) or mPa.

Analysis of Figure 3 shows that, depending on the units used (i.e. dB(A) or mPa in which noise is expressed) one can notice differences in the shape of both histograms, probability density functions and Q-Q charts for standardized values of the analyzed data. The calculated values of kurtosis and skewness for data (expressed in dB(A)) recorded by station S1 are 2.93 and -0.65, respectively, which confirms the validity of rejection of the H_0 hypothesis. Quantile charts are graphic illustrations of the fact that distributions of the analyzed data deviate from the normal distribution and that these distributions are left-skewed.

Statistical tests of the $L_{Aeq,T}$, determined from station S1 measurement data rejected the hypothesis H_0 for all the average annual time intervals given in Table 1, as in the case of analyzes for S2 stations. Values of the medians of the $L_{Aeq,T}$, expressed in dB(A) for each time sub-interval presented in Table 1 are similar for both stations. The values of the medians of $L_{Aeq,T}$ for each time sub-interval, presented in Table 1, exceed values applicable in Poland in accordance with the law, especially for the time sub-interval night, i.e. by about 11 dB.

Type A uncertainty of measurements of the traffic noise, calculated according to Equation (2), is about 0.2 dB(A).

Examples of diagrams, showing calculated according to Equation (3), split into 24-hour period sub-intervals, are

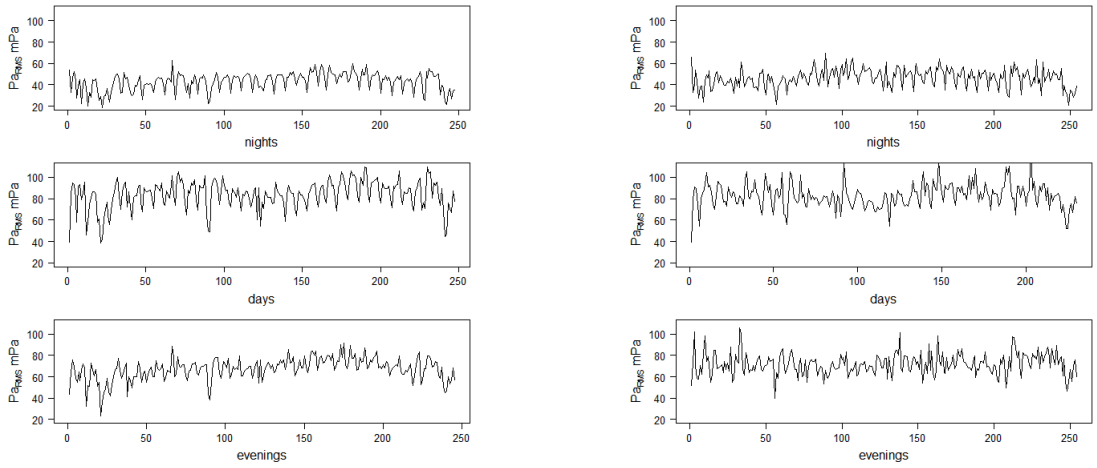

a) *b)*

Figure 4 *Sound pressure values p_{ARMS} expressed in mPa calculated for all the measurement days, split into time sub-intervals; a) S1 station, b) S2 station*

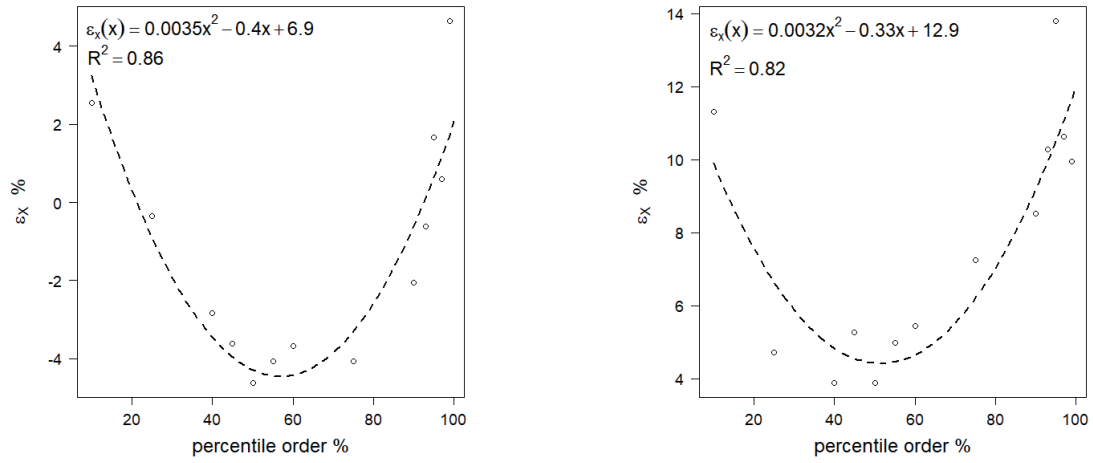

a) *b)*

Figure 5 *The average annual values of the coefficient ε_X of the relative difference in the sound pressure percentiles between the S1 and S2 stations, determined for the time sub-interval a) days, b) nights*

presented in Figure 4a for station S1 and in Figure 4b for station S2.

Results of the statistical tests of acoustic pressure p_{ARMS} allows concluding that only for the S2 station and for the time sub-interval nights - there are no grounds to reject the H_0 hypothesis (at the significance level of 0.05). The pressure diagrams, presented in Figure 4, are varied both for each time sub-interval and for each monitoring station. These differences rely both on other values of constant and variable components of pressure and the nature of their changes, which is confirmed by values of the statistical parameters presented in Table 1. For the 24 h periods, the median sound pressure for the S1 station is about 67 mPa and for the S2 station about 68 mPa. Type A expanded uncertainty (u_A) is about 1 mPa. Coefficients of variation of sound pressure for these periods and for both stations are in the range: for COV from 27.50% to 31% and for V_{Q31} from 21% to 25%.

Depending on the time sub-interval, the median sound pressure for both stations assumes similar values, which are in the range for: nights from 45 mPa to 47 mPa, days from 82 mPa to 86 mPa and evenings from 69 mPa to 71 mPa. However, the coefficients of variation of pressure for these time sub-intervals are in the following ranges: for COV - from 13% to 19%, for V_{Q31} - from 8% to 12%.

The calculated values of the C_{90} and C_{99} parameters of the noise pressure, determined for the 24 h periods, are similar for both stations and are approximately 90 mPa and 105 mPa, respectively. The average annual coefficients of relative percentile differences of the order X = 99 and Y = 90, calculated according to Equation (6), are always greater for the S2 station and their maximum value is about $\varepsilon_{99-90}(S2) = 20\%$ - for the time sub-interval evenings. However, for the S1 station and for the time sub-interval evenings $\varepsilon_{99-90}(S1) = 12\%$. The maximum value of the C_{99} parameter always occurs for the S2 station and for the time sub-interval days is about 112 mPa. The minimum value of the C_{99} parameter is for the S1 station and is about 59 mPa. Figure 5 presents the average annual values of the coefficient ε_X (calculated according to Equation (7)) of the relative difference in pressure percentiles between stations S1 and S2.

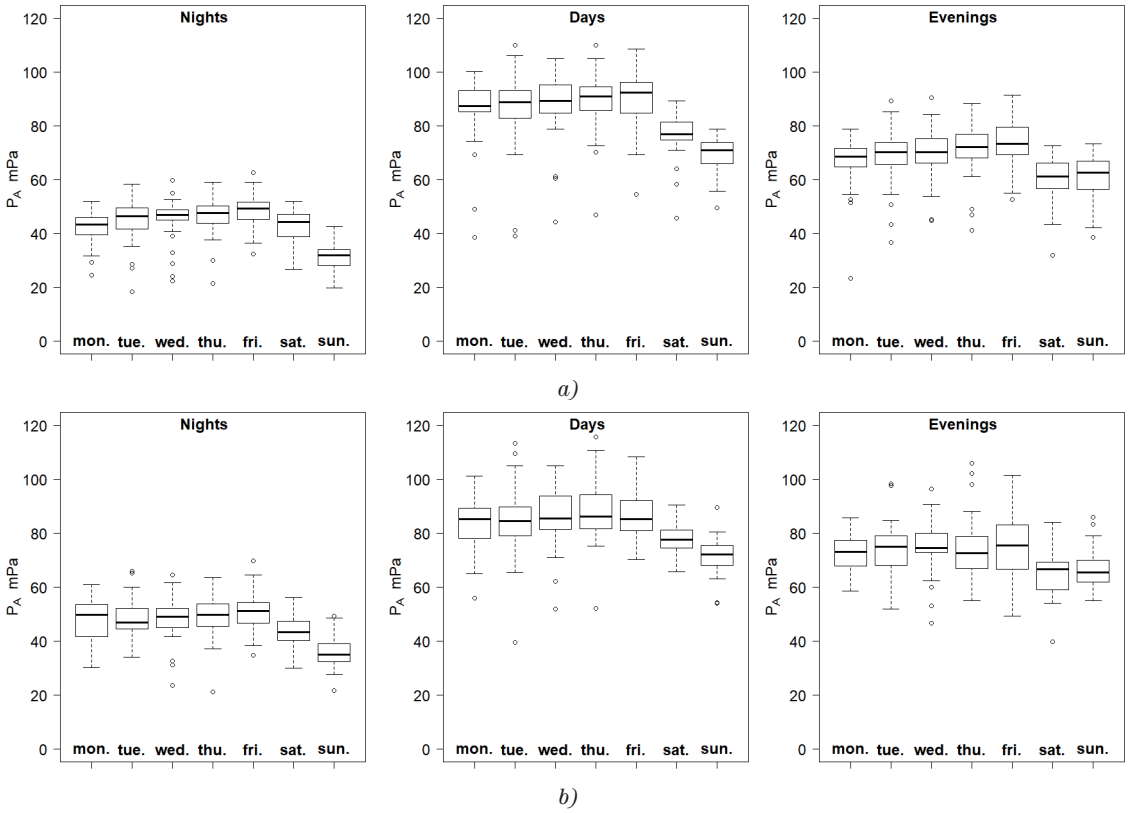

Figure 6 *Box plots of average annual sound pressure p_{ARMS} for individual days of the week and for time sub-intervals: nights, days, evenings: a) S1 station, b) S2 station*

The coefficient ε_X takes both positive and negative values. A change in the sign of this factor indicates that some pressure percentiles for station S1 have higher values than for station S2 - this occurs especially for the time sub-interval days. Figure 5 shows that the minimum values occur near the 50-th percentile. The variation range from minimum to maximum is around 10%. The maximum value is around $\varepsilon_{99} = 13\%$ for the time sub-interval evenings. The analyzed relationships can be described by a second-degree polynomial. Values of the coefficients of this polynomial depend on the time sub-interval. Values of the correlation coefficients R are high and amount to about 0.80. The analyzes conducted so far have not revealed significant large differences between the average annual values of a median and C_{90} noise pressure, determined for stations S1 and S2. However, for parameter C_{99} (for the evenings) the maximum relative pressure differences are around: $\varepsilon_{99} = 13\%$ (between stations S1 and S2), $\varepsilon_{99-90}(S1) = 12\%, \varepsilon_{99-90}(S2) = 20\%$. For any time sub-interval, regardless of the station, the noise parameter values are higher than the normative ones. For the time sub-interval day - these differences are around 11dB(A).

In order to conduct further more detailed comparative analyzes of the two stations, it was decided to calculate the average annual values of the sound pressure parameters for individual days of the week [1]. Figure 6 presents box plots prepared for average annual pressures p_{ARMS} calculated for individual days of the week and for time sub-intervals: nights, days and evenings. These plots show how the median and the interval between the first and third quartiles change during the week. They also show that the set of data analyzed contains values that can be considered atypical. The only period when there is no unusual data is time sub-interval - nights - on Saturdays. Since no causes were identified for occurrence of the atypical data, these data were taken into account in further analysis of the recorded samples of the traffic noise. This phenomenon is thus characterized by high randomness, which is consistent with the findings reported in the literature [12].

These graphs show that changes in the median value on weekdays are different in nature depending on the economic function of the section of road being studied, i.e. location of the measuring station. At station S1, the median values increase gradually from Mondays to Fridays. At station S2, the median value increases slightly or decreases from Mondays to Fridays. However, on weekend days, for both stations, the nature of changes in median p_{ARMS} is similar. On Saturdays and Sundays, the median value of p_{ARMS} for time sub-interval nights and days decreases and for the evenings the differences are insignificant - even then, the permissible noise values are exceeded. The statistical tests for data expressed in mPa showed that for some of the weekdays and for certain time sub-intervals within a 24-hour period there was not enough evidence to reject the hypothesis H_0. For the S1 and S2 stations, such days are Fridays, Saturdays and Sundays. Saturdays and Sundays are the weekend days and the traffic parameter values of road vehicles are different from on the business days.

As previous analyzes have shown, the largest exceedances of permissible noise occur for the time sub-

Table 2 *Average annual values of the statistical measures p_{ARMS} determined for individual days of the week for stations S1 and S2, time sub-interval - nights*

days of the week	median mPa	$\overline{p_{ARMS}}$ mPa	σ_{pARMS} mPa	COV %	V_{Q31} %	C_{90} mPa	C_{99} mPa	u_A mPa
station S1								
mondays	43.25	41.84	6.28	15.00	7.41	46.88	52.00	1.06
tuesdays	46.35	44.81	8.26	18.43	8.48	53.34	57.46	1.40
wednesdays	46.88	45.32	7.80	17.20	4.03	51.41	58.14	1.32
thursdays	47.70	46.28	6.69	14.46	6.50	52.30	56.78	1.12
fridays	49.38	48.51	6.02	12.41	6.35	54.47	61.30	1.00
saturdays	44.26	42.87	5.80	13.53	9.47	48.87	51.80	0.98
sundays	32.06	31.35	5.07	16.18	9.47	37.46	42.10	0.86
station S2								
mondays	49.78	48.24	7.94	16.46	11.98	58.00	61.00	1.34
tuesdays	46.94	48.30	7.47	15.46	8.05	59.39	65.70	1.23
wednesdays	48.98	48.33	8.08	16.71	7.04	56.74	63.48	1.35
wednesdays	49.70	49.11	7.88	16.04	7.92	56.89	63.63	1.31
fridays	51.13	50.65	6.95	13.72	7.47	56.90	67.86	1.13
saturdays	43.30	43.34	5.95	13.73	8.32	50.50	55.79	0.99
sundays	35.00	36.18	6.48	17.90	8.77	46.94	49.32	1.08

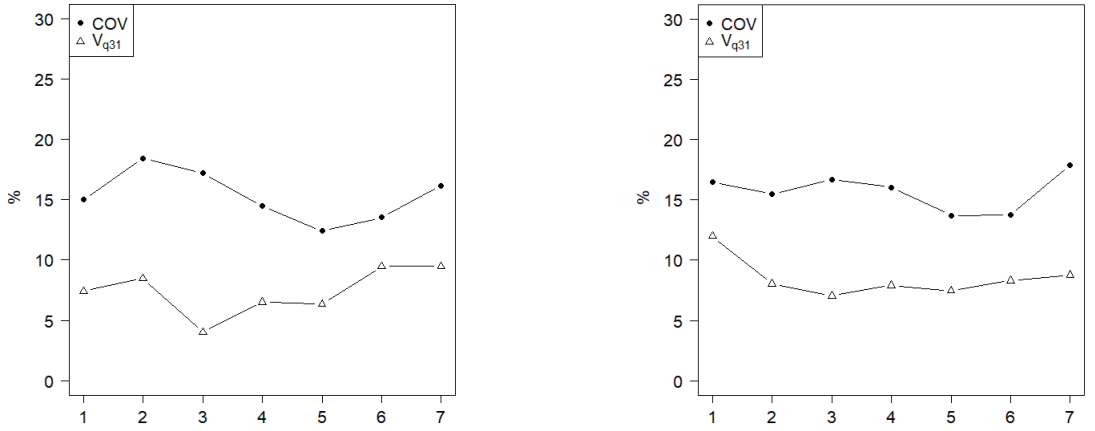

a) *b)*

Figure 7 *Changes in the coefficient of variation of the sound pressure on particular days of the week for the time sub-interval - nights a) S1 station, b) S2 station (designations; 1 - 7 - consecutive days of the week, from Monday to Sunday)*

interval - nights, which is particularly burdensome for residents [13]. Therefore, the authors decided to conduct further analysis for nights and on individual days of the week. Some values of the noise parameters at night and for individual days of the week are given in Table 2.

Median p_{ARMS} is in the range: for the S1 station from 32 mPa (on Sundays) to about 49 mPa (on Fridays), for the S2 station from 35 mPa (on Sundays) to 51 mPa (on Fridays). Pressure percentiles C_{90} and C_{99} have the lowest values on Sundays: for the S1 station - 37 mPa and 42 mPa, respectively and for the S2 station - 47 mPa and 49 mPa, respectively. However, values of the largest pressure percentiles C_{90} and C_{99} are: for the S1 station on Fridays - 54 mPa and 61 mPa, respectively and for the S2 station on Tuesdays - 59 mPa and on Fridays, 68 mPa.

The maximum relative differences between the values of parameters C_{90} and C_{99} for S1 station are $\varepsilon_{99-90} = 13\%$ (on Wednesdays) and for S2 station $\varepsilon_{99-90} = 19\%$ (on Fridays). The maximum relative differences in the C_{50}, C_{90} or C_{99} parameter values between stations, regardless of the day of the week for the nights, are approximately: $\varepsilon_{50} = 15\%$, $\varepsilon_{90} = 25\%$, $\varepsilon_{99} = 17\%$.

Figure 7 shows the mutual relations between values of the coefficients of relative changes in the median pressure p_{ARMS} on individual days of the week, for the nights for the stations S1 and S2. The COV coefficient values are several percent higher than the V_{Q31} coefficient. The nature of changes in their value during the week is varied for each station. For the S1 station, values of these coefficients increase from Mondays to Tuesdays and decrease from

Tuesdays to Fridays, after which from Fridays to Sundays they increase again. On the other hand, for the S2 station, values of these ratios decrease from Mondays to Tuesdays, from Tuesdays to Fridays they decrease or increase, after which from Fridays to Sundays they increase again.

Analysis of Figure 7 shows that nature of changes in the COV values from Monday to Wednesday for each station is different. However, from Wednesday to Sunday, the nature of the changes is similar. In the case of the V_{Q31} coefficient values, the qualitative differences occur from Monday to Tuesday and from Tuesday to Sunday the nature of the changes is similar.

5 Conclusions

The study evaluated and compared results of measurements recorded by the two stationary road noise-monitoring stations, located on one road. For this purpose, the arithmetic mean and median, as well as the variable components of the signals tested were calculated. For analysis of these signals, the acoustic pressure p_{ARMS} and the classical COV and positional V_{Q31} coefficients of variation were used. Use of the relative difference coefficients between pressure percentiles p_{ARMS} has been proposed.

Annual average median and C_{90} percentile of the sound pressure p_{ARMS} (depending only on 24-hour sub-periods) showed no significant differences between the S1 or S2 stations. For the 24h periods the median, C_{90} and C_{99} percentile of the sound pressure p_{ARMS} for both stations S1 and S2 are similar and are about 67 mPa, 90 mPa and 105 mPa, respectively. However, for both stations, depending on the time sub-interval, the median pressure p_{ARMS} assume similar values, which are around: for nights 46 mPa, for days from 84 mPa and for evenings 70 mPa. The maximum values of the C_{99} parameter are always present for the S2 station and for the time sub-interval days are about 112 mPa. The minimum value of the C_{99} parameter is for the S1 station and is about 59 mPa. At any time sub-interval, regardless of the monitoring station, values of the noise parameters are higher than normative. For the night, these differences are the largest and amount to about 11dB(A). The relative differences between the C_{90} and C_{99} parameter values are always greater for the S2 stations and their maximum value is approximately $\varepsilon_{X-Y}(S2) = 20\%$ - for the evenings. However, for the S1 station and for the evenings $\varepsilon_{X-Y}(S1) = 12\%$. The maximum relative differences in C_{99} percentile pressure between the stations S1 and S2 are approximately 13% for the evenings. Pressure variation coefficients for the 24h periods and for both stations are in the range: for the COV from 27.50% to 31% and for V_{Q31} from 21% to 25%. Whereas the coefficients of pressure variation for: nights, days, evenings are in the range: for COV from 13% to 19%, for V_{Q31} from 8% to 12%.

In order to conduct more detailed comparative noise analyzes for the stations tested, the average annual values of the sound pressure parameters on particular days of the week were calculated. At station S1, the median values increase gradually from Mondays to Fridays. At S2, the median value increases slightly or decreases from Mondays to Fridays. This nature of the median value changes on weekdays is due to location of the measuring stations. However, at weekends, the nature of changes in median p_{ARMS} is similar for both stations.

As previous analyzes for the time sub-interval night have shown: the structure of vehicle traffic for both stations is similar and the largest exceedances of permissible noise occur. It has been shown that at nights for stations S1 and S2: the minimum median p_{ARMS} occur on Sundays and the maximum on Fridays. Percentile C_{90} and C_{99} for station S1 have the lowest values on Sundays and the highest on Fridays. Whereas for S2 station - C_{90} and C_{99} percentiles have the smallest values on Sundays and the highest ones on Tuesdays and Fridays, respectively. The maximum relative differences between the C_{90} and C_{99} percentiles for the S1 station are $\varepsilon_{99-90} = 13\%$ (on Wednesdays, nights) and for the S2 station $\varepsilon_{99-90} = 19\%$ (on Fridays, nights). The maximum relative differences in the C_{50}, C_{90} or C_{99} percentiles between stations, regardless of the day for the nights, are approximately: $\varepsilon_{50} = 15\%$, $\varepsilon_{90} = 25\%$, $\varepsilon_{99} = 17\%$. It should be noted that the median values of p_{ARMS} for both stations are in ranges with similar boundaries and a span of about 16 mPa. On the other hand, for parameter C_{99}, the differences between the lower boundaries of the ranges are 7 mPa and the values of the lower and upper boundaries for each station differ by 19 mPa (for nights).

Minimal values of the coefficients of variation for the time sub-interval night occur on different days: for V_{Q31} on Wednesdays and for COV on Fridays. The nature of the change in COV value from Mondays to Wednesdays for each station is different. However, from Wednesdays to Sundays, the nature of the changes is similar. In the case of the V_{Q31} coefficient value, qualitative differences occur from Mondays to Tuesdays and from Tuesdays to Sundays, the nature of the changes is similar.

References

[1] GERAGHTY, D., O'MAHONY, M. Investigating the temporal variability of noise in an urban environment. *International Journal of Sustainable Built Environment* [online]. 2016, **5**(1), p. 34-45. ISSN 2212-6090. Available from: https://doi.org/10.1016/j.ijsbe.2016.01.002

[2] KHAIWAL, R., SINGH, T., TRIPATHY, J. P., MOR, S., MUNJAL, S., PATRO, B., PANDA, N. Assessment of noise pollution in and around a sensitive zone in North India and its non-auditory impacts. *Science of the Total Environment* [online]. 2016, **566-567**, p. 981-987. ISSN 0048-9697. Available from: https://doi.org/10.1016/j.scitotenv.2016.05.070

[3] VOGIATZIS, K., REMY, N. Environmental noise mapping as a smart urban tool development. In: *Smart Urban Development* [online]. IntechOpen, 2019. Available from: https://doi.org/10.5772/intechopen.88449

[4] CZYZEWSKI, A., KOTUS, J., SZCZODRAK, M. Online urban acoustic noise monitoring system. *Noise Control Engineering Journal* [online]. 2012, **60**(1), p. 69-84. ISSN 0736-2501. Available from: https://doi.org/10.3397/1.3670102

[5] MIHAJLOV, D. I., PRASCEVIC, M. R. Permanent and semi-permanent road traffic noise monitoring in the city of Nis (Serbia). *Journal of Low Frequency Noise, Vibration and Active Control* [online]. 2015, **34**(3), p. 251-268. ISSN 1461-3484, eISSN 2048-4046. Available from: https://doi.org/10.1260/0263-0923.34.3.251

[6] PETROVA, M., NENKO, A. Urban emptiness as a resource for sustainable urban development. *Management of Environmental Quality: An International Journal* [online]. 2018, **29**(3), p. 388-405. ISSN 1477-7835. Available from: https://doi.org/10.1108/MEQ-01-2018-0004

[7] FIGLUS, T., GNAP, J., SKRUCANY, T., SZAFRANIEC, P. Analysis of the influence of different means of transport on the level of traffic noise. *Scientific Journal of Silesian University of Technology. Series Transport* [online]. 2017, **97**, p. 27-38. ISSN 0209-3324, eISSN 2450-1549. Available from: https://doi.org/10.20858/sjsutst.2017.97.3

[8] BASNER, M., MCGUIRE, S. WHO environmental noise guidelines for the European region: a systematic review on environmental noise and effects on sleep. *International Journal of Environmental Research and Public Health* [online]. 2018, **15**(3), p. 519. eISSN 1660-4601. Available from: https://doi.org/10.3390/ijerph15030519

[9] JANDACKA, D., DECKY, M., DURCANSKA, D. Traffic related pollutants and noise emissions in the vicinity of different types of urban crossroads. In: IOP Conference Series: Materials Science and Engineering: proceedings. IOP Publishing, 2019. p. 012152.

[10] BAKOWSKI, A., RADZISZEWSKI, L., DEKYS, V. Urban noise recorded by stationary monitoring stations. In: IOP Conference Series: Materials Science and Engineering: proceedings. Vol. 245. Iss. 4. IOP Publishing, 2017. p. 042045. Available from: https://doi.org/10.1088/1757-899X/245/4/042045

[11] BOCHATKIEWICZ, J. *Acoustic maps of the city of Kielce - updated 2013 / Mapy akustyczne miasta Kielce - aktualizacja 2013* (in Polish) [online]. Available from: http://www.um.kielce.pl/gfx/kielce2/userfiles/files/srodowisko/opracowania/mapa_akustyczna_aktualizacja_2013.pdf

[12] PRZYSUCHA, B., BATKO, W., SZELAG, A. Analysis of the accuracy of uncertainty noise measurement. *Archives of Acoustics* [online]. 2015, **40**(2), p. 183-189. ISSN 0137-5075, eISSN 2300-262X. Available from: https://doi.org/10.1515/aoa-2015-0020

[13] SLAVIK, R., GNAP, J. Selected problems of night-time distribution of goods within city logistics. *Transportation Research Procedia* [online]. 2019, **40**, p. 497-504. ISSN 2352-1465. Available from: https://doi.org/10.1016/j.trpro.2019.07.072

DYNAMIC PROPERTIES AND WEAR ANALYSIS OF A RAIL VEHICLE WITH WHEELS' SELF-LUBRICATING COATINGS

Rafał Melnik[1,*], Andrzej Chudzikiewicz[2], Seweryn Koziak[3], Michał Opala[3], Ján Dižo[4]

[1]Faculty of Computer Science and Food Science, Lomza State University of Applied Sciences, Lomza, Poland
[2]Faculty of Transport, Electrical Engineering and Computer Science, Kazimierz Pulaski University of Technology and Humanities in Radom, Radom, Poland
[3]Faculty of Transport, Warsaw University of Technology, Warsaw, Poland
[4]Department of Transport and Handling Machines, Faculty of Mechanical Engineering, University of Zilina, Zilina, Slovakia

*E-mail of corresponding author: rmelnik@pwsip.edu.pl

Resume

The problem of wheel and rail wear in railway transport generates costs of reprofiling and availability of vehicles and infrastructure. One of the possibilities of wear minimizing is decreasing of the friction coefficient in wheel-rail contact by means of lubricants. Such a solution has drawbacks from which the most crucial are: decrease of tractive/braking forces and difficulties with the precise spreading of the lubricant. These disadvantages may be avoided by modern, innovative self-lubricating coatings, applied at the production stage on the wheel flanges. The aim of the study is to investigate the effect of self-lubricating coatings on a rail vehicle's dynamic behaviour, safety against derailment and predicted wheel wear. The numerical study was performed using the wagon multibody model with simulated self-lubricating coating on wheel flanges.

Article info

Received 31 March 2020
Accepted 19 June 2020
Online 30 October 2020

Keywords:

rail vehicle,
goods wagon,
self-lubricating coating,
dynamics,
multi-body system,
safety against derailment,
wear

Available online: https://doi.org/10.26552/com.C.2021.1.B22-B32

ISSN 1335-4205 (print version)
ISSN 2585-7878 (online version)

1 Introduction

Since the beginning of the rail transport expansion, wheel and rail wear has been one of the most significant technical problems in this mode of transport. Wear is not only a great economic burden for vehicles and tracks operators, yet it gives rise to the additional actions for wheels reprofiling and rails grinding, hence it may limit the availability of infrastructure and the rolling stock. Another adverse feature, related to the worn wheels' profiles, is affecting the vehicle dynamic behaviour, which may lead to reduction of safety against derailment [1]. Minimizing the phenomenon of wear has become a common goal of vehicle and rail infrastructure operators. Unfortunately, with the global tendency to increase the axle loads in railway goods transport, accelerated degradation of tracks and vehicle wheels should be expected, especially on routes with numerous small-radii curves. In such conditions (small-radii curves), the wheel slip values are high and additional frictional forces arise due to the wheel flange-rail head contact, what in turn increases the total resistive force and wear of the contacting surfaces.

The most common solution to the problem of the wheel/rail wear, used worldwide, is lubrication. In the case of goods, rail transport is nowadays the only economically acceptable means for the wheel-rail wear reduction, without running gear modification. Passenger rolling stock, especially trams, metro and multiple units are subject of studies aiming to develop the new running gear solutions facilitating curves negotiation [2-4]. To eliminate the problems of external lubricants and exploit advantages of decreased friction coefficient, it was decided to focus on the possibility of applying an innovative thin layer of self-lubricating coating on the wheel flange. The wheelsets with self-lubricating coatings are a new, innovative solution and thus neither has been adopted in the railway transport nor tested in real conditions. However, with decrease of the friction coefficient, depending on the wheels' lateral position relative to rails, vehicle's dynamic behaviour may be affected, since friction is a crucial factor in the process of contact forces generating. The aim of the presented study was to investigate dynamic responses and predict the wear rate of a two-axle goods wagon multibody model with simulated self-lubricating layers applied on wheels' flanges. This novel application of coating reducing friction required to include its mathematical description in the wheel-rail contact modelling.

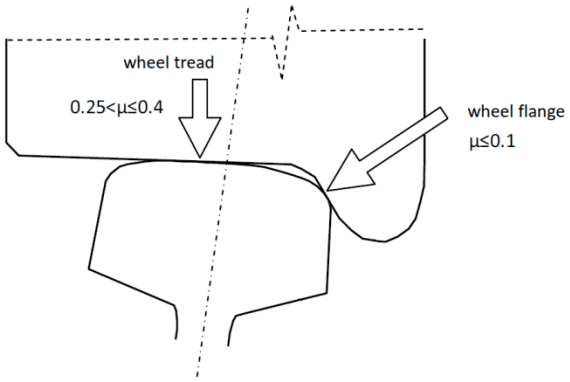

Figure 1 *Required friction coefficient values in the wheel-rail contact*

2 Wheel-rail friction modification

The necessity of friction coefficient modification of the wheel-rail contact is related to wear phenomenon. The rate of wear is strongly influenced by the values of the contact stresses, size of the contact being in slip and use of lubricants applied intentionally or occurring naturally (water, snow, etc.). Wear, as a result, leads to the changes of wheel and rail profiles. If the tangential force, generated in the contact patch, were greater than adhesion, determined by the friction coefficient, there will be a slip resulting in a significant increase of wear of the elements. Wear minimisation through friction modifiers is effective, nevertheless, it should be kept in mind that improper application may lead to the intensification of the wear process in a contact zone [5]. The required friction coefficient values, being a trade-off between low wear and ability to exert the high tractive/braking forces in the wheel-rail contact, are depicted in Figure 1.

In order to apply lubricant to area of the slipping contacting surfaces, three types of systems are usually used [6]:

- mobile systems - commonly in the form of specially adapted railway vehicles that lubricate rails,
- trackside devices - mounted in the vicinity of track in which the release of the lubricant is triggered by the passing vehicle and
- on-board devices - eject lubricant directly to the wheel flange, from where it flows into the area of contact between the wheel and the rail.

Effectiveness of some solutions of applying a lubricant is limited, as evidenced by Nilsson [7], to a distance of about 200 m from the last application. The way to eliminate disadvantages of using current methods of reducing the friction coefficient, which are:

- limited range of impact;
- the need for calibration;
- requirement for precise dosing;
- danger of failure of the lubricant distributing to the entire rolling surface, resulting in a critical decrease of tractive/braking forces;

the need to refill the lubricant, etc.

could be use of the self-lubricating coatings applied to the wheel flange. The self-lubricating coatings have been successfully utilized in many cases in which the friction coefficient modification is required, without interfering the materials of contacting surfaces. Preliminary laboratory test stand studies on a full-scale wheelset carried out by the Plasma Systems have shown significantly lower flange wear by using thin brass layer - from 0.89 mm to 0.09 mm [8]. Similar effects are observed in the case of the rail.

3 Rail vehicle dynamics modelling

3.1 General approach

In the case of a simulation analysis of the rail vehicle dynamics and wheel profile wear, it is necessary to create mathematical models of a vehicle, rolling contact and the track. Literature on modelling the rail-track vehicle system is abundant and diverse. One can distinguish three basic subsystems of the aforementioned system, such as track, contact zone with rail and rail vehicle. The problem of the track modelling can be found in such works as [9-11]. The issues of rail vehicle dynamics and wheel-rail contact modelling are discussed in the works, e.g. [12-18]. Damages of vehicles' running gear elements and their effect on dynamic behaviour are analysed by [19-22]. The mechanism of phenomena, occurring in the contact zone, is an interest of tribologists and researchers dealing with wearing of materials in the contact area [23-26]. It should be noted that there is no global theory explaining the mechanism of wear in general, also including the wheel-rail contact.

Investigation of dynamic properties of a rail vehicle as a mechanical system should begin with presentation of its physical model (Figure 2), whose dynamic properties are described by equations of motion.

This general model belongs to the group of the "low-frequency" models. It is assumed that the upper limit of the low-frequency vibration range is about 25 Hz [13]. Inertial objects of the vehicle - wheelsets and body - performing low-frequency vibrations behave like rigid bodies. These solids are connected by means of massless suspension elements: springs and dampers, whose characteristics can be linear or nonlinear. Sources of vibrations in the rail vehicle-track system are, in the considered issue, geometric irregularities of the track and inertial forces.

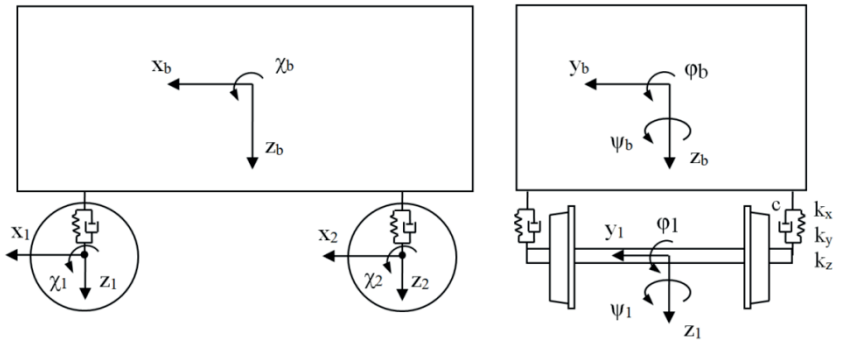

Figure 2 *Physical model of a double wheelset wagon*

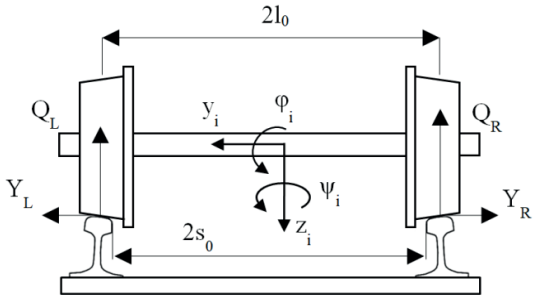

Figure 3 *Illustration of a wheelset in track*

The presented problem of a vehicle's dynamic behaviour and wheel wear requires including vibrations of the body and wheelsets, because they affect changes of the wheel loads on the rails and consequently the variations of the contact forces values. The general structure of the system of equations, describing the vibrating motion, is represented by Equation (1):

$$M\ddot{q} + C\dot{q} + Kq = p(t,q,\dot{q}) \tag{1}$$

where: M - inertia matrix, C - damping matrix, K- stiffness matrix, q - vector of generalised coordinates describing motion of a solid (translations and rotations), $\dot{q}$ - vector of generalised velocities, $p(t,q,\dot{q})$ - vector of forces (moments), which can be treated as the sum of two vectors:

$$p(t,q,\dot{q}) = f(t) + h(q,\dot{q}) \tag{2}$$

where: $f(t)$ - vector of exciting forces, $h(q,\dot{q})$ - vector of forces depending nonlinearly on displacements and velocities of the system, including the contact forces.

Kinematic constraints on the wheelset are a result of its interaction with a rigid track. As a consequence, the vertical displacement z and roll angle φ are related to lateral displacement of the wheelset y and its yaw angle ψ. Angle of rotation χ accounts for the coordinate describing position of the wheelset's mass centre along track x. The form of constraints is nonlinear and depends on the geometric parameters of the wheelset and track, including track gauge, track cant, wheel and rail profiles and the wheelset tape circle distance.

To express equations of motion of a wheelset, its schematic illustration is depicted in Figure 3, containing the selected force vectors and geometric quantities.

Equations of a wheelset in motion, including the elements of primary suspension, may have a different form, bearing in mind the number of degrees of freedom or the model of contact between the wheel and the rail. Following Chudzikiewicz [27], the simplified equations of motion of the i-th wheelset can be written in the form:

$$m\ddot{y}_i = Y_{Li} + Y_{Ri} - (Q_{Li} + Q_{Ri})\Theta_t + P_{yi} - m\frac{v^2}{R_i}, \tag{3}$$

$$I_z\ddot{\psi}_i = (F_{xLi} - F_{xRi})s_i + M_{zi} - I_z\left(\frac{1}{R_i} - \frac{1}{R_{i+1}}\right)\frac{v^2}{2l_0}, \tag{4}$$

$$I_y\ddot{X}_i = F_{xLi}\cdot r_{Li} + F_{xRi}\cdot r_{Ri}, \tag{5}$$

where:
v - vehicle velocity [m/s], m - wheelset mass [kg], I_y, I_z - wheelset polar and yaw moment of inertia [kg·m^2], l_0 - half of the wheels' tape circles distance [m], s_i - current semi track gauge [m], R_i - track curve radius (in i-th wheelset position) [m], r_{Li}, r_{Ri} - left and right wheel rolling radii [m], Y_{Li}, Y_{Ri} - left and right wheel/rail lateral forces (parallel to the track plane) [N], Q_{Li}, Q_{Ri} - left and right wheel/rail vertical forces [N], F_{xLi}, F_{xRi} - left and right wheel/rail longitudinal creep forces [N], Θ_t - track cant [rad], P_{yi} - lateral wheelset suspension forces [N], M_{zi} - yaw bogie suspension moment [Nm].

3.2 The wheel-rail contact

The wheel-rail contact zone, whose area is approximately 1 cm^2, is an interface of the two subsystems: vehicle and track. The forces generated in the contact area and transmitted to both subsystems are vital from the point of view of a vehicle dynamics, since in general,

they determine vehicle's behaviour in track and properties such as running stability and wear of wheels and rails. Their unfavourable distribution, e.g. due to wear of a wheel and/or rail profiles, can increase the risk of derailment. Mathematical description of the contact force generation mechanism is complicated due to the fact that all the contact parameters strongly depend on the wheel and rail geometry and that in some circumstances multiple points of contact may occur.

In general, the current approach to the study of contact between the wheel and rail can be divided into two problems:

- normal problem - location and size of the contact patch and normal stresses distribution (solution based mainly on Hertz contact theory [12-13]),
- tangential problem - calculation of tangent stresses and values of tangent forces.

Analysis of the normal problem and its solution is necessary for the formulation of the tangent problem. Mechanism of contact forces generation, tangent to the contact plane, can be explained due to a difference in strain rates of the two bodies in the contact region [28], caused by deviations of a wheel from pure rolling. Such forces are exerted by a wheel on a rail when a tractive/braking torque is applied to the wheel, in the case of curving (yaw angle) or when suspension lateral forces act on a wheelset. As a result, the contact area is thus divided into an adhesion zone (stick) and a slip zone. Depending on the conditions, the contact patch is divided into different proportions, into the area in which the stick and the slip area occur. The size of the slip area depends on the geometry of the wheel and rail in the contact patch, normal and lateral forces, as well as the friction coefficient. The zone, in which slip of interacting surfaces occurs, has a direct effect on their wear. To express the relative difference of pure rolling and rolling with sliding, Carter defined creep (or creepage) in the longitudinal direction, which the term was later extended to the lateral direction along with spin creep. Longitudinal γ_x, lateral γ_y and spin creepage ω_{sp} can be defined, basing on Wickens [17], as follows:

$$\gamma_x = \frac{V_x^w - V_x^r}{\frac{1}{2}(V_x^w + V_x^r)}, \tag{6}$$

$$\gamma_y = \frac{V_y^w - V_y^r}{\frac{1}{2}(V_y^w + V_y^r)}, \tag{7}$$

$$\omega_{sp} = \frac{\Omega_z^w - \Omega_z^r}{\frac{1}{2}(V_y^w + V_y^r)}, \tag{8}$$

where:
$V^w{}_x$, $V^w{}_y$ - rigid body velocities of the wheel in the x and y directions [m/s], respectively; $V^r{}_x$, $V^r{}_y$ - rigid body velocities of the contact point of the rail in y-direction [m/s]; $\Omega^w{}_z$, $\Omega^r{}_z$ - angular velocities of the wheel and rail about z-axis [rad/s].

The contact forces F_x (longitudinal), F_y (lateral) are functions of creep and thus also called the creep forces. The algorithms of creep forces generation emerged in the 20th century and have established the basis for the codes implemented in the rail vehicle dynamics simulation software. Kalker's simplified algorithm FASTSIM [29], based on the 'stripes theory', is the most widely used in simulations due to sufficient accuracy for engineering purpose and low computational costs. In this algorithm, the elliptical contact zone is divided into parallel longitudinal stripes of width Δy_i and length along the x-axis dependent on the ellipse size. Moreover, all the stripes are divided into the same number of elements and stress calculation is initiated from ellipse edge, element by element [12].

For small values of the creepages and spin, there is a linear relationship between the creep forces and the creepages. Values of those forces can be calculated using other Kalker's algorithm, the so-called Linear Theory [12-13, 27]:

$$\begin{bmatrix} F_x \\ F_y \\ M \end{bmatrix} = -Gab \begin{bmatrix} C_{11} & 0 & 0 \\ 0 & C_{22} & \sqrt{ab}\,C_{23} \\ 0 & -\sqrt{ab}\,C_{23} & abC_{33} \end{bmatrix} \begin{bmatrix} \gamma_x \\ \gamma_y \\ \omega_{sp} \end{bmatrix}, \tag{9}$$

where:
C_{11}, C_{22}, C_{23}, C_{33} - tabularized Kalker's microslip coefficients; G - shear modulus [Pa]; a and b -contact ellipse semi-axes [m].

The lateral components of creep forces must be projected onto the track plane and summed up to give the guiding force Y [12].

4 Simulation conditions

4.1 Vehicle model

Study of the effect of self-lubricating coatings on vehicle dynamics and wheel wear was carried out on a multibody model representing a two-axle goods wagon. Parameters of the model are derived from the Es series 3W/1 goods wagon, fully laden (Table 1). The axle load is 22.3 tons and the wheels have a standard S1002 profile.

The vehicle model was created in the VI-Rail software, which is based on ADMAS multibody simulation environment. The model consists of inertial elements (rigid bodies) representing wheelsets, axle boxes and body, which are connected by means of joints and massless spring and damping elements. The ADAMS software generates automatically and solves equations of motion for individual inertial elements of a complex mechanical system. The dynamic behaviour of the elements of the system is described in ADAMS environment by means of a system of differential-algebraic equations derived from the Euler-Lagrange formalisms presented in a general form [30]:

$$\frac{d}{dt}\left(\frac{\partial L}{\partial \dot{q}}\right) - \frac{\partial L}{\partial q} + \boldsymbol{\Phi}_q^T \boldsymbol{\lambda} = Q, \tag{10}$$

where:
q - vector of generalized coordinates; L - Lagrangian (difference of kinetic and potential energy: $L = T - V$);

Table 1 *Parameters of the two-axle good wagon*

parameter	value	unit
body mass	40770	kg
body moment of inertia I_{xx}	$35 \cdot 10^3$	kg·m^2
body moment of inertia I_{yy}	$220 \cdot 10^3$	kg·m^2
body moment of inertia I_{zz}	$220 \cdot 10^3$	kg·m^2
wheelset mass	1925	kg
wheelset moment of inertia I_{xx}	950	kg·m^2
wheelset moment of inertia I_{yy}	150	kg·m^2
wheelset moment of inertia I_{zz}	950	kg·m^2
spring longitudinal stiffness k_x	$12 \cdot 10^6$	N/m
spring lateral stiffness k_y	$640 \cdot 10^3$	N/m
spring vertical stiffness k_z	$1.8 \cdot 10^6$	N/m
vertical damping (one damper)	$100 \cdot 10^3$	Ns/m
wheelset base	5.2	m
wheel radius	0.5	m

Φ_q - Jacobian matrix of constraints; $\boldsymbol{\lambda}$ - vector of Lagrange multipliers;
Q - vector of external forces.

Systems of nonlinear differential equations are solved by the ADAMS solver numerically, mainly using the Newton-Raphson method. The method of creep-force computation, implemented in the simulation software, is based on the Kalker's FASTSIM algorithm. The code uses the actual wheel and rail profile and calculates the actual contact kinematics at each simulation step. Moreover, it models non-elliptical contact zones, as well as multiple contact patches. Contact stiffness is found according to Boussinesq formulation.

4.2 Self-lubricating coating model

In general, the simulation wear analyses of the wheel and rail profiles known from literature, assumed constant value of the wheel-rail coefficient of friction profiles, not taking into account lateral position of the wheelset relative to the track. In the case of applying the self-lubricating coating to the wheel flange, contact conditions will change depending on the location of the point (area) of contact. In this case, the coefficient of friction, for the area covered with the coating, is different, while the other coefficient value is along the wheel tread profile. Undoubtedly, this will have a significant impact on the wear rate of wheel and rail profiles.

The proposed model of the self-lubricating layer describes two values of friction coefficient [31-32]:

- $\mu_1 = 0.4$ for the wheel tread-rail contact,
- $\mu_2 = 0.1$ for the wheel flange-rail contact.

In order to express it mathematically, it is assumed that the coatings would be applied on the wheels' flanges to minimize friction and as a consequence wheel/rail wear:

$$\mu = \begin{cases} \mu_1 & \text{for } -6\text{mm} < y < 6\text{mm} \\ \mu_2 & \text{for } y \leq -6\text{mm} \wedge y \geq 6\text{mm} \end{cases}. \tag{11}$$

The transition between μ_1 and μ_2 is smoothed with software's in-built spline function. The value of 6 mm has been set based on the analysis of the wheel-rail contact points location with respect to the wheelset lateral displacement. The wheelset lateral shift of 6 mm corresponds to location of a contact point on a flange root [13]. Preliminary simulation tests have shown that for values lower than 6 mm there exists a very high risk of derailment, expressed in higher values of Y/Q (Nadal formula - quotient of lateral to vertical force).

The starting point for considering the wear model of a wheelset with a self-lubricating coating is the measure called the wear number (W_n) based on the widely used T-gamma energy model, whose assumption is the proportional relationship between the amount of worn material and the dissipated energy in the wheel-rail contact zone [33]:

$$W_n = F_x \gamma_x + F_y \gamma_y, \quad [\text{N}]. \tag{12}$$

The spin component $M\omega_{sp}$ in Equation (12) is neglected due to its low value compared to longitudinal and lateral components. In contrast to the classic wear model of Archard [34], the T-gamma model comprises friction coefficient between wheel and rail implicitly. The values of the developed creep forces F_x and F_y are limited by the friction coefficient μ and normal force N in the contact zone:

$$F_{\max} = \mu N, \quad [\text{N}]. \tag{13}$$

In the simulation tests, a simplifying assumption, based on immutability of material parameters, such as Young's modulus or Poisson's coefficient, was adopted - i.e. the thin

Table 2 *Track profiles (TC - transition curve)*

scenario 1		scenario 2	
distance (m)	radius (m)	distance (m)	radius (m)
0	∞	0	∞
29.75	∞/TC	50	∞/TC
30	150 (right)	85	1200 (right)
109.75	150 (right)/TC	485	1200 (right) /TC
110	∞	510	∞
120.92	∞/TC	560	∞/TC
120.98	-150 (left)	595	-1200 (left)
200.92	-150 (left)/TC	995	-1200 (left) /TC
200.98	∞	1030	∞
220	∞	1080	∞

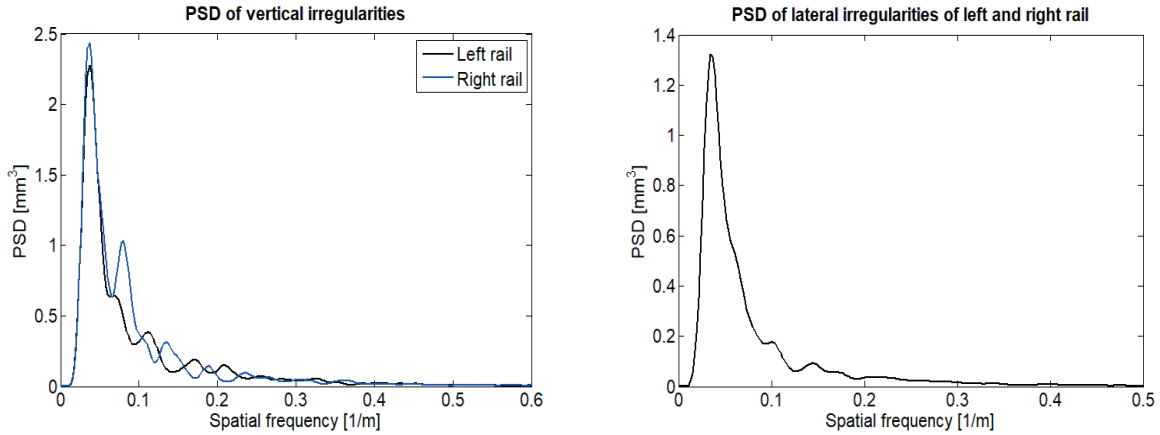

Figure 4 *Power spectral densities of the track irregularities*

self-lubricating bronze layer has the same properties as a wheel material.

4.3 Simulation scenarios

Simulation experiments have been carried out according to the following scenarios:

- Scenario 1 - vehicle moving on track with curves of R = 150 m radii at v = 30 km/h.
- Scenario 2 - vehicle moving on track with curves of R = 1200 m radii at v = 80 km/h.

The proposed scenarios reflect the curve radii characteristic for mountain routes (scenario 1, e.g. route Cracow-Zakopane in Poland) and common in lowland and hilly areas (scenario 2). The routes were designed to comprise a tangent track and S curve sections of normal gauge (1435 mm). The track cant in both scenarios is equal to 15 cm and rail profile is standard, unworn UIC60. Track profiles are described in Table 2.

The track vertical stiffness was assumed as infinite. The vertical and lateral track irregularities correspond to a medium quality of maintenance level. Statistical parameters of the track irregularities are shown in Table 3, whereas the power spectral densities of irregularities are depicted in Figure 4. Apart from the track geometry, track irregularities are an additional source of the wheelset-track dynamic interaction, causing vibrations of the model's inertial elements and thus grater variations of the contact forces.

5 Simulation study results

A quantitative comparison of the dynamic behaviour of the wagon with the standard wheelsets and the wagon with wheelsets covered with self-lubricating coatings is shown in Figures 5-7. Particularly important in a rail vehicle dynamics analysis is lateral displacement of the wheelset relative to the track centreline. In curves without gauge widening (radius R > 250 m) values exceeding 9 mm might indicate severe wheel flange-rail contact and high risk of derailment. In the case of scenario 1 (R = 150 m), lateral shifts of the leading and trailing wheelset with self-lubricating coatings are lower, however, these wheelsets are displaced in opposite directions compared to the standard wheelsets (Figure 5). Unfortunately, in the curves of greater radii (R = 1200 m, scenario 2), results obtained for the vehicle with coatings are worse, i.e. 3 - 4 mm higher displacements for both wheelsets are observed (Figure 6).

Developed lateral forces are crucial to guiding the wheelset in track, albeit too high values negatively affect

Table 3 *Height of the track irregularities*

height (mm)	left Y	left Z	right Y	right Z
min.	-8.1	-11.1	-8.1	-11.5
max.	8.8	13.2	8.8	12.5
standard dev.	3.0	4.2	3.0	4.5

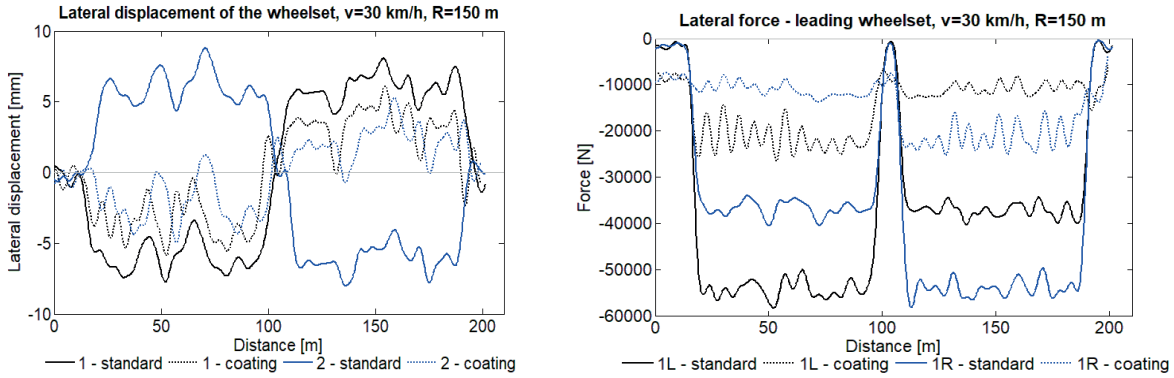

Figure 5 *Lateral displacement of both wheelsets (left) and lateral force of the leading wheelset (right) - scenario 1*

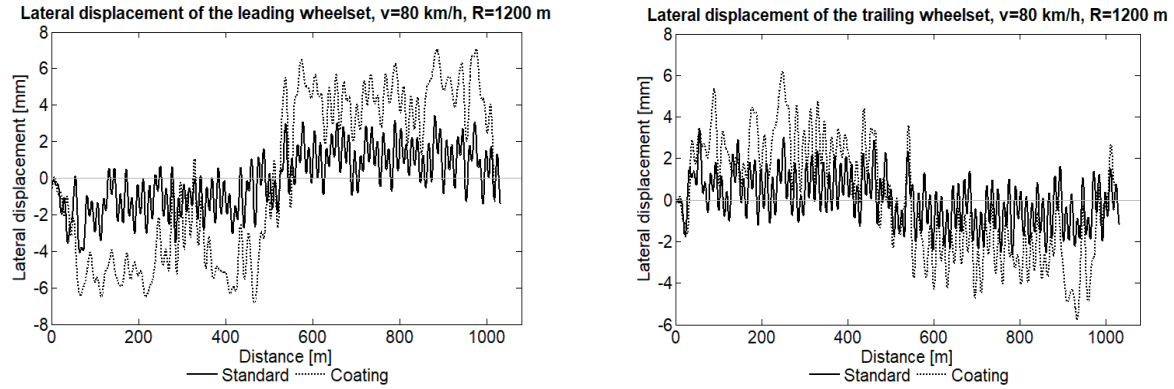

Figure 6 *Lateral displacement of the leading (left) and trailing wheelset (right) - scenario 2*

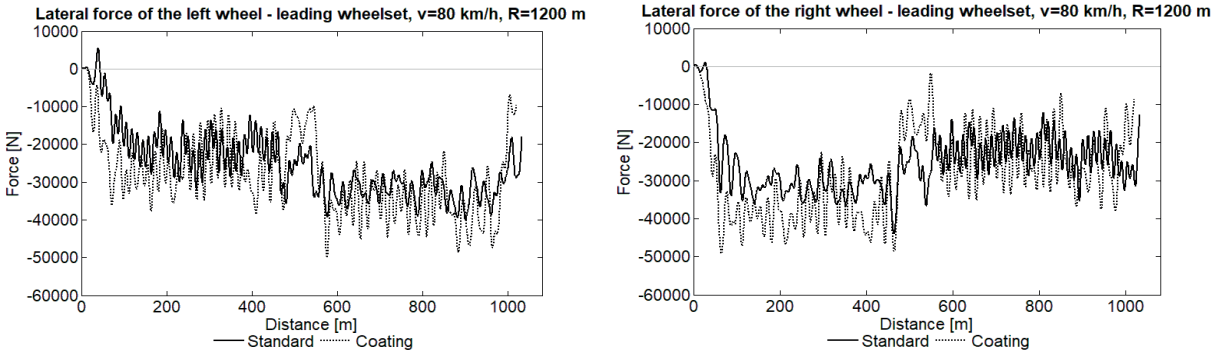

Figure 7 *Lateral force of the left and right wheel of the leading wheelset - scenario 2*

safety against derailment and contribute to accelerated wheel wear. In scenario 1 a significant decrease of lateral forces is observed, which is the result of the lower friction coefficient and lateral displacement (Figure 7 bottom). On the other hand, in the curves of R = 1200 m, the wheelsets with self-lubricating coatings are affected by noticeably higher lateral forces, being an objectionable feature. The differences in force values for both wheelsets are up to cca. 10 kN.

Following analysis of the lateral forces, one can investigate the lateral acceleration of the wheelsets. The greater lateral forces in the case of wheelset with coating entail the higher values of acceleration (Figure 8). This fact could have a negative effect on the ride comfort in the case

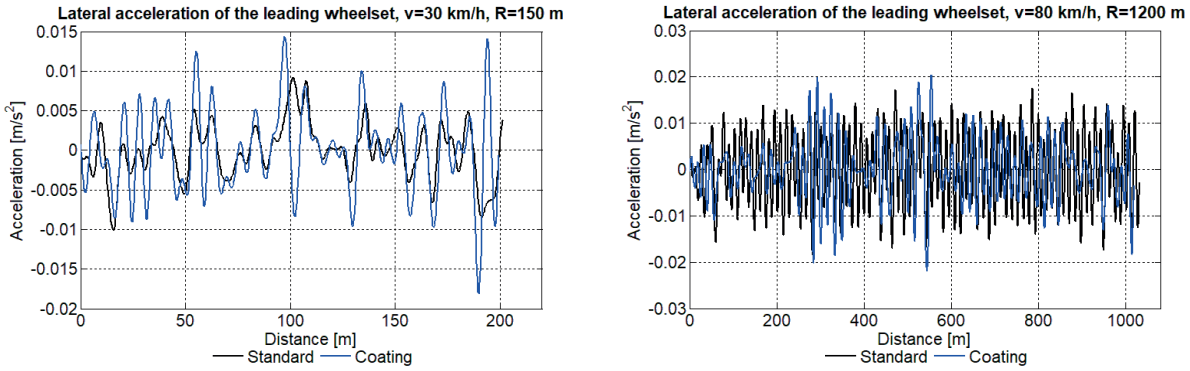

Figure 8 *Lateral acceleration of the leading wheelset - scenario 1 (left), scenario 2 (right)*

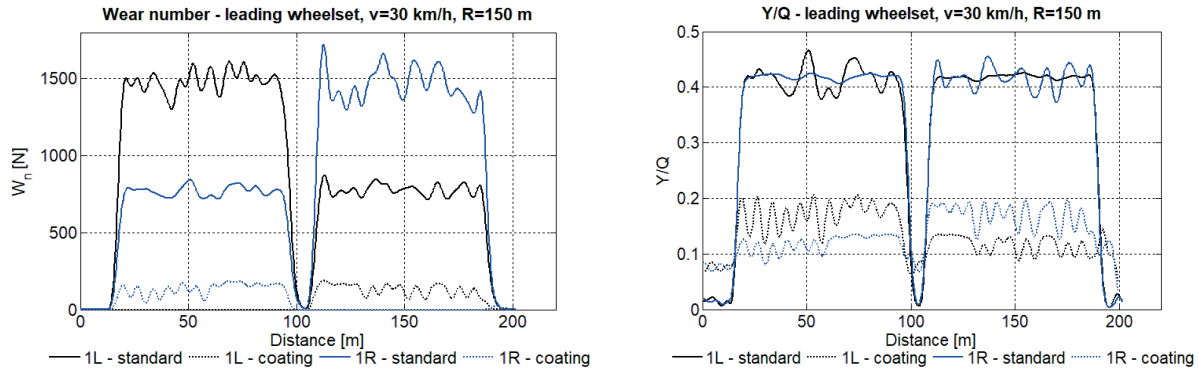

Figure 9 *Comparison of the wear number and mean Y/Q values - scenario 1*

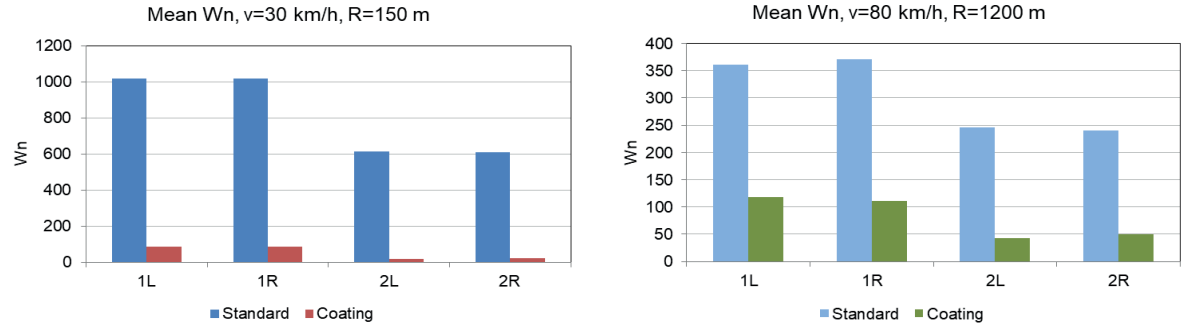

Figure 10 *Comparison of the mean wear number W_n values - scenario 1 (left), scenario 2 (right)*

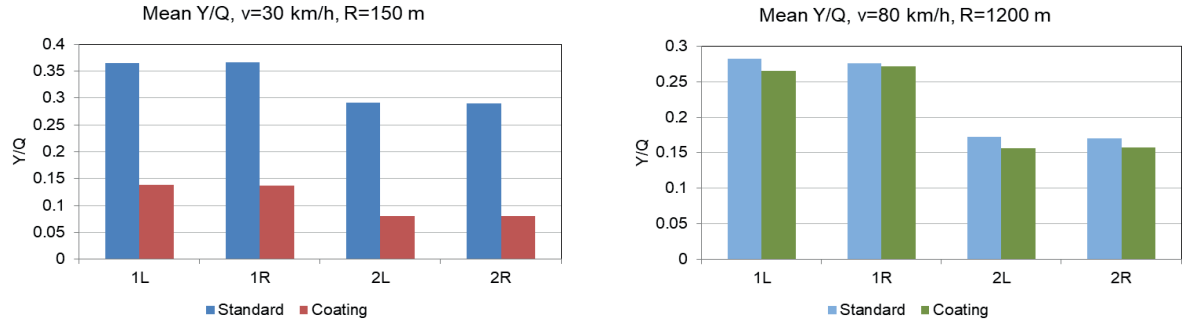

Figure 11 *Comparison of mean Y/Q values - scenario 1 (left), scenario 2 (right)*

of passenger coaches, nonetheless, it can be omitted when dealing with the transport of goods.

The next part of the analysis focuses on parameters estimating the wheel wear - W_n and safety against derailment - *Y/Q*. Examples of recorded values of W_n and *Y/Q* from scenario 1 are presented in Figure 9.

Predicted mean wear rate of the wheels' profiles, based on the T-gamma model, is lower for the wheelsets

with coatings. Especially low values of W_n are calculated for scenario 1, in which the wear is expected to be reduced up to cca. 10 times for the wheels of the leading wheelset (Figure 10 left). The wear number, obtained in scenario 2 for the wheelsets with coatings, is also lower despite the higher lateral forces (Fig. 10 right). In this case, the favourable W_n values are obtained due to the lower creep than in scenario 1. Along with increasing curve radius, application of the self-lubricating coatings should still be beneficial - the wear would be up to 5 times lower (for the wheels of the trailing wheelset).

In order to assess influence of the self-lubricating coatings on safety against derailment, the mean values of *Y/Q* forces ratio are compared in Figure 11. A similar dependence is noticed as in the case of W_n comparison - the smaller curve radius the greater the benefit of using coatings. In scenario 1 safety against derailment was substantially improved, yet the results obtained from scenario 2 show that coatings have only slightly positive effects on the *Y/Q* ratio.

6 Conclusions

Phenomenon of the wheel and rail wear generates significant operating costs and is a problem from the point of view of availability of the transport means and infrastructure. One of the most recent and potential solutions to reduce wear is application of the self-lubricating coatings on the wheel flange. These coatings reduce the friction coefficient of the wheel-rail interface.

Dynamic properties of the rail vehicle cannot remain unaffected due to modification of the friction coefficient. The aim of the study presented herein was an assessment of the self-lubricating coatings impact on dynamic behaviour of a vehicle, with special regard to safety against derailment and wheel wear.

The simulation tests were performed on a two-axle goods wagon, considering randomly generated geometrical track irregularities, in order to model the medium maintenance level. The simulation results allow formulating the conclusion that dynamic properties of a vehicle with wheels covered with the self-lubricating coatings enable the use of such a vehicle in safe conditions, not worse than in the case of a vehicle with standard wheels.

In the case of wagons with wheelsets covered with the self-lubricating coatings, the wear of the wheels' surface should be at least 2 times lower compared to wagons in which the wheels have not been covered with such a coating. Consequently, the lifecycle of the wheelset should be extended, taking into account only wear of the wheel profiles. Benefits, resulting from applying the self-lubricating coatings, will be particularly evident during the operation of vehicles on routes containing a significant number of low-radii curves, where the predicted wear would be up to 5 times lower.

The next actions taken in the study of the self-lubricating coatings should focus on evaluating their durability in operational conditions and comparing the costs and frequency of applying/replacing the new layers to the costs of the wheel reprofiling.

References

[1] POMBO, J. Application of a computational tool to study the influence of worn wheels on railway. *Journal of Software Engineering and Applications* [online]. 2012, **5**(2), p. 51-61. ISSN 1945-3116. Available from: https://doi.org/10.4236/jsea.2012.52009

[2] HAUSER, V., NOZHENKO, O., KRAVCHENKO, K., LOULOVA, M., GERLICI, J., LACK, T. Impact of three axle boxes bogie to the tram behaviour when passing curved track. *Procedia Engineering* [online]. 2017, **192**, p. 295-300. ISSN 1877-7058. Available from: https://doi.org/10.1016/j.proeng.2017.06.051

[3] MACIEJEWSKI, I., KRZYZYNSKI, T., CHUDZIKIEWICZ, A., SOWINSKA, M. Concept of the control system for a single wheelset with independently rotating wheels driven by induction motors. *Machine Dynamics Research*. 2016, **40**(1), p. 53-63. ISSN 2080-9948.

[4] MELNIK, R., SOWINSKI, B. Analysis of dynamics of metro vehicle model with differential wheelsets. *Transport Problems* [online]. 2017, **12**(3), p. 113-124. ISSN 1896-0596. Available from: https://doi.org/10.20858/tp.2017.12.3.11

[5] OLOFSSON, U., ZHU, Y., ABBASI, S., LEWIS, R., et al. Tribology of the wheel-rail contact - aspects of wear, particle emission and adhesion. *Vehicle Systems Dynamics* [online]. 2013, **51**(7), p. 1091-1120. ISSN 1744-5159. Available from: https://doi.org/10.1080/00423114.2013.800215

[6] SUNDH J. *On wear transitions in the wheel-rail* contact. Doctoral thesis. Stockholm, Sweden: KTH Royal Institute of Technology, 2009.

[7] NILSSON, R. *On wear in rolling/sliding contacts*. Doctoral thesis. Stockholm, Sweden: KTH Royal Institute of Technology, 2005.

[8] Plasma Systems [online] [accessed 2020-02-18]. Available from https://www.plasmasystem.pl/en/industries/rail-transport

[9] DROZDZIEL, J., SOWINSKI, B. Simulation of railway track deterioration influenced by ballast stiffness and dry friction. In: *Computers in railways XI*. Southampton (UK): WIT Press, 2008. ISBN 978-1-84564-126-9, p. 693-702.

[10] TUTUMLUER, E., QIAN, Y., HASHASH, Y. M. A., GHABOUSSI, J., DAVIS, D. D. Discrete element modelling of ballasted track deformation behaviour. *International Journal* of *Rail Transportation* [online]. 2013, **1**(1-2), p. 57-73. ISSN 2324-837, eISSN 2324-8386. Available from: https://doi.org/10.1080/23248378.2013.788361

[11] KOZIAK, S., CHUDZIKIEWICZ A., OPALA, M., MELNIK, R. Virtual software testing and certification of railway vehicle from the point of view of their dynamics. *Transportation Research Procedia* [online]. 2019, **40**, p. 729-736. ISSN 2352-1465. Available from: https://doi.org/10.1016/j.trpro.2019.07.103

[12] IWNICKI, S. *Hanbook of railway vehicle dynamics.* Boca Raton (FL): CRC Press, 2006. ISBN 9780849333217.

[13] KNOTHE, K., STICHEL, S. *Rail vehicle dynamics* [online]. Cham, Switzerland: Springer 2017. ISBN 978-3-319-45376-7. Available from: https://doi.org/ 10.1007/978-3-319-45376-7

[14] KONOWROCKI, R., WALCZAK, S. Influence of flexibility parameters of wheels and wheelset on the railway bogie dynamics. Experimental and theoretical investigations. *Machine Dynamics Research*. 2017, **41**(1), p. 41-53. ISSN 2080-9948.

[15] LACK, T., GERLICI, J. A modified strip method to speed up the tangential stress between wheel and rail calculation. *Applied Mechanics and Materials* [online]. 2014, **486**, p. 371-378. ISSN 1662-7482. Available from: https://doi.org/10.4028/www.scientific.net/AMM.486.371

[16] OPALA, M. Evaluation of bogie centre bowl friction models in the context of safety against derailment simulation predictions. *Archive of Applied Mechanics* [online]. 2018, **88**(6), p. 943-953. ISSN 0939-1533. Available from: https://doi.org/10.1007/s00419-018-1351-4

[17] WICKENS, A. *Fundamentals of rail vehicle dynamics: guidance and stability*. 1 ed. Lisse: Swets, 2003. ISBN 902651946X.

[18] ZBOINSKI, K., DUSZA, M. Bifurcation analysis of 4-axle rail vehicle models in a curved track. *Nonlinear Dynamics* [online]. 2017, **89**(2), p. 863-885. ISSN 1573-269X. Available from: https://doi.org/10.1007/s11071-017-3489-y

[19] FIRLIK, B., CZECHYRA, B., CHUDZIKIEWICZ, A. Condition monitoring system for light rail vehicle and track. *Key Engineering Materials* [online]. 2012, **518**, p. 66-75. ISSN 1662-9795. Available from: https://doi.org/10.4028/www.scientific.net/KEM.518.66

[20] DIZO, J., STEISUNAS, S., BLATNICKY, M. Vibration analysis of a coach with the wheel-flat due to suspension parameters changes. *Procedia Engineering* [online]. 2017, **192**, p. 107-112. ISSN 1877-7058. Available from: https://doi.org/10.1016/j.proeng.2017.06.019

[21] DUMITRIU, M., GHETI, M. A. Evaluation of the vertical vibrations behaviour of the bogie at failure of the dampers in the primary suspension of the railway vehicle. *MATEC Web of Conferences* [online]. 2018, **178**, p. 1-6. ISSN 2261-236X. Available from: https://doi.org/10.1051/matecconf/201817806001

[22] MELNIK, R., KOZIAK, S. Rail vehicle suspension condition monitoring - approach and implementation. *Journal of Vibroengineering* [online]. 2017, **19**(1), p. 487-501. ISSN 2538-8460. Available from: https://doi.org/10.21595/jve.2016.17072

[23] CHUDZIKIEWICZ, A., KORZEB, J. Simulation study of wheels wear in low-floor tram with independently rotating wheels. *Archive of Applied Mechanics* [online]. 2018, **419**(88), p. 175-192. ISSN 0939-1533. Available from: https://doi.org/10.1007/s00419-017-1301-6

[24] LEWIS, R., DWYER-JOYCE, R. S., LEWIS, S. R., HARDWICK, C., GALLARDO-HERNANDEZ, E. A. Tribology of the wheel-rail contact: the effect of third body materials. *The International Journal of Railway Technology* [online]. 2012, **1**(1), p. 167-194. ISSN 2049-5358. Available from: http://dx.doi.org/10.4203/ijrt.1.1.8

[25] TOMBERGER, C., DIETMAIER, P., SEXTRO, W., SIX, K. Friction in wheel-rail contact: a model comprising interfacial fluids, surface roughness and temperature. *Wear* [online]. 2011, **271**(1-2), p. 2-12. ISSN 0043-1648. Available from: https://doi.org/10.1016/j.wear.2010.10.025

[26] ZHU, Y. *Adhesion in the wheel-rail contact under contaminated conditions.* Licentiate thesis. Stockholm, Sweden: KTH Royal Institute of Technology, 2011.

[27] CHUDZIKIEWICZ, A. Evolution of the simulation study of a railway wheel profile through wear. In: 2nd Mini Conference on Contact Mechanics and Wear of Rail/Wheel Systems: proceeding. Budapest: University of Technology and Economics, 1996. ISBN 963-420-509-7, p. 207-214.

[28] GARG, V. K., DUKKIPATI, R. V. *Dynamics of railway vehicle systems.* Toronto (T.O.): Academic Press, 1984. ISBN 0-12-275950-8.

[29] KALKER, J. J. Fast algorithm for the simplified theory of rolling contact. *Vehicle System Dynamics* [online]. 1982, **11**(1), p. 1-13. ISSN 1744-5159. Available from: https://doi.org/10.1080/00423118208968684

[30] MCCONVILLE, J. B., MCGRATH, J. F. *Introduction to ADAMS theory*. Ann Arbor (MI): Mechanical Dynamic Inc., 1998.

[31] CHUDZIKIEWICZ, A., MELNIK, R., GORA, I. Wheelsets' self-lubricating coatings in terms of rail vehicle dynamic properties. *Prace Naukowe Politechniki Warszawskiej - Transport* [online]. 2019, **124**, p. 19-30. ISSN 1230-9265.

Available from: https://www.wt.pw.edu.pl/Badania-i-nauka/Prace-Naukowe-Politechniki-Warszawskiej-Transport/Zeszyty/Zeszyt-124

[32] GORA, I. *Modeling and simulation testing of dynamic properties of a railway wheelset using innovative self-lubricating coatings*. Doctoral thesis. Warsaw, Poland: Warsaw University of Technology, 2018.

[33] PEARCE, T. G, SHERRATT, N. D. Prediction of wheel profile wear. *Wear* [online]. 1991, **144**, p. 343-351. ISSN 00431648. Available from: https://doi.org/10.1016/b978-0-444-88774-0.50027-4

[34] ARCHARD, J. F. Contact and rubbing of flat surfaces. *Journal of Applied Physics* [online]. 1953, **24**, p. 981-988. ISSN 1089-7550. Available from: https://doi.org/110.1063/1.1721448

MODELLING OF CRITICAL VELOCITIES OF THE CARDAN MECHANISM USING TRANSFER MATRIX METHOD

Petr Hrubý[1], Tomáš Náhlík[2,*]

[1]Department of Mechanical Engineering, Institute of Technology and Business, Ceske Budejovice, Czech Republic
[2]Department of Informatics and Natural Sciences, Institute of Technology and Business, Ceske Budejovice, Czech Republic

*E-mail of corresponding author: nahlik@mail.vstecb.cz

Resume
The presented paper focuses to rotating components of mechanical constructions. The problem of the spatial combined bending-gyratory vibration and calculation of the Eigen frequencies is studied. The model of Cardan Mechanism is solved by the transfer matrix method. Transfer matrices were derived for shaft, concentrated mass and elastic bearing. The physical and mechanical properties of each part of the mechanism are hidden in these matrices. A procedure for calculating Eigen frequencies was proposed.

Article info
Received 9 April 2020
Accepted 17 June 2020
Online 10 November 2020

Keywords:
critical velocities,
cardan mechanism,
transfer matrix method,
eigen frequencies,
vibrations,
automotive

Available online: https://doi.org/10.26552/com.C.2021.1.B33-B38

ISSN 1335-4205 (print version)
ISSN 2585-7878 (online version)

1 Introduction

In mechanical constructions, the most endangered parts are rotating components, e.g. shafts [1]. Reliability of a shaft is endangered in particular in the two limit states. In the vicinity of resonance, there is an enormous increase in the amplitudes of the state variables and reaching of the yield strength of a material. These conditions often occur with the coupling shafts of Cardan mechanisms. The torque is transmitted here over long distances. Shafts are long and slender and are prone to transverse bending. The gearbox shafts are compact and operate at a sufficient distance from the resonant area. In that case, they are threatened by fatigue fractures; they need to be checked for safety to fatigue. A similar situation to gearboxes is with the gear pump shafts.

Mathematical models of the Cardan mechanism lead to solutions from the field of linear algebraic equations. In the case of bending oscillations, the motion equation of the basic element is a partial differential equation of the 4th order for the variables x and t [2]. An analytical solution for simpler cases can be used.

It seems appropriate, for this case, to use the transfer matrix method. This method does not increase the matrix size (matrix 4 x 4 for planar oscillation, 8 x 8 for spatial oscillation), resulting in the lower hardware requirements. The transfer matrix method uses a combination of analytical and numerical methods. The benefit of this calculation is a possibility to obtain deformations caused by external excitation and dynamic deformation and stress analysis. Using the transfer matrix method is relatively easy to get a solution to the whole system (the whole Cardan mechanism). Another advantage is that it can be combined with the method of the imaginary slice, which analytically solves the differential equations of motion for a smooth shaft (smooth continuum - a constant diameter), the transfer matrices for the shaft, matrices of concentrated mass and the elastic bearing, which are the basic structural elements of a dynamic model of shafts, are derived.

This paper is devoted to studying the problem spatial combined bending-gyratory vibration and calculation of the Eigen frequencies using the transfer matrix method.

2 Spatial combined bending-gyratory vibration

The element (see Figure 1) is an one-dimensional continuum with geometrical parameters as inner radius r_1, outer radius r_2 and length l. The physical parameters are E module of elasticity and density ρ. The whole system is rotating with angular velocity ω.

External forces, acting on the element, create a state of the combined bending-gyratory vibration. The continuum element is making general spatial motion which is composed

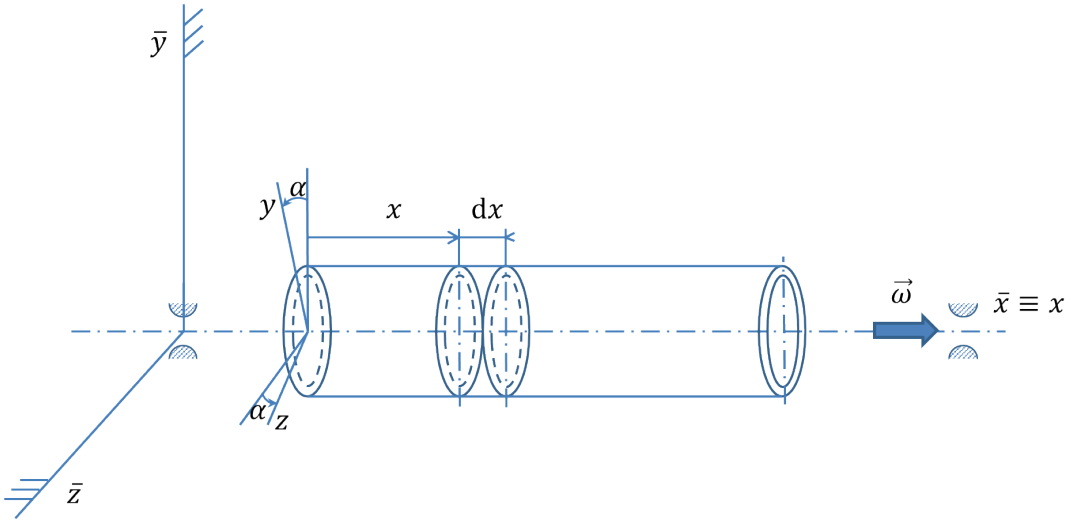

Figure 1 *The element of the continuum*

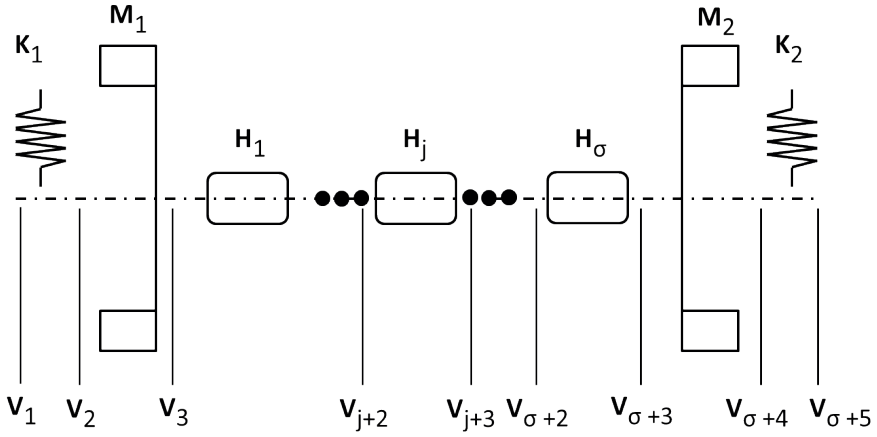

Figure 2 *Model of the whole Cardan mechanism*

of three simple movements - namely rotation, shift and spherical motion.

The following formula represents the equation of motion in the state of spatial combined bending-gyratory vibrations [2]

$$\frac{\partial^4 v}{\partial x^4} - \frac{\rho}{E}\left(\frac{\partial^4 v}{\partial x^2 \partial t^2} + \omega^2 \frac{\partial^2 v}{\partial x^2}\right) + \\ + \frac{4\rho}{E(r_2^2 + r_1^2)}\left(\frac{\partial^2 v}{\partial t^2} - \omega^2 v + 2i\omega \frac{\partial v}{\partial t}\right) = 0, \tag{1}$$

where

$$v(x,t) = y(x,t) + iz(x,t). \tag{2}$$

For more details see [2].

3 Derivation of the transfer matrix

The Transfer Matrix Method (TMM) is a combination of numerical and analytical methods and comes from the exact analytical solution (PDE of 4^{th} order) (see Equation 1).

It is necessary to derive the transfer matrices (matrices are denoted by bold letters, e.g. **H, M, K**) for each of the basic structural elements of the Cardan mechanism: shaft **H**, concentrated mass **M** and elastic bearing **K** (see Figure 2).

One needs to define the vector of state $\mathbf{V}_i$ on the edge cuts of each element based on amplitudes of state variables.

Vector of state (see Equation (2)):

$$\mathbf{V}(x,t) = \mathbf{V}(x)e^{i\omega t}, \mathbf{V}(x) = [\mathbf{Y}(x)|\mathbf{Z}(x)], \tag{3}$$

$$\mathbf{V}(x) = \begin{bmatrix} y(x) \\ y'(x) \\ -M_z(x) \\ -Q_y(x) \end{bmatrix}, \mathbf{Z}(x) = \begin{bmatrix} z(x) \\ z'(x) \\ -M_y(x) \\ -Q_z(x) \end{bmatrix}, \tag{4}$$

where $y(x)$ is the amplitude of deflection, $y'(x)$ is the slope of deflection, $M_z(x)$ is the amplitude of the bending moment and $Q_y(x)$ is the moving force.

Relationship between neighbouring state vectors is $\mathbf{V}_{i+1} = \mathbf{H}_j\mathbf{V}_i$, where $j = 1, ..., \sigma$, i, $i = j + 2$, $\mathbf{V}_2 = \mathbf{K}_1\mathbf{V}_1$, $\mathbf{V}_3 = \mathbf{M}_1\mathbf{V}_2$..., $\mathbf{V}_{\sigma+5} = \mathbf{P} \cdot \mathbf{V}_1$.

The method uses knowledge of boundary conditions of the state vectors of the joint shaft. The frequency

equation can then be determined from the coupling relations between the edge state vectors. The first and the last state vectors of the dynamic model are $\mathbf{V}_1$, resp. $\mathbf{V}_{\sigma+5}$, $\mathbf{V}_1[v_1(0), v_1'(0), 0, 0]^T$, $\mathbf{V}_{\sigma+5} = [0, 0, v_0(l_0), v_0'(l_0)]$.

States vectors $\mathbf{V}_1$ and $\mathbf{V}_{\sigma+5}$ are joint

$$\mathbf{V}_{\sigma+5} = \mathbf{P} \cdot \mathbf{V}_1 \tag{5}$$

The Transfer Matrix $\mathbf{P}$ is:

$$\mathbf{P} = \mathbf{K}_2 \cdot \mathbf{M}_2 \cdot \mathbf{H}_\sigma \ldots \mathbf{H}_j \ldots \mathbf{H}_1 \cdot \mathbf{M}_1 \cdot \mathbf{K}_1. \tag{6}$$

$$\mathbf{P} = \begin{bmatrix} \mathbf{P}_y & 0 \\ 0 & \mathbf{P}_z \end{bmatrix}, \mathbf{P}_y = \mathbf{P}_z = [p_{ij}]_1^4. \tag{7}$$

All the matrices in Equation (5) are of the 8×8 type. Equation (5) describes a system of eight equations of eight unknowns. The matrix $\mathbf{P}$ is blocked diagonal, so this system can be divided into two systems of 4 equations by 4 unknowns. Each system describes the movement of individual axes.

After entering the edge vectors, the transfer matrix and matrix multiplication are

$$\mathbf{A}_y \cdot \mathbf{B}_y = \mathbf{D}_y, \mathbf{A}_z \cdot \mathbf{B}_z = \mathbf{D}_z. \tag{8}$$

4 Solution to the problem

The following matrices, concerning Equations (5) to (7), are obtained.

$$\mathbf{A}_y = \mathbf{A}_z \begin{bmatrix} p_{11} & p_{12} & -1 & 0 \\ p_{21} & p_{22} & 0 & -1 \\ p_{31} & p_{32} & 0 & 0 \\ p_{41} & p_{42} & 0 & 0 \end{bmatrix}. \tag{9}$$

$$\mathbf{B}_y = \begin{bmatrix} y_1(0) \\ y_1'(0) \\ y_0(l_0) \\ y_0'(l_0) \end{bmatrix}, \mathbf{B}_z = \begin{bmatrix} z_1(0) \\ z_1'(0) \\ z_0(l_0) \\ z_0'(l_0) \end{bmatrix}. \tag{10}$$

$$\begin{aligned} \mathbf{D}_y &= M_{1z} \cdot \begin{bmatrix} p_{13} \\ p_{23} \\ p_{34} - M_{2z}/M_{1z} \\ p_{43} \end{bmatrix}, \\ \mathbf{D}_z &= M_{1y} \cdot \begin{bmatrix} p_{13} \\ p_{23} \\ p_{34} - M_{2y}/M_{1y} \\ p_{43} \end{bmatrix}. \end{aligned} \tag{11}$$

The solution of the left edge of the joint shaft is:

$$y_1(0) = \frac{p_{42}(p_{33}M_{1z} - M_{2z}) - p_{32}p_{43}M_{1z}}{p_{31}p_{42} - p_{32}p_{41}}. \tag{12}$$

$$y_1'(0) = \frac{p_{31}p_{43}M_{1z} - p_{41}(p_{33}M_{1z} - M_{2z})}{p_{31}p_{42} - p_{32}p_{41}}. \tag{13}$$

$$z_1(0) = \frac{p_{42}(p_{33}M_{1y} - M_{2y}) - p_{32}p_{43}M_{1y}}{p_{31}p_{42} - p_{32}p_{41}}. \tag{14}$$

$$z_1'(0) = \frac{p_{31}p_{43}M_{1y} - p_{41}(p_{33}M_{1y} - M_{2y})}{p_{31}p_{42} - p_{32}p_{41}}. \tag{15}$$

5 The transfer matrix for a shaft

The transfer matrices for shafts parts have the following form

$$\begin{aligned} &\mathbf{H}(x) = \begin{bmatrix} \mathbf{H}_y(x) & 0 \\ 0 & \mathbf{H}_z(x) \end{bmatrix}, \mathbf{H}_y = \mathbf{H}_z = \\ &= [\mathbf{H}_{11} | \mathbf{H}_{12} | \mathbf{H}_{13} | \mathbf{H}_{14}] \end{aligned}, \tag{16}$$

$$\mathbf{H}_{11} = \frac{1}{\beta_1^2 + \beta_2^2} \begin{bmatrix} \beta_2^2 \cosh\beta_1 l + \beta_1^2 \cos\beta_2 l \\ \beta_1\beta_2(\beta_2 \sinh\beta_1 l - \beta_1 \sin\beta_2 l) \\ EJ\beta_1^2\beta_2^2(\cosh\beta_1 l - \cos\beta_2 l) \\ EJ\beta_1^2\beta_2^2(\beta_1 \sinh\beta_1 l + \beta_2 \sin\beta_2 l) \end{bmatrix}, \tag{17}$$

$$\mathbf{H}_{12} = \frac{1}{\beta_1^2 + \beta_2^2} \begin{bmatrix} \beta_2^2/\beta_1 \sinh\beta_1 l + \beta_1^2/\beta_2 \sin\beta_2 l \\ \beta_2^2 \cosh\beta_1 l + \beta_1^2 \cos\beta_2 l \\ EJ\beta_1\beta_2(\beta_2 \sinh\beta_1 l - \beta_1 \sin\beta_2 l) \\ EJ\beta_1^2\beta_2^2(\cosh\beta_1 l + \cos\beta_2 l) \end{bmatrix}, \tag{18}$$

$$\mathbf{H}_{13} = \frac{1}{\beta_1^2 + \beta_2^2} \begin{bmatrix} 1/EJ(\cosh\beta_1 l - \cos\beta_2 l) \\ 1/EJ(\beta_1 \sinh\beta_1 l + \beta_2 \sin\beta_2 l) \\ \beta_1^2 \cosh\beta_1 l + \beta_2^2 \cos\beta_2 l \\ \beta_1^3 \sinh\beta_1 l + \beta_2^3 \sin\beta_2 l \end{bmatrix}, \tag{19}$$

$$\mathbf{H}_{14} = \frac{1}{\beta_1^2 + \beta_2^2} \begin{bmatrix} 1/EJ(1/\beta_1 \sinh\beta_1 l - 1/\beta_2 \sin\beta_2 l) \\ 1/EJ(\cosh\beta_1 l + \cos\beta_2 l) \\ \beta_1 \sinh\beta_1 l + \beta_2 l \\ \beta_1^2 \cosh\beta_1 l + \beta_2^2 \cos\beta_2 l \end{bmatrix}, \tag{20}$$

where:

$$J = \frac{\pi}{4}(r_2^4 - r_1^4), \tag{21}$$

$$\begin{aligned} \beta_1 = \Bigg\{ &-\frac{\rho}{2E}(\overline{\omega^2} - \omega^2) + \\ &+ \left[\frac{\rho^2}{4E^2}(\overline{\omega^2} - \omega^2)^2 + \frac{4\rho(\overline{\omega} - \omega)^2}{E(r_2^2 + r_1^2)} \right]^{\frac{1}{2}} \Bigg\}^{\frac{1}{2}}. \end{aligned} \tag{22}$$

$$\begin{aligned} \beta_2 = \Bigg\{ &\frac{\rho}{2E}(\overline{\omega^2} - \omega^2) + \\ &+ \left[\frac{\rho^2}{4E^2}(\overline{\omega^2} - \omega^2)^2 + \frac{4\rho(\overline{\omega} - \omega)^2}{E(r_2^2 + r_1^2)} \right]^{\frac{1}{2}} \Bigg\}^{\frac{1}{2}}. \end{aligned} \tag{23}$$

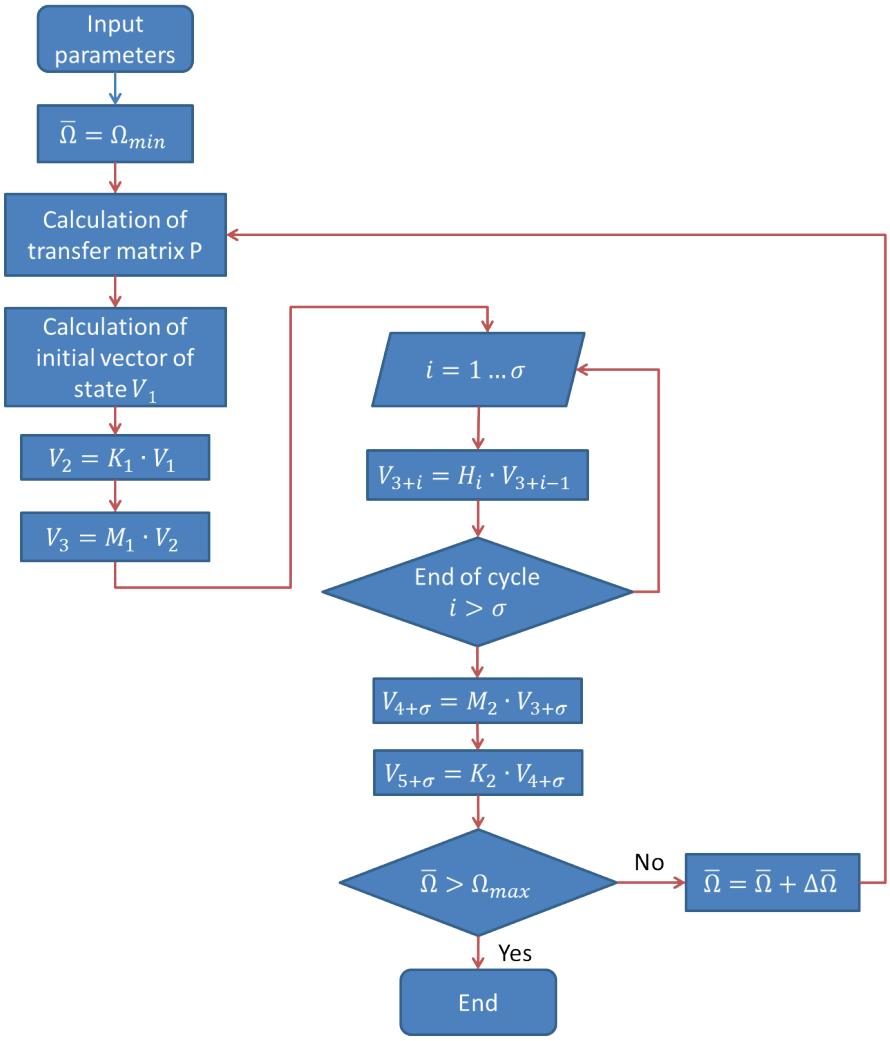

Figure 3 *Process of the Eigen frequencies calculations*

6 The transfer matrix for the concentrated mass

The matrices for concentrated masses are:

$$\mathbf{M} = \begin{bmatrix} \mathbf{M}_y & 0 \\ 0 & \mathbf{M}_z \end{bmatrix}. \tag{24}$$

$$\mathbf{M}_y = \mathbf{M}_z = \begin{bmatrix} 1 & 0 \\ 0 & 1 \\ 0 & -J_1\omega^2 + (J_0 - J_1)\omega^2 \\ m(\overline{\omega} + \omega^2) & 0 \\ 0 & 0 \\ 0 & 0 \\ 1 & 0 \\ 0 & 1 \end{bmatrix} \tag{25}$$

7 Transfer matrix for elastic bearing

Matrices for the elastic bearing can be expressed as:

$$\mathbf{K}(x) = \begin{bmatrix} \mathbf{K}_y & 0 \\ 0 & \mathbf{K}_z \end{bmatrix}. \tag{26}$$

$$\mathbf{K}_y = \mathbf{K}_z = \begin{bmatrix} 1 & 0 & 0 & 0 \\ 0 & 1 & 0 & 0 \\ 0 & 0 & 1 & 0 \\ -k & 0 & 0 & 1 \end{bmatrix}. \tag{27}$$

8 Eigen frequencies

Rewriting of Equation (8) leads to the following equation

$$\mathbf{F} \cdot \mathbf{V} = 0\,, \tag{28}$$

and

$$\mathbf{V} = [v(0), v'(0), v_0(l_0), v_0'(l_0)]^T\,. \tag{29}$$

One obtains set of equations (4 homogeneous equations of 4 unknowns) with matrix

$$\mathbf{F} = \begin{bmatrix} p_{11} & p_{12} & -1 & 0 \\ p_{21} & p_{22} & 0 & -1 \\ p_{31} & p_{32} & 0 & 0 \\ p_{41} & p_{42} & 0 & 0 \end{bmatrix}. \tag{30}$$

Eigen frequencies are the non-trivial solutions of the above sets of equations with matrix Equation (31). Calculation of these solutions goes in a standard way

$$\mathrm{Det}\,\mathbf{F} = 0\,. \tag{31}$$

Frequency determinant $\det \mathbf{F} = f(\Omega)$ is a function of Ω. Eigen frequencies of system are solutions of nonlinear algebraic equation $f(\Omega) = 0$ (i.e., intersections with axis). The number of solutions is indefinite. Appropriate solutions are found only in the interval $(\Omega_{\min}, \Omega_{\max})$.

Process of calculation of Ω is done in several steps (see Figure 3).

It is sufficient to take $\Delta\Omega$ of the order of one hundredth to a thousandth of the length $(\Omega_{\max} - \Omega_{\min})$ of the frequency interval.

If the signum of the function $f(\Omega)$ changes between $\Omega_{\min} + j \cdot \Delta\Omega$ and $\Omega_{\min} + (j+1) \cdot \Delta\Omega (j = 0,1,2\ldots)$, $\Delta\Omega$ must be reduced to $\frac{1}{10}$ and the process is repeated with the value $\frac{\Delta\Omega}{10}$. The calculation is finished when $\left|\frac{f}{f_{\min}}\right| < \varepsilon < 1$.

More frequently separated movements of the shaft are studied (see [1, 7-9]). Sinitsin and Shestakov [10] present a comprehensive analysis of the angular and linear accelerations of moving elements (shafts, gears) by wireless acceleration sensor of moving elements. The combined motions are presented in paper [2].

A procedure for vibration analysis of the device, based on measured data in simulated operating modes in mechanisms, is studied in [11]. In [12], these new trends in torsional vibration calculation for various vehicles are briefly described, with attention paid not only to practical use but above all to how and to what extent these themes should be presented to students.

In the paper, the following problems are presented:

- Calculation the vector of state in every part of the shaft based on known physical characteristics;
- Calculation of transfer matrix **P** and all the other amplitude-frequency characteristics of the state quantity are done in Octave 4.2.0;
- Assessing the resistance of the shaft to transverse oscillation during the design by application of the transfer matrix method.

9 Conclusions

Modelling of the rotating shaft is influenced by many factors, such as workspace of universal joints [3], vibration noise [4], flexibility of a shaft [5], increasing rotation velocity [6].

Acknowledgement

The work presented in this paper was supported by project IGS-8210-006/2020 of the Institute of Technology and Business in Ceske Budejovice.

References

[1] ARAB, S. B., RODRIGUES, J. D., BOUAZIZ, S., HADDAR, M. A finite element based on Equivalent Single Layer Theory for rotating composite shafts dynamic analysis. *Composite Structures* [online]. 2017, **178**, p. 135-144. ISSN 0263-8223. Available from: https://doi.org/10.1016/j.compstruct.2017.06.052

[2] HRUBY, P., SMETANOVA, D., NAHLIK, T. Spatial combined bending-gyratory vibration - equations of motion. In Mathematics, Information Technologies and Applied Sciences 2018: post-conference proceedings of extended versions of selected papers. 2018. p. 64 - 69.

[3] ZHANG, G., DU, J., TO, S. Study of the workspace of a class of universal joints. *Mechanism and Machine Theory* [online]. 2014, **73**, p. 244-258. ISSN 0094-114X. Available from: https://doi.org/10.1016/j.mechmachtheory.2013.11.004

[4] ERTURK, A. T., KARABAY, S., BAYNAL, K., KORKUT, T. Vibration noise harshness of a light truck driveshaft, analysis and improvement with six sigma approach. *Acta Physica Polonica A* [online]. 2017, **131**(3), p. 477-480. ISSN 0587-4246. Available from: https://doi.org/10.12693/APhysPolA.131.477

[5] RODRIGUEZ-CIANCA, D., RODRIGUEZ-GUERRERO, C., VERSTRATEN, T., JIMENEZ-FABIAN, R., VANDERBORGHT, B., LEFEBER, D. A Flexible shaft-driven Remote and Torsionally Compliant Actuator (RTCA) for wearable robots. *Mechatronics* [online]. 2019, **59**, p. 178-188. ISSN 0957-4158. Available from: https://doi.org/10.1016/j.mechatronics.2019.04.004

[6] XU, H.-B., TANG, S., XI, H. F., GAO, P.-Y., LI, M.-Y. Joint interface during arc milling brazing of aluminium alloy to low carbon steel with cutter milling at various rotation speeds. *Rare Metals* [online]. 2017, **36**(11), p. 872-877. ISSN 1001-0521, eISSN 1867-7185. Available from: https://doi.org/10.1007/s12598-017-0957-y

[7] GUO, Y., LI, W., YU, S., HAN, X., YUAN, Y., WANG, Z., MA, X. Diesel engine torsional vibration control coupling with speed control system. *Mechanical Systems and Signal Processing* [online], 2017, **94**, p. 1-13. ISSN 0888-3270. Available from: https://doi.org/10.1016/j.ymssp.2017.01.017

[8] HRUBY, P.; NAHLIK, T.; SMETANOVA, D. Mathematical modelling of shafts in drives. *Communications-Scientific letters of the University of Zilina* [online]. 2018, **20**(4), p. 36-40. ISSN 1335-4205, eISSN 2585-7878. Available from: http://komunikacie.uniza.sk/index.php/communications/article/view/637

[9] HRUBY, P.; NAHLIK, T. Application of the transfer matrix method for modelling Cardan mechanism of a real vehicle. Extended abstract [online] [accessed 2020-04-01]. Available from: https://www.imm.upv.es/wp-content/uploads/2019/03/Modelling2018.pdf

[10] SINITSIN, V. V.; SHESTAKOV, A. L. Wireless acceleration sensor of moving elements for condition monitoring of mechanisms. *Measurement Science and Technology* [online]. 2017, **28**(9), 094002. ISSN 0957-0233, eISSN 1361-6501. Available from: https://doi.org/10.1088/1361-6501/aa7ab6

[11] DEKYS, V., KRISKA, P., LIETAVA, L. KOPAS, P. STALMACH, O. Simplified estimate of fatigue damage based on dynamic analysis. *Scientific Journal of Silesian University of Technology. Series Transport* [online]. 2018, **99**, p. 15-23. ISSN 0209-3324, eISSN 2450-1549. Available from: https://doi.org/10.20858/sjsutst.2018.99.2

[12] ZOUL, V., KOVAC, P. A brief overview about the development of torsional vibration calculation and education of methods for their calculation. *Scientific Journal of Silesian University of Technology. Series Transport* [online]. 2018, **99**, p. 205-211. ISSN 0209-3324, eISSN 2450-1549. Available from: https://doi.org/10.20858/sjsutst.2018.99.19

AN EXAMPLE OF REPARATORY SURFACE WELDING OF THE MINING MACHINE VITAL PART

Dušan Arsić[1], Ružica Nikolić[2,*], Vukić Lazić[1], Srbislav Aleksandrović[1], Ljubica Radović[3], Nada Ilić[3], Branislav Hadzima[2]

[1]Faculty of Engineering, Kragujevac, Serbia
[2]Research Center, University of Zilina, Zilina, Slovakia
[3]Military Technical Institute, Belgrade, Serbia

*E-mail of corresponding author: ruzicarnikolic@yahoo.com

Resume

Mining machines' components, or the whole structure, are prone to frequent premature damages and fractures what is explained either by inadequate design and construction or by insufficient knowledge of the material's and welded joints' properties and oversights in manufacturing. Here is considered the bucket-wheel excavator, i.e. the fracture of the tooth of the girth gear, which enables the circular motion of the excavator's upper structure (which was in operation for 5000 hours). The gear was made of the cast steel GS 40 MnCrSi3 V. The reparatory hard-facing (HF) technology of the fractured tooth required specification of numerous operations including the preparation works. The reparation realized the two-fold savings, in time and money - the new girth gear costs over 500 000 € and its manufacturing lasts 6 to 9 months, while the safety and quality of the repaired tooth was guaranteed.

Article info

Received 7 May 2020
Accepted 7 July 2020
Online 19 November 2020

Keywords:

bucket-wheel excavator,
girth gear,
tooth fracture,
reparatory surface welding,
financial gains

Available online: https://doi.org/10.26552/com.C.2021.1.B39-B45

ISSN 1335-4205 (print version)
ISSN 2585-7878 (online version)

1 Introduction

The Bucket wheel excavators (BWE) are in exploitation subjected to stresses that appear in manufacturing of parts and mounting of equipment (residual stresses), as well as during their functioning (stationary and dynamic loadings) and during the disrupted exploitation (non-stationary dynamic loadings) [1-2]. Thus, the loading of the bucket wheel excavators' parts and assemblies cannot be formulated by a simple form mathematical function. That loading cannot be represented by a model where the variables and/or parameters would be uniformly varying in the working conditions, for a model like that would have to include a series of approximations resulting from the real exploitation conditions [1]. Those are the reasons why only testing of a BWE in the real working conditions would make possible to completely estimate its state and to obtain all the data necessary for comparing the quality of the machine and its structure and for estimating the influence of the working environment on the carrying capacity of its parts and assemblies. Numerous failures of the BWE structures are presented in papers [3-8] and of similar structures in papers [9-18]. It should be emphasized that the presented procedure can successfully be applied to other machine parts and technical systems, like: transport mechanisms [12], parts of boilers [13-14], forging dies [15-16], stone crushers' mills and parts of the construction mechanization [17], turbine elements etc. In addition, each executed reparation requires prior extensive preparation procedure, which would enable successful execution of the reparation itself [18].

The bucket wheel excavator TAKRAF SRs 2000×32/5.0 [19], which operates at the open pit mine "Kostolac" (Serbia), is shown in Figure 1 and its basic techno-technological characteristics are given in Table 1. It was employed on excavation of the barren soil for 5.000 h (a few weeks more than a year after the assembly) when the fracture of the tooth of the girth gear, which enables the circular motion of the upper structure of the bucket-wheel excavator, occurred.

It was established, through analysis of the fracture surface that the fracture occurred during the fatigue loading and due to existence of an initial crack in the tooth base. That crack was created during the girth gear manufacturing and it was not detected prior to gear's mounting onto the BWE's structure.

In Figures 2 to 4 are shown the gear, the broken tooth and the girth gear fracture surface, respectively. Analysis of the broken tooth fracture surface clearly shows that the very small portion of the tooth was loaded in fatigue (smooth fracture surface of the girth gear) and that the much larger portion was subjected to static fracture (the rough fracture surface of the girth gear), Figure 4.

According to the manufacturer's documentation, the girth gear was made of the cast steel GS 40 MnCrSi3 V [19].

Figure 1 *Bucket wheel excavator SRs 2000×32/5.0*

Table 1 *Basic technical characteristics of the bucket wheel excavator TAKRAF SRs 2000×32/5.0*

characteristics	notation/units
volume of a bucket with a ring space	W_{buck} = 2000 (m^3)
maximum cut height	H = 32 (m)
maximum cut depth	L = 5 (m)
diameter of the rotor wheel	D_r = 12 (m)
number of buckets	z = 20
installed engine power for rotor drive (2 x 670 kW)	N = 1340 (kW)
motor voltage	6000 (V)
specific resistance to excavation per knife length	k_L = 100 (N/mm)
speed of the upper construction	30 (m/min)
peripheral speed of the rotor wheel	2.7 (m/s)
teeth number of the pinion for rotation of the excavator's upper structure	z_p = 16
teeth number of the girth gear for rotation of the excavators' upper structure	z_{gg} = 312
teeth module of the pinion for rotation of the excavator's upper structure	m = 36
outside diameter of girth gear	D_{gg} = 11232 (mm)
outside diameter of the pinion	D_p = 576 (mm)
output rpm on the pinion	N_p = 2.28 (rpm)
Rpm of the girth gear rotation	N_{gg} = 0.12 (rpm)

Figure 2 *Appearance of the girth gear and the pinion for rotation of the excavator's upper structure*

Figure 3 *Appearance of the broken tooth and its dimensions*

Figure 4 *Appearance of the girth gear fracture surface at the broken tooth spot*

Table 2 *Chemical composition of the cast steel GS 40 MnCrSi3 V, values in %*

C	Si	Mn	Cr	P	S	Cu
0.35- 0.45	0.50-0.75	0.60-0.90	0.50-0.80	≤ 0.040	≤ 0.040	≤ 0.30

Table 3 *Mechanical properties of the cast steel GS 40 MnCrSi3 V*

yield stress $R_{0.2}$ (N/mm^2)	tensile strength R_m (N/mm^2)	elongation A5 (%)	impact energy KCU 3 (J/cm^2)	contraction Z (%)
390	740	10	min 24	20

Its chemical composition and mechanical properties are given in Tables 2 and 3, respectively.

To predict the cast steel GS 40 MnCrSi3 V resistance to crack propagation, the fracture parameters were calculated, namely the critical value of the stress intensity factor - the facture toughness K_{Ic} and the critical crack length a_{cr}, based on the obtained values of the material's impact energy and the yield stress, according to the Barsom-Rolfe model [20]. The calculated value of the critical crack length was 61.9 mm. The detailed procedure for calculation of given parameter is presented in [21-22].

2 Methodology of the new tooth manufacturing by the reparatory hard-facing

Due to the complex construction solution of the girth gear and its function in exploitation, it was necessary to precisely define a large number of details and carefully consider and execute all the operations in the methodology of manufacturing the new tooth. This was an imperative in order to ensure the safety of the repaired girth gear exploitation, since the smallest oversight, underestimate or improper execution could cause serious problems in the operation of the BWE as a whole. This is the reason why the preparation procedure for the hard-facing technology is presented, as well.

2.1 Analysis of the girth gear material's weldability

According to equivalent carbon formula - Equation (1) - of the International Welding Institute [23], the limiting value for the good weldability of this material should not be greater than 0.45. For the maximal values of the chemical elements composition of the GS 40

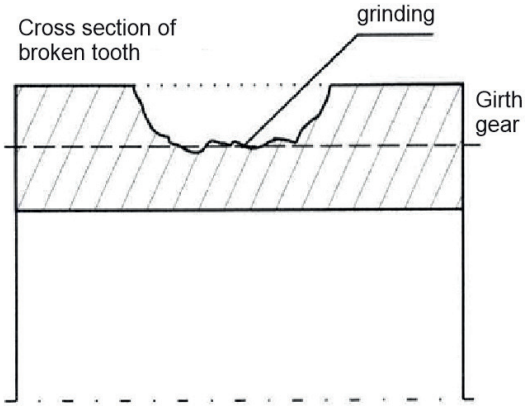

Figure 5 *Schematic presentation of the girth gear cross section at the broken tooth spot*

MnCrSi3 V, given in Table 1, that value is 0.57. The value obtained by the Ito-Bessyo formula - Equation (2) - of 0.68, also surpasses the limiting value for the good weldability of 0.30 [24]. The presented data point to the fact that this steel is prone to cold cracks appearance, what prompted the necessity for the hard-facing of the broken tooth to be performed with preheating and controlled cooling.

$$CEV = C + \frac{Mn}{6} + \frac{Cr + Mo + V}{5} + \frac{Ni + Cu}{15}. \quad (1)$$

$$CEV = C + \frac{Si}{30} + \frac{Mn + Cu + Cr}{20} + \\ + \frac{Mo}{15} + \frac{Ni}{60} + \frac{V}{10}. \quad (2)$$

According to Equation (3) for the Hot Cracking Susceptibility (or Sensitivity) (HCS) [23], it was established that this material is prone to appearance of the hot cracks, as well, since the obtained value for HCS was 21.52, which is greater than 4 - the limiting value for this type of steels with tensile strength of about 700 N/mm^2.

$$HSC = \frac{C \cdot \left(S + P + \frac{Si}{25} + \frac{Ni}{100}\right) \cdot 10^3}{3 \cdot Mn + Cr + Mo + V}. \quad (3)$$

Due to the girth gear construction (dimensions and mass) and conditions of the hard-facing execution without the heat treatment, for the filling volume greater than 500 cm^3, the recommended preheating temperature is within range 100 °C to 150 °C. The preheating temperature was determined according to Seferian's formula [25-26].

2.2 Preparation operations for the reparatory hard-facing of the girth gear tooth

The hard-facing preparation procedure included the following operations:

- Providing the means of protection at work
- Preparing the copper templates for various purposes and corresponding geometries
- The first measurement of the girth gear deformation (planarity test) by the appropriate template (measures' controller)
- Grinding of the fracture surface of the girth gear in the zone of the broken tooth by the corresponding grinders until the complete removal of all the unevenness and cracks, Figure 5
- Cleaning of surfaces prepared for welding the new tooth of the anti-corrosion protection (ACP) and the corrosion products
- Shaping the ground pieces, in order to remove the sharp edges, for welding of the new tooth
- Processing of ground pieces with brushless sand papers to provide the necessary quality of surfaces for testing by the non-destruction methods
- Testing of the ground pieces by magnetic particles [27-28] and penetrants [29-30]
- Precise definition (by adequate template) of the position, width, length, depth and volume of the ground places
- Providing that the ground surfaces are degreased, clean and dry
- Placing the adequate templates at the position of the tooth hard-facing

2.3 Order of operations of the girth gear tooth reparatory hard-facing

Reparatory hard-facing included the following operations:

- Placing the corresponding references for control of the girth gear deformation (planarity test)
- Depositing of the I (first - initial) hard-facing layer at the ground spot by austenitic filler metal with forging by the round tip pneumatic hammer of 3 mm diameter
- Shaping of the I hard-faced layer of the new tooth by adequate template, with respect to the base material plane (Figure 6) with overfill of order 0.2 to 0.3 mm
- Repeating of the welding if the non-destructive test showed necessity for it

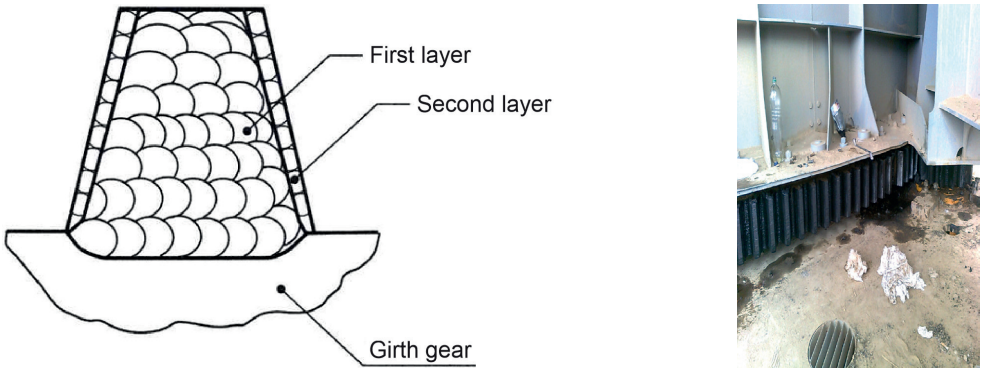

(a) (b)

Figure 6 *Order of the hard-facing layers deposition (a) and appearance of the new tooth (b)*

Table 4 *Chemical composition of the E 18 8Mn B 22 electrode, values in [%]*

C	Si	Mn	Ni	Cr
0.12	0.80	7.00	9.00	18.00

Table 5 *Mechanical properties of the pure weld metal*

yield stress Rp0.2% (N/mm^2)	tensile strength R_m (N/mm^2)	elongation A5 (%)	toughness Av (J)
> 350	590 - 690	> 40	> 60 (+20)

Table 6 *Chemical composition of the E 1-UM-300 electrode, values in [%] and hardness*

C	Mn	Ni	Hardness (HB)
0.18	1.3	1.2	280-330

- Testing of the I layer with respect to the base metal (BM) plane by magnetic particles [27-28] and penetrants [29-30]
- Processing of surfaces by the sand paper in the zones of the new tooth welding up to reaching the machining quality of Ra_{max} = 1.6 μm (permissible overfill and underfill up to 0.03 mm)
- In the case of the satisfying tests results, after each layer deposition, forging of ground surfaces by the round tip pneumatic hammer of 3 mm diameter for the purpose of reducing the residual stresses in the weld metal (WM) and the heat affected zone (HAZ)
- Control of the filler metal, welding parameters and deposited layers dimensions during the welding
- Depositing of the II (second - final) layer of the new tooth by the basic filler metal with forging by the round tip pneumatic hammer of 3 mm diameter
- Final measurement of the girth gear deformation (planarity test) by the appropriate template (measures controller)
- Final testing of the new tooth by magnetic particles and penetrants [27-30]
- Manual machining of the girth gear in the case of unsatisfactory planarity.

The order of the hard-facing layers deposition and appearance of the new tooth are shown in Figure 6.

2.4 Technology of the girth gear tooth reparatory hard-facing

This hard-facing technology is completely defined by the presented preparatory and depositing operations. Depositing of the I layer was executed by the austenitic electrode marked E 18 8Mn B 22 [31], while the II layer was deposited by the basic electrode marked E 1-UM-300 (DIN 8555) [32]. The chemical composition of the E 18 8Mn B 22 electrode is presented in Table 4, mechanical properties of the weld metal in Table 5 and the chemical composition of the E 1-UM-300 electrode in Table 6.

3 Conclusions

Reparation of the girth gear tooth of the bucket wheel excavator SRs 2000×32/5.0, by the presented methodology, was executed in 14 days in 2013. Considering that the excavator is still in operation at the open pit mine "Kostolac" (Serbia), it could be concluded that the reparation was successful.

It should be emphasized that in this way the large financial effect was realized since the construction of the new girth gear would cost over 500 000 €. If the time, needed

for manufacturing the new girth gear, which is about 6 to 9 months, would also be included in this calculation, as well as effect of the electric power that would not be produced in such a long period, the total positive financial effect is about 8 000 000 €.

The presented methodology of the reparatory hard-facing, as well as the welding procedure, can be applicable, with necessary adjustments, for recovery of other parts and structures of the bucket wheel excavator or other machines at open pit mines.

Acknowledgment

This research was partially financially supported by the project "Innovative Solutions for Propulsion, Power and Safety Components of Transport Vehicles" ITMS 313011V334 of the Operational Program Integrated Infrastructure 2014 – 2020 and co-funded by the European Regional Development Fund and projects TR35006 and TR35024 financed by the Ministry of education, science and technological development of Republic of Serbia.

References

[1] ARSIC, M., BOSNJAK, S., ZRNIC, N., SEDMAK, A., GNJATOVIC, N. Bucket wheel failure caused by residual stresses in welded joints. *Engineering Failure Analysis* [online]. 2011**,** **18**(2), p. 700-712. ISSN 1350-6307. Available from: https://doi.org/10.1016/j.engfailanal.2010.11.009

[2] SEDMAK, S., SEDMAK, A., ARSIC, M., TUMA, J. V. An experimental verification of numerical models for the fracture and fatigue of welded structures. *Materiali in Tehnologije - Materials and Technology*. 2007, **41**(4), p. 173-178. ISSN 1580-2949.

[3] DJURDJEVIC, D. J., MANESKI, T., MILOSEVIC, V., MITIC-ANDJELIC, N., IGNJATOVIC, D. Failure investigation and reparation of a crack on the boom of the bucket wheel excavator ERS 1250 Gacko. *Engineering Failure Analysis* [online]. 2018, **92**, p. 301-316. ISSN 1350-6307. Available from: https://doi.org/10.1016/j.engfailanal.2018.05.015

[4] ZRNIC, N., BOSNJAK, S., GASIC, V., ARSIC, M., PETKOVIC, Z. Failure analysis of the tower crane counterjib. *Procedia Engineering* [online]. 2011, **10**, p. 2238-2243. ISSN 1877-7058. Available from: https://doi.org/10.1016/j.proeng.2011.04.370

[5] SEDMAK, S., JOVICIC, R., SEDMAK, A., ARANDJELOVIC, M., DJORDJEVIC, B. Influence of multiple defects in welded joints subjected to fatigue loading according to SIST EN ISO 5817:2014. *Structural Integrity and Life*. 2018, **18**(1), p. 77-81. ISSN 1451-3749, eISSN 1820-7863.

[6] ARSIC, M., BOSNJAK, S., ODANOVIC, Z., DUNJIC, M., SIMONOVIC, A. Analysis of the spreader track wheels premature damages. *Engineering Failure Analysis* [online]. 2012, **20**(1), p. 118-136. ISSN 1350-6307. Available from: https://doi.org/10.1016/j.engfailanal.2011.11.005

[7] BOSNJAK, S., ARSIC, M., SAVICEVIC, S., MILOJEVIC, G., ARSIC, D. Fracture analysis of the pulley of a bucket wheel boom hoist system. *Eksploatacja i Niezawodnosc - Maintenance and Reliability* [online]. 2016, **18**(2), 155-163. ISSN 15072711. Available from: https://doi.org/10.17531/ein.2016.2.1

[8] BOSNJAK, S., ARSIC, M., GNJATOVIC, N., MILENOVIC, I., ARSIC, D. Failure of the bucket wheel excavator bucket. *Engineering Failure Analysis* [online]. 2018, **84**, p. 247-261. ISSN 1350-6307. Available from: https://doi.org/10.1016/j.engfailanal.2017.11.017

[9] LAZIC, V., SEDMAK, A., ALEKSANDROVIC, S., MILOSAVLJEVIC, D., CUKIC, R., GRABULOV, V. Reparation of damaged mallet for hammer forging by hard facing and weld cladding. *Technical Gazette*. 2009, **16**(4), p. 07-113. ISSN 1330-3651.

[10] MEDJO, B., ARSIC, M., MLADENOVIC, M., SAVIC, Z., GRABULOV, V., RADOSAVLJEVIC, Z., RAKIN, M., Influence of defects on limit loads and integrity of the pipeline at hydropower plant "Pirot". *Structural Integrity and Life*. 2020, **20**(1), p. 82-86. ISSN 1451-3749, eISSN 1820-7863.

[11] ARSIC, D., NIKOLIC, R., LAZIC, V., ARSIC, A., SAVIC, Z., DJACIC, S., HADZIMA, B. Analysis of the cause of the girth gear tooth fracture occurrence at the bucket wheel excavator. *Transportation Research Procedia* [online]. 2019, **40**, p. 413-418. ISSN 2352-1465. Available from: https://doi.org/10.1016/j.trpro.2019.07.060

[12] TANASKOVIC, D., DJORDJEVIC, B., TATIC, U., SEDMAK, S., GAJIN, M. Cracking due to repair welding of the treiber roll. *Structural Integrity and Life*. 2017, **17**(2), p. 133-138. ISSN 1451-3749, eISSN 1820-7863.

[13] TANASKOVIC, D., DJODRJEVIC, B., GAJIN, M., ARANĐELOVIC, M., GOSTOVIC, N., Damages of burner pipes due to the working conditions and its repair welding, *Procedia Structural Integrity* [online]. 2018, **13**, p. 404-409. ISSN 2452-3216. Available from: https://doi.org/10.1016/j.prostr.2018.12.067

[14] MILOVANOVIC, N., DJORDJEVIC, B., TATIC, U., SEDMAK, S., STRBACKI, S. Low-temperature corrosion damage and repair of boiler bottom panel tubes. *Structural Integrity and Life*. 2017, **17**(2), p. 125-131. ISSN 1451-3749, eISSN 1820-7863.

[15] ARSIC, D., LAZIC, V., SAMARDZIC, I., NIKOLIC, R., ALEKSANDROVIC, S., DJORDJEVIC, M., HADZIMA, B. Impact of the hard facing technology and the filler metal on tribological characteristics of the hard faced forging dies. *Tehnicki Vjesnik - Technical Gazette* [online]. 2015, **22**(5), p. 1353-1358. ISSN 1330-3651, eISSN 1848-6339. Available from: https://doi.org/10.17559/TV-20150408152638

[16] ARSIC, D., LAZIC, V., SEDMAK, A., NIKOLIC, R., ALEKSANDROVIC, S., DJORDJEVIC, M., BAKIC, R., SAMARDZIC, I. Selection of the optimal hard facing (HF) technology of damaged forging dies based on cooling time $t_{8/5}$. *Metalurgija - Metallurgy*. 2016, **55**(1), p. 103-106. ISSN 0543-5846.

[17] LAZIC, V., ARSIC, D., NIKOLIC, R., MUTAVDZIC, M., MESKO, J. Reparation by hard facing of the damaged secondary stone crushers. *Manufacturing Technology* [online]. 2016**,** **16**(1), p. 375-380. ISSN 1213-2489. Available from: https://doi.org/10.21062/ujep/x.2016/a/1213-2489/MT/16/2/375

[18] LAZIC, V., CUKIC, R., ALEKSANDROVIC, S., MILOSAVLJEVIC, D., ARSIC, D., NEDELJKOVIC, B., DJORDJEVIC, M. Techno-economic justification of reparatory hard facing of various working parts of mechanical systems. *Tribology in Industry* [online]. 2014, **36**(3), p. 287-292. ISSN 0354-8996, eISSN 2217-7965. Available from: http://www.tribology.rs/journals/2014/2014-3/7.pdf

[19] TAKRAF, Gmbh. Bucket wheel excavator SRs 2000 in Serbia. Tenova, Germany, 2007.

[20] HERTZBERG, R. W. *Deformation and fracture mechanics of engineering materials*. John Wiley & Sons, Inc., 1995. ISBN 13: 9780471012146.

[21] ARSIC, D., GNJATOVIC, N., SEDMAK, S., ARSIC, A., UHRICIK, M. Integrity assessment and determination of residual fatigue life of vital parts of bucket-wheel excavator operating under dynamic loads. *Engineering Failure Analysis* [online]. 2019, **105** p. 182-195. ISSN 1350-6307. Available from: https://doi.org/10.1016/j.engfailanal.2019.06.072

[22] ARSIC, M., BOSNJAK, S., SEDMAK, S., VISTAC, B., SAVIC, Z., Repair of cracks detected in cast components of vertical Kaplan turbine rotor hub. *Structural Integrity and Life*. 2019, **19**(3), p. 243-250. ISSN 1451-3749, eISSN 1820-7863.

[23] KARPICHEV, V., SERGEEV, K., BOLOTINA, A., Modeling of technological processes of machine-building and repair manufacture. *Communications - Scientific Letters of the University of Zilina* [online]. 2019, **21**(4), p. 59-62. ISSN 1335-4205, eISSN 2585-7878. Available from: http://komunikacie.uniza.sk/index.php/communications/article/view/1518

[24] ITO, Y., BESSYO, K. Weld crackability formula of high strength steels. *Journal of Iron and Steel Research International*. 1972, **13**, p. 916-930. ISSN 1006-706X, eISSN 2210-3988.

[25] LAZIC, V., ALEKSANDROVIC, S., NIKOLIC, R., PROKIC-CVETKOVIC, R., POPOVIC, O., MILOSAVLJEVIC, D., CUKIC, R. Estimates of weldability and selection of optimal procedure for welding of high strength steel. *Procedia Engineering* [online]. 2012, **40**, p. 310-315. ISSN 1877-7058. Available from: https://doi.org/10.1016/j.proeng.2012.07.100

[26] NEJKOVIC, V., MILICEVIC, M., RADAKOVIC, Z., New method for determining cooling time and preheating temperature in arc welding. *Thermal Science* [online]. 2019, **23**(6), p. 3975-3984. ISSN 0354-9836, eISSN 2334-7163. Available from: https://doi.org/10.2298/TSCI180330297N

[27] ISO 17638:2016. Non-destructive testing of welds - magnetic particle testing. European Committee for Standardization, 2013.

[28] ISO 23278. Non-destructive testing of welds - magnetic particle testing of welds - acceptance levels. European Committee for Standardization, 2009.

[29] ISO 3452-1:2013. Non-destructive testing. Penetrant testing. Part 1: general principles. European Committee for Standardization, 2013.

[30] ISO 23277. Non-destructive testing of welds. Penetrant testing of welds. Acceptance levels. European Committee for Standardization, 2016.

[31] EN 1600: E 18 8 Mn B 22. Austenite basic electrode for welding of stainless Cr and CrNi steels. Classification, 1997.

[32] DIN 8555: E 1-UM-300. Basic electrode alloyed with Cr and Mn for medium hard surfacing. Classification, 1997.

DEVELOPMENT OF A METHOD FOR DIAGNOSING INJECTORS OF DIESEL ENGINES

Ildar Gabitov*, Andrei Negovora, Shamil Nigmatullin, Arseny Kozeev, Mahmut Razyapov

Department of Automobiles and Machine-Tractor Complexes, Federal State Budgetary Educational Establishment of Higher Education "Bashkir State Agrarian University", Ufa, Russia

*E-mail of corresponding author: gabitovilda@rambler.ru, bgau@ufanet.ru

Resume

The purpose of this study was to improve the diagnostics efficiency of modern diesel engine injectors with electronic controls. Experimental studies, performed using certified specialized equipment of injectors' manufacturers and standard software packages for data analysis, made it possible to prove adequacy of theoretical research and get results that are more accurate. Those results contribute to development of a software product that allows identifying a particular faulty element during the defective injector's operation by using mathematical processing of the diagnostic data obtained when testing the injector. Thus, the time spent to repair the fuel injection system reduces. The developed software product also helps to predict the remaining injector's operational life and prevent possible technical failures during operation.

Article info

Received 6 April 2020
Accepted 20 July 2020
Online 19 November 2020

Keywords:

acceptable values,
diagnostic table,
injector,
nozzle parameters,
test mode

Available online: https://doi.org/10.26552/com.C.2021.1.B46-B57

ISSN 1335-4205 (print version)
ISSN 2585-7878 (online version)

1 Introduction

Common Rail fuel injection system is widely used in modern automotive and agricultural machinery. In engines with this system, the fuel pressure creation and fuel distribution inside the cylinder occur over time. Since this system is relatively new, manufacturers do not disclose diagnostic technologies. They can give such information only to certified specialized maintenance representatives. Thus, there is a need to develop ways for detecting the elements' working capacity, especially when speaking about the injector, which is the main executive element [1-4].

Various diagnostic methods are used to assess the technical conditions of the fuel supply system (Table 1). These methods are applied in accordance with the diagnostics tasks.

Different diagnostic methods, identifying certain failures and damages (e.g. reduced injection pressure, instability of fuel supply parameters, etc.), are used when checking the working capacity of fuel injection system elements without specifying the location and cause of the failure.

When checking the correct functioning, diagnostics is aimed at determining all the defects in technological adjustments and settings that cause an unacceptable decrease in technical, economic and environmental indicators [5-7].

When searching for defects, diagnostic methods allow identifying the location, type and cause of the defect (wear of plunger elements, fuel delivery and consumption, etc.).

According to the degree of disassembly of an object, there are disassembly and unassembled diagnostic methods.

Disassembly diagnostics is used to assess the mobility of the plunger elements, the spray needle and to measure the wear of various parts of the fuel-delivery systems.

Unassembled diagnostics is usually based on indirect measurements of structural parameters, when installing sensors or diagnostic devices outside the object being diagnosed, without removing it from the diesel engine or on a test stand for fuel-delivery systems [8-11].

Depending on the diagnostic parameters, all the methods are divided into three groups. Thus, some methods are based on measurement parameters, which characterize operation of the entire fuel-delivery system and its component parts, or the co-process. Other methods are based on a direct structural parameter of a part or parts mating.

Diagnostic methods based on work process parameters allow checking the fuel-delivery system output parameters (fuel pressure in the high-pressure line, the stroke of the spray nozzle needle, etc.) and numerous technical characteristics of this system's components (phase parameters of fuel supply and pressure, needle movement speed, flow rate, etc.). Usually, the measurement accuracy of these parameters

Table 1 *Classification of methods for diagnosing the battery fuel-delivery systems*

classification parameters	diagnostic methods
diagnosing tasks	functionality test tests for proper operation search for defects
character of parameter measurement	direct indirect
diagnostics conditions	field service station motorless
use of diagnostic facilities	organoleptic instrumental
the mode of operation of the object	in steady state on non-steady state in static-dynamic mode
diagnostic parameters	work process-related parameters parameters of related processes structural parameters
the frequency of diagnosing	routine required continuous
by the degree of disassembly of the device under test	disassembly diagnostics unassembled
the physical process being used	vibro-acoustic magneto electric spectrographic; thermal hydraulic gas analytical kinematic; other

is quite high, since in most cases a direct measurement of the controlled physical quantity is performed.

Diagnostic methods based on parameters of related processes make it possible to determine indirectly the same parameters of the work processes, as well as structural parameters of parts and interfaces, if they cannot be directly measured or if their measurement is useless. In this case, the processes' indicators generated by the work processes, are measured. Among these processes are vibration and noise, heating or cooling. This also includes the diagnostic methods for analyzing the fuel contamination by wear products and gas analysis. The accuracy of this measurement of the state parameters is lower than when diagnosing with use of the work process parameters [12-13].

Diagnostic methods, based on the structural parameters, allow determining the wear of parts and gaps in their interfaces and values of the adjustment parameters, by means of direct measurements. Among the parts subject to wear can be precision parts, regulator parts, the housing of the high-pressure fuel pump, camshaft, injection timing coupling, etc. These methods are based on measurement of parts relative motion or geometric dimensions of a part.

According to the physical process used, diagnostic methods are divided into vibro-acoustic, spectrographic, magneto-electric, thermal, hydraulic, gas-analytical and kinematic and some others.

Each method is designed to control a specific physical process and is based on application of a specific physical phenomenon. Classification by the physical process used allows the most complete identification of capabilities and technical characteristics of the corresponding diagnostic method.

A physical process is characterized by a change in physical quantity over time. Hydraulic process is based on pressure; thermal - on temperature; vibro-acoustic-on the amplitude of vibrations at certain frequencies, etc. [14-15].

Currently, many tools for diagnosing injectors have been developed, but they only measure the cycle injection and control flow. If the injector does not meet the requirements, it must be replaced or repaired. The diagnostic methods do not specify procedures for identifying a specific injector fault and the tools used in this case are not designed for its element-by-element study and forecasting the residual life of their operation [16-19].

Quality of the diesel engine operation depends directly on quality of the fuel supply system and each of its elements. Quality of those elements is determined by a set of technical parameters that depend on a number of factors: climate conditions, the adopted system of maintenance and repair, the volume and nature of the work performed, quality of implementation of the rules of operation and maintenance of machines, quality and availability of technical means of

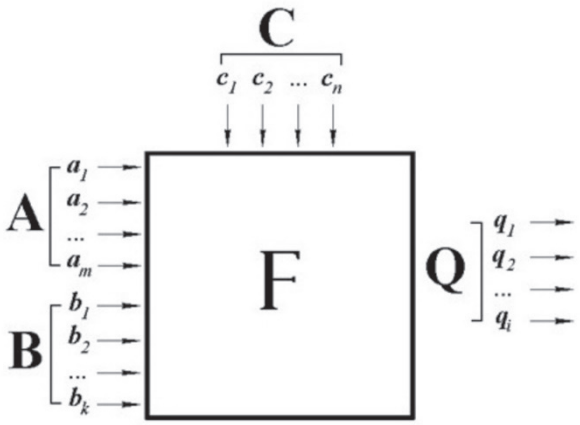

Figure 1 *Information model of injector operation*

service and technical documentation, etc. Because of this, the control over the technical parameters conditions can be considered as a way and method of influencing these indicators of the work quality and reliability of the node during its service life.

By the control over the technical conditions of the fuel equipment elements, as well as injectors, warning failures, manipulations aimed at restoring nominal values and maintaining all the parameters within the tolerance of the operational state should be meant. Thus, a diesel injector can be considered as an object that is affected by various operational factors and has certain patterns of changes in technical conditions.

Effective methods implemented in various automated installations, diagnostic devices and testers cannot be applied in practice without preliminary measures to improve suitability of both diagnostic tools and diesel engine and its fuel-delivery systems. Improving the suitability of fuel-delivery systems to basic diagnostic tools allows reducing the number of adapter units, to make sensors installation on the object easier and to increase efficiency of diagnostics [20-22].

In general, it should be noted that these devices and diagnostic tools make it possible to evaluate only one delivery line for one inspection cycle. They neither provide specific data on the resource and the probable defect, nor indicate a specific defect. They do not provide a full picture of many diagnostic parameters. As a result, it is difficult to analyze the information received when diagnosing an element of the fuel-delivery systems. Thus, it is necessary to develop modern diagnostic tools and their software, i.e. electronic automated systems.

Electronic automated systems create conditions that allow solving problems of diagnostics on a fundamentally new industrial basis. It means that nearly all the operations of technical diagnostics will be performed by electronic installation blocks. The end result on the composition of the object will inform of the object quality class by means of such words as “fit” “unfit”, “normal”, “less than normal”, “more than normal” etc. At the same time, the diagnostics process can be carried out continuously according to a preset optimal program in a particular logical sequence [4, 23-24].

A brief review and analysis of the problem showed that a certain scientific and technical basis has been created for ensuring reliability and evaluating the quality of fuel equipment while in operation. At the same time, existing technologies and methods for diagnosing, monitoring and evaluating the technical condition of electrically-controlled elements of modern fuel-delivery systems do not take due account of their performance features.

Improving the reliability and reducing the complexity of diagnostic work can be achieved by developing automated tools capable to digitize data obtained by direct determination. The data are then processed using a mathematical apparatus ensuring diagnosis that is more accurate by increasing the number of compared parameters while the number of sensors is constant.

The study aims at analyzing the injector work process to define the influence of its various design parameters on performance, conducting theoretical and experimental studies of an effect of the injector structural parameters on diagnostic parameters, developing an effective way of injector diagnosing to estimate the injector working parameters and predict its residual resource based on scientific research.

2 Material and Methods

2.1 Mathematical model

The information model of the diesel injector operation should be presented in the form of a multi-parameter system (Figure 1).

To analyze the injector operation, A, B, C correction factors are considered. They are determined by structural and diagnostic parameters. In this case, in the system under consideration, input A (a_1, a_2, … , a_n) is unmanaged. Components of vector A should include: natural and climatic conditions, air humidity, environmental temperature fluctuations, fuel quality, etc. Components of the input B vector (b_1, b_2, … , b_m) are corrective and change during operation. They are the spring force, the value of moving elements displacement, the hydraulic density of precision

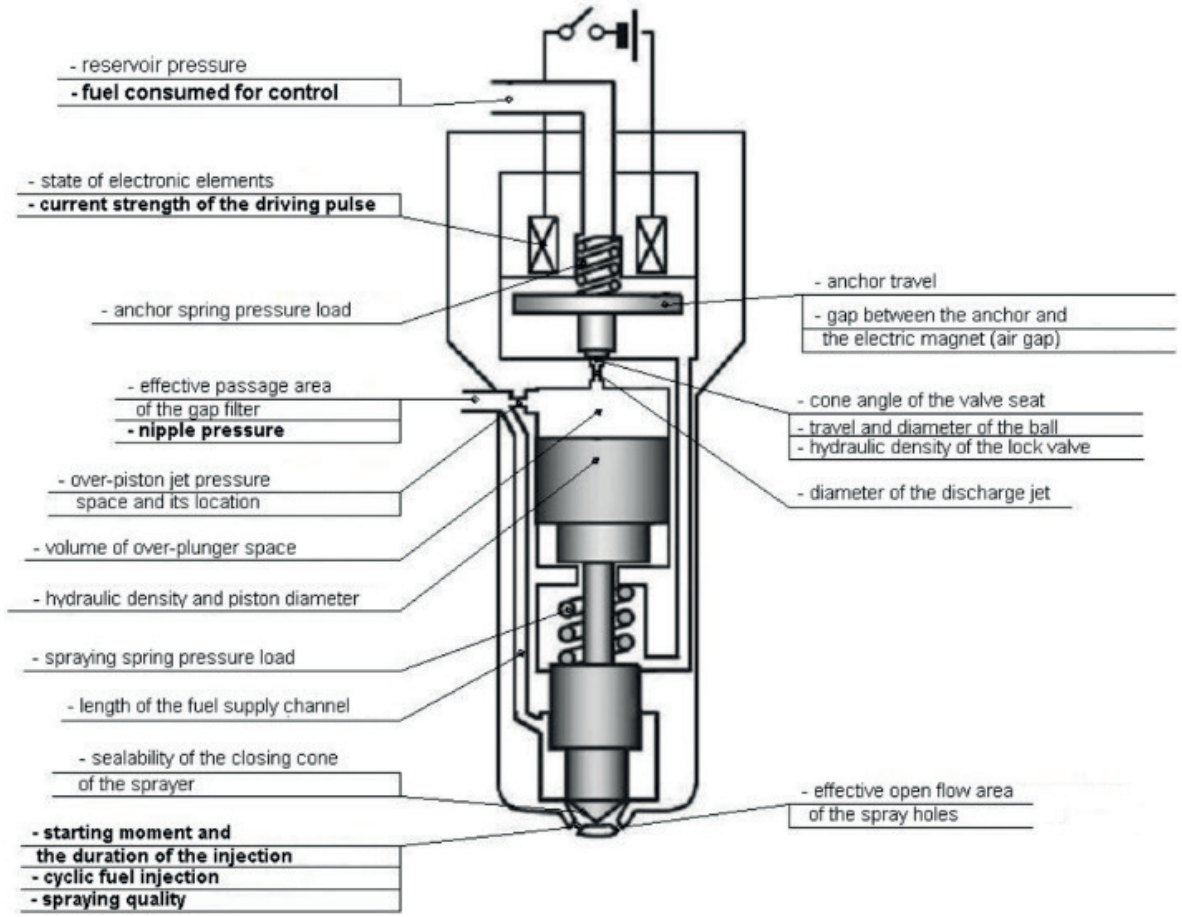

Figure 2 *Structural and diagnostic (bold type) parameters of the diesel engine injector*

parts, etc. Among control factors of the model are such components of the C vector (b_1, b_2, …, b_k) as pulse frequency and duration, ramp fuel pressure, etc. [1, 4, 14].

The value of the output Q vector depends on the state of the input parameters according to a certain pattern:

$$Q = F\{A, B, C\}, \quad (1)$$

where F is a conversion operator for the three vector arguments that defines the system's optimization criterion.

If the actual generalized estimator of the injector state quality Q_f and the set of its estimators q_{fi} are less than or equal to its tolerance values $_{Qtol}$ and $q_{i\,tol}$, respectively, then it can be considered that the injector functions in accordance with the established requirements and is in good technical condition.

Criteria for the normal functioning of the system can be defined as follows:

$$q_{fi} \le [\,q_{i\,tol}]; \; Q_f \le [\,Q_{tol}]. \quad (2)$$

To improve the quality of diagnostics, injector operation parameters, determined by diagnostics, must contain quantitative characteristics that can be evaluated within the tolerance values. Any deviation of the system parameters from the acceptable values that occurs during operation is compensated by the influence of C control factors. If this is not sufficient, the system can return to normal operation both by changing B corrective factors and by performing repair or adjustment actions.

2.2 Operation analysis

The tolerance values of the structural and diagnostic injector parameters were accepted as the operation estimators of the system under consideration.

In this paper, the object of research is a BOSCH injector of the battery fuel-delivery system. This injector was completely demounted in order to analyze its working surfaces, the principle of its operation and the purpose of its each part. For example, a ball lock valve controls the pilot piston movement. When the lock valve is closed, the fuel pressure in the over-plunger cavity affects the upper surface of the pilot piston, which makes it move towards the closed atomizer. When the valve opens, the pressure in the over-plunger cavity drops and the fuel is dumped. When the fuel pressure in the cavity under the needle increases, the spray needle and the pilot piston are lifted. The working surface of the lock ball valve is the "cone seat - ball" coupling surface, which is determined by the state of the seat and ensures that high pressure is maintained

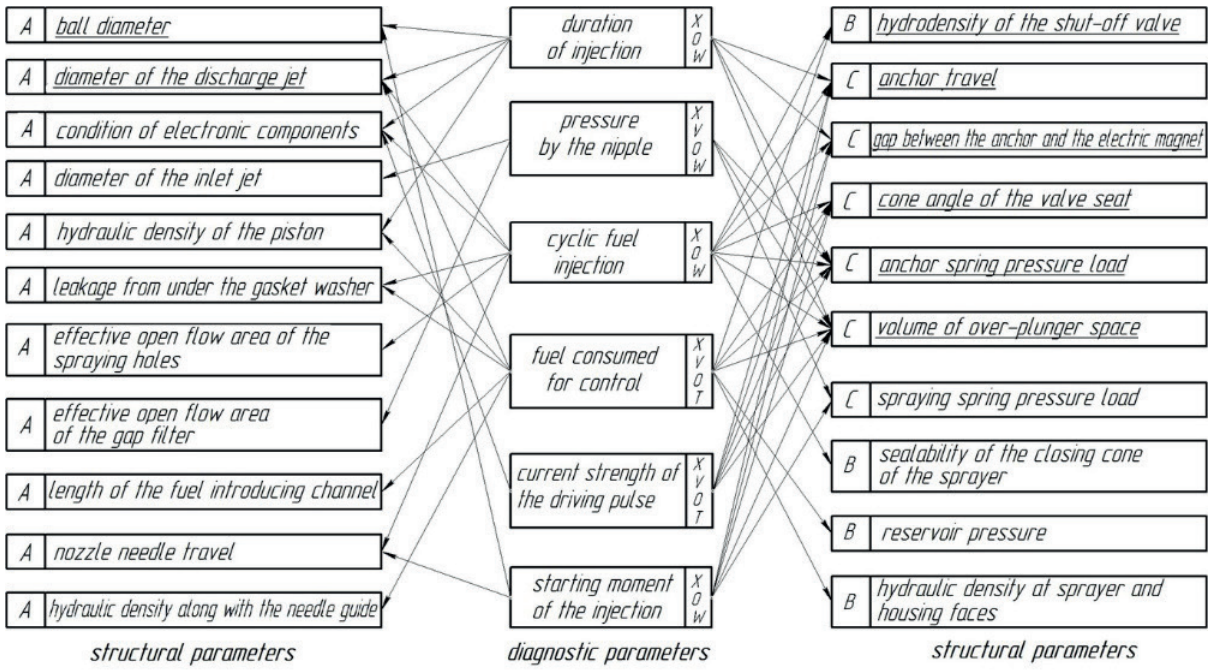

Figure 3 *Mutual effects of diagnostic and structural parameters*

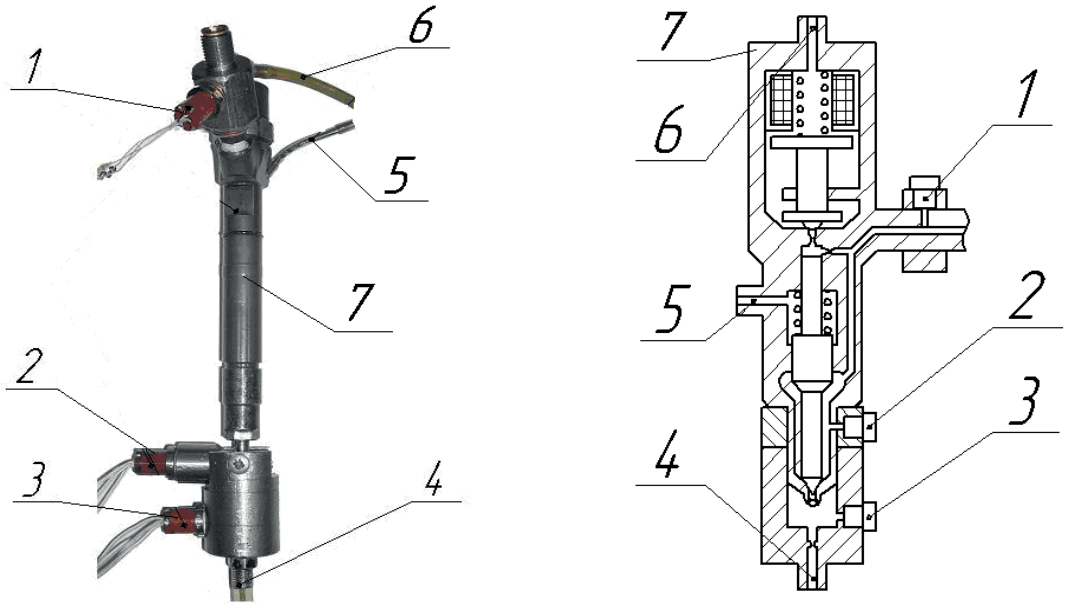

Figure 4 *General view of the experimental injector (a) and sensors location on the nozzle (b): 1, 2, 3 - pressure sensors at the inlet, under the needle sensors and the beginning of injection sensors, respectively; 4, 5, 6 - measurement of the cyclic supply, leaks on the sealing washers, the fuel consumption for control; 7 - the injector*

in the over-plunger cavity. The amount of fuel needed for control is also determined by the lock valve range, which is adjusted by changing the thickness of the washers installed between the valve-stem guide housings and the tapered seat. Other parts were reviewed in a similar way. A detailed analysis of a BOSCH injector design allowed describing 21 structural and 6 diagnostic parameters (Figure 2).

Parameters that change spontaneously during the operation, or are corrected using adjustments during the maintenance, were taken as structural parameters. For example, the spray needle hydro-density is reduced due to wear, or the gap between the anchor and the electromagnet, which is adjusted using washers. Diagnostic parameters are those that can be measured without disassembling the injector. For example, injection rate can be determined using a stand flow meter. A clamp meter is used to measure the current strength of the driving pulse [13, 25-26].

To improve efficiency of the repair work, methods for assessing the state of each structural parameter were determined. For example, they can be determined directly on the engine (V), on stands (X) or by disassembling (O), respectively. At the same time the need to dismantle and install the injector (W), as well as the possibility of abandoning these operations were considered (T). Each of

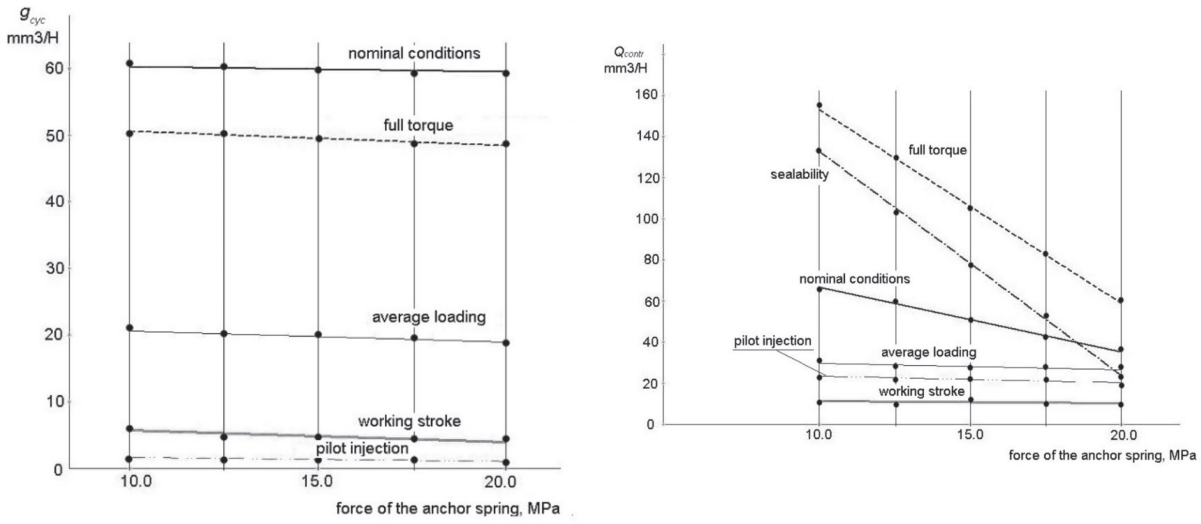

Figure 5 *Dependence of the cyclic fuel injection g_c in mm^3 / cycle (a) and fuel consumption for control Q_{contr} in mm^3/cycle (b) on the anchor spring force in different modes*

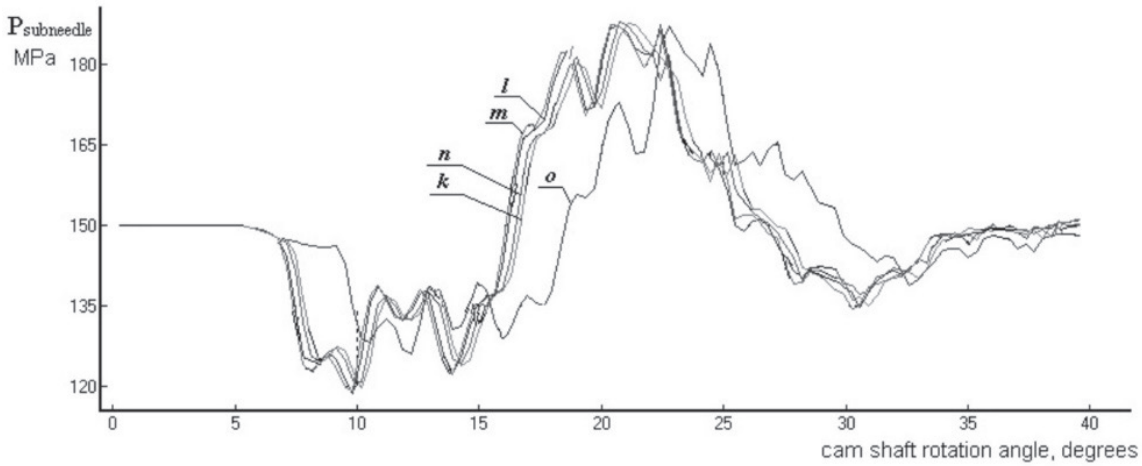

Figure 6 *Change of pressure in the sub needle space in one cycle depending on the half angle of the cone α: k - α = 30°; l - α = 40°; m - α = 55°; n - α = 60°; o - α = 70°*

the structural parameters can be changed by replacing (A), restoring (B), or adjusting parts (C).

In order to determine the effect of changes in each structural parameter on changes in diagnostic parameters, an additional analysis was performed. During this analysis, the processes occurring inside the injector was studied. The analysis showed that the parameters have mutual influence according to diagram in Figure 3.

2.3 Experimental studies

The next stage of scientific work consisted of experimental studies of changes in all the diagnostic parameters under the influence of one of the structural parameters. Non-motor tests were carried out in accordance with ISO 9002 test plans using a specialized EPS 815 diesel-fuel equipment stand, used for adjusting and testing and a Bosch KMA 802 electronic measuring system with a CRI retrofit kit used for the Common Rail injectors testing. For experimental studies, some changes were made to design of the injector (Figure 4). A distinctive feature of this injector is its ability to determine the moment of injection start, measure the pressure under the injector needle and leaks on the sealing washers of the nozzle body, regardless of the fuel consumption for control.

As an example, some of the numerous dependencies obtained are shown.

Dependence of the value of cyclic injection and fuel consumed for control on the force of the anchor spring is shown in Figure 5. Analyzing the graph of dependence of the GC fuel cyclic injection and the fuel consumption, for the Qcontr control from the spray spring force, one can say that when the starting torque of the injector nozzle needle increases, the cyclic injection decreases and in some modes, there is a complete stop of the GC fuel supply. This is due to an increase in the load acting on the spray needle, which in some modes exceeds the force from the pressure in the fuel system. Thus, the spray needle does not open the spray holes. The most informative modes for this structural parameter are the cyclic injection at medium loads and the fuel consumption for control at maximum

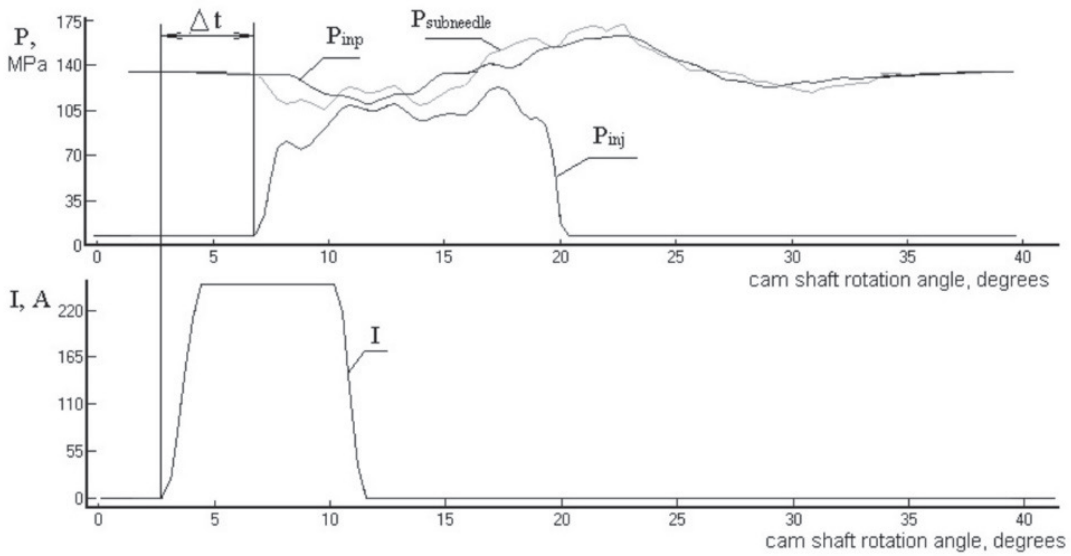

Figure 7 *Determining the injection delay parameter from the moment the control pulse is applied: I - current strength; p_{overpl} - pressure in the over-plunger cavity; p_{inp} - pressure at the nipple; p_{inj} - fuel injection pressure; $p_{subneedle}$ - pressure in the sprayer*

Table 2 *Changes in the EGF diagnostic parameters when the structural parameters in the nominal mode are changed*

structural parameter	diagnostic parameter					
	Q_{contr}	I_{em}	Δt	g_c	t_{inj}	P_{inp}
the force of the sprayer spring	↑	-	↑	↓	↓	↑
hydraulic density of the sprayer	↑	↑	-	-	↑	-
effective passage area of the sprayer	↓	-	↓	↑	↑	↓
sealability of the closing cone of the sprayer	↑	-	↑	↓	↑	↑
anchor travel	↑	-	↓	↑	↑	-
air gap	↑	↑	↑	↑	-	-
effective passage area of the gap filter	↑	-	↑	↑	↑	↓
angle of the valve seat cone	↑	↓	↑	↓	-	↑
ball diameter	↓	↓	↑	↓	-	-
length of the fuel introducing channel	-	-	-	-	-	-
hydraulic density at the front surface of the sprayer	↑	-	↓	↓	↓	↓
nozzle needle travel	↑	-	-	↑	↑	↓
drain pressure	↑	-	-	↓	↓	-
condition of electronic parts	↑	-	↑	↓	-	-
force of the anchor spring	↓	-	↑	↓	↓	↑
diameter of the spraying nozzle in the over-piston space	↑	-	↑	↓	↓	-
hydraulic density of the piston	↓	-	↓	↓	↓	↑
leaks on the sealing washer	↑	-	↑	↓	↓	↓
volume of over-plunger space	↑	-	↑	↑	-	↑

torque. Graphs show that the force of the anchor spring has a pronounced effect on the fuel consumption for control. This is influenced by an increase in the force on the ball valve bases and consequently on the reaction to the fuel pressure in the over-plunger cavity.

To clarify the scientific research, measurements of the pressure values in the injector cavities, at different operating modes of fuel supply systems, were made. The graph shows one of the many graphs obtained when changing the structural parameters of the injectors (Figure 6).

Analysis of the average injection characteristics for different values of the half-angle of the valve seat cone showed that when the angle of the valve seat of the cone increases, the characteristic first improves, but after

Table 3 *Influence of the injector structural parameters exceeding the limits on the injector diagnostic parameters (idle mode)*

structural parameter	diagnostic parameter					
	Q_{contr}	I_{em}	Δt	g_c	t_{inj}	P_{inp}
the force of the sprayer spring	↑	-	↑	↓	↓	↑
hydraulic density of the sprayer	↑	-	↓	↓	↑	↓
effective passage area of the sprayer	↓	-	↓	↑	↑	-
sealability of the closing cone of the sprayer	↑	-	-	↓	↑	-
anchor travel	↑	-	-	↑	↑	-
air gap	↑	↑	↑	↑	-	-
effective passage area of the gap filter	↑	-	-	↑	↑	-
angle of the valve seat cone	↑	↓	-	↓	-	-
ball diameter	↓	↓	↑	↓	-	-
length of the fuel introducing channel	-	-	-	-	-	-
hydraulic density at the front surface of the sprayer	↑	-	↓	↓	↓	↓
nozzle needle travel	↑	-	-	↑		-
drain pressure	↑	-	-	↓	↓	-
condition of electronic parts	↑	-	-	↓	-	-
force of the anchor spring	↓	-	↑	↓	↓	↓
diameter of the spraying nozzle in the over-piston space	↑	-	-	↓	↓	-
hydraulic density of the piston	↓	-	-	↓	↓	-
leaks on the sealing washer	↑	-	↑	↓	↓	↓
volume of over-plunger space	↑	-	-	↑	↓	-

α = 55° it decreases again. The critical value for this structural parameter is α > 65°, since it is at this value that the fuel supply parameter leaves the tolerance zone. This is due to a decrease in fuel consumption through the shut-off valve, since its effective flow section reduces together with the flow capacity of the valve, which leads to a delay in lifting the control plunger and, accordingly, a delay in the start of fuel injection.

When performing experiments and processing results, a new diagnostic parameter "injection delay Δt" was introduced that characterizes the period from the start of the pulse to the start of injection. This period depends on the speed of the processes in the injector and directly characterizes the state of some of its elements. The retardation value depends mainly on the mobility of the elements (hanging, jamming) and the channels and valve transport capacity (Figure 7). A new concept of injection delay is introduced to obtain the updated data for diagnosing injectors. It depends on the speed of the injector elements. This diagnostic parameter shows the condition of the holes and the mobility of the elements.

3 Results and discussion

The data obtained made it possible to conduct a complete analysis of influence of each diagnostic parameter on the structural change in different operating modes of the diesel engine (nominal, start-up, maximum torque and idling). If value of the diagnostic parameter does not exceed the allowed deviations, then a particular diagnostic parameter in this mode is not informative in relation to a particular structural parameter, then the "- " sign is written. If the value is higher than the allowed value and this is due to an increase in the structural parameter, then the sign " ↑ " is written in the Table 2 (direct dependence), if it is lower than the allowed value, then the sign " ↓ " is used (inverse dependence). If the value exceeds the limit, which is caused by an increase in the structural parameter then the sign is written in the Table 3. If the dependence is reversed, then the ↓ sign is used [4, 12-13, 25].

As a result, for the first time, fault Tables 2-3 with corrected structural parameters in the course of experimental studies were obtained. Table 4 allows analyzing the state of the injector for different operating modes.

The full cycle of diagnostics is performed by determining diagnostic indicators for the three main modes of injector operation, which can be completed on the engine and on specialized stands. Experimental studies have shown that use of the full volume injector tests for diagnosis of certain defects may be excessive. During the data processing from initial tests, after obtaining a guaranteed conclusion about the state of the diesel injector, the diagnosis process may be completed ahead of time.

Table 4 *Influence of the injector structural parameters exceeding the limits on the injector diagnostic parameters (start mode)*

structural parameter	diagnostic parameter					
	Q_{contr}	I_{em}	Δt	g_c	t_{inj}	P_{inp}
the force of the sprayer spring	↑	-	↑	↓	↓	↑
hydraulic density of the sprayer	↑	-	↓	↓	↑	↑
effective passage area of the sprayer	↓	-	↓	↑	↑	-
sealability of the closing cone of the sprayer	↑	-	-	↓	↑	-
anchor travel	↑	-	↓	↑	↑	-
air gap	↑	↑	↑	↑	-	-
effective passage area of the gap filter	↑	-	-	↑	↑	-
angle of the valve seat cone	↑	↓	↑	↓	-	↑
ball diameter	↓	↓	↑	↓	-	-
length of the fuel introducing channel	-	-	-	-	-	-
hydraulic density at the front surface of the sprayer	↑	-	↓	↓	↓	↓
nozzle needle travel	↑	-	-	↑	↑	-
drain pressure	↑	-	-	↓	↓	↓
condition of electronic parts	↑	-	-	↓	-	-
force of the anchor spring	↓	-	↑	↓	↓	-
diameter of the spraying nozzle in the over-piston space	↑	-	↓	↓	↓	↓
hydraulic density of the piston	↓	-	↓	↓	↓	↓
leaks on the sealing washer	↑	-	↑	↓	↓	↓
volume of over-plunger space	↑	-	-	↑	↓	-

Based on results of Tables 2-4, a specific injector fault can be pointed out. In other words, when the diagnostic parameter exceeds the limit in one direction or another, a structural parameter that has gone out of the permissible deviation limit from the set value and requires adjustment or replacement can be identified. For example, an increase in fuel consumption for control may be caused by wear on the seat of the ball valve or by a decrease in the anchor spring force.

In this study, a well-known method for diagnosing elements of diesel fuel equipment was applied. This method is used by manufacturers for their products and it represents a common hydrodynamic calculation of fuel injection systems [25-34]. A distinctive feature of this method compared to traditional methods is addition of a detailed analysis of the closing valve of the injector into theoretical studies. This made it possible to obtain more accurate tolerance values for the structural parameters of the injector, which allowed preserving its performance, as well as the diesel engine working capacity as a whole. Implementation of the obtained data into the standard software of diagnostic stands of fuel equipment will increase efficiency of the injectors diagnostics and will provide a more accurate diagnosis of state of its elements. As mentioned above, this method of research can be applied to other units of the engine and fuel system of various manufacturers.

Currently various stands for testing injectors of the battery fuel injection systems are being developed. These stands assess the quality of their operation using only a few parameters: cyclic injection, fuel consumed for control, sometimes injection quality [1, 5, 8-9, 11, 17, 24, 28]. These technological recommendations are provided by the manufacturers. However, this method of diagnosis only gives two test results - a "working" and a "non-working" injector. This diagnostics is sufficient for employees of specialized services, but it increases the detection of a specific injector fault and working hours for troubleshooting. Reduction in the cost of operations is due to an accurate diagnosis of the injector condition, which in turn reduces the time spent on its repair.

4 Conclusions

As a part of the study, the injector's work process was examined and theoretically described, taking account wear of parts during its operation. Based on this, the classical hydrodynamic calculation process of fuel injection was refined. The resulting mathematical model of injector's operation allowed calculating the permitted deviations of specific structural parameters of the injector and determining the test modes in which this effect is most pronounced. Because of a comprehensive analysis of the design and work process of the BOSCH injector,

20 structural and 6 diagnostic parameters were identified. By studying these parameters, Tables 2-4 of faults for different modes of operation of the diesel engine (nominal, start, idling) were made, which also contains justification of the conditions for ensuring the injector operability by adjusting, restoring or replacing any part.

Experimental studies have corrected and confirmed values of allowed deviations of structural parameters and revealed their relationship with diagnostic parameters. Using the obtained results, made it possible to identify a specific faulty element based on data obtained during the random diagnostics of the injector. Results allow not only to identify a specific faulty element in the case of the bad injector operation, which reduces the complexity of repair of the resistant temperature device, but also to predict the remaining injector life, to prevent possible failures and downtime of equipment during the hard agricultural work.

The resulting method of diagnostics makes it possible to carry out tests for the malfunctions of individual units of the fuel-delivery systems and injectors of other manufacturers such as Denso and Delphi. For the first time, the permitted deviations of structural parameters for the BOSCH injector were obtained. All of the tolerance values of the injector's structural parameters are noticeable, and the test mode in which its influence is most observed is determined for each of them.

References

[1] ANANIN, A. D., MIKHLIN, V. M., GABITOV, I. I. *Diagnostics and maintenance of machines.* Textbook. Moscow: Academy, 2015. ISBN 978-5-4468-0769-7.

[2] GABITOV, I. I., INSAFUDDINOV, S. Z., KHARISOV, D. D., SAFIN, F. R., NEGOVORA, A. V., YUNUSBAEV, N. M., AKHMETOV, A. F., FARHUTDINOV, T., SHARAFEEV A. Diagnostics and regulation of fuel equipment of diesels on stands with injection to medium with counter-pressure. *Journal of Engineering and Applied Sciences* [online]. 2018, **13**(S11), p. 8782-8788. ISSN 1816-949X, eISSN 1818-7803. Available from: https://doi.org/10.3923/jeasci.2018.8782.8788

[3] GABITOV, I. I., SAIFULLIN, R. N., FARHSHATOV, M. N., NEGOVORA, A. V., MUDARISOV, S. G., KHASANOV, E. R., GALIULLIN, R. R., GABDRAFIKOV, F. Z., YUNUSBAEV, N. M., VALIEV A. R. Hardening of electrohydraulic injectors valve units of diesels at repair. *Journal of Engineering and Applied Sciences* [online]. 2018, **13**(S8), p. 6478-6486. ISSN 1816-949X, eISSN 1818-7803. Available from: https://doi.org/10.3923/jeasci.2018.6478.6486

[4] SKAKOV, M., RAKHADILOV, B., SCHEFFLER, M., BATYRBEKOV, E. Microstructure and tribological properties of electrolytic plasma nitrided high-speed steel. *Materials Testing* [online]. 2015, **57**(4), p. 360-364. ISSN 0025-5300. Available from: https://doi.org/10.3139/120.110709

[5] GRITSUK, I. V., ZENKIN, E. Y., BULGAKOV, N., GOLOVAN, A., KURIC, I., MATEICHYK, V., SAGA, M., VYCHUZHANIN, V., SYMONENKO, R., RABINOVICH, E., PAVLENKO, V., POHORLETSKYI, D. The complex application of monitoring and express diagnosing for searching failures on common rail system units *SAE Technical Paper* [online], 20182018-01-1773. ISSN 0148-7191, eISSN 2688-3627. Available from: https://doi.org/10.4271/2018-01-1773

[6] KULMANAKOV, S. P., LEBEDEVAS, S., KULMANAKOV, S. S., LAZAREVA, N., RAPALIS, P. Comparative studies of the biodiesel fuel jet development dynamics in common rail and conventional design fuel systems. *Transport* [online]. 2019, **34**(1), p. 67-74. ISSN 1648-4142, eISSN 1648-3480. Available from: https://doi.org/10.3846/transport.2019.7223

[7] MALASTOVSKII, N. S., BARCHENKO, F. B., GREKHOV, L. V., KULESHOV, A. S., DENISOV, A. A., STARKOV, E. E. Formation of requirements for high-speed diesel injection characteristics in order to reduce toxicity. *Engineering Journal: Science and Innovation* [online]. 2017, **3**(63), p. 1-19. ISSN 2308-6033. Available from: https://doi.org/10.18698/2308-6033-2017-3-1594

[8] POGULYAEV, Y. D., BAITIMEROV, R. M., ROZHDESTVENSKII, Y. V. Detailed dynamic modeling of common rail piezo injector. *Procedia Engineering.* [online]. 2015, **129**, p. 93-98. ISSN 1877-7058. Available from: https://doi.org/10.1016/j.proeng.2015.12.014

[9] MAIORANA, G., SEBASTIANO, G. R., UGAGLIA, C. Common rail system for passenger car / Die common-rail-motoren von Fiat (in German). *MTZ-Motortechnische Zeitschrift* [online]. 1998, **59**(9), p. 582-588. ISSN 0024-8525. Available from: https://doi.org/10.1007/BF03251382

[10] WU, D. W., SUN, B. G., XU D. Deformation of nozzle, needle, and control plunger of solenoid fuel injector under high injection pressure. *Proceedings of the Institution of Mechanical Engineers*, *Part D: Journal of Automobile Engineering* [online]. 2019, **233**(7), p. 1767-1782. ISSN 0954-4070, eISSN 2041-2991. Available from: https://doi.org/10.1177%2F0954407018786354

[11] HOFFMANN, K.-H., HUMMEL, K., MADERSTEIN, T. The common rail injection system - a new chapter in diesel injection technology / Das Common-Rail-Einspritzsystem -ein neues Kapitel der Dieseleinspritz-Technik (in German). *MTZ: Motortechnische Zeitschrift.* 1997, **10**(58), p. 572-582. ISSN 0024-8525.

[12] MALASTOWSKI, N. S., BARCHENKO, F. B., GREKHOV, L. V., KULESHOV, A. S. Shaping of injection rate for reducing emission level of high-speed engine. *International Journal of Applied Engineering Research.* 2016, **11**(23), p. 11189-11198. ISSN 0973-4562.

[13] MARCOV, V., GLADYSHEV, S., DEVIANIN, S. Injector tip design improvement of the diesel injectors. *SAE Technical Paper* [online], 2011, 2011-01-1397. ISSN 0148-7191, eISSN 2688-3627. Available from: https://doi.org/10.4271/2011-01-1397

[14] NIGMATULLIN, S. F., KOSTAREV, K. V., KARACHURIN, B. S. Studies on the effect of the process fluid temperature on the cycle flow of an electrohydrocontrolled nozzle. *Bulletin of Bashkir State Agrarian University.* 2015, **3**(35), p. 69-71.

[15] WIARTALLA, A., RUHKAMP, L., KOERFER, T., TOMAZIC, D., TATUR, M., KOEHLER, E. Future emission demands for ship and locomotive engines-challenges, concepts and synergies from HD-applications. In: 26th CIMAC World Congress on Combustion Engine: proceedings. 2010. Paper No. 174.

[16] JOCANOVIC, M. T., KARANOVIC, V. V., KNEZEVIC, D. M., OROSNJAK, M. D. Diesel fuel filtration problems with modern common rail injection systems. *Vojnotehnicki Glasnik.* [online]. 2017, **65**(4), p. 968-993. ISSN 0042-8469, eISSN 2217-4753. Available from: https://doi.org/10.5937/vojtehg65-11577

[17] RAJAK, U., NASHINE, P., VERMA, T. N., PUGAZHENDHI, A. Performance, combustion and emission analysis of microalgae Spirulina in a common rail direct injection diesel engine. *Fuel.* [online]. 2019, **255**, 115855. ISSN 0016-2361. Available from: https://doi.org/10.1016/j.fuel.2019.115855

[18] SAPIO, F., PIANO, A., MILLO, F., PESCE, F. C. Digital shaping and optimization of fuel injection pattern for a common rail automotive diesel engine through numerical simulation. *SAE Technical Paper* [online], 2017, 2017-24-0025. ISSN 0148-7191, eISSN 2688-3627. Available from: https://doi.org/10.4271/2017-24-0025

[19] TZANETAKIS, T., VOICE, A. K., TRAVER, M. L. Durability study of a high-pressure common-rail fuel injection system using lubricity additive-dosed gasoline-like fuel. *SAE International Journal of Fuels and Lubricants* [online]. 2018, **11**(4), p. 319-336. ISSN 2641-9637, eISSN 2641-9645. Available from: https://doi.org/10.4271/2019-01-0263

[20] ABRAMEK, K. F., STOECK, T., OSIPOWICZ, T. Statistical evaluation of the corrosive wear of fuel injector elements used in common rail systems. *Strojniski vestnik - Journal of Mechanical Engineering* [online]. 2015, **61**(2), p. 91-98. ISSN 0039-2480, eISSN 2536-2948. Available from: https://doi.org/10.5545/sv-jme.2014.1687

[21] LAZAREV, V. E., WLOKA, J. A., WACHTMEISTER, G. A Method for the estimation of the service life of a precision guiding interface "Needle-Nozzle Body" of a common-rail-injector for high rail pressures. *SAE Technical Paper* [online], 2011, 2011-01-2020. ISSN 0148-7191, eISSN 2688-3627. Available from: https://doi.org/10.4271/2011-01-2020

[22] RICCO, M., DE MATTHAEIS, S., OLABI, A. G. Simulation of the magnetic properties for common rail electro-injector. *Journal of Materials Processing Technology.* [online]. 2004, **155**, p. 1611-1615. ISSN 0924-0136. Available from: https://doi.org/10.1016/j.jmatprotec.2004.04.343

[23] KURCZYNSKI, D., LAGOWSKI, P. Performance indices of a common rail-system CI engine powered by diesel oil and biofuel blends. *Journal of the Energy Institute* [online]. 2019, **92**(6), p. 1897-1913. ISSN 1743-9671. Available from: https://doi.org/10.1016/j.joei.2018.11.004

[24] ZHAO, J., YUE, P., GREKHOV, L., MA, X. Hold current effects on the power losses of high-speed solenoid valve for common-rail injector. *Applied Thermal Engineering* [online]. 2018, **128**, p. 1579-1587. ISSN 1359-4311. Available from: https://doi.org/10.1016/j.applthermaleng.2017.09.123

[25] GREKHOV, L. V., DENISOV, A. A., STARKOV, E. E. Requirements justification for fuel injection system, energy-efficient low-emission diesel engines. *VSTU News.* 2014, **6**(18), p. 7-11. ISBN 978-5-9948-1574-8.

[26] IVASHCHENKO, N. A., GREKHOV, L. B., TSZIANKHUEI, CH. Method of calculating the quick-operating drive of the control valve of the fuel supply equipment. *Internal Combustion Engines (All-Ukrainian Scientific and Technical Journal)*. 2012, **1**, p. 65-69. ISSN 0419-8719.

[27] CHIATTI, G., CHIAVOLA, O., PALMIERI, F. Phenomenological approach for common rail diesel engine emission and performance prediction. *SAE Technical Paper* [online], 2010, 2010-01-0874. ISSN 0148-7191, eISSN 2688-3627. Available from: https://doi.org/10.4271/2010-01-0874

[28] COPPO, M., DONGIOVANNI, C., NEGRI, C. A linear optical sensor for measuring needle displacement in common-rail diesel injectors. *Sensors and Actuators A: Physical* [online]. 2007, **134**(2), p. 366-373. ISSN 0924-4247. Available from: https://doi.org/10.1016/j.sna.2006.05.038

[29] GREKHOV, L. V., DRAGAN, Y. E. E., DENISOV, A. A., STARKOV, E. Injection rate shaping with possibilities of conventional design common rail system. *International Journal of Applied Engineering Research.* 2015, **10**(5), p. 3979-3986. ISSN 0973-4562.

[30] GREKHOV, L., MAHKAMOV, K., KULESHOV, A. Optimization of mixture formation and combustion in two-stroke OP engine using innovative diesel spray combustion model and fuel system simulation software. *SAE Technical Paper* [online], 2015, 2015-01-1859. ISSN 0148-7191, eISSN 2688-3627. Available from: https://doi.org/10.4271/2015-01-1859

[31] KULESHOV, A., GREKHOV, L. Multidimensional optimization of DI diesel engine process using multi-zone fuel spray combustion model and detailed chemistry NOx formation model. *SAE Technical Paper* [online], 2013, 2013-01-0882. ISSN 0148-7191, eISSN 2688-3627. Available from: https://doi.org/10.4271/2013-01-0882

[32] LAU, K., JUNK, R., KLINGBEIL, S., SCHUUMANN, U., STREIBEL, T. Analysis of internal common rail injector deposits via thermo desorption photon ionization time of flight mass spectrometry. *Energy and Fuels* [online]. 2015, **29**(9), p. 5625-5632. ISSN 0887-0624, eISSN 1520-5029. Available from: https://doi.org/10.1021/acs.energyfuels.5b01114

[33] SHATROV, M. G., GOLUBKOV, L. N., DUNIN, A. U., YAKOVENKO, A. L., DUSHKIN, P. V. Experimental research of hydrodynamic effects in common rail fuel system in case of multiple injection. *International Journal of Applied Engineering Research.* 2016, **11**(10), p. 6949-6953. ISSN 0973-4562.

[34] WROBLEWSKI, A. Modeling of hydrodynamic processes in diesel injector nozzle. *Mechanics* [online]. 2019, **25**(2), p. 128-133. ISSN 1392-1207, eISSN 2029-6983. Available from: https://doi.org/10.5755/j01.mech.25.2.19326

CALCULATION OF THE VEHICLES STRESS-DEFORMED STATE WHILE TRANSPORTING THE LIQUID CARGO

Oleksii Grevtsev[1], Ninel Selivanova[1], Pavlo Popovych[2], Liubomyr Poberezhny[3,*], Oksana Shevchuk[2], Igor Murovanyi[4], Andrii Hrytsanchuk[3], Liubov Poberezhna[3], Vasyl Zapukhliak[3],Galyna Hrytsuliak[4]

[1]National Transport University, Kyiv, Ukraine
[2]West Ukrainian National University, Ternopil, Ukraine
[3]Ivano-Frankivsk National Technical University of Oil and Gas, Ivano-Frankivsk, Ukraine
[4]Lutsk National Technical University, Lutsk, Ukraine

*E-mail of corresponding author: lubomyrpoberezhny@gmail.com

Resume
To calculate the stress-deformed state of road-tanker metal structures during the liquid cargo transportation, the solution for bending axially and symmetrically loaded circular plates is proposed, which is based on the theory of elasticity approach. Dependencies for calculating stresses and displacements under arbitrary load law and support type are substantiated. Deformation of the support under the action of axisymmetric loading leads to appearance of a temperature field.

Article info
Received 31 January 2020
Accepted 14 July 2020
Online 19 November 2020

Keywords:
trailers,
metal structures of vehicles,
liquid cargoes,
axisymmetric problem,
thermodynamically reverse process,
bend of a circular plate

Available online: https://doi.org/10.26552/com.C.2021.1.B58-B64

ISSN 1335-4205 (print version)
ISSN 2585-7878 (online version)

1 Introduction and literature review

According to analysis of operation conditions of vehicles for transporting the liquid cargoes, the dynamic loads and influence of external environment, in particular temperature and precipitation, are the main factors that cause destruction of assembly units (load-bearing systems and tanks of vehicles), their parts (supports of tanks, etc.), as well as connections [1-7]. This fact contributes to formation of wet films on surfaces of vehicles, with regard to condition of surfaces: coating, roughness, hardness etc. The constant impact of combinations of these factors causes damage with subsequent destruction, the most characteristic of which are [8-17]: fatigue damage, atmospheric corrosion, corrosion-mechanical wear, corrosion fatigue, corrosion cracking, fretting - corrosion. The study of the vehicles' condition after 1-3 years of operation makes it possible to conclude: more than 70-80% of constituent units and machine parts are subjected to corrosion in one way or another, [1-17]. Therefore, the corrosion damage and fatigue fracture are objective and logical results of influence of the environment, dynamic loads and thermodynamically unstable metal materials of the vehicles' parts. The fatigue damage to metal structures, as well as the corrosive one, causes vehicle failure and weight loss, intensifies joint wear, changes in the surface roughness of parts, reduces fatigue strength, causing various cracks and metal breaks. As a result, the reliability, efficiency and resource of the machines and their components are reduced; the cost of repair and the elimination of the consequences of failures increase. The service life of parts often reduces in practice up to 50% due to fatigue fractures. According to analysis of fractures of parts, knots and details of thin sheet steel, the inner surfaces of containers for toxic chemicals are destroyed most quickly [9-17]. Therefore, during the operation of vehicles, especially when transporting the liquid cargo, the random complex combinations of different power factors affects the tank and elements of the bearing systems. This fact is stipulated by the random nature of the sources of disturbances (transport modes, inequalities of the road, geometry, etc.).

Based on the research results of metal structures of tanks (including their supports) for transporting the liquid cargoes, the following tasks can be solved:

- estimation of the stress strain state of metal structures (in particular tanks and their supports during the transportation of the liquid cargoes) in order to identify and improve the maximum loaded elements to reduce the metal structure;

- distribution of stresses in the maximum loaded cross sections of elements to predict the reliability of vehicles.

Deformation of the solid elastic medium is not always purely a mechanical phenomenon. Nearly every deformation is accompanied by thermal effects and therefore an attempt to describe the behavior of the environment, ignoring the thermo-mechanical interaction within the environment, is not always feasible. Temperature change in the body can occur as a result of a deformation process, as well as for extraneous reasons. External load (surface, volume) causes the body deformation and at the same time causes the change of the temperature field in it. The change in temperature is $\theta = T - t_0$, where T is the absolute temperature points of the body, t_0 is the temperature of the unstressed body. Therefore, during the deformation the temperature changes of the points of the body and can lead to the absorption or release of heat by elastic uninsulated body and its interaction with the environment. The deformation process is very slow, i.e., it is thermodynamically reversible. The temperature change θ is very small and does not cause changes in existing physical and mechanical characteristics of the material body. Its accounting allows to accurately solve the equation of elasticity for bending of round plates under the action of forces normally applied according to arbitrary loading law with any type of section, which previously was impossible to do.

2 Methodology

The exact solution of equations of the theory of elasticity in the closed form for round plates with axisymmetric loading is possible only taking into account the temperature change, which appears at deformation from action of normally added forces. The magnitude of the temperature change is very small ($\approx 2 \div 3$ K), but its consideration makes it possible to accurately solve the problem of the theory of elasticity for bodies of rotation with axisymmetric deformation without any simplified hypotheses, except for the general linear theory of elasticity. There is no need to use different approximate numerical methods of solution, such as FEM.

Therefore, in order to solve these problems with maximum accuracy, it is advisable to apply the provisions of the theory of elasticity, which will provide adequate simulation of stresses and displacements under arbitrary loads and types of supports.

The exact solution of elasticity problem is known [18] to be available only for the case of a solid round plate loaded with a uniformly distributed pressure of constant intensity. Thus, the form of loading is assumed arbitrary, as well as the type of plate resistance.

Differential equilibrium equations in a cylindrical coordinate system are deduced [18]:

$$\begin{aligned} &\Delta u_1 - \frac{u_1}{r^2} + \frac{e,_1}{1-2v} - 2\frac{(1+v)}{(1-2v)}\alpha\theta,_1 = 0; \\ &\Delta u_3 - \frac{u_1}{r^2} + \frac{e,_3}{1-2v} - 2\frac{(1+v)}{(1-2v)}\alpha\theta,_3 = 0; \end{aligned} \tag{1}$$

$$\begin{aligned} &\sigma_{11,1} + \sigma_{13,1} + \frac{\sigma_{11} - \sigma_{22}}{r} = 0; \\ &\sigma_{13,1} + \sigma_{33,3} + \frac{1}{r}\sigma_{13} = 0. \end{aligned} \tag{2}$$

In Equations (1) and (2), the index after the comma denotes the partial derivative with respect to the corresponding coordinate: r or z; u_1 and u_3 are components of radial and axial movements, respectively; Δu - Laplace operator for movements $u_i (i = 1,3)$; σ_{11}, σ_{12}, σ_{13} - respectively, the components of radial, circumferential, axial and tangential stresses; σ_{33} is explained in Equation (6).

The Hooke's law [19] determines the stress components

$$\begin{aligned} &\sigma_{ij} = 2G\left(e_{ij} + \frac{v}{1-2v}e\delta_{ij} - \frac{1+v}{1-v}\alpha\theta\delta_{ij}\right), \\ &i,j = 1,2,3; \end{aligned} \tag{3}$$

based on the well-known dependencies between deformations and movements:

$$e_{11} = u_{1,1}; e_{22} = \frac{1}{r}u_1; e_{33} = u_{3,1}; 2e_{13} = u_{1,3} + u_{3,1}, \tag{4}$$

where δ_{ij} - Kronecker delta symbol; α and v - respectively, coefficients of linear thermal expansion and Poisson's ratio; $e = e_{11} + e_{22} + e_{33}$ - volumetric expansion; $G = \frac{E}{2(1+v)}$ - shear module; E - modulus of elasticity.

To solve the system of equilibrium Equations (1), the equation of thermal conductivity should be considered [19]:

$$\Delta\theta + \frac{1}{\lambda}W = 0, \tag{5}$$

where W - amount of heat that is released or absorbed per unit of the body volume during the deformation; λ - thermal conductivity; $\Delta\theta = \theta,_{11} + \frac{1}{r}\theta,_{11} + \theta,_{33}$.

To solve the problem of bending the round plates under the action of an arbitrary axisymmetric intensity load $P(r)$, the normal axial stress σ_{33} should be determined. Therefore, the method based on translational approximations should be applied. Thus, after the transformations, we obtain:

$$\sigma_{33} = -P(r)\frac{12}{h^3}\left(\frac{z^3}{6} - \frac{zh^2}{8} - \frac{h^3}{24}\right). \tag{6}$$

Equation (6) meet conditions:

$$\begin{aligned} &\sigma_{33} = -P(r), \text{ if } z = -\frac{h}{2} \text{ and } \sigma_{33} = 0, \\ &\text{where } z = -\frac{h^2}{2}, \end{aligned} \tag{7}$$

where h - the thickness of the round plate.

3 Results and discussion

Based on Equation (6), the problem of bending the plate is further solved applying the function $\phi_{(r,z)}$. To solve this problem accurately, a polytrophic thermodynamic process (neither isothermal nor adiabatic) is studied. The function $\psi_{(r,z)}$ is related to the thermoelastic movement potential by the formula [19]:

$$\phi_{(r,z)} = \frac{1+v}{1-x}\psi(r,z). \tag{8}$$

For this case, the movement is defined:

$$\begin{aligned} u_1(r,z) &= \frac{1+v}{1-v}\psi_{,1}; \\ u_3(r,z) &= \frac{1+v}{1-v}\psi_{,3}. \end{aligned} \tag{9}$$

The volumetric expansion e is derived from Equation (4), with taking into account Equation (9):

$$\begin{aligned} e &= e_{11} + e_{22} + e_{33} = \\ &= \frac{1+v}{1-v}\left[\psi_{,11} + \frac{1}{r}\psi_{,1} + \psi_{,33}\right] = \\ &= \frac{1+v}{1-v}\Delta\psi \end{aligned} \tag{10}$$

Substituting Equations (9) and (10) into the system of Equations (1), one obtains:

$$\begin{aligned} &\frac{2(1+v)}{1-v}(\Delta\psi)_{,1} - \frac{2(1+v)}{1-v}2\theta_{,1} = 0 \\ &\frac{2(1+v)}{1-v}(\Delta\psi)_{,3} - \frac{2(1+v)}{1-v}2\theta_{,3} = 0. \end{aligned} \tag{11}$$

Integrating Equation (11) the first equation with respect to r and the second equation with respect to z, the formula for definition of a temperature variable is deduced:

$$2\theta = \Delta\psi. \tag{12}$$

Based on the Hooke's law [20], the elasticity is found. The temperature change θ is derived from Equation (12).

Then:

$$\begin{aligned} &\sigma_{13} = \frac{E}{1-v}\psi_{,13}; \sigma_{33} = -\frac{E}{1-v}\frac{1}{r}(r\psi_{,1})_{,1}; \\ &\sigma_{11} = -\frac{E}{1-v}\left(\frac{1}{r}\psi_{,1} + \psi_{,3}\right); \\ &\sigma_{11} = -\frac{E}{1-v}(\psi_{,11} + \psi_{,3}3). \end{aligned} \tag{13}$$

To solve the elasticity theory equations, the movement function $\psi(r,z)$ should be chosen in such a way as to satisfy the boundary conditions for a specific problem.

Thus, the curvature of the round plates in the exact formulation of the problem from the standpoint of the theory of elasticity is considered below. The given plates are loaded symmetrically with respect to the axis of rotation z by forces $P(r)$ applied perpendicular; forms of loading and types of supports are arbitrary.

The stress σ_{33} in Equation (6), which satisfies Equation (7), is compared to stress σ_{33} in Equation (13). After transformations, the differential equation for determining the function $\psi(r,z)$ is developed:

$$(r\psi_{,1})_{,1} = \frac{1-v}{E}\frac{12}{h^3}\left(\frac{z^3}{6} - \frac{zh^2}{8} + \frac{h^3}{24}\right)rP(r). \tag{14}$$

Integrating Equation (14) with respect to r in the range from a_1 to r, the formula is deduced:

$$\begin{aligned} &\psi_{,1} = \frac{1-v}{E}\frac{12}{h^3}\left(\frac{z^3}{6} - \frac{zh^2}{8} + \frac{h^3}{24}\right)\frac{1}{r}\cdot \\ &\cdot\int_{a1}^{r} rP(r)dr + \frac{1}{r}f_1(z), \end{aligned} \tag{15}$$

where $f_1(z)$ - arbitrary integration function; a_1 - radius of the central hole of the plate.

For the case, if there is no hole in the metal plate under study ($a_1 = 0$), then, $f_1(z)$ is equal to zero for finite movements $u(r)$. Therefore, Equation (15) is integrated with respect to r in the range from a_1 to r, resulting in:

$$\begin{aligned} &\psi_{(r,z)} = \frac{1-v}{E}\frac{12}{h^3}\left(\frac{z^3}{6} - \frac{zh^2}{8} + \frac{h^3}{24}\right)\times \\ &\times\int_{a1}^{r}\frac{1}{r}\int_{a1}^{r} rP(r)drdr + f_1(z)\ln\frac{r}{a} + f_2(z), \end{aligned} \tag{16}$$

where $f_2(z)$ - arbitrary integration function.

To rationally simplify calculations, a solid plate $[a_1 = 0; f_1(z) = 0]$ should be considered. Then:

$$\begin{aligned} &\psi_{(r,z)} = \frac{1-v}{E}\frac{12}{h^3}\left(\frac{z^3}{6} - \frac{zh^2}{8} + \frac{h^3}{24}\right)\times \\ &\times\int_{0}^{r}\frac{1}{r}\int_{0}^{r} rP(r)drdr + f_2(z). \end{aligned} \tag{17}$$

Differentiating Equation (17) with respect to r and z:

$$\psi_{(r,z)} = \frac{1-v}{E}\frac{12}{h^3}\left(\frac{z^3}{6} - \frac{h^2}{8}\right)\frac{1}{r}\int_{0}^{r} rP(r)dr \tag{18}$$

and substituting $\psi_{,13}$ into Equation (13), one obtains:

$$\sigma_{13} = \frac{6}{h^3}\left(z^2 - \frac{h^2}{4}\right)\frac{1}{r}\int_{0}^{r} rP(r)dr. \tag{19}$$

The boundary conditions for Equation (19) are satisfied integrally at the edge of the round plate. Therefore, to meet the boundary conditions providing, $r = a$, the stress σ_{13} at the edge of the plate should be reduced to the support reaction:

a

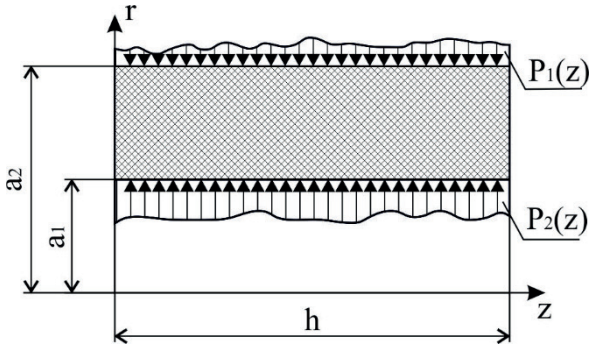

b

Figure 1 *a - tank of a vehicle for transporting the liquid cargoes; b - schematization of the tank element, solid round plate with an arbitrary type of support, loaded* $P(r)_x$

$$A = \left[\int_{-\frac{h}{2}}^{\frac{h}{2}} \sigma_{13} dz \right]_{r=a} = -\frac{1}{a} \int_0^r rP(r)dr . \tag{20}$$

Thus, the stresses in Equation (19) satisfy the boundary conditions on the planes $z = \pm\frac{h}{2}$ integrally at the edge of the surface.

Substituting Equation (17) into Equation (13) for the normal radial stress σ_{11} and deriving the function $f_2(z)$ from the boundary conditions $\sigma_{11} = 0$, providing $r = a$, one obtains:

$$\sigma_{11} = \frac{12}{h^3} \times \left\{ \left(\frac{z^3}{6} - \frac{zh^2}{8} + \frac{h^3}{24} \right) \times \left\{ \times \left[\frac{1}{r^2} \int_0^r rP(r)dr - \frac{1}{a^2} \int_0^a rP(r)dr \right] + \right. \right. \left. \left. + Z \left[\int_0^r \frac{1}{r} \int_0^r rP(r)drdr - \int_0^a \frac{1}{r} \int_0^a rP(r)drdr \right] \right\} . \tag{21}$$

For the stress σ_{22} in Equations (13):

$$\sigma_{22} = -\frac{12}{h^3} \times \left\{ \left(\frac{z^3}{6} - \frac{zh^2}{8} + \frac{h^3}{24} \right) \times \left\{ \times \left[P(r) - \left(\frac{1}{r^2} \int_0^r rP(r)dr - \frac{1}{a^2} \int_0^a rP(r)dr \right) \right] + \right. \right. \left. \left. + z \left[\int_0^r \frac{1}{r} \int_0^r rP(r)drdr - \int_0^a \frac{1}{r} \int_0^a rP(r)drdr \right] \right\} . \tag{22}$$

The obtained stresses satisfy the equilibrium Equation (2) and the boundary conditions: $\sigma_{33} = -P(r)$ if $z = -\frac{h}{2}$; $\sigma_{33} = 0$ where $z = \frac{h}{2}$; $\sigma_{13} = 0$ where $z = \pm\frac{h}{2}$; and integrally on the edge of the plate: $\sigma_{11} = 0$ where $r = a$.

The plate support conditions make it possible to determine the exact values of movements by Equation (8) using Equation (17).

Movements u_1 and u_2:

$$\begin{aligned} u_1(r,z) &= \frac{1+V}{1-V} \left[\psi_{,1} + \frac{1}{r}(A_5 z - A_3) \right] + \\ &+ r\left(A_4 z + A_6 \frac{1}{2} \right) \\ u_1(r,z) &= \frac{1+V}{1-V} [\psi_{,3} + A_5 \ln r] - \\ &- A_4 \left(\frac{V}{1-V} z^2 + \frac{r^2}{2} \right) - \frac{V}{1-V} z A_6 + A_7 . \end{aligned} \tag{23}$$

where A_i - arbitrary integration constants.

Based on Equation (23), the formula is developed:

$$\begin{aligned} \sigma_{13} &= \frac{E}{1-V} \psi_{,13}; \sigma_{33} = -\frac{E}{1-V} \frac{1}{r} (r\psi_{,1})_{,1} \\ \sigma_{11} &= \frac{E}{1-V} \left[\begin{array}{l} -\frac{1}{r}\psi_{,1} - \psi_{,33} - \frac{1}{r^2} \times \\ \times (A_5 z - A_3) + A_4 z + A_6 \frac{1}{2} \end{array} \right] \\ \sigma_{22} &= \frac{E}{1-V} \left[\begin{array}{l} \psi_{,11} - \psi_{,33} - \frac{1}{r^2} \times \\ \times (A_5 z - A_3) + A_4 z + A_6 \frac{1}{2} \end{array} \right] . \end{aligned} \tag{24}$$

Equations (23) and (24) are exact solutions of equilibrium Equations (1) and (2); after substitution, Equations (1) and (2) are transformed into identities. The function $\psi(r,z)$ must satisfy Equation (12). Based on this equation, the temperature variable $\theta(r,z)$, occurred due to the action of external loads, could be determined, as well as the dependence $\psi(r,z)$ on the boundary conditions.

To illustrate the elastic and thermodynamic reflexivity of the above-considered problems of the theory of elasticity for axisymmetric deformation of plates, the solution should be simplified by assuming that $P(r) = P_0 = const$ (see Figure 1).

Then, for the movement in Equation (17) one gets:

$$\psi(r,z) = \frac{1-V}{E} \frac{12}{h^3} P_0 \left(\frac{z^3}{6} - \frac{zh^2}{8} + \frac{h^3}{24} \right) \times \times \frac{r^2}{4} + f_2(z), \tag{25}$$

while for stresses in Equation (19) is obtained:

$$\sigma_{13} = \frac{3}{h^3} P_0 \left(z^3 - \frac{h^2}{4} \right) r . \tag{26}$$

The magnitude of the support reaction at the edge of the plate:

$$A = -\frac{a}{2}P_0. \tag{27}$$

Radial stresses in Equation (21) and circular stresses in Equation (22) coincide:

$$\sigma_{11} = \sigma_{22} = \frac{3z}{h^3}P_0(a^2 - r^2). \tag{28}$$

For the function $f_2(z)$ one obtains:

$$f_2(z) = \frac{1-V}{E}\frac{6}{h^3}P_0\left(\frac{z^5}{120} - \frac{z^3h^2}{48} + \frac{z^3a}{12}\right) + \\ + C_1C_1z + C_2. \tag{29}$$

where C_1 and C_2 - arbitrary integration constants.

Based on Equation (9), the displacements are found:

$$u_1(r,z) = \frac{1+V}{1-V}\psi_{,1} = \frac{1+V}{E}\frac{12}{h^3}P_0\times \\ \times\left(\frac{z^3}{6} - \frac{z^8h^2}{8} + \frac{h^3}{24}\right)\frac{r}{2}u_3(r,z) = \frac{1+V}{1-V}\psi_{,3} = \\ = \frac{1+V}{E}\frac{3}{2h^3}P_0\times \\ \times\left[r^2\left(z^2 - \frac{h^2}{4}\right) - \left(\frac{z^3}{6} - \frac{h^2z^2}{4} + \frac{zh^3}{6} + z^2a^2\right)\right] + \\ + \frac{1+V}{1-V}C_1. \tag{30}$$

The radial movement in Equation (30) affects the resistance of the plate in such a way that it allows the movement of the plate in the direction of the vertical axis (Figure 1).

The normal movement in Equation (31) allows fixing the points of the plate edges in different ways to prevent their vertical displacement.

As an example, the hinge fixing of the plate contour points, in the middle plane, could be considered, $u_3 = 0$; $r = a; z = 0$. Satisfying these boundary conditions for movement in Equation (30) and an arbitrary integration constant C_1, the formula is deduced:

$$\frac{1+V}{1-V}C_1 = \frac{1+V}{E}\frac{3}{2h^3}P_0\frac{a^2h^2}{4}. \tag{31}$$

After substitution Equation (31) into Equation (30), one obtains:

$$u_3(r,z) = \frac{1+V}{E}\frac{3}{2h^3}P_0\times \\ \times\left[\begin{array}{l} r^2\left(z^2 - \frac{h^2}{4}\right) + \frac{a^2h^2}{4} - \\ -\left(\frac{z^3}{6} - \frac{h^2z^2}{4} + \frac{zh^3}{6} + z^2a^2\right)\end{array}\right]. \tag{32}$$

The stresses corresponding to movements in Equations (28) and (32) are developed:

$$\sigma_{33} = -\frac{6}{h^3}P_0\left(\frac{z^3}{3} - \frac{h^2z}{4} + \frac{h^3}{12}\right); \\ \sigma_{13} = \frac{3}{h^3}P_0\left(z^2 - \frac{h^2}{4}\right)r; \\ \sigma_{11} = \sigma_{22} = \frac{3}{h^3}P_0(a^2 - r^2)z. \tag{33}$$

Based on Equations (25) and (29), follows:

$$\psi(r,z) = \frac{1-V}{E}\frac{6}{h^3}P_0\times \\ \times\left[\begin{array}{l}\left(\frac{z^3}{6} - \frac{zh^2}{8} + \frac{h^3}{24}\right)\frac{r^2}{4} - \\ -\left(\frac{z^5}{120} - \frac{z^3h^2}{48} + \frac{z^2h^3}{48} + \frac{a^2z^2}{12}\right) + \frac{a^2z^2}{16}z\end{array}\right] + \\ + C_2. \tag{34}$$

where C_2 - arbitrary integration constant.

The temperature variable $\theta(r,z)$ occurred due to the action of external loads P_0 in the plate under study is developed

$$\alpha\theta = \Delta\psi_{,11} + \frac{1}{r}\psi_{,1} + \psi_{,33}. \tag{35}$$

Substituting Equation (34) into Equation (35), one obtains:

$$\theta(r,z) = \frac{(1-V)}{E\alpha}\frac{6}{h^3}P_0\times \\ \times\left[\frac{z^3}{6} - \frac{zh^2}{8} + \frac{h^3}{24} - (a^2 - r^2)\frac{z}{2}\right]. \tag{36}$$

External surface and volume loads cause the body deformation and the occurrence of temperature changes in it [20]. Temperature change is $\theta = T - T_0$, where T - the absolute temperature of the body point; T_0 - the temperature of the unstressed body when t = 0.

Therefore, during the deformation, temperature of an arbitrary point of the body changes. As a result, an elastic uninsulated body absorbs or releases heat during its interaction with the environment [21]. This temperature change of the bent round plate is determined by the dependence in Equation (36).

Providing that the load P_0 = 0 is reset, voltage in Equation (33) and temperature change in Equation (36) disappear. Then, the plate acquires the initial unstressed and undeformed state. The deformation process is very slow, i.e. it is thermodynamically reversible [22].

The deformation of the plate and the temperature change in it under external load are under study. Substituting $z = -\frac{h}{2}$ into Equation (32), the dependence describing the compression ratio of the upper layers of the plate in the given direction is developed:

$$u_3\left(r_1 - \frac{h}{2}\right) = \frac{1+V}{E}\frac{3h}{64}P_0 > 0. \tag{37}$$

For the case of a lower surface of the plate where $z = +\frac{h}{2}$:

$$u_3\left(r_1 \frac{h}{2}\right) = -\frac{1+V}{E}\frac{3h}{64}P_0 < 0\,. \tag{38}$$

Resulting in a stretching area.

Based on Equation (32), for the compressed section of the plate, the temperature change is deduced as:

$$\begin{aligned}\theta\left(r_1 - \frac{h}{2}\right) &= \frac{1-V}{E\alpha}\frac{3}{h^2}P_0\left(\frac{h^2}{3} + a^2 - r^2\right) \geq 0, or\\ T\left(r_1 - \frac{h}{2}\right) &= T_0 + \frac{1-V}{E\alpha}\frac{3}{h^2}P_0\left(\frac{h^2}{3} + a^2 - r^2\right)\times\\ &\times (r \leq a),\end{aligned} \tag{39}$$

while for the stretched, area due to the bending, it is:

$$\begin{aligned}\theta\left(r_1 \frac{h}{2}\right) &= -\frac{1-V}{E\alpha}\frac{3}{h^2}P_0(a^2 - r^2) \leq 0, or\\ T\left(r_1 \frac{h}{2}\right) &= T_0 - \frac{1-V}{E\alpha}\frac{3}{h^2}P_0(a^2 - r^2)(r \leq a).\end{aligned} \tag{40}$$

Therefore, the temperature of the compressed area will be slightly higher than the temperature of the stretched area. In other words, the compressed zone releases heat $(T > T_0)$ and the stretched zone absorbs it $(T < T_0)$, i.e. there is a heat exchange of the plate with the external environment. K. Zener [23] developed a similar theory; it was experimentally confirmed for a thin plate with bending deformations.

Substituting the temperature variable in Equation (36), which appears when the round plate is bent under the action of a uniformly distributed load of constant intensity, into Equation (5), the power of the heat flow in the sections of the plate is found.

$$W = -\lambda\Delta\theta = -\lambda\frac{(1-V)}{E\alpha}\frac{18z}{h^3}P_0\,. \tag{41}$$

For the case of a compressed section of the plate, where $z = -\frac{h}{2}$.

The heat released:

$$W = \lambda\frac{(1-V)}{E\alpha}\frac{9}{h^2}P_0 > 0\,. \tag{42}$$

For the stretched area due to the bending $z = \frac{h}{2}$.

The heat absorbed:

$$W = -\lambda\frac{(1-V)}{E\alpha}\frac{9}{h^2}P_0 < 0\,. \tag{43}$$

As a result, due to the thermal conductivity, a heat flow occurs, due to bending, from the compressed to the stretched area.

4 Conclusion

In the analytical calculations of the stress strain state of metal structures of vehicles for the transportation of the bulk cargo, the theory of elasticity approach should be applied. The problem solution for the case of bending of the axisymmetrically loaded round plates is presented. Analytical dependences for calculation of stresses and movements in metal plates at arbitrary forms of loading and types of supports are substantiated. The obtained solutions prove that the action of external forces leads to the temperature change and heat flow occurrence due to the deformation of the bent tank metal structure.

Deformation and change in the temperature fields in the plate due to the external axisymmetric loading were considered first. The results indicate that the temperature of the compressed zone of the bent plate will be slightly above the temperature of the stretched zone, that is, the compressed area generates heat ($T > t_0$), while the stretched area absorbs it ($T < t_0$) and there is the heat exchange with the external environment.

References

[1] GAYDAR, S. M. *Protection of agricultural machinery from corrosion and wear using nanotechnology*. Dissertations for Doctor of technical sciences. Moscow, 2011.

[2] POPOVYCH, P., SHEVCHUK, O., DZYURA, V., POBEREZHNA, L., DOZORSKYY, V., HRYTSANCHUK, A. Assessment of the influence of corrosive aggressive cargo transportation on vehicle reliability. *International Journal of Engineering Research in Africa* [online]. 2018, **38**, p. 17-25. ISSN 1663-3571, eISSN 1663-4144. Available from: https://doi.org/10.4028/www.scientific.net/JERA.38.17

[3] POPOVYCH, P. V., LYASHUK, O. L., SHEVCHUK, O. S., TSON, O. P., POBEREZHNA, L. Y., BORTNYK, I. M. Influence of organic operation environment on corrosion properties of metal structure materials of vehicles. *INMATEH Agricultural Engineering* [online]. 2017, **52**(2), p. 113-118. ISSN 2068-4215, eISSN 2068-2239. Available from: https://inmateh.eu/volumes/old-volume/volume-52-no-2-2017/article/influence-of-organic-operation-environment-on-corrosion-properties-of-metal-structure-materials-of-vehicles.

[4] POPOVYCH, P. V., LYASHUK, O. L., MUROVANYI, I. S., DZYURA V. O., SHEVCHUK O. S., MYNDYUK, V. D. The service life evaluation of fertilizer spreaders undercarriages. *INMATEH Agricultural Engineering* [online]. 2016, **50**(3), p. 39 -46. ISSN 2068-4215, eISSN 2068-2239. Available from: https://inmateh.eu/volumes/old-volume/volume-50-no-3-2016/article/the-service-life-evaluation-of-fertilizer-spreaders-undercarriages

[5] LYTVYNENKO, I. V., MARUSCHAK, P. O., LUPENKO, S. A., POPOVYCH, P. V. Modeling of the ordered surface topography of statically deformed aluminum alloy. *Materials Science* [online]. 2016, **52**, p. 113-122. ISSN 1068-820X, eISSN 1573-885X. Available from: https://doi.org/10.1007/s11003-016-9933-1

[6] POPOVICH, P. V., BARNA, R. A. Influence of operating media on the fatigue fracture of steels for elements of agricultural machines. *Materials Science* [online]. 2014, **50**(3), p. 377-380. ISSN 1068-820X, eISSN 1573-885X. Available from: https://doi.org/10.1007/s11003-014-9729-0

[7] MARUSCHAK, P., PANIN, S., DANYLIUK, I., POBEREZHNYI, L., PYRIG, T., BISHCHAK, R., VLASOV, I. Structural and mechanical defects of materials of offshore and onshore main gas pipelines after long-term operation. *Open Engineering* [online]. 2015, **5**(1), p. 365-372. eISSN 2391-5439. Available from: https://doi.org/10.1515/eng-2015-0045

[8] POBEREZHNYI, L. Y., MARUSHCHAK, P. O., SOROCHAK, A. P., DRAGANOVSKA, D., HRYTSANCHUK, A. V., MISHCHUK, B. V. Corrosive and mechanical degradation of pipelines in acid soils. *Strength of Materials* [online]. 2017, **49**(4), p. 539-549. ISSN 0039-2316, eISSN 1573-9325. Available from: https://doi.org/10.1007/s11223-017-9897-x

[9] MARUSCHAK, P., POBEREZNY, L., PRENTKOVSKIS, O., BISHCHAK, R., SOROCHAK, A., BARAN, D. Physical and mechanical aspects of corrosion damage of distribution gas pipelines after long-term operation. *Journal of Failure Analysis and Prevention* [online]. 2018, **18**(3), p. 562-567. ISSN 1547-7029. Available from: https://doi.org/10.1007/S11668-018-0439-Z

[10] SHCHURIN, K. V. *Prediction and increase of fatigue life of bearing systems of agricultural tractor machinery*. Dissertations for Doctor of technical sciences. Orenburg: OPI. 1994.

[11] POBEREZHNY, L., MARUSCHAK, P., HRYTSANCHUK, A., POBEREZHNA, L., PRENTKOVSKIS, O, STANETSKY, A. Impact of gas hydrates and long-term operation on fatigue characteristics of pipeline steels. *Procedia Engineering* [online]. 2017, **187**, p. 356-362. ISSN 1877-7058. Available from: https://doi.org/10.1016/J.Proeng.2017.04.386

[12] HEVKO, B. M., POPOVICH, P. V., DIACHUN, A. Y., LYASHUK, O. L., LIUBACHIVSKYI, R. O. The Study of bulk material kinematics in a screw conveyor-mixer. In: International Symposium of ISB-INMA TEH. Agricultural and Mechanical Engineering: proceedings. 2015.

[13] YAVORSKYI, A. V., KARPASH, M. O., ZHOVTULIA, L. Y., POBEREZHNY, L. Y., MARUSCHAK, P. O., PRENTKOVSKIS, O. Risk management of a safe operation of engineering structures in the oil and gas sector. In: 20th International Scientific Conference Transport Means: proceedings. 2016. p. 370-373.

[14] PATIL, M. R. B., KULKARNI, V. V. (2018). Finite element analysis of support designs for road tankers. *International Research Journal of Engineering and Technology.* 2018, **5**(2), p. 836-843. ISSN 2395-0056, eISSN 2395-0072.

[15] ROMERO, J. A., OTREMBA, F., LOZANO-GUZMAN, A. A. Simulation of liquid-cargo-vehicle interaction under lateral and longitudinal accelerations. In: 9th International Conference on Computational Methods: Proceedings. 2018. p. 6-10.

[16] HAN, M., DAI, J., WANG, C. M., ANG, K. K. Hydrodynamic analysis of partially filled liquid tanks subject to 3d vehicular manoeuvring. *Shock and Vibration* [online]. 2019, 6943879. ISSN 1070-9622, eISSN 1875-9203. Available from: https://doi.org/10.1155/2019/6943879

[17] POPOVYCH, P. V., MAHLATYUK, L. ., KUPOVYCH, R. B. Influence of organic fertilizers on the corrosion-electrochemical characteristics of low-carbon steels. *Materials Science* [online]. 2014, **50**(2), p. 284-289. ISSN 1068-820X, eISSN 1573-885X. Available from: https://doi.org/10.1007/s11003-014-9719-2

[18] NOVOZHILOV, V. V. *Foundations of the nonlinear theory of elasticity*. Courier Corporation, 1999. ISBN 0-486-40684-9.

[19] SEDOV, L. I. *Mechanics of continuous media.* 4. ed. World Scientific, 1997. ISBN 978-9971-5-0728-2.

[20] LANDAU, L. D., LIVSHYTS, Y. M. *Theory of elasticity*. 7. ed. Nauka, 1987. ISBN 978-0750626330.

[21] PARKUS, H. *Thermoelasticity*. Springer Science & Business Media, 2012. ISBN 978-3-7091-8447-9.

[22] TIMOSHENKO, S. P., GOODIER, J. N. *Theory of elasticity*. 3. ed. New York: Mcgraw Hill, 1970. ISBN 9780070647206.

[23] FENG, J. *Machines, energy, entropy* (in Russian). Moscow: Mir, 1986. ISBN 978-0966081381.

USE OF THE BEZIER CURVES FOR A VEHICLES DRIVING CYCLES' MODELING

Valerii Dembitskyi

Department of Automobiles and Transport Technologies, Lutsk National Technical University, Lutsk, Ukraine

*E-mail of corresponding author: dvm2@meta.ua

Resume

While performing the research of the vehicles operating characteristics in real operating conditions, a question of creation or correction of a movement driving cycle always appears. An absence of a mathematical model rather complicates the research process and makes a quick correction of movement conditions impossible. To solve the given problem, it was proposed to model a driving cycle using the Bezier curves. As a result of this research, it is stated that the most advantageous is to use the Bezier curves of the second and third degrees. During the analysis of results of driving cycles modeling and their comparison to the standardized and real movement cycles, a satisfactory coincidence of results was obtained. The conducted thematic research confirms the previous results, directed to creation of a universal dynamic model of a vehicle's driving cycle.

Article info

Received 30 June 2020
Accepted 4 August 2020
Online 27 November 2020

Keywords:

driving cycle,
movement,
vehicle,
modeling,
Bezier curve,
coordinate

Available online: https://doi.org/10.26552/com.C.2021.1.B65-B75

ISSN 1335-4205 (print version)
ISSN 2585-7878 (online version)

1 Introduction

In spite of an intensive development of vehicles with an electric drive, during their exploitation many questions, concerning an electric energy consumption by such vehicles in concrete operating conditions, appear. The mentioned question is particularly acute during the exploitation of commercial transport, namely the buses that run the city routes. Very often, there is a problem of considerable deviation of an electric energy consumption by the same vehicle in different operating conditions. Besides, the electric energy consumption, declared by the manufacturers, noticed in official documents, is usually rather lower than the real one. In addition, these differences do not allow unique evaluating of the electric drive vehicles exploitation efficiency. Appearance of such arguments and non-conformities is associated with the difference between the driving cycle applied during the test and the real operating conditions. In such a way, a question arises of creation of such a driving cycle that could be easily adapted to the necessary operating conditions. Its application should allow getting the real figures of electric energy consumption and evaluating efficiency of one or another vehicle. This problem is rather actual and the researches that are proposed to be made within the framework of a programme Horizon 2020, give evidence to this [1].

Analysis of the previously conducted researches, connected with the research and modeling of a driving cycle and concerning the energy consumption by vehicles according to driving cycles, testify to a great interest of scientists for solving the given problem. In the research work [2], the authors have investigated multi-factors model of movement and have made the corresponding experimental research with the aim to minimize the electric energy consumption, taking into account the concrete vehicles operating conditions. A driving cycle for a passenger car in Mashhad city, Iran, compared to the standard driving cycles in Europe and America, showed a significant distinction about the speed of movement [3].

A great number of the driving cycles, offered in literature, are corrected to the concrete operating conditions and do not allow to adapt them to the other conditions or to change the cycle parameters [4-10]. Besides a problem of creating a driving cycle for the concrete operating conditions and the movement modes, also appears a problem of changeability of a driving cycle in the same locality depending on the time of day [11].

The authors in a research work [12] have investigated different driving cycles that are used to find a consumption of fuel, electric energy and the levels of the vehicles exhaust gases emissions. All the investigated driving cycles have significant differences in time, movement speed and movement modes. Along with that, the authors draw attention to necessity of matching a driving cycle for concrete cities, regions.

A similar situation also occurs with the driving cycles for buses, besides it becomes complicated due to absence of a unique standardized cycle with help of which it would

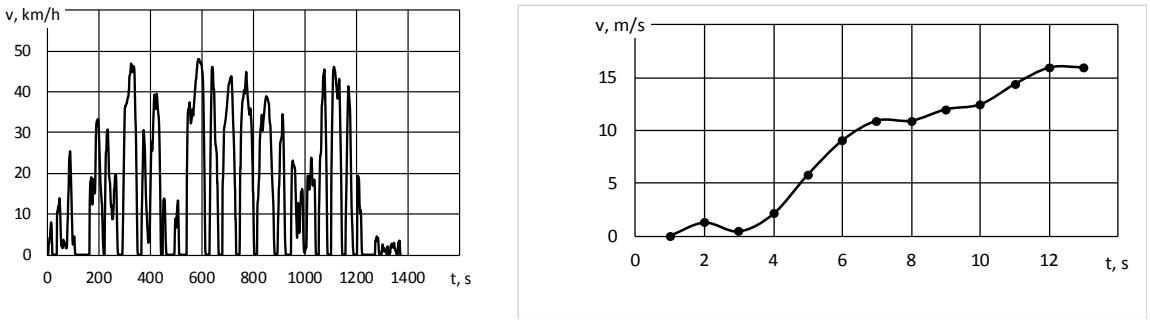

a) *b)*

Figure 1 *Driving cycle of urban bus movement, obtained by experiment in Lutsk city (a); speed-up section (b)*

Table 1 *Equations of Bezier curves and level of validity of their approximation for a real vehicle movement cycle on the example of Lutsk city*

Bezier curve	equation	validity level
linear, $n = 1$	$V = 1.3333t - 1.3333$	1
quadratic, $n = 2$	$V = -0.0285t^2 + 1.821t - 1.7689$	1
cubic, $n = 3$	$V = -0.0031t^3 + 0.0212t^2 + 1.6207t - 1.9949$	0.9987
quartic, $n = 3$	$V = -0.0033t^4 - 0.1174t^3 + 1.3298t^2 - 3.5439t + 2.3598$	0.9966

be possible to compare the research results. That is why many researches in separate cities and regions in order to determine a representative driving cycle were conducted [13-15]. A driving cycle is determined as a numeric series of speeds and a scheme of movement is reproduced by a number of parameters and operation characteristics [16].

2 Research methods

A problem of the driving cycles' creation is being solved for a long time. There are four main methods of the driving cycles' creation, namely: microtrip-based, segment-based, pattern classification and modal cycle construction. Each of them has its own advantages and disadvantages and discerns by different complexity [17-19].

It is a common knowledge that a driving cycle in a graphic interpretation is a set of segments that include an acceleration of a vehicle, a movement with constant speed and braking (deceleration). The researches of real driving cycles, previously published [17, 20-24], are based on determination of extreme indices of the elementary sections of a cycle and of their deviation from standardized driving cycles.

A great problem today is still a possibility to build a driving cycle according to given data, the main of which can be the acceleration of speed-up and braking, the durability of every elementary section, the number of sections of speed-up, braking, acceleration. Results of analysis of the standardized and experimental driving cycles, described in literature sources, [20-24] demonstrate that any driving cycle can be shown as a set of curves that describe some of its section. It was proposed to take the Bezier curves as a base for building the driving cycles. The analysis of literature sources testifies about an effective usage of Bezier curves during the modeling of a vehicle mechanical trajectory [25-26], in the automatized vehicles control systems [27-28], modeling and prediction of the route of vehicle movement and avoidance of collision for pilotless vehicles [29].

3 Research results

During the creation of a driving cycle it is advantageous and the most optimal to use:

1) for modeling of constant movement sections - linear Bezier curves, at $n = 1$,

$$B(t) = (1-t)P_0 + tP_1,\ t \in [0;1], \tag{1}$$

where
P_0 - position of the zero point,
P_1 - position of the finishing point,
t - the time parameter.

2) for modeling of sections of speed-up and braking;
- quadratic Bezier curves, at $n = 2$,

$$B(t) = (1-t)^2 P_0 + 2t(1-t)P_1 + t^2 P_2,\ t \in [0;1], \tag{2}$$

where
P_0 - position of the zero point,
P_1 - position of the intermediate point,
P_2 - position of the finishing point.
- cubic Bezier curves, at $n = 3$,

$$B(t) = (1-t)^3 P_0 + 3t(1-t)^2 P_1 + \\ + 3t^2(1-t)P_2 + t^3 P_3,\ t \in [0;1], \tag{3}$$

where
P_0 - position of the zero point,
P_1,P_2 - position of the intermediate points,

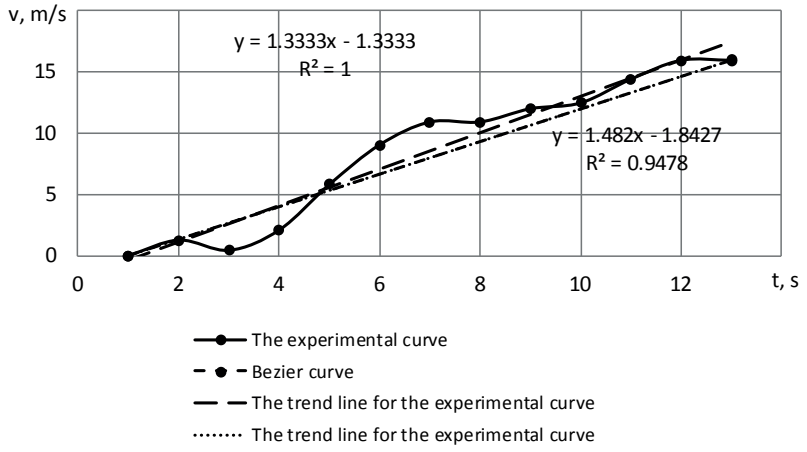

a) The linear Bezier curve

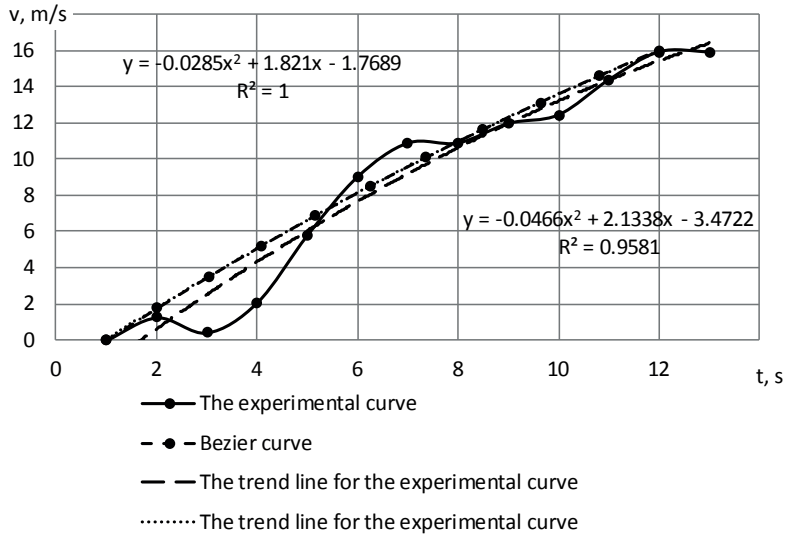

b) The quadratic Bezier curve

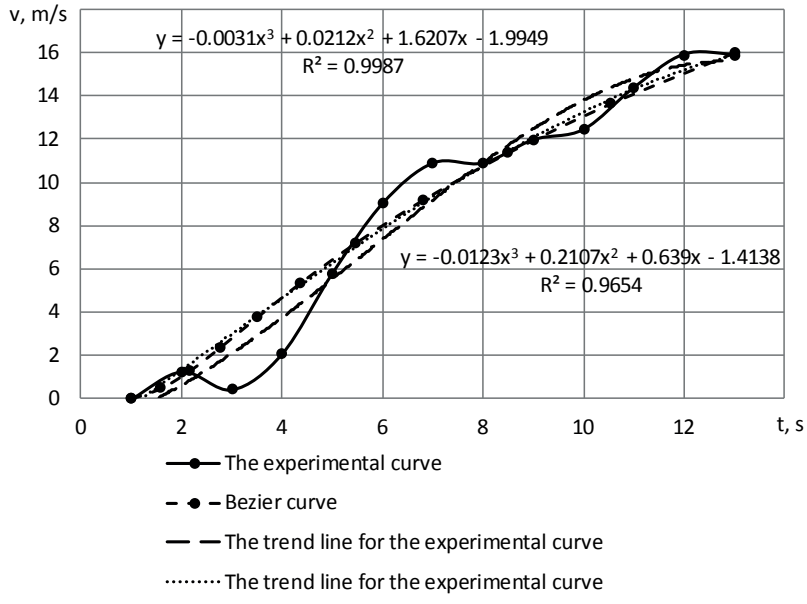

c) The cubic Bezier curve

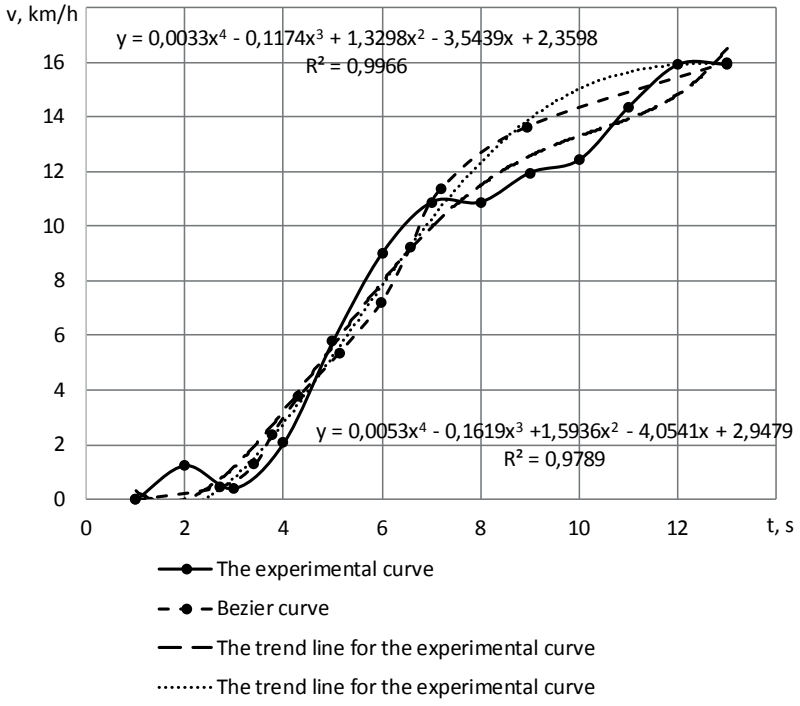

d) The quartic Bezier curve

Figure 2 *Results of the driving cycle speed-up section modeling*

Table 2 *Equations of a real driving cycle and a level of validity of their approximation*

Bezier curve	equation	validity level
linear approximation	$V = 1.482t - 1.8427$	0.9478
polynomial curve of second degree	$V = -0.0466t^2 + 2.1338t - 3.4722$	0.9581
polynomial curve of third degree	$V = -0.0123t^3 + 0.2107t^2 + 0.639t - 1.4138$	0.9654
polynomial curve of fourth degree	$V = -0.0053t^4 - 0.1619t^3 + 1.5936t^2 - 4.0541t + 2.9479$	0.9789

P_3 - position of the finishing point.
- quartic Bezier curves, at $n = 3$,

$$B(t) = (1-t)^3 P_0 + 3t(1-t)^2 P_1 + 3t^2(1-t)\cdot \cdot P_2 + 4t^3(1-t)P_3 + t^4 P_4,\ t \in [0;1], \quad (4)$$

where
P_0 - position of the zero point,
P_1, P_2, P_3- position of the intermediate points,
P_4 - position of the finishing point.

A speed-up section, extracted from a driving cycle of urban bus movement, obtained by experiment in Lutsk city is shown in Figure 1.

While building the driving cycles, a speed is measured in m/s, because a change of speed by time is an acceleration. It was made with an aim to get the unique results. A vehicle speed on the graphs that demonstrate the driving cycles, is given in km/h, according to the common rules, including standards.

Using the Bezier curves of the first, second, third and fourth degrees, made a modeling of the speed-up section for an experimental driving cycle, shown at Figure 1. In Table 1 are given the appropriate equations and a level of validity of their approximation. The corresponding graphs are shown at Figures 2 (*a*) to (*d*).

In Table 2 there are shown the curves of approximation and the levels of validity for a real vehicle movement cycle graph on the example of Lutsk city.

To compare the obtained dependences, the appropriate calculations were conducted and their results are shown in Table 3. In the course of calculations, values of speeds were determined according to dependences shown in Tables 1 and 2. After that, the obtained data were compared to real speeds recorded directly during the movement.

The minimum deviation of speed, according to Table 3, is seen in the course of using the Bezier curves of the second and third degrees.

As far as an average acceleration is concerned, another indicator of the driving cycle, analogical calculations were conducted, as well, for values of average acceleration. Results are shown in Table 4.

In Tables 3 and 4 there are some inaccuracies that are caused by external influence of the environment and by the vehicle's operating conditions, for example: speed

Table 3 *Deviations of modeling results from their real driving cycle for speed*

real speed (m/s)	approximation							
	linear		curve of second degree		curve of third degree		curve of fourth degree	
	approximation by real dependence	Bezier curve	approximation by real dependence	Bezier curve	approximation by real dependence	Bezier curve	approximation by real dependence	Bezier curve
0.00	-1.84	1.33	3.47	1.77	1.41	1.99	-2.95	-4.47
1.25	-2.08	1.25	2.63	1.23	1.83	1.61	0.92	1.14
0.42	-4.39	-0.92	-0.19	-1.34	-0.19	-0.89	0.41	1.04
2.08	-4.21	-0.58	-0.43	-1.36	0.01	-0.89	0.90	1.18
5.80	-1.97	1.80	1.48	0.74	2.08	1.17	2.58	2.27
9.03	-0.22	3.69	3.00	2.40	3.52	2.78	3.44	2.64
10.88	0.15	4.22	3.23	2.75	3.53	3.06	2.99	2.03
10.88	-1.33	2.88	1.70	1.30	1.72	1.56	1.03	0.34
11.96	-1.74	2.63	1.34	0.98	1.07	1.22	0.64	0.62
12.43	-2.75	1.77	0.48	0.12	0.00	0.38	0.14	1.05
14.36	-2.30	2.36	1.16	0.77	0.62	1.13	1.50	3.29
15.91	-2.24	2.57	1.55	1.09	1.17	1.63	2.62	4.88
15.91	-3.72	1.24	0.48	-0.07	0.57	0.76	1.99	3.74

and direction of wind, road cutting in a plan, its roughness and vehicle suspension, driver's behaviour. Those factors sometimes have a great influence [30]. The least deviation of the vehicle's acceleration, according to Table 4, is noticed during application of the Bezier curves of the second and third degrees.

In such a way it was determined that it would be optimal to use the Bezier curves of the second and third degrees, with the aim to model and build the movement driving cycle. Along with that, using of the Bezier curves of the first degree is advantageous on the sections of a cycle with constant speeds.

During the building of the Bezier curves of the second and third degrees that describe the movement driving cycle, the biggest problem was determination of the intermediate points' P_1, P_2, positions. At first, it is necessary to investigate a simpler version, namely searching of point P_1 positions for the quadratic curve. Since a point P_1 on intervals $[P_0; P_1]$ characterizes the linear Bezier curves, its position would be the position of intersection of the corresponding lines. As the initial and final points of a vehicle movement process are known, so the equation of a line could be written out using a formula:

$$\frac{t-t_1}{t_2-t_1}=\frac{v-v_1}{v_2-v_1}, \tag{5}$$

where

t_1, t_2 - time of the beginning and the end of movement correspondingly, s,

v_1, v_2 - initial and final vehicle speed, m/s.

From that dependence, equations for lines of the speed-up v_a and braking v_b were obtained:

$$v_a=\frac{v_2(t-t_1)-v_1(t-t_2)}{(t_1-t_2)}, \tag{6}$$

$$v_b=\frac{v_4(t-t_3)-v_3(t-t_4)}{(t_3-t_4)}. \tag{7}$$

After the dependences 6 and 7 were compared, positions of lines' intersection point, which correspond to the positions of point P_1, were obtained as:

$$\frac{t(v_1-v_2)+v_2t_1-v_1t_2}{(t_1-t_2)}= =\frac{t(v_3-v_4)+v_4t_3-v_3t_4}{(t_3-t_4)}, \tag{8}$$

$$t_{P_1}=\frac{\begin{array}{c}v_2t_1t_3-v_1t_2t_3-v_2t_1t_4+v_1t_2t_4-\\-v_4t_1t_3+v_3t_1t_4+v_4t_2t_3-v_3t_2t_4\end{array}}{\begin{array}{c}v_2t_3-v_1t_3-v_2t_4+v_1t_4-\\-v_4t_1+v_3t_1+v_4t_2-v_3t_2\end{array}}. \tag{9}$$

Position v_{P_1} of a point P_1 is calculated by expression:

$$v_{P_1}=\frac{t_{P_1}(v_1-v_2)+v_2t_1-v_1t_2}{(t_1-t_2)}, \tag{10}$$

or

$$v_{P_1}=\frac{\left(\frac{v_2t_1t_3-v_1t_2t_3-v_2t_1t_4+v_1t_2t_4-v_4t_1t_3+v_3t_1t_4+v_4t_2t_3-v_3t_2t_4}{v_2t_3-v_1t_3-v_2t_4+v_1t_4-v_4t_1+v_3t_1+v_4t_2-v_3t_2}\right)(v_1-v_2)+v_2t_1-v_1t_2}{(t_1-t_2)}, \tag{11}$$

Table 4 *Deviations of modeling results from their real driving cycle for acceleration*

real acceleration (m/s^2)	Approximation							
	linear		curve of second degree		curve of third degree		curve of fourth degree	
	approximation by real dependence	Bezier curve	approximation by real dependence	Bezier curve	approximation by real dependence	Bezier curve	approximation by real dependence	Bezier curve
1.25	-0.23	-0.08	-0.84	-0.54	0.41	1.61	3.87	5.61
-0.83	-2.32	-2.17	-2.83	-2.57	-2.02	-2.14	-0.51	-0.11
1.67	0.18	0.33	-0.23	-0.01	0.21	-1.31	0.48	0.15
3.72	2.24	2.39	1.91	2.10	2.06	-0.91	1.68	1.09
3.23	1.74	1.89	1.51	1.66	1.44	-3.03	0.86	0.37
1.86	0.37	0.52	0.23	0.35	0.02	-5.97	-0.44	-0.61
0.00	-1.48	-1.33	-1.53	-1.45	-1.82	-9.33	-1.96	-1.69
1.08	-0.40	-0.26	-0.36	-0.32	-0.64	-9.66	-0.40	0.28
0.47	-1.01	-0.86	-0.87	-0.86	-1.08	-11.58	-0.50	0.43
1.93	0.45	0.60	0.68	0.65	0.62	-11.30	1.35	2.25
1.54	0.06	0.21	0.39	0.32	0.55	-12.73	1.12	1.58
0.00	-1.48	-1.33	-1.06	-1.17	-0.60	-15.15	-0.63	-1.14
	average acceleration values, m/s^2							
1.32	-0.16	-0.01	-0.25	-0.16	-0.07	-0.11	0.41	0.91
	average acceleration values, %							
100	-12.12	-0.76	-18.94	-12.12	-5.30	-8.33	31.06	68.94

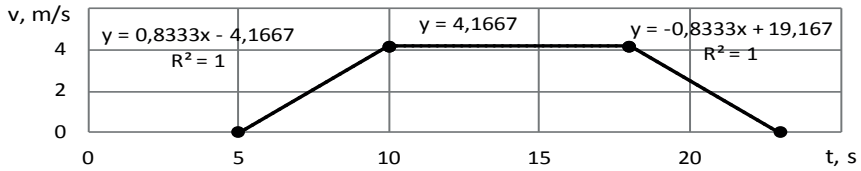

Figure 3 *Elementary driving cycle*

$$v_{P1} = \frac{2v_1^2t_2t_4 - 2v_1^2t_2t_3 - v_1v_4t_1t_3 + v_1v_3t_1t_4 + v_1v_4t_2t_3 - v_1v_3t_2t_4 - 2v_1v_2t_2t_4 + v_2v_4t_1t_3 - v_2v_3t_1t_4}{(t_1 - t_2)} -$$
$$- \frac{v_{P1}v_2v_4t_2t_3 + v_2v_3t_2t_4 - v_2v_4t_1^2 + v_2v_3t_1^2 + v_2v_4t_1t_2 - v_2v_3t_1t_2 - v_1v_4t_1t_2 + v_1v_3t_1t_2 + v_1v_4t_2^2 - v_1v_3t_2^2}{(t_1 - t_2)}. \quad (13)$$

Equations (9) and (12) give a possibility to find the positions of an intermediate point P_1 to build a Bezier curve.

If one builds a driving cycle with help of lines, so in a line equation $v = at + b$, the angular coefficient a stands for a value of average deceleration on a given segment of a driving cycle. This regularity should be taken into consideration during the building of driving cycles with the help of Bezier curves. Thus, a graph of a section «speed-up - braking», for a standardized driving cycle, shown in [31] (Figure 3) is obtained.

Taking into consideration that in the real driving cycles the sections of movement with a constant speed are actually absent, modeling of a part of the driving cycle, shown in Figure 3, was performed with help of the Bezier curves of the second degree. Results are shown in Figure 4.

Deviations of speed of the modeled driving cycle from the standardized one are shown in Table 5.

The maximum deviation is observed in points of passage from the speed-up to a constant speed and from the constant speed to braking. Along with that, taking into account that in real conditions of movement, the passages from one mode to another are made smoothly without abrupt changes, the given non-conformity can be neglected.

4 Discussion of results

The Bezier curves that are used for the driving cycles modeling (Figure 4) does not completely represent the necessary characteristics of a driving cycle. That is why it is advisable to build a driving cycle by parts, marking out the sections of the speed-up, deceleration and constant speed, using the quadratic Bezier curve during that the whole process. According to the given

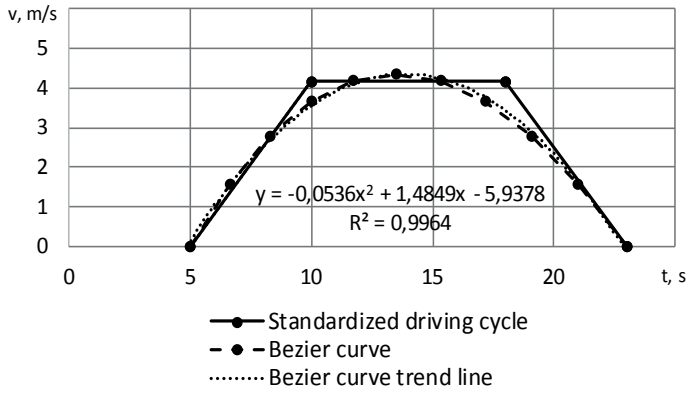

Figure 4 *Elementary driving cycle*

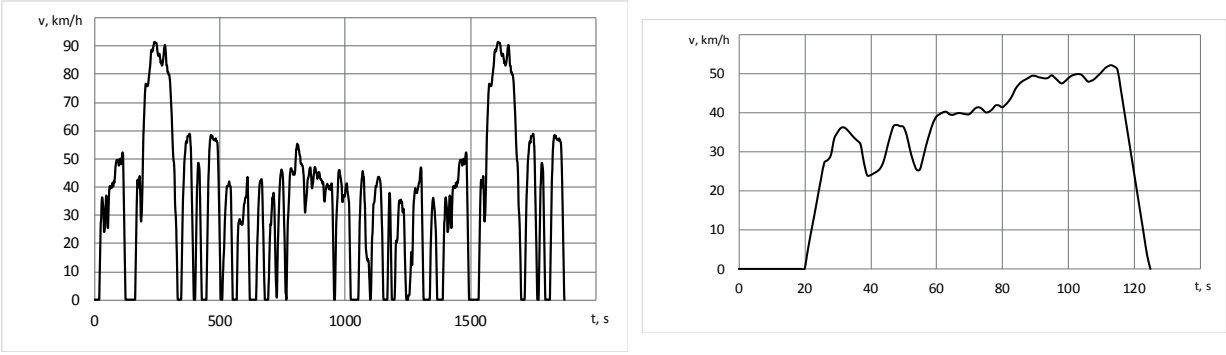

a) *b)*

Figure 5 *Standardized driving cycle (a) and its section that was modeled using the Bezier curves (b)*

Table 5 *Deviations of the modeled driving cycle from the standardized one*

time, s	speed of driving cycle (m/s)		deviations of a modeled driving cycle	
	standardized	modeled	m/s	km/h
5	0.000035	0.1092	-0.10925	-0.3933
6	0.83328	0.988	-0.15472	-0.55699
7	1.66661	1.7566	-0.08999	-0.32396
8	2.49994	2.415	0.08494	0.305784
9	3.33327	2.9632	0.37007	1.332252
10	4.1666	3.4012	0.7654	2.75544
11	4.1666	3.729	0.4376	1.57536
12	4.1666	3.9466	0.22	0.792
13	4.1666	4.054	0.1126	0.40536
14	4.1666	4.0512	0.1154	0.41544
15	4.1666	3.9382	0.2284	0.82224
16	4.1666	3.715	0.4516	1.62576
17	4.1666	3.3816	0.785	2.826
18	4.1676	2.938	1.2296	4.42656
19	3.3343	2.3842	0.9501	3.42036
20	2.501	1.7202	0.7808	2.81088
21	1.6677	0.946	0.7217	2.59812
22	0.8344	0.0616	0.7728	2.78208
23	0.0011	-0.933	0.9341	3.36276

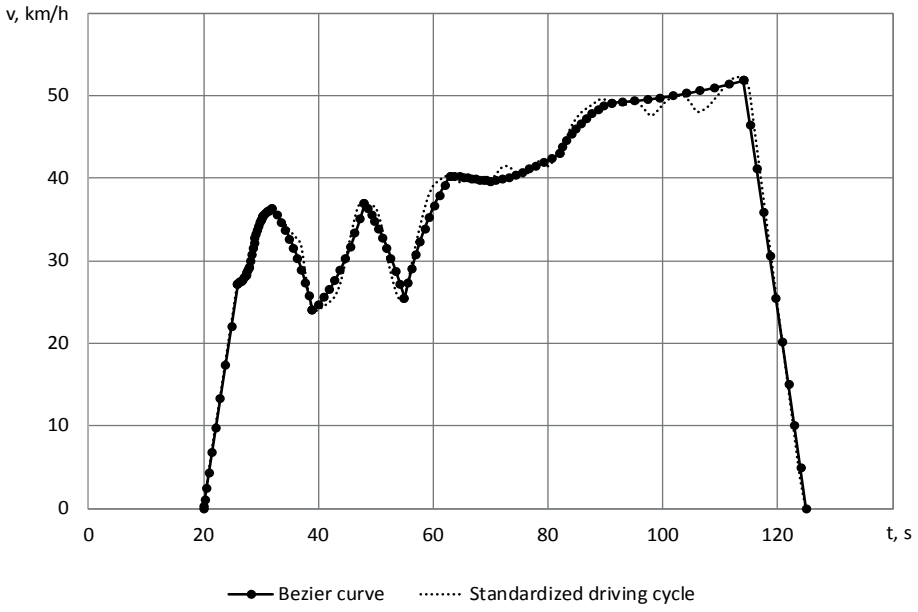

Figure 6 *Modeling of the standardized driving cycle by Bezier curves*

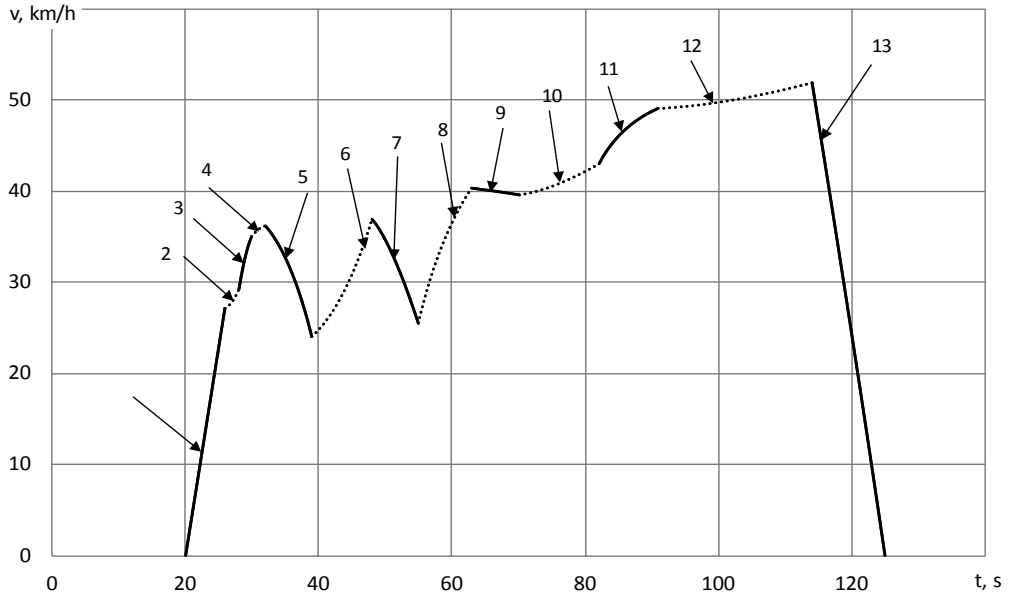

Figure 7 *Elementary parts of the modeled driving cycle*

method, a section of the driving cycle FTP was built, (Figures 5, 6).

While building a section of a driving cycle, for the initial point is taken a point of the vehicle movement beginning, while the final point, which at the same time is the initial point of the next section, has positions that correspond to the extreme value of speed (minimum and maximum).

During the modeling of a driving cycle, an FTP part was divided into 13 segments; each of them is in a model presented by the quadratic Bezier curve, shown in Figure 7. If in the quadratic Bezier curve the points P_1 and P_2 have the same positions, the Bezier curve of the second degree turns into a line. Some non-conformities of the modeled driving cycle with a standardized one can be eliminated by dividing these sections into smaller parts.

In Table 6 is given an extension for each part and the maximum speed deviation on a given part.

As a result of the research, the maximum deviation of speed between the standardized driving cycle and its model was found to be about 10 % (elementary parts 5 and 12). Along with that, taking into consideration that a sign of speed's difference between the given driving cycles can be either positive or negative, an average deviation by a part of a cycle is about 3 %. To decrease the speed deviation o from the standardized driving cycle, a part 12 was additionally divided in three elementary parts (Figure 8). As a result of this, the maximum deviation for the elementary part 12 was

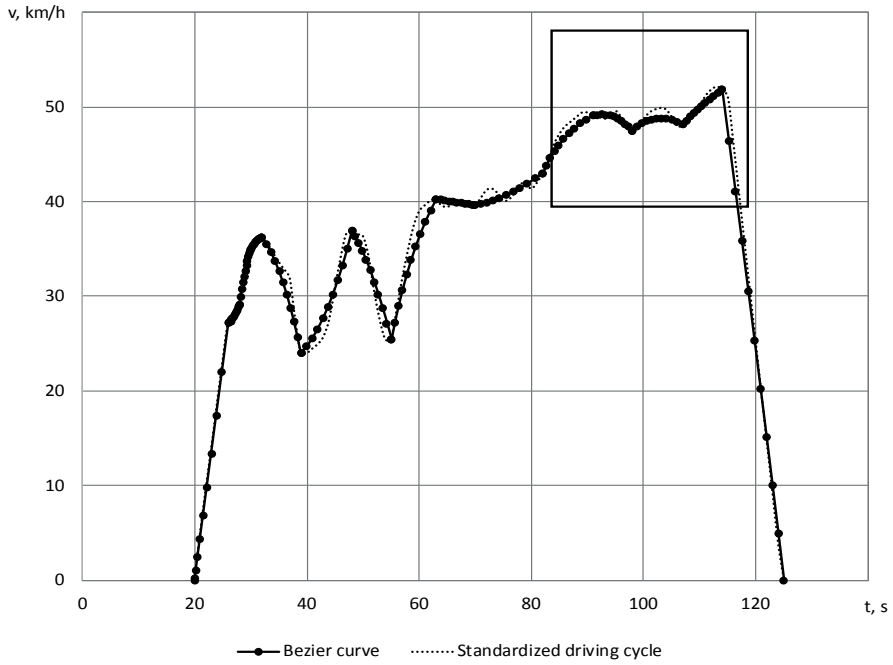

Figure 8 *Division of a part of the 12th driving cycle on the segments to get higher precision*

Table 6 *Extension for each part and the maximum speed deviation on an elementary part of the 12th driving cycle*

number of an elementary part of a cycle	extension of an elementary part of a cycle (s)	maximum deviation by speed (%)
1	6	0
2	2	0.011
3	2	1.926
4	2	0.670
5	7	9.629
6	11	7.297
7	7	4.475
8	8	6.012
9	7	1.464
10	12	3.196
11	9	2.603
12	23	9.101
13	11	0

2.2 %. In such a way, it was found that for increasing the length of an elementary part, the corresponding increasing of deviation is observed. A value of deviation would primarily depend on the length of an elementary part and a character of a curve on this part. As it was shown before, the polynomial curves of the second and third degrees gave the most accurate results.

An accuracy level, with the help of which a modeling was being made, should correspond to the accuracy level of the experimental research, i.e. the deviations of a modeled driving cycle should correspond to deviations that appear during the experimental research of vehicles using the given driving cycle.

5 Conclusions

The research objective was searching and investigation of possibilities for the vehicles driving cycles' modeling. To achieve this objective it was proposed to use the Bezier curves. The performed theoretic research has shown a possibility to realize the tasks of driving cycles' modeling using the mentioned curves. In addition to this, the optimal is to use the Bezier curves of the second degree and together with them - the linear Bezier curves.

A character of a proposed method of the driving cycle's modeling is a possibility to choose the desirable accuracy of the model, while using different lengths. As a result of

this research, the maximum and minimum differences of speed between the real driving cycle and a proposed model were determined, that amount to 10% and 3%, respectively. It was also set that decreasing of elementary parts increases accuracy of the model. Dividing one part into three smaller parts decreased the difference between cycles from 10% to 2.2 % of elementary driving cycle sections.

It is certain that this process of modeling is rather difficult and the higher is the accuracy, the more difficult would be to model, however, the created model would be rather dynamic and can be easily changed in a case of change of some external factors. The performed thematic research confirms the previous results, aimed at a creation of a universal dynamic model of vehicles' driving cycle.

References

[1] Reducing the environmental impact of hybrid light duty vehicles - European Commission [online] [accessed 2020-02-15]. Available from: https://ec.europa.eu/info/funding-tenders

[2] BRAUN, A., RID, W. The influence of driving patterns on energy consumption in electric car driving and the role of regenerative braking. *Transportation Research Procedia* [online]. 2017, **22**, p. 174-182. ISSN 2352-1465. Available from: https://doi.org/10.1016/j.trpro.2017.03.024

[3] POURESMAEILI, M., F., AGHAYAN, I., TAGHIZADEH, S., A. Development of Mashhad driving cycle for passenger car to model vehicle exhaust emissions calibrated using on-board measurements. *Sustainable Cities and Society*, [online]. 2018, **36**, p. 12-20. ISSN 2210-6707. Available from: https://doi.org/10.1016/j.scs.2017.09.034

[4] STEVES-BOOTH, A., MUNEER, T., KIRBY, H., KUBIE, J., HUNTER, J. The measurement of vehicular driving cycle within the city of Edinburgh. *Transportation Research Part D. Transport and Environment* [online]. 2001, **6**(3), p. 209-220. ISSN 1361-9209. Available from: https://doi.org/10.1016/S1361-9209(00)00024-9

[5] LIN, J., NIEMEIER, D., A. Regional driving characteristics, regional driving cycles. *Transportation Research Part D: Transport and Environment* [online]. 2003, **8**(5), p. 361-381. ISSN 1361-9209. Available from: https://doi.org/10.1016/S1361-9209(03)00022-1

[6] HUNG W. T., TONG H. Y., LEE, C. P., HA, K., PAO, L. Y. Development of a practical driving cycle construction methodology: a case study in Hong Kong. *Transportation Research Part D: Transport and Environment* [online]. 2007, **12**(2), p. 115-128. ISSN 1361-9209. Available from: https://doi.org/10.1016/j.trd.2007.01.002

[7] GUO, F., ZHANG, F. A study of driving cycle for electric cars on Beijing urban and suburban roads. In: IEEE International Conference on Power and Renewable Energy ICPRE: proceedings [online]. IEEE, 2016. p. 319-322. Available from: https://doi.org/10.1109/ICPRE.2016.7871224

[8] ANIDA, I. N., NORBAKYAH, J. S., ZULFADLI, M., NORAINIZA, M. H., SALISA, A. R. Driving cycle development of BAS KITe in Kuala Terengganu city to optimize the energy consumption and emissions. In: 1st International Postgraduate Conference on Mechanical Engineering IPCME 2018: proceedings [online]. IOP Conference Series: Materials Science and Engineering. 2019. Vol. 469. ISSN 1757-8981, eISSN 1757-899X. Available from: https://doi.org/10.1088/1757-899X/469/1/012112

[9] ARUN, N., H., MAHESH, S., RAMADURAI, G., NAGENDRA, S. Development of driving cycles for passenger cars and motorcycles in Chennai. *Sustainable Cities and Society*, [online]. 2017, **32**, p. 508-512. ISSN 2210-6707. Available from: https://doi.org/10.1016/j.scs.2017.05.001

[10] CHEN, Z., ZHANG, Q., LU, J., BI, J. Optimization-based method to develop practical driving cycle for application in electric vehicle power management: a case study in Shenyang, China. *Energy* [online]. **186**, 115766, ISSN 0360-5442. Available from: https://doi.org/10.1016/j.energy.2019.07.096

[11] YANG, Y., LI, T., ZHANG, T., YU, Q. Time dimension analysis: comparison of Nanjing local driving cycles in 2009 and 2017. *Sustainable Cities and Society*, [online]. 2020, **53**, 101949. ISSN 2210-6707. Available from: https://doi.org/10.1016/j.scs.2019.101949

[12] ACHOUR, H., OLABI, A. G. Driving cycle developments and their impacts on energy consumption of transportation. *Journal of Cleaner Production* [online]. 2015, **112**(2), p. 1778-1788. ISSN 0959-6526. Available from: https://doi.org/10.1016/j.jclepro.2015.08.007

[13] TONG, H., Y. Development of a driving cycle for a supercapacitor electric bus route in Hong Kong. *Sustainable Cities and Society* [online]. 2019, **48**, 101588. ISSN 2210-6707. Available from: https://doi.org/10.1016/j.scs.2019.101588

[14] YUHUI, P., YUAN, Z., HUIBAO, Y. Development of a representative driving cycle for urban buses based on the K-means cluster method. *Cluster Computing* [online]. 2019, **22**, p. 6871-6880. ISSN 1386-7857, eISSN 1573-7543. Available from: https://doi.org/10.1007/s10586-017-1673-y

[15] LAI, J., YU, L., SONG, G., GUO, P., CHEN, X. Development of city-specific driving cycles for transit buses based on VSP distributions: case of Beijing. *Journal of Transportation Engineering* [online]. 2013, **139**. p. 749-757. ISSN 2473-2907, eISSN 2473-2893. Available from: https://doi.org/10.1061/(ASCE)TE.1943-5436.0000547

[16] HUERTAS, J., GIRALDO, M., QUIRAMA, L., DIAZ-RAMIREZ, J. Driving cycles based on fuel consumption. *Energies* [online]. 2018, **11**(11), 3064. ISSN 1996-1073. Available from: https://doi.org/10.3390/en11113064

[17] GALGAMUWA, U., PERERA, L. BANDARA, S. A Representative driving cycle for the southern expressway compared to existing driving cycles. *Transportation in Developing Economies* [online]. 2016, **2**, 22. ISSN 2199-9287, eISSN 2199-9295. Available from: https://doi.org/10.1007/s40890-016-0027-4

[18] GALGAMUWA, U, PERERA, L, BANDARA, S. Developing a general methodology for driving cycle construction: comparison of various established driving cycles in the world to propose a general approach. *Journal of Transportation Technologies* [online]. 2015, **5**(4), p. 191-203. ISSN 2160-0473, eISSN 2160-0481. Available from: https://doi.org/10.4236/jtts.2015.54018

[19] KALT, S.; BRENNER, L.; LIENKAMP, M. Requirements for electric machine design based on operating points from real driving data in cities. *World Electric Vehicle Journal* [online]. 2019, **10**(4), 60. eISSN 2032-6653. Available from: https://doi.org/10.3390/wevj10040060

[20] CHINDAMO, D., GADOLA, M. What is the most representative standard driving cycle to estimate diesel emissions of a light commercial vehicle? *IFAC-PapersOnLine* [online]. 2018, **51**(5), p. 73-78. ISSN 2405-8963. Available from: https://doi.org/10.1016/j.ifacol.2018.06.213

[21] DREIER, D., SILVEIRA, S., KHATIWADA, D., FONSECA, K. V. O., NIEWEGLOWSKI, R., SCHEPANSKI, R. The influence of passenger load, driving cycle, fuel price and different types of buses on the cost of transport service in the BRT system in Curitiba. *Transportation* [online]. 2019, **46**, p. 2195-2242. ISSN 0049-4488, eISSN 1572-9435. Available from: https://doi.org/10.1007/s11116-018-9925-0

[22] FOTOUHI, A., MONTAZERI-GH, M. Tehran driving cycle development using the k-means clustering method. *Scientia Iranica* [online]. 2013, **20**(2), p. 286-293. ISSN 1026-3098. Available from: https://doi.org/10.1016/j.scient.2013.04.001

[23] GONG, H. M., GE, Y. S., WANG, J. F., YIN, H. Light-duty vehicle emissions control: a brief introduction to the China 6 emissions standard. *Johnson Matthey Technology Review* [online]. 2017, **61**(4), p. 269-278. ISSN 2056-5135. Available from: https://doi.org/10.1595/205651317X696199

[24] WU, T., HAN, X., ZHENG M., OU, X., SUN, H., ZHANG, X. Impact factors of the real-world fuel consumption rate of light duty vehicles in China. *Energy* [online]. 2020, **190**, 116388. ISSN 0360-5442. Available from: https://doi.org/10.1016/j.energy.2019.116388

[25] LATTARULO, R., GONZALEZ, L., MARTI, E., MATUTE-PEASPAN, J., MARCANO, M., PEREZ, J. Urban motion planning framework based on N-Bezier curves considering comfort and safety. *Journal of Advanced Transportation* [online]. 2018, 6060924, p. 1-13. ISSN 0197-6729, eISSN 2042-3195. Available from: https://doi.org/10.1155/2018/6060924

[26] THARWAT, A., ELHOSENY, M., HASSANIEN, A. E., et al. Intelligent Bezier curve-based path planning model using chaotic particle swarm optimization algorithm. *Cluster Computing* [online]. 2019, **22**, p. 4745-4766. ISSN 1386-7857, eISSN 1573-7543. Available from: https://doi.org/10.1007/s10586-018-2360-3

[27] LATTARULO, R., MARTI, E., MARCANO, M., MATUTE-PEASPAN, J., PEREZ, J. A speed planner approach based on Bezier curves using vehicle dynamic constrains and passengers comfort. In: 2018 IEEE International Symposium on Circuits and Systems ISCAS: proceedings [online]. IEEE, 2018. eISSN 2379-447X, p. 1-5. Available from: https://doi.org/10.1109/ISCAS.2018.8351307

[28] LATIP, A., BADARIYAH, N., ROSLI, O. Feasible path generation using Bezier curves for car-like vehicle. In: International Research and Innovation Summit IRIS2017: proceedings [online]. IOP Conference Series: Materials Science and Engineering. 2017. Vol. 226. ISSN 1757-8981, eISSN 1757-899X, 012133. Available from: https://doi.org/10.1088/1757-899X/226/1/012133

[29] ABDELAAL, M, SCHON, S. Predictive path following and collision avoidance of autonomous connected vehicles. *Algorithms* [online]. 2020; **13**(3), 52. eISSN 1999-4893. Available from: https://doi.org/10.3390/a13030052

[30] DEMBITSKYI, V., SITOVSKYI, O., PAVLIUK, V. Influence of a system "vehicle - driver - road - environment" on the energy efficiency of the vehicles with electric drive. In: 1st International Scientific Conference ICCPT 2019: Current Problems of Transport: proceedings. SciView. 2019. p. 162-173.

[31] EN 1987-1 Electrically propelled road vehicles - specific requirements for safety - part 1: On board energy storage.

University of Žilina

In its over 65 years of successful existence, the University of Žilina (UNIZA) has become one of the top universities in Slovakia.

Scientific conferences
organized by University of Žilina in the first half of the 2021

International Particle Physics Masterclases
Date and venue: 25. 2. 2021, University of Žilina, SK
Contact: melo@fyzika.uniza.sk
Web: http://www.physicsmasterclasses.org

Young Wings 2021
Date and venue: 25. 3. 2021, University of Žilina, Airport Žilina, SK
Contact: blaskova@fpedas.uniza.sk
Web: http://www.kld.uniza.sk

Sustainable Energy Forum
Date and venue: May 2021, Liptovský Mikuláš, SK
Contact: pavel.simon@uniza.sk
Web: https://www.energiaweb.sk/smart-energy-forum-slovakia

Crisis Situations Solution in Specific Environment
Date and venue: 19. 5. - 20. 5. 2021, University of Žilina, SK
Contact: crisis@uniza.sk; valeria.moricova@fbi.uniza.sk
Web: http://www.fbi.uniza.sk

International Scientific Conference on Sustainable, Modern and Safe Transport TRANSCOM 2021
Date and venue: 26. 5. - 28. 5. 2021, High Tatras, Horný Smokovec - Grand Hotel Bellevue, SK
Contact: transcom@uniza.sk
Web: http://www.transcom-conference.com

UNIVERSITY OF ŽILINA
Science & Research Department
Univerzitná 8215/1, 010 26 Žilina, Slovakia
Ing. Janka Macurová
tel.: +421 41 513 5143
e-mail: janka.macurova@uniza.sk

DESIGN AND CONSTRUCTION OF HIGH-QUALITY CAPACITOR FOR HIGH FREQUENCY AND POWER APPLICATION

Martin Zavřel[1], Vladimír Kindl[1,*], Tomáš Kavalír[2], Pavel Drábek[1]

[1]Regional Innovation Centre for Electrical Engineering, Faculty of Electrical Engineering, University of West Bohemia, Pilsen, Czech Republic
[2]Regional Technological Institute, Faculty of Mechanical Engineering, University of West Bohemia, Pilsen, Czech Republic

*E-mail of corresponding author: vkindl@kev.zcu.cz

Resume
The paper proposes a design and construction of a special plated capacitor exhibiting very good high-frequency characteristics. The capacitor is designed to minimize the parasitic parameters like ESR (equivalent series resistance) and ESL (equivalent series inductance) and to be suitable for power industry applications. The paper describes the fabrication process and discusses technical issues related to technology of manufacturing and assembling. It also provides an experimental verification and the quality evaluation based on frequency characteristics compared to existing commercial high-quality capacitor.

Article info
Received 26 May 2020
Accepted 8 June 2020
Online 27 October 2020

Keywords:
capacitor,
high quality,
high power,
high frequency,
parasitics,
construction design,
testing

Available online: https://doi.org/10.26552/com.C.2021.1.C1-C6

ISSN 1335-4205 (print version)
ISSN 2585-7878 (online version)

1 Introduction

Increasing the power density of electrical passive components, such as a capacitor [1-3], inductor or resistor, incorporated into modern power systems, is a common technical goal for many power applications. Higher power density brings better material utilization, lower weight and lower equipment cost. Many power applications are using the high frequency and sometimes the resonance, e.g. wireless power transfer [4-5], high-pass, low-pass and EMI (electromagnetic interference) filters [6-7], induction heating [8-9] etc.

In these applications, the compensation capacitors play a very important role, since they must carry very high electrical current and are being stressed with relatively high voltage. In that case, the quality factor (Q factor) of the capacitor is one of the most important characteristics in a power circuit design [10]. Besides the capacitance (the main parameter), the practical capacitor consists of equivalent series resistance (ESR), equivalent series inductance (ESL) and insulation resistance (R_g) [11-13]. The electrodes and the terminals of a capacitor contribute the resistive component and the inductive component, while the dielectric material contributes the insulation resistance.

The ESR component causes energy loss in a form of heat and the ESL parameter creates a magnetic field interfering with how the current rises to the peak and falls back. The Q factor then represents efficiency of a given capacitor in terms of its rate of energy loss. When neglecting influence of the insulation resistance (is too high), one may write:

$$Q = 2\pi \frac{\frac{1I_m^2}{2\omega^2 C}}{\frac{I_m^2 ESR}{2f}} = \frac{1}{\omega RC}. \quad (1)$$

In Equation (1), ω represents the angular frequency of the power supply, I_m is the magnitude of the current through the capacitor C and R represents its ESR. As obvious from Equation (1), the energy loss starts to dominate at higher frequencies, therefore the high Q *factor* capacitors must be used to prevent any performance issues. This could be achieved by special design having the ultra-low ESR and so ESL. This high-quality capacitor will find its purpose in any industrial-, electronics- or medicine application [14-17] that are using frequencies even higher than tens of MHz.

This paper proposes a design of high-quality, high-frequency and high-power capacitor and describes step-by-step manufacturing and assembling process. The capacitor properties are compared to the equivalent high-quality capacitor available on the market [18].

2 Design of the capacitor

As mentioned in previous section, to demonstrate the quality of this design, the properties of the capacitor are compared to the existing one developed by Vishay

Table 1 *Typical properties for AD1000*

property	value	units	test method
dielectric constant	8.5	---	@10 GHz (IPC TM-650 2.5.5.5)
dissipation factor	0.0023	---	@10 GHz (IPC TM-650 2.5.5.5)
temperature coefficient	-380 (-40÷150 °C)	ppm/°C	@10 GHz (IPC TM-650 2.5.5.5)
volume resistivity	1.4×10^9	MΩcm	C96/35/90
surface resistivity	1.8×10^9	MΩ	C96/35/90
electrical strength	24.5	kV/mm	IPC TM-650 2.5.5.5
dielectric breakdown	> 45	kV	IPC TM-650 2.5.5.5
decomposition temperature	> 500	°C	for PCB
temperature withstand	60 min	220 °C	IPC TM-650 2.4.24.1
thermal conductivity	0.81	W/m K	ASTM E1461

Company. Capacitor PE 140 is chosen as a benchmark. This capacitor is widely used for resonance coupling, bypassing and feeding circuits in the high power radio transmitters, high-frequency tube welding equipment, high-frequency quenching and electric stoves, high-frequency driers, etc.

The main parameters are as follows: maximum voltage U_{peak} = 16 kV, ESR = 20 mΩ, ESL = 15 nH and C = 3 nF.

The targeted parameters of the newly designed capacitor are as follows: $U_{peak} \geq 10$ kV, ESR < 20 mΩ, ESL < 15 nH and C = 10 nF.

2.1 Electrical parameters and dimensions

To design similar parameters that can be compared, one can use Equation (2) to determine the required main dimensions in the case if a plated topology is assumed. Here, d is dielectric thickness, S is active electrode surface area and $\varepsilon_0, \varepsilon_r$ represent the relative permittivity (dielectric constant) of a free space and the dielectric materiel between plates, respectively.

$$C = \varepsilon_0 \varepsilon_r \frac{s}{d}. \tag{2}$$

The material selected for a capacitor dielectric is high dielectric constant substrate (AD1000) that permits circuit miniaturization compared to traditional low loss materials. It is a woven ceramic fiberglass reinforced laminate for microwave printed circuit boards (PCB's). As the material shows the perfect electrical and thermal parameters (seen in Table 1), it could be used for a wide range of applications.

The overall capacitance is determined from Equation (3) assuming nearly ideal parallel interconnection of N capacitor layers [19]:

$$C_{cap} = \varepsilon_0 \varepsilon_r \frac{s}{d} N. \tag{3}$$

Parallel connection also has beneficial impact to the current density - Equation (4) and parasitic values minimization.

$$JS_k k \geq \sqrt{\frac{\Delta T S_k}{R_{th} \rho_{Cu} \frac{a}{4}}}. \tag{4}$$

In Equation (4), J stands for the chosen current density (10 A/mm^2), S_k represents the usable current carrying cross-section, ΔT defines allowed warming, R_{th} represents the thermal conductivity for one layer, ρ_{Cu} is specific resistivity of copper, a is the electrode dimension (a = 130 mm) and k represents the safety coefficient (k = 0.5).

The current density in Equation (4) needs to be defined regarding to the current carrying capacity (maximum current, cooling ability, etc.). The final number of layers (N = 5) is then defined from both the requested physical dimensions (130 × 130 mm) and the overall capacitance C_{cap} ~10 nF.

As a consequence, a large electrode thickness (200 μm of copper foil), usable electrode surface and five-layers connected in parallel make the current density to fulfil condition in Equation (4) up to 50 A_{peak}.

2.2 Mechanical and construction design

The basic mechanical design comes out from chosen geometrical topology, i.e. number of layers, electrode dimensions, plate layer thickness, etc. As the minimization of ESR and ESL is of a great importance, the design must guarantee uniform distribution of the current density in the capacitor layers. Therefore, the physical interconnections between each layers must have the same impedance, which is moreover as small as possible. The same must be ensured within each standalone layer.

Since the AD1000 material shows relatively weak mechanical tolerance (soft and fragile), the structure of the capacitor must be supported by robust copper chassis. However, this gives the opportunity to lead the thermal loss out of the capacitor efficiently.

The basic technical drawing (Figure 1) shows the layout of the capacitor (upper) and the capacitor as a model (bottom).

The most important components, combining both the mechanical and the electrical function, are the electrical interconnections formed between individual layers. These pliable but relatively solid connections are fabricated of profiled copper sheets (0.5 mm thick). The terminals on

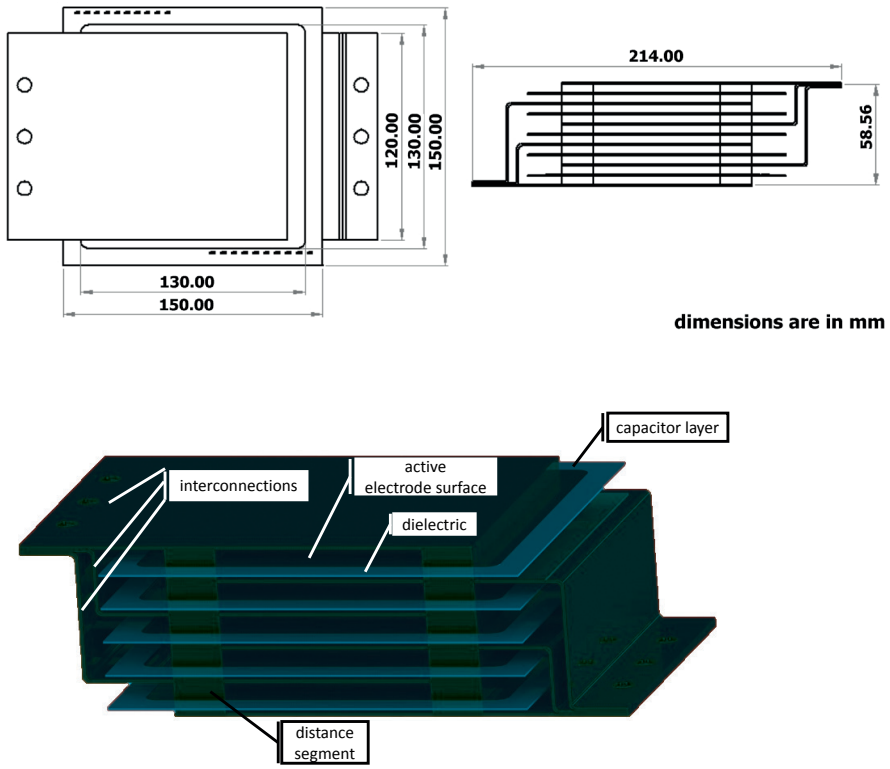

Figure 1 *Basic technical layout (top), model (bottom)*

Figure 2 *Capacitor prototype: in a soldering frame (left), finished (right)*

both sides are made asymmetrically to compensate the different length of individual interconnection legs. The structure is further supported by a distance segments (5×18×120 mm), which are also made of copper and which significantly improve the overall mechanical stiffness. Their other advantage lies in the future possibility of improving ventilation by installing forced air cooling ducts. As seen in Figure 1, the active area of the capacitor plates are purposely reduced to form a "dielectric enlarging" that will increase the voltage breakdown and simultaneously minimize the partial discharge activity.

3 Manufacturing process

3.1 Soldering and surface finishing

The interconnections between all the construction parts are made using soft soldering. During the soldering process the paste S6M-XM3S has shown perfect temperature behavior while reaching satisfactory low reflow temperature (182 °C) and good electrical properties of resulting interconnections. The solder paste was applied onto each contact surface in a very thin layer. The capacitor structure was stacked into the supporting frame (Figure 2 - left) to avoid layers to move during the soldering process (reflow).

The key issue is to find a proper heating source for the soldering process that will protect the surface from any damage. Direct resistance heating is not feasible due to the geometry issues. Indirect resistive heating (heating hotplate) is inappropriate because of really low thermal conductivity of dielectric material. Induction heating is possible, but it requires special equipment, which makes the technology very expensive for the prototype.

The high temperature air-flow heating cannot be used since it will irreversibly damage the surface, which was observed when manufacturing the first prototype. The best

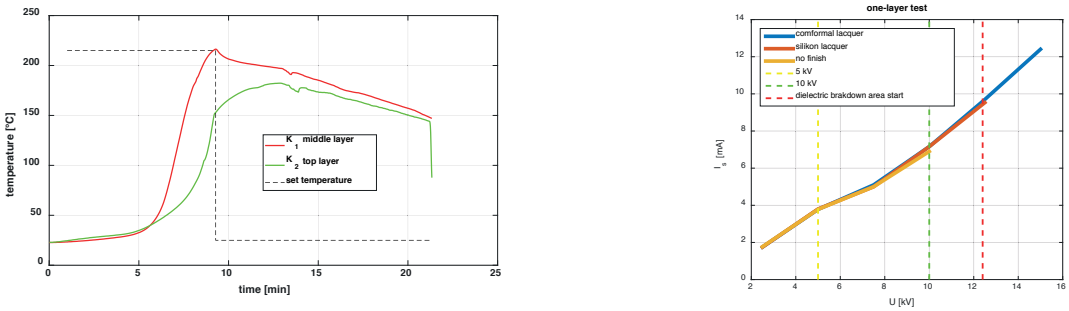

Figure 3 *Heating proces in Galden vapor; temperatures (color lines) measured with a high quality sensors (PT100) located in the center of the distance elements, required temperature (black dashed lines). Breakdown tests of one layer of the capacitor after the surface finishing (right)*

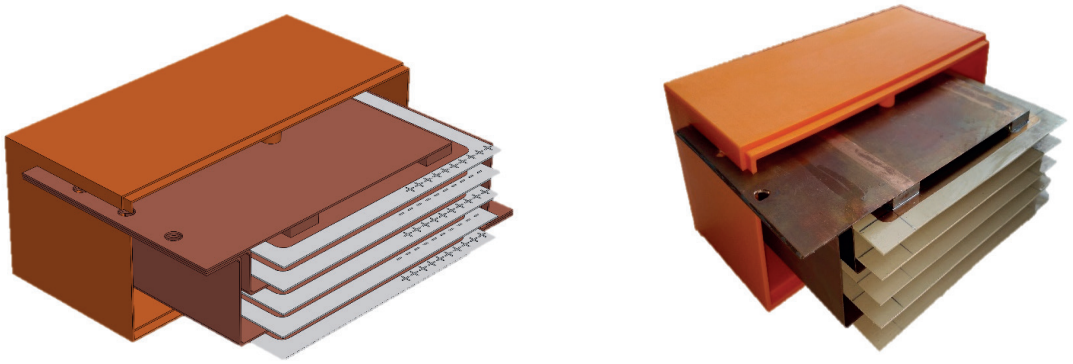

Figure 4 *Capacitor in one half of housing, 3D model (left) and photo (right)*

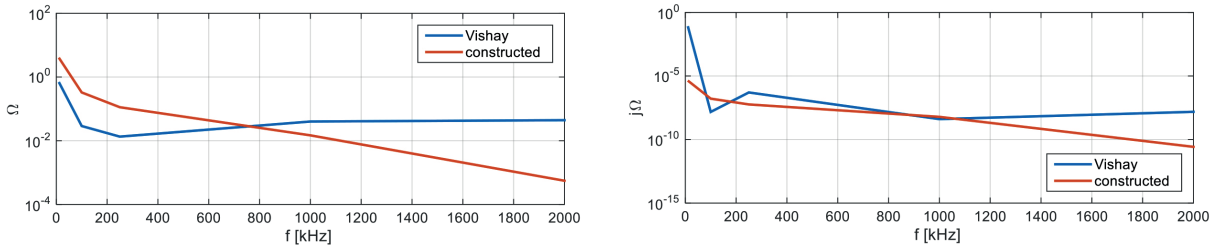

Figure 5 *Measured ESR (left) and ESL (right)*

Table 2 *Measured capacitor parameters*

parameter	symbol	frequency	value	units
maximum repeatable AC voltage	U_{peak}	100 kHz	12	kV
		1 MHz	12	kV
		2 MHz	12	kV
nominal capacitance	C_n	100 kHz	10.45	nF
		1 MHz	11	nF
		2 MHz	14	nF
equivalent series resistance	ESR	100 kHz	112	mΩ
		1 MHz	14	mΩ
		2 MHz	0.556	mΩ
equivalent series inductance	ESL	100 kHz	57.9	nH
		1 MHz	6.1	nH
		2 MHz	0.0266	nH
nominal current (RMS value)	I_n	100 kHz	50	A
		1 MHz	50	A
		2 MHz	50	A

results were finally reached using the Galden vapor heating seen in Figure 3 (left side).

The capacitor voltage breakdown is not directly given by a dielectric materials and thickness, but it is also influenced by the surface partial discharges. Application of the surface dielectric coating (silicon lacquer HCS Electrolube) will keep the partial discharge activity at the minimal level (Figure 3) and will protect the surface from moisture and pollution. The surface finishing was applied by soaking, dripping and curing after the soldering process.

3.2 Housing

The housing is the final step of the design and manufacturing process and is important due to protection against an electric shock. The housing is composed of the two components (4 mm thick wall) fabricated by a 3D printer using ABS material having sufficiently high electrical strength [20]. The capacitor placed in one half of housing is shown in Figure 4.

4 Experimental verification

The prototype has been tested in a wide frequency range (from 10 to 2000 kHz) using a precise laboratory RLC-meter (Keysight E4980A). The frequency characteristics of the constructed capacitor are compared to characteristics of existing commercial high-quality capacitor (Vishay PE 140).

Both the ESR and ESL in terms of frequency are shown in Figure 5. As obvious, the constructed capacitor shows better results starting the higher tested frequencies (> 750 kHz for ESR and > 200 kHz for ESL). This could be improved/adjusted by choosing another substrate for the capacitor plates. The material that was used is predicted mainly for very high frequencies. Compared to that, Vishay PE 140 (3 nF and more) is designed for frequencies up to 100 kHz only.

Measured parameters of the manufactures capacitor under different tested frequencies are given in Table 2. The data correspond to the graphs in Fig. 5.

5 Conclusions

Since the high-voltage high-frequency and high-quality capacitors are very expensive and usually not accessible on the market, a capacitor of the new design has been developed. The capacitor is constructed using the soft soldering and the geometry design allowing to increase the voltage breakdown and to minimize the partial discharge activity.

The capacitor housing works as the protection against the electric shock and forms a supporting mold for possible resin casting. As shown in Figure 5, the designed capacitor exhibits better performance compared to the Vishay capacitor starting at a frequency of 800 kHz and higher.

The parameters reached during the laboratory measurement are listed in Table 2.

The manufactured capacitor has also been successfully tested as a compensation capacitor for the 5 kW wireless power charger [21].

Acknowledgment

This research has been supported by the Ministry of Education, Youth and Sports of the Czech Republic under the RICE - New Technologies and Concepts for Smart Industrial Systems, project No. LO1607 and by funding program of the University of West Bohemia number SGS-2018-009.

References

[1] BANDALO, F. S., SINGH, B., SEVIGNY, R. Audible noise and high-voltage power capacitors. *IEEE Transactions on Power Delivery* [online]. 2018, **33**(5), p. 2437-2441. ISSN 0885-8977. Available from: https://doi.org/10.1109/TPWRD.2017.2774506

[2] SARJEANT, W. J., ZIRNHELD, J., MACDOUGALL, F. W. Capacitors. *IEEE Transactions on Plasma Science* [online]. 1998, **26**(5), p. 1368-1392. ISSN 0093-3813. Available from: https://doi.org/10.1109/27.736020

[3] BRAY, K. R., KOSAI, H., SCHWEICKART, D. L., RAY, B. High temperature capacitor performance. in a high power, high frequency converter. In: IEEE International Power Modulator and High Voltage Conference IPMHVC 2012: proceedings [online]. 2012. p. 276-279. Available from: https://doi.org/10.1109/IPMHVC.2012.6518733

[4] KINDL, V., FRIVALDSKY, M., SPANIK, P., PIRI, M., JAROS, V. Transfer properties of various compensation techniques for wireless power transfer system including parasitic effects. *COMPEL - The International Journal for Computation and Mathematics in Electrical and Electronic Engineering* [online]. 2017, **36**, p. 1198-1219. ISSN 0332-1649. Available from: https://doi.org/10.1108/COMPEL-04-2016-0143

[5] COVIC, G. A., BOYS, J. T. Modern trends in inductive power transfer for transportation applications. *IEEE Journal of Emerging and Selected Topics in Power Electronics* [online]. 2013, **1**(5), p. 28-41. ISSN 2168-6777, eISSN 2168-6785. Available from: https://doi.org/10.1109/JESTPE.2013.2264473

[6] WANG, R., BOROYEVICH, D., BLANCHETTE, H. F., MATTAVELLI, P. High power density EMI filter design with consideration of self-parasitic. In: 27th Annual IEEE Applied Power Electronics Conference and Exposition APEC 2012: proceedings [online]. 2012. ISSN 1048-2334, p. 2285-2289. Available from: https://doi.org/10.1109/APEC.2012.6166141

[7] WANG, X., RAVI, L., ALBERT, M. P., TALLAM, R. M. A novel configuration of DC link EMI filter capacitors in variable frequency drives. In: IEEE Applied Power Electronics Conference and Exposition APEC 2019: proceedings [online]. 2019. p. 2603-2607. Available from: https://doi.org/10.1109/APEC.2019.8721782

[8] PHADUNGTHIN, R., HAEMA, J. Application study on induction heating using half bridge LLC resonant inverter. In: 12th IEEE Conference on Industrial Electronics and Applications ICIEA 2017: proceedings [online]. 2017. eISSN 2158-2297, p. 1582-1585. Available from: https://doi.org/10.1109/ICIEA.2017.8283090

[9] CLARK, F. M., SCOVILLE, M. E. Capacitors for high-frequency induction-heating circuits. *Transactions of the American Institute of Electrical Engineers*. 1945, **64**(11), p. 791-796. ISSN 0096-3860, eISSN 2330-9431.

[10] BARTLEY, P. G., BEGLEY, S. B. Quality factor determination of resonant structures. In: IEEE Instrumentation and Measurement Technology Conference: proceedings [online] 2006. ISSN 1091-5281, p. 312-316. Available from: https://doi.org/10.1109/IMTC.2006.328435

[11] ZHANG, H., JIANG, Q. Accurate measurement of key parameters of film capacitors for EV power control unit. In: IEEE 4th International Future Energy Electronics Conference IFEEC 2019: proceedings [online]. 2019. p. 1-5. Available from: https://doi.org/10.1109/IFEEC47410.2019.9014981

[12] MOONMIRAT, P., HOMKLINTIAN, M., KUMTAWEE, C. Measurement of the frequency dependence of standard capacitors in the frequency range 10 kHz to 1 MHz. *In: Conference on Precision Electromagnetic Measurements CPEM 2016: proceedings* [online]. 2016. eISSN 2160-0171, p. 1-2. Available from: https://doi.org/10.1109/CPEM.2016.7540688

[13] WON, S. Y., JOO, J. H., KIM, H. S., HWANG, D. S., LEE, K. J. Performance analysis of single film electrode of the L-C resonance capacitors for using high-frequency induction heating processing equipment. In: *IEEE International Telecommunications Energy Conference INTELEC 2015: proceedings*. 2015. p. 1-5.

[14] IEEE standard, test code, and recommended practice for induction and dielectric heating equipment. In: *IEEE Std No 54-1955* [online]. IEEE, 1955. eISBN 978-1-5044-0389-4, p. 1-24, Available from: https://doi.org/10.1109/IEEESTD.1955.7430213

[15] AL BASTAMI, A., JURKOV, A., GOULD, P., HSING, M., SCHMIDT, M., HA, J. I., PERREAULT, D. J. Dynamic matching system for radio-frequency plasma generation. *IEEE Transactions on Power Electronics*. 2018, **33**(3), p. 1940-1951.

[16] HSIEH, M., KUO, L., WU, E., CHEN, J. Imaging adult zebrafish brain structures using micro-fabricated RF coil on 3T MRI system. In: Joint Meeting of the 6th International Symposium on Noninvasive Functional Source Imaging of the Brain and Heart and the International Conference on Functional Biomedical Imaging: proceedings. 2007. p. 98-100.

[17] IHNAT, P., RUDINSKA, L., ZONCA, P. Radiofrequency energy in surgery: state of the art. *Surgery today* [online]. 2013, **44**, p. 985-991. ISSN 0941-1291, eISSN 1436-2813. Available from: https://doi.org/10.1007/s00595-013-0630-5

[18] P. 70, P. 100, P. 140, P. 200 RF power plate capacitor with contoured rim - Vishay company [online]. Product datasheet. 2019. Available from: https://www.vishay.com/docs/22082/p70p100p140p200.pdf

[19] Capacitors and dielectric - Lumen Learning [online]. 2020. Available from: https://courses.lumenlearning.com/austincc-physics2/chapter/19-5-capacitors-and-dielectrics

[20] HOFF, B. W., MAESTAS, S. S., HAYDEN, S. C., HARRIGAN, D. J., GRUDT, R. O., OSTRAAT, M. L., HORWATH, J. C., LEONTSEV, S. Data on dielectric strength heterogeneity associated with printing orientation in additively manufactured polymer materials. *Data in Brief* [online]. 2018, **20**, p. 480-489. ISSN 2352-3409. Available from: https://doi.org/10.1016/j.dib.2018.07.070

[21] KINDL, V., ZAVREL, M., DRABEK, P., KAVALIR, T. High efficiency and power tracking method for wireless charging system based on phase-shift control. *Energies* [online]. 2018, **11**(8), p. 1-19. eISSN 1996-1073. Available from: https://doi.org/10.3390/en11082065

OPTIMIZED CONTROL OF ENERGY FLOW IN AN ELECTRIC VEHICLE BASED ON GPS

Matúš Danko*, Branislav Hanko, Peter Drgoňa

Mechatronics and Electronics, University of Zilina, Zilina, Slovakia

*E-mail of corresponding author: matus.danko@feit.uniza.sk

Resume

Presented paper deals with energy flow control of an electric vehicle with multiple energy storages. For efficiency control of energy flow is necessary to know the traction profile of the route. The Global Positioning System is used for observation of the traction profile. The first of the proposed algorithms uses the whole traction profile of a predetermined route, so the control algorithm can determine when the use of energy of the secondary energy storage is useful. The second proposed algorithm uses the GPS to determine the traction profile from routes stored in memory. If the route is not predetermined, or found in the memory of stored routes, the last algorithm controls the energy flow, based on the current of the primary energy storage. For verification of the proposed algorithm for control of the DC/DC converter, motor with inverter was replaced by the programmable power supply and programmable electronic load. The final evaluation shows that the proposed algorithm with the predetermined route saves about 5% more energy than the basic algorithm based on the battery current.

Available online: https://doi.org/10.26552/com.C.2021.1.C7-C14

Article info

Received 26 May 2020
Accepted 8 June 2020
Online 28 October 2020

Keywords:

electric vehicle,
energy flow,
multiple energy storages,
GPS

ISSN 1335-4205 (print version)
ISSN 2585-7878 (online version)

1 Introduction

Nowadays, electric vehicles and hybrid electric vehicles are more and more common. Although these vehicles are more environmentally friendly and more efficient than vehicles with internal combustion engines, they also have many technical problems, which prevent mass sales and production. One of the main disadvantages is the driving range. For extension of the driving range and increasing vehicle dynamics, multiple energy storages like batteries, supercapacitors, high-speed flywheels and fuel cells are used for powering the electric drive. One or multiple secondary energy storage assist to main energy storage, which leads to decrease of weight and volume of the main energy storage. Energy storages can be divided by their specific power and specific energy. The specific power represents how much power can be delivered per mass unit (W/kg). The specific energy defines how much energy can be stored per mass unit (Wh/kg). Batteries are the most common main energy storage because of their high specific energy and relatively high specific power. The supercapacitor is used most often as the secondary energy storage because it has high specific power. The simplest way of connection between the main and secondary energy storage is their parallel connection. The main disadvantage of this type of connection is that voltages of energy storages are the same, so the performance of the secondary energy storage is not fully utilized and control of energy flow is not possible [1-4].

The issue of inefficient energy utilization is the problem of current types of electric vehicles. Furthermore, the style of driving has a significant impact on the energy efficiency of the electric vehicle. In Table 1, the comparison between the presented and real driving range of electric vehicles is shown [3].

Configurations where active control of energy flow is possible, using the DC/DC converter at least for one of the energy storages. The DC/DC converter should be bidirectional to utilize regenerative braking for storing energy [5-6]. In this paper, serial active topology was chosen (Figure 1), because the energy flow is controlled trough one DC/DC converter of the secondary energy storage. Thus, the DC/DC converter is active only during the energy control i.e. during the acceleration and during regenerative braking [7-9].

2 Proposed algorithms

For the optimal energy flow control of the secondary energy storage, it is necessary to know the traction profile. If the traction profile of the whole track is known or part of the traction profile, the control algorithm can decide when to use the energy of secondary energy storage is useful. Proposed algorithms utilize GPS localization for detection of traction profile.

Table 1 *Claimed and a real range of electric vehicle [3]*

make	model	claimed range	real range	full charge €	cost per km €	km per kWh
Hyundai	Kona Electric 64 kWh	467.2	414.4	10.121	0.035	5.76
Jaguar	I-Pace	467.2	404.8	13.888	0.059	4.16
Kia	e-Niro 64 kw	481.6	404.8	10.226	0.047	5.6
Tesla	Model S 75D	486.4	326.4	11.805	0.059	3.84
Hyundai	Kona Electric 39 kWh	310.4	252.8	6.1659	0.035	5.76
Renault	Zoe R110	297.6	233.6	7.0551	0.047	4.64
Nissan	Leaf	268.8	204.8	6.318	0.047	4.48
BMW	i3 94 Ah	252.8	193.6	5.4639	0.047	4.96
Volkswagen	e-Golf	230.4	187.2	4.9959	0.047	5.28
Hyundai	Ioniq Electric	278.4	187.2	4.1769	0.035	6.24
Smart	Fortwo EQ	158.4	94.4	2.8431	0.047	4.64

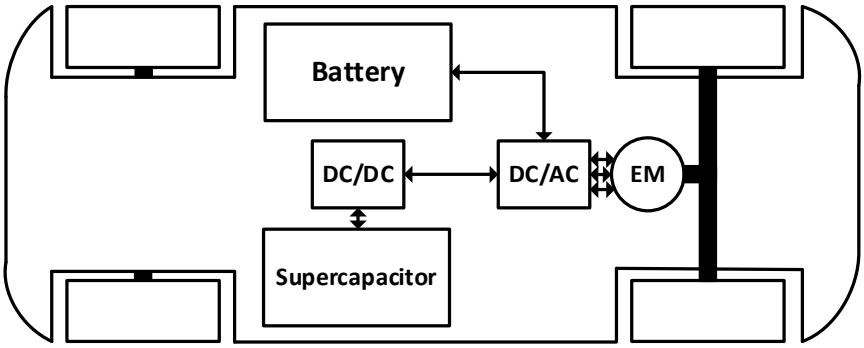

Figure 1 *Active serial topology*

2.1 Algorithm with use of the whole traction profile

In Figure 2 one can see that the first of the proposed algorithms, which uses the whole traction profile has one big disadvantage that the user must set the route on which the electric vehicle will move. On the other hand, a big advantage of this algorithm is that the whole traction profile is known so the algorithm decides on which uphill, the energy of the secondary energy storage will be used, based on the remaining energy of the secondary energy storage.

For example, if the route contains two uphills in a row and remaining energy in the secondary energy storage suffices only for one of uphills, the control algorithm uses energy for the bigger uphill. The same situation occurs at regenerative braking, algorithm decides during which downhill to store energy to the secondary energy storage based on how much energy the secondary energy storage can store.

2.2 Algorithm with use of a part of the traction profile

The second algorithm eliminates the disadvantage of the previous algorithm and the user does not have to set the route (Figure 3).

The route is set from memory where the routes, on which the vehicle was moving are stored, based on the GPS localization. At the start of the route, ten coordinates are acquired, which are searched in the routes in memory. Coordinates of singe points are not searched, because of the GPS accuracy, two routes can be searched, each in the opposite direction. The disadvantage is that the whole traction profile of the route is not known and the vehicle can change direction any time, so the energy of the secondary energy storage is used on every uphill. If a vehicle changes direction, coordinates of the new route are searched in the memory. If the new route is not in the memory, the route is saving it in memory until the vehicle stops, which means the end of the route or crossroad, which means the vehicle can continue on the known route.

2.3 Algorithm based on battery current

This basic algorithm is used when the route is not searched in the memory or the user does not set the route, so the energy control system cannot decide when to use the energy of the secondary energy storage. Energy usage of the secondary energy storage is based on the maximum specified current of batteries. During the fast acceleration or during the uphill driving, the current exceeds specified current of batteries. If the energy storage has enough energy, the

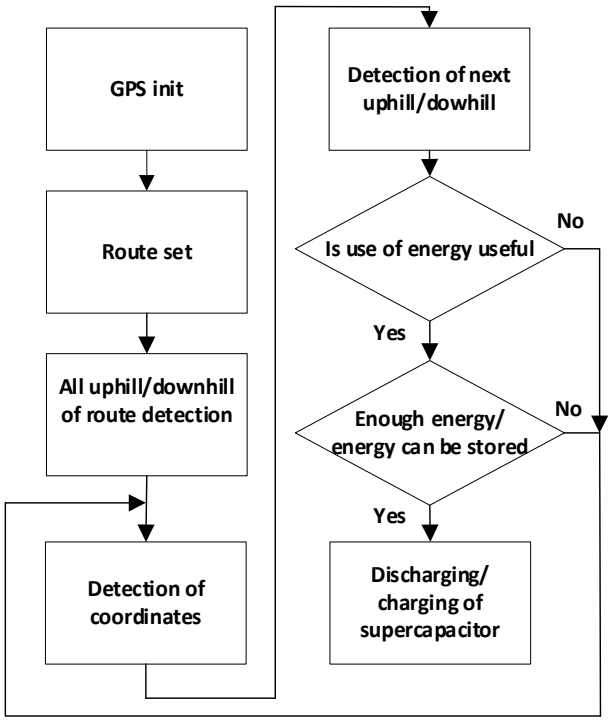

Figure 2 *Algorithm with use of the whole traction profile*

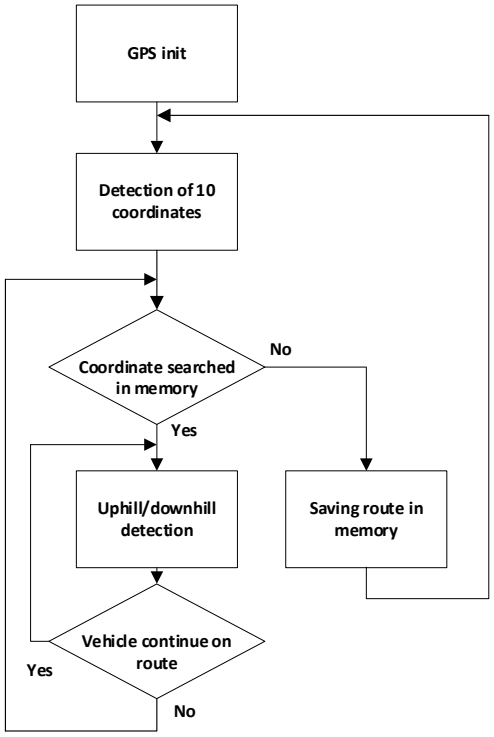

Figure 3 *Algorithm with use of a part of the traction profile*

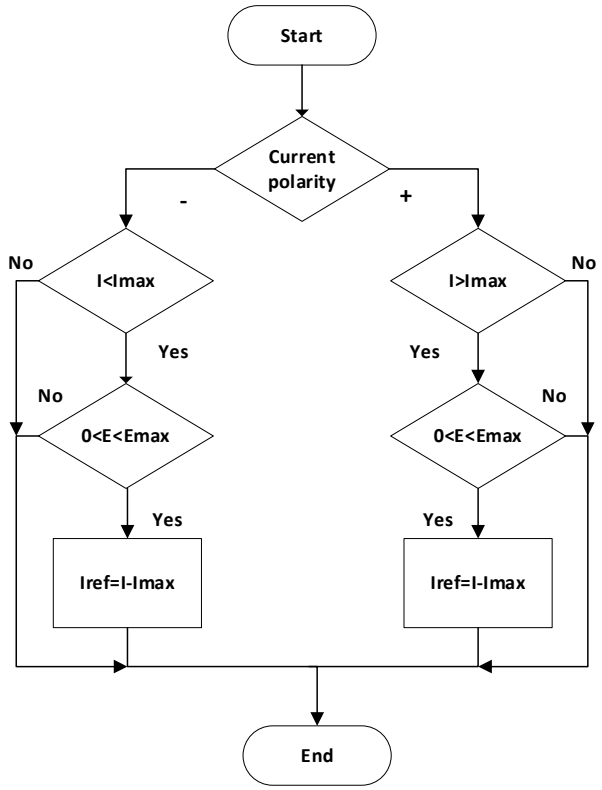

Figure 4 *Algorithm based on the battery current*

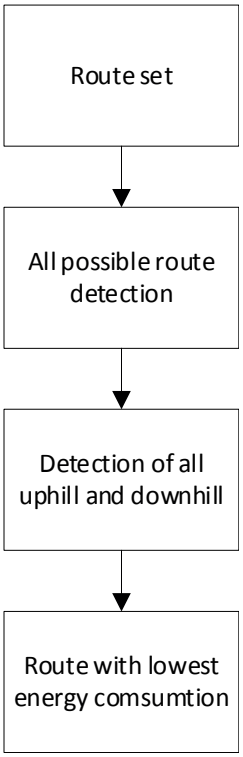

Figure 5 *Algorithm for searching for the least energy-consuming route*

current will be supplied from the secondary energy storage (Figure 4). The same situation occurs during deceleration and the downhill driving. If the current of regenerative braking exceeds the specified current and energy can be stored in the secondary energy storage, the remaining current would flow into the secondary energy storage.

2.4 Algorithm for search of the least energy-consuming route

This algorithm (Figure 5) can be used when energy in the primary energy storage is low. After the user sets destination, the route, which is least energy-consuming,

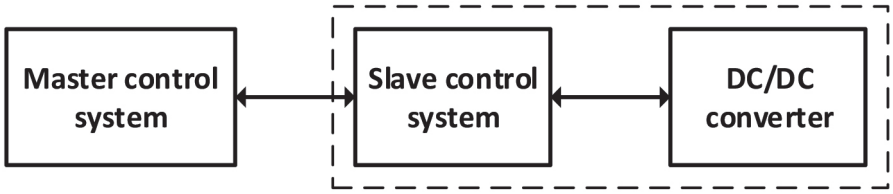

Figure 6 *Control system divided into subsystems*

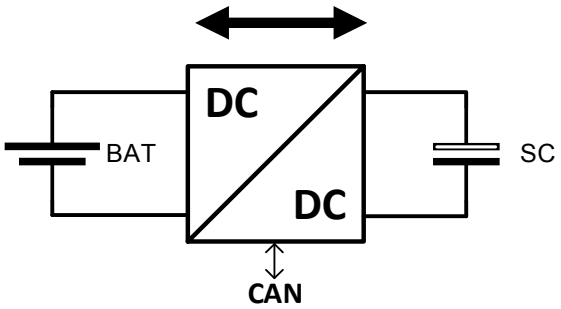

Figure 7 *Block diagram of the DC/DC converter connection*

that means, the route with the smallest number of the uphills and crossroads will be chosen from the memory.

3 The DC/DC converter control trough the CAN BUS

With using of a great amount of electronics in the modern vehicles, the requirement to divide the electronic system of the car to specific sections, by usefulness and reliability, arises. According to the importance of messages, these electronic subsystems have different speeds of the bus. The control system is divided into two subsystems, master and slave control system. The slave subsystem is implemented in the DC/DC converter (Figure 6). The master subsystem communicates with other systems like the infotainment of vehicles to observe the position of the vehicle [10].

3.1 The CAN BUS

To save material for cabling of the car and secure communication between sensors, electronic control units and actuators, a communication data bus, called Controller Area Network, abbreviated CAN, by German company Bosh GmbH at 1980 was proposed. The content of a message is described by an identifier. The Identifier does not indicate the destination of the message, but describes the meaning of the data, so that all the nodes in the network are able to decide by message filtering whether the data is to be acted upon by them or not. Within a CAN network, it is guaranteed that a message is accepted simultaneously either by all the nodes or by no node. Thus, the data consistency is a property of the system achieved by the concepts of multicast and by error handling [11].

Whenever the bus is free, any node may start to transmit a message. If the two or more nodes start transmitting messages at the same time, the bus access conflict is resolved by bit-wise arbitration using the Identifier. The mechanism of arbitration guarantees that neither information nor time is lost. If a Data frame and a Remote frame with the same Identifier are initiated at the same time, the Data frame prevails over the Remote frame. During the arbitration, every transmitter compares the level of the bit transmitted with the level that is monitored on the bus. If those levels are equal, the node may continue to send. When a recessive level is sent, but a dominant level is monitored, the node has lost arbitration and must withdraw without sending any further bits [11-12].

The message transfer is manifested and controlled by four different frame types:

- A Data frame carries data from a transmitter to the receivers;
- A Remote frame is transmitted by a bus node to request the transmission of the Data frame with the same Identifier;
- An Error frame is transmitted by any node on detecting a bus error;
- An Overload frame is used to provide for an extra delay between the preceding and the succeeding Data or Remote frames [11-12].

3.2 The DC/DC converter with an implemented control subsystem

The basis of the system is a bidirectional interleaved buck-boost converter, which controls the energy flow between supercapacitors and batteries, as can be seen in Figure 7. The DC/DC converter has three phases with phase shift 120°, which results in a smaller current ripple of energy storages.

The way of energy flow control is shown in Figure 8. If the voltage of the secondary energy storage E2 is half of the voltage of the primary energy storage E1 and duty

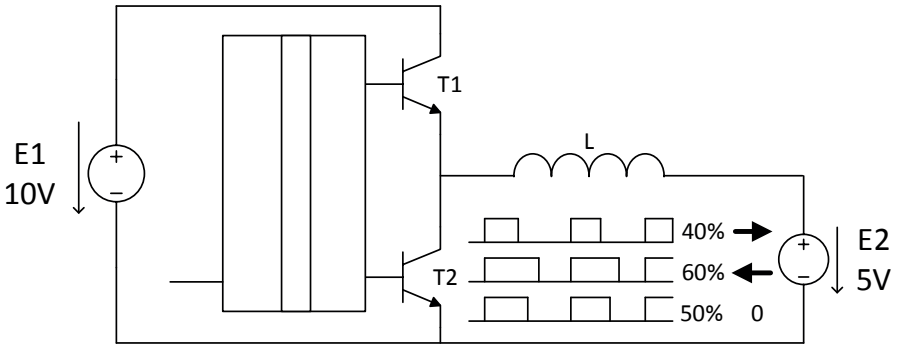

Figure 8 *Control of energy flow*

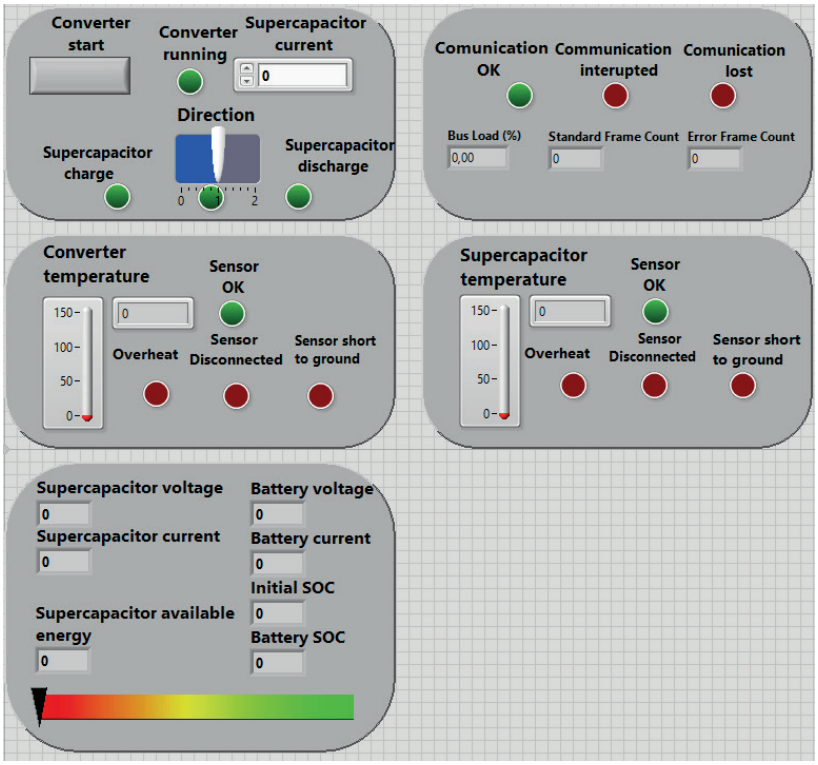

Figure 9 *The front panel of the master control system in the LabVIEW*

cycle is 50%, there is no transfer of energy. If the duty cycle is greater than 50%, energy from the secondary energy E2 storage will be transferred to the primary energy storage E1 (supercapacitors discharging). If the duty cycle is smaller than 50%, energy from the primary energy E1 storage will be transferred to the secondary energy storage E2 (supercapacitors charging).

The slave subsystem uses a feed-forward regulator for controlling the converter. This regulator uses a steady-state mathematical model. The current of the DC/DC converter is subsequently tuned by a PI (Proportional Integral) regulator. Action value is limited by next the PI regulators to secure maximal voltage of batteries and supercapacitor, supercapacitor minimal voltage and supercapacitor maximal current. Except for the control of the converter itself, the slave subsystem also provides protection and diagnostics of the converter. The slave subsystem monitors continuity of communication, which must be with period 20 ms at 500 kbps, like communication at powertrain of a real vehicle. If the period is greater, the status of communication is interrupted, while if the communication speed is different, communication status is "communication lost". Both statuses mean that the converter will be turned off. The slave system also monitors the temperature of the converter and supercapacitor. If these temperatures exceed the maximal temperature, the converter will be turned off. The slave subsystem sends the status of converter, temperatures of converter and supercapacitor, battery and supercapacitor voltages, battery and supercapacitor current, to the master subsystem through the CAN-BUS.

3.3 Master control subsystem

The master control subsystem was implemented in visual programing language LabVIEW, since it offers a graphical programming approach that helps to visualize every aspect of applications, including the hardware configuration, measurement data and debugging. The master subsystem sends commands (through the CAN-BUS) for start and stop

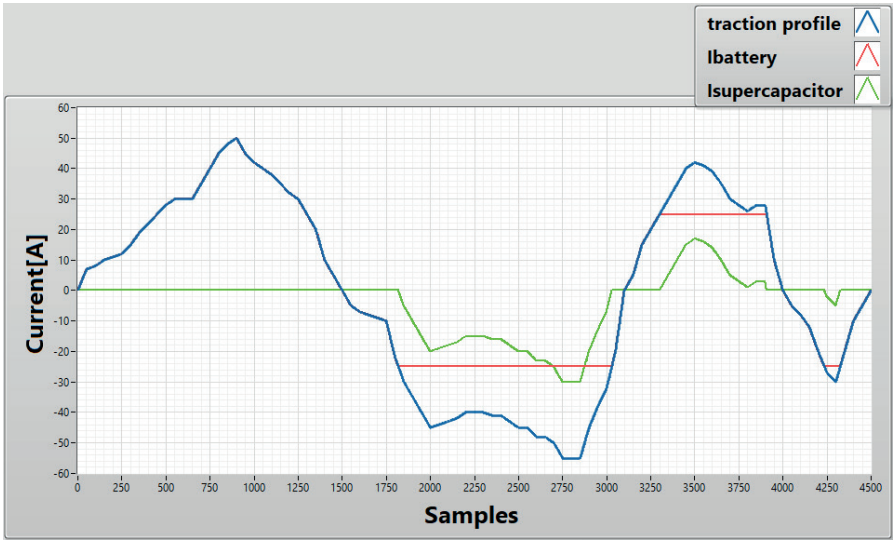

Figure 10 *Verification of algorithm based on the battery current*

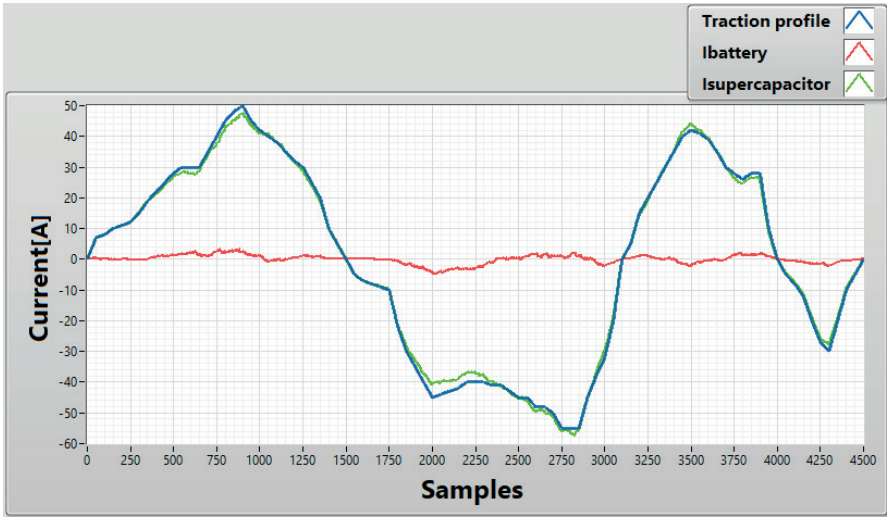

Figure 11 *Verification of algorithm using the whole traction profile*

of the converter and commands for polarity and size of the current flowing through the DC/DC converter, which are determined from the proposed algorithms. Figure 9 shows the GUI (Graphical User Interface) of master subsystem for manual control of the DC/DC converter. Kvaser Leaf SemiPro was chosen as the CAN bus interface. The Kvaser Leaf SemiPro is a single channel USB interface for the high speed CAN, with the bus speed up to 1000 kbps, with up to 15000 messages per second, synchronized with a precision of 25 microseconds. This interface has galvanic isolation, standard DB9 connector and supports both the standard 11-bit identifier and extended 29-bit identifier [13-15].

This control subsystem also estimates a state of charge of batteries that is important for control of power flow. State of Charge (SOC) estimation is realized as a combination of the open-circuit voltage (OCV) method and coulomb counting method. During the start of the program, when a current of batteries is zero, voltage is measured., The SOC is estimated from the lookup table where the dependency OCV on SOC is implemented. Important for this method is that the current must be zero, i.e. this method can be used only when the vehicle does not move. When the vehicle is moving, i.e. the battery current is not zero, the OCV method cannot be used, since the current will be integrated over time, to estimate the state of charge. The energy of the supercapacitor is calculated from its voltage. One of 19 interpreted sentences of the NMEA standard, the $GPGGA sentence, is used for observation of position and altitude of a vehicle. This sentence contains the time, latitude, longitude, number of satellites and altitude [16-17].

4 Testing of proposed algorithms

4.1 NI cRIO-90822

For the testing purposes, motor and inverter in the motor mode were simulated with programmable DC electronic load EA-EL 9500-60 and in the generator mode with programmable DC power supply EA-PSI 8060-60. Control was realized with visual programing language LabVIEW, as well. Electronic DC load was connected

through the USB, using the Modbus protocol, while the programmable power supply was connected by ethernet. Eight series-connected 40 Ah LiFePO4 traction cells were used as the primary energy storage. Supercapacitor with nominal voltage 16 V and nominal capacity 500 F was used as secondary energy storage. The algorithm, which uses part of the traction profile, was implemented for the test purposes as two look up tables (Figure 10). One look-up table is used for the saved traction profile and the second look-up table is used as an actual traction profile. Both look-up tables were saved from the GPS coordinates of the real route. The second implemented algorithm was algorithm based on the maximal battery current (Figure 11).

5 Conclusions

This paper has described a system for the energy flow control with multiple energy storages in serial active topology. The LiFePO4 traction cells were used as the primary energy storages and the supercapacitor was used as the secondary energy storage. The control system of a bidirectional DC/DC converter is divided into two subsystems that communicate through the CAN BUS. The slave subsystem is implemented directly into the DC/DC converter. The master subsystem sends direction and amplitude of current to the slave subsystem through the CAN BUS. Optimization of the energy flow, with proposed algorithms based on GPS, has extended the driving range for up to 5.11% more than the basic algorithm based on battery current. Extension of the driving range can be greater using a more accurate sensor for altitude detection or for correction of altitude from the GPS because altitude from the GPS is relatively inaccurate. The second way is using the GPS to observe the position and search altitude in the database.

Acknowledgment

This research was funded by a grant APVV-15-0571: Research of the optimum energy flow control in the electric vehicle system, APVV-17-0218: Investigation of biological tissues with electromagnetic field interaction and its application in the development of new procedures in the design of electrosurgical instruments and ITMS 26210120021- Modernization of research infrastructure in the field of electrical engineering, electrical materials and information and communication technologies.

References

[1] HUSAIN, I. *Electric and hybrid vehicles - design fundamentals*. Boca Raton, Florida: CRC PRESS LLC, 2003. ISBN 0-8493- 1466-6, eISBN 0-203-00939-8.

[2] SCHALZ, E. Electrical vehicle design and modeling. In: *Electric Vehicles - Modelling and Simulations*. SOYLU, S. (ed.). 1. ed. Aalborg University, Denmark: InTech, 2011. ISBN 978-953-307-477-1, p. 1-24.

[3] HULL, R. How far can you go in an alectric car? New test reveals the REAL ranges of models on sale todaz with one faliing 100 MILES SHORT of claims [online] [accessed 2019-11-08]. Available from: https://www.thisismoney.co.uk/money/cars/article-6337871/New-test-reveals-far-electric-cars-REALLY-travel-charge.html

[4] LINDEN, D., REDDY, T. B. *Handbook of batteries*. 3. ed. New York: McGraw-Hill, 1995. ISBN 0-07-135978-8.

[5] AL SAKKA, M., VAN MIERLO, J., GUALOUS, H. DC/DC converters for electric vehicle. In: *Electric Vehicles - Modelling and Simulations*. SOYLU, S. (ed.). 1. ed. Aalborg University, Denmark: InTech, 2011. INTECH, ISBN 978-953-307-477-1, p. 309-332.

[6] DOBRUCKY, B., KASCAK, S., PRAZENICA, M. A novel enhanced connection of AC/AC powertrain for hev - modelling and simulation results. *Advances in Electrical and Electronic Engineering* [online]. 2018, **16**(3), p. 253-260. ISSN 1336-1376, eISSN 1804-3119. Available from: https://doi.org/10.15598/aeee.v16i3.2874

[7] DOBRUCKY, B., KASCAK, S., PRAZENICA, M.; DRGONA, P., PAVLASEK, P. AC/AC powertrain control under different HEV supply network. In: 12th International Conference on Elektro 2018: proceedings. 2018.

[8] DOBRUCKY, B., KASCAK, S., PRAZENICA, M., JARABICOVA, M., KONARIK, R. Computation and comparison power losses of three- and five-phase converters (VSI) based on datasheet characteristics. In: 23rd International Conference Electronics 2019: proceedings [online. IEEE, 2019. Available from: https://doi.org/10.1109/ELECTRONICS.2019.8765583

[9] KASCAK, S., PRAZENICA, M., JARABICOVA, M., PASKALA, M. Interleaved dc/dc boost converter with coupled inductors. *Advances in Electrical and Electronic Engineering* [online]. 2018, **16**(2), p. 147-154. ISSN 1336-1376, eISSN 1804-3119. Available from: https://doi.org/10.15598/aeee.v16i2.2413

[10] BLAHO, M., ERNEK, M., SUROVCIK, T., MURGAS, T., FODREK, P.. Real-time communication subsystem for CAN bus. *International Journal on Communications Antenna and Propagation*. 2014, **4**(4), p. 108-112. ISSN 2039-5086.

[11] Bosch Controller Area Network (CAN) - Freescale Semiconductor, Inc. Version 2.0 [online] [accessed 2017-02-14]. Available from: https://www.nxp.com/docs/en/reference-manual/BCANPSV2.pdf

[12] Introduction to the Controller Area Network (CAN) - Texas Instrument [online] [accessed 2017-04-05] Available from: http://www.ti.com/lit/an/sloa101b/sloa101b.pdf

[13] KONIAR, D., HARGAS, L., LONCOVA, Z., DUCHON, F., BENO, P. Machine vision application in animal trajectory tracking. *Computer Methods and Programs in Biomedicine* [online]. 2016, **127**, p. 258-272. ISSN 0169-2607, eISSN 1872-7565. Available from: https://doi.org/ 10.1016/j.cmpb.2015.12.009

[14] SPANIK, P., HARGAS, L., HRIANKA, M., KOZEHUBA, I. Application of virtual instrumentation LabVIEW for power electronic system analysis. In: 12th International Power Electronics and Motion Control Conference EPE-PEMC 2006: proceedings. 2006.

[15] PANCIK, J., BENES, V. Emulation of wheel speed sensors for automotive electronic control unit. In: *Industry 4.0: trends in management of intelligent manufacturing systems*. KNAPCIKOVA, L., BALOG, M. (eds.). Springer International Publishing, 2019. ISBN 978-3-030-14010-6, eISBN 978-3-030-14011-3

[16] ABDUL-HAK, M., AL-HOLOU, N., MOHAMMAD, U. Predictive intelligent battery management system to enhance the performance of electric vehicle. In: *Electric Vehicles - Modelling and Simulations*. SOYLU, S. (ed.). 1. ed. Aalborg University, Denmark: InTech, 2011. ISBN 978-953-307-477-1, p. 365-384.

[17] ABU-SHARKH, S., DOERFFEL, D. Rapid test and non-linear model characterization of solid-state lithium-ion batteries. *Journal of Power sources* [online]. 2004, **130**, p. 266-274. ISSN 0378-7753. Available from: https://doi.org/10.1016/j.jpowsour.2003.12.001

ESTIMATING THE POSITION OF AN IMAGE WITH UNKNOWN INTENSITY SHAPE

Yury E. Korchagin[1], Viacheslav N. Vereshchagin[1], Alexander V. Terekhov[2], Kirill A. Melnikov[2,3,*]

[1]Department of Radio Physics, Voronezh State University, Voronezh, Russia
[2]Department of Electronics and Nanoelectronics, National Research University "Moscow Power Engineering Institute", Moscow, Russia
[3]International Laboratory of Statistics of Stochastic Processes and Quantitative Finance, National Research Tomsk State University, Tomsk, Russia

*E-mail of corresponding author: kirill.a.melnikov@mail.ru

Resume
The problem considered is to estimate the image position of a spatially extended object. It is assumed that the shape of the image intensity is a priori unknown, but it can be predicted with some error. In order to synthesize the estimate of the image position, the quasi-likelihood version of the maximum likelihood method is used. Behavior of the signal function in the neighborhood of the real image position is studied. Characteristics of the resulting estimate, such as bias and dispersion, are found by means of the local Markov approximation method. Influence of non-uniformity of the received image intensity upon the estimate accuracy is demonstrated by an example of receiving the rectangular image with linearly varying intensity.

Article info
Received 19 May 2020
Accepted 12 June 2020
Online 6 November 2020

Keywords:
image processing,
unknown intensity,
estimate of position,
quasi-likelihood approach,
local Markov approximation method,
characteristics of estimate

Available online: https://doi.org/10.26552/com.C.2021.1.C15-C22

ISSN 1335-4205 (print version)
ISSN 2585-7878 (online version)

1 Introduction

Systems for estimating (predicting) the position of a spatially extended object by its own image are widely used for security purposes, traffic monitoring and management, in railway transport and in other sectors [1-4]. However, the information processing algorithms, applied in the specified systems, can often provide the simplest operations only, such as detection of a moving object against a relatively simple background with a subsequent measurement of its speed. Thus, such systems, in fact, are video surveillance systems and not the measuring ones. A more complicated task is when realization of the two-dimensional random field $\xi(x,y)$ is processed, which, in general case, includes the image of an object with unknown coordinates to be measured, the background and the spatial noise [2-5]. The useful image is often described by a quasi-deterministic function $s(x,y)$ of the two variables determining the dependence of the image intensity upon the coordinates (x,y). One can call $s(x,y)$ the intensity distribution or the intensity profile of the image.

Depending on both the nature of the image and the resolution of the receiving system, the function $s(x,y)$ may be a regular or discontinuous one [5]. Discontinuous functions describe objects with well-defined boundaries.

Some tasks of optimal and suboptimal image processing of the spatially extended objects, with the statistical nature of the observed field $\xi(x,y)$ taken into account, are considered in [2-10]. It is presupposed that the useful image is distorted by both the spatial noise and the additive or applicative background. When using the additive model of interaction between the image and the background, the intensities of the quasi-deterministic image and the background are different from zero within the area occupied by the image. However, in the case of the applicative model use, the image shadows background, i.e. the background intensity is zero within the area occupied by the image. Algorithms for detecting the quasi-deterministic image in the presence of a background are studied in [8], while in [9-10] algorithms for processing the image with unknown position, observed in the presence of the additive Gaussian spatial white noise, are developed. In particular, in [10], efficiency of the non-uniform image position estimate is tested for the case when the image intensity distribution is a priori known. However, in practice, there may be cases where the image intensity distribution is unknown. Thus, it is of interest to consider a more general case including estimating the position of the image with an unknown varying intensity.

In order to estimate the image position, the quasi-likelihood (QL) measurer can be applied that is synthesized for some predicted (presupposed) intensity distribution of the image of the same shape and area. In this paper, both

synthesis and analysis of the QL algorithm for estimating the unknown position of the two-dimensional signal (image) with the unknown intensity distribution are carried out. Influence with a priori ignorance of the image parameters upon the efficiency of the resulting estimate is studied.

2 The problem statement

The image with the unknown intensity and position can be described by the function [5, 7-10]

$$s(x,y,\lambda,\eta) = f(x-\lambda, y-\eta) I(x-\lambda, y-\eta), \tag{1}$$

where $f(x,y)$ is the function differentiable in both arguments that describes the intensity distribution, while λ and η are values characterizing the image position in the plane two-dimensional observation area Ω. Equation (1) occupies the area $\Omega_s(\lambda,\eta) \subset \Omega$ described by the indicator function

$$\begin{aligned} I(x,y) &= \begin{cases} 1, & x,y \in \Omega_s(0,0), \\ 0, & x,y \notin \Omega_s(0,0), \end{cases} \\ I(x-\lambda, y-\eta) &= \begin{cases} 1, & x,y \in \Omega_s(\lambda,\eta), \\ 0, & x,y \notin \Omega_s(\lambda,\eta). \end{cases} \end{aligned} \tag{2}$$

Let the realization of the Gaussian random field

$$\xi(x,y) = s(x,y,\lambda_0,\eta_0) + n(x,y), \quad x,y \in \Omega \tag{3}$$

be observed within the area Ω. Here λ_0 and η_0 are the unknown position parameters and $n(x,y)$ is the spatial Gaussian white noise with zero mathematical expectation and the one-side spectral density N_0.

In the observation area Ω, one chooses the coordinate system so that the equality [9-10]

$$\iint\limits_{\Omega} xI(x,y)dxdy = \iint\limits_{\Omega} yI(x,y)dxdy \tag{4}$$

is satisfied, that is, the origin is located in the centre of the area $\Omega_s(0,0)$ described by the indicator $I(x,y)$. Then λ and η are coordinates of the centre of the area $\Omega_s(\lambda,\eta)$ occupied by the image and described by the indicator function $I(x-\lambda, y-\eta)$, while λ_0 and η_0 are the unknown real coordinates of the centre of the image presented in the observable realization in Equation (3), they determine its position.

Let it be assumed that the parameter η_0 is a priori known. Then, without loss of generality, one can presume that $\eta_0 = 0$ and rewrite expressions (3) and (1) as follows

$$\xi(x,y) = s(x,y,\lambda_0) + n(x,y), \quad x,y \in \Omega, \tag{5}$$

$$s(x,y,\lambda) = f(x-\lambda, y) I(x-\lambda, y). \tag{6}$$

The abscissa λ_0 of the centre of the area $\Omega_s(\lambda_0,0) \equiv \Omega_s(\lambda,y)$, occupied by the image, is a priori unknown. Let it takes values from the interval $[-\lambda_{\max}/2, \lambda_{\max}/2]$. By observations in Equation (5), it is necessary to estimate the unknown position λ_0 of the image $s(x,y,\lambda_0)$ with the unknown intensity distribution $f(x,y)$.

3 The estimation algorithm synthesis

If the distribution intensity $f(x,y)$ of Equation (6) is known, then it is possible to find the logarithm of the functional of the likelihood ratio (FLR) and then develop the maximum likelihood (ML) estimation algorithm. According to the ML method [11-12], in order to obtain an estimate $\hat{\lambda}$ of the position λ_0 of Equation (6), it is necessary to form the component of the FLR logarithm depending on the current value λ of the unknown parameter λ_0 as follows [13-14]

$$\begin{aligned} L_m(\lambda) &= \frac{2}{N_0} \iint\limits_{\Omega} \xi(x,y) s(x,y,\lambda) dxdy, \\ &\lambda \in [-\lambda_{\max}/2, \lambda_{\max}/2]. \end{aligned} \tag{7}$$

The ML estimate λ_m of the image position coincides with the position of the greatest maximum of the decision statistics in Equation (7), that is, $\lambda_m = \arg\sup L_m(\lambda)$.

If the image intensity $f(x,y)$ is a priori unknown, then one can use the estimation algorithm synthesized for some presupposed image intensity distribution $g(x,y) \geq 0$. Then, the output of the receiver produces some function

$$L(\lambda) = \frac{2}{N_0} \iint\limits_{\Omega} \xi(x,y) \tilde{s}(x,y,\lambda) dxdy. \tag{8}$$

Here $\tilde{s}(x,y)$ is the reference image and, in general case, $f(x,y) \neq g(x,y)$. The QL algorithm, for finding the estimate $\hat{\lambda}$ of the position λ_0, includes the search of the position of the greatest maximum of the signal in Equation (8) at the receiver output:

$$\hat{\lambda} = \arg\sup L(\lambda), \quad \lambda \in [-\lambda_{\max}/2, \lambda_{\max}/2]. \tag{9}$$

If the function $f(x,y)$ is a priori known so that

$$f(x,y) = g(x,y), \tag{10}$$

then Equation (8) coincides with the FLR logarithm when implementing the optimal reception in Equation (7) and the QL estimate in Equation (9) coincides with the ML estimate λ_m.

4 The statistical characteristics of the decision statistics

In order to determine the characteristics of the QL estimate in Equation (9), the statistical properties of the decision statistics in Equation (8) are examined. By substituting Equation (3) into Equation (8), the functional in Equation (8) is presented as the sum of signal and noise components [12]:

$$L(\lambda,\lambda_0) = S(\lambda,\lambda_0) + N(\lambda). \tag{11}$$

Here

$$S(\lambda,\lambda_0) = \frac{2}{N_0}\iint\limits_{\Omega} f(x-\lambda_0,y)g(x-\lambda,y)\cdot \\ \cdot I(x-\lambda_0,y)I(x-\lambda,y)dxdy, \tag{12}$$

$$N(\lambda) = \frac{2}{N_0}\iint\limits_{\Omega} n(x,y)g(x-\lambda,y)I(x-\lambda,y)dxdy \tag{13}$$

are the signal and noise components, respectively.

Similarly to [15], let it be supposed that in the neighborhood of the point λ_0 the signal function satisfies the conditions

$$S(\lambda,\lambda_0) > 0,\ dS(\lambda,\lambda_0)/d\lambda|_{\lambda=\lambda_0+0} < 0, \\ d(\lambda,\lambda_0)/d\lambda|_{\lambda=\lambda_0+0} > 0, \tag{14}$$

while the functions $f(x,y)$ and $g(x,y)$ do not vanish at the boundary of the area $\Omega_S(\lambda,\eta)$. Then, position of the maximum of the signal function $S(\lambda,\lambda_0)$ by the variable λ coincides with the real value λ_0 of the image position and the QL estimate in Equation (9) is consistent.

Let $S_m = \sup\limits_{\lambda} S(\lambda,\lambda_0) = S(\lambda,\lambda_0) = \frac{2}{N_0}\iint\limits_{\Omega_S(0)} f(x,y)\times$ $\times g(x,y)dxdy$ denote the maximum value of the signal component(12)and $\sigma_N^2 = \langle N^2(\lambda)\rangle = \frac{2}{N_0}\iint\limits_{\Omega_S(0)} g^2(x,y)dxdy$ denote the dispersion of the noise component in Equation (13). Taking into account the last representations, one can rewrite Equation (11) in the form

$$L(\lambda) = S_m\hat{S}(\lambda,\lambda_0) + \sigma_N\hat{N}(\lambda) = \\ = \sigma_N[\tilde{z}\hat{S}(\lambda,\lambda_0) + \hat{N}(\lambda)], \tag{15}$$

where

$$\hat{S}(\lambda,\lambda_0) = S(\lambda,\lambda_0)/S_m = \\ = \iint\limits_{\Omega_{\min}(\lambda,\lambda_0)} f(x-\lambda_0,y)g(x-\lambda,y)dxdy/ \\ \iint\limits_{\Omega_S(0)} f(x,y)g(x,y)dxdy, \tag{16}$$

$$\hat{N}(\lambda) = N(\lambda)/\sigma_N = \\ = \sqrt{\frac{2}{N_0}}\iint\limits_{\Omega_S(\lambda)} n(x,y)g(x-\lambda,y)dxdy/ \\ \sqrt{\iint\limits_{\Omega_S(\lambda)} g^2(x,y)dxdy}, \tag{17}$$

are the normalized signal component in Equation (16) and noise component in Equation (17), $\Omega_{\min}(\lambda,\lambda_0) = \Omega_S(\lambda)\cap\Omega_S(\lambda_0)$, $\tilde{z}^2 = S_m^2/\sigma_N^2 = z^2K_{fg}^2$ is the power signal-to-noise ratio (SNR) at the output of the QL receiver,

$$z^2 = \frac{2}{N_0}\iint\limits_{\Omega_S(0)} f^2(x,y)dxdy \tag{18}$$

is the power SNR at the output of the ML receiver while Equation (10) is satisfied (i.e. the image intensity distributions coincide) and

$$K_{fg} = \iint\limits_{\Omega_S(0)} f(x,y)g(x,y)dxdy/ \\ \sqrt{\iint\limits_{\Omega_S(0)} f^2(x,y)dxdy\iint\limits_{\Omega_2(0)} g^2(x,y)dxdy} \tag{19}$$

is the value that characterizes the difference between the forms of intensities of the received and the reference images.

The noise component in Equation (17) is realization of the centered Gaussian random process with the correlation function

$$K(\lambda_1,\lambda_2) = \langle\hat{N}(\lambda_1)\hat{N}(\lambda_2)\rangle = \\ = \iint\limits_{\Omega_{\min}(\lambda_1,\lambda_2)} g(x-\lambda_1,y)g(x-\lambda_2,y)dxdy/ \\ \iint\limits_{\Omega_S(0)} g^2(x,y)dxdy. \tag{20}$$

In the case of the optimal reception, functions in Equations (16) and (20) coincide, that is,

$$\hat{S}(\lambda_1,\lambda_2)|_{f=g} = K(\lambda_1,\lambda_2)|_{f=g} \tag{21}$$

for $\lambda = \lambda_1, \lambda_0 = \lambda_2$.

If value of the SNR $\tilde{z}$ is big enough, then the characteristics of the estimation algorithm in Equation (9) are defined by the behavior of the signal function in the small neighborhood of the real value λ_0 of the image position. The signal function in Equation (16) is then expanded into the Taylor series by the variable λ in the neighborhood of the point λ_0 and only the term containing the first derivative is taken into account there. According to (16), the signal function is continuously differentiable to both the right and the left of the neighborhood of the point λ_0, excluding the point $\lambda = \lambda_0$ where the derivative has the discontinuity of the first kind. Therefore, expansion of the function (16) has the form

$$\hat{S}(\lambda,\lambda_0) = 1 + \\ + \begin{cases} d_1(\lambda-\lambda_0) + o(|\lambda-\lambda_0|) & \lambda < \lambda_0, \\ -d_2(\lambda-\lambda_0) + o(|\lambda-\lambda_0|) & \lambda > \lambda_0, \end{cases} \tag{22}$$

where

$$d_1 = d\hat{S}(\lambda,\lambda_0)/d\lambda|_{\lambda=\lambda_0-0}, \\ d_2 = d\hat{S}(\lambda,\lambda_0)/d\lambda|_{\lambda=\lambda_0+0}, \tag{23}$$

and $o(|\lambda-\lambda_0|)$ denotes the higher-order infinitesimal terms compared to $|\lambda-\lambda_0|$.

Let, for example, the area , occupied by the image and set by the indicator $I(x,y)$, has the form shown in Fig. 1. Then, one projects this area on the axis *Oy*. Here $y_{\min}$, $y_{\max}$ are the minimum and maximum values of the y coordinate of the projection of the area $\Omega_S(0,0)$ on the ordinate axis, respectively. Now, the minimum and maximum values of the coordinate on the axis *Oy* on the border of the area $\Omega_S(0,0)$ are denoted as points *A* and *B*, respectively, while the parametric descriptions of the left

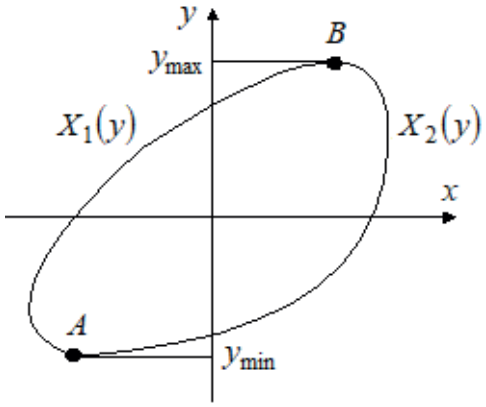

Figure 1 *The type of the area occupied by the image*

and right parts of the border of the area occupied by the image relative to the line AB are described as $X_1(y)$ and $X_2(y)$, respectively.

Using the introduced notations (see Figure 1), one can rewrite the signal function in Equation (16) in the form

$$\hat{S}(\lambda,\lambda_0) = \int_{y_{min}}^{y_{max}} \int_{X_1(y)+\max(\lambda,\lambda_0)}^{X_2(y)+\min(\lambda,\lambda_0)} f(x-\lambda_0,y)g(x-\lambda,y)dxdy \Big/ \iint_{\Omega S(0)} f(x,y)g(x-\lambda,y)dxdy. \quad (24)$$

Differentiating (24) by the variable λ and taking into account the finite size of the image existence area, one obtains expressions for the expansion coefficients in Equation (22):

$$d_i = (-1)^{i+1} \int_{y_{min}}^{y_{max}} \left\{ - \int_{X_1(y)}^{X_2(y)} f(x,y)\frac{\delta g(x,y)}{\delta x}dx + f(X_2(y),y)g(X_2(y),y)\delta_{1i} - f(X_1(y),y)\cdot g(X_1(y),y)\delta_{2i} \right\} dy \Big/ \iint_{\Omega S(0)} f(x,y)g(x-\lambda,y)dxdy, \quad (25)$$

where δ_{ij} is the Kronecker delta symbol. In practice, different combinations of types of intensity distribution of the real and presupposed (reference) images are possible. Therefore, carrying out the integration of Equation (25) by parts, one can present the expansion coefficients in Equation (25) in an alternative way:

$$d_i = (-1)^{i+1} \int_{y_{min}}^{y_{max}} \left[- \int_{X_1(y)}^{X_2(y)} g(x,y)\frac{\delta f(x,y)}{\delta x}dx + f(X_1(y),y)g(X_1(y),y)\delta_{1i} - f(X_2(y),y)\cdot g(X_2(y),y)\delta_{2i} \right] dy \Big/ \iint_{\Omega S(0)} f(x,y)g(x,y)dxdy, \quad (26)$$

Now are considered several special cases of the intensity distribution. If $g(x,y) = \text{const}$ and $f(x,y) \neq \text{const}$, then, for the expansion coefficients in Equation (23), Equation (25) is convenient because the integral by the variable x is reduced to zero and one gets

$$d_i = (-1)^{i+1} \frac{\int_{y_{min}}^{y_{max}} \left[f(X_2(y),y)g(X_2(y),y)\delta_{2i} - f(X_1(y),y)g(X_2(y),y)\delta_{1i} \right] dy}{\iint_{\Omega S(0)} f(x,y)g(x,y)dxdy}. \quad (27)$$

When $f(x,y) = \text{const}$ and $g(x,y) \neq \text{const}$, it is convenient to determine the expansion coefficients (23) of the signal function according to Equation (26) as follows

$$d_i = (-1)^{i+1} \frac{\int_{y_{min}}^{y_{max}} \left[f(X_1(y),y)g(X_1(y),y)\delta_{1i} - f(X_2(y),y)g(X_2(y),y)\delta_{2i} \right] dy}{\iint_{\Omega S(0)} f(x,y)g(x,y)dxdy}. \quad (28)$$

In the case of the optimal reception, the intensity distributions of the received and reference images coincide, that is, Equation (10) is satisfied and the expansion coefficients in Equation (23) of the signal function take the form

$$d_1 = d_2 = \int_{y_{min}}^{y_{max}} [f^2(X_1(y),y) + f^2(X_1(y),y)]dy \Big/ 2\iint_{\Omega S(0)} f^2(x,y)dxd. \quad (29)$$

The same result has been obtained in [10].

Now consider properties of the correlation function in Equation (20). Taking into account equality in Equation (21) of the signal in Equation (16) and correlation in Equation (20) functions under $f(x,y) = g(x,y)$, one can obtain an asymptotic expansion in Equation (20), while $|\lambda_2 - \lambda_1| \to 0$ as a special case of Equation (22). By substituting $g(x,y)$ instead of $f(x,y)$ in Equation (29), for the expansion coefficients in Equation (22) one gets

$$d_1 = d_2 = \int_{y_{min}}^{y_{max}} [g^2(X_1(y),y) + g^2(X_1(y),y)]dy \Big/ 2\iint_{\Omega S(0)} g^2(x,y)dxdy, \quad (30)$$

while $d_0 > 0$. Therefore, if $|\lambda_2 - \lambda_1| \to 0$, then the correlation function (20) allows the following asymptotic representation:

$$K(\lambda_1,\lambda_2) = \hat{S}(\lambda_1,\lambda_2)|_{f=g} = \\ = 11 + d_0|\lambda_2 - \lambda_1| + o(|\lambda_2 - \lambda_1|). \quad (31)$$

If intensity of the reference image is constant, that is, $g(x,y) = \text{const}$, then $d_0 = l_y/G_s$, where $l_y = y_{\max} - y_{\min}$ is the length of the image projection on the axis *Oy* (see Fig. 1), G_s is the image area [10]. While $|\lambda_2 - \lambda_1|$ increases, the correlation function in Equation (20) decreases and becomes zero, if $|\lambda_2 - \lambda_1| > l_x$. Here l_x is the length of the image projection on the axis *Ox*.

In view of the above, one can conclude that the decision statistics in Equation (15) of the QL estimation algorithm in Equation (9) is the Gaussian random process, for which the mathematical expectation and the correlation function, under conditions of high a posteriori accuracy, allow the representations in Equations (22) and (31), respectively. The statistical properties of such a process are studied in details in [10, 15]. Taking into account Equation (22), relations in Equation (14) conditioning the consistency of the QL estimate in Equation (9), can be rewritten in a more convenient form: $S_m > 0$, $d_i > 0$, $i = 1,2$. Thus, the conditions in Equations (14) are satisfied and the QL estimate in Equation (9) is consistent, if for all $y \in [y_{\min}, y_{\max}]$ the following inequalities hold:

$$\iint\limits_{\Omega_s(0)} f(x,y)g(x,y)dxdy > 0, \quad (32)$$

$$-f(X_1(y),y)g(X_1(y),y) < \\ < \int\limits_{X_1(y)}^{X_2(y)} g(x,y)\frac{\partial f(x,y)}{\partial x}dx < \quad (33) \\ < f(X_2(y),y)g(X_2(y),y).$$

5 The characteristics of the quasi-likelihood estimate of the image position

Next, one seeks characteristics of the image position QL estimate in Equation (9), assuming that this estimate is consistent. Taking into account the set properties of the signal in Equation (22) and correlation in Equation (31) functions, the conditional bias $b(\hat{\lambda}|\lambda_0) = \langle \hat{\lambda} - \lambda_0 \rangle$ and variance $V(\hat{\lambda}|\lambda_0) = \langle (\hat{\lambda} - \lambda_0)^2 \rangle$ of the reliable estimate in Equation (9) can be found by applying the local Markov approximation method as it is described in [16-17]. As a result, one gets

$$b(\hat{\lambda}|\lambda_0) = \frac{z_1^2 R(R+2) - z_2^2(2R+1)}{z_1^2 z_2^2 (R+1)^2}, \quad (34)$$

$$V(\hat{\lambda}|\lambda_0) = 2\frac{z_1^4 R(2R^2+6R+5) + z_2^4(5R^2+6R+2)}{z_1^4 z_2^4 (R+1)^3}, \quad (35)$$

where

$$R = d_1/d_2, \ z_1^2 = \tilde{z}^2 d_i^2/d_0, \ i = 1,2. \quad (36)$$

By substituting Equation (36) into Equations (34) and (35), for the required bias and variance, one obtains

$$b(\hat{\lambda}|\lambda_0) = \frac{d_0(d_1^2 - d_2^2)}{\tilde{z}^2 d_1^2 d_2^2}, \quad (37)$$

$$V(\hat{\lambda}|\lambda_0) = \frac{2d_0^2}{\tilde{z}^4} \cdot \\ \cdot \frac{2(d_1^6 + d_2^6) + 4d_1d_2(d_1^4 + d_2^4) + d_1^2 d_2^2 (d_1^2 + d_2^2) - d_1^3 d_2^3}{d_1^4 d_2^4 (d_1 + d_2)^2}. \quad (38)$$

If shapes of the received and the reference images coincide (the condition in Equation (10) is satisfied), then according to Equations (29) and (30), $d_1 = d_2 = d_0$ and the bias in Equation (37) and variance in Equation (38) take the form

$$b(\hat{\lambda}|\lambda_0) = 0, \quad V(\hat{\lambda}|\lambda_0) = 13/2z^4 d_0^2, \quad (39)$$

respectively.

It should be noted that these expressions coincide with characteristics of the ML estimate of the image position obtained in [10].

Then, one considers, for example, estimate of the rectangular image position. Let in the observation area of the image be present a rectangle with sides l_x and l_y, parallel to the axes *Ox* and *Oy*, respectively. In this case, one selects the coordinate system so that its origin is located at the intersection of the rectangle diagonals. One assumes that the image intensity is described by a linear function that increases in the direction of the angle θ with the side l_x (axis *Ox*):

$$f(x,y) = \\ = AS_0\left[\frac{(q-1)(x\cos\theta + y\sin\theta)}{l_x\cos\theta + l_y\sin\theta} + \frac{q+1}{2}\right]. \quad (40)$$

Here, the multiplier

$$A = \left[\frac{(q-1)^2}{12}\frac{l_x^2\cos^2\theta + l_y^2\sin^2\theta}{(l_x\cos\theta + l_y\sin\theta)^2} + \left(\frac{q+1}{2}\right)^2\right]^{-1/2}$$

is introduced to provide the constancy of the image energy for different values of q and θ. The value $q = s_{\max}/s_{\min}$ characterizes the slope, while S_0 - the magnitude of the change in the image intensity; $s_{\max} = \max f(x,y)$, $s_{\min} = \min f(x,y), x,y \in \Omega$, are the maximum and minimum intensity values, respectively. For a uniform image that has the same area and shape as the non-uniform one, the slope is $q = 1$, so that $f(x,y) = S_0$. One chooses the uniform image with the intensity $g(x,y) = S_0$ as the expected one. This corresponds to the case when a receiver synthesized for estimating the position of a uniform image is applied for the position estimate of a non-uniform image in Equations (1), (40). By substituting Equation (40) and $g(x,y) = S_0$ into Equation (27), one finds expressions for the expansion coefficients in Equations (22), (31)

$$d_0 = 1/l_x, \ d_1 = (1+a)/l_x, d_2 = (1-a)/l_x, \\ a = \frac{q-1}{q+1}\frac{\cos\theta}{\cos\theta + \gamma\sin\theta}, \gamma = l_y/l_x. \quad (41)$$

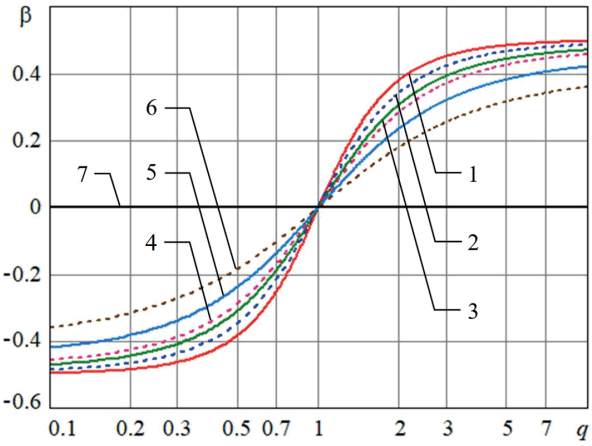

Figure 2 *Dependences of the normalized bias of the image position QL estimate*

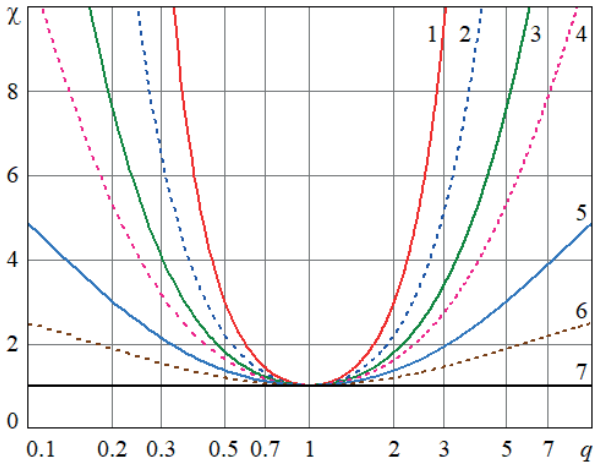

Figure 3 *Dependences of the loss in the accuracy of the image position QL estimate due to the ignorance of the image intensity*

Taking into account Equation (41), expressions for estimation characteristics in Equations (37) and (38) take the form

$$b(\hat{\lambda}|\lambda_0) = 4al_x/\tilde{z}^2(a^2-1)^2, \tag{42}$$

$$V(\hat{\lambda}|\lambda_0) = \frac{l_x^2}{2\tilde{z}^4}\frac{13+15a^4+101a^2-a^6}{a^8-4a^6+6a^4-4a^2+1}. \tag{43}$$

For the case when $q=1$ in Equations (41)-(43), one obtains expressions for the bias and the variance of the ML estimate of the uniform image position that coincide with the expressions in Equation (39):

$$b(\hat{\lambda}|\lambda_0) = 0,\ V_0(\hat{\lambda}|\lambda_0) = 13l_x^2/2z^4, \tag{44}$$

respectively.

Comparing Equations (42) and (43) to Equation (44), one can estimate influence of the non-uniformity of the image brightness distribution upon the accuracy of the QL estimate of the image position. Unlike the ML estimate, the QL estimate is biased as it follows from Equation (42). While the deviation of the parameter q from unity increases, the absolute magnitude of the estimate bias increases too. When the bias is a significant part of the mean-root-square error, it significantly reduces the accuracy of the estimate. Therefore, one introduces the normalized bias

$$\beta(\hat{\lambda}|\lambda_0) = b(\hat{\lambda}|\lambda_0)/\sqrt{V(\hat{\lambda}|\lambda_0)}, \tag{45}$$

that shows what proportion of the mean-root-square is the bias of the QL estimate.

Graphs of dependence of the normalized bias in Equation (45) of the QL estimate upon the parameter q under $\gamma=1$ and the varied values of the parameter θ are presented in Figure 2. Here, the curve 1 corresponds to value $\theta=0$, the curve 2 - to $\theta=\pi/16$, the curve 3 - to $\theta=\pi/8$, the curve 4 - to $\theta=\pi/6$, the curve 5 - to $\theta=\pi/4$, the curve 6 - to $\theta=\pi/3$, the curve 7 - to $\theta=\pi/2$ (the last curve coincides with the abscissa axis). From Figure 2 can be seen that the QL estimate is unbiased under $q=1$. If $q\neq 1$, then, for the same value of q, accuracy of the estimate decreases with increasing θ, and that corresponds to the increasing degree of difference between the received and the presupposed images.

In order to characterize the loss in accuracy of the QL estimate, while comparing it to the same kind of loss in case of the ML estimate, one introduces the relation

$$\chi(\hat{\lambda}|\lambda_0) = V(\hat{\lambda}|\lambda_0)/V_0(\hat{\lambda}|\lambda_0), \tag{46}$$

where $V(\hat{\lambda}|\lambda_0)$ and $V_0(\hat{\lambda}|\lambda_0)$ are determined in Equations (43) and (44), respectively.

In Figure 3, the graphs demonstrate dependence of the loss in the QL estimate accuracy (46) upon the parameter q under $\gamma=1$ and the varied values of the parameter θ. Here the notations coincide with the ones introduced in Figure 2. From Figure 3, it follows that under $q=1$, there is no loss in the QL estimate accuracy. However, under the fixed $q\neq 1$, the loss increases with the increasing θ and that corresponds to the increasing degree of difference between the intensities of the received and the reference (presupposed) images. When the value q increases and the value θ is fixed, the loss increases.

6 Conclusion

Synthesis and analysis of the rather simple QL algorithm have been carried out for estimating the position of the image with the unknown intensity distribution. As a result, the expansion is found of the signal function of the decision statistics in the neighborhood of the image position real value. Expressions are obtained for the bias and variance of the resulting estimate of the measured image coordinate. The dependence of the estimate characteristics upon the non-uniformity of the image intensity distribution is examined on an example of an image with the set intensity distribution. The relations

obtained allow determining the loss in accuracy of the image position estimate due to a priori ignorance of the image intensity distribution.

In the case when the intensity profiles of the received and the reference images differ significantly, so that the loss in the QL estimate accuracy becomes significant, an adaptation of the estimation algorithm, by the unknown intensity profile that leads to the improvement in the accuracy of the image position estimate, can be applied. One of the possible ways to implement adaptation is to expand the intensity profile function in terms of an orthogonal function system basis with a further estimation of the expansion coefficients. The nonparametric estimate of the intensity profile can also be used [18].

These results can be used in design of the measuring systems for object monitoring in the field of transport services, security, process and production control, etc.

Acknowledgement

This study was financially supported by the Ministry of Education and Science of the Russian Federation (research project No. FSWF-2020-0022).

References

[1] DOBRUCKY, B., MARCOKOVA, M., POKORNY, M., SUL, R. Prediction of periodical variable structure system behaviour using minimum data acquisition time. In: 26th IASTED International Conference on Modelling, Identification, and Control (MIC): proceedings. Calgary: ACTA Press, 2007. ISBN 978-0-8898-6633-1, p. 440-445.

[2] OSTROVITYANOV, R. V., BASALOV, V. F., BARTON, W. F., BARTON, D. K. *Statistical theory of extended radar targets*. 1. ed. Norwood, MA: Artech House, 1985. ISBN 0890061440.

[3] REFREGIER, P., GOUDAIL, F. *Statistical image processing techniques for noisy images. An application-oriented approach*. New York: Springer, 2004. ISBN 1461346924.

[4] FIEGUTH, P. *Statistical image processing and multidimensional modeling*. New York: Springer, 2011. ISBN 1441972935.

[5] TRIFONOV, A. P., KUTSOV, R. *Dynamic image processing* (in Russian). Moscow: LAP Lambert Academic Publishing, 2011. ISBN 3845474068.

[6] BYCHKOV, A. A., PON'KIN, V. A. Detection of random images of lengthy in space objects shadowing the background. *Avtometriya* [online]. 1992, **28**(6), p. 33-40 [accessed 1992-09-01]. ISSN 0320-7102. Available from: https://www.iae.nsk.su/images/stories/5_Autometria/5_Archives/1992/4/33-40.pdf

[7] TRIFONOV, A. P., PRIBYTKOV, Y. N., CHERNOYAROV, O. V., MIKHAILOV, B. B. Estimating the image area with unknown parameters of the image and background. *Journal of Communications Technology and Electronics* [online]. 2015, **60**(11), p. 852-859 [accessed 2015-08-18]. ISSN 1064-2269. Available from: https://doi.org/10.1134/S1064226915080185

[8] TRIFONOV, A. P., PRIBYTKOV, Y. N. Quasi-deterministic image detection in the presence of background with unknown parameters. *Avtometriya* [online]. 2002, **38**(6), p. 19-31 [accessed 2002-09-01]. ISSN 0320-7102. Available from: https://www.iae.nsk.su/images/stories/5_Autometria/5_Archives/2002/4/19-31.pdf

[9] TRIFONOV, A. P., SAVIN, S. A. Effectiveness of detection of images with unknown position. *Radioelectronics and Communications Systems* [online]. 2006, **49**(12), p. 1-8 [accessed 2019-09-30]. ISSN 0735-2727. Available from: https://doi.org/10.3103/S0735272706090019

[10] TRIFONOV, A. P., SAVIN, S. A. Effectiveness of detection and estimation of position of heterogeneous image. *Radioelectronics and Communications Systems* [online]. 2007, **50**(16), p. 647-656 [accessed 2007-12-30]. ISSN 0735-2727. Available from: https://doi.org/10.3103/S0735272707120011

[11] VAN TREES, H. L., BELL, K. L., TIAN, Z. *Detection, estimation, and modulation theory. Part I. Detection, estimation, and filtering theory*. 2. ed. New York: Wiley, 2013. ISBN 9780470542965.

[12] CHERNOYAROV, O. V., VACULIK, M., SHIRIKYAN, A., SALNIKOVA, A. V. Statistical analysis of fast fluctuating random signals with arbitrary-function envelope and unknown parameters. Communications - Scientific Letters of the University of Zilina [online]. 2015, 17(1A), p. 35-43 [accessed 2015-04-30]. ISSN 1335-4205. Available from: http://komunikacie.uniza.sk/index.php/communications/article/view/410

[13] CHERNOYAROV, O. V., BREZNAN, M. Optimal and quasioptimal algorithms of distinction of the compressed images in bases of orthogonal polynomials. *Communications - Scientific Letters of the University of Zilina* [online]. 2012, **14**(3), p. 22-26 [accessed 2012-06-30]. ISSN 1335-4205, eISSN 2585-7878. Available from: http://komunikacie.uniza.sk/index.php/communications/article/view/742

[14] CHERNOYAROV, O. V., BREZNAN, M., TEREKHOV, A. V. Restoration of deterministic and interference distorted signals and images with use of the generalized spectra in bases of orthogonal polynomials and functions. *Communications - Scientific Letters of the University of Zilina* [online]. 2013, **15**(2A), p. 71-77 [accessed 2013-07-31]. ISSN 1335-4205, eISSN 2585-7878. Available from: http://komunikacie.uniza.sk/index.php/communications/article/view/658

[15] TRIFONOV, A. P., SMORGONSKY, A. V. Quasiprobable estimation of arrival instant of finite signal. *Radioelectronics and Communications Systems* [online]. 2008, **51**(1), p. 40-49 [accessed 2008-01-31]. ISSN 0735-2727. Available from: https://doi.org/10.3103/S0735272708010068

[16] CHERNOYAROV, O. V., ZAKHAROV, A. V., TRIFONOV, A. P., SALNIKOVA, A. V., MAKAROV, A. A., The common approach to calculating the characteristics of the signal parameters joint estimates under the violation of the decision statistics regularity conditions. *Engineering Letters* [online]. 2020, **28**(2), p. 492-503 [accessed 2020-05-28]. ISSN 1312-885X. Available from: http://www.engineeringletters.com/issues_v28/issue_2/index.html

[17] CHERNOYAROV, O. V., SALNIKOVA, A. V., ROZANOV, A. E., MARCOKOVA, M. Statistical characteristics of the magnitude and position of the greatest maximum of Markov random process with piecewise constant drift and diffusion coefficients. *Applied Mathematical Sciences* [online]. 2014, **8**(147), p. 7341-7357 [accessed 2014-10-22]. ISSN 1312-885X. Available from: https://doi.org/10.12988/ams.2014.49740

[18] PCHELINTSEV, E. A., PERGAMENSHCHIKOV, S. M. Model selection method for efficient signals processing from discrete data. In: 31st European Modeling and Simulation Symposium (EMSS): proceedings. Genoa: Dime University of Genoa, 2019. ISBN 978-8-8857-4126-3, p. 90-95.

TECHNICAL FEASIBILITY OF DECEIT WHILE A VEHICLE IS WEIGHED IN MOTION WITH A VERY LOW SPEED

Zbigniew Lozia

Faculty of Transport, Warsaw University of Technology, Warsaw, Poland

*E-mail of corresponding author: zbigniew.lozia@pw.edu.pl

Resume

The study concerns the problem of overloading the vehicles driven on public roads. The gross vehicle mass and individual axle loads are limited by legal regulations. However, a tricking method, applicable to most popular designs of motor vehicles and multiaxial tractor-semitrailer units, has been shown that the weighing inspectors, even if provided with precise scales, may be deceived without any interference in the scale operation. In such a method, the current vehicle state may be changed by modifying the stiffness of individual pneumatic suspension springs, which is now technically feasible. The author used two authorial vehicle models and a simulation program. Calculation results obtained for a four-axle motor vehicle and a five-axle tractor-semitrailer unit, taken as an example, have been demonstrated. They show that a deceit is possible when a vehicle is weighed in motion with a very low speed.

Article info

Received 6 March 2020
Accepted 6 June 2020
Online 26 October 2020

Keywords:

vehicle weighing,
WIM,
Weigh-In-Motion,
road surface load,
vehicle overload,
deceit at vehicle weighing

Available online: https://doi.org/10.26552/com.C.2021.1.D1-D14

ISSN 1335-4205 (print version)
ISSN 2585-7878 (online version)

1 Introduction

The motor transport of passengers and goods plays a key role in economies of most countries in Europe and other continents. However, the bearing capacity of land roads is not unlimited. Therefore, the legal regulations have been adopted to restrict the acceptable gross vehicle mass and the normal forces exerted by wheels of individual vehicle axles on the road surface [1]. The limits thus imposed depend on specific road class (traffic service level), vehicle type, position of a specific axle in the suspension system structure and vehicle's running gear. Transportation companies and their drivers try to make use of vehicle's load capacity to the maximum possible extent. They reduce the "idle mileage" to the minimum, which is a reasonable trend. Simultaneously, however, it happens quite often that they overload (unconsciously or intentionally) their vehicles by exceeding the acceptable gross mass of the vehicle or the tractor-semitrailer unit or by incorrectly arranging the cargo. In both cases, that causes the axle loads to exceed the acceptable limits. As a consequence, the overloaded road surface undergoes more intensive wear. According to [2], the 10% exceedance of the acceptable limit of the road surface load may raise the road-destroying effect by 45%. Another negative effect of the vehicle overloading is increased traffic accident hazard arising from higher loads on vehicle's running gear and on its braking and steering systems. In Poland, like in many other (especially East European) countries, there are still shortages in the network of modern roads with high load capacity; as a consequence, the traffic of heavy vehicles takes place in a considerable part on the lower-class roads. It also happens that drivers, trying to avoid the payment of a toll, choose local highways and the progressing deterioration of such roads constitutes a serious problem for local authorities. The Minister of Infrastructure and Development and the Road Transport Inspection (ITD) in Poland receive many related questions, appeals and requests, which sometimes have the form of parliamentary questions [3] and are formulated in result of analyses carried out by institutions subordinated to legislative authorities [4]. The said Road Transport Inspection (ITD) has adequate equipment necessary to carry out continuous and periodic inspections of vehicle loading.

This paper's aim is to present the problem of a possibility of the ITD inspectors being cheated when measuring the vehicle axle loads and even if instruments of the highest possible accuracy are used at that. Thus, apart from the problem exploration aspect, the purpose of this study is to direct inspectors' attention to the possible hazard of deceit.

2 Systems for weighing vehicles in motion

The systems for weighing vehicles in motion have been developed as a result of many years of research, experiments and construction of measuring equipment

and as an effect of experience gained from multiannual operation of such devices in the USA and in many European countries. They were first built in the USA in 1951 [5]. In Europe, the earliest one was made in the UK in 1978 [6] and intensive research and engineering works aimed at construction of systems intended to determine the weight of a vehicle in motion, referred to as weigh-in-motion (WIM) systems, have been done since 1990s. In publications [2, 6-9], such projects as COST323 (1993-1999), WAVE (1996-1999), TOP TRAIL (2000-2002), REMOVE (2004-2006) and FiWi (2007-2009) have been mentioned. The researchers and scientists involved in exploring such issues meet together at cyclic conferences named ICWIMi (the most recent one, ICWIM8, was held in Prague in May 2019).

Publication [6] presents division of the WIM systems into on-board and road WIM systems and the latter are divided into non-invasive (seismic) and embedded systems. The embedded systems may use a bridge structure as the measuring device (they are referred to as Bridge-WIM or B-WIM systems) or may be installed in or under the pavement (Pavement WIM systems), which in turn are divided into Low Speed (LS-WIM) and High Speed (HS-WIM) systems operating at vehicle speeds of up to 10 $km.h^{-1}$ and higher (even up to 80-120 $km.h^{-1}$), respectively. The latter may be made as one- or two-sensor devices or as multi-sensor (Multi-Sensor WIM or MS-WIM) systems. A matter of critical importance here is the measurement accuracy, specified as about 2% for the LS-WIM systems and 7-20% for the HS-WIM ones. For the most modern MS-WIM systems, where even as many as 16 sensors may be employed, the accuracy is 2% [6].

To determine vehicle weights, static (or quasi-static) scales with an accuracy of the order of ±1% [10] are also used (some manufacturers even declare an accuracy of 0.03% [11]). They are made as weighbridges (or platform scales) for vehicles as a whole [10-19] and stationary or mobile scales for determining the loads on individual vehicle wheels or on two wheels of the same vehicle axle [12, 16, 20-21]. The measurement results obtained from this equipment may provide grounds for imposing penalties for overloading of vehicles in relation to the requirements specified in the applicable normative document [1]. The measurements in this case take more time than required when other equipment is used and the vehicle must pull in. Therefore, such measurements are carried out when a suspicion of a vehicle overload is indicated by the road WIM system (chiefly an HS-WIM system). Therefore, the HS-WIM systems are treated as intended for in-motion preselection of overloaded vehicles [2, 5-9, 22-23].

In the USA, the ASTM E1318 standard is in force [5], according to which the WIM systems have been divided into types I, II, III and IV. Type I and Type II systems are used for collecting traffic data (at vehicle speeds of 10-80 $mi.h^{-1}$). For Type III systems (10-80 $mi.h^{-1}$), requirements corresponding to the European pre-selection systems (HS-WIM) have been formulated. Type IV is also mentioned, although not approved yet for use in the USA, but built to enforce the vehicle loading regulations (suitable for vehicle speeds of 2-10 $mi.h^{-1}$).

Since 2014, a nationwide WIM network has been under construction in Poland. By 2015, 300 stations to weigh pre-selected vehicles were to be built, according to GDDKiA (General Directorate for National Roads and Motorways in Poland) [2]. The WIM network administered by ITD (Road Transport Inspection) is provided with mobile systems, i.e. scales for determining the loads on individual vehicle wheels or on two wheels of the same vehicle axle [12, 16, 20-21].

3 Essence of the feasible method of deceiving when a vehicle is weighed in motion with a very low speed

Figure 1 shows a schematics that explains the way how a deceit can be committed when a vehicle is weighed in motion with a very low speed. Here, a four-axle vehicle standing on a horizontal road surface, with its axles being situated symmetrically to each other, will be used as an example. The vehicle load is so arranged that the gross vehicle weight 4F causes identical normal reactions F to act on the wheels of individual vehicle axles (see the top part of the drawing). In this example, axle scales (simultaneously measuring the load on two wheels of the same axle) is used. Thus, four F values are measured (with accuracies of individual scales). If the measurement, carried out for the wheels of a specific axle (marked with a red ring in the drawing) of the vehicle under test, is immediately preceded by a reduction in the stiffness of suspension springs of the said axle (caused by e.g. the vehicle driver) then the load value actually read for this axle will be lower than F. If such a fraudulent driver's action is repeated when the loads on other axles are measured, a similar effect will be obtained. The drop in the normal reaction value determined for the axle under measurement will be accompanied by growths in the values of such reactions at the axles situated nearby (where the load is not measured at that time). In consequence, the sum of the readouts will be less than 4F and the measuring inspector will record a total result lower than the actual vehicle weight (4F), in spite of precise stationary scales being used. Instead of reducing the stiffness of the suspension system of the axle under measurement, the suspension stiffness at the other (or neighbouring) axles may be raised to obtain a similar effect. A schematic similar to the one presented in Figure 1 may also be drawn for a multiaxial tractor-semitrailer unit.

The following questions arise:

- Can the suspension stiffness be changed during the slow vehicle motion on the measuring stand?
- Can the possible changes in the suspension stiffness at individual vehicle axles be big enough for the difference between the actual vehicle weight and the sum of individual readings to be such that the driver would avoid punishment for vehicle overloading?

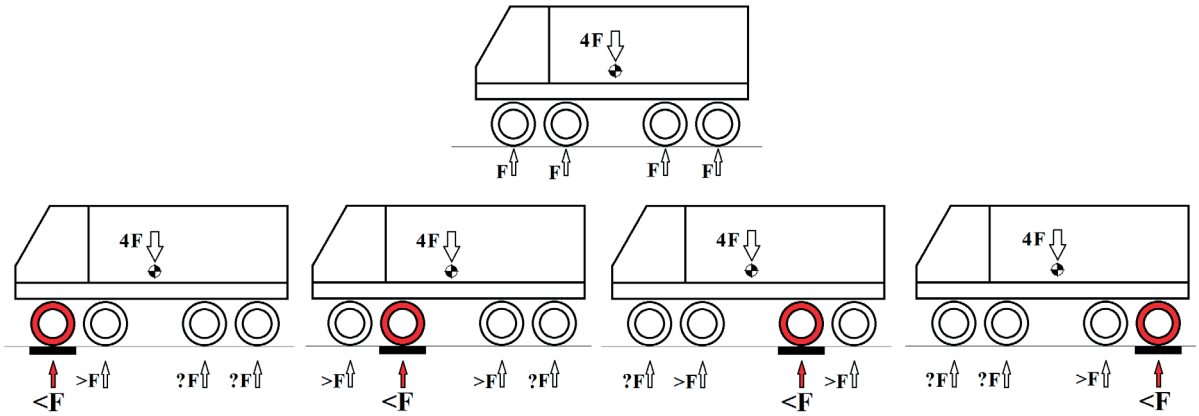

Figure 1 *Schematics to explain the possibility of deceit when a vehicle is weighed in motion with a very low speed. The red rings indicate the axles where the suspension spring stiffness is temporarily reduced.*

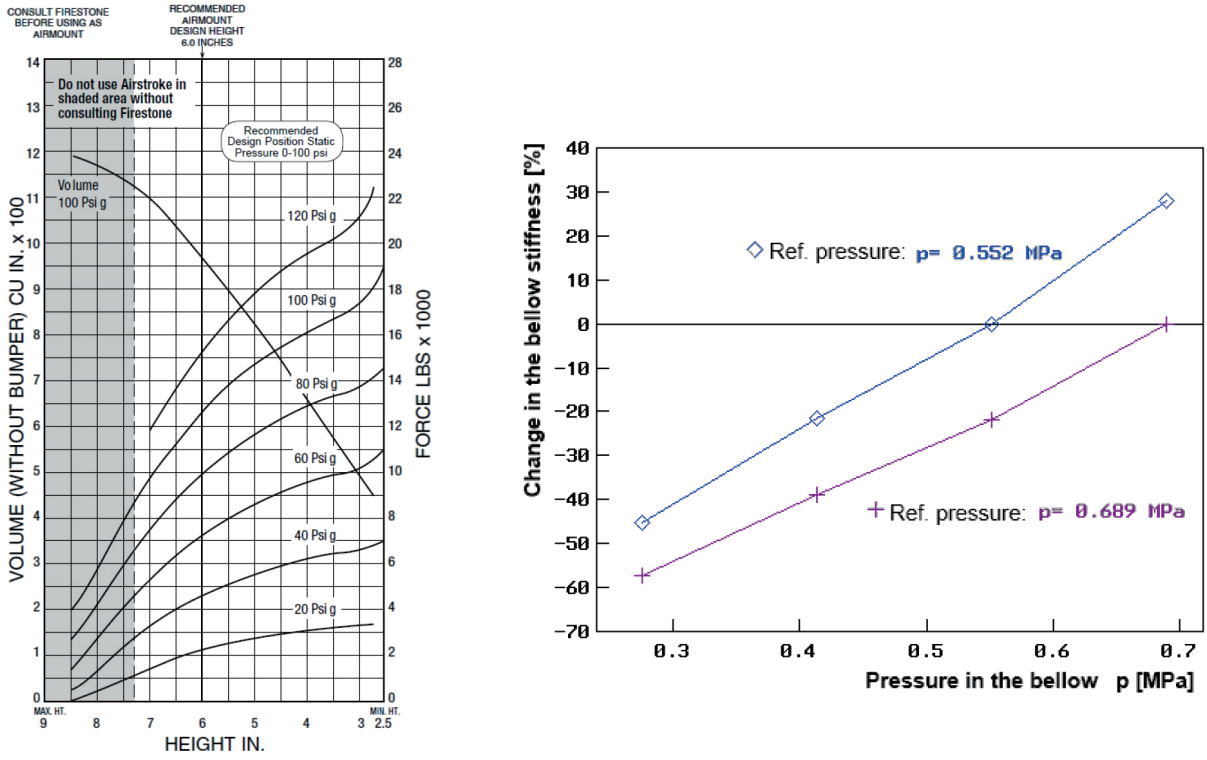

a. *b.*

Figure 2 *a. Example characteristics of the pneumatic suspension spring (air bellow) of a motor truck: force (lbs×1 000=4.54×1 000 N) vs current bellow height (in = 0.0254 m) for various constant values of bellow inflation pressure (above atmospheric, e.g. 100 psig=0.689 MPa) [25], b. Relative changes in the air bellow stiffness for two different reference pressure values (0.552 MPa and 0.689 MPa in this case, as specified)*

- Similar questions may be asked in the case of examining a single axle and comparing the measurement result with the legally acceptable limit.

The computer systems (LAN) and on-board diagnostic systems used in motor vehicles provide technical possibilities that the first question may be answered affirmatively.

For the "YES" answer to be given to the second question, some preconditions must be met. First, the vehicle under consideration must be provided with a suspension system with controllable stiffness, e.g. a pneumatic one. At present, there are many vehicles with such systems [24-26], especially those designed for the long-range operation, where driver's comfort and reduction of vibrations, having an impact on the cargo transported, are a matter of importance. This particularly applies to suspension systems of semitrailers (e.g. Wielton, Fruehauf, Schmitz, Kogel), as well as trucks and truck-tractors (in the latter case, not all the vehicle axles are so equipped). Even the manufacturers of the four-axle motor trucks, designed for operation in the building industry and driven on unpaved roads (e.g. Scania, Volvo, Iveco and Renault), provide selected

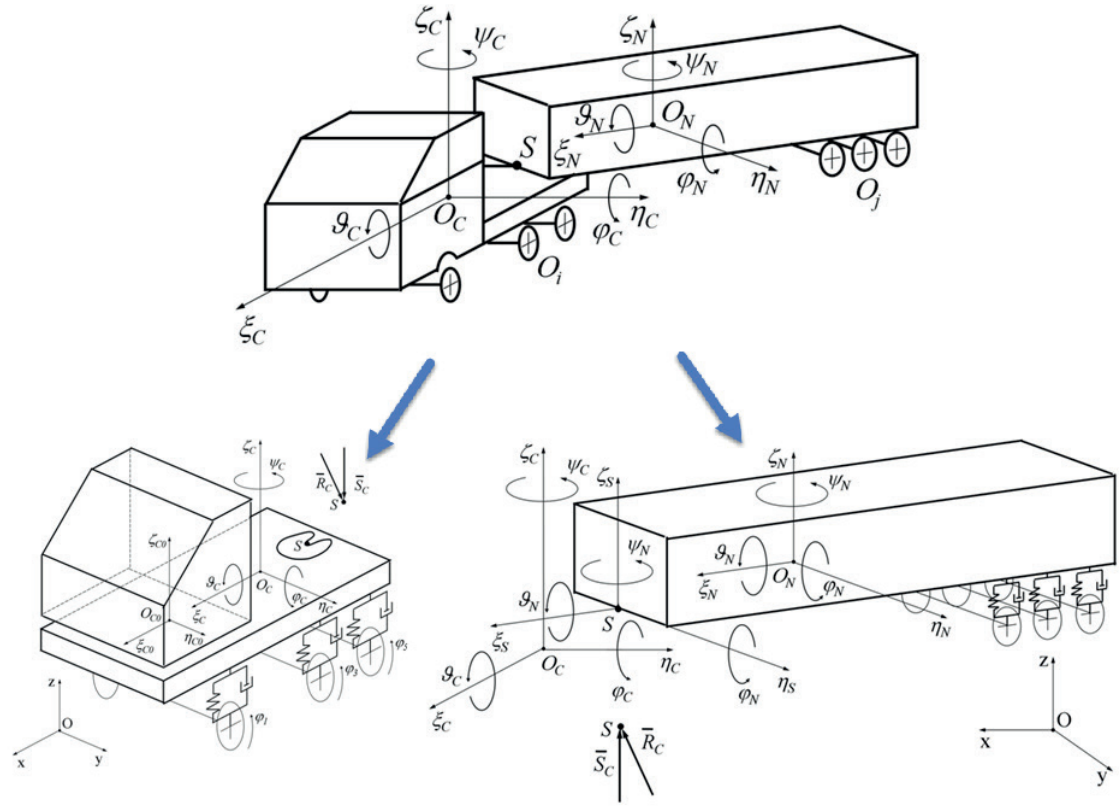

Figure 3 *Model of a tractor-semitrailer unit for the simulation of the vehicle motion and dynamics, including real time simulation. 29 degrees of freedom, i.e.* x_{O1}, y_{O1}, z_{O1}, ψ_1, φ_1, ϑ_1, ζ_{C1}, ζ_{C2}, ζ_{C3}, ζ_{C4}, φ_1, φ_2, φ_3, φ_4, ψ_N, φ_N, ϑ_N, ζ_{N1}, ζ_{N2}, ζ_{N3}, ζ_{N4}, ζ_{N5}, ζ_{N6}, φ_7, φ_8, φ_9, φ_{10}, φ_{11}, φ_{12}. *Vehicle modelled: Mercedes Actros 1841L [29]*

vehicle axles with pneumatic suspension systems. Figure 2a shows an example of characteristics of the pneumatic suspension spring (air bellow) of a motor truck [25]. Figure 2b illustrates relative changes in the air bellow stiffness for the two different reference pressure values (0.552 and 0.689 MPa in this case, as specified). The characteristic curves in Figure 2a represent the axial forces transmitted by the bellow as functions of the current bellow height for various inflation pressure values. As it can be seen, the slope of the curves, i.e. the suspension stiffness, increases with a growth in the bellow inflation pressure.

As an example: for the bellow height of 5 in. (0.127 m), a pressure change from 40 psig to 100 psig (i.e. from 0.276 MPa to 0.689 MPa) will cause the suspension stiffness (slope of the bellow force vs height curve) to rise more than 2.34 times (i.e. by 134%). For the same bellow height, a reduction in the pressure from 100 psig to 40 psig (i.e. from 0.689 MPa to 0.276 MPa) will cause a drop in the suspension stiffness by about 57.3%. This is illustrated by the curve plotted in Figure 2b for the reference bellow pressure of 100 psig (0.689 MPa). Thus, the suspension stiffness may be considerably changed by modifying the bellow inflation pressure.

Second, it should be checked by calculation whether the obtainable change in the suspension stiffness would cause a sufficient lowering of the measurement results for the cheating effect in question to be achieved. And this is exactly the objective of this study.

4 Physical models used in the calculations

Originally, the author planned to use his authorial MBS (Multi-Body System) models presented in [27-29]. An example model of this type, used to study dynamics of an articulated vehicle, has been shown in Figure 3. This model has 29 degrees of freedom and requires a lot of data to be predetermined, including performance curves characterizing the operation of individual vehicle component systems. Actually, the objective of the calculations carried out was to verify the hypothesis formulated in Section 3; therefore, the two simpler models were chosen, which were to be used at first for qualitative research and then for quantitative tests. The fact was taken into account that during the quasi-static measurement carried out on single-wheel scales (determining the loads on individual vehicle wheels) or on axle scales, the vehicle is moving rectilinearly with a very low speed.

Pursuant to the rule that the model adopted should chiefly represent the main vehicle characteristics in the test conditions [28, 30-31], a decision was made to reduce the complexity of structures of the models built.

Figure 4 shows the model of a four-axle motor truck moving rectilinearly with a very low speed. The model has the form of a beam representing the mass of the vehicle body solid supported by four springs that describe the elasticity of individual wheel suspension systems and pneumatic tyres (arranged in series). The masses of vehicle

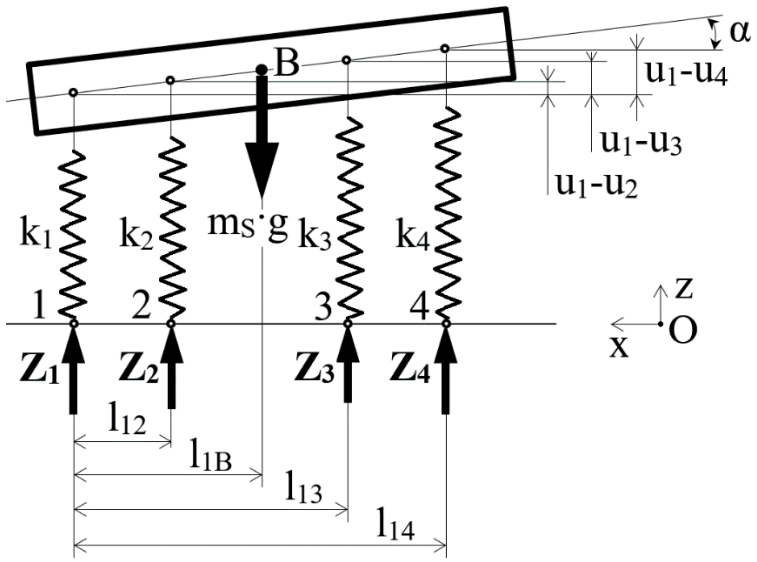

Figure 4 *Model of a four-axle motor truck moving rectilinearly with a very low speed (for the meaning of the symbols used see the text)*

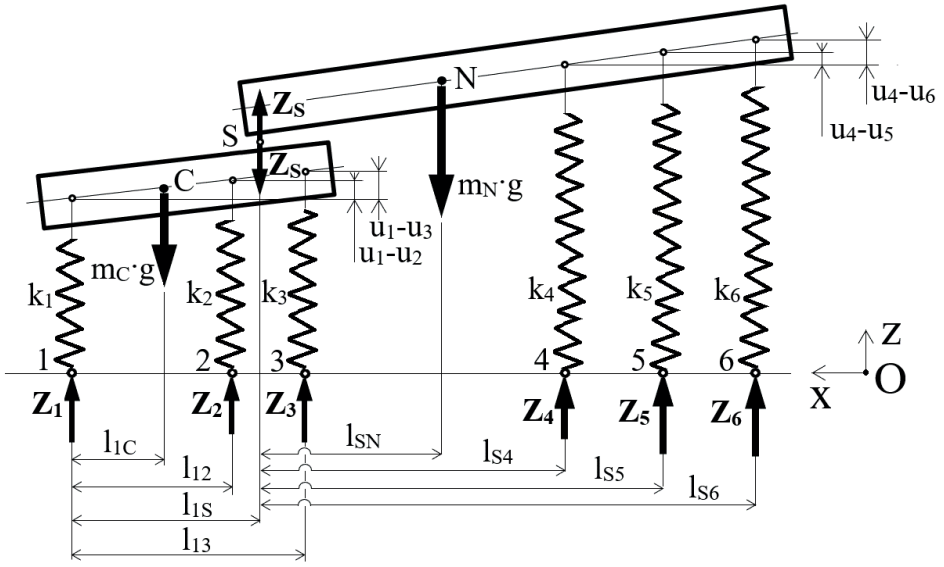

Figure 5 *Model of a three-axle truck-tractor with a three-axle semitrailer moving rectilinearly with a very low speed (for the meaning of the symbols used see the text)*

wheels and axles and the propulsion forces have been ignored. In the model so designed, point B represents the centre of a vehicle mass; m_S [kg] is vehicle mass; g = 9.81 m.s^{-2} is acceleration of gravity; numerals i = 1, 2, 3, 4 denote tyre-road contact points; Z_i [N] is normal reaction at the ith tyre-road contact point (equal to the load on the ith axle); k_i [N.m^{-1}] is resultant stiffness of the suspension system and tyres of the ith axle; l_{ij} [m] is a horizontal distance between point "i" and point "j" (here, i = 1 and j = 2, B, 3, 4); u_i [m] is deflection of the suspension system of the ith axle (here, i = 1, 2, 3, 4); α [rad] is a pitch angle of the vehicle body solid. Oxy is the coordinate system attached to the road, where Ox is the horizontal axis and Oz is the vertical axis.

Figure 5 shows a similar model of a three-axle truck-tractor with a three-axle semitrailer. Here, the two beams can be seen that represent masses of the tractor and semitrailer body solids. They are coupled to each other by a rotary joint representing the fifth-wheel joint in the tractor-semitrailer unit. The beams are supported by springs describing the elasticity of individual wheel suspension systems and pneumatic tyres (arranged in series as above). Masses of the vehicle wheels and axles and the propulsion forces have been ignored here, as well. In the model so designed, points C and N represent centres of mass of the truck-tractor and semitrailer, respectively; S is a centre of the rotary coupling between the truck-tractor and semitrailer (centre of the fifth-wheel kingpin head, i.e. the "fifth-wheel centre"); m_C [kg] is the truck-tractor mass; m_N [kg] is the semitrailer mass; g = 9.81 m.s^{-2} is acceleration of gravity; numerals i = 1, 2, 3, 4, 5, 6 denote tyre-road contact points; Z_k [N] is normal reaction at the kth tyre-road contact point (equal to the load on the kth axle); k_k [N.m^{-1}] is resultant stiffness of the suspension system and tyres of the kth axle; Z_S [N] is vertical reaction at the fifth-wheel centre (point S); l_{kl} [m] is horizontal distance

between point "k" and point "l" (here, k = 1, S; and l = C, 2, S, N, 4, 5, 6); u_k [m] is deflection of the suspension system of the k^{th} axle (here, k = 1, 2, 3, 4, 5, 6). Oxy is the coordinate system attached to the road, where Ox is the horizontal axis and Oz is the vertical axis.

5 Mathematical models for the physical models adopted

For the physical models illustrated in Figures 4 and 5, mathematical models have been built, which describe the state of the static equilibrium of vehicles moving rectilinearly with a constant very low speed (close to zero) on a horizontal even road surface.

5.1 Mathematical model of a four-axle motor truck

The following additional assumptions were adopted for the model shown in Figure 4:

- differences $u_i - u_j$ in suspension system deflections are small in comparison to the l_{ij} dimensions specified;
- suspension system deflections u_i are vertical (in the Oz direction);
- pitch angle α of the vehicle body solid is small (up to a few degrees);
- Z_i reactions are non-negative.

Equations that describe the state of the static equilibrium of the vehicles moving rectilinearly, with a constant very low speed, have the form of equations of forces acting in the vertical direction Oz, equations of the moments of forces relative to point l, tangent of the pitch angle α of the vehicle body solid determined from deflections of the suspension systems of axles 1, 2 and 4 and tangent of this angle determined from deflections of the suspension systems of axles 1, 3 and 4. After transformations, they take a matrix form:

$$\mathbf{AS}_{4x4} \times \mathbf{ZS}_{4x1} = \mathbf{WPSS}_{4x1}. \quad (1)$$

The non-zero elements of the **AS** matrix are represented by a group of relations:

$$\begin{aligned} &AS(1,1) = AS(1,2) = AS(1,3) = AS(1,4) = 1,\\ &AS(2,2) = l_{12},\ AS(2,3) = l_{13},\ AS(2,4) = l_{14},\\ &AS(3,1) = (l_{12}-l_{14})/k_1,\ AS(3,2) = l_{14}/k_2,\ AS(3,4) = -l_{12}/k_4,\\ &AS(4,1) = (l_{13}-l_{14})/k_1,\ AS(4,3) = l_{14}/k_3,\ AS(4,4) = -l_{13}/k_4. \end{aligned} \quad (2)$$

Vector **ZS** has the form in Equation (3) and vector **WPSS** is defined by:

$$\mathbf{ZS}_{4x1} = \mathrm{col}[Z_i],\ i = 1, 2, 3, 4. \quad (3)$$

$$\mathbf{WPSS}_{4x1} = \mathrm{col}[m_S \times g,\ m_S \times g \times l_{1B},\ 0,\ 0]. \quad (4)$$

The vector **ZS** to be found (Equation (3)), representing the normal reactions (axle loads) Z_i at the i^{th} tyre-road contact points, can be obtained by solving Equation (1).

5.2 Mathematical model of a three-axle truck-tractor with a three-axle semitrailer

Additional simplifying assumptions were also adopted for the model shown in Figure 5:

- differences $u_i - u_j$ in suspension system deflections are small in comparison to the l_{kl} dimensions specified;
- suspension system deflections u_i are vertical (in the Oz direction);
- pitch angles of the tractor and semitrailer body solids are small (up to a few degrees);
- Z_i reactions are non-negative.

Equations that describe the state of static equilibrium of the truck-tractor moving rectilinearly, with a constant very low speed, have the form of equations of forces in the vertical direction Oz, equations of the moments of forces relative to point l and tangent of the pitch angle of the tractor body solid determined from deflections of the suspension systems of axles 1, 2 and 3. Similar equations that describe the state of static equilibrium of the semitrailer have the form of equations of forces acting in the vertical direction Oz, equations of the moments of forces relative to point S and tangent of the pitch angle of the semitrailer body solid determined from deflections of the suspension systems of axles 4, 5 and 6. After transformations, they take a matrix form:

$$\mathbf{AZ}_{6x6} \times \mathbf{ZZ}_{6x1} = \mathbf{WPSZ}_{6x1}. \quad (5)$$

The non-zero elements of the **AZ** matrix are represented by a group of relations (6):

$$\begin{aligned} &AZ(1,1) = AZ(1,2) = AZ(1,3) = AZ(1,4) = AZ(1,5) =\\ &= AZ(1,6) = 1,\\ &AZ(2,1) = -l_{1S},\ AZ(2,2) = l_{12} - l_{1S},\ AZ(2,3) = l_{13} - l_{1S},\\ &AZ(3,1) = (l_{12}-l_{13})/k_1,\ AZ(3,2) = l_{13}/k_2,\ AZ(3,3) = -l_{12}/k_3,\\ &AZ(4,2) = l_{12}/l_{1S},\ AZ(4,3) = l_{13}/l_{1S},\ AZ(4,4) = AZ(4,5) =\\ &= AZ(4,6) = 1,\\ &AZ(5,4) = l_{S4},\ AZ(5,5) = l_{S5},\ AZ(5,6) = l_{S6},\\ &AZ(6,4) = (l_{S6}-l_{S5})/k_4,\ AZ(6,5) = -(l_{S6}-l_{S4})/k_5,\ AZ(6,6) =\\ &= (l_{S5}-l_{S4})/k_6, \end{aligned} \quad (6)$$

Vector **ZZ** has the form in Equation (7) and vector **WPSZ** is defined by Equation (8).

$$\mathbf{ZZ}_{6x1} = \mathrm{col}[Z_i],\ i = 1, 2, 3, 4, 5, 6. \quad (7)$$

$$\mathbf{WPSZ}_{6x1} = \mathrm{col}[(m_C + m_N) \times g,\ m_C \times g \times (l_{1C} - l_{1S}),\ 0,\ (m_C \times l_{1C}/l_{1S} - m_N) \times g,\ m_N \times g \times l_{SN},\ 0]. \quad (8)$$

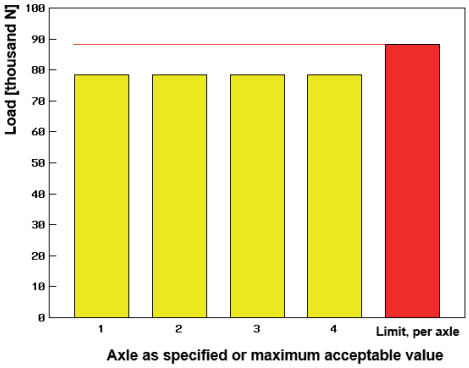

Figure 6 *Calculation results obtained for the nominal data of the example four-axle motor truck in comparison to the maximum acceptable axle load values ("Limit, per axle")*

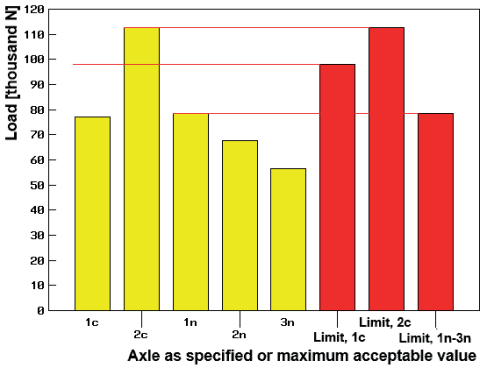

Figure 7 *Calculation results obtained for the nominal data of the example two-axle truck-tractor with a three-axle semitrailer in comparison to the maximum acceptable values for the 1st tractor axle ("Limit,1c"), 2nd tractor axle ("Limit,2c") and a semitrailer axle ("Limit, 1n-3n")*

The vector **ZZ** to be found (Equation (7)), representing the normal reactions (axle loads) Z_i at the i^{th} tyre-road contact points, can be obtained by solving Equation (5).

6 Data adopted for the example calculations

For the motor truck calculations, the data adopted as an example represent a four-axle vehicle with an 8×8 drive system (all-wheel drive eight-wheeler) with a design similar to that of at least several truck types used in Poland, chiefly in the building industry.

The data taken for the example calculations, concerning a truck-semitrailer unit, correspond to a two-axle truck-tractor with a three-axle semitrailer. The structure of such a vehicle combination is somewhat less complicated than that shown in Figure 5, but it was chosen because of being very popular in Poland. The low road gradients prevail (except for the southern regions) and transport companies usually choose truck-tractors with 4×2 drive systems (four wheels, two of them being driven), which is less expensive than the 6×4 type (six wheels, four of them being driven). The tractor-semitrailer model, as discussed in the foregoing sections, makes it possible to analyse the five-axle vehicle combinations instead of the six-axle ones, as such a model reduction would not disturb the computation algorithm. Equation (9) illustrates a modified system of denoting individual vehicle axles and tyre-road contact points, which enables the said model reduction:

$$\begin{aligned} &1 \Rightarrow 1c \quad 2 \Rightarrow 2c \quad 3 \Rightarrow 3c \text{ (omitted)} \\ &4 \Rightarrow 1n \quad 5 \Rightarrow 2n \quad 6 \Rightarrow 3n, \end{aligned} \tag{9}$$

where: "c" and "n" means "tractor" and "semitrailer, respectively.

Point 3 (i.e. 3c in the new notation) would be omitted in the case of the said reduction. The mathematical model would still have the form as described by Equations (5)-(8), but the method of presenting the calculation results would be modified according to Equation (9).

6.1 Nominal data of the motor truck and the tractor-semitrailer unit

The following data were adopted for the four-axle 8×8 motor truck taken as an example: m_S =32 000 kg, $k_1 = k_2 = k_3 = k_4$ = 300 000 N.m^{-1}, l_{12} = 1.7 m, l_{13} = 4.8 m, l_{14} = 6.15 m, l_{1B} = 3.1625 m. The maximum acceptable values are: m_{Sdop} = 32 000 kg (i.e. $G_{Sdop} = m_{Sdop} \times g$ = 313 920 N) and $Z_{1dop} = Z_{2dop} = Z_{3dop} = Z_{4dop}$ = 9 000 kg×g = 88 290 N, according to the applicable normative document [1]. As it can be seen, the vehicle mass is equal to the maximum acceptable gross vehicle mass ($m_S = m_{Sdop}$). Figure 6 shows the calculation results obtained for the nominal data of the example four-axle motor truck in comparison to the maximum acceptable values. At none of the vehicle axles, the normal reactions (axle loads) exceed the limits.

For the example truck-semitrailer unit (two-axle truck-tractor with a three-axle semitrailer), the following data were adopted: m_C = 7 500 kg, m_N = 32 500 kg, k_1 = 412 000 N.m^{-1}, k_2 = 1 500 000 N.m^{-1}, k_4 = 1 340 000 N.m^{-1}, k_5 = 1 340 000 N.m^{-1}, k_6 = 1 340 000 N.m^{-1}, l_{12} = 3.595 m, l_{1C} = 0.567 m, l_{1S} = 3.13 m, l_{SN} = 3.849 m, l_{S4} = 4.89 m, l_{S5} = 6.20 m, l_{S6} = 7.51 m.

The maximum acceptable values are [1]: $m_{Zdop} = (m_C + m_N)_{dop}$ = 40 000 kg (i.e. $G_{Zdop} = m_{Zdop} \times g$ = 392 400 N), Z_{1cdop} = 10 000 kg × g = 98 100 N, Z_{2cdop} = 11 500 kg × g = 112 815 N, $Z_{1ndop} = Z_{2ndop} = Z_{3ndop}$ = 8 000 kg × g = 78 480 N. The mass of the truck-semitrailer unit is equal to the maximum acceptable gross vehicle mass ($m_Z = m_C + m_N = m_{Zdop}$). Figure 7 shows the calculation results obtained for the nominal data of the example two-axle truck-tractor with a three-axle semitrailer in comparison to the maximum acceptable values. At none of the vehicle axles, the normal reactions exceed the limits.

6.2 Data of the motor truck and the tractor-semitrailer unit when overloaded

The model of the four-axle motor truck taken as an example was overloaded by 20% and the centre of its mass

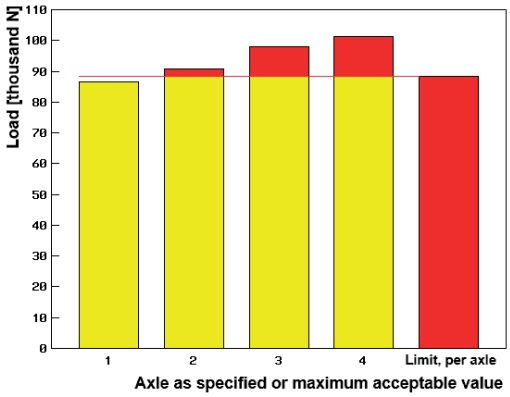

Figure 8 *Calculation results obtained for the four-axle motor truck overloaded by 20%, shown in comparison to the maximum acceptable axle load values ("Limit, per axle")*

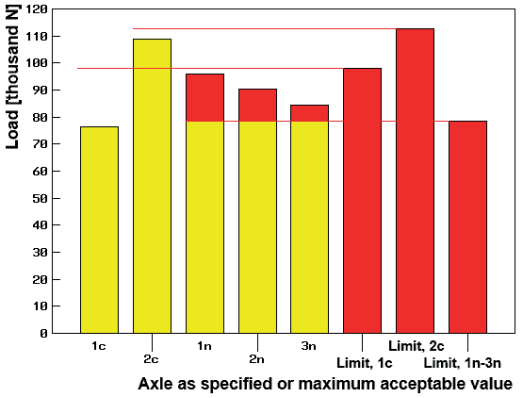

Figure 9 *Calculation results obtained for the truck-semitrailer unit overloaded by 20%, shown in comparison to the maximum acceptable values for the 1st tractor axle ("Limit, 1c"), 2nd tractor axle ("Limit, 2c") and a semitrailer axle ("Limit, 1n-3n")*

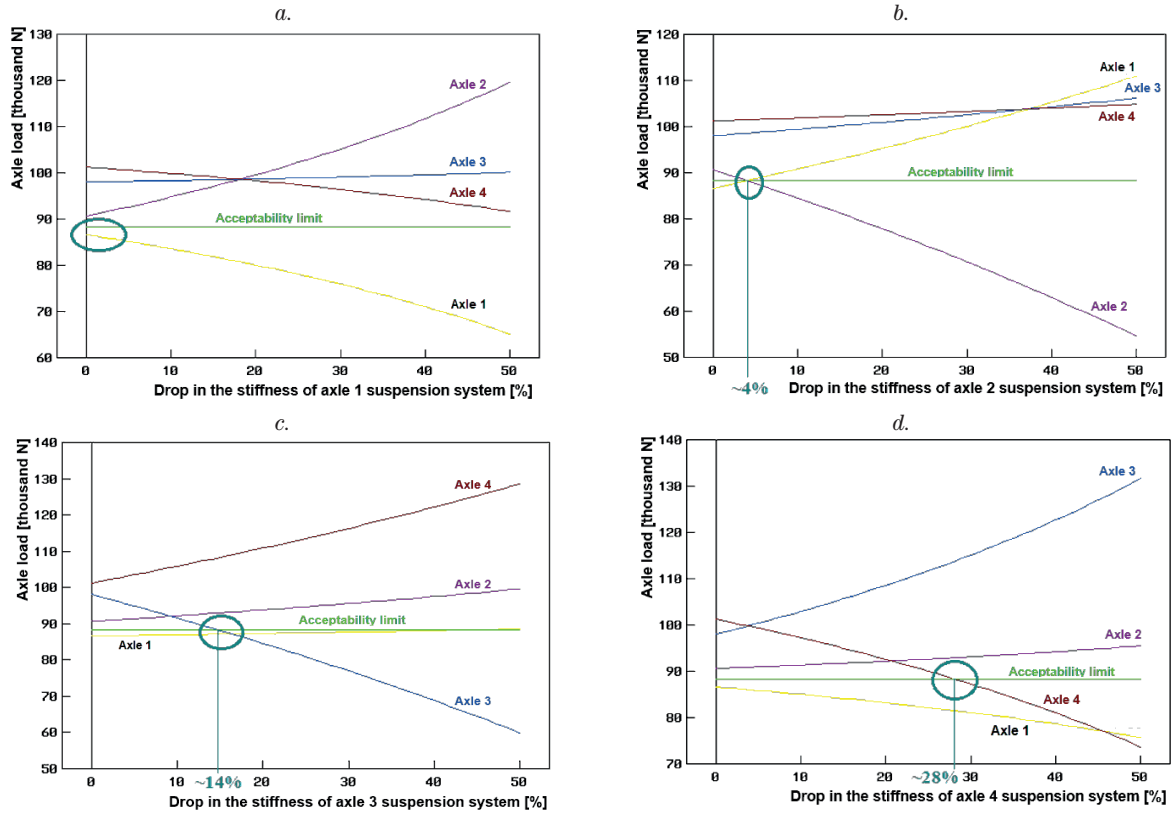

Figure 10 *Motor truck. Impact of a reduction in the stiffness of suspension systems of axles 1 (a), 2 (b), 3 (c) and 4 (d) on the normal road reactions (axle loads) at pneumatic tyres of all the four vehicle axles*

was shifted rearwards by 0.15 m. Thus, the two parameters of the model were changed (cf. Figure 4): m_S = 38 400 kg, l_{1B} = 3.3125 m. Figure 8 shows the calculation results obtained for the overloaded four-axle motor truck in comparison with the maximum acceptable values. The normal reactions (axle loads) exceed the limits at axles 2, 3 and 4.

In the model of the truck-semitrailer unit taken as an example (two-axle truck-tractor with a three-axle semitrailer), the semitrailer was overloaded by 20% and the centre of its mass was shifted rearwards by 0.5 m. Thus, the two parameters of the model were changed (cf. Figure 5): m_N = 39 000 kg, l_{SN} = 4.349 m. Figure 9 shows the calculation results obtained for the overloaded truck-semitrailer unit in comparison to the maximum acceptable values. The normal reactions at the semitrailer axles (1n, 2n and 3n) exceed the limits.

7 Potential capabilities of the method of deceiving when the example vehicles are weighed

The analysed method of deceiving when the loads on individual vehicle axles are measured consists (as described above) in reducing the stiffness of specific axle's

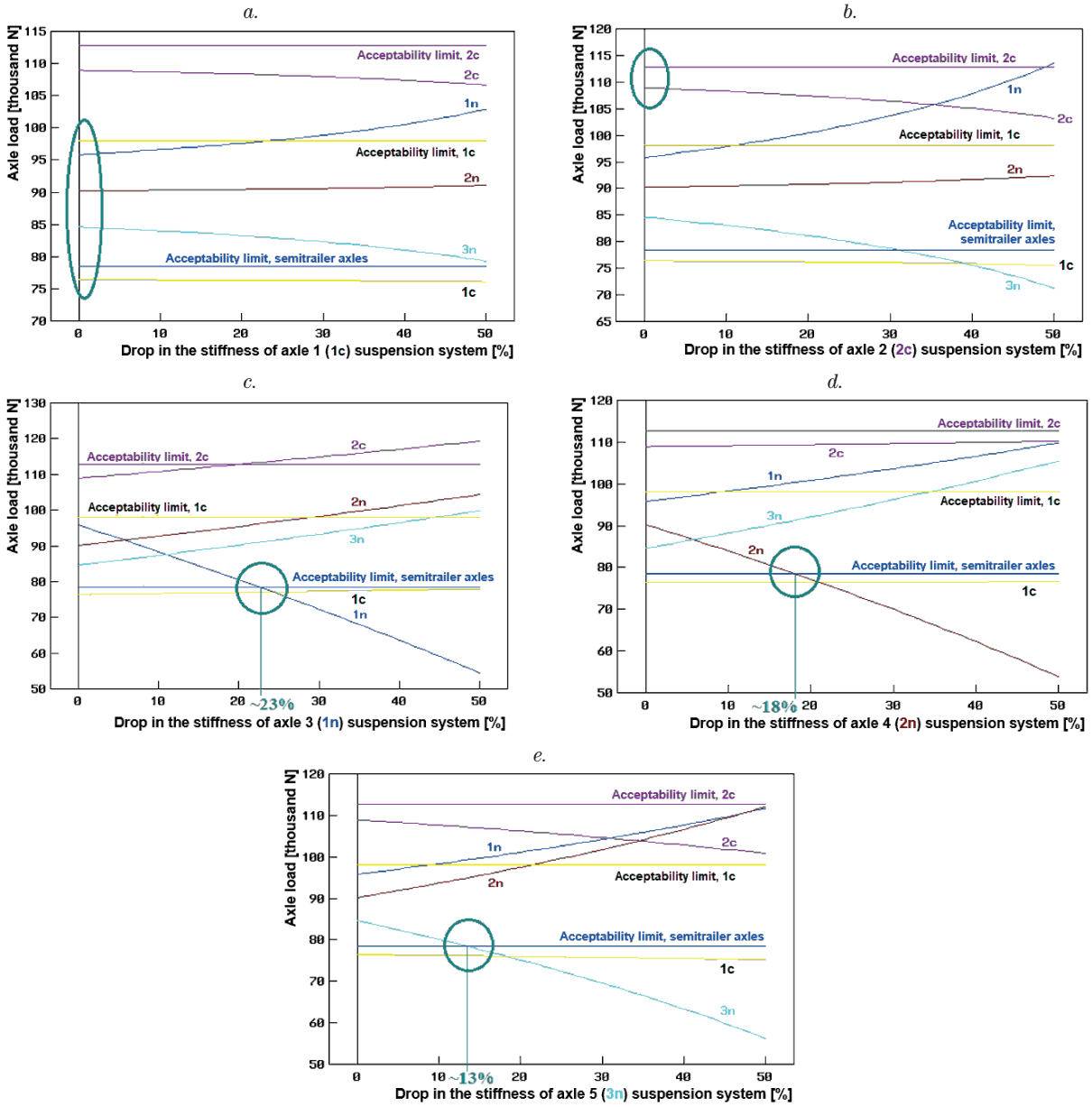

Figure 11 *Tractor-semitrailer unit. Impact of a reduction in stiffness of the suspension systems of axles 1 (a), 2 (b), 3 (c) 4 (d) and 5 (e) on the normal road reactions (axle loads) at pneumatic tyres of all the five vehicle axles*

suspension springs immediately before the axle load is measured. In consequence, a part of this load is taken over by the other vehicle axles, chiefly those next to the one under measurement.

7.1 The case with overloading the example motor truck

As mentioned before, the four-axle motor truck taken as an example for the calculations has an 8×8 drive system (it is an all-wheel drive eight-wheeler). Usually, the front axle of such vehicles is not provided with pneumatic bellows because of the confined space available, restricted by the design and mounting of vehicle's engine and steering system components. An air suspension system, whose stiffness may be varied, is provided at the 2nd, 3rd and 4th axle or at the two rearmost axles. Figure 10 shows impact of a reduction in stiffness of the suspension systems of individual vehicle axles on the normal road reactions (axle loads) at pneumatic tyres of all the four axles. The 1st axle (Figure 10a) is not overloaded. Should, however, a reduction in the stiffness of the suspension system of this axle be possible then the normal road reaction (axle load) would decline with the said drop in the stiffness of this suspension system. The load on the 4th axle would also decrease, at the expense of a growth in the loads on axles 2 and 3. Since the front axles of vehicles of this type are not usually provided with pneumatic bellows, the interference in the front axle suspension system will not be discussed here. The 2nd axle (Figure 10b) is overloaded. A decline in the stiffness of its suspension system causes a drop in the normal road reaction (axle load); namely, if this stiffness declines by as little as about 4%, the axle load drops to the

acceptability limit. A decrease in this load is accompanied by growths in the loads on the other vehicle axles. The 3rd axle (Figure 10c) is overloaded, too. Again, a decline in the stiffness of its suspension system causes a drop in the normal road reaction (axle load). Here, a load drop to the acceptability limit is achieved when the suspension stiffness is reduced by about 14%. Consistently, growths are observed in the loads on the other axles, with the lowest value of this growth being observed at the 1st axle. Overloading also takes place at the 4th axle (Figure 10d). This overload also declines with a drop in the stiffness of the suspension system of this axle, but this stiffness must be reduced by about 28% for the acceptability limit of the axle load to be achieved. In this case, the load on the 1st axle declines as well, with the loads on axles 2 and 3 increasing at the same time. Results shown in Figure 10 indicate a high potential of the presented method of interfering in measurements of normal road reactions, i.e. in determination of the loads on individual vehicle axles.

7.2 The case with overloading the example tractor-semitrailer unit

The model of a tractor-semitrailer unit, taken as an example for calculations, represents a combination of a two-axle truck-tractor having a 4×2 drive system (four wheels, two of them being driven) with a three-axle semitrailer. Here, Equation (9) should be recalled, which was adopted when the six-axle model of Figure 5 was replaced by a five-axle one. As in the motor truck case, the truck-tractor's front axle is not provided with pneumatic bellows because of confined space available, restricted by the design and mounting of vehicle's engine and steering system components. An air suspension system, whose stiffness may be varied, is sometimes provided at the 2nd tractor's axle only. On the other hand, such systems very often occur at semitrailer axles. Figure 11 shows the impact of a reduction in the stiffness of suspension systems of individual vehicle axles on the normal road reactions (axle loads) at pneumatic tyres of all the five axles. The 1st axle of the tractor (Figure 11a) is not overloaded. Should, however, a reduction in the stiffness of the suspension system of this axle be possible, then the normal road reaction (axle load) would decline (at a very low rate, hardly noticeable) with the said drop in the stiffness of this suspension system. A decrease in the load would also take place at the 2nd axle of the tractor and the 3rd (rearmost) axle of the semitrailer. Conversely, the load on the other semitrailer axles would increase (with the rate of this growth being higher at the 1st axle). As mentioned above, truck-tractors' front axles are not usually provided with pneumatic bellows; therefore, the interference in the suspension system of this axle will not be discussed here. The 2nd axle of the tractor (Figure 11b) is not overloaded, either. With declining stiffness of its suspension system, the normal road reaction (axle load) decreases and so does the load on the 3rd axle of the semitrailer and the 1st axle of the tractor (although at an insignificant rate in the latter case). This is accompanied by an increase (slight in this case) in the loads of semitrailer axles 1 and 2.

The 3rd axle of the tractor-semitrailer unit, i.e. the 1st semitrailer axle (Figure 11c) is markedly overloaded. With a decline in the stiffness of its suspension system, the load of this axle decreases, as well. The load drops to its acceptability limit when the suspension stiffness is reduced by about 23%. This process is accompanied by an increase in the load on the other vehicle axles, especially on the 2nd axle of the tractor and on the 2nd and 3rd semitrailer axle. The 2nd semitrailer axle (Figure 11d) is overloaded, too. A reduction in the stiffness of its suspension system results in a decline in the axle load, with the load acceptability limit being achieved when the stiffness is lowered by about 18%. This takes place at a simultaneous growth in the load on other vehicle axles, especially on the 1st and 3rd semitrailer axle. The 3rd semitrailer axle (Figure 11e) is overloaded and, as it is in the other cases, a reduction in its suspension stiffness causes a drop in its load, which crosses the acceptability limit when the stiffness decreases by about 13%. In such a situation, the load drops on the 2nd tractor axle and slightly declines on the 1st tractor axle, while the loads increase on the 1st and 2nd semitrailer axles. Results shown in Figure 11 indicate a considerable potential of the presented method of interfering in the measurements of normal road reactions, i.e. in determination of the loads on the axles of a vehicle combination consisting of a two-axle truck-tractor with a three-axle semitrailer. This particularly applies to the semitrailer axles.

8 Results of weighing the example vehicles while the presented methods of interfering in the stiffness of vehicle suspension systems are employed

The method of deceiving when the loads on individual vehicle axles are measured, described in Section 7, was verified for the example data adopted here to represent a four-axle motor truck and a two-axle truck-tractor with a three-axle semitrailer. Due to the vehicle design constraints (air suspension systems are mainly provided at the 2nd, 3rd and 4th axle or at the two rearmost axles of the four-axle motor trucks and at semitrailer axles), hypothetical interference (of persons wanting to affect the weighing results) was only considered for the 2nd, 3rd and 4th axle of the motor truck and for the three semitrailer axles in the tractor-semitrailer unit. This means a lower number of the vehicle axles where the suspension stiffness could be altered. An assumption was made that the suspension stiffness was reduced by 50%.

Figure 12 shows calculation results obtained for overloading of the example four-axle motor truck. They include loads on individual vehicle axles, actual vehicle weight, maximum acceptable value of the vehicle load and result of a measurement with the said interference in

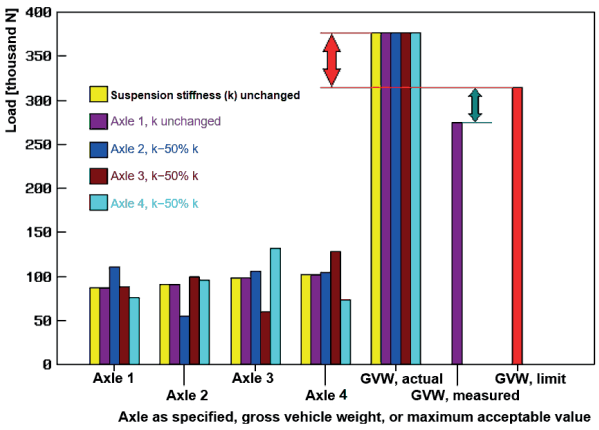

Figure 12 *Calculation results for the example four-axle motor truck overloaded by 20%, compared to the maximum acceptable load values. Loads on individual axles ("Axle 1", "Axle 2", "Axle 3", "Axle 4"), actual gross vehicle weight ("GVW, actual"), gross vehicle weight limit ("GVW, limit") and gross vehicle weight measurement result obtained with changing the suspension stiffness at axle 2, 3 and 4 as described ("GVW, measured")*

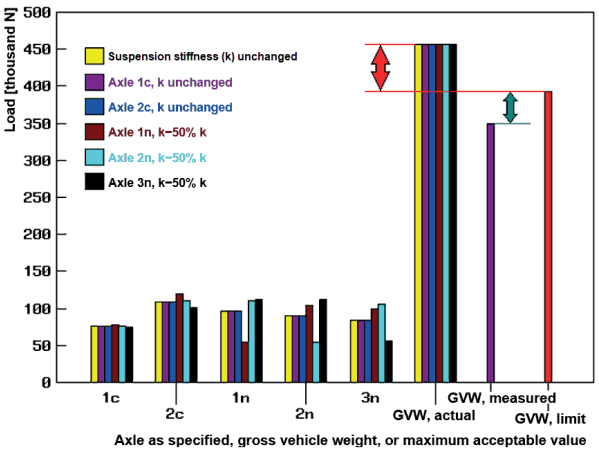

Figure 14 *Calculation results for the example tractor-semitrailer unit where the semitrailer was overloaded by 20%, compared to the maximum acceptable load values. Loads on individual axles ("1c", "2c", "1n", "2n", "3n"), actual gross weight of the vehicle combination ("GVW, actual"), maximum acceptable gross weight of the vehicle combination ("GVW, limit") and gross weight of the vehicle combination as measured with changing the suspension stiffness at semitrailer axles 1n, 2n and 3n as described ("GVW, measured")*

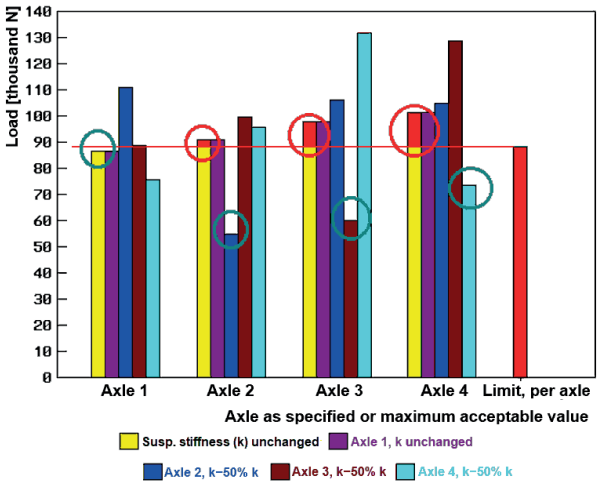

Figure 13 *Calculation results for the example four-axle motor truck overloaded by 20%, compared to the maximum acceptable load values. Loads on individual axles ("Axle 1", "Axle 2", "Axle 3", "Axle 4") and maximum acceptable axle load ("Limit, per axle"). The red rings indicate the state of overloading and the green rings indicate either the state that the acceptability limit is actually not exceeded (axle 1) or the effect of changing the suspension stiffness (axles 2, 3 and 4)*

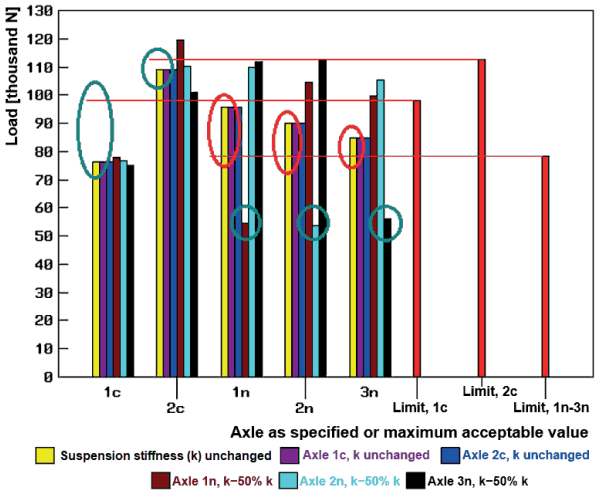

Figure 15 *Calculation results for the example tractor-semitrailer unit where the semitrailer was overloaded by 20%, compared to the maximum acceptable load values. Loads on individual axles ("1c", "2c", "1n", "2n", "3n"), maximum acceptable values for the 1st tractor axle ("Limit, 1c"), 2nd tractor axle ("Limit, 2c") and a semitrailer axle ("Limit, 1n-3n"). The red rings indicate the state of overloading and the green rings indicate either the state that the acceptability limit was actually not exceeded (tractor axles 1c and 2c) or the effect of changing the suspension stiffness (semitrailer axles 1n, 2n and 3n)*

the form of altering the stiffness of suspension systems of axles 2, 3 and 4. The vehicle weight remained unchanged during the measurements. The vehicle weight considerably exceeded the acceptability limit, which has been indicated by a double red arrow. However, the sum of results of measurements of individual vehicle axle loads was lower than the acceptability limit and this in turn has been indicated by a double green arrow. This means that the effect of seemingly lower gross vehicle weight, translated into the gross vehicle mass subject to assessment, was achieved.

Figure 13 shows the same results but rearranged to focus on the loads on individual axles compared to the applicable acceptability limits. The red rings indicate the state of overloading without any interference in the suspension stiffness. The green rings indicate either the

state that the acceptability limit was actually not exceeded (axle 1), or the effect of changing the suspension stiffness (axles 2, 3 and 4), where the load measured (scale readout) was lower than the applicable acceptability limit. In the example shown, the said interference in the stiffness of vehicle axle suspensions may be assessed as successful. For the example motor truck, the measurement results presented in Figures 12 and 13 fraudulently show that the total vehicle load and the loads on individual vehicle axles did not exceed the acceptability limits.

Figure 14 shows calculation results obtained for overloading of the example tractor-semitrailer unit. They include loads on individual tractor and semitrailer axles, actual weight of the complete vehicle combination, maximum acceptable values of the vehicle load and result of a measurement with the said interference in the form of changing the stiffness of suspension systems of the semitrailer axles (1n, 2n and 3n). The weight of the vehicle combination remained unchanged during the measurements. The vehicle weight considerably exceeded the acceptability limit, which has been indicated by a double red arrow. However, the sum of results of measurements of individual vehicle axle loads was lower than the acceptability limit and this in turn has been indicated by a double green arrow. This means that the effect of seemingly lower gross vehicle weight, translated into the gross vehicle mass subject to assessment, was achieved.

Figure 15 shows the same results but rearranged to focus on the loads on individual axles compared to the applicable acceptability limits. The red rings indicate the state of overloading without any interference in the suspension stiffness. The green rings indicate either the state that the acceptability limit was actually not exceeded (truck-tractor axles 1c and 2c), or the effect of changing the suspension stiffness (semitrailer axles 1n, 2n and 3n), where the load measured (scale readout) was lower than the applicable acceptability limit. For the tractor semitrailer unit taken as an example, the said interference in the stiffness of suspensions of the semitrailer axles specified, may be assessed as successful. The measurement results presented in Figures 14 and 15 fraudulently show that the total vehicle load and the loads on individual vehicle axles did not exceed the acceptability limits.

9 Closing conclusions

The possibility of deceit while a vehicle is weighed in motion with a very low speed has been discussed. Two authorial linear vehicle models were used in the analysis. Calculation results obtained with using a dedicated author's own simulation program ZL_WIM19 have been presented. For the calculations, data representing an example four-axle motor truck and a five-axle tractor-semitrailer unit were assumed.

The calculations show that a deceit as mentioned above is feasible. A conclusion may be formulated that a trick described herein, i.e. alteration of the suspension stiffness at predefined axles of the example four-axle motor truck, may successfully distort the vehicle weighing results, which would then fraudulently show that the axle loads and gross weight of the vehicle do not exceed the acceptable limits. For the example truck-semitrailer unit, the deceit under consideration has also been found possible and the weighing results may fraudulently show that the axle loads and gross weight of the vehicle are within the acceptable limits.

The calculation results quoted in the study should be mainly considered as qualitative only; nevertheless, their error may be expected not to be very big for the assumptions adopted as regards the example vehicles and measurement conditions.

References

[1] Announcement of the Minister of Infrastructure and Building Industry of 27 October 2016 on the publishing of a consolidated text of the Regulation of the Minister of Infrastructure and Building Industry on the technical requirements for vehicles and their necessary equipment. Warszawa: Journal of Laws of the Republic of Poland of 15 December 2016, item 2022.

[2] BURNOS, P. Weighing of road vehicles in motion. Part 1, Impact of overloaded vehicles on the pavement / Wazenie pojazdow samochodowych w ruchu. Czesc 1: Oddzialywanie pojazdow przeciazonych na nawierzchnie (in Polish). *Drogownictwo*. 2014, **6**, p. 192-196. ISSN 0012-6357.

[3] ZIOBRO, K. (Member of Parliament of the Republic of Poland). Parliamentary Question No 34607 to the Minister of Infrastructure and Development on the poor condition of road infrastructure caused by excessive vehicle loading [online] [accessed 2019-09-09]. Lancut, 2015. Available from: http://www.sejm.gov.pl/sejm7.nsf/InterpelacjaTresc.xsp?key=6BDF5971

[4] MARCZAK, P. *The impact of heavy vehicles on the condition of local roads / Wplyw ciezkich pojazdow na stan drog lokalnych* (in Polish). Warszawa: Analyses and Research Unit, Analyses, Documentation and Correspondence Office, Chancellery of the Senate of the Republic of Poland, 2009.

[5] FHA - Federal Highway *Administration. LTBP Program's literature review on Weigh-in-Motion Systems*. Publication No FHWA-HRT-160024. Georgetown Pike, 2016.

[6] BURNOS, P. Weighing of road vehicles in motion. Part 2., Types and characteristics Weigh in Motion systems / Wazenie pojazdow samochodowych w ruchu. Czesc 2: Rodzaje i charakterystyka systemow Weigh in Motion (WIM) (in Polish). *Drogownictwo*. 2014, **7-8**, p. 240-244. ISSN 0012-6357.

[7] JACOB, B., O'BRIEN, E. J. WAVE - a European research project on Weigh-in-Motion. In: National Traffic Data Acquisition Conference NATDAQ '96: proceedings [online] [accessed 2019-06-13]. 1996. Available from: http://ntl.bts.gov/lib/jpodocs/proceedn/443.pdf

[8] JACOB, B., O'BRIEN, E. Weigh-in-Motion: recent developments in Europe. 4th International Conference on WIM: proceedings. 2005.

[9] LYNDON, M., TAYLOR, S. E., ROBINSON, D., MUFTI, A., O'BRIEN, E. J. Recent developments in bridge weigh in motion (B-WIM). *Journal of Civil Structural Health Monitoring* [online]. 2016, **6(1)**, p. 69-81. ISSN 2190-5452, eISSN 2190-5479. Available from: https://doi.org/10.1007/s13349-015-0119-6

[10] Mettler Toledo. Industrial weighing and measuring. Vehicle weighing. Newsletter 13**.** Nanikon, Switzerland: Mettler-Toledo GmbH Industrial Division, 2017.

[11] Truck scales / Wagi samochodowe (in Polish) – Wagotechnika [online] [accessed 2019-06-15]. Available from: http://www.wagotechnika.pl/katalog/produkty/wagi-przemyslowe/wagi-samochodowe?gclid=Cj0KCQiAw5_fBRCSARIsAGodhk9f02 Pn3ikHaTkbTYGx3Ln_WN4uZiPYSL_Vs5wIdzYkq7X4lpygIPYaAmKyEALw_wcB

[12] Truck scales. Electronic truck scales. - Factory Wag Kalisto [online] [accessed 2018-11-11]. Available from: http://www.kalisto.pl/wagi-samochodowe/

[13] Company's publicity materials - GS Software [online] [accessed 2018-11-11]. Available from: www.gs-software.pl

[14] Truck scales: characteristics and specifications – Herkules [online] [accessed 2018-11-11]. Available from: http://herkules-wagi.pl/wagi-samochodowe/

[15] All-embracing weighing systems / Kompleksowe systemy wazace (in Polish) - MASA Zenon Kolankowski [online] [accessed 2019-06-14]. Available from: www.masa.com.pl

[16] Truck scales. Weighing platforms for road vehicles / Wagi samochodowe dla pojazdow drogowych. Pomosty wagowe dla pojazdow drogowych (in Polish) - Mettler Toledo [online] [accessed 2018-11-11]. Available from: https://www.mt.com/pl/pl/home/products/Transport_and_Logistics_Solutions/Truck_Scales/road_bridge.html

[17] Weighbridge DFT-E – Schenck [online] [accessed 2018-11-11]. Available from: https://www.schenckprocess.com/pl/products/truck-pit-scale-dft-e

[18] Truck scales / Wagi samochodowe (in Polish) – Uniwag [online] [accessed 2018-11-11]. Available from: https://uniwag.pl/Oferta/wagi_samochodowe_-_elektroniczne/1/

[19] Innovative truck scales - a way to a success / Innowacyjne wagi samochodowe - droga do sukcesu (in Polish) - Wagen-Mont Pawel Montowski [online] [accessed 2018-11-11]. Available from: http://www.wagen-mont.pl/?gclid=Cj0KCQiAw5_fBRCSARIsAGodhk_D-TfXj365g5DIindF_-PTNMvIxJLI0FsE3OpKsx6mwI44hzyGAJ8aAq38EALw_wcB

[20] Truck scale INPT011 - Aliexpress [online] [accessed 2018-11-11]. Available from: https://pl.aliexpress.com/item/20t-capacity-wireless-dynamic-portable-vehicle-axle-weighing-truck-scale-weigh-bridge-weight-pads-weighing-scale/32702594284.html

[21] Portable truck scales. WWS system - Dini Argeo [online] [accessed 2018-11-11]**.** Available from: http://www.ewp.com.pl/wagi-samochodowe/wagi-przenosne

[22] DANIEK, S. *System of vehicle preselection by weight on roads administered by ZDW Lodz. Intelligent system of vehicle preselection by weight on roads administered by ZDW Lodz as an example of the "SMART" integrated system of road traffic management and meteorological protection / System preselekcji wagowej pojazdow w ZDW Lodz. Inteligentny system preselekcji wagowej pojazdow na drogach ZDW Lodz jako przyklad zintegrowanego systemu oslony meteorologicznej i zarzadzania ruchem „SMART"* (in Polish). Krakow: TRAX elektronik Sp. J., 2010.

[23] WIM PRO 2.0 system - APM PRO sp. z o.o. [online] [accessed 2019-06-14]**.** Available from: https://apm.pl/systemy/wim/

[24] Electronic catalogues - DTR VMS Italy [online] [accessed 2019-06-17]. Available from: https://www.dtrvms.it/en/market-and-products/trucks

[25] Engineering Manual and Design Guide 2013 – Firestone [online] [accessed 2019-03-08]. Available from: www.firestoneip.com https://www.firestoneip.com/content/dam/fsip/pdfs/airide/commercial-air-spring-catalog-EU-east.pdf

[26] Design manuals - Saf-Holland Group [online] [accessed 2019-03-08]. Available from: https://corporate.safholland.com/en/company/about-us/history

[27] LOZIA, Z. Vehicle dynamics model as road-pavement load generator. *Engineering Transactions*. 2000, **48**(3), p. 243-259. ISBN 0867-888X.

[28] LOZIA, Z. *Analysis of biaxial car motion based upon dynamic models / Analiza ruchu samochodu dwuosiowego na tle modelowania jego dynamiki* (in Polish). A monograph. Warszawa: Prace Naukowe Politechniki Warszawskiej, 1998. ISSN 1230-9265.

[29] LOZIA, Z. Examples of authorial models for the simulation of motor vehicle motion and dynamics. *Proceedings of the Institute of* Vehicles. 2015, 104(4), p. 9-27. 1642-347X.

[30] ARCZYNSKI, S. *Mechanics of motion of the motor vehicle / Mechanika ruchu samochodu* (in Polish). Warszawa: WNT, 1993. ISBN 83-204-1488-1.

[31] KAMINSKI, E., POKORSKI, J. *Automobile theory. Dynamics of suspension systems and powertrains of motor vehicles / Teoria samochodu. Dynamika zawieszen i ukladow napedowych pojazdow samochodowych* (in Polish). Warszawa: WKL, 1983. ISBN 832060348X.

METHOD OF THE FINITE-ELEMENT MODEL FORMATION CONTAINING THE 3D ELEMENTS FOR STRUCTURAL CALCULATIONS OF THE REINFORCED CONCRETE STRUCTURES CONSIDERING THE CRACK OPENING

Sergei N. Nazarenko*, Galina A. Grudcina

RUT (MIIT), Moscow, Russia

*E-mail of corresponding author: s.nazarenko@mail.ru

Resume

This article presents the 3D computational modeling method for reinforced concrete structures. An example of calculation of the reinforced concrete beam, using the Finite Element Method in SCAD++ following proposed algorithm, is given. Results comparison to the analytical calculation of the model with selected reinforcement is presented. For concrete, the 3D solid Finite Elements are used and the 3D beam elements for reinforcement. The model is formed using AutoCAD and AutoLISP, which creates a text data file in SCAD format for the description of model. In addition, computation of the 3D model of the crossbar with a crack is performed. Crack sizes are set in the stretched zone based on data from initial calculation. Graphic results obtained in SCAD++ are presented.

Article info

Received 5 May 2020
Accepted 10 August 2020
Online 30 November 2020

Keywords:

concrete structures,
finite element method,
3D elements,
cracks in concrete,
SCAD++,
AutoCAD,
AutoLISP

Available online: https://doi.org/10.26552/com.C.2021.1.D15-D25

ISSN 1335-4205 (print version)
ISSN 2585-7878 (online version)

1 Introduction

The reinforced concrete (RC) structures can have various applications in construction, such as beams, slabs, shells, massive structures, often of a complex shape, defined by the architectural features of the designed structure and construction process. The reinforced concrete structures calculation, based on standard approaches, does not define an adequate model for the stress-strain state, both in concrete and in reinforcement due to multiple reasons, such as crack propagation in concrete, complex geometry and structural dimensions, not allowing the use of beam theory.

Currently, engineers use the rod elements for calculations of the reinforced concrete structures, as a creation of volumetric elements and complex shape, is a very difficult and time-consuming process. Appearance of cracks is allowed by standards [1]. However, as shown in results of simulation performed in this article, appearance of even minor cracks noticeably increases stresses in the reinforcement rebars. Such consequences cannot be considered in calculations without using the 3D elements.

Calculation of the crack formation and size of the crack opening is important to ensure the bearing capacity of the reinforcement and durability of the reinforced concrete structures. The paper [1] presents a comparative analysis of the existing SP calculation methods for the normal crack formation, based on a nonlinear deformation model. For simple types of structures, the joint venture allows calculation according to a simplified method (by limiting forces). Usually, an assumption to perform calculations, using simplified methods, is organized in such a way that the obtained results provide a margin of reliability. However, that is not valid in the case of the normal crack opening width analysis, as shown in the article [1].

Remaining within the same normative document, the spread of acceptable crack opening values can exceed 50 % [1].

If one considers problems with reinforcement in a compressed zone and stronger concrete, the discrepancies between the deformation and force approach can increase up to 200 - 300 % [1].

As a result, it can be concluded that in order to solve the described problem, the development of methodology that allows to determine as accurately as possible the value of crack opening in reinforced concrete structures is needed.

The purpose of this article is to present a method of a complex strength calculation of reinforced concrete elements, allowing to consider the factors mentioned above and to obtain more precise values of the elements stress-strain state, including reinforcement, considering

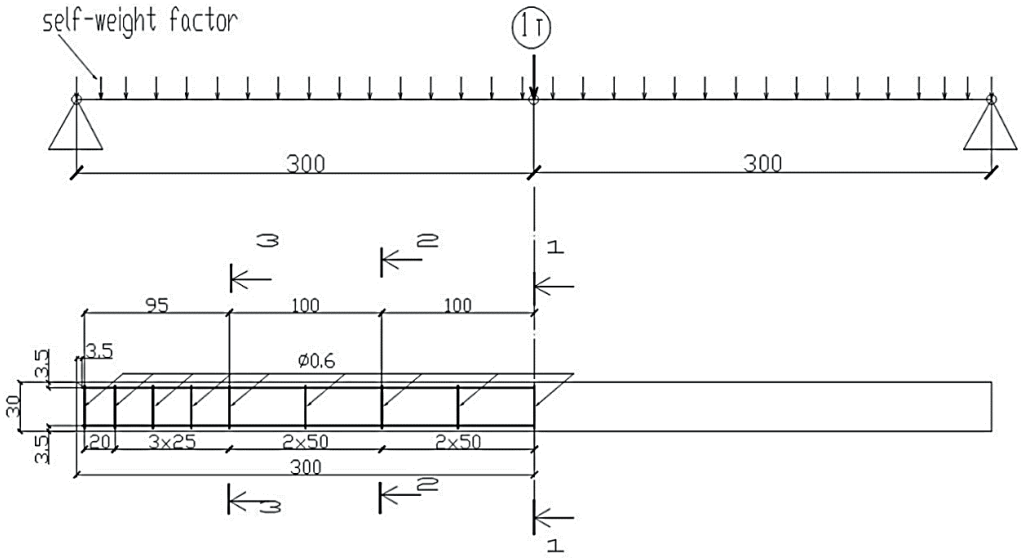

Figure 1 *Scheme of the reinforced concrete beam (dimensions in cm) loaded with distributed load from the self- weight factor and concentrated load on the symmetry axis*

occurrence and opening of cracks. The method is based on application of the 3D solid finite elements with maximum automation of labor-intensive processes of the 3D model creation.

2 Methodology

To solve the problem of specifying the calculated values of stress-strain state in reinforced concrete structures, it is proposed to define their models as the 3D objects for the FEM calculation, with use of Solid 3D Finite Elements (FE) for modeling concrete and Beam FE for modeling reinforcement. The resulting difficulties can be divided into three categories:

1. The large number of the 3D finite elements required to obtain enough accuracy of the FEM calculations when forming the 3D model.
2. The complex geometry of a structure, which causes difficulties in forming input data of the FEM model.
3. Difficulties of the model assembling when joining nodes of the 3D FE modeling concrete and Truss FE modeling rebars.

To solve these problems, the following is used:

SCAD FEM complex for strength analysis and solid-state eight-node iso-parametric 3D finite element from SCAD++ library, other possibilities used for solid-state modeling, given in article [2]. SCAD is an integrated system for the finite element structural analysis and design. Software is chosen because of its wide range of finite elements and calculation modes available and, at the same time, the possibility to use the standard documents for reinforcement and cross-section. As a result, the software is well-ranked and widely used in engineering practice [3-11]. Multiple comparative results analyses proved calculations accuracy compared to other software: SAP2000 [12], ETABS [13], MIDAS GTS NX [14], Tekla Structures [15-16], PLAXIS [17].

1. SCAD provides data exchange with other programs using:
- universal formats (IFC, CIS/2, DXF, DWG, TXT);
- data formats of Advance Steel, ANSYS, STAAD, Abaqus, Femap, GMSH, NetGen;
- plugins for Revit, ArchiCAD, Tekla.

2. AutoCAD software to define a beam reinforcing frame of RC models, networks in the foundation of solid 3D models and their nodal coordinates using AutoCAD graphic database.
3. Program, developed by S. N. Nazarenko using AutoLISP language, embedded in AutoCAD, which is also described in the article [18], automatically creating a text data file in SCAD format [18-19] for a FE model, consisting of 3D FEs.

This program automatically generates arrays of topology and coordinates for the finite element model, then generates text data file in SCAD format for definition of the 3D model sub-structures. Volumetric sub-structures are then joined together, merging with the core elements in SCAD++ assembly procedure, as well. More details about program realization on AutoLISP for formation of covers are also available in [2, 18-19]. Problems of modeling and calculating massive structures of bridges, supports and other 3D structures, based on their parametric dimensions, were solved by this program. Using this program in conjunction with AutoCAD allows optimizing SCAD 3D modeling of structures and reducing time consumed.

3 Example

The developed method is demonstrated using an example of the reinforced concrete beam with rectangular cross-section. It should be mentioned that the proposed method can be used for calculation of the reinforced concrete structures with more complex cross-sections, as well.

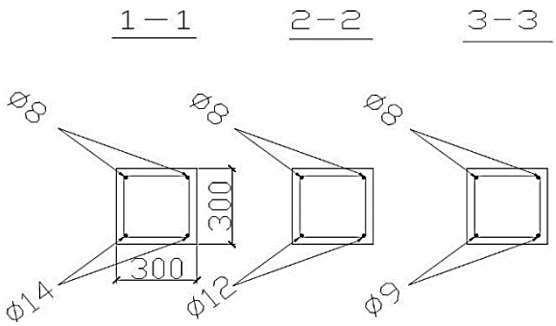

Figure 2 *Results of selection of the longitudinal rebars and structural transverse armature of reinforced concrete beam from Figure 1, specified according to the standards (dimensions in mm)*

Table 1 *Concrete working conditions ratios*

concrete	concrete type: heavy	concrete class: B25
	concrete working conditions ratios	
γ_{b1}	considering long-acting loads	0.9
γ_{b2}	considering the nature of the destruction	1
γ_{b3}	considering the vertical position when constructing	1
γ_{b5}	considering freezing/thawing and negative temperatures	1

For the girder shown in Figure 1, calculation is done in system SCAD++ for the purpose of the subsequent comparison of results for two models:

The first model: the beam model, results of deflection determination for this model are shown in Figure 3;

The second model: the 3D model formed by solid 3D finite elements used for concrete, which were combined in SCAD++ by means of assembly with beam elements simulating reinforcement. The process of forming the 3D model of the girder is shown in Figures 4-6. Results of its calculation are shown in Figures 7-14.

4 Standard method

At the first step, the calculation of the girder is performed and modeling it with the rod elements, using the standard methodology described in SP [20-22].

Selection of reinforcement was carried out by SP 63.13330.2012.

The following parameters were used:

- element type - bendable beam element;
- load case - uniaxial bending;
- maximum reinforcement percentage- 10%.

Longitudinal reinforcement of class A400steel rebars and transverse reinforcement of class A240 steel rebars were used for calculation. Concrete working conditions ratio 1 was applied.

For the concrete, the parameters specified in Table 1 were used.

By iteration and meeting the above conditions, the maximum value of crack opening, equal to 0.388 mm, is obtained.

For the girder shown in Figure 1, the calculation was carried out in the SCAD++ system to compare the results of calculations of two versions model: the beam and 3D.

Next is presented an analysis of the SP recommendations [20-22]. The width of opening of normal cracks is calculated by formula:

$$a_{crc,i} = \varphi_1\varphi_2\varphi_3\psi_s \cdot \frac{\sigma_s}{E_s} l_s. \quad (1)$$

where:

σ_s - is the stress in a longitudinal rebars in tension in its normal cross-section with a crack from the corresponding external load;

ψ_s - the coefficient considering the non-uniform distribution of relative deformations of stretched reinforcement between cracks;

l_s - basic (without considering the influence of the rebars surface type) distance between adjacent normal cracks;

φ_1 - coefficient taking into account duration of the load;

φ_2 - coefficient taking into account profile of the longitudinal fitting;

φ_3 - coefficient taking into account nature of the load.

The stress values in the tensioned rebars of the bending elements are determined by the formula:

$$\sigma_s = \frac{M(h_0 - y_c)}{I_{red}} \cdot \alpha_{sl}, \quad (2)$$

where:

I_{red} and y_c - moment of inertia and height of the compressed zone of the element's reduced cross-section, respectively, defined taking into account the cross-section area only of the compressed zone of concrete, areas of section of the stretched and compressed armature, taking into account

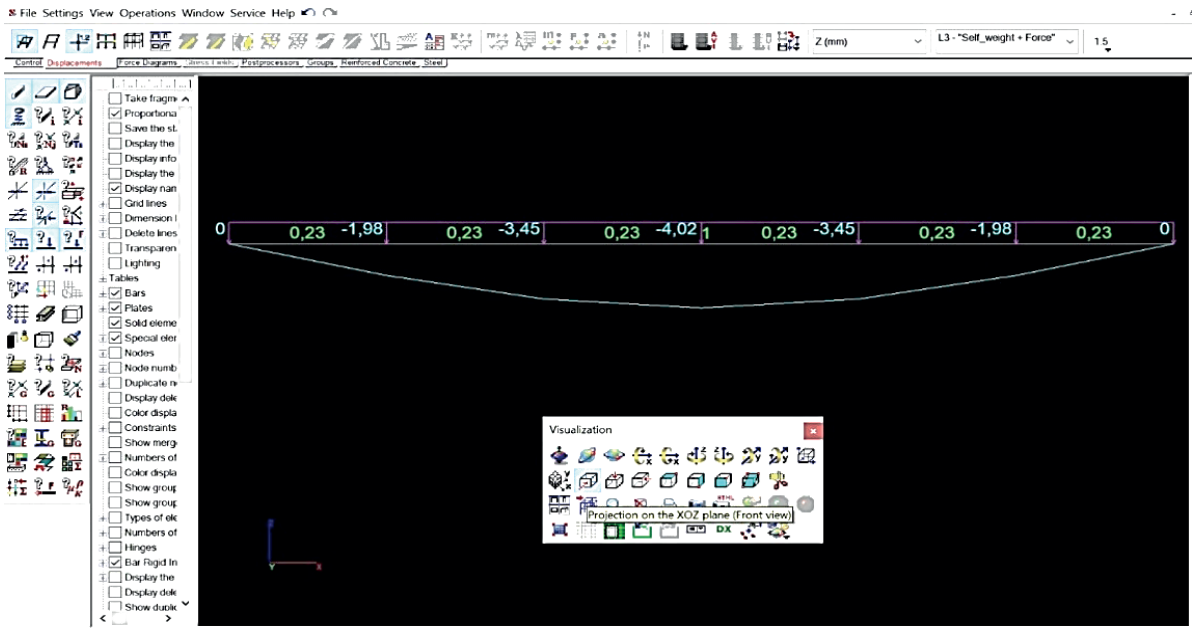

Figure 3 *Results of the beam deflection calculation using SCAD*

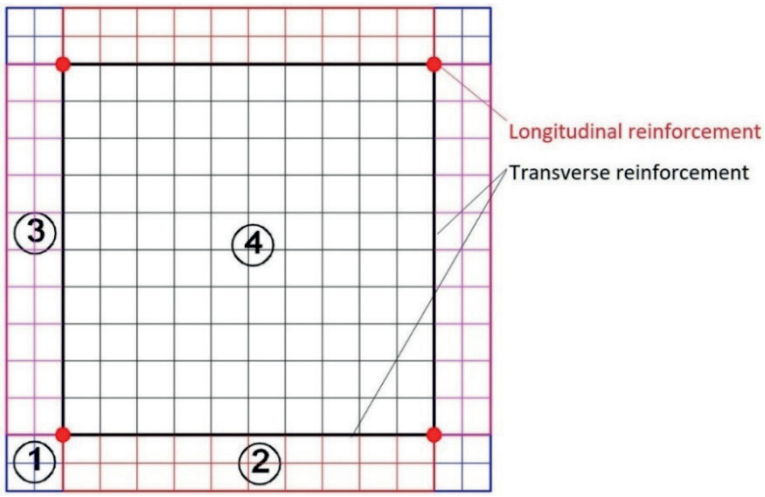

Figure 4 *Networks AutoCAD with numbers of separated segments of the RC beam, used to create the 3D FE model*

values of factor of reduction of armature to concrete, in corresponding formulas;

h_0 - operational height;

y_c - for bending elements $y_c = x$, where x is the height of the compressed concrete zone.

α_{sl} - coefficient of adduction.

According to SP, the following options can be applied:

- The coefficient $\psi_s = 1 - 0.8\frac{\sigma_{s,crc}}{\sigma_s}\cdot$ or $\psi_s = 1 - 0.8\frac{M_{crc}}{M}$
- Crack initiation moment $M_{crc} = 1.3R_{bt,ser}W_{red}$ (W_{red} defined with or without assuming the reinforcement);
- Stress $\sigma_s = \frac{M(h_0 - y_c)}{I_{red}}\cdot\alpha_{sl}$ or $= \frac{M}{z_s \cdot A_S}$
- the distance from the center of gravity of the stretched rebars to the point of application of resulting force in the compressed zone of the element $z_s = h_0 - \frac{x}{3}$ or $z_s = 0.8h_0$

Similarly, $\sigma_{s,crc}$ - tension in the longitudinal stretched reinforcement in the section with a crack immediately after the formation of normal cracks.

5 New method

After obtaining the stress-strain state and cracks opening by the standard method, following are the stages of formation and calculation of the 3D model of a beam with application of the 3D solid FE and crack modeling, using axial symmetry for a beam from Figure 1, what reduces the number of FE twice. We use the AutoCAD software. The cross-section in the middle of the beam is given in Figure 4. For formation of model of the 3D FE, it is necessary

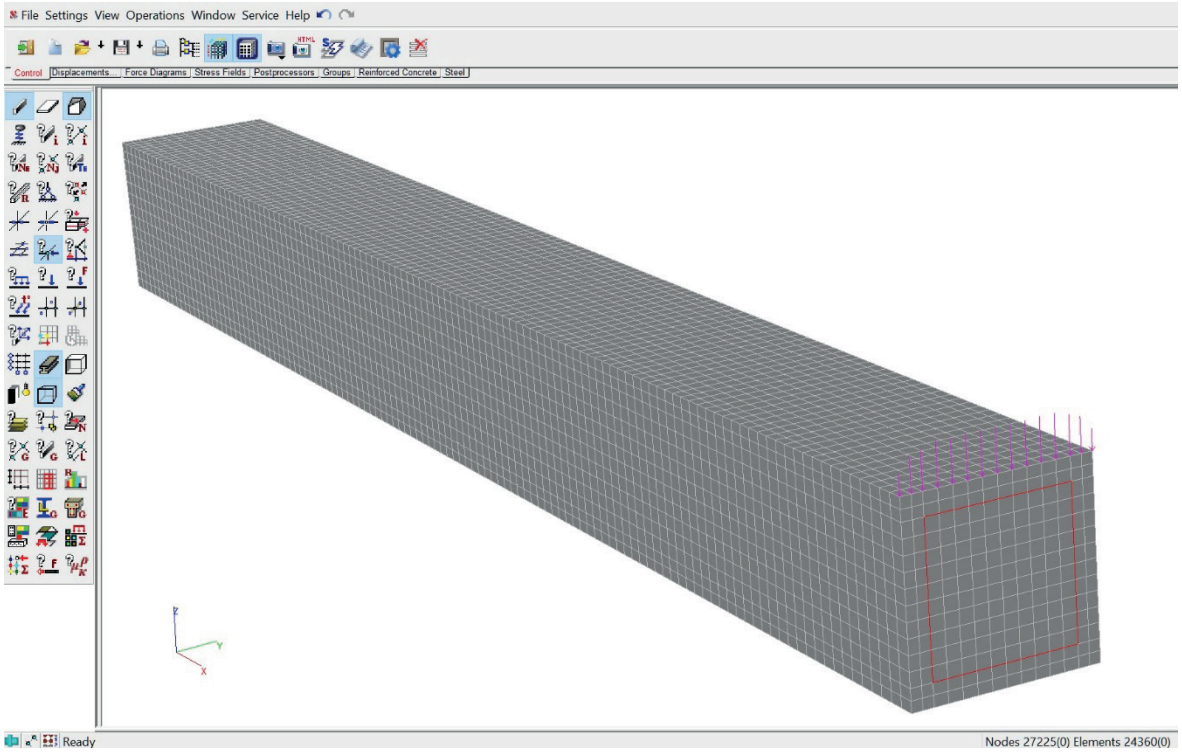

Figure 5 *Visualization in SCAD++ of a concrete part assembled from substructures of the 3D model. Reinforcement rebars in the middle section of beam and concentrated load are also given.*

to divide section into segments filled with primitives NETWORK in AutoCAD as it is shown in Figure 4.

In Figure 4, four contours represented by different colors in cross-section of a beam are filled by networks on AutoCAD edges using EDGESURF command. The number of splits on two adjacent overlapping edges of a network can be set randomly by assigning values of AutoCAD SURFTAB1 and SURFTAB2 system variables, but these values should be the same in the connected contours. AutoCAD accurately divides the boundary edges of network contours into a specified number of sections of equal length, even if the boundaries are curved. Possible small errors in definition of coordinates by AutoCAD are eliminated in SCAD during the assemblage with the set accuracy. Grids 1,2,3 in Figure 4 have the symmetric sites marked by identical colors. Thus, it is sufficient to form four structures from sub-networks, all the other parts of model are formed in SCAD using the assemblage procedure.

The number of divisions in the cross-section in this example is relatively small, but after setting the number of the 3D FE along the axis of the beam, even considering the symmetry, the total number of finite elements was 24360. However, that is far from exceeding the possibilities of system SCAD and can be increased by an order of magnitude.

In a longitudinal direction, the length of the 3D FEs is chosen such that:

The nodes of the 3D elements along the longitudinal axis of the structure coincide with the nodes of the transverse structural reinforcement, the location of which is shown in Figures 1, 2 and 6;

Dimensions of the 3D finite elements would be close to the topological cube, which gives better accuracy of calculations in the FEM procedures.

In other possible cases of modeling reinforced concrete structures with more irregular placement of the transverse rebars than in this example, additional 3D sub-structures by length can be introduced, which can be grouped into separate parts that are joined during the assembly in SCAD.

Further, each separate sub-network, shown in Figure 4, by dismembering of an initial network by a command AutoCAD, is filled with primitives 3DFACE. The program AutoLISP, forming the text description of each substructure, is started. The resulting sub-structure is then uploaded into SCAD and saved as a separate SCAD project file. Then, it is proceeded to the final assembly of the model from 3D parts of the structure modeling concrete. The description of this process can be found in the article [18]. Result of an assembly for this example, is presented in Figure 5. For the created model, it is possible to set in SCAD the missing calculation components such as rigidity of 3D elements, units with support, load, before the further final assembly with the substructure modeling the reinforcement.

To simulate the rebar, the AutoCAD LOCK and MASSIVE commands were initially used. To make the nodes of 3D beam (AutoCAD segments) and the nodes of the 3D solid elements coincide, the MASSIVE command is used (Figure 6). Then, after receiving the two files of the AutoCAD drawing with the segments simulating longitudinal and transverse rebars, they are exported to SCAD in DXF format for the subsequent assemblage with substructure (Figure 5), simulating concrete. Each of the two drawings

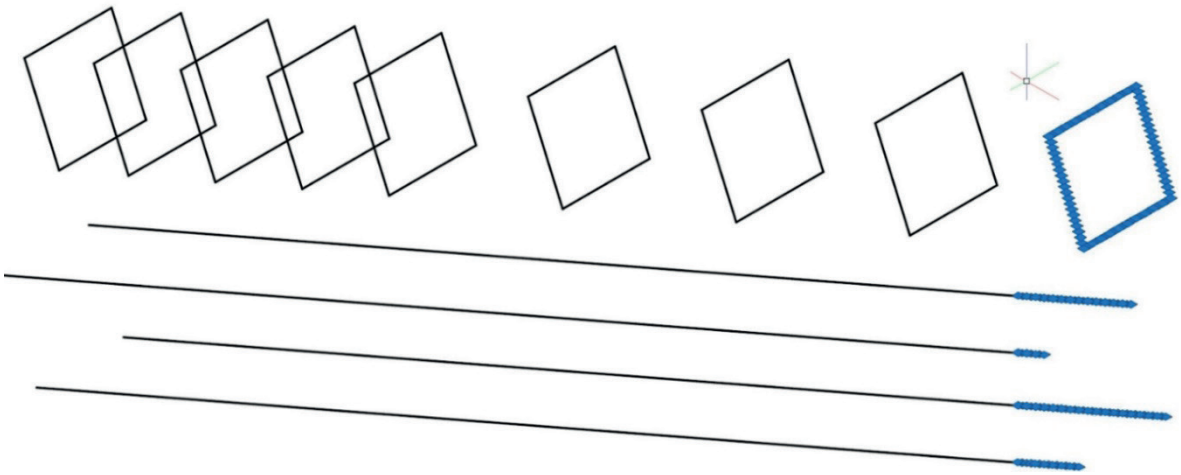

Figure 6 *AutoCAD drawing, showing the rebar, longitudinal and transverse, a total of 480 lines. Some of them are marked with grips on the right-hand side in the drawing*

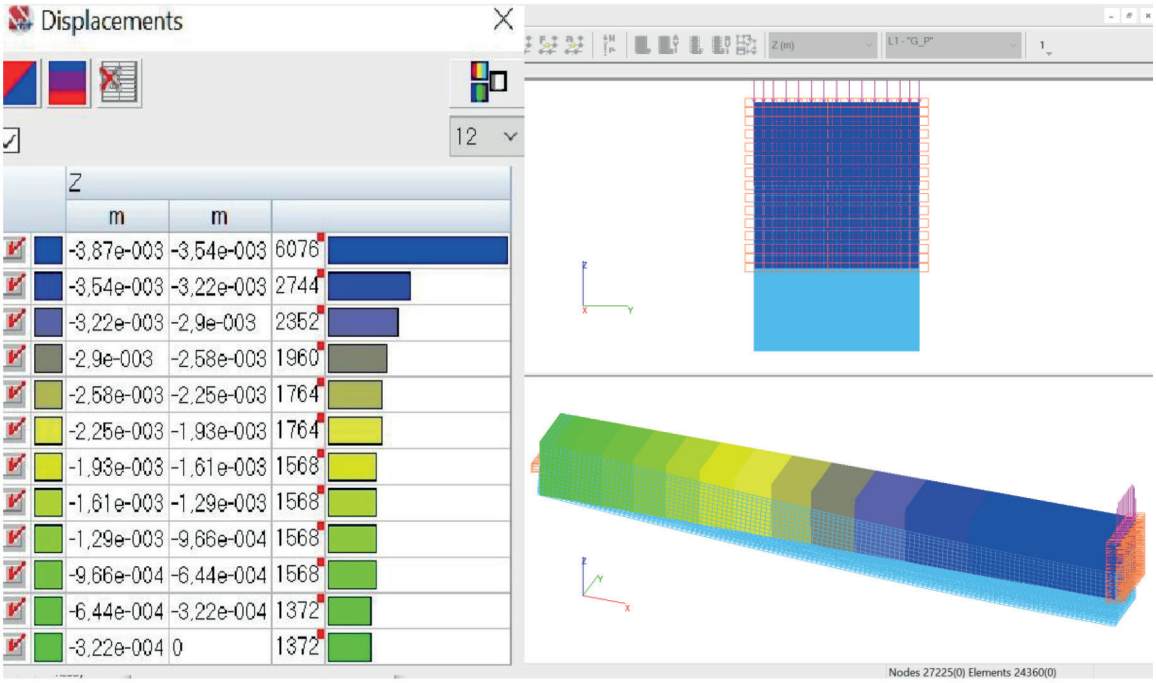

Figure 7*Projections of displacements on the Z axis from the self-weight factor and from the load, simulating the concentrated force from Figure 1, the deformed scheme of the 3D calculation concrete + rebars model, in SCAD*

of the reinforcement, longitudinal and transverse, in order to facilitate the task of rigidity definition in SCAD, is exported separately, then combined with the model of concrete in the assembly procedures in SCAD.

6 Results

Some results of calculation in SCAD for the 3D model of the concrete beam, combined in assemblage with steel rebars, are shown in Figures 7-10.

The maximum value of displacement in the Z-axis direction, obtained in the model calculation, is equal to $-3.87e^{-003}$ m, or 3.87 mm in the downwards direction. The comparative analysis of difference in deflection values of the beam (calculated numerically) and 3D model gave 0.05 mm or 1.25%. The smaller deflection value obtained for the 3D model in comparison to the beam model can be explained by considering the rigidity of the transverse rebar and more accurate distribution of rigidity in the volume of the 3D model compared to the beam theory.

In Figure 7 are also shown the fixed nodes and the axial load (Figure 1), distributed along the transverse line of symmetry in the upper part.

Figures 8 and 9 display the load replacing the concentrated force shown in Figure 1 with calculated force values, considering the symmetry and the unequal spacing between the units, applied to the concrete. The table allows to determine the height of the stretched zone in the critical cross-section along the axis of symmetry of the girder with the maximal internal forces (right-hand end with the applied load).

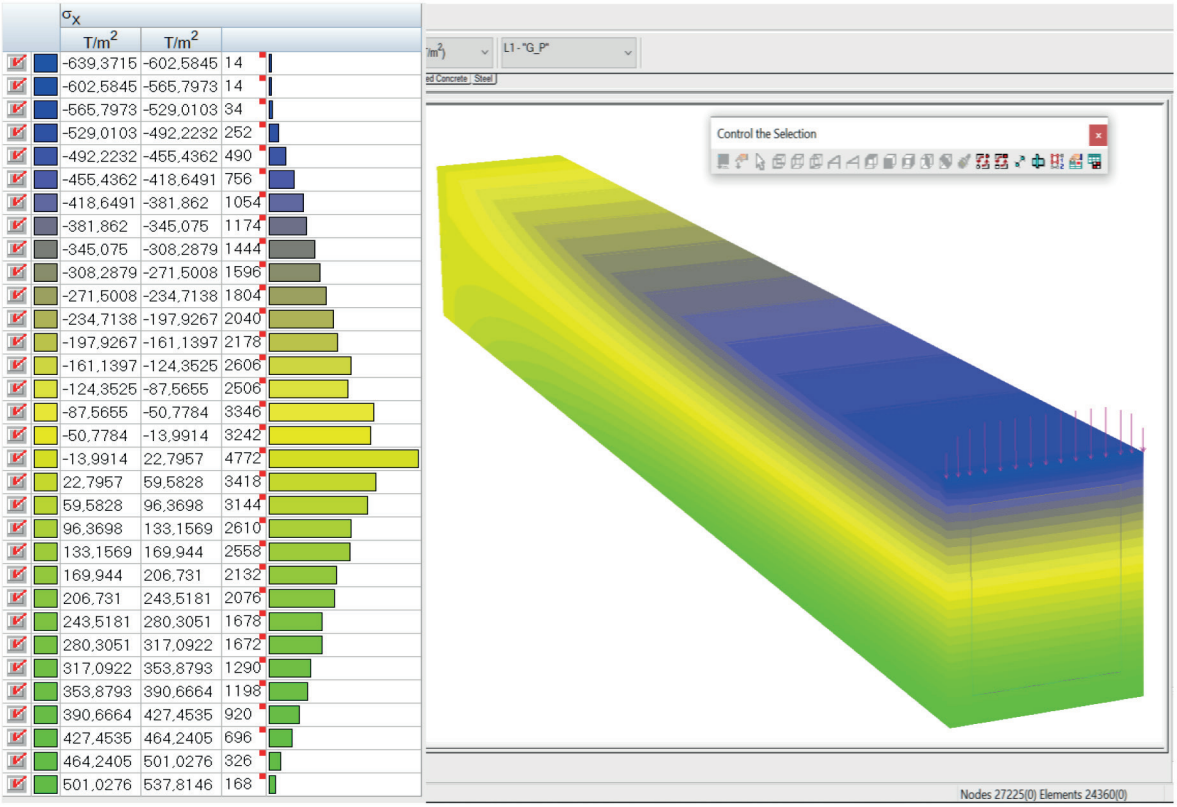

Figure 8 *SCAD stress isofields of σ_x in the direction of the longitudinal axis X on a 3D model*

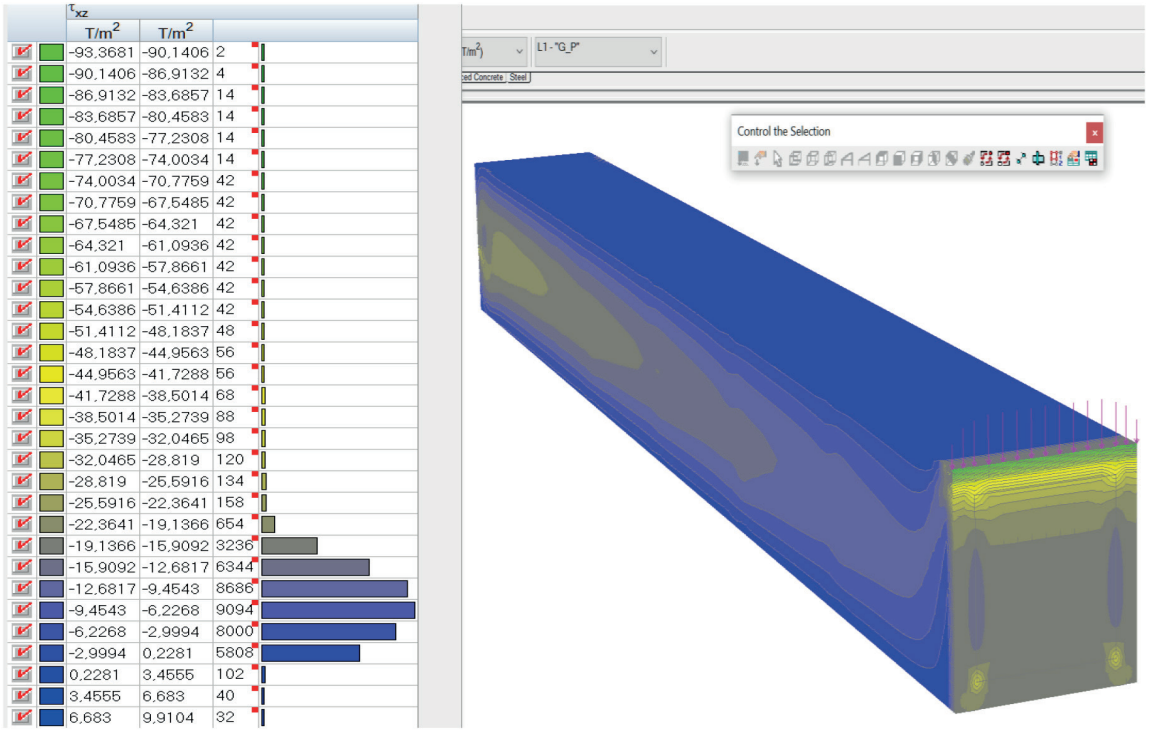

Figure 9 *Isofields and isolines of tangential stresses τ_{xz} in the model*

In determining the stress-strain state, the plot of the tangential stress τ_{xz} distribution can be of interest. In comparison to the theoretical formulas of materials resistance, a significant difference between the τ_{xz} plot and the picture shown in Figure 9, is obtained, which can be explained by influence of the transverse reinforcement.

After obtaining the precise stress-strain state using the 3D solid FE for the concrete modeling and beam FE for the reinforcement, it is proceeded to the cracks modeling and their opening determination.

Then, it is proceeded to modeling of a crack located in the most loaded cross-section, along the axis of symmetry

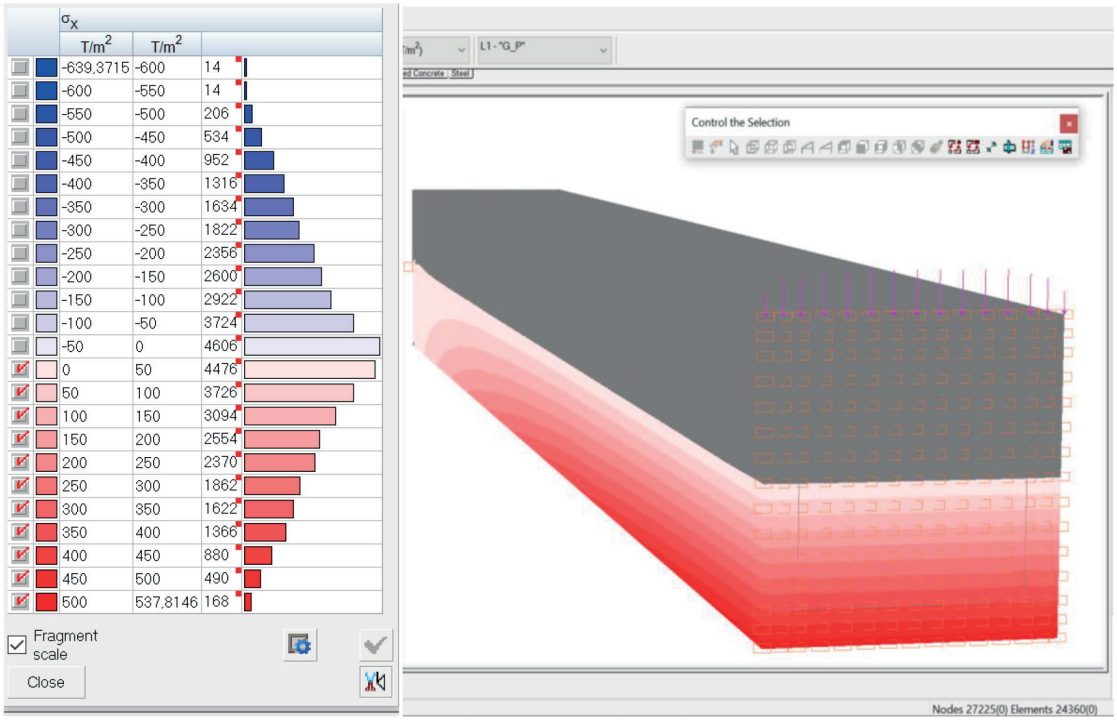

Figure10 *Isofields and isolines σ_x in the structure without crack. Coloring in the compressed and compressed-stretched zone is switched off*

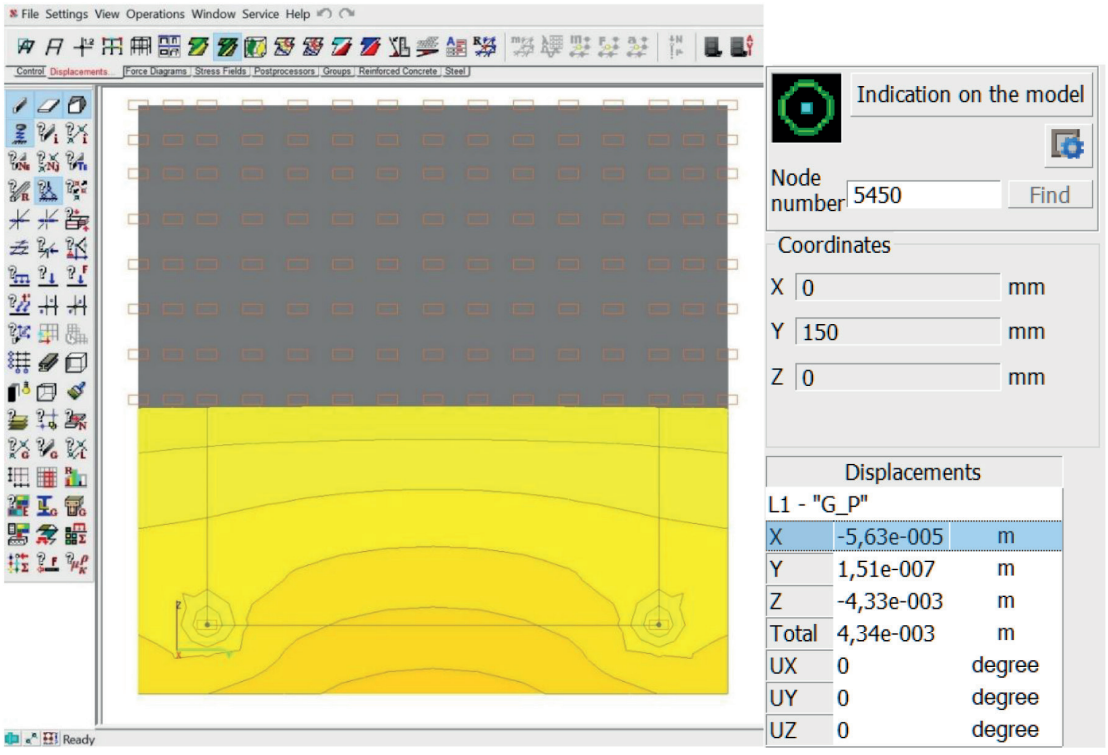

Figure 11 *Isofields and isolines of X displacement in cross-section with modeled crack at the first stage of crack development*

of the reinforced concrete beam (see Figures 8, 10). The height of a crack development is determined by stress σ_x isopolls preliminary calculated in SCAD++. In Figure 10, obtained based on the calculation results, coloring of the model in a compressed and compressed-strained zone is disabled by means of SCAD++. The stretched zone of the structure, in the right cross section, as it follows from Figure 8, extends to the middle of the section height.

The crack is modeled by removing the longitudinal connections at the right-hand end of the beam, along the symmetry axis, to the height of the lower half of cross-section. In this case, appearance of a crack in this section

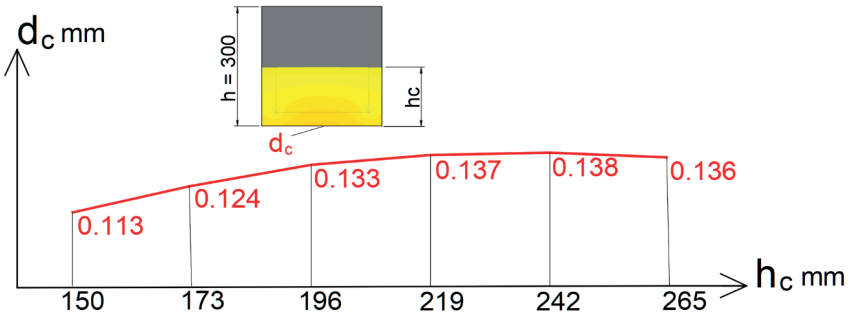

Figure 12 *Relation between the maximum crack opening value d_c and crack height h_c*

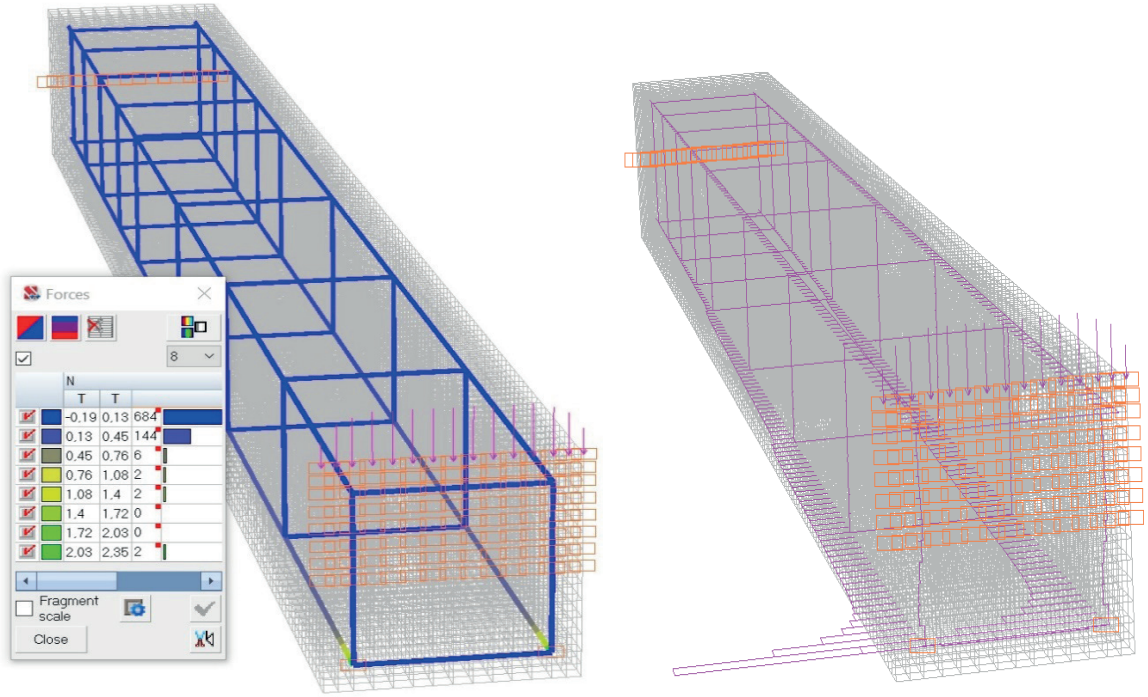

Figure13 *Diagrams of longitudinal forces N in the reinforcement rebars of the calculated RC structure with a crack*

will lead to displacement of the lower edge to the left, because this accepted section with the crack is located in the symmetry plane. The calculation of this structure is performed.

As a result of the structure calculation, with a modeled crack, the obtained value of maximum deflection - displacement in the Z-axis, has increased by 11.9 %, up to - 4.33 mm.

Some other calculation results in SCAD++ 3D model with a crack are shown in Figures 11 and 12. Longitudinal movements in the section along the axis of symmetry of the beam - opening of the assumed crack, are shown in Figure 11.

Figure 11 also shows regions in the area of the bottom longitudinal rebars, painted grey, with zero displacement along the X axis due to longitudinal bonds defined in these nodes. The connections in the assumed stretched area are also shown in the form of rectangles above the cross-section. The maximum value of the crack opening as given in the table in Figure 11, is: 0.0563×2 = 0.113mm (multiplied by 2 assuming displacements in the symmetrical part of structure). Six calculations were performed, with longitudinal connections with the assumed crack being removed on one row above at each of the subsequent steps.

The graph of the d_c maximum crack opening values variation, obtained in calculation for each stage of crack development, is presented in Figure 12.

The longitudinal forces N in the reinforcement rebars in the cross section with a crack have increased significantly compared to the calculated values obtained in calculation of the beam without a crack. The N-plots in rebar are shown in two views in Figure13 with the table of values N, also the fixation points are indicated.

It should be noted that the location of cracks in the proposed 3D model of reinforced concrete structures, their length and direction of development, require additional theoretical and experimental justification. Cracks can also be simulated by dividing in SCAD++ the neighboring bulk finite elements by their contact boundaries.

The two models' calculations results were compared by the crack opening values: 0.388 mm according to the standard method and its maximum value 0.138 mm obtained from the 3D model calculation.

Results of the modeling were compared to results obtained by the method established in [22], which is based on stochastic and probabilistic approaches for the characteristics of reinforcement and concrete and is confirmed by extensive practical tests [23-24]. The characteristics used in the calculations with 95% probability will not exceed the characteristics in real constructions. Safety factors are applied. Thus, this technique provides a guarantee that the results obtained from it will not exceed the critical values included in the SP [22]. According to the standards for this type of construction and operating conditions, the crack opening value should not exceed 0.4 mm [22]. The crack growth to a compressed zone (opening width 0.1126 mm) and then to the moment when the crack stopped (0.138 mm), is simulated. Multiple cracks were modeled, at each stage, the crack opening value was fixed and the most dangerous crack was selected (Figure 12). At the maximum length of the crack, the opening value was 0.138 mm. This corresponds to the criterion defined by standards and is less than those obtained using the method mentioned above [20-22].

The results obtained are less than those calculated according to the standard method, possibly due to the fact that the model took into account the volume work of concrete, longitudinal reinforcement in the compressed and stretched part of the structure, transverse reinforcement.

Results of the two models' calculations are compared according to the crack opening values: 0.388 mm according to the standard method and 0.1126 mm obtained from the 3D model calculation. These results showed that the obtained value of the crack opening is more than 3 times less than calculated according to the norms, which may be due to the fact that the model that was built took into account the volume action of concrete, longitudinal reinforcement in the compressed and stretched part of the structure, transverse reinforcement.

7 Conclusions

Result of the work, presented in this article, is development of methods for formation of the 3D finite element models of reinforced concrete structures with use of the bulk finite elements for the modeling of concrete and rod elements, modeling rebar, allowing strength calculation of reinforced concrete beams, taking into account crack opening. This applies not only to beam structures, but to the reinforced concrete structures almost of any shape, as well. The proposed method allows modeling cracks in concrete and obtaining the values of crack opening considering the work of longitudinal reinforcement located in a stretched and compressed zone of the structure, transverse reinforcement, which cannot be done using the existing standards. The stress-strain state parameters, obtained by the precise model, allow optimization reinforcement parameters, analyze and consider stress concentrators with possible reinforcement and reinforcement of non-standard cross-sections. Developed program, applied in this article, can be also applied into another FEM software supporting the corresponding file exchange formats. It allows to optimize as much as possible the process of modeling of the massive reinforced concrete structures and thus to reduce time costs.

References

[1] PERELMUTHER, M. A., POPOK, K. V., SKORUK, L. N. *Calculation of the width of disclosure of normal cracks under SP63.13330.2012 ocncrete and reinforced concrete* (in Russian). Vol. 1. 2014, p. 21-22.

[2] KARPILOVSKIY, V. S., KRIKSUNOV, E. Z., MALYARENKO, A. A., FIALKO, S. Y., PERELMUTER, A. V., PERELMUTER, M. A. *SCAD Office. Ver. 21. Computer complex SCAD++ / Vychislitelnyy kompleks SCAD++* (in Russian). Izdatelstvo SKAD SOFT, Izdatelskiydom ASV, 2015.

[3] FIALKO, S., KARPILOVSKYI, V. Multithreaded parallelization of the finite element method algorithms for solving physically nonlinear problems. In: Federated Conference on Computer Science and Information Systems: proceedings.2018. Vol. 15. p. 311-318.

[4] FIALKO, S., KARPILOVSKYI, V. Triangular and quadrilateral flat shell finite elements for nonlinear analysis of thin-walled reinforced concrete structures in SCAD software. In PIETRASZKIEWICZ, W., WITKOWSKI, W. (eds.) *Shell structures: theory and applications* [online]. Vol. 4. London, New York: CRC Press Taylor & Francis Group,2017, p. 367-370. eISBN 9781315166605. Available from: https://doi.org/10.1201/9781315166605

[5] 11th international conference Shell structures: theory and applications SSTA 2017: proceedings. CRC Press, 2017. ISBN 978-1138050457.

[6] GAVRILENKO, I. S., GIRENKO, S. V., PERELMUTER, A. V., PERELMUTER, M. A., YURCHENKO, V. V. Load-bearing capacity as an interactive analysis tool in SCAD Office. In: METNET Seminar 2017 in Cottbus: proceedings. 2018. p. 112-127.

[7] NAZARENKO, S. N., GRUDCINA, G. A. Methods of generation of calculation models of structures with monolithic ceiling panels of an arbitrary form (in Russian). *Design Bureau*. 2016,**12**(125), p. 18-23.

[8] FIALKO, S., KARPILOVSKYI, V. Spatial thin-walled reinforced concrete structures taking into account physical nonlinearity in SCAD software. Rod finite element. In: 13th International Conference Modern building materials, structures and techniques: proceedings.2020.p. 728-735.

[9] NUZHDIN, L. V., MIKHAYLOV, V. S., VOSKRESENSKIY, M. N. Methods for subsoil modeling under dynamic impacts and multicomponent damping in SCAD FEA software with geophysical monitoring.*Journal of Physics: Conference Series* [online]. 2020,**1425**, 012096. ISSN 1742-6588.Available from: https://doi.org/10.1088/1742-6596/1425/1/012096

[10] FIALKO, S. Y. Dynamic analysis of the elasto-plastic behaviour of buildings and structures in the SCAD++ software package. *Journal of Physics: Conference Series* [online]. 2020,**1425**, 012041. ISSN 1742-6588. Available from: https://doi.org/10.1088/1742-6596/1425/1/012041

[11] FIALKO, S., KARPILOVSKYI, V. Time history analysis formulation in SCAD FEA software. *Journal of Measurements in Engineering*[online].2018, **6**(4), p. 173-180. ISSN 2335-2124, eISSN 2424-4635. Available from: https://doi.org/10.21595/jme.2018.20408

[12] GRUDCINA, G. A., SOKOLOVA, I. I., BATURKIN, D. A. TUN TUN, U. Methods of graphic information transmission for modeling of complex transport infrastructure structures operation using CAD systems. *Quality. Innovations. Education*. 2017, p. 32-37.

[13] BATURKIN, D. A., GRUDCINA, G. A., REZNIKOVA, E. R. Methods of formation and transfer of graphic information for modeling of objects of a transport infrastructure. Priority directions of science development in the modern world. In: Collection of articles on the materials of the international scientific-practical conference: proceedings. Part 1. 2019. p. 89-93.

[14] SEMENOV, A. A., KILDIBAEV, R. S. Integration of software complexes MIDAS GTS NX and SCAD 21.1 for the solution of interdisciplinary design problems. *Industrial and Civil Construction*. 2016, **5**, p. 72-75.

[15] KUKUSHKIN, I. S., LYUBIMOV, I. Y. Ways to automate the design of supporting structures for equipment using communication technology: SMART 3D - Tekla Structures - SCAD Office. *International Journal for Computational Civil and Structural Engineering*. 2015, **11**(3), p. 126-132. ISSN 2587-9618, eISSN 2588-0195.

[16] KUKUSHKIN, I. S. Implementation of Bilateral Communication between Software Complexes Tekla Structures and SCAD Office v.21.*Industrial and Civil Construction*. 2014, **9**, p. 63-65.

[17] MANGUSHEV, P. A., SAKHAROV, I. I., KONYUSHKOV, V. V., LANKO, S. V. Comparative analysis of numerical modeling of "building-basis" system in SCAD and PLAXIS software packages. *Vestnik Civil Engineers*. 2010, **3**, p. 96-101.

[18] NAZARENKO, S. Automation of creation of volume models for strength calculation in SCAD by means of AutoCAD AutoLISP (in Russian). *CAD and Graphics* [online]. 2015,**6**, p. 90-94. Available from: https://sapr.ru/article/24935.

[19] NAZARENKO, S. Automation of strength calculations in SCAD shells - models created in AutoCAD (in Russian). *CAD and Graphics* [online]. 2010, **2**, p. 69-70.Available from: https://sapr.ru/article/21196

[20] Methodical manual calculation of reinforced concrete structures without prestressed reinforcement. NIISF RAASSN. Moscow, 2015.

[21] SP.63.13330.2012. Standard. Concrete and reinforced concrete structures. General provisions. Updated edition of SNiP 52-01-2003 (approved by Order of Ministry of Regional Development of Russia dated 29.12.2011 N 635/8).

[22] Manual for the design of concrete and reinforced concrete structures from heavy concrete without prestressed reinforcement (to SP 52-101-2003), 2005, p. 155.

[23] GOST 24452-80 Concrete. Methods for determination of prismatic strength, modulus of elasticity and Poisson's coefficient.

[24] GOST 26633-91 Concretes heavy and fine-grained. Technical specifications (as amended N 1, 2).

komunikácie
COMMUNICATIONS

Dear colleague,

Journal Communications - Scientific Letters of the University of Zilina are a well-established open-access scientific journal aimed primarily at the topics connected with the field of transport. The main transport-related areas covered include Civil engineering, Electrical engineering, Management and informatics, Mechanical engineering, Operation and economics, Safety and security, Travel and tourism studies. The full list of main topics and subtopics is available at: *http://komunikacie.uniza.sk/index.php/communications/topics*

Journal Communications - Scientific Letters of the University of Zilina are currently indexed by EBSCO and SCOPUS.

We would like to invite authors to submit their papers for consideration. We have an open-access policy and there are no publication, processing or other fees charged for published papers. Our journal operates a standard double-blind review procedure, the successful completion of which is a prerequisite for paper publication.

The journal is issued four times a year (in January, in April, in July and in October).

I would also like to offer you the opportunity of using already published articles from past issues as source of information for your research and publication activities. All papers are available at our webpage: *http://komunikacie.uniza.sk*, where you can browse through the individual volumes.

For any questions regarding the journal Communications - Scientific Letters of the University of Zilina please contact us at: *komunikacie@uniza.sk*

We look forward to future cooperation.

Sincerely

Branislav Hadzima
editor-in-chief

IMPROVING INITIAL POPULATION FOR GENETIC ALGORITHM USING THE MULTI LINEAR REGRESSION BASED TECHNIQUE (MLRBT)

Esra'a Alkafaween[1,*], Ahmad B. A. Hassanat[1,2,3], Sakher Tarawneh[1]

[1]IT Department, Mutah University, Karak, Jordan
[2]Computer Science Department, Community College, University of Tabuk, Tabuk, Saudi Arabia
[3]Industrial Innovation and Robotics Center, University of Tabuk, Tabuk, Saudi Arabia

*E-mail of corresponding author: esrakafaween86@gmail.com

Resume

Genetic algorithms (GAs) are powerful heuristic search techniques that are used successfully to solve problems for many different applications. Seeding the initial population is considered as the first step of the GAs.

In this work, a new method is proposed, for the initial population seeding called the Multi Linear Regression Based Technique (MLRBT). That method divides a given large scale TSP problem into smaller sub-problems and the technique works frequently until the sub-problem size is very small, four cities or less. Experiments were carried out using the well-known Travelling Salesman Problem (TSP) instances and they showed promising results in improving the GAs' performance to solve the TSP.

Article info

Received 9 March 2020
Accepted 11 May 2020
Online 20 October 2020

Keywords:

genetic algorithm,
population seeding,
TSP,
multi linear regression

Available online: https://doi.org/10.26552/com.C.2021.1.E1-E10

ISSN 1335-4205 (print version)
ISSN 2585-7878 (online version)

1 Introduction

Genetic Algorithm (GA) is one of effective and robust machine learning algorithms [1]. Many studies were concerned with Genetic Algorithms (GA) and exploited its capabilities in designing smart systems and solving problems [2-4]. The genetic algorithms are concerned, in general, with how to produce new chromosomes (individuals) that possess certain features through recombination (crossover) and mutation operators [5-6]. Therefore, individuals with appropriate characteristics have the strongest chance of survival [7]. Typically, the GAs start with a number of random solutions (initial population); this is the first phase in the GA. This phase generates a set of possible solutions randomly or by heuristic initialization. Although the initial population seeding phase is executed only once, it has an important role to improve the GA performance.

The GA aims to produce many solutions to solve specific problems, such as a problem of the TSP, which is a common issue in Artificial Intelligence area [8-9]. Several previous studies dealt with insight in the GA procedure to indicate its procedure and how it can be exploited to solve sophisticated problems, such as finance, medical, mathematical and technical ones [10-11].

Efficiency of the GA is based on many factors, such as initial population, crossover operator, mutation operator and selection strategy [12]. In this paper, a new enhanced initial population is proposed to increase the GA performance.

The proposed technique distinguishes from other previous techniques, where it divides the problem into sub problems using the regression line, which indicates the relationship between the points in the xy coordinates. Each sub problem results from intersection between the regression line and the rotated line at the center point. Then, the initial population is determined by reconnecting each sub problem. Results of experiments show that the proposed technique is of high efficiency through different aspects: improvement in error rate, average convergence and convergence diversity. This work contribution is in proposing a new enhanced approach to generate the initial population to be used in solving the decision-making problems, especially the TPS problem. Each individual in population is called chromosome, which will be presented as a solution [13]. Then, sampling this initial population will generate an intermediate population. Therefore, it is possible to apply reproduction, crossover and mutation on the new intermediate population [14]. This process is repeated until reaching the desired number of generations or a convergence adopted in the design is reached. Hence, initializing population is necessary in order to start the process of evolution in the GA [15].

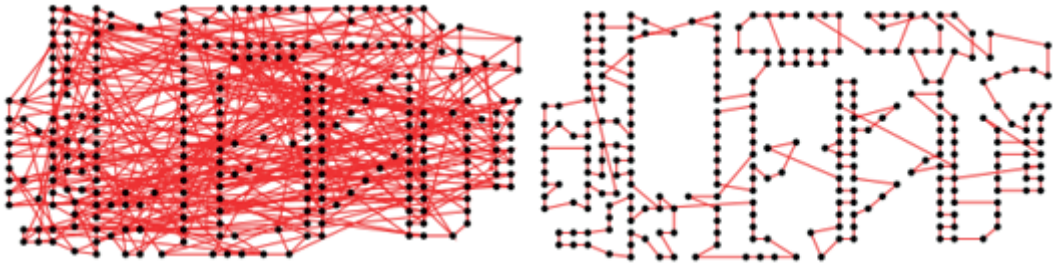

Figure 1 *Random Initialization and K-mean initialization*

2 Related work

Various initialization techniques have been introduced since the GA concepts appeared, such as random technique, nearest neighbor technique, Gene Bank (GB) technique, K-means clustering technique and Initialization Mechanism Based on Regression techniques. The randomization technique is considered as one of the most suitable and most used technique for generating the seed of the initial population. However, it may contain a poor fitness solution that reduces the possibility of finding the optimal solution.

Here is briefly presented a background review of several of the initial population seeding techniques that are used for the GAs.

A. Random initialization technique

This technique is widely used in machine learning algorithms and it is used widely in GA because it is the simplest way to initialize population seeding. In addition, the researchers prefer this technique especially when the prior data about expected optimal solution is trivial. As shown on the left-hand side of Figure 1, the successive cities of the initial solutions are chosen randomly, where the right-hand side shows initializing using the K-means [16]. This figure shows the difference between the random initialization and any other initialization techniques such as K-means. Most researchers use the sentence "generate an initial population" to indicate that they use random initialization technique. In the case of the TSP, random initialization selects the cities randomly and it generates random numbers from 1 up to (n) for each city. As shown in study [17], "if the current individual already contains the generated number, then it generates a new number. Otherwise, the generated number is added to the current individuals". Hence, this process is repeated until reaching the desired individual size (n).

B. Gene bank initialization technique

The Gene Bank is considered as a database of initial population to be used as solutions based on quality and diversity [18]. In the case of the TSP, each city that the salesman travels to is called N and permuted and assembled to build a gene bank. Then, encoding the nearest cities C to the city in order to be encoded to build a gene bank and noting that C should be less than (N-1). As a result, the Gene bank is given as a matrix A where its size is (C × N). For example, A[i][j] is an element in the matrix (Gene Bank) is the j-th city to city i. Therefore, the first row in the Gene Bank includes the C closest cities for city i. For each solution, the initial city i is initialized randomly from the row i in the Gene Bank. "After that, the method selects city j, where j is the nearby one in the unvisited elements of the i-th row. Then, city k is selected from the j-th row of gene bank as the next city. If all the city codes of the j-th row have been selected, then next city is chosen randomly from the set of unvisited cities" as mentioned by [18]. Thus, this process is repeated until generating the solution of the size N.

C. Nearest neighbor initialization technique

The nearest neighbor (NN) is known as the most common initial population seeding technique. In addition, NN can be used as an efficient random initial population method to be used for the purpose of generating initial population solutions, especially in the case of the TSP (to be solved with GA). The process of generating each individual begins by randomly selecting a city to be the starting city; then, adding the nearest city to the starting city as the new starting city. Thus, the nearest city that was not added to the current city is added to the individual until all the cities are included in the individual. Therefore, as the next generations that were created from a city nearest to the current city, the generated individuals would enhance the evolving search process [19].

D. K-means initial population (KIP)

To improve the process of initializing population of the GA, several studies used K-means clustering algorithm, especially in the case of the TSP problem, such as [20-22]. These studies used the k-means clustering to split a large-scale of the TSP into small groups k, where $K = [\sqrt{N} + 0.5]$ and N denotes number of cities. Then, the KIP is applied to the GA to find the local optimal path for each group and a global optimal path that connects each local optimal solution.

E. Initialization mechanism based on the regression techniques

A new initialization technique has been designed to improve the GA for solving the well-known TSP. It is based on the the Regression line and the perpendicular line that crosses the regression line at the center point to divide a large-scale TSP problem to small sub-problems. The resulting sub-problems are repeatedly classified to fit

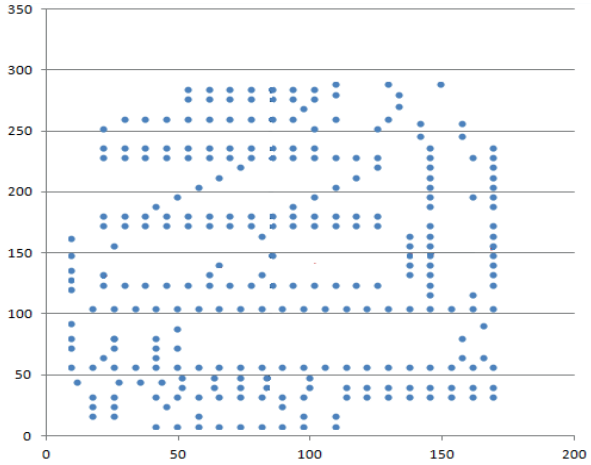

Figure 2 *The (x, y) scatter for the TSP city (a280)*

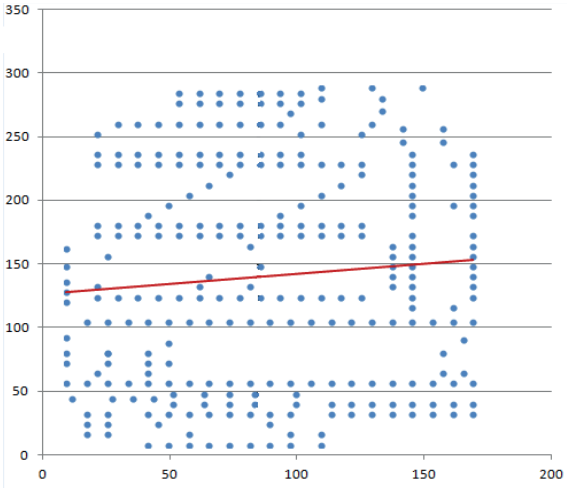

Figure 3 *The regression line*

into the four categories to obtain local optimal solutions [23].

Procedures of the proposed method **firstly** start with dividing the large-scale TSP into the four small sub-problems using Regression line and the perpendicular line and then classify the points into four categories. Each category is divided into four new categories recursively, by using the Regression line and the perpendicular line. The process carries on until having the target category that contains a small number of instances (x, y points). Maximum four cities or x, y points are assigned to each category that are considered as initial population for the TSP sub-problem. The process ends up when the local optimal solution is obtained for each category.

Second, rebuild the initial populations seeding by reconnecting all the local optimal solutions together. Finally, mutate the initial population N times to obtain N solutions, where N is the population size.

The research, presented in this paper, is compared to that research, because it already outperformed the two methods of seeding the population: random and the nearest neighbor.

3 The proposed method

This paper aims to propose a new initialization technique, which has been designed to enhance the GA at the aim of solving the problem of the TSP. The proposed technique is called (Multi Linear Regression Biased Techniques (MLRBT). This technique aims to divide the TSP problem into small sub-problems. In addition, it works depending on the Regression line on X and Regression line on Y, where it crosses the regression line at a point, which is not necessary to be in the center. Then, the previous process is repeated on the resulted sub-problems and classified in order to fit into the four categories to obtain local optimal solutions.

The main procedures of the proposed method include two main steps:

- Initially, the large-scale TSP problem is divided into four small sub-problems by using regression line on X and the regression line on Y. Then, the method classifies the resulting points into four categories. Then, recursively, dividing each category into new four sub-categories through the Regression line on X and Regression line on Y. The previous process will continue until reaching the optimal target category, which includes a small number of instances (x, y) points. Maximum is four cities or (x, y) points assigned to each category that are considered as initial population for TSP sub-problem. The process ends up when the local optimal solution is obtained for each category.
- Secondly, reconnecting all the local optimal solutions together in order to rebuild the initial populations seeding. Finally, to obtain N solutions, the method mutates the initial population N times, where N denotes the population size.

To show how regression population seeding works, Figure 2 shows the main steps by using one of the TSP cities (a280).

The following steps illustrate design of the MLRBT:

Step 1: dividing the points into two categories by using the regression line equation ($y=a + bx$). As shown in Figure 3, each section includes almost an equal number of nodes.

Step 2: this step aims to divide the points into two sections using the regression line equation ($x = a + by$), then, the diagram is divided into four equal sections where each section includes an equal number of cities as shown in Figure 4.

Step 3: In this step, the diagram is divided into four sections as shown in Figure 5:

- Section 1: (A is all the points above the positive x-axis and to the right of the positive y- axis).
- Section 2: (B is all the points above the negative x- axis and to the left of the positive y- axis).
- Section 3: (C is all the points below the negative x- axis and to the left of the negative y- axis).
- Section 4**:** (D is all the points below the positive x-axis and to the right of the negative y- axis).

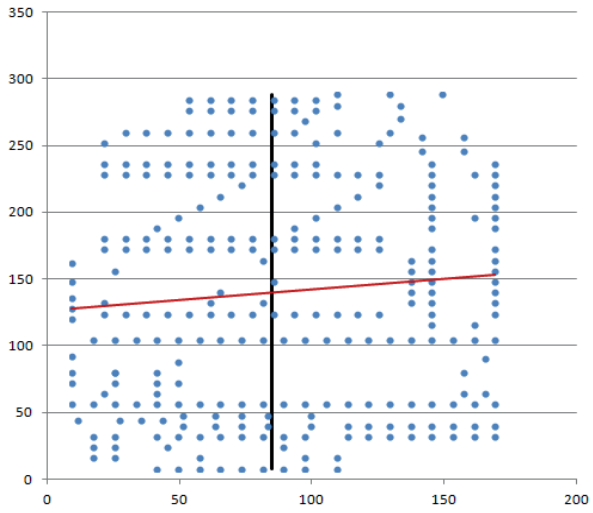

Figure 4 *Regression on x line, which intersects with the regression y line*

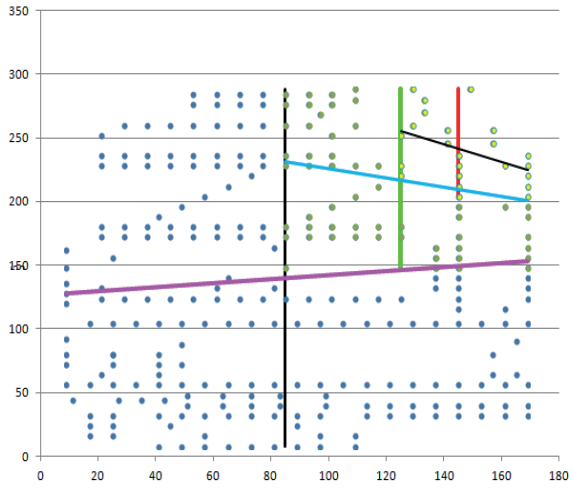

Figure 6 *Implementation of the regression line algorithm on category A (+, +)*

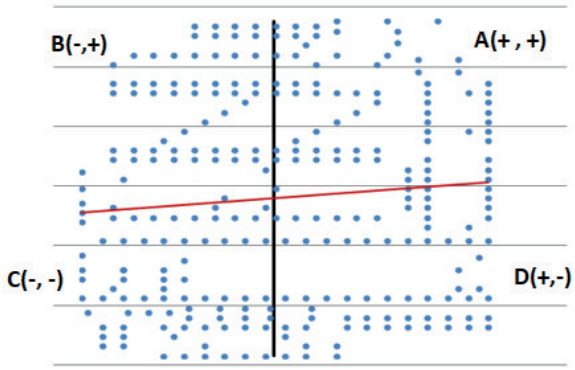

Figure 5 *A, B, C and D categories that generated from the intersect between regression line on x and y*

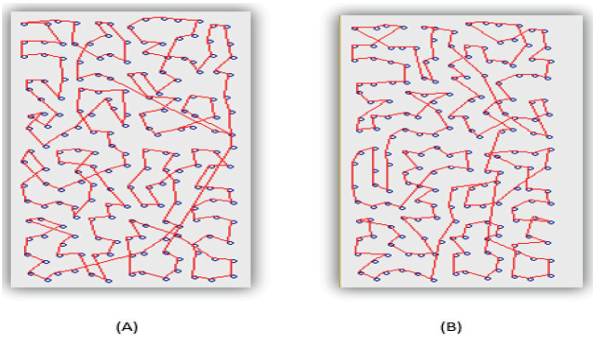

Figure 7 *(A) The initial solution for a280 using [23], (B) The initial solution for a280 using MLRBT*

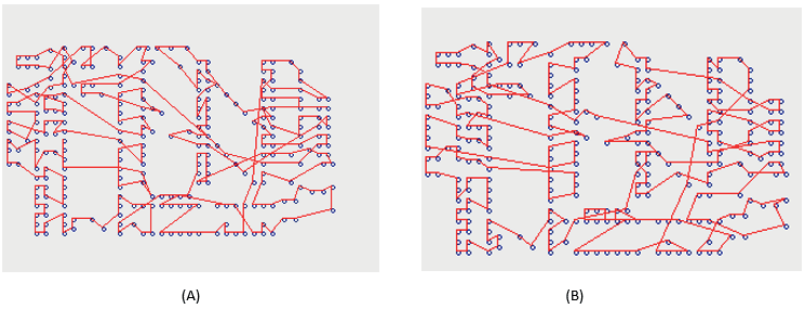

Figure 8 *(A) The initial solution for rat195 using [23], (B) the initial solution for rat195 using MLRBT*

Step 4: repeating the method recursively four times on all categories: (A), (B), (C) and (D), as shown in Figure 6.

Step 5: Terminate the recursive call, if the number of points (cities) is less than or equal four. Since the algorithm uses the regression line, it guarantees that the small number of cities that it ends with are more likely to be neighbors and closer to each other from the other cities. Therefore, connecting them with each other is better than connecting any of them with further cities, as these local links are minimized and minimizing the local links attributes in finding a smaller global route.

Step 6: Select a random city to be the starting city and then add the nearest city as a new starting city until having all the cities connected in the category of the local path. The group in each category is connected with the nearest group in other categories until all the groups are connected in a global path.

This method gives only one solution, and to derive solutions with a specific population size, the mutation process is used. It is used to mutate the seed solution (n-1) times, in order to derive the other solutions, where n is e size of the population.

Table 1 *GA configuration parameters for experiments*

no.	parameter	value/technique
1	population size	100
2	generation limit	3000
3	initialization technique	regression based technique [23] for GA's population initialization techniques and multi linear regression based technique (MLRBT)
4	crossover method	one-point modified crossover
5	crossover probability	0.82
6	mutation method	exchange mutation
7	mutation probability	1.0
8	selection	roulette wheel
9	termination condition	generation limit

Table 2 *Experimental results for the MLRBT and RBT*

city	optimal solution	MLRBT			regression based technique		
		best solution before GA	best sol	average	best solution before GA	best sol	average
KroA100	21282	32210	27493	29440.8	40675	29234	30506.2
eil51	426	550	465	478.6	680	475	500.6
pr76	108159	156926	128039	133572.8	209897	132694	139536.6
KroA200	29368	51191	46269	47877.4	64374	51427	52770.8
lin318	42029	73676	68490	70237.6	81754	75180	76764.7
pr144	58537	152275	124763	131974.3	213332	124881	136572.1
att532	27686	160340	145128	157423.6	184976	178600	182420.33
rat783	8806	15711	14659	15308.1	16730	16214	16355.8
d2103	80450	172550	169253	171890	175701	175147	175573.5
fnl4461	182566	361538	351280	358443	365414	363900	364567.5

Figures 7 and 8 show a comparison of the two initialization population methods: Initialization Mechanism Based on regression Techniques [23] and MLRBT, applied to two TSP instances: a280 and rat195.

As shown in Figures 7 and 8, the process of the GA is continuing to enhance and optimize the solutions.

4 Results and analysis

To evaluate the proposed methods, he experiments on different TSP problems were conducted. Experiments include conducting the proposed method, which includes implementing the Multi Linear Regression Based Technique MLRBT together with the Regression based technique in [23], which was found superior to both the Random and the NN techniques. Table 1 shows the selected GA parameters.

Experiments include applying each technique 10 times for each of the TSP instances. Then, computing the average of all the executions results for the purpose of experimental analysis. To conduct the experiments, Microsoft visual studio 2008 tool was used, as well as the TSP benchmark datasets obtained from TSPLIB [24]. Results of experiments are shown in Table 2. Hence, the results are divided into three different solutions: best solution, worst solution and the average solution as well.

Ten TSP instances were selected to implement the experiment; these instances include KroA100, eil51, pr76, KroA200, in318, pr144, att532, rat783, d2103, fnl4461 and e experiments were repeated ten times for each instance. It resulted in that the MLRB technique was more beneficial than the Regression Based Technique [21] across all the instance categories (small, medium and large) using the same parameters, which have been fixed according to the previous research, i.e. the Regression Based Technique [21]. The RBT was previously compared to other techniques, the random and the NN in different researches and was found superior. In addition, Table 2 shows that the MLRB is found to have advantage for all the cities in terms of the best solution. It can also result in that these techniques are more beneficial than the random and the NN techniques, where the successful performance has been achieved by the proposed solution and the achieved performance was close to the optimal solution.

It is necessary to consider the performance factors (which have been identified as measurements) when investigating several initialization techniques such as error rate, average convergence and convergence diversity.

Table 3 *Error Rate (%)*

problem	optimal solution	random		NN		regression based T		MLRBT	
		best	worst	best	worst	best	worst	best	worst
KroA100	21282	5.70759	6.15248	3.11968	6.03017	0.83437	0.93065	0.40767	0.54403
eil51	426	2.12911	2.43897	0.94366	1.11972	0.46714	0.61502	0.17606	0.32629
pr76	108159	3.41266	3.70083	0.87348	1.03310	0.88179	1.04367	0.28720	0.50809
KroA200	29368	9.11206	9.74299	5.11244	5.25940	1.19021	1.31865	0.53790	0.76202
lin318	42029	11.64106	12.19720	5.21618	5.68427	0.91615	0.95808	0.70366	0.78900
pr144	58537	10.81328	11.65166	1.26527	1.56317	0.84842	0.90172	0.79873	0.84839
att532	27686	28.14841	54.83620	27.91581	54.87900	5.75349	6.14578	4.36174	5.29621
rat783	8806	18.01306	18.65478	9.13570	9.41154	0.87247	0.90427	0.78605	0.83046
d2103	80450	38.15525	38.67478	10.16072	38.59516	1.16288	1.20272	1.13421	1.16910
fnl4461	182566	22.10100	43.99948	22.06794	43.88047	1.01834	1.03906	0.97270	0.98494

Table 4 *Average Error rate (100%)*

city	MLRBT	regression based T
KroA100	0.339273518	0.476779348
eil51	0.225454545	0.373529412
pr76	0.310764309	0.484704403
KroA200	0.426305405	0.543790972
lin318	0.429542863	0.485908946
pr144	0.615583648	0.725606098
att532	0.827329425	0.850326529
rat783	0.439500987	0.473640167
d2103	0.533758331	0.542119851
fnl4461	0.495029568	0.500385864

However, in any problem, the error rate denotes the percentage difference between the known optimal solution and the fitness value of the solution [19]. The Error Rate can be given by the following formula:

$$Error\ Rate(\%) = \frac{Fitness - Optimal\ fitness}{Optimal\ fitness} \times 100\,. \quad (1)$$

This factor measures the quality of the generated population by finding the effect of applying initial population technique on the GAs' performance to obtain a solution near to optimal one. The error rates are also classified into two types, depending on the fitness values in the given problem population. In other words, individuals with high error rate are given according to the initial population with the worst fitness value. In addition, individuals with low error rate are given according to the initial population with the best fitness. The experimental results of error rate for random, NN, RTB and MLRBT are given in Table 3.

From Table 3 follows that MLRBT technique achieved the minimum error rate likened to Random, NN and RBT techniques. It can be noted that the Multi Linear Regression based technique for GA's achieved lower error rate than the other seeding techniques, which are "Random and NN and RBT". Hence, it indicates that the produced individuals by the MLRBT for GA's are better fit the quality measures than the individuals that were produced by each of: NN, Random and RBT techniques. Since the proposed technique divides the problem (which is improvement for the RBT), this difference occurred. Table 3 also shows the experimental results of ("the initial population techniques w.r.t. error rate for the best individuals and the worst individuals in the initial population for each technique").

The results of Table 3 are extracted from Table 2, which includes the error rate for the MLRBT and RBT [23] for each city and there is a clear superiority in ratios in the table in favor of the MLRBT.

The Average error rates, obtained from both initial population techniques (RBT and MLRBT), for different problems are given in Table 4.

Besides on the size of cities, Table 5 shows the selected TSP examples, which were classified into three classes according to their problem size. The error rates of several initial population techniques are given for different classes of a problem example by Class A and Class B.

As shown in Figure 9, the error rates of several initial population techniques are given for different classes of a problem example by Class A and Class B.

Average Convergence (%) is the convergence rate of solutions in the initial population, and it is given by the following formula [25]:

Table 5 *Different sized TSP problem*

Class	Size	city
Class 1	Size<= 100	KroA100, pr76, eil51
Class 2	100 <Size<= 500	KroA200, pr144, lin318
Class 3	500<Size<= 1000	att532, rat783, fnl4461, d2103

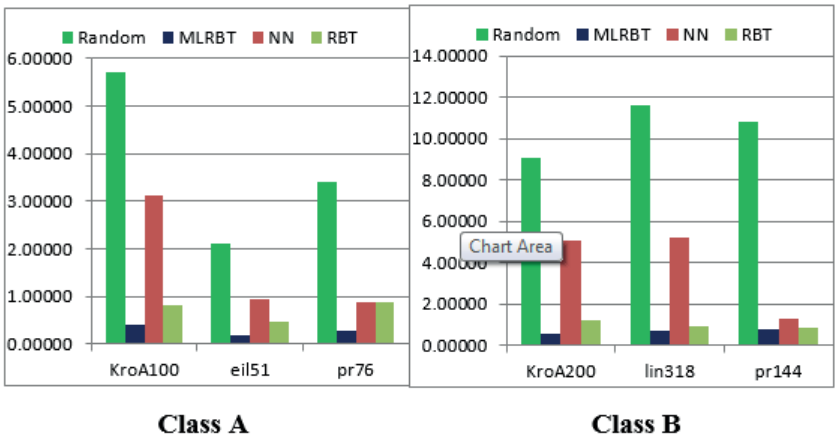

Figure 9 *Performance of initialization techniques*

Table 6 *The Average Convergence (%)*

city	MLRBT	RBT
KroA100	0.660726482	0.523220652
eil51	0.774545455	0.626470588
pr76	0.689235691	0.515295597
KroA200	0.573694595	0.456209028
lin318	0.570457137	0.514091054
pr144	0.384416352	0.274393902
att532	0.172670575	0.149673471
rat783	0.560499013	0.526359833
d2103	0.466241669	0.457880149
fnl4461	0.504970432	0.499614136

$$Average\ convergence = \\ = 1 - \frac{Average\ Fitness - Optimal\ fitness}{Optimal\ fitness} \times 100. \quad (2)$$

Optimal fitness denotes the recognized optimal value of identical instance, and Average fitness denotes the average value of the initial population fitness.

From the results, it was found that the MLRBT regression based technique for the GA's population initialization had average convergence rate higher than the RBT. In addition, it was noted that the MLRBT works in better way, especially in the case of large size problems. Hence, it can result that individuals that are produced by the MLRBT are the closest to the optimal solution. Moreover, Table 6 includes the experimental results of the initial population techniques w.r.t. average convergence (%).

As shown in Figure 10, the Multi Linear Regression Based Technique (MLRBT) achieved larger convergence than the Regression based technique. Hence, the MLRBT was found slightly greater than Random and NN, especially the RBT, [23] is better than Random and NN technique.

Furthermore, the final solution error rate denotes the difference between the known optimal solution and the final solution that resulted when applying the GAs on the TSP instances using one of initial population techniques. This can be given by the following formula:

$$Final\ Solution\ Error\ Rate\,(\%) = \\ = \frac{final\ solution - Optimal\ fitness}{Optimal\ fitness} \times 100. \quad (3)$$

In addition, this factor aims to compute the produced population quality and this can be conducted by determining

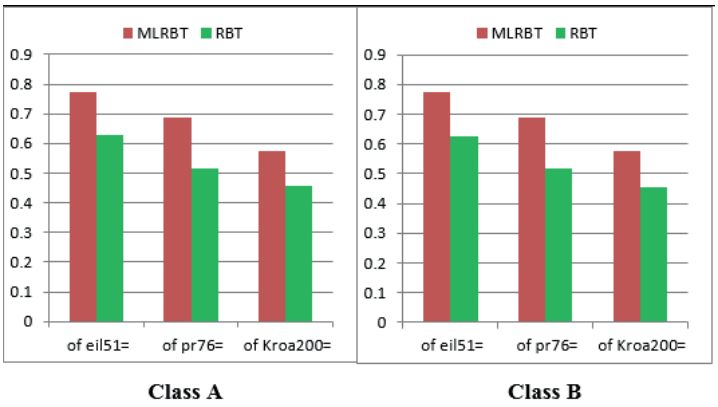

Figure 10 *The Average Convergence (%)*

Table 7 *Final Solution Error Rate (%)*

city	MLRBT	RBT
KroA100	0.291842872	0.373649
eil51	0.091549296	0.115023
pr76	0.183803475	0.226842
KroA200	0.57549033	0.751124
lin318	0.629589093	0.788765
pr144	1.13135282	1.133369
att532	4.241927328	5.450914
rat783	0.664660459	0.841245
d2103	1.103828465	1.177091
fnl4461	0.924126069	0.993252

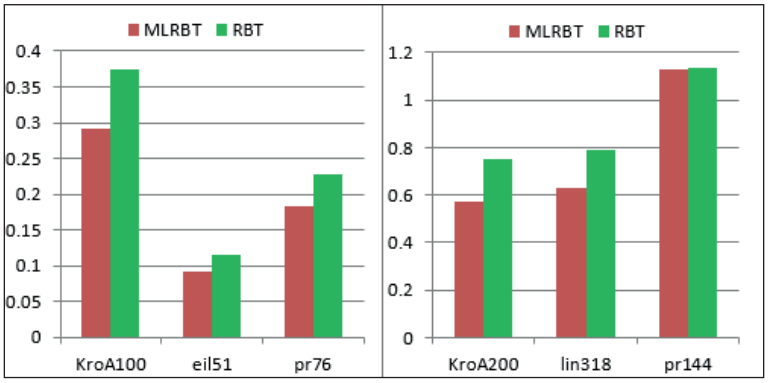

Figure 11 *Final solution error rates for MLRBT and RBT [23]*

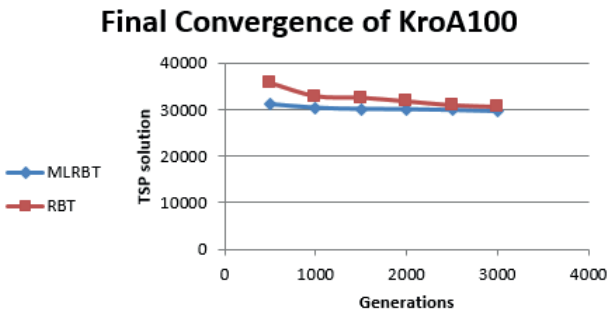

Figure 12 *KroA100 - overview of performance*

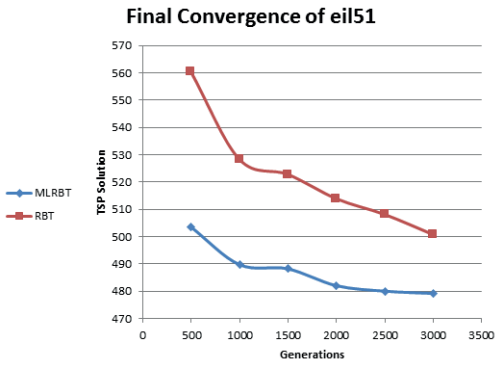

Figure 13 *eil51- overview of performance*

the impact of applying initial population technique on the GAs performance for obtaining a solution, which is close to the optimal one. However, the error rate of the final solutions indicated that the MLRBT for the GA's population initialization achieved error rate lower than the RBT. In other words, this indicates that the produced individuals from the MLRBT achieved a higher fit quality more than the individuals that are produced from RBT. This is evaluated in Table 7.

Figure 11 shows the final solution error rate obtained from several initial population techniques used for different classes of problem instances. The Multi Linear Regression Based Technique (MLRBT) achieved the maximum final solution error rate over the Regression based technique [23].

The performance MLRBT and RBT [23] techniques' was observed from the instances: kroA100 and eil51 as shown in Figures 12 and 13. In addition, the two figures show the produced initial population from the MLRBT, RBT and the final solution after 3000 generations.

5 Conclusion

This paper introduced a new, enhanced, initial population technique for genetic algorithm in order to solve the problem of the TSP and this technique was called the Multi Linear Regression Based Technique for GAs population initialization. In addition, the proposed technique has been implemented and analyzed, and to test the efficiency of the proposed technique, it has been compared to three other population techniques: Random, Nearest Neighbor (NN) initial population and Regression based techniques.

In this context, a set performance criteria were considered in order to compute the performance factors for the proposed technique and the other seeding techniques including the convergence diversity, error rate, and average convergence.

Moreover, to conduct experiments, the study extracted several TSP examples from the standard TSPLIB. After conducting experiments, the results indicated that the proposed Multi Linear Regression Based Technique for the GA's population initialization achieved the higher efficiency than the other initial population techniques to be depended in developing GA-based applications. Hence, it can be concluded that the Multi Linear Regression Based Technique for the GA's population initialization produces the high quality and efficient fittest individuals, which enable the GA to enhance the solution using the best-fit individuals.

References

[1] HENDRICKS, D., GEBBIE, T., WILCOX, D. High-speed detection of emergent market clustering via an unsupervised parallel genetic algorithm. *South African Journal of Science* [online]. 2016, **112**(1/2), p. 1-9. eISSN 1996-7489. Available from: https://doi.org/10.17159/sajs.2016/20140340

[2] GOLBERG, D. E. *Genetic algorithms in search, optimization, and machine learning*. Boston: Addion - Wesley Longman Publishing Co., 1989. ISBN 978-0-201-15767-3.

[3] MOHAMMED, A. A., NAGIB, G. Optimal routing in Ad-Hoc network using genetic algorithm. *International Journal of Advanced Networking and Applications*. 2012, **3**(5), p. 1323-1328. ISSN 0975-0290, eISSN 0975-0282.

[4] AYALA, H. V. H., DOS SANTOS COELHO, L. Tuning of PID controller based on a multiobjective genetic algorithm applied to a robotic manipulator. *Expert Systems with Applications* [online]. 2012, **39**(10), p. 8968-8974. ISSN 0957-4174. Available from: https://doi.org/10.1016/j.eswa.2012.02.027

[5] HOLLAND, J. H. Genetic algorithms. *Scientific American* [online]. 1992, **267**(1), p. 66-72. ISSN 0036-8733. Available from: http://dx.doi.org/10.1038/scientificamerican0792-66

[6] EIBEN, A. E., SMITH, J. E. *Introduction to evolutionary computing* [online]. Berlin Heidelberg: Springer Science & Business Media, 2003. ISBN 978-3-642-07285-7, eISBN 978-3-662-05094-1. Available from: https://doi.org/10.1007/978-3-662-05094-1

[7] GENDREAU, M., POTVIN, J.-Y. *Handbook of metaheuristics*. Vol. 2. Springer International Publishing, 2010. ISBN 978-1-4419-1663-1.

[8] HASSANAT, A., ALMOHAMMADI, K., ALKAFAWEEN, E., ABUNAWAS, E., HAMMOURI, A., PRASATH, V. B. Choosing mutation and crossover ratios for genetic algorithms - a review with a new dynamic approach. *Information* [online]. 2019, **10**(12), 390. ISSN 2078-2489. Available from: https://doi.org/10.3390/info10120390

[9] HASSANAT, A. B., ALKAFAWEEN, E. A., AL-NAWAISEH, N. A., ABBADI, M. A., ALKASASSBEH, M., ALHASANAT, M. B. Enhancing genetic algorithms using multi mutations: experimental results on the travelling salesman problem. *International Journal of Computer Science and Information Security*. 2016, **14**(7), p. 785-801. ISSN 1947-5500.

[10] HUSSAIN, A., MUHAMMAD, Y. S., SAJID, M. N. A simulated study of genetic algorithm with a new crossover operator using traveling salesman problem. *Journal of Mathematics*. 2019, **51**(5), p. 61-77. ISSN 1016-2526.

[11] ZHONG, J., HU, X., GU, M., ZHANG, J. Comparison of performance between different selection strategies on simple genetic algorithms. In: International Conference on Computational Intelligence for Modelling, Control and Automation

CIMCA ´05 and International Conference on Intelligent Agents, Web Technologies and Internet Commerce CIMCA-IAWTIC´06: proceedings. Vol. 2. 2005. p. 1115-1121.

[12] ALKAFAWEEN, E., HASSANAT, A. Improving TSP solutions using GA with a new hybrid mutation based on knowledge and randomness. arXiv preprint arXiv:1801.07233. 2018.

[13] HASSANAT, A., ALKAFAWEEN, E. On enhancing genetic algorithms using new crossovers. *International Journal of Computer Applications in Technology* [online]. 2017, **55**(3), p. 202-212. ISSN 0952-8091. Available from: https://doi.org/10.1504/IJCAT.2017.10005868

[14] ALKAFAWEEN, E. O. *Novel methods for enhancing the performance of genetic algorithms*. Master´s degree thesis. Karak: Mutah University, 2018.

[15] VEDAT, T., DALOGLU, A. T. An improved genetic algorithm with initial population strategy and self-adaptive member grouping. *Computers and Structures* [online]. 2008, **86**(11-12), p. 1204-1218. ISSN 0045-7949. Available from: https://doi.org/10.1016/j.compstruc.2007.11.006

[16] YUGAY, O., KIM, I., KIM, B., KO, F. I. Hybrid genetic algorithm for solving traveling salesman problem with sorted population. In: 3rd International Conference on Convergence and Hybrid Information Technology: proceedings [online]. IEEE, 2008. ISBN 978-0-7695-3407-7. Available from: https://doi.org/10.1109/ICCIT.2008.373

[17] WAGSTAFF, K., CARDIE, C., ROGERS, S., SCHRODL, S. Constrained K-means clustering with background knowledge. In: 8th International Conference on Machine Learning ICML´01: proceedings. 2001. p. 577-584.

[18] WEI, Y., HU, Y., GU, K. Parallel search strategies for TSPs using a greedy genetic algorithm. In: 3rd International Conference on Natural Computation ICNC 2007: proceedings [online]. Vol. 3. IEEE, 2007. Available from: https://doi.org/10.1109/ICNC.2007.537

[19] RAY, S. S., BANDYOPADHYAY, S., PAL, S. K. Genetic operators for combinatorial optimization in TSP and microarray gene ordering. *Applied Intelligence* [online]. 2007, **26**(3), p. 183-195. ISSN 0924-669X, eISSN 1573-7497. Available from: https://doi.org/10.1007/s10489-006-0018-y

[20] PAUL, P. V., RAMALINGAM, A., BASKARAN, R., DHAVACHELVAN, P., VIVEKANANDAN, K., SUBRAMANIAN, R., VENKATACHALAPATHY, V. Performance analyses on population seeding techniques for genetic algorithms. *IJET International Journal of Engineering and Technology*. 2013, **5**(3), p. 2993-3000. ISSN 2319-8613, eISSN 0975-4024.

[21] CHANG, D.-X., ZHANG, X.-D., ZHENG, C.-W. A genetic algorithm with gene rearrangement for K-means clustering, Pattern Recognition. 2009, **42**(7), p. 1210-1222. ISSN 0031-3203. Available from: https://doi.org/10.1016/j.patcog.2008.11.006.

[22] SALLABI, O. M., EL-HADDAD, Y. An improved genetic algorithm to solve the traveling salesman problem. World Academy of Science, Engineering and Technology. 2009, **52**(3), p. 471-474. ISSN 2010-376X, eISSN 2010-3778.

[23] HASSANAT, A., PRASATH, V., ABBADI, M., ABU-QDARI, S., FARIS, H. An improved genetic algorithm with a new initialization mechanism based on regression techniques. *Information* [online]. 2018, **9**(7), 167. ISSN 2078-2489. Available from: https://doi.org/10.3390/info9070167

[24] REINELT, G. TSPLIB [online] [accessed 2018]. University of Heidelberg 1996. Available from: http://comopt.ifi.uni-heidelberg.de/software/TSPLIB95

[25] DENG, Y., LIU, Y., ZHOU, D. An improved genetic algorithm with initial population strategy for symmetric TSP. *Mathematical Problems in Engineering* [online]. 2015, **2015**, 212794. ISSN 1024-123X, eISSN 1563-5147. Available from: https://doi.org/10.1155/2015/212794

STUDY ON THE VEHICLE LINEAR DYNAMIC INTERVAL IN A TRAFFIC FLOW

Oleg Fyodorovich Danilov, Victor Ivanovich Kolesov, Denis Alexandrovich Sorokin*, Maxim Leonidovich Gulaev

Federal State Budget Educational Institution of Higher Education "Industrial University of Tyumen" (IUT), Tyumen, Russian Federation

*E-mail of corresponding author: sorokinda@tyuiu.ru

Resume

The transportation industry of a modern city involves the effective systems for the road traffic management. To manage any object is impossible without understanding its specifics. The tasks of road traffic management are based on mathematical models of traffic flows. The "following the leader" model based on the linear dynamic interval of vehicles has become widely accepted in the model analysis. The paper discusses the mathematical model of the linear dynamic interval of vehicles; the model is identified structurally and parametrically. Coefficients of the model are analyzed in detail; a generalized assessment of the dynamic performance of the traffic flow, evolved in various road conditions, is given. The study has resulted in the proposed basic models for traffic flows that can be used for algorithmic support of the model analysis of traffic flows and the road traffic management.

Article info

Received 8 March 2020
Accepted 11 July 2020
Online 13 November 2020

Keywords:

smart city,
dynamic interval,
traffic flow,
speed,
intensity,
density,
road coverage

Available online: https://doi.org/10.26552/com.C.2021.1.E11-E22

ISSN 1335-4205 (print version)
ISSN 2585-7878 (online version)

1 Introduction

Strong promotion of the Smart City concept is a current trend in Russia. As a rule, the approach to growth strategy of cities is based on the idea of their sustainable development which is the systemic basis of "Smart Cities" [1-6]. The present Smart Cities include Smart Mobility as a key component; in here, in terms of importance, the "weight" of the component is estimated at no less than 20%. The success in this field is achieved due to the depth of understanding of the technological process, the traffic flow (TF) being its "spring".

The authors have proposed a method that makes it possible to comprehensively assess efficiency of the traffic flows comprehensively [7]. Theoretical and experimental studies have been carried out based on the mathematical model of the TF developed by the authors and considered in detail in the reference [8]. The paper, being a logical continuation of the mentioned references, presents a comprehensive study of the linear dynamic interval (DI) of vehicles.

The "following the leader" model describes how a led vehicle reacts to a leading vehicle in a single lane. Over the past 60 years a large number of investigations have been made, the main purpose of which was simulation modelling of traffic flow [8-20]. Existing mathematical models have significant accuracy obtained during the continuous development of the subject domain at hand. However, there are some models' elements that require additional research and improvements of the mathematical representations.

2 Dynamic performance study

The dynamic interval is recorded as follows [21-23]:

$$L(V) = m_2 \cdot V^2 + m_1 \cdot V + m_0, \quad (1)$$

where
L - linear dynamic interval, m;
V - speed, m.s^{-1};
m_2 - coefficient, s^2.m^{-1};
m_1 - coefficient, s;
m_0 - coefficient, m.

The linear dynamic interval of a vehicle is widely used in mathematical modeling and represents the distance between the leading and led vehicles, ensuring the safe operation of the traffic flow.

This makes it possible to evaluate the density of the TF

$$q(V) = 1/L(V) = 1/(m_2 \cdot V^2 + m_1 \cdot V + m_0), \quad (2)$$

where
q - density, TU.km^{-1};
TU - traffic unit.

The basic equation of the TF [22-24] determines its intensity

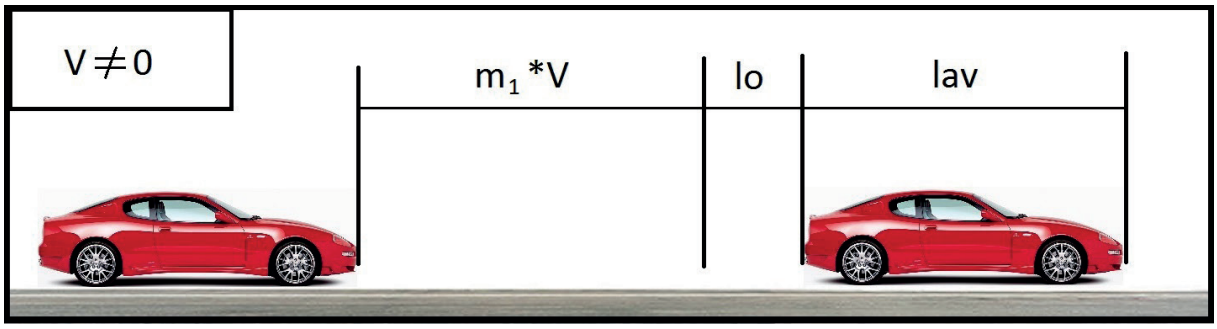

Figure 1 *Interval determined between the two adjacent vehicles*

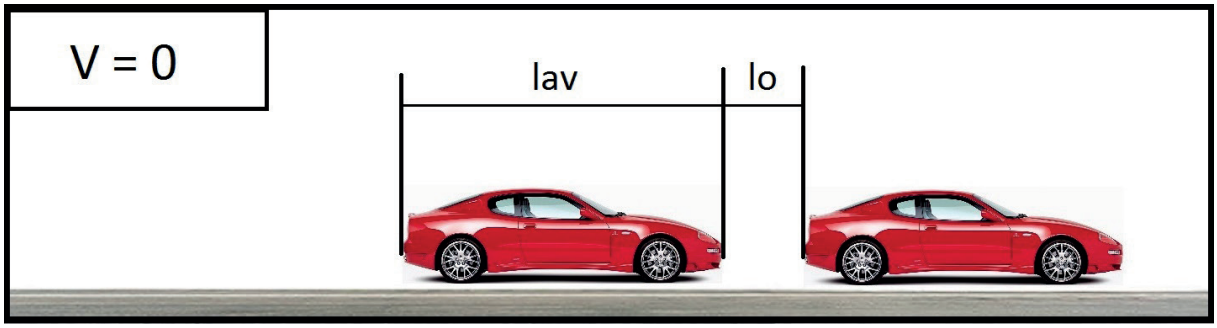

Figure 2 *Minimum interval between the two adjacent vehicles in a traffic jam*

$$N(V) = V \cdot q(V) = V/(m_2 \cdot V^2 + m_1 \cdot V + m_0), \quad (3)$$

where
N - intensity, TU.h^{-1}.

The extreme point of intensity is reached when on the assumption $dN(V)/dV = 0$. When considering Equation (3), one can find the derivative of the function with respect to speed

$$\frac{(V^2 \cdot m_2 + V \cdot m_1 + m_0) - V(m_1 + 2 \cdot V \cdot m_2)}{(V^2 \cdot m_2 + V \cdot m_1 + m_0)^2} = 0.$$

The root of equation corresponds to the speed of the maximum intensity

$$V_{\max N} = \sqrt{m_0/m_2}. \quad (4)$$

The density reaches its peak when the traffic flow does not move, i.e. when $V = 0$. Here, L takes the minimum value $L_{\min} = m_0$, which corresponds to the density

$$q_{\max} = 1/m_0. \quad (5)$$

Thus, the main dynamic characteristics of the TF are functionally related to the DI and, in fact, are evaluated by the coefficients included in Equation (1).

3 Coefficient m_0 study

Figure 1 shows the actual interval between two vehicles, which is the sum

$$l_0 + m_1 \cdot V + l_{av}, \quad (6)$$

where
l_0 - arbitrary interval, m;
l_{av} - average length of the vehicle, m.

The coefficient m_1 is characterized by the stopping time value and depends on the driver's response and the rapidity of the brake system [25-27]. The sum in Equation (6) is valid if the vehicles have the same values of deceleration developed by the brake system in operation. Then, when the "leading" driver slows down, the real interval between vehicles will be reduced by a distance $m_1 \cdot V$.

Value of the interval l_0 depends on the "degree of cohesion" of the TF and is minimized in the maximum density. Figure 2 shows the flow as a "traffic jam" ($V = 0$). Here, l_0 can be defined as the minimum distance between vehicles, which ensures safety of the flow. In fact, if the "leading" driver slows down urgently, the TF transits from the state of movement (Figure 1) to the full stopping (Figure 2) and the interval l_0 remains the only obstacle for a vehicle collision.

Thus, the expression for the coefficient m_0 takes the form

$$m_0 = l_{av} + l_0, \quad (7)$$

where
l_{av} - average length of the vehicle, m;
l_0 - safety interval between two vehicles in a traffic jam, m.

Taking into account Equations (1) and (7), the DI can be recorded as

$$L(V) = m_2 \cdot V^2 + m_1 \cdot V + l_{av} + l_0. \quad (8)$$

It is necessary to note that L in Equation (8) evolves into the classical interval of Tanaka - Equation (1) [21-22]

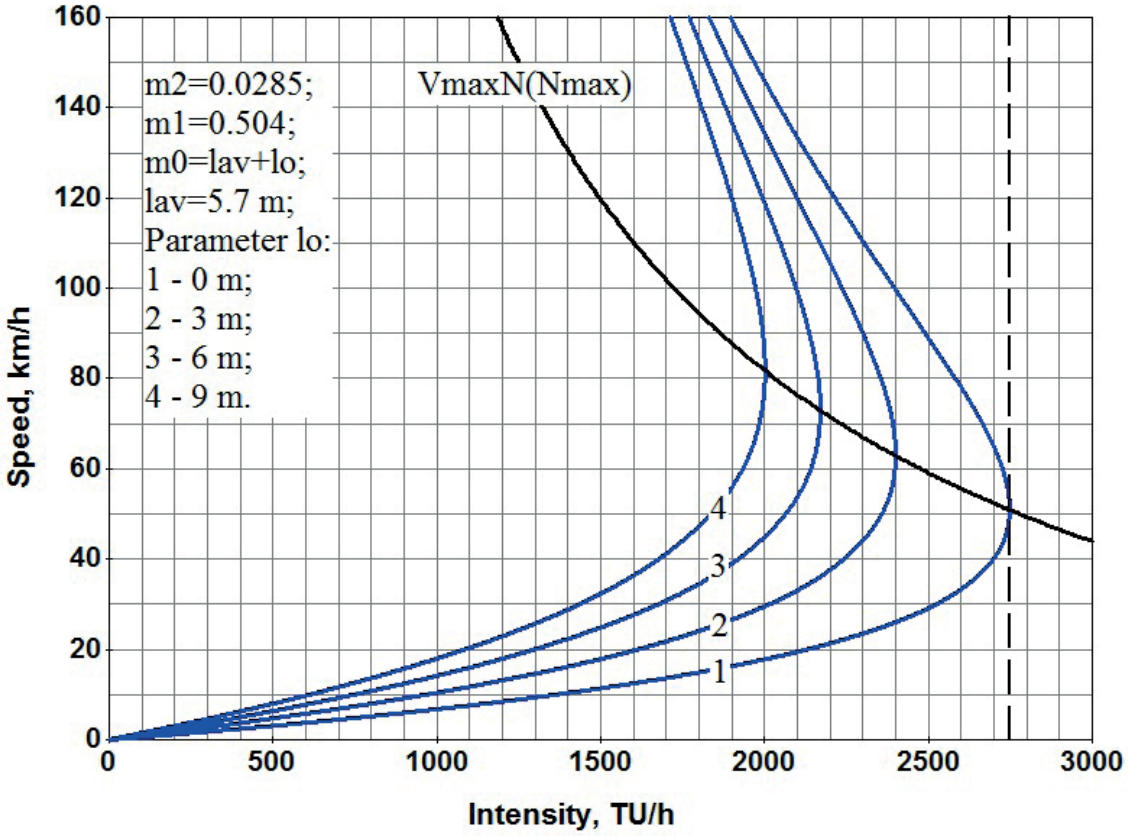

Figure 3 *V_{maxN} versus maximum intensity N_{max}*

if $l_0 \to 0$ (in $l_0 = 0$ $m_0 = l_{av}$). In here, the changed dynamic performance of the TF results from direct connection of the values and L. To study the sensitivity of the extreme point intensity to value of l_0, Equation (4) is transformed, taking into account Equation (7), to

$$V_{\max N} = \sqrt{(l_{av} + l_0)/m_2}\,. \tag{9}$$

In given values of l_{av} and m_2, it is easy to evaluate the following

$$l_0 = m_2 \cdot V_{\max N}^2 - l_{av}\,. \tag{10}$$

On the other side, from Equation (3) follows that

$$l_0 = V/N - (m_2 \cdot V^2 + m_1 \cdot V + l_{av})\,. \tag{11}$$

If to evaluate Equation (10) integrally, with Equation (11), provided that the real intensity corresponds to the maximum one, one obtains the equation

$$m_2 \cdot V_{\max N}^2 - l_{av} = V_{\max N}/N_{\max} - \\ -(m_2 \cdot V_{\max N}^2 + m_1 \cdot V_{\max N} + l_{av}),$$

from which one obtains

$$V_{\max N} = (1/N_{\max} - m_1)/(2 \cdot m_2)\,. \tag{12}$$

The calculation data of Equation (12) are illustrated in Figure 3; in here, the parameters of the DI correspond to the Tanaka model for the standard road conditions [22] (m_2 = 0.0285; m_1 = 0.504; l_{av} = 5.7 m).

If the interval l_0 increases, the position of the extreme point N_{max} drifts towards the increased speed V_{maxN}, in here, the real value of the maximum intensity decreases. Analysis of Equation (12) suggests that the drift is sensitive to the parameters m_1 and m_2.

The minimum interval l_0 is widely used in mathematical modeling of the TF, in particular in references [25, 27]. Impact of l_0 on the road safety can be assessed using the safety criterion K_s proposed in [25]. The criterion takes the form

$$K_s = \frac{m_2 \cdot V^2 + m_1 \cdot V + l_0}{m_2 \cdot V^2 + m_1 \cdot V}\,. \tag{13}$$

Figure 4 illustrates the two operating modes of the flow. The upper curve illustrates the distance observed by the drivers as prescribed by L with l_0 = 0. The maximum intensity N_{max} = 2747 TU.h^{-1} (point 1) is reached at V_{maxN} = 51.61 km.h^{-1}. The lower curve has been plotted taking into account l_0 = 2.22 m. Here, the position of the extreme point N_{max} = 2475 TU.h^{-1} (point 2) shifts to the maximum permissible speed limit in the city - 60 km.h^{-1}. Performance of the safety criterion in the changed V_{maxN} is shown in Figure 5. If K_s = 1 at point 1 (in l_0=0), as it follows from Equation (13), then its value reaches K_s = 1.1359 at point 2, i.e. the maximum provided $V \leq 60$ km.h^{-1}.

Thus, to find a rational value of the interval l_0, the algorithmic support has been created; it suggests that

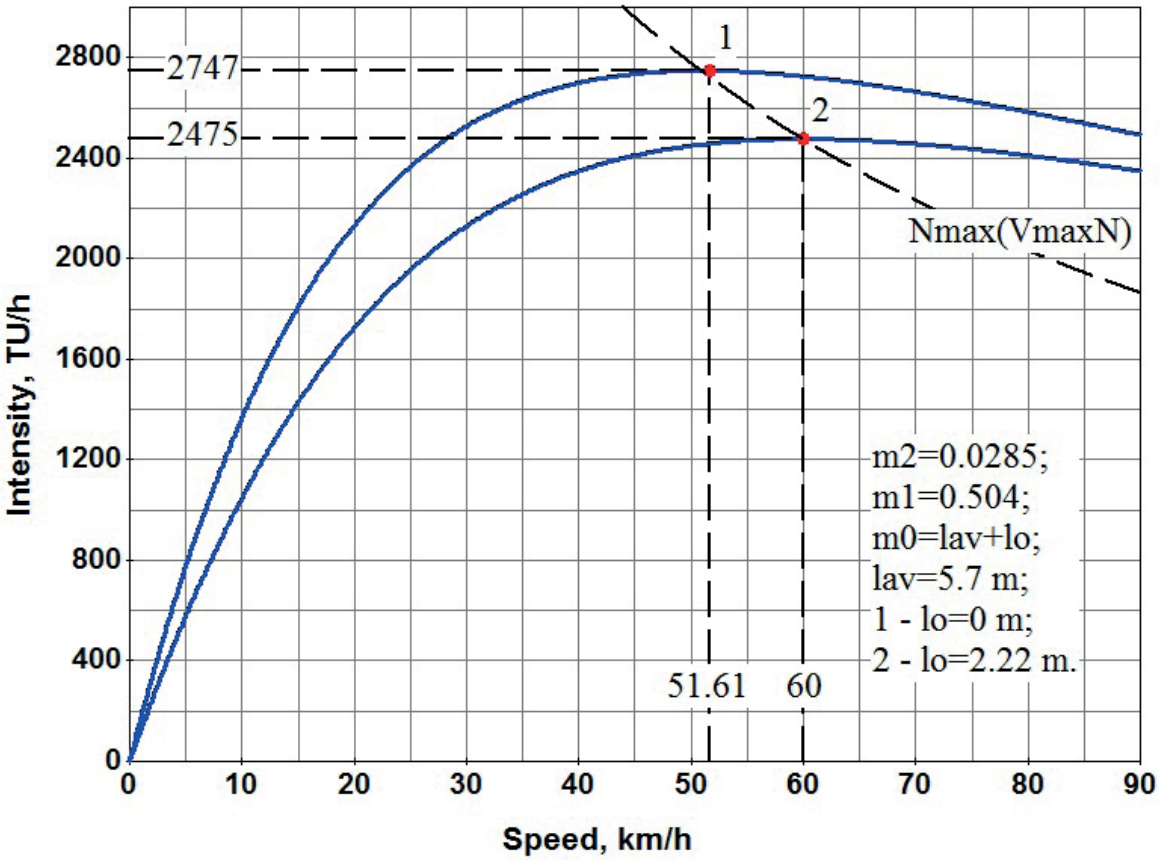

Figure 4 *Analysis of the two operating modes of the TF*

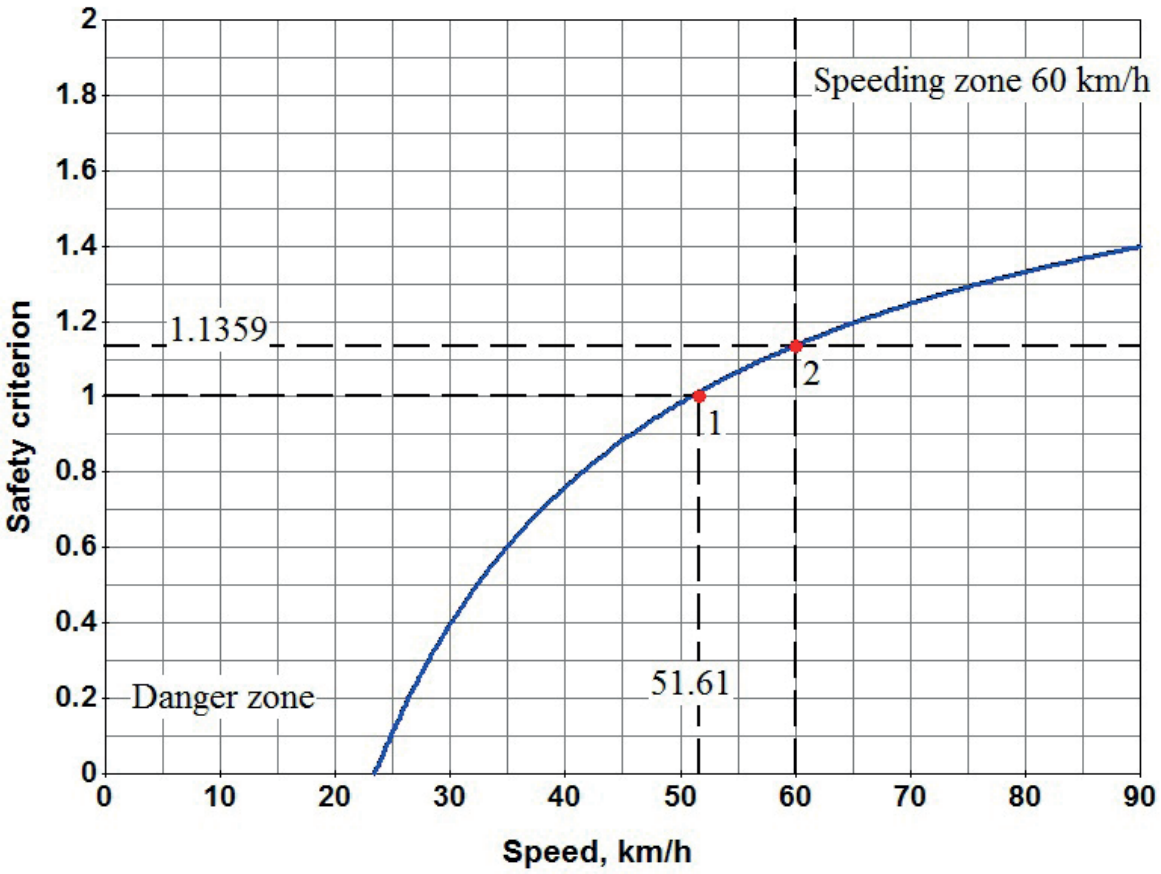

Figure 5 *Safety criterion K_s versus V_{maxN}*

Table 1 *Confidential intervals of the driver's response for lognormal distribution*

confidential interval reliability (%)	case 1 "unexpected obstacle" (s)	case 2 "expected signal" (s)
50	1.18	0.53
85	1.87	0.64
95	2.45	0.72
99	3.31	0.82

Table 2 *Standards for effective braking of the TU with a brake system in operation when checking in the travel conditions*

TU	category of TU	rapidity of the brake system (max.), (s)
passenger and utility vehicles	M1	0.6
	M2, M3	0.8
trailer cars	M1	0.6
trucks	N1, N2, N3	0.8
tractor-trailers	N1, N2, N3	0.9

the maximum intensity is reached only in the interval 1-2 (Figure 4). On one side, this segment is limited by the "danger zone" (Figure 5); in here, V_{maxN} at point 1 is evaluated by Equation (9) in $l_0 = 0$. On the other side, l_0 is evaluated by Equation (10) in the permissible speed limit. The position of points 1 and 2 (Figure 4), relative to the axis of speed, is determined by the DI parameters and the value of the permissible speed limit in the city.

If it is possible to control the speed, then (within the search strategy for the value of l_0) two approaches are available: either to increase the safety of the flow and decrease its maximum intensity, or to increase N_{max} if the level of danger increases. Figure 4 illustrates the position of N_{max} at point 2 as the most preferable from the point of view of safety; in here, l_0 = 2.22 m and it is an entirely "traditional" value. The minimum interval between the adjacent vehicles in a traffic jam is usually l_0 = 1 - 3 m in mathematical modeling [27]. The average length of the TU is determined by structure of the TF.

4 Coefficient m_1 study

When analyzing the stopping time, the rapidity of the brake system is usually taken into account alongside with the driver's response [25-27]. In here, the response is usually differentiated into two intervals: the deceleration of the brake system and increase of the deceleration time [26]. Thus, the coefficient m_1 can be represented as [25-26]

$$m_1 = t_{dr} + t_{bl} + 0.5 \cdot t_{si}\,, \tag{14}$$

where
t_{dr} - driver's response, s;
t_{bl} - brake lag, i.e. deceleration of the brake system, s;
t_{si} - slow down increase, i.e. rise time of the deceleration, s.

The response time depends on a number of factors: the driver's qualification, his age and health, traffic conditions, etc. At present, there is no any strict specification of the t_{dr} value; therefore, in assessing the brake system performance of the TU, the following ranges of possible values are used: in [26] t_{dr} = 0.3 - 2.5 s, in [24] t_{dr} = 0.6 - 0.8 s, in [27] t_{dr} = 0.1 - 0.6 s.

The report [23] presents results of experimental study obtained by Lerner. During the experiment, two situations were considered. In the first case, the driver did not know that an unexpected obstacle, which would make him to slow down, would arise in the way. In the second case, the driver expected a signal, but he did not know exactly when this would happen. The obtained confidential intervals, with the corresponding reliability indicators, are given in Table 1. Results of the study show that the driver's response is caused by the need to predict the travel conditions.

Deceleration of the brake system performance is determined by the time when the driver begins to slow down versus the time when deceleration begins; in here, the vehicle continues to move uniformly with the initial speed. Value of t_{bl} depends on the type, design and physical situation of the brake system and varies in the average ranges: for a hydraulic drive gear t_{bl} = 0.1 - 0.4 s [26], t_{bl} = 0.05 - 0.15 s [24]; for a pneumatic drive gear t_{bl} = 0.6 - 0.8 s [26], t_{bl} = 0.2 - 0.4 s [24]. For monorails with pneumatic drive gear, the deceleration time can reach t_{bl} = 2 - 3 s [26].

The rise time of deceleration is characterized by a continuous increase in braking forces, which results in a fixed value of deceleration. Value of the t_{si} depends on the brake drive type, weight of the car and the adhesion coefficient. Generally, the time of blocking out is proportional to the weights falling upon the axles of the front and rear wheels [25]. On average, for a standard dry road coverage, t_{si} = 0.4 - 0.6 s [24].

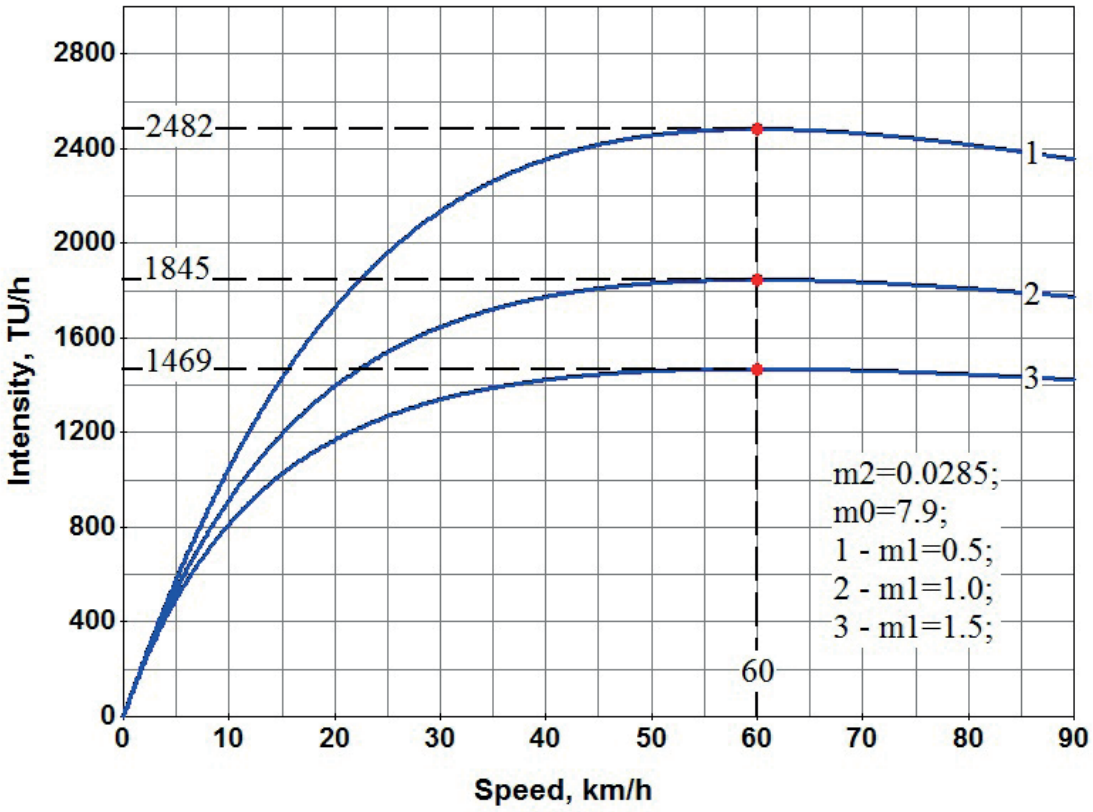

Figure 6 *Position of the extreme point N_{max} versus m_1*

The standards for effective braking of the TU, with a brake system in operation, are regulated by the GOST [28]. The maximum permissible values of the brake operation, when checking in the travel conditions, are shown in Table 2.

As for the effect of m_1 on the dynamic characteristics of the TF, L increases if the value of m_1 increases, as can be seen from Equation (1), and the density decreases at a fixed speed, as shown in Equation (2). The intensity versus speed, with a changing value of m_1, is illustrated in Figure 6. The speed V_{maxN} remains constant, which is due to the no effect of m_1 on V_{maxN} in Equation (4) and the maximum intensity decreases if m_1 increases. In here, the real value of m_1 can be evaluated using Equations (12) and (4), and the simultaneous solution results in the expression

$$m_1 = 1/N_{\max} - 2 \cdot \sqrt{m_0 \cdot m_2}\,. \tag{15}$$

Analysis in Equation (15) makes it possible to state that when N_{max} increases, the coefficient m_1 decreases to its minimum value, determined by its constituent parameters.

Thus, the decrease in the parameter values of the coefficient m_1 in Equation (14) can be considered as a reserve to increase the TF capacity.

5 Coefficient m_2 study

The value of m_2 can be evaluated using equation of the trip mileage during the mean fully developed deceleration of the TU. The equation is as follows [24, 26-27]:

$$S_{ss} = V^2/(2 \cdot j)\,, \tag{16}$$

where

S_{ss} - trip mileage during the mean fully developed deceleration, m;

j - mean fully developed deceleration of the TU, m.s^{-2}. In here, value of j is evaluated by expression:

$$j = g \cdot \varphi\,, \tag{17}$$

where

g - gravitational acceleration, m.s^{-2};

φ - adhesion coefficient.

The standard situation shown in Figure 7 is considered next. Two vehicles move at a certain speed; the drivers observe a safe interval equal to the linear DI (position “a”). The “leading” vehicle (number “1”) begins to slow down, covers the distance S_{ss1} and stops. The stopping distance of the “driven” car (number “2”) consists of two sections: the first one is covered during the driver’s response and rapidity of the brake system (due to the value of m_1) and the second one, S_{ss2} - during the mean fully developed deceleration. Thus, the distance between the vehicles decreased to l_0 (position “b”). Besides, the situation is modeled in such a way that the deceleration value of the “leading” vehicle exceeds the same value of the “driven” one, or they are equal ($j_1 \geq j_2$). This is due to the fact that value of L increases in the given conditions and it is the most relevant for safety. In this case, using Equation (16), one obtains that $S_{ss2} \geq S_{ss1}$.

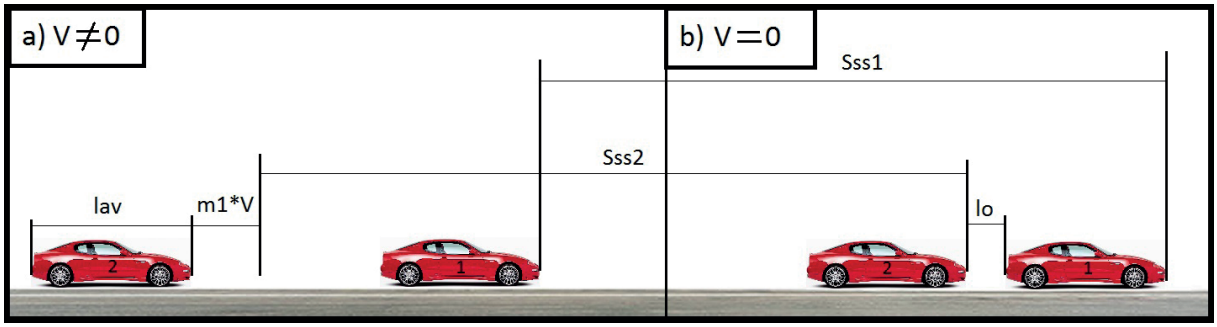

Figure 7 *Interval determined between the two adjacent vehicles*

Table 3 *Values of adhesion coefficients and changed adherence characteristics*

order of the road coverage k	rank of the road coverage state r											
	1		2		3		4		5		6	
	φ_{20}	β	φ_{20}	β	φ_{200}	β	φ_{20}	β	φ_{20}	β	φ_{20}	β
1	0.825	0.002	0.675	0.0035	0.425	0.0025	0.25	0.0025	0.35	0.0025	0.115	0.002
2	0.825	0.002	0.55	0.0035	0.375	0.0025	0.25	0.0025	0.35	0.0025	0.115	0.002
3	0.825	0.0035	0.625	0.0035	0.5	0.0035	0.25	0.0025	0.35	0.0025	0.15	0.002
4	0.65	0.005	0.45	0.004	0.325	0.0025	0.21	0.0025	0.35	0.0025	0.115	0.002

Table 4 *Values of k and r for different types and states of the road coverage*

k	type of road coverage	r	state of road coverage
1	cement concrete	1	standard dry
2	hot asphalt concrete without rough finish	2	wet clean
		3	wet dirty
3	rough asphalt concrete	4	dense snow
		5	loose snow
4	cold asphalt concrete	6	ice crusted

Table 5 *Results of the regression analysis φ_{20}*

regression equation: $\varphi_{20} = a_k - b_k \cdot r = a_k \cdot \left(1 - \frac{b_k}{a_k} \cdot r\right)$				
order k	a_k	b_k	b_k/a_k	R^2
1	0.9300	0.14000	0.15053	0.9702
2	0.8636	0.13128	0.15201	0.9325
3	0.9150	0.13280	0.14513	0.9845
4	0.6700	0.08786	0.13113	0.9024

Table 6 *Results of the regression analysis β/φ_{20}*

regression equation: $\beta/\varphi_{20} = A_k/(7-r)^{Bk}$			
order k	A_k	B_k	R^2
1	0.01902	0.9449	0.9024
2	0.01872	0.8846	0.8216
3	0.01726	0.7492	0.9788
4	0.01577	0.4549	0.7657

The DI section characterized by the coefficient m_2, represents the difference

$$S_{ss2} - S_{ss1} = \frac{V^2}{2 \cdot j_2} - \frac{V^2}{2 \cdot j_1} = V^2 \left[\frac{j_1 - j_2}{2 \cdot j_i \cdot j_2}\right]. \quad (18)$$

Thus, m_2 can be evaluated from expression

$$m_2 = \frac{j_1 - j_2}{2 \cdot j_1 \cdot j_2}, \quad (19)$$

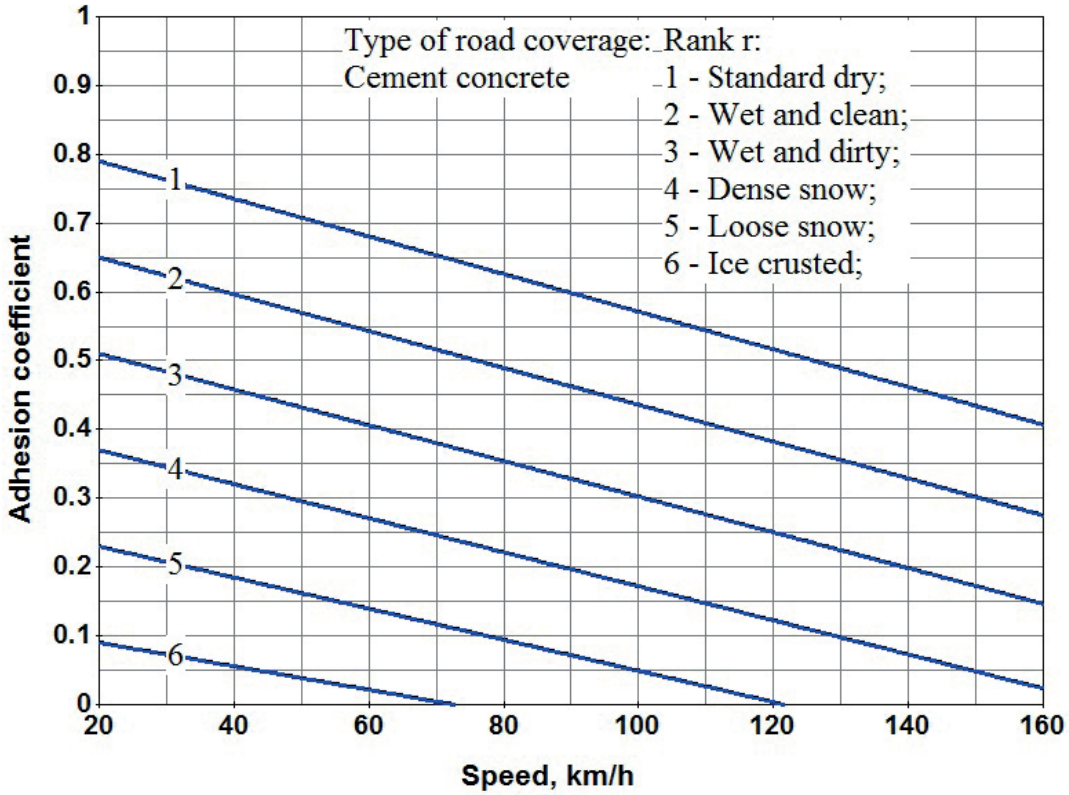

Figure 8 *Adhesion coefficient versus speed*

where

j_1 and j_2 - deceleration of the two adjacent vehicles, m.s^{-2}.

The adhesion coefficient depends on the speed, type of the road coverage and its condition, as it is shown in [29]

$$\varphi = \varphi_{20} - \beta \cdot (V - 20) = \varphi_{20} \cdot \left[1 - \frac{\beta}{\varphi_{20}} \cdot (V - 20)\right], \quad (20)$$

where

φ_{20} - adhesion coefficient at a speed of 20 km.h^{-1};

β - the changed adhesion coefficient due to the speed.

In order to create a generalized assessment of φ, the data given in [29] have been used; in here, the ranges have been replaced by the average values (Table 3). Each type of the road coverage is given the order of k and the state of the road coverage is ranked by r (Table 4). The effect of the road coverage on φ_{20} and β/φ_{20} is assessed in the ordinal scale (as rank r). The regression analysis has shown that the relationship between φ and rank r is linear (Table 5) and β/φ_{20} with r corresponds to Zipf's law (Table 6). The value of φ versus the speed on different road surfaces is illustrated in Figure 8.

Then, dependence of the adhesion coefficient on the type of the road coverage is analyzed. Structural and parametric identification of the model φ has resulted in a generalized assessment of the adhesion coefficient, taking into account the Equation (20),

$$\varphi(k, r, V) = a_k \cdot \left(1 - \frac{b_k}{a_k} \cdot r\right) \cdot \cdot \left[1 - A_k/(7 - r)^{B_k} \cdot (V - 20)\right], \quad (21)$$

where

$a_k = 0.93 - 0.003677 \cdot \exp[1.4263 \cdot (k - 1)]$;

$b_k/a_k = 0.152 - 0.0008 \cdot \exp[1.08 \cdot (k - 1)]$;

$A_k = 0.0193 - 0.00035 \cdot \exp[0.76 \cdot (k - 1)]$;

$B_k = 0.99 - 0.02 \cdot \exp[0.8252 \cdot (k - 1)]$.

It is assumed that φ equals to V = 20 km.h^{-1} for V < 20 km.h^{-1}.

If one takes the adhesion coefficient for the dry road coverage as a reference (r = 1) at V = 20 km.h^{-1}, then Equation (21) can be represented as

$$\varphi(k, r, V) = \varphi_s(k) \cdot K_\varphi(r, V), \quad (22)$$

where

φ_s - reference adhesion coefficient (r = 1, V = 20 km.h^{-1});

K_φ - coefficient characterized by the state of road coverage and speed.

Values of φ_s, evaluated for each type of coverage, are given in Table 7.

When transforming expression for deceleration of the TU - Equation (17) and taking into account Equation (22), one obtains

$$j = g \cdot \varphi_s \cdot K_\varphi = j_s \cdot K_\varphi, \quad (23)$$

where

j_s - reference deceleration of the TU (r = 1, V = 20 km.h^{-1}), m.s^{-2}.

Then, substituting Equation (23) in Equation (19), one can obtain the formula to evaluate m_2, taking into account the adhesion coefficient

Table 7 *Values of φ_s for different types of the road coverage*

k	type of coverage	φ_s
1	cement concrete	0.786
2	hot asphalt concrete without rough finish	0.778
3	rough asphalt concrete	0.742
4	cold asphalt concrete	0.583

Table 8 *Performance standards for braking with brake system in operation during the road conditions management*

TU	category of TU	mean fully developed deceleration of the TU (min.), ($m.s^{-2}$)
passenger and utility vehicles	M1	5.8
	M2, M3	5.0
trailer cars	M1	5.8
trucks	N1, N2, N3	5.0
tractor-trailers	N1, N2, N3	5.0

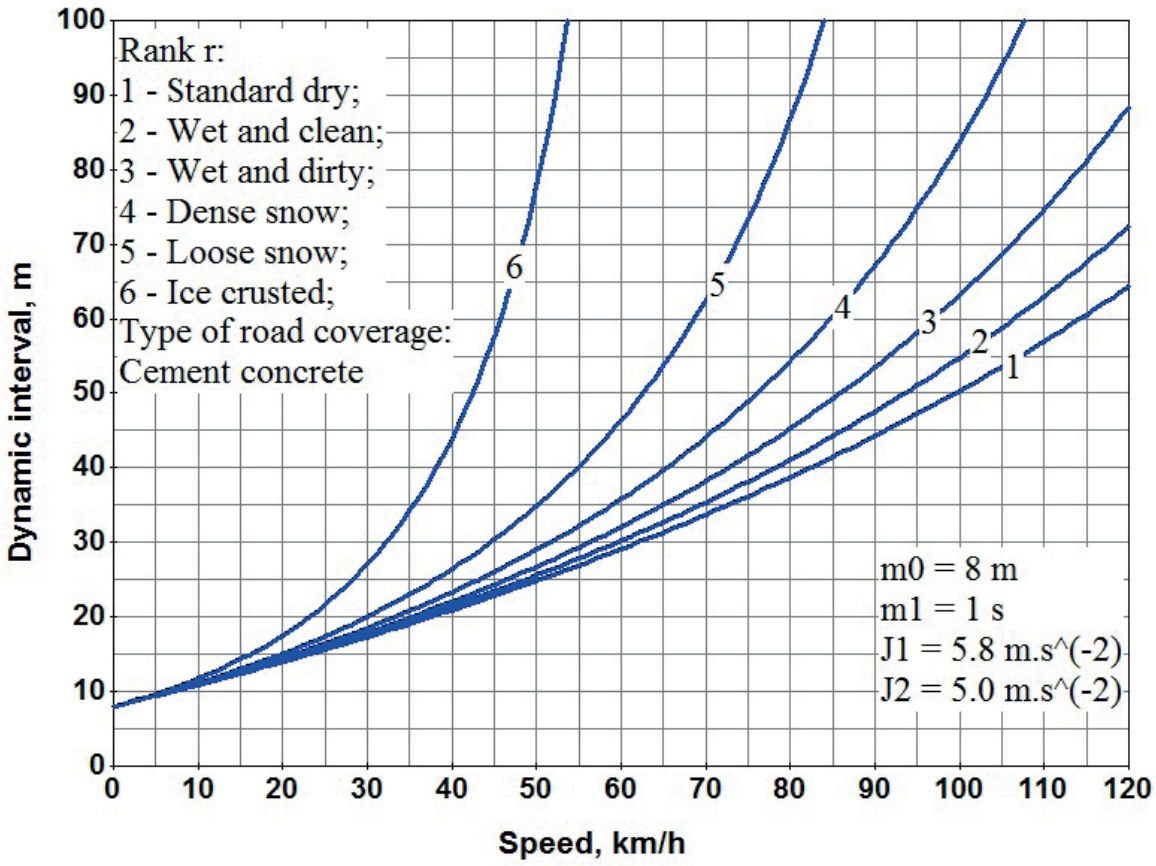

Figure 9 *L versus speed under different states of the road coverage*

$$m_2 = \frac{1}{K_\varphi} \cdot \left[\frac{j_{s1} - j_{s2}}{2 \cdot j_{sl} \cdot j_{s2}}\right] = \left[\frac{\varphi_s}{\varphi}\right] \cdot \left[\frac{j_{s1} - j_{s2}}{2 \cdot j_{sl} \cdot j_{s2}}\right], \quad (24)$$

where j_{s1} and j_{s2} - reference deceleration of two adjacent vehicles, $m.s^{-2}$.

Thus, the adhesion coefficient included in Equation (24) depends on the type of the road coverage, its state and speed of the TU. Values of j_{s1} and j_{s2} depend on the structure of the TF; in here, in order to ensure safety, j_{s1} is suitable to vehicles with the greater braking efficiency in the flow and j_{s2} - with the smaller one. Values of deceleration are taken in accordance with GOST [28] for passenger vehicles of M1 and M2 categories, respectively (Table 8).

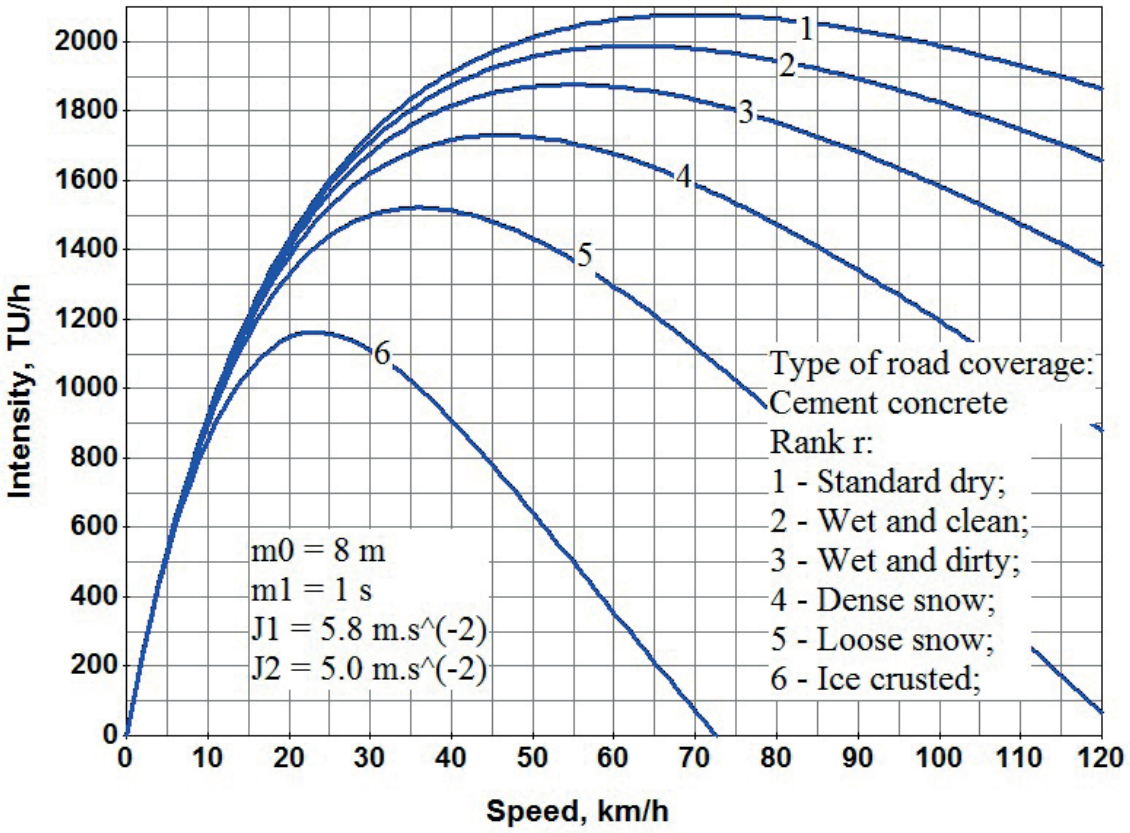

Figure 10 *N versus speed under different states of the road coverage*

6 Basic models of the traffic flow

The study has resulted in identifying the effective diagrams of the traffic flow. Dependence of the L and intensity on the speed under different states of the road coverage is illustrated in Figures 9-10, m_0 = 8 m, m_1 = 1 s are taken in calculations.

The complete algorithmic support reflects the variability of the DI coefficients, making it possible to track the dynamics of the TF characteristics in a wide palette of travel conditions.

7 Conclusions

The article presents research that extends the existing mathematical representations of the linear dynamic interval model of the vehicle. The authors would like to highlight the main results (authors' contribution):

1. The method of rational choice of the interval l_0 for simulation modelling has been developed;
2. Parametric identification of the linear dynamic interval model has been performed, including a generalized estimation of the adhesion coefficient, allowing to study the dynamics of the traffic flow in various road conditions;
3. Influence of the model parameters on the traffic flow intensity has been studied.

Results are focused on development of promising engineering solutions in the field of mathematical modeling of the traffic flows and road traffic management [30]. The proposed algorithmic support is of interest to specialists involved in the problems of synthesis of the traffic safety control systems, efficiency of traffic flows and intelligent transport systems.

References

[1] DIRKS, S., KEELING, M. A vision of smarter cities: how cities can lead the way into a prosperous and sustainable future [online]. U.S.A.: IBM Corporation, 2009. Available from: https://www.ibm.com/downloads/cas/2JYLM4ZA

[2] FOSTER, M. *Building and managing an intelligent city. Accenture* [online]. 2011, p. 24-25. Available from: http://www.fm-house.com/wp-content/uploads/2015/01/Building-Managing-Intelligent-City.pdf

[3] HEDLUND, J. *Smart city 2020: technology and society in the modern city.* Microsoft Service Enterprise Architecture paper. 2012, 1, p. 12.

[4] GIFFINGER, R., FERTNER, C., KRAMAR, H., KALASEK, R., PICHLER-MILANOVIC, N., MEIJERS, E. Smart cities ranking of European medium-sized cities [online]. Final report of Centre of Regional Science in Vienna. 2007, p. 7. Available from: http://www.smart-cities.eu/download/smart_cities_final_report.pdf

[5] NEIROTTI, P., DE MARCO, A., GAGLIANO, A., MANGANO, G., SCORANNO, F. Current trends in smart city initiatives: some stylized facts. *Cities* [online]. 2014, **38**, p. 25-36. ISSN 0264-2751. Available from: https://doi.org/10.1016/j.cities.2013.12.010

[6] BEGICH, Y. E., SHERSTOBITOVA, P. A. The concept of smart city as a strategy to manage urban infrastructure. *Construction of Unique Buildings and Structures* [online]. 2017, **8**(59), p. 27-40. ISSN 2304-6295. Available from: https://doi.org/10.18720/CUBS.59.2

[7] DANILOV, O. F., KOLESOV, V. I., SOROKIN, D. A. Development of criteria for transport flow efficiency assessments of the city street road network. *MATEC Web of Conferences* [online]. 2016, **73**, 01010. ISSN 2261-236X. Available from: https://doi.org/10.1051/matecconf/20167301010

[8] DANILOV, O. F., KOLESOV, V. I., SOROKIN, D. A. Development of mathematical model for traffic flow within speed limitation. *MATEC Web of Conferences* [online]. 2016, **73**, 01028. ISSN 2261-236X. Available from: https://doi.org/10.1051/matecconf/20167301028

[9] CHANDLER, R. E., HERMAN, R., MONTROLL, E. W. Traffic dynamics: studies in car following. *Operations Research* [online]. 1958, **6**(2), p. 165-184. ISSN 0030-364X, eISSN 1526-5463. Available from: https://doi.org/10.1287/opre.6.2.165

[10] GAZIS, D. C., HERMAN, R., ROTHERY, R. W. Nonlinear follow-the-leader models of traffic flow. *Operations Research* [online]. 1961, **9**(4), p. 545-567. ISSN 0030-364X, eISSN 1526-5463. Available from: https://doi.org/10.1287/opre.9.4.545

[11] DREW, D. R. *Traffic flow theory and control*. New York: McGraw-Hill, 1968. ISBN 978-0070178311.

[12] WIEDEMANN, R. *Road traffic flow simulation / Simulation des Strassenverkehrsflusses* (in German). Karlsruhe: Series of publications from the Institute of Transportation at the University of Karlsruhe / Schriftenreihe des Instituts fur Verkehrswesen der Universitat Karlsruhe, 1974. Available from: https://www.worldcat.org/title/simulation-des-straenverkehrsflusses/oclc/634105860

[13] GIPPS, P. G. A behavioural car-following model for computer simulation. *Transportation Research Part B: Methodological* [online]. 1981, **15**(2), p. 105-111. ISSN 0191-2615. Available from: https://doi.org/10.1016/0191-2615(81)90037-0

[14] FRITZSCHE, H. T. A model for traffic simulation. *Traffic Engineering and Control*. 1994, **35**(5), p. 317-321. ISSN 0041-0683. ISSN 0041-0683.

[15] SEARLE, J. Equations for speed, time and distance for vehicles under maximum acceleration. In: Safety Technology session of the 1999 SAE International Congress and Exposition and is included in the SAE Special Publication, "Advances in Safety Technology 1999" (SP-1433): proceedings. Society of Automotive Engineers. 1999. ISBN 0768003652, p. 1-11.

[16] TREIBER, M., HENNECKE, A., HELBING, D. Congested traffic states in empirical observations and microscopic simulations. *Physical Review E* [online]. 2000, **62**(2), 1805. ISSN 2470-0045, eISSN 2470-0053. Available from: https://doi.org/10.1103/PhysRevE.62.1805

[17] JIANG, R., WU, Q., ZHU, Z. Full velocity difference model for a car-following theory. *Physical Review E* [online]. 2001, **64**(1), 017101. ISSN 2470-0045, eISSN 2470-0053. Available from: https://doi.org/10.1103/PhysRevE.64.017101

[18] NEWELL, G. F. A simplified car-following theory: a lower order model. *Transportation Research Part B: Methodological* [online]. 2002, **36**(3), p. 195-205. ISSN 0191-2615. Available from: https://doi.org/10.1016/S0191-2615(00)00044-8

[19] OLSTAM, J. J., TAPANI, A. *Comparison of car-following models* [online]. Swedish National Road and Transport Research Institute, 2004. Available from: https://www.researchgate.net/publication/265198439_Comparison_of_Car-following_models

[20] RAKHA, H. Validation of Van Aerde's simplified steady state car-following and traffic stream model. *Transportation Letters - The International Journal of Transportation Research* [online]. 2009, **1**(3), p. 227-244. ISSN 1942-7867, eISSN 1942-7875. Available from: https://doi.org/10.3328/TL.2009.01.03.227-244

[21] INOSE, H., HAMADA, T. *Traffic management*. Moscow: Transport, 1983.

[22] GASNIKOV, A. V. *Introduction to mathematical modeling of traffic flows*. Moscow: MIPT, 2010. ISBN 978-5-7417-0334-2.

[23] NATHAN, G., CARROLL, J., AJAY, K. Traffic flow theory: a state of the art report [online]. Washington DC, 2001. Available from: https://www.academia.edu/39779635/Traffic_Flow_Theory_A_State-of-the-Art_Report

[24] PUGACHEV, I. N., GOREV, A. E., OLESHENKO, E. M. *Organization of road traffic and traffic safety. manual for graduate students*. Moscow: Academia Publishing House, 2009. ISBN 978-5-7695-4662-4.

[25] SOTSKOV, D. A., NUZHDIN, R. V., KUNAKOV, A. P., NAZAROV, A. G. *Modeling of emergency brake application in traffic flow* [online]. Analytical and expert support for road traffic safety system: collection of reports. St. Petersburg: GASU, 2006, p. 16-21. Available from: http://www.adf.spbgasu.ru/Conference2006/section_4.pdf

[26] GUDKOV, V. A. *Safety of transport units (vehicles)*. Manual for graduate students. Moscow: Hotline - Telecom, 2010. ISBN 978-5-9912-0090-5.

[27] BAKHTINA, O. N. *Study on characteristics of traffic flow in conditions prior to traffic congestion* [online]. Organization of road traffic and traffic safety in large cities: collection of reports. St. Petersburg: GASU, 2008, p. 168-171. Available from: http://lib.madi.ru/fel/fel1/fel10B008.pdf

[28] GOST R 51709 Motor vehicles. Safety requirements for technical condition and verification methods [online]. Introduced 2002-01-01. Moscow: Publishing House of Standards, 2001. Available from: http://docs.cntd.ru/document/gost-r-51709-2001

[29] VASILIEV, A. P. Reference encyclopedia of a road builder. Book 2. Repair and maintenance of roads [online]. Moscow, 2004. Available from: http://science.totalarch.com/book/0502.rar

[30] KAPSKI, D., KASYANIK, V., LOBASHOV, O., VOLYNETS, A., KAPTSEVICH, O., GALKIN, A. Estimating the parameters of traffic flows on the basis of processing of localization data on the movement of vehicles. *Communications - Scientific Letters of the University of Zilina* [online]. 2019, **21**(2), p. 89-99. ISSN 1335-4205, eISSN 2585-7878. Available from: http://komunikacie.uniza.sk/index.php/communications/article/view/1474

"ROAD SAFETY SEQUENCE" - A NEW CONCEPT OF THE ROAD SAFETY MANAGEMENT IN POLAND

Andrzej Szymanek

Faculty of Transport and Electrical Engineering, Kazimierz Pulaski University of Technology and Humanities in Radom, Radom, Poland

*E-mail of corresponding author: a.szymanek@uthrad.pl

Resume

The article shows a fragment of the results of the author's concept of road safety management in Poland. The article shows the "program sequence" of the construction action of road safety management system in Poland. The main component of this "sequence" of actions to improve the road safety - should be the "road risk management model". It should be widely used in Poland as an element of knowledge and practices of international road safety management. It is primarily about the model of the Office for Land Transport Safety Authority in New Zealand adopted by the EU in its road safety policy. The article also presents other components of the author's concept, including the "3 levels" model of risk management, the idea of which is to isolate three categories of the risk associated with any transport system.

Article info

Received 23 February 2020
Accepted 30 March 2020
Online 21 October 2020

Keywords:

road safety sequence (RSS),
road risk management (RRM),
LTSA model

Available online: https://doi.org/10.26552/com.C.2021.1.F1-F10

ISSN 1335-4205 (print version)
ISSN 2585-7878 (online version)

1 Introduction

The average annual probability of a fatal traffic accident (approximately $2{\cdot}10^{-4}$) is 10 to 100 times higher than in other modes of transport. It is also higher in relation to occupational accidents in many industries. The annual costs of traffic accidents at the rate of 1-2% of GDP (depending on the level of development of the country) are a big economic problem. In the road transport is the largest potential of risk reduction of fatal and serious accidents. These are just some of the important reasons to become a subject of interest to road safety (RS). However - what is paradoxical - until the end of 2012, there was no standard for the road safety management - it has become only the ISO 39001 [1].

For years, there is a call for construction of a solid theoretical basis for road safety research. For example, the OECD document indicated the need for construction of theories and models for the road safety [2]: "no theoretical basis is unfortunately more common in road safety research than in many other areas of research". Since then, there has been considerable progress in study of the road safety, but still there is a need to develop a theoretical basis and a consistent methodology in this regard. These are the foundations for construction of national and international road safety management systems.

The risk of road accidents is the primary way of measuring the road safety, while "risk management of the road accidents", is the primary means of influencing the level of road safety. This interpretation arises from the "safety operationalization", that is, the ability to measure and control the risk. In turn, the acceptance of the thesis of the "acceptable level" of risk is the cornerstone of the methodology for the risk managed and tip for regulators in the various modes of transport. Thus, the risk management is a central concern of each project to improve the road safety. The research paradigm is also the basis of the concept of the road safety management in Poland, presented in this article.

2 The main reasons and thesis for development of the concept of the road safety management in Poland

Analysis of the state of research in the field of the road risk management (RRM) allows for the formulation of the rationale for development of the concept of the road safety management (RSM) in Poland [3]; here are some of them.

(1) In development of a research methodology for the road safety can be seen both evolution and jumps. Formulated new objectives and new research criteria

RS would consolidate in the form of „good practices" and then other unsuitable would disappear. In projects relating to RS an important role carried out terms such as: prioritising objectives, determine scopes of competence and responsibility, improve the allocation of resources, the mechanisms for financing transport investments, institutional management [4]. The strategic approach to eliminating of fatal and serious road accidents and formulation of the principle of shared responsibility for the status of the RS turned out to be important. Large national programs: The Dutch Sustainable Safety and Swedish Vision Zero were created [5-6].

(2) Until recently, there were no risk management standards in the road transport commonly recognized as the „best". Only the ISO 39001 Road Traffic Safety Management standard, published at the end of 2012, was dedicated strictly to the road safety management.

(3) In connection with the fourth EU Road Safety Programme and the United Nations Decade project; neither Action for Road Safety 2011-2020 created better opportunities to work on new management concepts RS in Poland.

(4) Projects to improve the RS should take into account the so-called „Gerondeau paradox" [7]: „Anyone road user is responsible for his behavior, but only the authorities are responsible for the overall level of road accidents"

(5) Projects to improve the RS should take into account the Adams' idea that the balance in risk management is the basis of its effective management. Disregarding this thesis can cause two opposite errors: 1. error of ignoring the costs of risk reduction; 2. error of ignoring environmental and social risk factors [8].

(6) New projects of the road risk management should take into account:

- The ability to control the primary and secondary risk factors.
- The role of the transport infrastructure for emergence of threats.
- The role of traffic processes and control processes on formation of risks.
- Scale of the impact on the population groups (social risk context).
- Scale of the impact on the environment (environmental risk context).

The construction of each project to improve the road safety requires formulation of numerous working theses, to classify problems and directs research in the field of construction models and the road risk management methodology. Theses such as shown in [3]; here are the most important of them:

(1) The nature of safety in different systems is often identical, sometimes similar, it is advisable to use a legitimate analogy and the theoretical results of constituting science of safety. This is the thesis of W. J. Geysen and it can be adapted to needs of the road safety management concept in Poland [9]: safety in road transport can be shaped through the risk management and road events and management of losses on the road traffic, using the methodologies known from other systems risk management techniques.

(2) Accidents are effects of the existence gaps in the system of management, and therefore safety prevention must rely on locating, defining and removing these gaps. This thesis is based on the theory of J. Reason that - especially in the Swiss Cheese Model, (SChM) - postulated the need for a study of two kinds of gaps, that is latent conditions and active failures, as the main causes of accidents [10]. The idea that one can use to develop a defense-in- depth strategy in the road safety management.

(3) The road transport is a complex system, in structure and working processes of which one can find different „varieties of safety", such as: a) Safety of traffic processes; b) Safety load processes; c) Functional safety (safety control devices); d) Safety (and reliability) of the human factor; e) Occupational safety in the road transport sector; f) Safety of critical infrastructure (bridges, tunnels, etc.); g) Safety of means of road transport; h) Environment safety.

(4) Road transport is a complex system, in the structure and working processesof which one can find that the principles and general methodology of the road transport risk management are the same as for other technical areas of human activity. Therefore, the risk management process steps are the same road as the general steps of the risk management process. What is specific for the road transport is included in all of this „superstructure" risk management processes.

(5) Traffic road safety can be interpreted as „product", whose final form are observable results of safety outcomes, in particular road accidents. This is the thesis related to the LTSA (Land Transport Safety Authority) model, which is currently an international model for the construction of the national road risk management models.

(6) All the kinds of risks that are associated with the road transport can be classified in three levels of the road safety system - this is a thesis related to the author's concept of the „three levels" of the risk management in the road transport system, [11]:

- Structural risks - derived from interaction of structure system elements.
- Functional risks - derived from operation of the system.
- Behavioral risks - derived from effects (negative) of behaviors of the system.

3 Road safety system concept in Poland

The concept of the road safety management in Poland was described in the monograph Szymanek [3] and in this article shows its improved version, but limited to the main items.

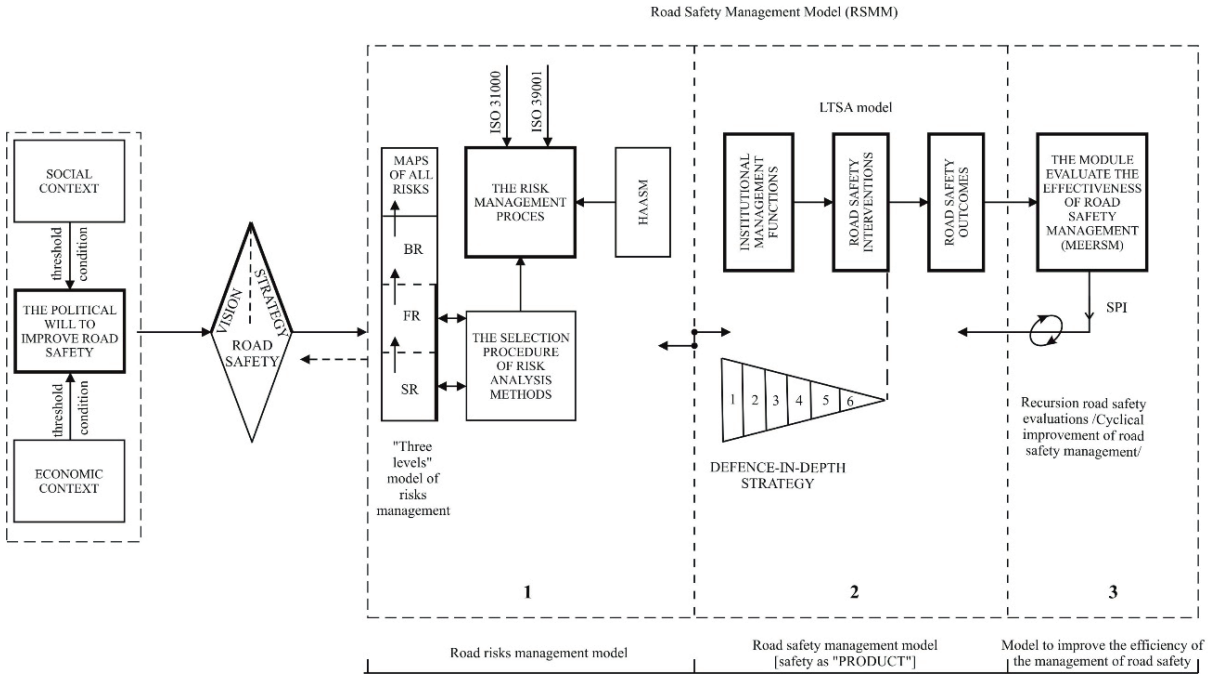

Figure 1 *The concept of road safety management system in Poland*

Program sequence of building the road safety management system in Poland (RS SEQUENCE) begins a strategy to improve the road safety (RS STRATEGY), which should be developed within the current Polish transport policy. Formulating a vision and road safety policy is always a *conditio sine qua non* for the construction of a road safety program and basically every process and system of road safety management starts from that. A factor that initiates creation of a vision, then the road safety strategy is the political will to improve road safety in the country (political will RS). It appears when the „threshold conditions", associated with the socio-economic environment (context), are exceeded. As an example of the „threshold condition", a popular interpretation of the „ Smeed's right" can be quoted: „the number of deaths in any country is the number the country is willing to tolerate" [12].

This interpretation has been confirmed a few times: each country has achieved its "Smeed's point" at some moment of development. So it was in Poland after a critical 1991 year - the „critical mass" of road accidents was reached. And a few years later, GAMBIT was developed, the first national program to improve the road safety in Poland.

The road safety strategy enforces construction of the road safety management system (RSMS). According to the concept RSMS, presented here, the model can be described by:

- Road risks management model (RRMM);
- Road safety management model (RSMM);
- Module evaluate the effectiveness of road safety management (MEERSM).

A diagram of the proposed safety management system is shown in Figure 1. Into the RSMS should enter The following elements of knowledge and practice of international road risk management, previously widely used in Poland, should enter the RSMS:

- LTSA model of the road safety management [13]; this model is adopted by the European Union in its road safety policy.
- Road safety management model (RSMM).
- "Three levels" model of risk management (3RM*)*, whose idea is to develop "maps of all risks" associated with the road transport (further: with any transport system); there are three levels of risk of system characterization: structure, work processes and "behavior" of system [3, 13].
- Defense-in-depth strategy. A Polish methodology of building-in the road safety management system of various protections in all the critical points of the transport system and at all the levels of the management of such a system should be developed.
- Standard AS/NZS ISO 31000: here that means use of the overall RMP [14].
- Standard ISO 39001 - dedicated exclusively to the management of safety in the road transport, at the same time a little yet known [1].

In the draft „ efforts to improve road safety" the final product are the results of the safety outcomes. These include, first of all, the road traffic accidents, especially fatal and serious accidents. These results must be evaluated independently and reliably. This is to be the module to evaluate effectiveness of the road safety management, (MEERSM). Measures of effectiveness of this would be, of course, Safety Performance Indicators (SPI), whose methodology was developed in the framework of the project SafetyNet. Based on, inter alia, the SPI module this should force a RSMS modification. This means the correction in the management of the road/transport risks,

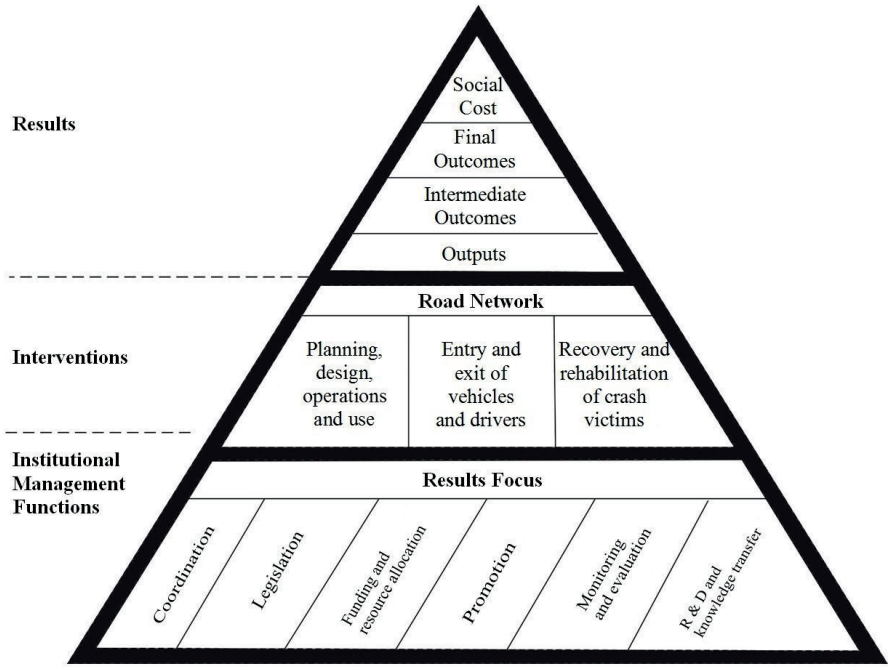

Figure 2 *LTSA model of the traffic safety management [13]*

thus that means modifications of the RSMS, which must of be a recursion type (Figure 1).

It comes to cyclical improvement of the RSMS, that is, efficiency improvement of the road safety. Information about the SPI values, arising from MEERSM module, should cause positive feedbacks, continuously improving the working RSMS system, Figure 1.

4 LTSA model as the basis for the construction of a system for the road safety management in Poland

The road safety management model in Poland must be built on the modern methodology foundation - conformity with the guidelines of the EU transport policy. These conditions meet the New Zealand Land Transport Safety Authority, which has been adapted by the European Safety Transport Council and is recommended by the World Bank.

It should be noted that the concept of the road safety management described in the LTSA model found its reflection in the standard ISO 39001. It has a double and important meanings:

- Meanings that the LTSA philosophy of the road safety management has been recognized by ISO experts in the right direction for the construction of the road safety management systems.
- Meanings that the Polish model of the road safety management, described here, is a part of the latest international trends in this area.

According to the LTSA, the road safety management should be seen as a 3-level process, in which the „product" is the „road safety". This „processing of road safety" has to rely on the continued improvement of the intermediate and the final results of the road safety. The idea is a continuous improvement of the fatalities and serious road accidents reduction process. This philosophy should also set the goal for a future Polish road safety management system.

In the LTSA model there are three levels of the road safety management, Figure 2:

- Management by institutional management functions (IMF), which have run specific interventions to improve road safety.
- Managing through the road safety interventions (RSI) - that is actions improving results of the road safety.

Managing through evaluation of intermediate and final outcomes.

What is needed is a Polish version of the LTSA model. A preliminary description of the Polish version of the IMF is shown in [3]. For example, in terms of the IMF1 it is proposed to include:

- The term national and regional objectives of improving the road safety by the year 2020 and beyond based, inter alia, on the results of the research programs GAMBIT (2005) and ZEUS (2009-2010); see [15].
- Development of Polish versions of road safety indicators by the National Road Safety Council.
- To determine the value of the maximum individual/personal risk of death in traffic at $5.2 \cdot 10^{-5}$ [1/year], by 2020, which means about 2000 deaths, that is a reduction of about 50% in comparison to the year 2011.
- To determine the acceptable social risk of death in traffic in accordance with the criteria of the EU.

The specification of the „Polish" institutional management functions, proposed in works by Szymanek [3, 16], will be helpful to the inventory of „holes" in the RSMS.

Adaptive treatments also require the „road safety interventions" as the second-level components of the management model of the LTSA. Such interventions are the result of implementation of the IMF and will depend on

the circumstances of the Polish RSMS system. That is why their specification should be the subject of wider discussion among people dealing with the road safety research in Poland. Reference material is contained in results of GAMBIT (2005) [17].

The third management level "road safety effects" - these include results of the intermediate and final road safety. The final road safety outcomes show final performance built and implemented road safety management system (RSMS). The LTSA management Safety Performance Indicators apply to the effectiveness rate, SPI, in the third stage. In the next Polish RSMS the SPI indicators developed in the EU project SafetyNet and saved in the "Handbook of SPI", should be used [18-19].

In SafetyNet project, the SPI methodology is developed for the seven key problem areas of the road safety: 1) alcohol, medicines, drugs; 2) speed; 3) protective systems (passive); 4) the use of headlights during the day; 5) vehicles; 6) roads; 7) management of trauma.

Areas 1 and 2 relate to behavior of the road users and are the direct causes of traffic accidents. Areas 3 and 4 relate to prevention of accidents and their consequences, which relate to the reduction of the risk of accidents. Areas 5 and 6 are related to design and technical safety interventions. Area 7 relates to the road accident care and rescue systems.

In the report of the 2005 SafetyNet, the construction schemes and calculations of these seven key indicators of the SPI are provided [20].

It is also proposed to adopt the main EU macro-factors of exposure, risk and consequences of the road accidents. They are a tool for reliable and readable information on the impact of the various measures and remedial action on the level of road safety. The basis for discussions about the future of the Polish macro-indicators of the road safety should be a wide list of indicators of this kind adopted in EU road transport security policy [3, 21].

5 General model of the road risk management in Poland

The road risk management has specific characteristics, but does not differ essentially from the risk management of other systems. This issue concerns the working thesis No. 4 posted earlier. It follows that the risk management process model in Poland should be supported on two pillars:

1. The overall risk management process formula technique - adaptation of the latest formulas, "the overall risk management process" from the standard [1, 14].
2. "Superstructure" risk management process, which is the specificity of the road safety in Poland. The superstructure components that form the LTSA, thus the IMF, interventions and the results of road safety. In addition, the "superstructure" components will be measurable components of the risk management process, as the risk indicators, indicators of risk exposure and the macro-parameters of the road safety.

These ingredients of the Polish road safety management system will be distinguished from other such systems. Conclusion: the risk management processes in different technological systems have similar "general topology of process", but at the same time have a "variety of the process superstructures".

An essential ingredient of the road safety management concept, presented here, is the general scheme of the risk management process. It is the result of an analysis of several risk management standards and it has many borrowings from the standard AS/NZS ISO 31000. The risk management scheme is concurrent with the concept of the Enterprise Risk Management.

5.1 The concept of "three levels" of the road risks management

In transport, there are different risks; some of them generate a starting „accident sequence", which may or may not end in a transport accident. These risks appear in three „places" of the road transport system:

- The structure of the transport system,
- Work processes of transport system and
- Behaviour of the transport system.

It is the main idea of the "three levels" model [11]. It shows three interpretations of any general system:

1. Interpretation of the definition of "structure" (internal construction system).
2. Interpretation of the definition of "function" system, which are identified by the work processes changing ownership.
3. Interpretation that defines the "behaviour" of the system.

The structural interpretation of the system refers to definition of L. von Bertalanffy, according to which the system is a "collection of items remaining in their relations" [22]. Definitions of this type describe the system by means of: a collection of components; a collection of relationships between elements and objective - as a system relationship.

Interpretation system is derived from the functional definition by M. Mesarovic: "the system is a set of relationships between its characteristics" [23]. By studying these relationships one can determine whether the system is abnormal or not. Each system has certain characteristics and changing one or more characteristics is the event. A string of such events determines the functioning of the system and its effects (here: road accidents).

Here is a working thesis of the „three levels" model of the risk management: risk management takes place on three levels of road safety management system:

1. At the level of structure by managing interactions of structure elements,
2. At the level of processes, through the management of work processes in the road traffic and
3. At the level of "behaviours" through risk management, to minimize the negative effects of transport (NET).

Table 1 *Possible structural risks in the road transport. Fragment of theoretical classification*

risk type	interaction of risk factors	structural risk factor
	1-argument mathemat. relations	
R1	HF→A	faults and dangerous behaviors of traffic participants
R2	MRT→A	damage means of road transport
R3	TI →A	defect/damage of transport infrastructure
R4	CRE →A	influence of natural environment factors
R5	N→A	wrong norms, bad rules
	2-argument mathemat. relations	
R6	HF∧MRT → A	wrong fit of means of transport to human-operator
R7	HF∧TI → A	wrong reading of transport infrastructure elements
R8	HF∧CRE→A	influence of natural environment on human operator
R9	HF∧N→A	wrong norms, bad rules
R10	MRT∧TI→A	effects at: means of transport - transport infrastructure, e.g. aquaplaning effect
R11	MRT∧CRE→A	influence of natural environment on mean of transport
R12	MRT∧N→A	norms of reliability and safe for means of transport
R13	TI∧CRE→A	influence of natural environment on transport infrastructure
R14	TI∧N→A	norms of designing and IT exploitation
R15	CRE∧N→A	rules of environmental conditions of transport safety

From the above arguments three levels transport risks are due:

- The 1st level - "structural risk" (SR); therefore a need arises of a logical classification of risks. Helpful is here the classification proposed in [11].
- The 2nd level - "functional risks" (FR) - generated by unwanted changes in traffic, traffic control processes and load processes.
- The 3rd level - "behavioral risks" (BR) - those are the risks of emergence of the "negative effects of transport" (NET), i.e. transport accidents, traffic congestion, environmental degradation.

Structural risks - SR. At a structural approach to interpretation of the road transport system (basically any system) can be considered risks at the level of „the structure of the system". They are conventionally called the „structural risks" and defined as follows: structural risks come from the risks which are the effects of such changes in the interactions between the elements of the system, that can generate losses in the system and environment. Sources of structural risks are undesirable operating transport infrastructures and means of transport, as well as dangerous errors and infringements, in those places of the system where there is a cooperation with a man (human factor is also an element of the structure of the transport system).

Need arises for classification of risks. A method that relies on a review of the logical implications is proposed in [11]: **risk factor (RF) accident (A).**

Consider the five main groups of risk factors present in the road transport system: **HF** - the human factor; **MRT** - means of road transport; **TI** - transport infrastructure; **CRE** - close road environment; **N** - standard, norms.

Each of these risk factors may occur either alone or jointly with others, which conventionally can be saved by the logical conjunction operator (traditionally denoted by a symbol $\wedge$). Then the total number of structural interactions NSI in the system is the sum of combinations without repetition - rows 1 to 5, namely:

$$NSI = \sum_{i=1}^{5} \frac{1}{i!} \cdot \frac{5!}{(5-i)!} = 31\,. \tag{1}$$

Equation (1) above gives a theoretical number of structural types of risks in the system, in which it identified the five main groups of risk factors. To the structural risk factors here concerned one needs to add five others that are defined by implications of the same arguments. The general classification of 33 structural categories of the risk factors is presented in [3, 11]; here is shown a small portion of it, Table 1.

The author cannot name aggregate risks R16-R33. One can only say that these risks are the result of a greater number of aggregated risk factors. So, these risks are more and more "systemic".

Functional risks FR. Structural risks can transform into danger of the „2nd level". It's about the risks of such changes of ownership of a road system that the system and environment can be losses generated. Risks associated with changes in these properties is „functional risk" - that is, the risk of undesirable changes important for safety of the working processes in the system.

Therefore, the interpretation „of the process approach to transport system" is used. According to it transport activity consists of three basic processes:

1. Process of shaping the transport infrastructure: a. planning of infrastructure; b. implementation of infrastructure; c. the operation of the infrastructure.
2. The process of providing a transport service aimed at the flow of people, goods and information. This process

includes organizational, regulatory and administrative elements.

3. Process of creation of the transport policy - is a process of management that ensures the integration and coordination of all elements of the transport system.

Functional risks in transport system may be classified as follows:

- FR1 - the risk of faulty infrastructure formation:
- $FR1_1$: the risk of faulty planning of infrastructure - depend on: an incorrect location; erroneous predictions; disadvantages of financing plans;
- $FR1_2$: the risk of poor implementation of infrastructure - dependent on such risks as: wrong selection of contractors; defective construction work; errors in works monitoring;
- $FR1_3$: the risk of incorrect operation of the transport infrastructure - dependent on: faulty repairs and modernization; erroneous analysis of investment effects.
- FR2 - the risk of faulty transport services - dependent on:
- $FR2_1$ - the risk of faulty organization of the transport process;
- $FR2_2$ - executive risk in the transport process;
- $FR2_3$ - administrative risk in the transport process;
- $FR2_4$ - risk cargo in transport process;
- $FR2_5$ - the risk of traffic (road, rail, sea, air).
- FR3 - the risk of erroneous transport policy - depends on:
- $FR3_1$ - the risk of erroneous macro-forecasts of transport development;
- $FR3_2$ - faulty risk management (the impact of state public-law bodies on transport users).

Behavioral risks BR. Functional threats initiate unwanted behavior of transport and these, in turn, can result in appearance of the negative effects of transport (NET); these are primarily accidents and collisions, but one can also consider other road traffic systems. The NET-s are on the 3rd floor of the related behavioral risks. They can be applied in road safety policy of the EU, through the SPI.

5.2 Defense-depth strategy in the road safety management

Management of safety in transport is a management of „loss avoidance" that can occur at any level and in any place of the specific transport system. Such a management requires methodology of multiple levels of security, in all of the identified critical points of the transport system and at all the levels of the management of such a system. It is a methodology consistent with the strategy of deep defense [24].

To the concept of „defense-in-depth" connect Reason's *Swiss cheese model* - accidents are effects of gaps in the management of the system [25]. In this model, the crucial importance have layers of protection („cheese slices") with differently situated „holes", which is the two-fold gaps: 1) active faults (failures); 2) latent conditions. Reason postulated the need to study such loopholes as major causes of accidents. This model was used, inter alia, in investigation of traffic accidents [26].

In this model is the interpretation is the following: an accident may occur as a result of imposition of dangerous behavior and actions of the driver, road management problems, the vicious traffic and surveillance and the so-called latent conditions, that is „holes" in the Swiss cheese. If at some point of time and the point of the road network „holes" (sometimes called the „windows way") would be simultaneous - it would cause a traffic accident.

Within the deep defense safety strategy there are integral safety barriers, which play a big role in understanding and prevention of accidents. The standard IEC 61511-1 defines a protective layer: "any independent mechanism that reduces the risk by the control, prevention, and weakness" [26]. The main message of the barrier analysis is the password: „hold the threat away from the target."

The deep defense strategy can be interpreted by the blunt-sharp-end model. It specifies the next phases to prevent activation of remote threats (closer to the „blunt end") and stopping local threats („here and now") on the „sharp end". This can be implemented in the next layers of defense that correspond to the levels of safety management. Impact on the risk of an accident is remote in time („blunt end") and the nearby at the time („sharp end"). The strategy of „deep defense" is avoiding errors and use of defense - as soon as possible, from the blunt end.

In the road transport, one can specify the following levels of the road safety management [3]:

1. Creation of a high safety culture - reducing the social consent for high risk of the road accidents,
2. Safety policy planning - development and implementation of vision and improving programs of the safety transport,
3. Management of the road safety at the level of regional and local authorities and road administrations,
4. Safety management work of transport operators,
5. Risk management of road accidents and
6. Reducing the effects of road accidents.

5.3 The concept of the analysis methods selection for the functional and structural risks

The risk analysis methods describe identification of probabilities and consequences/losses associated with the adverse events in the considered system.

For analysis of risks in a particular road transport system crucial is reliable, that is complete and accurate identification of potential threats. Choosing the right method for the hazard identification and risk analysis is a critical moment in the procedure for risk assessment. Success depends on relevancy of this selection. There is no one criterion for selection of methods. Which of the methods one would choose depends on the purpose

Table 2 *The concept of the risk analysis methods selection for the structural and functional risks in the road transport*

methods	areas of risk						layers of management in the road transport system									
	HF	MT	TI	NE	N	EF	CA			RLA		TB		C		PCT	
	structural risks						functional risks										
							FR1					FR2				FR3	
							the risk of faulty infrastructure formation					the risk of faulty transport services				the risk of erroneous transport policy	
							1_1	1_2	1_3	2_1	2_2	2_3	2_4	2_5	3_1	3_2
what -if analysis							x	x	x	x	x	x	x	x	x	x
checklist											x	x	x	x	x	x
risk score											x	x	x	x		
relative ranking													x	x	x	x
preliminary hazard analysis											x	x				
HAZOP																
FMEA																
PRA/OSA/PSA										x	x	x	x	x		
FTA				x			x	x	x							
ETA				x			x	x	x							
CCA				x												
human reliability analysis	x: risks: R1, R6-9, R16-21, R26-27, R31-R32															
barrier analysis							x	x	x	x	x	x				
black spot analysis							x	x	x	x	x	x	x	x		
bow-tie analysis											x	x	x	x		
brainstorming							x	x	x	x	x	x	x	x		
change analysis											x	x	x	x		
swiss cheese model										x	x	x	x	x	x	x

x - is a possible method to apply

and scope of the risk analysis, as well as the preferences of a team undertaking an analysis, its experience and availability of similar analysis objects (sometimes called as referred objects).

There is no „the best" method assigned to specific applications. It is therefore entitled to declare: the selection of an appropriate method of risk analysis is more art than science.

Guided by the above criteria, very preliminary proposals for selection of the analysis methods for the functional and structural risks for road transport were developed. Table 2 was published in the papers [11, 25].

Selection of methods of risk analysis in the road transport system depends on the conventional "areas of risk" and "layers of management in the road transport system". Those areas are identified by the five main groups of risk factors present in the road transport system, described in this article: HF - the human factor; MT - means of transport; TI - the transport infrastructure; NE - natural environment; N - standard, norms. In addition, the area: EF - external factors (floods, terrorist acts) was considered, as well.

Layers of the transport system: CA - central authorities; RLA - regional and local authorities; TB - transport boards; C - carriers; PCT - producing companies for transport.

6 Conclusions

The main interest in this work was to answer the question: what should be the program "sequence of actions to improve the status of road safety" in Poland? Attempt to answer to question is contained in the work [3]. In this text, a "sequence" in summary form version is shown, but as newer and essentially enriched.

Any project for the road safety improvement is located in the wider project - a project to improve quality of the road transport. In order to realize that, it is necessary to ensure: 1. Minimum nuisance for the natural environment. 2. The maximum level of safety.

Realization of the above objectives means the need of implementation of the 5E methodology (Education-Engineering-Enforcement-Encouragement-Evaluation).

Construction of projects to improve the road safety (widely: the road transport safety) in Poland must be supported by scientific research. That research is defficient or even unknown in Poland. Here is a brief list of suggestions in this regard:

1. Development of a Polish methodology of identification of gaps in the traffic management system. It is about latent failure conditions in the management and active management errors; based on the Reason's theory;
2. Continue work on selection criteria and methods of risk analysis, the most useful for transport systems and traffic;
3. Interpretation and adaptation to the conditions of Institutional Management Features IMF known from the LTSA model road safety management;
4. Development of model "3-levels of road risks management"; the excerpt is shown in this article;
5. Adaptation of the "deep defence strategy" for the road safety management.

References

[1] ISO 39001. Road traffic safety (RTS) management systems - requirements with guidance for use. 2012.

[2] OECD. Integrated strategies for safety and environment Road Transport Research. Paris, 1997.

[3] SZYMANEK, A. *Theory and methodology of traffic risk management / Teoria i metodologia zarzadzania ryzykiem w ruchu drogowym* (in Polish). Radom: Wyd. Polit. Radomskiej, 2012. ISBN 978-83-7351-505-5.

[4] BLISS, T. *Implementing the recommendations of the world report on road traffic injury prevention*. Transport Note No. TN-1. Washington D.C.: The World Bank, 2004.

[5] TINGVALL, C. The zero vision. In: 1st International Conference Transportation, Traffic Safety and Health: The New Mobility: proceedings. Springer-Verlag, 1995. p. 35-57.

[6] WEGMAN, F., ELSENAAR, P. *Sustainable solutions to improve road safety in the Netherlands*. SWOV Report D-97-8. Leidschendam, 1997.

[7] ABOURAAD, S., ELSENAAR, P. Road safety management in ESCWA countries critical issues in implementation. In: ESCWA-WHO Regional Conference: proceedings [online] [accessed 2020-02-18]. 2006. Geneve, Switzerland: Global Road Safety Partnership. Available from: http://www.grsproadsafety.org

[8] ADAMS, J. Complexity and uncertainty in a risk averse society. Three framing devices for managing risk. In: For Omega Conference: proceedings [online] [accessed 2020-02-18]. 2007. Available from: http://john-adams.co.uk

[9] GEYSEN, W. J. The structure of safety science: definitions, goals and instruments. In: 1st World Congress on Safety Science: proceedings. Vol. 1. 1990. p. 44 - 80.

[10] REASON, J. *Managing the risks of organizational accidents*. Aldershot: Ashgate, 1997. ISBN 978-1840141054.

[11] SZYMANEK, A. Conception of 4 goals and 3 levels of risk management in road transport systems. *Archives of Transport* [online]. 2010, **22**(3), p. 359-375. ISSN 0866-9546, eISSN 2300-8830. Available from: https://doi.org/10.2478/v10174-010-0022-1

[12] SMEED, R. J. The usefulness of formulae in traffic engineering and road safety. *Accident Analysis and Prevention* [online]. 1972, **4**(4), p. 303-12. ISSN 0001-4575. Available from: https://doi.org/10.1016/0001-4575(72)90029-2

[13] Land Transport Safety Authority. Road Safety to 2010. Wellington, New Zealand, 2003.

[14] ISO-DIS 31000. Risk management - principles and guidelines on implementation [online] [accessed 2020-02-20]. Draft International Standard ISO/DIS 31000. International Organization for Standardization, 2008. Available from: http://rmia.org.au

[15] KRYSTEK, R. *Integrated transport safety system / Zintegrowany system transportu* (in Polish). Vol. 1-3. Warszawa-Gdansk: WKL, 2009-2010.

[16] SZYMANEK, A. *The concept of using SCh-M and LTSA models to identify management gaps in the Polish road safety system (Koncepcja wykorzystania modeli SCh-M I LTSA do identyfikaacji luk zarządzania w polskim systemie bezpieczeństwa drogowego)*. In: 23rd International Scientific Conference TRANSPORT MEANS 2019: proceedings. Sustainability: Research and Solution. Part III, 2019, ISSN 2351-7034, p. 1170-1174.

[17] GAMBIT 2005. *National Road Safety Program 2005-2007-2013 / Krajowy program bezpieczenstwa ruchu drogowego 2005-2007-2013* (in Polish). Warszawa: Ministry of Infrastructure / Ministerstwo Infrastruktury, 2005.

[18] HAKKERT, A. S., GITELMAN, V. *Road safety performance indicators* [online] [accessed 2020-02-20]. Manual. Deliverable D 3.8 of the EU FP6 project SafetyNet. 2007. Available from: http://erso.swov.nl/safetynet

[19] VIS, M. A., VAN GENT, A. L. *Road Safety performance indicators: country comparisons*. Deliverable D3.7a of the EU FP6 project SafetyNet. 2007.

[20] VIS, M. A., AMELINK, M. Safety performance indicators. In: 1st SafetyNet Conference: poster [online] [accessed 2020-02-21]. Deliverable No: D 3.5. 2006. Available from: http://ec.europa.eu/transport/

[21] Al-HAJI, G. *Traffic safety in developing countries-new approaches in technology transfer by using distance education technique*. Master's thesis. LITH-ITN-EX-2001:156-SE. Linkoping University, 2001.

[22] VON BERTALANFFY, L. *General systems theory: foundations, development, applications*. New York: George Braziller Inc., 1968. ISBN 978-0807604533.

[23] MESAROVIC, M. D., TAKAHARA, Y. *General systems theory: mathematical foundations*. 1. ed. Elsevier Science, 1975. ISBN 9780080956220.

[24] SZYMANEK, A. Defence-in-depth strategy in transport risk management. *Communications in Computer and Information Science*. 2010, **104**, p. 51-58. ISSN 1865-0929.

[25] REASON, J. *Human error* [online]. Cambridge: Cambridge University Press, 1990. eISBN 9781139062367. Available from: https://doi.org/10.1017/CBO9781139062367

[26] SALMON, P., REGAN, M., JOHNSTON, I. *Human error and road transport: phase two - a framework for an error tolerant road transport system* [online] [accessed 2020-02-21]. Monash University Accident Research Centre Report Documentation Page. Report No. 257, 2006. ISBN 0732623278. Available from: www.monash.edu.au

SAFETY OF OPERATION AND MAINTENANCE ACTIVITIES OF ROLLING STOCKS BY THE EXAMPLE OF ELECTRIC MULTIPLE UNITS EN96

Artur Kalinowski[1], Norbert Radek[1,*], Jozef Bronček[2]

[1]Faculty of Mechatronics and Mechanical Engineering, Kielce University of Technology, Kielce, Poland
[2]Faculty of Mechanical Engineering, University of Zilina, Zilina, Slovakia

*E-mail of corresponding author: norrad@tu.kielce.pl

Resume
This paper deals with importance of executing maintenance activities of rolling stocks by the example of the electric multiple unit EN96 series and with influence of repairing rolling stocks on the transport safety. It also discusses Poland's Supreme Audit Office report for the 2017 year that concerns the condition of safety of the rail transport in Poland. It describes the way in which the maintenance operations are performed with a division of the maintenance levels that depend of time of utilization and distance travelled by a vehicle.

Article info
Received 25 March 2020
Accepted 13 May 2020
Online 6 November 2020

Keywords:
technological process,
operational safety,
maintenance activities,
EN96 series

Available online: https://doi.org/10.26552/com.C.2021.1.F11-F19

ISSN 1335-4205 (print version)
ISSN 2585-7878 (online version)

1 Introduction

The physical condition of rolling stocks is a very important factor that affects the railway traffic safety. The necessity of performing regular maintenance operations comes from the reason that technical objects are subjected to inevitable wear processes. To prevent malfunctions that can lead to accidents on the railroad, periodic inspections are carried out. In the case of the electric multiple units, such as EN96 series vehicles, requirements of these inspections are included in the Ordinance of the Minister of Infrastructure of October 12, 2005 *On general technical conditions for the use of railway vehicles*. It also includes a list of other documents that describes term of technological and organizational conditions about exploitation of rolling stocks (for example relevant technical specifications and standardization documents, The Regulation concerning the International Carriage of Dangerous Goods by Rail - RID, Regulations concerning the International Haulage of private owner's wagons by Rail - RIP). The concept of operational maintenance of the rolling stocks is defined as organizational and technical activities that are designed to provide safe and economical utilization of technical objects as a part of a given transport service organization, as well as the part of the maintenance plan and applied maintenance level. The maintenance plan is a plan of projects and intensions of such elements as [1]:

- a range and types of inspections and services of rolling stocks;
- a range and frequency of operations that are connected with a preventive maintenance process, whose mainly purpose is to diminish probability of occurring a failure;
- a range and frequency of activities that are connected with a repairing process after declaration of inability of the whole rail vehicle or just its part to operate as intended;
- operations that result from specific maintenance conditions;
- the maintenance level of rolling stocks.

The main purpose of the paper is to present a description of maintenance operations of rolling stocks with the emphasis on safety of these operations, based on the previously created technological process for the EN96 series electric multiple unit. The article presents a comprehensive overview of the maintenance of rolling stocks in Poland. The proper performance of such operations is one of the factors for increasing safety in the rail transport.

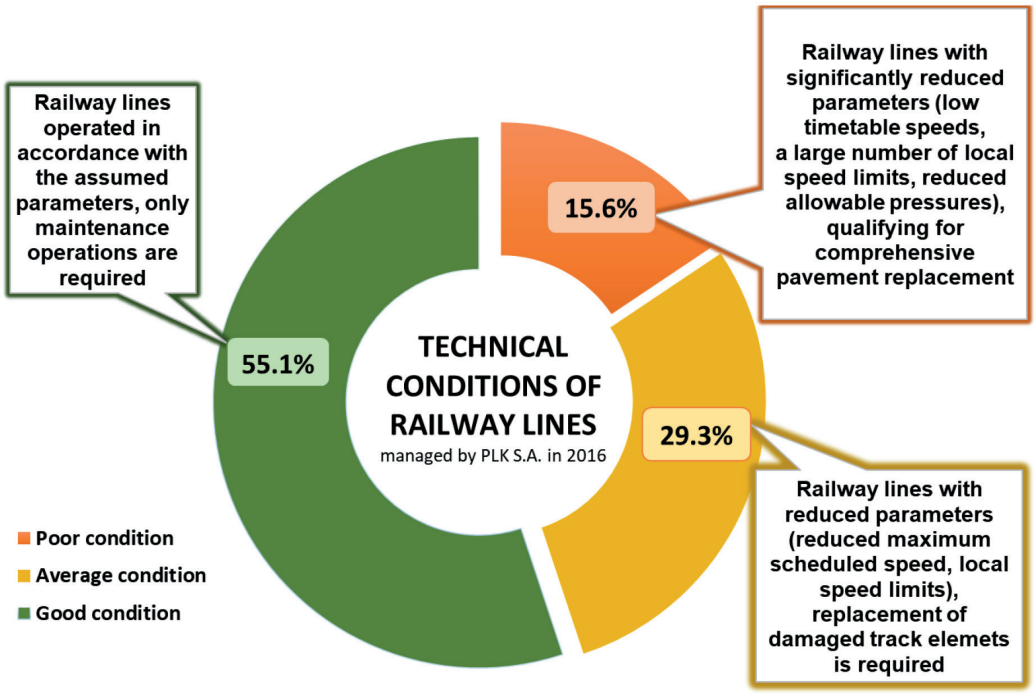

Figure 1 *Technical conditions of railway lines in 2016 [2]*

2 Railway traffic safety in Poland

Technical efficiency of the rolling stocks is one of the basic components of railway safety. The other elements are technical efficiency of the point and line rail infrastructure, transport organization, staff competence and experience, as well as implementing of proper anti-accident legal acts. All the entities involved in the transport process should follow these rules. These entities can be as follows [2]:

- executive entities such as:
  - ❑ railway infrastructure managers,
  - ❑ railway siding users,
  - ❑ railway carriers,
  - ❑ plants and workshops dealing with the maintenance processes of the rolling stock vehicles,
- supervising and controlling entities:
  - ❑ Office of Rail Transport,
  - ❑ State Commission for the Investigation of Railway Accidents,
  - ❑ Ministry of Infrastructure and Development.

The Supreme Audit Office report from 2017 shows that in comparison to 2014 significant improvement in the rail traffic safety did not occur. In the years 2010 - 2014, the railway safety level was very low in comparison to other Europe countries. It was determined not only by poor technical conditions of the rail infrastructure and rolling stock vehicles, but by multiple errors in a transport organization as well and by insufficient protection of transported commodities and passengers from criminal activities. However, the rail transport is still one of the safest means of the land transport with a constant decrease in number of serious accidents year by year. This report, which is concerned with the biggest national railway infrastructure managers, railway stations and 23 biggest rail carriers in Poland, shows the following conclusions [2]:

- the Number of railway accidents has decreased from 638 in 2015 to 581 in 2016, as well as the number of death tolls from 228 in 2015 to 169 in 2016;
- the number of individuals hit by the rolling stock who passed through the railroad in unauthorized places has decreased;
- in the years 2012 - 2016 there was a decrease in crimes committed inside the rolling stocks or in the rail area, such as stealing packages (by 16%), stealing other people's property (by 64.5%), extortion and robberies (by 57%) and beatings (by 72%).

The report discovered improprieties in 23 railway track development and construction units that are responsible for the railway lines in Poland. This led to a significant decline in the safety level of the railway traffic. The reason of this incongruities was, among others, unreliable performance of the line infrastructure maintenance tasks, as well as maintenance of the rail traffic control and monitoring equipment, which is a crucial factor to safety (in the 2017 year 1044.6 km of rail lines were in operation). Another reason was a lack of the radio-stop system encryption. This system is used to prevent the rail accidents. Encryption of this system should be introduced in 2023. The average age of a rolling stock vehicle is also high - for freight carriages - 27 years, for passenger carriages - 26 years and for locomotives - 32 years [2].

Many unused rolling stock vehicles limit utilization possibility of the railroad tracks for maneuvering purposes. Another factor that decreases safety is a lack of the formal settlement of obligations related to passenger carriage, electric rolling stock vehicles maintenance processes

similar to one that regulate freight carriages - MMS System an EMC system. Another problem is a great diversity of types and series of carriages that are in possession in the biggest carriers. This makes difficult for unification and specialization of vehicles maintenance processes. The lack of relevant permissions for the Railway Protection Service to perform tasks included in the Polish Railway Transport Act from 2003, in the case of an event that requires intervention, also causes the low safety level of the rail traffic. Moreover, the railway stations are not considered as a part of the linear infrastructure in the Polish Railway Transport Act, which means that they are not included in the railway Safety Management System (SMS). Another root of the problem is that the PKP PLK S.A. (Polskie Koleje Panstwowe Polskie Linie Kolejowe) still uses the railway lines in a bad condition status and many of the railway platforms are not adjusted to the EU Regulation [3] in the terms of the height and distance of the platform edge from the railway line axis. More than 15% of used railway lines are classified for replacement (Figure 1). This has a major impact on the travel time of rolling stocks. The Supreme Audit Office requested PKP PLK S.A. to develop and implement a program to modernize these railway lines as a part of the company's own supervision [2].

The paper [4] describes the conditions and development of a safety criterion to prevent derailment of rolling stocks. The problem of preventing vehicle derailment should be considered as early as it is possible - at the design stage. Both during the testing and during operation, this is an essential factor for qualifying a vehicle for operation. If it is not met, there is no need for other tests (such as brake tests, strength tests of individual rolling stock components and dynamic tests). The safety criterion against derailment was introduced in 1908 as Nadal's formula and it is still used today to assess the safety of rolling stocks. An assessment of the vehicle's safety against derailment is determined from Equation (1) for the maximum ratio of the leading force Y to the vertical force Q. These forces take variable values when the vehicle is moving. The formula for the safety ratio is as follows:

$$\frac{Y}{Q} = \frac{tg\gamma - \mu}{1 + \mu \times tg\gamma}, \tag{1}$$

where:
γ - angle of inclination of the wheel flange,
μ - friction coefficient between wheel and rail.

After many tedious calculations, focused on selection of the optimal wheel profile, it was assumed that the angle of inclination of the wheel flange for the majority of rolling stocks should be 70 degrees. With a coefficient of friction of 0.36, the safety factor can be calculated - it should not exceed the value of 1.2. In summary, the author of the paper points out that too strict requirements result in a significant increase in vehicle manufacturing costs, high maintenance costs of railway infrastructure and low competitiveness of rail in relation to other modes of transport [4].

In [5] authors presented selected constructions of devices designed to increase passive safety of a rolling stock. These are various types of collision-absorbing elements designed for wagons-tanks, which meet the regulations of UIC (fr. Union internationale des chemins de fer - The International Union of Railways) cards. Development of material engineering and modern construction methods has an increasing influence on the properties of these elements. However, authors also point out the economic aspect - introduction of modern materials and methods will be associated with increased costs.

The safety aspect of rolling stocks also involves adapting the infrastructure to modern high-speed rails. Authors of [6] describe the technological process of adopting the main track and track-bed by using modern machines. On the CMK (Central Railway Main Line in Poland) lines, which are part of European high-speed rails, vehicles will be able to travel up to 250 km/h. Therefore, that imposes the high quality requirements for infrastructure preparation.

Another aspect of the railway traffic safety is an adequate control system. With development of the railway, those systems have improved technical solutions. Devices of the system are [7]:

- stationary equipment,
- rail locking systems,
- rail-road crossing protection systems.

When the physical conditions of such systems worsens excessively, they need to be renewed. Otherwise, damage will occur, which may cause a significant breach of their structure and result in a safety hazard. Due to the need to maintain an appropriate level of the railway traffic safety in Poland, systematic inspections of the physical condition of used railway traffic control devices are carried out. Authors of paper [7] point out that in most cases during the inspection in 2016 the conditions of these devices were unsatisfactory.

The rail transport is one of the safest modes of passenger transport. In the paper [8] the author, draws attention to the statistics of the rail accident mortality. In relation to train-kilometers, Poland is at the second place among countries with the highest mortality risk in the EU. It amounts to 1.5 fatalities per million train-kilometers, when the European average is 0.31. In relation to passenger-kilometers, Poland is at the 8th place with mortality rate of 0.5 victims per million train-kilometers. The European average is 0.16.

The paper [9] assesses the general physical conditions of rolling stock vehicles in Poland. It was stated that despite its constant improvement (which is the result of EU funds and projects implemented in cooperation with them) there are still many problems affecting safety of the rail transport in Poland. The author mentions, among other things, problems with obsolete rolling stock vehicles (30-40-year-old locomotives and wagons not meeting safety requirements). He also compares the physical condition of rolling stock vehicles in Western countries and mentions the difficult access of the new carriers to rolling stock in Poland, as well as the lack of an appropriate purchasing strategy for the new rolling stock vehicles.

Table 1 *Rolling stocks maintenance levels*

maintenance level	tasks characteristic	protocol	execution frequency
P1	checking or monitoring actions performed before the rolling stock goes on the line, after leaving it or while driving. most of the activities can be performed by employees of the carrier	1. assessment of the condition of main assemblies, subassemblies and other systems that have impact on driving safety 2. provision of the rolling stock spare parts 3. replacement of the fast-wearing assemblies and parts during operation	3000 km or 4 days
P2	actions to prevent exceeding wear limits they are performed in specialized workstations during the technical breaks between planned utilizations	1. detailed evaluation of the rolling stock physical condition by inspection of its circuits, examination of components without dismantling and diagnostic tests described in documentation 2. repairs performed by replacing standard components	30 000 km or 60 days
P3	actions to prevent wear limits from being exceeded they are performed in specialized workstations and with excluding the vehicle from intended exploitation	1. detailed evaluation of the rolling stock technical condition by inspection of its circuits, examination of components with dismantling and diagnostic tests described in documentation 2. planned subassembly replacements and small functional assembly repairs that are performed in specialized workstations	210 000 km or 13 months
P4	repair maintenance operations performed in specialized workstations	1. detailed physical condition verification of assemblies and subassemblies included in technical documentations, combined with their dismantling 2. planned replacement of assemblies and subassemblies 3. planned repairments of assemblies and subassemblies performed in specialized workshops	1 100 000 km or 5 years
P5	actions that improve the rolling stock conditions	1. dismantling of assemblies and subassemblies from the rolling stock and their replacement with new or regenerated parts 2. modifications to body of the rolling stocks and gearbox systems	3 300 000 km or 15 years

3 Rolling stocks maintenance levels

According to the guidelines included in the Ordinance of the Minister of October 12, 2005 *on general physical conditions for the operation of railway vehicles*, five levels of the rolling stocks maintenance can be distinguished [1]. They differ in time of performing tasks and in degree of their complexity. Although 15 years have passed since the guidelines were introduced, they are up to date and there is no need to amend them, as they are universal. Table 1 presents maintenance levels of rolling stock and description of maintenance operations that are covered in this Ordinance [1].

Paragraph 2 of [1] defines maintenance levels as a list of maintenance operations performed for a given rolling stock. Realization of this task requires proper technical equipment of the rolling stock maintenance point, relevant employees' qualifications and the proper certification range. Performing particular maintenance level depends on the distance travelled or the service life of the rolling stock. For each of them a technological process is created in which a list of performed maintenance tasks are included. It also contains a list of documents involved, a list of all the tasks that are outsourced to other workshops, a sketch of the rolling stock maintenance point, a list of specialized workstations, a list of relevant personnel competence and skills and required safety precautions. There is also the rule that during the performed maintenance activities from higher level, activities from lower levels should be executed as well.

Moreover, it is required to perform seasonal inspections twice a year. They are designed to prepare the vehicle and all its assemblies and components for changed weather conditions. In the event of malfunction during the normal exploitation, the vehicle should be delivered for repair outside the normal maintenance cycle. The main purpose of this repairment is to reinstate the physical conditions before the malfunctioning. During this repair, documentation and procedures from maintenance level P4 and P5 should be applied.

4 EN96 series electric multiple unit

An electric multiple unit is a railway rolling stock vehicle designed to transport passengers. It consists of:

- assemblies,
- subassemblies,
- elements that can be connected into circuits and systems.

Figure 2 *EN96 during course*

EN96 series 34WE vehicles are the two-part vehicles manufactured and constructed by PESA Bydgoszcz S.A. in 2011. The EN96 is a railway literal code and 34WE is a construction code. Those vehicles were constructed on behalf of the Marshal's Office of the Swietokrzyskie Voivodship in the amount of 4 units. Each of the vehicles has an assigned number EN96-001, EN96-002, EN96-003 or EN96-004. All the units were painted to white-grey. They are called ELFs (ELF - Electric Low Floor) and they are operated by Przewozy Regionalne sp. z o.o. Swietokrzyskie Department with headquarters in Kielce [10]. The EN96 series vehicles were designed to operating in a local passenger transport between big urban areas and in a suburban passenger transport. Their construction was adjusted to high and low rail stations (in the range of 300-960 mm). The vehicle consists of two parts - A and B, it was adapted to operate by two workers and its operating speed is 160 km/h. It could be powered with direct current 1.5 kV/3 kV as well as 15 kV/25 kV AC. The vehicle has two drive bogies and one rolling bogie. A modular body allows to freely arranging the multifunctional spaces - for example a bar corner, space for transport bicycles, bigger luggage [11]. It has 107 standing places and 123 sitting places. Driver's cabs are equipped with ergonomic remote panels and driver's assistant seats, fire extinguishers and air conditioning. Cabins are separated by doors from the passenger compartment. The passenger compartment is equipped with vandal-proof, permanent seats, luggage racks above the seats and handrails. Each part of the vehicle is heated by the floor convection heaters mounted under the seats in special covers. The heat is supplied by two heating and air conditioning units. There is one pair of entrance doors. The vehicle is powered by four asynchronous electric motors with a total active power of 1600 kW. The vehicle has two pneumatic braking systems [10]:

- indirect action pneumatic brake functioning as an emergency brake - it is a classic pneumatic brake, controlled by distributor valves by changing the pressure in the brake cylinders;
- direct-acting electro-pneumatic brake, functioning as the vehicle's main brake, used during its normal utilization. Braking power is regulated from the driver's desk and it depends on the actual operating conditions. Electrodynamic brake is supported by a pneumatic brake or all the braking power could be transferred to the electro pneumatic brake.

The vehicle is equipped by automatic coupling and spring devices for dampening. Powder fire extinguishers are located in the driver's cab and in passenger compartments. The fire protection meets the requirements of the Polish Standards and UIC cards. The vehicle is presented in Figure 2.

5 Safety of maintenance operations performed during technological process on the example of electrical multiple unit EN96

Paragraph 6 of [1] contains information that the maintenance of a vehicle should be performed by entities with qualified staff and by using of relevant technical infrastructure. It is important to provide organizational conditions that guarantee the correct performance of the tasks specified in the maintenance system documentation. Article 14a of [12] describes that each vehicle, before being released to utilization, must be assigned to an entity responsible for its maintenance. According to [13] it could be a railway enterprise, owner or an infrastructure manager. Its objective is to provide the safe vehicle transport by using the maintenance systems. To that purpose, this entity uses own workshops or other with whom it has a contract. Vehicle maintenance is executed according to:

- documentation, which contains maintenance processes for each vehicle,
- requirements that are in force such as maintenance standards and TSL (Transport-Spedition-Logistics) provisions.

Degree of complication and advance of maintenance activities in technical processes depends of individual

Table 2 *List of tests performed in accordance to the P3 maintenance level*

no.	test name
1.	pneumatic system tightness test
2.	the main, auxiliary and parking brake tests
3.	anti-slip traction control test
4.	rail current collector test
5.	air conditioning system test
6.	heating system test
7.	lighting system test
8.	vehicle control systems test
9.	dead-man's vigilance device test
10.	radiotelephone and radiostop test
11.	drive system test
12.	static break and pneumatic system tests
13.	leak tightness test
14.	test drive

maintenance process. In the case of the P3 level assemblies and subassemblies that should be reviewed as follows [10]:

- complete electrical multiple unit - this applies to maintenance operations related to the general condition of the vehicle,
- rolling stock frame,
- body and internal equipment;
- bogies,
- traction motor,
- automated coupling,
- rolling and drive wheelsets,
- brake and pneumatic systems,
- axial gear,
- heating,
- air conditioning for the passenger compartment and for the driver's compartment,
- drive system,
- cooling system of traction motors,
- pantograph,
- doors,
- sanitary equipment and water installation,
- batteries,
- electrical multiple unit systems.

In addition, the auxiliary equipment such as transport trolleys, pullers for dismantling the axle boxes and multimeters, are used. In the case of the P3 maintenance level list of tests are shown in Table 2.

The EN96 vehicle maintenance activities of the P3 level are carried out at a given rolling stock maintenance point at the following workstations [10]:

1. Brake tests workstation,
2. Repair and inspection workstation of rolling stocks in the tent hall.
3. Assembly and disassembly track with an inspection channel,
4. ABP equipment workstation.
5. Workstation for checking the vehicle axis geometry and for grinding the vehicle,
6. Workstation for repairing mechanical speedometers,
7. Workstation for air conditioning repair and maintenance,
8. Workstation for repairing electric and electronic devices,
9. Workstation for analyzing saved vehicle's operational parameters from electronic recorders,
10. Workstation for performing welding operations on vehicles,
11. Workstation for washing and cleaning the rolling stocks,
12. Trackside dead-man's vigilance device checking workstation,
13. Workstation for lifting the rolling stock boxes,
14. Workstation for regulating lighting of the vehicle front,
15. Workstation for washing bogies and other components,
16. Workstation for testing safety valves, pneumatic and electro-pneumatic devices,
17. Battery charging station.
18. Workstation for repairment of current collectors and electric machines,
19. Locksmith's workstation,
20. Workstation for on-board monitoring recording analysis and
21. IT and control workstation.

In order to perform the maintenance operations safely, the rules contained in the technological process for a given vehicle must be strictly observed. All the necessary precautions are listed, as well as special equipment and relevant repair workstations, according to which all the processes should be carried out. Not all of the maintenance activities are performed at the particular rolling stock maintenance point. Some assemblies and subassemblies require specialized equipment and devices that maintenance points do not have either for economic reasons or for need

for the special staff qualifications. Hence, these activities are outsourced to external entities and documents concerning this operation are included in the maintenance process. Test reports are also included in this documentation and the entire process should be carried out in accordance with them. During the inspection-repairing operations, the staff are obligated to [10]:

- use the personal protection equipment,
- abide by rules of Occupational Health and Safety.

Inspection and repair tasks should be preceded by securing the vehicle from the uncontrolled rolling and in the case of operating on pneumatic systems, pressure in these systems must be reduced to the atmospheric level. Regulation of brakes should be performed after completion of work on the chassis and tests of vehicle systems must not be performed until other inspection were not be finished. During the operation, the rolling stock workers should pay particular attention to equipment and devices that are essential to traffic safety. An important aspect that greatly affects safety is monitoring the state of wear of given parts, assemblies and subassemblies in order to determine whether the maximum wear limit has not been exceeded. Parts that are especially prone to exceed the wear limit are [10]:

- rolling surfaces of wheelsets,
- pneumatic systems, their tightness,
- brake blocks,
- bumper suspension devices.

In documentation, provided with the vehicle, there is also a list of subassemblies that are under special technical supervision performed by the Office of Technical Inspection. Those are elements such as air tanks, safety valves etc. The basic requirements for performing maintenance operations by the personnel is a good knowledge of the technical documentation and maintenance systems, as well as a proper training for operation and maintenance of a given rolling stock. These maintenance operations must be carried out by qualified staff e.g. welding tasks should be performed by workshops that are certified according to the Polish Norm PN-M-69009 and employees performing the non-destructive testing should have at least the level 2 qualification in accordance with the PN-EN 473:2002 [10].

6 Technological process P3 of EN96

The technological process for a rolling stock should be performed in accordance with the maintenance system documentation. For the EN96 series vehicles, documentation is provided for employees of the headquarters of Przewozy Regionalne sp. z o.o. and for employees of the rolling stock workshops. The technological process based on design, whose author is Przewozy Regionalne sp. z o.o., consists of the following elements:

- introduction,
- guidelines for the technological process creating,
- change sheet,
- list of related documents,
- situational sketch of the rolling stock maintenance point,
- list of specialized workstations,
- list of personnel,
- performed maintenance activities,
- list of outsourced operations,
- process of acceptance of performed maintenance activities,
- required safety precautions.

Introduction and guidelines for creation of the technological process describe the basic requirements of the technological process. The change sheet should be filled in each case of change to the process. List of related documents contains a list of all the documents that are related to the technological process. Another element of the technological process is a situational sketch of the rolling stock maintenance point. In the case of Przewozy Regionalne sp. z o.o. Swietokrzyskie Department, the rolling stock maintenance point is located in Skarzysko-Kamienna. The sketch contains the workstation layout and a diagram of the track system. The next item in documentation is a list of tools and equipment that are used in the process. The other item is a list of specialized stations with a detailed description of each of them. The list of employees should include the necessary competences of employees and the required number of them that are involved in the maintenance process. The most important element is a list of performed maintenance activities. Then, there is a list of outsourced operations, the process of acceptance of performed operations and required safety precautions. Execution of maintenance process of the rolling stock vehicles is performed in accordance with specific chains of action, known as algorithms or procedures. Each process starts with a description of a specific vehicle, an identification of assemblies and components and possible damages or malfunctions that are not involved in the specific maintenance level process. Maintenance activities start with cleaning assemblies and components, carrying out diagnostic tests, verifying and inspection of the parts concerned, as well as issuing the work instructions. Issuing of instructions concerns the repair of individual components and assemblies, regeneration of certain elements, as well as installing new parts in case of scrapping up the old ones. Once assemblies and components are installed, they must be tested to assess their proper functioning. If the inspection was negative, the repair cycle should be repeated; in the case of a positive inspection, the components should be mounted on a vehicle and a running test should be carried out. Then, if not no additional malfunctions occur, the vehicle is put into service. In each step, the proper documentation should be filled out. Figure 3 presents an example algorithm that describes in general the technological P3 process. This algorithm was prepared according to the EN96 documentation and [10].

The process is carried out every 210 000 km or 13 months of exploitation. This ensures that the technical efficiency of a vehicle is maintained. Its proper performance is crucial for operation safety and, from a practical point

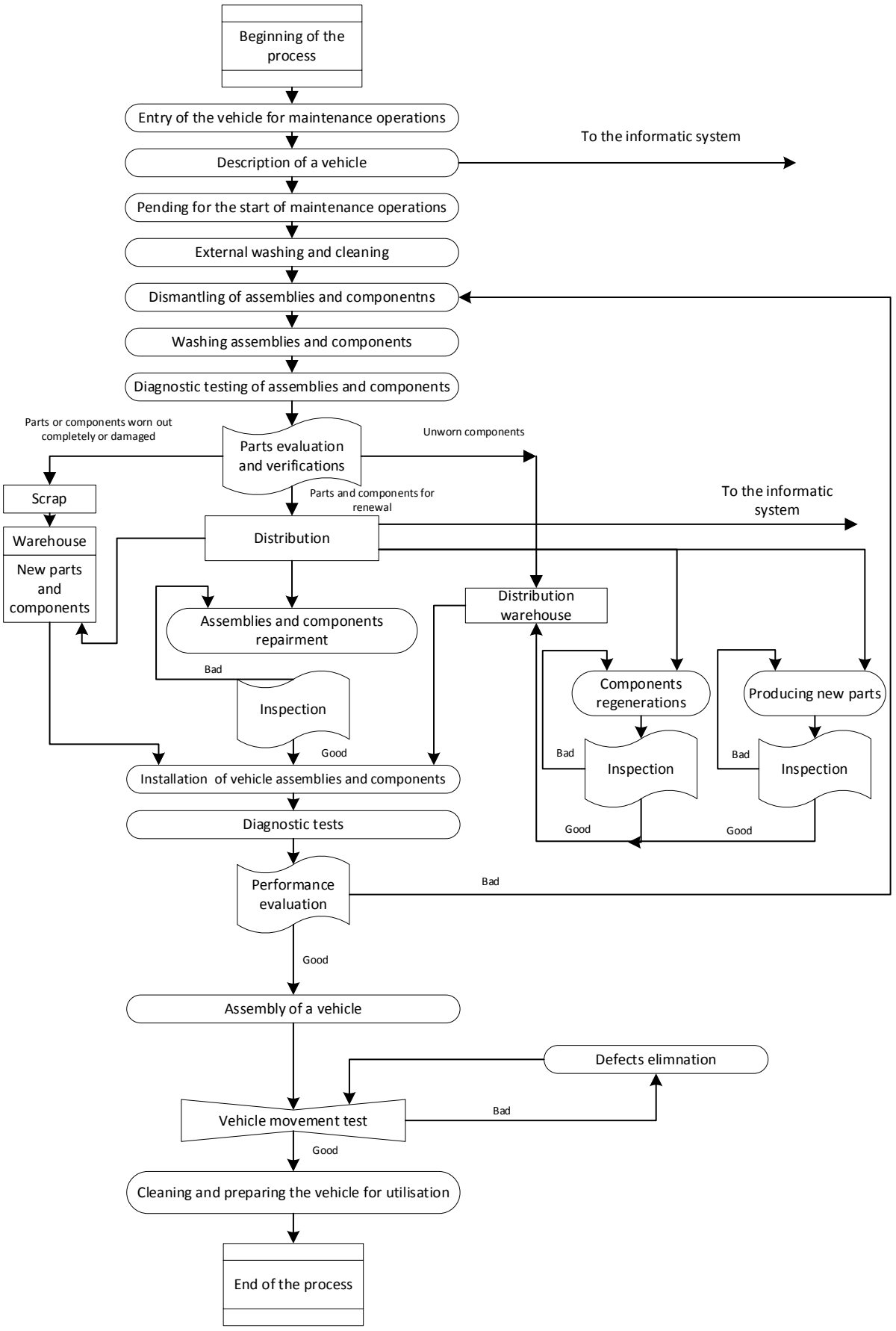

Figure 3 *Algorithm of the technological P3 process*

of view, prevents expensive consequences of unexpected malfunctions. The rolling stocks transport heavy and large loads, which means that their reliability is very important. Breakdowns of these vehicles are not frequent. However, their results can be severe.

7 Conclusions

Safety of the rail transport mainly depends of the physical condition of vehicles and the rail infrastructure conditions. Maintenance activities are performed to reduce the risk of a vehicle malfunction, which directly impacts the operational and rail transport safety, to a minimum. It is crucial to perform those operations in accordance with instructions included in the individual technological processes. The 2017 Supreme Audit Office's report states that the level of the rail transport safety in Poland is not sufficient and that there are many problems that must be eliminated. The most important problem is not the quality of performed maintenance operations but a poor rail line infrastructure conditions and a high age of utilized vehicles. Electrical multiple units of the EN96 series, that have been produced by PESA Bydgoszcz SA, are not worn out in comparison to other rolling stocks in Poland - there were first inspection and repair activities of the P4 level conducted, as well as many operational services that were designed to improve the vehicle's use safety. The P3 maintenance level, discussed in this paper, is a comprehensive vehicle inspection that contains a detailed check of its technical conditions and planned replacements of important vehicle components affecting its operational safety. Result of this paper is a design of an algorithm of the P3 technological process for the rolling stock maintenance. It shows the complexity of performing the maintenance operations that are crucial for safety of the rail transport.

References

[1] Ordinance of the Minister of October 12, 2005 on general physical conditions for the operation of railway vehicles [online] [accessed 2020-01-28]. Available from: http://prawo.sejm.gov.pl/isap.nsf/DocDetails.xsp?id=WDU20052121771

[2] Najwyzsza izba kontroli. Bezpieczenstwo przewozow kolejowych / Audit Office. Railway transport safety (in Polish). [online] [accessed 2019-11-15]. 2018, No. 199/2017/P/17/031/KIN Available from: https://www.nik.gov.pl/plik/id,16137,vp,18659.pdf

[3] Commission Regulation (EU) No 1300/2014 of 18 November 2014 on the technical specifications for interoperability relating to accessibility of the Union's rail system for persons with disabilities and persons with reduced mobility [online] [accessed 2020-01-11]. Available from: http://data.europa.eu/eli/reg/2014/1300/oj

[4] SOBAS, M. Stan i doskonalenie kryteriow bezpieczenstwa przed wykolejeniem pojazdow szynowych / State and improvement of the safety criteria against derailment of the rail vehicles (in Polish). *Pojazdy Szynowe*. 2005, **4**, p. 1-13. ISSN 0138-0370.

[5] NOWICKI, J., SOBAS, M. Przedsiewziecia materialowe i konstrukcyjne zwiekszajace bezpieczenstwo pojazdow szynowych przed skutkami zderzen / Material and constructional undertakings increasing the safety of the rail vehicles against the results of collisions (in Polish). *Pojazdy Szynowe*. 2007, **2**, p. 14-27. ISSN 0138-0370.

[6] CIESLAKOWSKI, S., DULEBA, P. Proces technologiczny naprawy glownej toru i podtorza zespolem PUN dla predkosci pociagow 250 km/h / Technological process of the repair of the main track and substructure with the PUN unit for train speeds of 250 km/h (in Polish). *TTS Technika Transportu Szynowego*. 2000, **7**(10), p. 30-36. ISSN 1232-3829.

[7] SITARZ, M., CHRUZIK, K., GRABON, M., GAMON, W. Stan bezpieczenstwa na kolei w Unii Europejskiej 2013 / State of the safety in the European Union Railways 2013 (in Polish). *TTS Technika Transportu Szynowego*. 2013, **20**(9), p. 45-55. ISSN 1232-3829.

[8] KORNASZEWSKI, M. Analysis of the technical condition of railway traffic control devices using on Polish railways (in Polish). *AUTOBUSY - Technika, Eksploatacja, Systemy Transportowe* [online]. 2018, **19**(6). p. 513-517. ISSN 1509-5878. Available from: https://doi.10.24136/atest.2018.123

[9] BARTCZAK, K. Analiza taboru kolejowego w Polsce / Analysis of rolling stock in Poland (in Polish). *TTS Technika Transportu Szynowego*. 2015, **22**(12), p. 1780-1785. ISSN 1232-3829.

[10] KALINOWSKI, A. *Optimization of maintenance activities of the rolling stock vehicle on example of a vehicle of the EN 96 series (in Polish)*. Master thesis. Kielce: Kielce University of Technology, 2019.

[11] PESA ELF [online] [accessed 2019-11-14]. Available from: http://www.pesa.pl/produkty/elektryczne-zespoly-trakcyjne/elf/

[12] Directive 2004/49/EC of The European Parliament and of The Council of 29 April 2004 on safety on the Community's railways and amending Council Directive 95/18/EC on the licensing of railway undertakings and Directive 2001/14/EC on the allocation of railway infrastructure capacity and the levying of charges for the use of railway infrastructure and safety certification (Railway Safety Directive) [online] [accessed 2020-01-28]. Available from: http://data.europa.eu/eli/dir/2004/49/oj

[13] Directive (EU) 2016/797 of The European Parliament and of The Council of 11 May 2016 on the interoperability of the rail system within the European Union [online] [accessed 2020-01-28]. Available from: http://data.europa.eu/eli/dir/2016/797/oj

OPTIMAL ROUTE DETERMINATION TO PROVIDE RELIEF FOLLOWING AN EARTHQUAKE USING THE TRAFFIC DENSITY RATIO (CASE STUDY: ISFAHAN'S FIRE STATIONS)

Seyed Ahmad Almasi[1], Mohammad Mehdi Khabiri[1,*], Mehdi Fallah Tafti[1], Meisam Akbarzadeh[2]

[1]Department of Civil Engineering, Faculty of Engineering, Yazd University, Yazd, Iran
[2]Department of Transportation Engineering, Isfahan University of Technology, Isfahan, Iran

*E-mail of corresponding author: mkhabiri@yazd.ac.ir

Resume

Despite the very important role of primary arteries and transportation network in providing relief for regions affected by an earthquake and black spots, they have received less attention. Therefore, in the current study, at first, the status quo of the traffic black spots and safe regions was identified to predict the movement direction, evacuation of residents from their habitat and temporary residence using the region zoning. The trips were assigned to the network based on the trip distribution matrix and their relevant travel times both related to the crisis state. The results indicated that out of 94 traffic regions, located in the area under investigation, 7 regions were put in the very low risk or safe regions group and 10 traffic regions were put in a very high-risk group. Additionally, the results indicated that out of 794 links, located in the area under investigation, about 32 links will have a very undesirable status following an earthquake.

Article info

Received 1 May 2020
Accepted 2 July 2020
Online 12 November 2020

Keywords:

earthquake,
crisis management,
emergency evacuation,
optimal route selection,
fire stations

Available online: https://doi.org/10.26552/com.C.2021.1.F20-F32

ISSN 1335-4205 (print version)
ISSN 2585-7878 (online version)

1 Introduction

The occurrence of severe earthquakes, especially in large cities, can lead to widespread human loss. The transportation network is essential for saving lives of injured and providing them with quick medical care. In order to reduce the possible human damages in an earthquake in any city or region, it would be necessary to assess the performance of the transportation network in response to demands to provide relief to travels following an earthquake. One of the issues, which most cities in the world are facing, is natural disasters [1]. These disasters have already killed three million people during the last 25 years and have imposed $23 billion costs in financial damages. Meanwhile, earthquake is one of the most common disasters worldwide and in 2001 was reported as the deadliest event in the world. In Iran, from 1955 to 1995, more than 150,000 people have lost their lives due to earthquakes. The majority of new technologies allow the user to select the best route depending on numerous factors, including road length, grade and speed [2]. Today, as the density of big cities grows and the city's outskirts expand, a dangerous situation occurs in the event of a crisis. The main part of the reaction operation in an earthquake event is relief effort and its main purpose is to reduce casualties during the first hours after the earthquake. In previous earthquakes, the importance of speeding and reducing the time required for relief vehicles to pass through the traffic following an earthquake is highlighted. Goretti et al. [3] took note of the importance of the post-earthquake safety assessments by the European Union Civil Protection Team (EUCPT) after the Ecuadorian 7.8Mw earthquake on April 16, 2016. Helderop and Grubesic [4] explored the implications of network disturbance in their study to provide vulnerability analysis and emergency response in the event of an exacerbation of an alternative network that maintains important information in the network. Extensive research with simulation software has been used to model drivers' traffic behavior, for example, in assessing the capacity of urban roads according to the Slovak standard of simulations in PTV VISSIM and other software, [5].

Various views have been expressed on the vulnerability of the road network and the disruption of traffic after the crisis [6]. In order to find the best possible network, optimal methods for comparing failure scenarios have been used [7]. Result of identifying the critical situations is the approach used to evaluate the different possibilities of degradation of a network in an event [6]. The critical positions of a traffic area in a network are said to be the most effective on the network access flow [8]. In the present study, a vulnerability zoning map related to the transport network risk is obtained and with it, the network reliability, the traffic volume, the risk of each link and its serviceability are calculated. Bell et al. [9] conducted

extensive research on network reliability. In addition, Gunnec and Salman [10] conducted a network reliability review study and defined reliability as the ability of the network to continue service in degradation conditions. Reliability of the travel time was first introduced to account for the reduction in capacity resulting from the road failures and as a function of the travel times ratio is expressed in abnormal (faulty) and normal modes [10]. When this ratio is close to one, the link operates in an ideal capacity and if it approaches infinity, the destination is not accessible due to the severity of congestion on some links. The sudden demand on the network, with the aim of uncertain travel, especially in times of crisis, is also a matter in considering the travel time reliability, but less attention has been paid to it [11]. Generally, the travel-time reliability criterion is useful for evaluation of the network performance based on the quality of service that should be maintained in daily traffic performance. In 2004, Yao et al. [12] studied the vital arteries functions in earthquake conditions and interaction of the vital arteries Poorzahedy and Shetab Bushehri calculated reliability of a small network and provided a criterion for the importance of links, based on the surplus of the user's interest in the simple deterministic route selection models or the non-deterministic (random) balance of the user [13-14]. Khademi et al. studied a post-earthquake response and determined the optimum route for cars in the network [15].

Lu et al. (2016) planned to rebuild the urban road network caused by rain, snow and other adverse weather conditions, traffic accidents and the daily urban network conditions. They used greedy algorithm to retrieve the network after the crisis. The results have shown that this method is the most effective solution for identifying the critical links on the network [16].

The above review indicates that in previous studies, only one of the following two methods has been used for computation of the network reliability, i.e. either the hazard zonation maps have been used or the traffic flow on the road network has been analyzed. However, it seems to be more appropriate to use a combination of both methods and therefore, this innovative approach was adopted in this study. Thus, both network zoning maps and the traffic flow on the road network, obtained from a trip assignment processes, based on the links travel times in crisis situations, have been adopted in this study. As a case study, the performance of the street network of the city of Isfahan has been investigated against a hypothetical earthquake. This street network comprises all the major and minor arterial streets and a number of local access streets in general, the network conditions were considered as close as possible to reality to produce reliable results.

In this study, serviceability is defined as a combination of the street network vulnerability and the zoning map, using criteria such as the height of the buildings - the life period of the buildings, which is a number between zero and one for each rig. In the serviceability index or SC, the higher the vulnerability of the surrounding buildings, i.e. closer to one, the lower the serviceability of their surrounding streets. If the serviceability of the streets were close to zero, it means that the buildings around are not in the good condition and would fall due to an earthquake and due to street blockage the traffic flow on the street would be reduced to zero. This coefficient is calculated by:

$$serviceability = 1 - vulnerability. \quad (1)$$

Due to the fact that an earthquake of magnitude 5 Richter does not destroy the buildings of medium risk, low risk and very low risk, the vulnerability is calculated as:

$$vulnerability = \frac{\text{the number of cells with very vulnerability around the crossing}}{\text{total of the surrounding cells}}. \quad (2)$$

In order to calculate the serviceability of links, located along the paths between the origin-destination pairs, the post-crisis network simulation methods were used in the following steps.

The transportation network of Isfahan was modeled in TransCad software using 2015 census information.

Using a questionnaire based survey, the amount of travel demand after the earthquake and the impact of the local discharges on the traffic network, the magnitude of traffic crisis was calculated.

Traffic flows on the network links were estimated using the trip production and attraction data values obtained for 15 areas of Isfahan using the TransCad software.

Based on the location of the network links on the city's vulnerability map, the serviceability index for each link was determined.

Using the effect of serviceability on the travel time, the critical travel time was calculated for each network link.

Using the critical travel time for each link, the optimal routes for relief vehicles to reach the high-risk areas, which were identified by the TransCad software.

Based on the results, the network traffic shortcomings under current conditions were evaluated and discussed.

Regarding the innovation of this study, it can be said that so far no similar study has been carried out for Isfahan and no TransCad software has been used in previous studies.

2 Research method

2.1 An overview of the city of Isfahan

Isfahan Province with a total area of 107045 square kilometers, accounts for 6.25% of the total area of Iran. This province is located between 30 to 34 degrees and 30 minutes' north latitude and 49 degrees and 36 minutes to 55 degrees and 32 minutes' east longitude in the center of Iran. According to the 2015 census, the population of the city of Isfahan has reached around 2 million. The central district of Isfahan has the highest population density in comparison to the other districts in the city. Most of the traffic passes through the central district that represents the old city

and majority of historic sites are located in this district. Moreover, about 70% of the city's relief centers are located in this area. Therefore, the purpose of this area selection was to reduce human casualties due to the high population density and risk assessment of urban roads. The research method is a combination of documentary, descriptive and analytical research methods. The study area is main streets (major distributors, minor collectors and local access streets) in the central area of Isfahan City. This information is obtained through detailed results of the general population and housing census, a 1.2000 map of Isfahan, detailed plans of the city of Isfahan as well as through documents and journals and related books. The results of this study have been obtained through the ArcGIS, Transcad, Excel software, as well as AHP and Expert Choice software for weight measurement and determination of vulnerability and efficiency of roads and vital transport routes. According to the vulnerability coefficient of each link in the ArcGIS software and importing into the TransCad software, the serviceability of each link for the central area of Isfahan, has finally been identified as the optimal route for any relief vehicle to reach the accident areas. Using the ArcGIS software, land use maps, building density, population density, building life, distance from fault, type of building, number of construction floors and degree of enclosure were modeled. The vulnerability map is then generated in three steps. At the first stage, the main maps that are effective in the destruction of the earthquake are ranked and scored in importance and are also ranked according to the criteria for each major criterion. In the second stage, these criteria are gathered in the ArcGis software using the Raster Composite Computation Function. In the third step, according to the scores of each map, the maps are merged with the ArcGis software using the weighted sum of orders. In the following, the map is divided into 5 codes from the very low risk to high risk. Since in the magnitude 5 earthquake, the high-risk buildings have a high probability of falling, by division of the area of building code 5 into the total area of the surrounding buildings, the coefficient of vulnerability of each link is calculated as a link failure probability.

After zoning the studied area, vulnerable buildings were identified in each section and the probability of blockage of each link was calculated. The links that were able to handle high traffic (serviceability less than 25%) were removed from the network links. After reviewing the opinion of the experts, since the travel time increases with reduction of serviceability, it tends to infinity and with the close availability of service, there is no change in the number of free travel time. Therefore, in general, one can consider three hypotheses for free service life and free travel time as follows: a) inverse relation of degree 2, b) logarithmic relationship, c) linear inverse relationship.

2.2 Principles and method of research

Assuming the inverse relationship between the free travel time and the probability of the link obstruction, probability of the link obstruction was applied as a coefficient in the travel time function to calculate the critical travel time. After allocating traffic, each bow is affected by the traffic from the adjacent links obstruction, based on the same link obstruction probability [17]. After loading the network, the optimal route has been obtained for any desired source-destination:

$$C_0 = \sum_{i=1}^{n} t_i * x_i. \quad (3)$$

In this case t_i is the travel time of each link in normal mode and x_i is the flow rate per link in normal mode and C_0 are the link costs in the normal mode. Therefore, the greater the flow of traffic or the travel time, the greater the costs of travel on the link:

$$C_0^e = \sum_{i=1}^{n-1} t_i^e * x_i^e. \quad (4)$$

In this case, t_i^e is the travel time of the link in the event that one of the network links is interrupted and x_i^e xi e is the traffic flow on the link in the event that one of the network links is cut off and C_0^e are the costs of the link travel in the event that one of the network links is deleted.

Due to the linkage obstruction, the travel time of all links increases. As a result, the friction of the traffic of each link increases [17]. On the other hand, travel time links depends on link service capabilities. Therefore, the lower the link functionality is, the higher travel time or travel costs are:

$$t_{critical} = \frac{t_0}{sc}, \quad (5)$$

where *sc* is a service function and shows that the less service the link is, the higher its free travel time. In fact, in links with the serviceability close to zero, the travel time has increased significantly and when allocating traffic that link was removed from the competition and the traffic was not allocated, i.e. the link was actually blocked. In the links for which the serviceability is close to 1, the buildings around the streets have no effect on changing the link conditions and the traffic allocation in those links are behaving like normal.

In order to calculate the link failure, the information was obtained from the seismic zonation of the city of Isfahan. In these calculations, assumptions were made to simplify and rationalize the process of calculations, which are as follows:

- Only the failure of the buildings located adjacent to the street links would affect the damage caused by the link tissue.
- Another failure of the link is the inability to withstand the link traffic load due to adjacent arcing obstruction.
- The probability of destruction of buildings in each area for all the links is equal to the percentage of buildings damaged in links.
- It was assumed that the network was affected by a magnitude 5 earthquake and its focal point was in the center of Isfahan, with major disruptions in the regions

Table 1 *Weighting results of one of the AHP selective criteria*

criteria	building type	weight factor
building quality	concrete-steel	0.49
	metal-brick	0.13
	brick- adobe	0.22
	wooden- adobe	0.25
	adobe	0.32
building age	0-10	0.10
	10-20	0.16
	20-30	0.31
	>30	0.42
population density	<50	0.02
	50-100	0.06
	100-150	0.09
	150-200	0.13
	200-250	0.16
	250-300	0.24
	>300	0.29
building density	15-50	0.06
	50-75	0.08
	75-100	0.13
	100-150	0.138
	150-250	0.24
	250-300	0.31
land use	very low risk	0.04
	low risk	0.10
	medium risk	0.16
	high risk	0.29
	very high risk	0.41
distance from fault (m)	<1000	0.06
	1000-2000	0.08
	2000-4000	0.13
	4000-6000	0.138
	6000-8000	0.24
	8000-10000	0.31

1 and 3 and part of other areas and percentage of the damaged buildings that caused the link obstruction were considered with this assumption. Therefore, buildings outside the study area are not affected by this earthquake.

3 Data and analysis

In order to investigate the role of communication networks and vulnerability of the building components in traffic areas, it is necessary to examine factors such as population and construction densities, land use, quality of buildings, etc. Thus, the effective index of vulnerability of the building components in the traffic areas of the central area of the city of Isfahan against an earthquake, including the quality of buildings, population density, construction density, land use risk, distance from fault, building life, as well as vulnerabilities in network paths including degree of confidentiality, building quality, building life, fault separation by traffic areas and network links, were investigated. In each study, the selected criteria should be proportional to the purpose of the study and be selected with the opinion of the experts. In this study, the main goal is to relieve and reduce casualties after earthquakes. Therefore, the criteria such as construction density and population density are of a great importance, as well as distance from faults and building life. Moreover, the type of building is the most

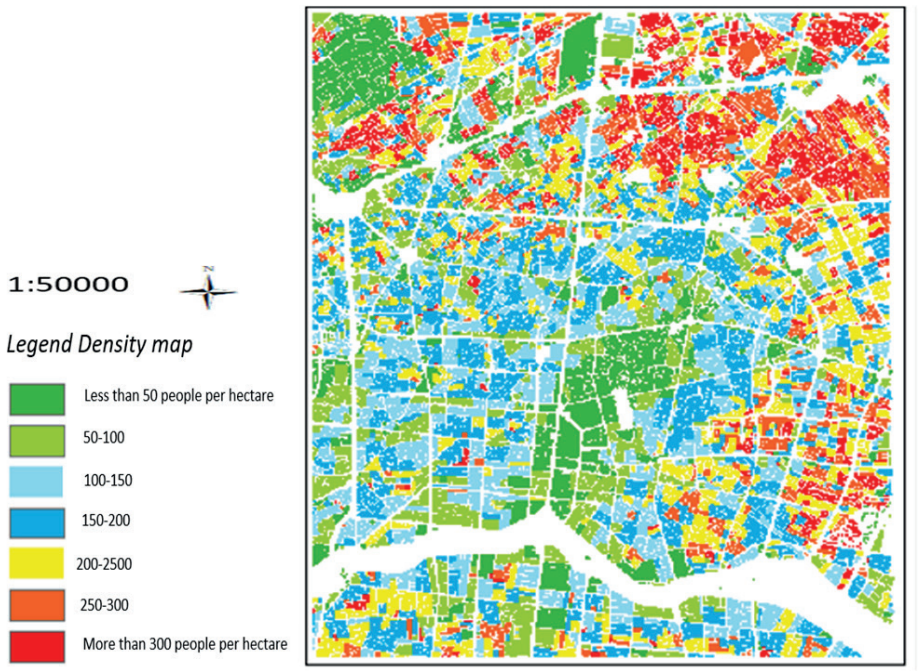

Figure 1 *Density GIS map indicators for the risk assessment*

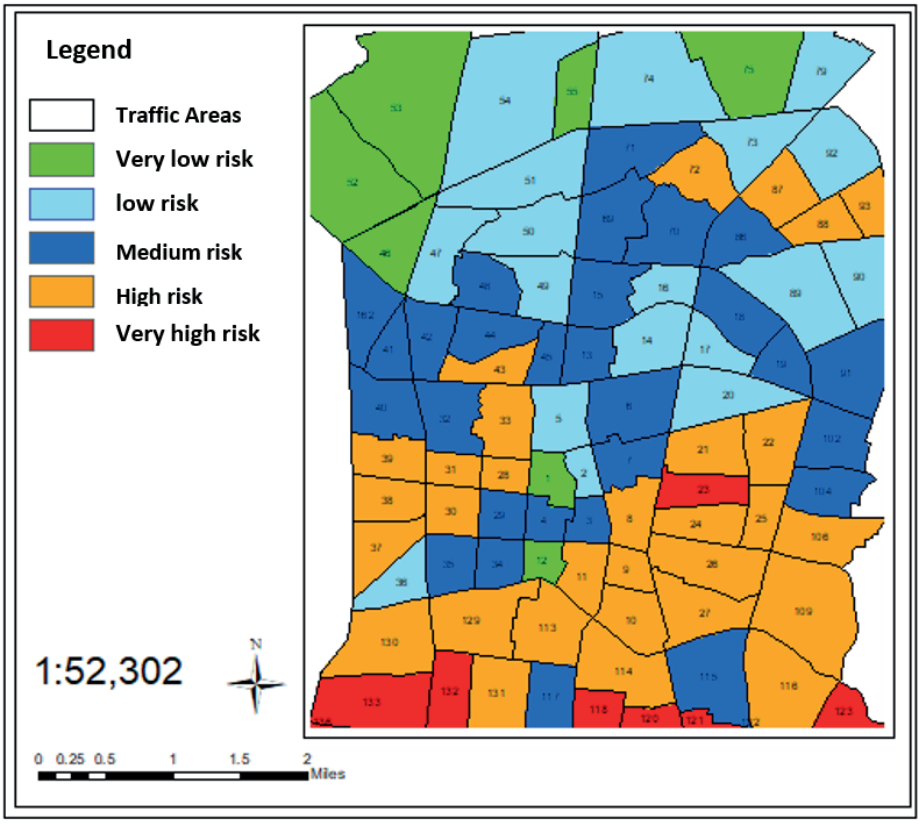

Figure 2 *Zoned map of the study area divided by the traffic areas*

important criterion for vulnerability studies, which is also shown in Table 1 [17-18]. On the other hand, the criterion of degree of confinement (elevation to the width of the passageway) and land use is a good indicator for identifying high-risk passages, which has been used in most studies in the field of this indicator. Figures 1-4 show the steps that were described.

The criteria for weighting factors are based on a combination of Resource Criteria 15, 16 and 17. The method considered in this paper for weighing risk factors is the analytic hierarchy process (AHP) method. That is a structured technique for organizing and analyzing complex decisions, based on mathematics and psychology. It was developed by Taylor, M. I. Page 6 - t represents an

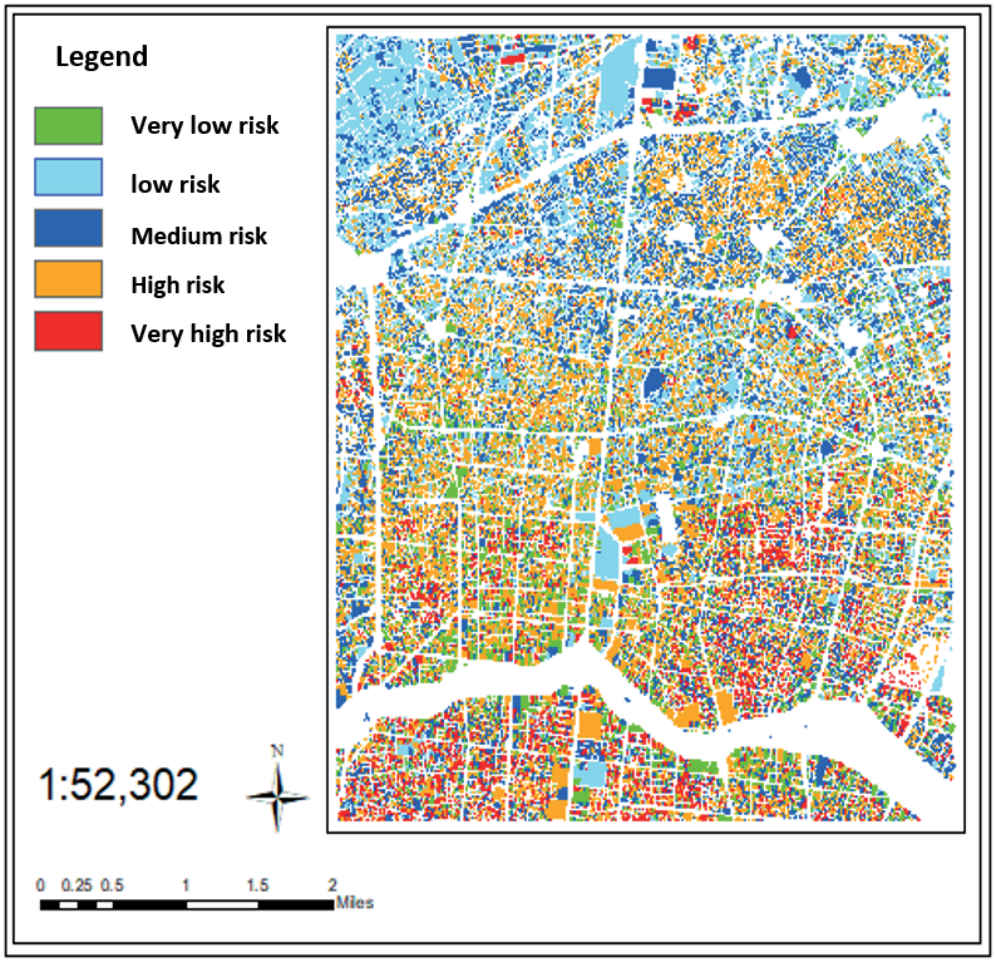

Figure 3 *Earthquake vulnerability zoning map of the investigation area*

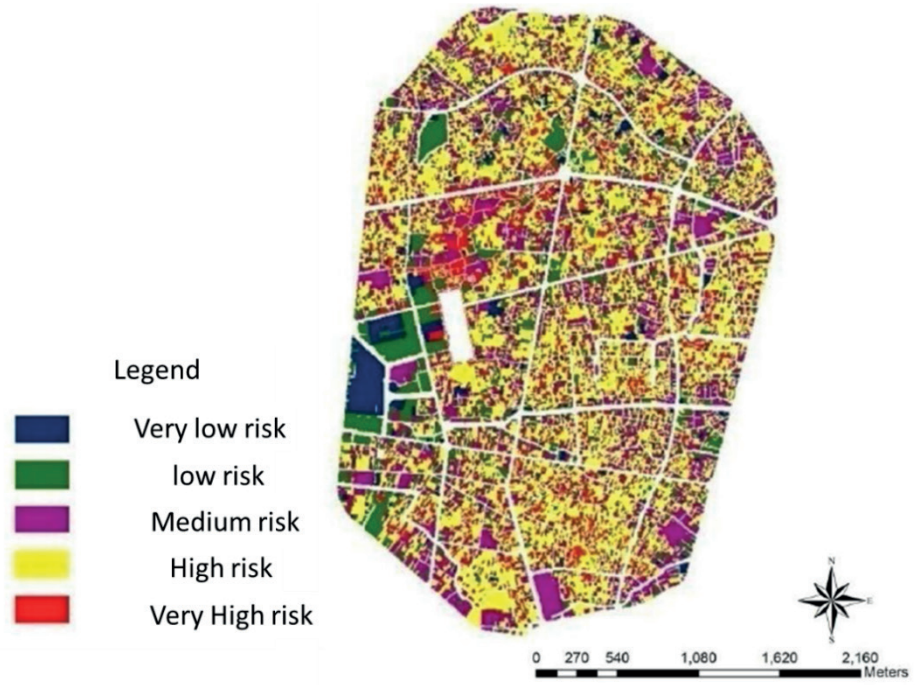

Figure 4 *Sample GIS map indicators for the risk assessment [18]*

Table 2 *An example of the vulnerability situation of secure traffic areas for temporary and post-discharge risk per unit pixel (1m*1m)*

row	traffic area number	very low risk	low risk	medium risk	risky	very risky	sum
vulnerability status of secure traffic areas for temporary accommodation							
1	1	13093	133004	8967	46927	30	202021
	Area (%)	6.48	65.84	4.44	23.23	0.01	100
2	12	26201	19835	18535	20078	6478	91127
	Area (%)	28.75	21.77	20.34	22.03	7.11	100
3	46	18776	150103	77604	68951	2092	317526
	Area (%)	5.91	47.27	24.44	21.72	0.66	100
vulnerability status of hazardous traffic areas							
4	23	23085	7749	65142	87752	75011	258739
	Area (%)	8.92	2.99	25.18	33.92	28.99	100
5	118	10044	25294	20216	61621	126749	243924
	Area (%)	4.12	10.37	8.29	25.26	51.96	100
6	119	46911	14124	47705	55778	109626	274144
	Area (%)	17.11	5.15	17.40	20.35	39.99	100

Table 3 *An example of the serviceability of links with high vulnerability (relation 2) after an earthquake*

link code	very low risk	low risk	medium risk	risky	very risky	sum	link failure probability (percent)	serviceability (percent)
6823039	0	0	0	141	2420	2561	94.49	5.51
10411042	0	0	0	2	30	32	93.75	6.25
10426994	0	0	0	18	1658	1676	98.93	1.07
10591061	2336	1129	9	1188	20295	24957	81.32	18.68
11126266	0	4	0	0	6623	6627	99.94	0.06
12071208	4	2451	0	2	10110	12567	80.45	19.55
12321233	0	0	0	1	114	115	99.13	0.87
12621263	0	0	0	0	845	845	100.0	0.00
12731266	0	7	0	8	2813	2828	99.47	0.53
14561457	1615	0	0	143	7235	8993	80.45	19.55
15151553	236	0	0	0	1248	1484	84.10	15.90
15321545	719	1695	454	2708	32503	38079	85.36	14.64
23387019	7	0	0	1	315	323	97.52	2.48

accurate approach for quantifying the weights of decision criteria. Individual experts' experiences are utilized to estimate the relative magnitudes of factors through pair-wise comparisons [19].

4 Results and discussion

Using the map analysis, it can be seen that the traffic areas 1-12 are based on criteria that are considered good, that is, the vulnerability in these areas is very low and areas 23-123 are very vulnerable. Table 2 shows the vulnerability of the safe areas and high-risk areas of traffic units in terms of pixel units.

Based on results of the proposed criteria, it is predicted that after the earthquake, the traffic area No 75 of the Isfahan Municipality is at risk of being in a very low risk and has higher safety than other traffic areas. The traffic area No 23 does not have a good status and after earthquakes, there would be a lot of damages. Regarding the role of the body of communication networks in the area, streets with sufficient width to provide better access to relief centers

Table 4 *Network link vulnerability status*

number of links	vulnerability status
438	very low risk
164	low risk
111	medium risk
48	risky
33	very risky
794	sum

are in a better position in terms of vulnerability. In other words, these streets are ranked "too low" or "low" due to the division of the role of into 5 parts. In general, the existing trails in the north and center of the region are more vulnerable than the rest of the studied parts. Moving from south to north of the region increases the vulnerability (Table 3). This is due to the fact that the south of the region has a fairly large passageway and buildings of low ages.

According to the classification (Table 4), links with a vulnerability of less than 20% were very low vulnerable in the vulnerability category, links with between 20% and 40% in the low vulnerability category, links with a vulnerability of between 40% and 60% in the normal vulnerability, links whose vulnerability was between 60% and 80% in the high vulnerability group and links, whose vulnerability was higher than 80% were categorized in the very high vulnerable group.

The total number of links analyzed in the surveyed network was 794, since the number of these links and the segregation to the points are highly responsive and serviceable, so only links vulnerable to earthquakes in the high vulnerability category (vulnerability between 60 and 80 percent) and very high (vulnerability between 80% and 100%), so as to identify these links, measures will be taken to manage the pre-crisis situation.

In the normal network mode, regardless of the effect of the link failure caused by the seismicity, Equation (4) was used to calculate travel time per link and to find the shortest travel time between a destination-destination pairs:

$$T_t = t_0\left(1 + \beta\left(\frac{v}{c}\right)^{\alpha}\right), \tag{6}$$

where:
T_t: link travel time in minutes,
t_0: free travel time in minutes,
v: Traffic volume at the link (in terms of vehicle equal to a car for 1 meter wide pass),
c: link capacity.

In this case, the alpha value is equal to 4 and the beta value is equal to 0.15.

In this study, to evaluate the impact of an earthquake on the link failure, the post-earthquake serviceability for each link is specified. In addition to the overwhelming effect of breaking down the network links, due to collapse of the surrounding buildings, links to a network that did not suffer from the critical traffic load and with reduced capacity were revealed, as well. For this reason, by assuming an inverse relationship between serviceability and free travel time, the critical travel time during the earthquake is calculated as:

$$t_{critical} = \frac{t_0}{sc}, \tag{7}$$

where:
$t_{critical}$: Critical free travel time in minutes,
t_0: initial free travel time in minutes,
sc: Serviceability between zero and one.

This relationship shows that the less service a link is, the higher its free travel time. In fact, for the links with serviceability close to zero, travel time have increased significantly. When allocating traffic, that link was eliminated from the competition and the traffic was not allocated, that is, the link is actually blocked. In links where their serviceability is close to 1, that is, the buildings around the traffic jams have no effect on change of the link conditions and the traffic allocation in that link behaves like normal.

Since the impact of the traffic demand outside the scope of the study cannot be considered, it is assumed that the earthquake is strong - magnitude 5 and its focal area is investigated in the center of the range. Therefore, the impact of the buildings around the street outside the studied area is negligible and the serviceability for these links is considered 1. Thus, the travel time in the crisis mode is calculated from:

$$T_{critical} = t_{critical}\left(1 + \beta\left(\frac{v}{c}\right)^{\alpha}\right). \tag{8}$$

In this case, the alpha value is 4 and the beta value is equal to 0.15

- The nodes of their priests end up in the traffic signal. The delay of the link is calculated from:

$$d_1(v) = \frac{(ct - g)^2}{2ct\left(1 - \frac{v}{s}\right)} + 32\left(\frac{v}{\left(\frac{g}{s}\right)}\right)^2 + 5, \tag{9}$$

where:
$d_1\ (v)$: Average delay time for crossing the intersection in the desired street entrance to the intersection,
v: The volume of the traffic flow at the intersection of the intended street entrance,
s: discharge rate in saturation mode,
g: The length of the green light in the direction of the desired street,
C_i: The period of the light at the intersection.

Table 5 *Street transport quality index*

quality level	ratio(V/C)	index
very favorable	< 0.35	A
favorable	0.35-0.5	B
fairly favorable	0.5-0.75	C
unfavorable	0.75-0.9	D
very unfavorable	0.9-1	E
obstruction and congestion	>1	F

Table 6 *Number of fire stations in Isfahan city*

number of fire and rescue stations	median reach for the incident	number of fire lanterns
22	6 minutes and 20 seconds	1375

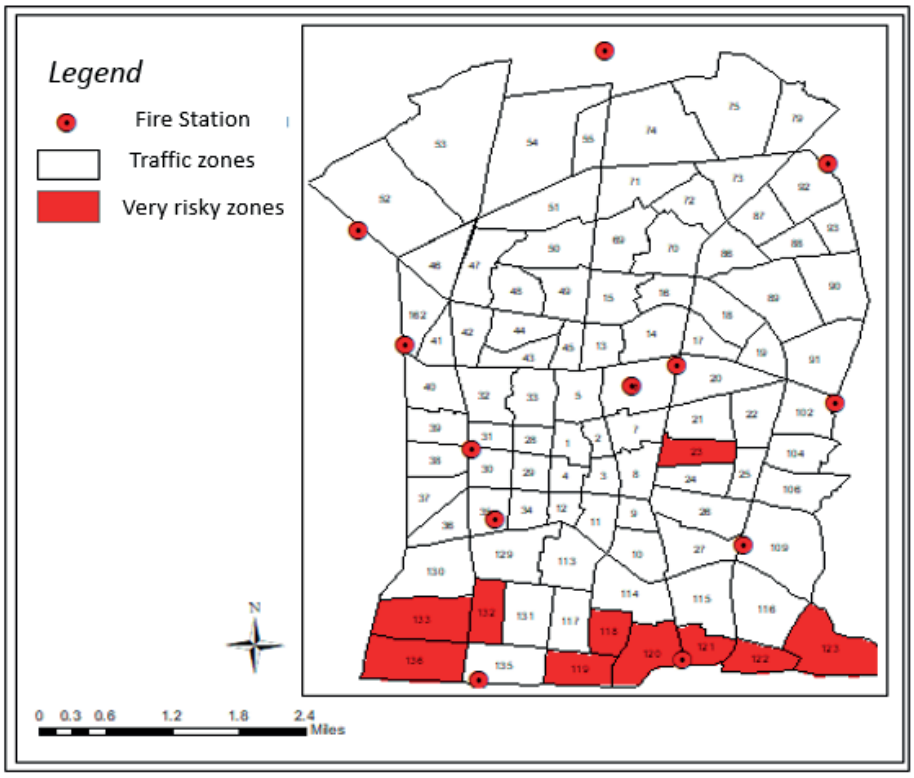

Figure 5 *Location map of the fire stations and high risk areas in GIS*

- The nodes, which their ancestors do not stop at the traffic signal, the link delay is calculated from:

$$d_2(v) = d_0\left(2.5 + 2\left(\frac{v}{Q}\right)^2\right), \quad (10)$$

where:
$d_2(v)$: Average delay time for crossing the intersection,
Q: Practical capacity of intersecting streets,
v: The volume of traffic flow in the desired street inlet to the intersection,
d_0: Fixed coefficient of the delay time at an intersection without lights for streets entering the intersection.
In the above relation, the value of d_0 is calculated as:

$$d_0 = a \times m, \quad (11)$$

where:
m: number of permitted movements at the intersection (except bypassing),
a: Delay coefficient.

In this part of the study, the traffic volume indicator and street capacity using the traffic model (V/C) (traffic to capacity ratio) have been used to determine the level of service and quality of traffic in the streets of Isfahan. The following describes the (V/C) coefficient and the quality of commuting.

Based on the standard classification (Table 5), the quality of the item is categorized into 6 classes based on different values. In this categorization, the quality of service at the service level A is in very favorable conditions and with increasing (V/C), this quality decreases to the service level F.

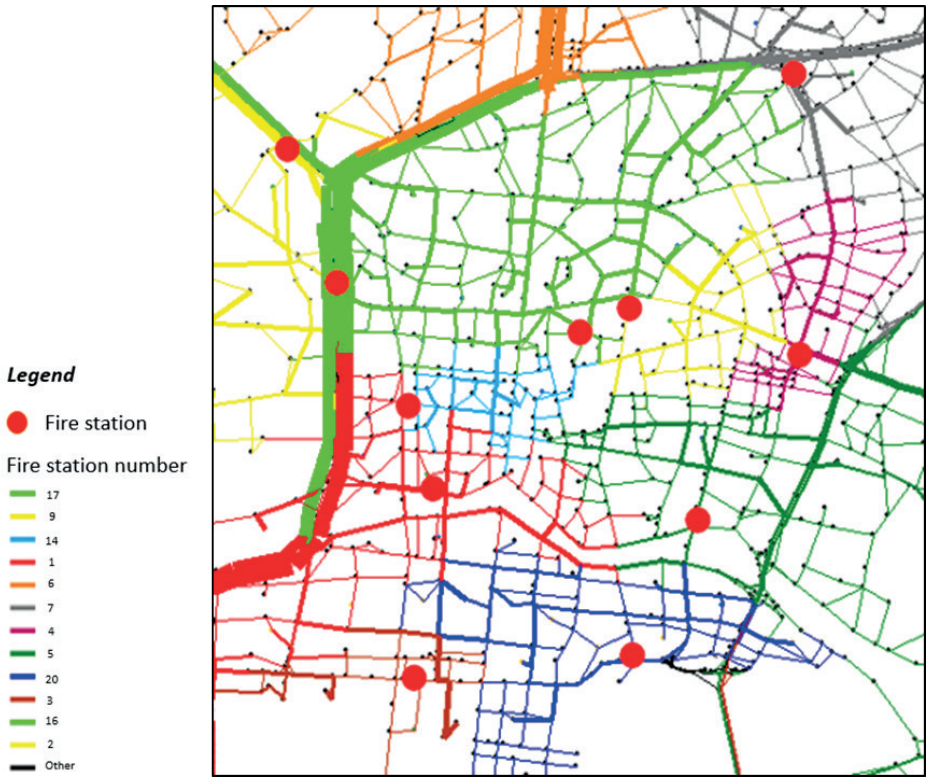

Figure 6 *Traffic density of access routes between the fire stations and the high-risk traffic areas in TransCad software*

Table 7 *Examples of links that have been blocked due to vulnerability*

link name	link code	vulnerability rate (percent)	serviceability (percent)	initial free travel time (seconds)	critical free travel time (seconds)
Kamal Ismail	6823039	94.49	5.51	28	500
Taleghani	10411042	93.75	6.25	10	150
Flower garden	10426994	98.93	1.07	20	700
Flower garden 2	10591061	81.32	18.68	18	70
Kamal	11126266	99.94	0.06	8	5850
Khayyam is heading south	12071208	80.45	19.55	8	30
Khayyam moves north	12321233	99.13	0.87	12	950
Sheikh Baha'i	12621263	100.0	0.00	13	20000000
Saeb	12731266	99.47	0.53	12	1952
Ibn Sina	15321545	85.36	14.64	30	208
Dashtestan	23387019	97.52	2.48	15	325
Bozorgmehr	24012413	96.67	3.33	17	320
Bridge Bozorgmehr	24272630	100.0	0.00	20	29000000
Mofateh	24332432	82.80	17.2	28	152

In order to investigate the relief organizations in the area under study, they were surveyed in a radius of 1000 meters outside the study area in Isfahan, as Table 6. The city of Isfahan now has 22 stations, which should serve the entire city. According to the available statistics, the average reach for the incident is 6 minutes and 20 seconds. The city of Isfahan now has 1375 firefighters.

4.1 Application of the proposed model

After identifying the highly vulnerable areas and location of the fire stations to a radius of 1000 meters outside the scope of the study, it is necessary to determine the optimal route of these vehicles to reach the traffic areas (Figure 5). This path is determined by the final time travel

Table 8 *The shortest path from the fire stations to the traffic area of the incident during the earthquake*

fire station number	risky traffic area	shortest path (seconds)	fire station number	risky traffic area	shortest path (seconds)
5	23	560	20	118	95
5	122	3150	20	119	210
5	123	14250	20	121	621
1	133	625	20	132	535
1	138	1820	3	120	1812

Table 9 *Important fire stations in the investigation range in the earthquake scenario*

fire station number	the number of risky traffic areas covered	stage coverage radius (percent)	the status of the traffic area in which the station is located
20	4	40	very risky
5	3	30	risky
1	2	20	medium risk
3	1	10	medium risk

function after allocation of the network in a critical state. In fact, according to the travel time, the shortest route is the optimal route.

As shown in Figure 6, the coverage radius of all the relief centers and fire stations is shown in the entire range. This coverage radius is partitioned based on the shortest travel time.

In this allocation, streets are divided into 5 categories according to the (V/C) ratio and are graphically plotted. Following the allocation of traffic, critical links were identified. Black links are the links, which have the capacity of crashing after the earthquake and disturb the network. Up to this point, links have been found to be critical and blocked due to the vulnerability of body parts, as well as links that have been identified due to the excessive traffic load of the network (both due to the people's behavioral crisis and the traffic load of the adjacent links blocked by the destruction of the body parts).

Based on the time of the final critical journey (after allocation), it has begun to reroute the relief vehicles. That is, at each stage, an accidental traffic area is considered as the destination and all the relay stations are selected as the source of the trip. After the implementation of the program, the closest area to the traffic area is specified based on the shortest travel time.

In Table 8 the travel time of all the link of the network, which is covered by the traffic area has been calculated and the shortest path between the two points has been identified. The priority is shorter, but if the emergency station does not have the capacity for relief, it will be reset from the nearest station.

According to information in Tables 6 and 7, Station 20, located in Traffic Area 109, has a very good position to access the high-risk areas and can provide assistance to 40% of the total risk areas, but it may suffer from a lack of capacity as it should be sent to 4 traffic areas simultaneously. On the other hand, placing this station in the traffic area 109, which is shown in Figure 5 as a high-risk traffic area, should be considered to prevent the station from being deactivated in the crisis state to reduce losses and provide quicker relief by appropriate measures, according to Table 9.

Studies on the post-earthquake network serviceability so far have not addressed the exact vulnerability and traffic congestion separately, in fact, most of these investigations have addressed either tissue vulnerability or traffic congestion. Therefore, in this study, in addition to carefully examining the vulnerability of traffic areas and urban passages, providing a relationship of this capability has affected the free travel time.

5 Conclusion

In this research, the ArcGIS software first determined the role of the traffic areas of the studied area as well as the vulnerability of each traffic area. Then, by providing the role of the ability to serve each link was identified. After applying the service capability to free travel time, the critical travel time was obtained for each link. Finally, using the TransCad software and considering the location of the fire and air stations in the study area, the shortest route for the relief vehicles to reach each high-risk area of traffic was identified for earthquake scenario.

- The traffic area's physical quality is not enough to determine its vulnerability. Some other factors such as the construction and demolition densities, quality of the building and the building age are also very effective.

- The secure traffic areas are located in the north of the studied area, while the accidental traffic areas are situated in the south. After the earthquake, it is expected that a relatively large traffic wave would be created in the network for evacuation and temporary accommodation. This is the same result as the zoning of the Saidian study for District 3 of the municipality of Isfahan has been achieved and the accuracy of the study is acceptable.

- The high-risk traffic areas are located in close proximity, thus putting relief effortlessly.

- The wider the width of the tunnel, the lower the degree of confinement and eventually the link vulnerability decreases.

Applying the results of this study could also help managers and decision makers to prioritize, refine and strengthen the urban transport network links, so they would be able to make the better decisions.

Acknowledgement

The present paper is extracted from a master dissertation at the Yazd University and funded by the Municipality of Isfahan, No. 121/96/2226.

References

[1] NTZEREMES, P., KIRYTOPOULOS, K. Evaluating the role of risk assessment for road tunnel fire safety: a comparative review within the EU. *Journal of Traffic and Transportation Engineering* [online]. 2019, **6**(3), p. 282-296. ISSN 2095-7564. Available from: https://doi.org/10.1016/j.jtte.2018.10.008

[2] SIUHI, S., MWAKALONGE, J. Opportunities and challenges of smart mobile applications in transportation. *Journal of Traffic and Transportation Engineering* [online]. 2016, **3**(6), p. 582-592. ISSN 2095-7564. Available from: https://doi.org/10.1016/j.jtte.2016.11.001

[3] GORETTI, A., HUTT, C. M., HEDELUND, L. Post-earthquake safety evaluation of buildings in Portoviejo, Manabi province, following the Mw7. 8 Ecuador earthquake of April 16, 2016. *International Journal of Disaster Risk Reduction* [online]. 2017, **24**, p. 271-283. ISSN 2212-4209. Available from: https://doi.org/10.1016/j.ijdrr.2017.06.011

[4] HELDEROP, E., GRUBESIC, T. H. Streets, storm surge and the frailty of urban transport systems: a grid-based approach for identifying informal street network connections to facilitate mobility. *Transportation Research Part D: Transport and Environment* [online]. 2019, **77**, p. 337-351. ISSN 1361-9209. Available from: https://doi.org/10.1016/j.trd.2018.12.024

[5] CELKO, J., KOVAC, M., HUSZAROVA, K. (2019). Influence of Selected Vehicle Maneuvers on Reduction of the Urban Roads Capacity. *Communications-Scientific Letters of the University of Zilina* [online]. 2019, **21**(4), p. 81-89. ISSN 1335-4205, eISSN 2585-7878. Available from: http://komunikacie.uniza.sk/index.php/communications/article/view/1522

[6] TAYLOR, M., SEKHAR, S., D'ESTE, G. Application of accessibility based methods for vulnerability analysis of strategic road networks. *Network Spatial Economy* [online]. 2006, **6**, p. 267-291. ISSN 1566-113X, eISSN 1572-9427. Available from: https://doi.org/10.1007/s11067-006-9284-9

[7] SHEN, W., NIE, Y., ZHANG, H. Dynamic network simplex method for designing emergency evacuation plans. *Transportation Research Record: Journal of the Transportation Research Board* [online]. 2007, **2022**(1), p. 1-25. ISSN 0361-1981, eISSN 2169-4052. Available from: https://doi.org/10.3141/2022-10

[8] HOLLY, M., SHULMAN, L. *Estimating evaluation vulnerability of urban transportation systems using GIS*. A thesis submitted to the Department of Geography in conformity with the requirements for the degree of Master of Arts. Ontario. Canada: Queen's University Kingston, 2008.

[9] BELL, M.G.H. AND Y. IIDA. Transportation Network Analysis. John Wiley & Sons, New York. 1997.

[10] GUNNEC, D., SALMAN, F. S. *Assessing the reliability and the expected performance of a network under disaster risk*. Istanbul: College of Engineering, Koc University, 2006.

[11] RECKER, W., CHUNG, Y., CHEN, A., PARK, J., WANG, L., JI, Z., LIU, H., HORROCKS, M., OH, J.-S. *Considering risk-taking behavior in travel time reliability*. California Partners for Advanced Transit and Highways (PATH). Research report. Berkeley: University of California, 2005.

[12] YAO, B, XIE, L, HUO, E. Study effect of lifeline interaction under seismic conditions. In: 13th World Conference on Earthquake Engineering: proceedings. 2004. 3152.

[13] POORZAHEDY, H., SHETAB BUSHEHRI, S. N. Network performance improvement under stochastic events with long term effects. *Transportation* [online]. 2005, **32**(1), p. 65-85. ISSN 0049-4488, eISSN 1572-9435. Available from: https://doi.org/10.1007/s11116-004-1139-y

[14] CHEN, A., YANG, H., LO, H. K., TANG, W. H. Capacity reliability of a road network: an assessment methodology and numerical results. *Transportation Research Part B: Methodological* [online]. 2002, **36**(3), p. 225-252. ISSN 0191-2615. Available from: https://doi.org/10.1016/S0191-2615(00)00048-5

[15] KHADEMI, N., BALAEI, B., SHAHRI, M., MIRZAEI, M., SARRAFI, B., ZAHABIUN, M., MOHAYMANY, A. S. Transportation network vulnerability analysis for the case of a catastrophic earthquake. *International Journal of Disaster Risk Reduction* [online]. 2015, **12**, p. 234-254. ISSN 2212-4209. Available from: https://doi.org/10.1016/j.ijdrr.2015.01.009

[16] LU, G., XIONG, Y., DING, C., WANG, Y. An optimal schedule for urban road network repair based on the greedy algorithm. *PLOS ONE* [online]. 2016, **11**(10), e0164780. eISSN 1932-6203. Available from: https://doi.org/10.1371/journal.pone.0164780

[17] ALMASI, S. A., KHABIRI, M. M., FALLAH TAFTI, M, AKBARZADEH, M. Development of a methodology to identify crucial emergency stations for quick relief response to the damaged urban areas following an earthquake (case study: Isfahan City Center). *Health in Emergencies and Disasters Quarterly* [online]. 2018, **3**(3), p. 131-142. ISSN 2345-4210. Available from: https://doi.org/10.29252/NRIP.HDQ.3.3.131
[18] SAIDIAN, Z. *Evaluation and evaluation of critical transport arteries in the event of an earthquake: district 3 of Isfahan*. Master's thesis. Yazd: Yazd University, 2014.
[19] TAYLOR, M.; SEKHAR, S. AND D ESTE, G. "Application of Accessibility Based Methods for Vulnerability Analysis of Strategic Road Networks", Network Spatial Economy. (2006), 6: 267-291.

Notations

lists all the symbols	the meaning of the explanatory symbols
SC	the serviceability index
t_i	the travel time of each link in the normal mode
x_i	the flow rate per link in the normal mode
c_0	the link costs in the normal mode
$t_i^{\ e}$	the travel time of the link in the event that one of the network links is interrupted
$x_i^{\ e}$	the traffic flow on the link in the event that one of the network links is cut off
$C_0^{\ e}$	the costs of the link travel in the event that one of the network links is deleted
T_t	the link travel time in minutes
t_0	the free travel time in minutes
v	traffic volume at the link (in terms of vehicle equal to car for 1 meter wide pass)
C	link capacity
$t_{tcritical}$	critical free travel time in minutes
$d_2\ (v)$	average delay time for crossing the intersection
Q	practical capacity of intersecting streets
d_0	fixed coefficient of delay time at an intersection without lights
$d_1\ (v)$	average delay time for crossing the intersection in the desired street entrance
s	the discharge rate in the saturation mode
g	the length of the green light in the direction of the desired street
C_t	the period of the light at the intersection

komunikácie
COMMUNICATIONS

VEDECKÉ LISTY ŽILINSKEJ UNIVERZITY
SCIENTIFIC LETTERS OF THE UNIVERSITY OF ZILINA

VOLUME 23 Number 1

https://doi.org/10.26552/com.J.2021.1

Author guidelines

- All papers have to deal with the topic of transport and be submitted strictly within one of the listed subtopics. Please, refer to list of topics and subtopics here and indicate it clearly when submitting your paper.
- Submitted papers must be unpublished and must not be currently under review for any other publication.
- Manuscripts written in good English must include abstract and keywords also written in English. The abstract should not exceed 10 lines. Please provide minimum three up to maximum seven keywords which express the principal topics of the paper.
- Submitted manuscripts should not exceed 20 pages including figures and graphs.
- Submission should be sent by e-mail – as an attachment – to the following address: komunikacie@uniza.sk.
- The author‘s exact mailing address, full names, E-mail address, telephone or fax number, the name and address of the organization and workplace (also written in English) must be enclosed.
- For all manuscripts a double-blind peer review by at least two independent reviewers and language correction is mandatory.
- After reviewing and incorporating the editor‘s comments, the final draft (before printing) will be sent to authors for final review and minor adjustments.

The full author quidelines are available at:
http://komunikacie.uniza.sk/index.php/communications/guidelines

Address of the editorial office:
University of Zilina
EDIS – Publishing House
Univerzitna 8215/1
010 26 Zilina, Slovakia

E-mail: komunikacie@uniza.sk

Individual issues of the journal can be found on:
http://komunikacie.uniza.sk

Each paper was reviewed by two reviewers.

Journal is excerpted in **SCOPUS** and **EBSCO host**.

Published quarterly by University of Zilina
in EDIS – Publishing House of University of Zilina

Registered No: EV 3672/09

ISSN (print version) 1335-4205
ISSN (online version) 2585-7878

ICO 00397 563

January 2021